

# AEROFOIL SECTIONS

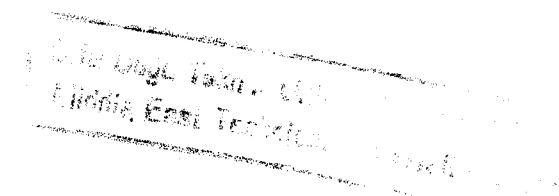
RESULTS FROM WIND-TUNNEL INVESTIGATIONS

THEORETICAL FOUNDATIONS

BY DR. FRIEDRICH WILHELM RIEGELS

Translated from the German by

D. G. RANDALL



LONDON  
BUTTERWORTHS

1961

R513

TL574 A4 R513

METU LIBRARY

Aerofoil sections, results



0020084290

Originally published under the title  
Aerodynamische Profile  
by Verlag R. Oldenbourg, Munich  
© R. Oldenbourg, Munich, 1958

Suggested U.D.C. Number : 533.6.01

English Translation

©

Butterworth & Co. (Publishers) Ltd.  
1961

44546

Made and printed by offset in Great Britain by  
William Clowes and Sons, Limited, London and Beccles

7-84 (Chuvet) 11 Oct 3, 1966 F 101-1-

## LIST OF CONTENTS

<b>Foreword</b>	vii
<b>Preface to the English Edition</b>	ix
<b>Abbreviations</b>	xi
<b>Notes on the References</b>	xiii
<b>1 Nomenclature. Geometry. Survey</b>	
1.1 Definitions. Scope of book	1
1.2 Characteristic Geometrical Quantities	1
1.2.1 Thickness Distribution and Camber Line	1
1.2.2 Parameters	2
1.2.3 Introduction of the Parametric Angle	3
1.3 Experimentally Investigated Families of Profiles	3
1.3.1 Göttingen Profiles	3
1.3.2 Four-figure NACA Profiles	4
1.3.3 Five-figure NACA Profiles	5
1.3.4 First Extension of the Four-figure and Five-figure NACA Series	6
1.3.5 Extension of the NACA Series by the DVL	7
1.3.6 Extension of the NACA Series with regard to the Pressure Distribution. Laminar Profiles	7
1.4 Theoretically Developed Families of Profiles	10
1.4.1 Joukowsky Profiles and Generalisations	10
1.4.2 Kármán-Trefftz and Betz-Kuene Profiles	11
1.4.3 The Hyperbola Family	12
1.4.4 Remarks on Further Families of Profiles	12
1.5 References	12
1.5.1 Books	12
1.5.2 Comprehensive Reports	13
1.5.3 Specialised Reports	13
<b>2 On Experimental Methods. Wind Tunnels and Corrections</b>	
2.1 Some Details of Wind Tunnels used for Profile Measurements	15
2.1.1 Göttingen Wind-tunnels	15
2.1.2 Wind Tunnels of the DVL	16
2.1.3 Wind Tunnels of the NACA	16
2.1.4 British Wind-tunnels	18
2.1.5 Some Other Wind-tunnels	18
2.2 On the Turbulence of Wind-tunnels	18
2.2.1 Degree of Turbulence and Scale of Turbulence	18
2.2.2 The Critical Reynolds Number for Turbulence	19
2.2.3 The Turbulence Factor	19
2.2.4 Influence of the Diameter of the Sphere. More Exact Definition of the Turbulence Factor	19
2.2.5 Comparison Between Hot-wire and Sphere Measurements	20
2.3 General Remarks on Experimental Investigations	21
2.3.1 On Profile Measurements in Wind Tunnels	21
2.3.2 On Wind-tunnel Corrections	21
2.3.3 Influences of Wing-tips and Supports	22
2.3.4 Influence of Turbulence in the Air	22
2.4 References	23
<b>3 Force and Moment Coefficients</b>	
3.1 Characteristic Aerodynamic Quantities	24
3.2 Review of Experimental Results	26
3.2.1 Angle of Incidence Ranging from 0° to 360°	26
3.2.2 Normal Range of Angle of Incidence	26
3.3 Behaviour of the Lift	28
3.3.1 Lift-curve Slope	28
3.3.2 Angle of Zero Lift	29
3.3.3 Effect of Increase in Mach Number on the Relation between Lift and Angle of Incidence	29
3.4 Maximum Lift	30
3.5 Profile Drag	31
3.5.1 Incompressible Flow. Minimum Drag	31
3.5.2 Incompressible Flow. Dependence on Lift Coefficient	32
3.5.3 Compressible Flow	32
3.6 Moment Coefficient, Centre of Pressure, and Aerodynamic Centre	35
3.6.1 Incompressible Flow	35
3.6.2 Compressible Flow	35
3.7 References	37
3.7.1 Incompressible Flow	37
3.7.2 Compressible Flow	38
<b>4 Special Problems</b>	
4.1 Influence of Quality of Surface	40
4.1.1 Older Results	40
4.1.2 Surface Roughness	40
4.1.3 Standard Roughness	40
4.1.4 Isolated Disturbances	42
4.1.5 Permissible Size of Grain and Critical Height of Roughness	44
4.1.6 Waviness	45
4.2 Problems of High Speed in Liquid Media: Cavitation	45
4.3 References	46
4.3.1 Quality of Surface	46
4.3.2 Cavitation	47
<b>5 Profiles with Flaps</b>	
5.1 Survey	48
5.2 Plain Flaps	48
5.3 Split Flaps	48
5.4 Slotted Flaps	48
5.5 Nose Flaps and Slats	49
5.6 References	50
<b>6 Boundary Layer Control</b>	
6.1 Suction as a Means of Increasing the Lift	53
6.2 Blowing as a Means of Increasing the Lift	55

6.3 Suction as a Means of Reducing Drag . . . . .	56	9.3.2 Amplification and Transition . . . . .	95
6.3.1 Keeping the Boundary Layer Laminar . . . . .	56	9.3.3 Keeping the Boundary Layer Laminar at Higher Reynolds Numbers . . . . .	95
6.3.2 Control of the Turbulent Boundary Layer . . . . .	57		
6.4 Pressure and Power Requirements for Boundary Layer Control . . . . .	58	9.4 Calculation of the Profile Drag . . . . .	96
6.5 References . . . . .	59	9.4.1 Preliminary Remarks . . . . .	96
<b>7 The Theory of Wing Profiles I</b>		9.4.2 Drag of the Flat Plate with and without Boundary Layer Control . . . . .	96
Profile Shape and Pressure Distribution in Inviscid Incompressible Flow . . . . .	62	9.4.3 Drag of an Arbitrary Profile . . . . .	97
7.1 General Remarks . . . . .	62	9.5 Calculation of Polars . . . . .	99
7.2 Camber Line and Velocity Distribution . . . . .	62	9.5.1 Calculation of the Maximum Lift . . . . .	99
7.2.1 Simple Special Cases . . . . .	62	9.5.2 Behaviour of the Pitching Moment . . . . .	100
7.2.2 Various Types of Camber Line . . . . .	63	9.6 References . . . . .	100
7.3 Thickness Distribution and Velocity Distribution . . . . .	67		
7.3.1 Simple Special Cases . . . . .	67	<b>10 The Theory of Wing Profiles IV</b>	
7.3.2 More General Thickness Distributions . . . . .	68	Compressible Flow . . . . .	103
7.3.3 Influence of a Sudden Change in Curvature of the Profile Contour . . . . .	70	10.1 General Remarks . . . . .	103
7.4 Cambered Profiles . . . . .	72	10.2 Relation between Speed and Pressure . . . . .	103
7.5 References . . . . .	72	10.3 Subsonic Flow . . . . .	104
<b>8 The Theory of Wing Profiles II</b>		10.3.1 The Prandtl-Glauert Rule . . . . .	104
Numerical Methods . . . . .	74	10.3.2 Higher Approximations . . . . .	105
8.1 The Flow Field . . . . .	74	10.4 Mixed Subsonic and Supersonic Flows . . . . .	107
8.2 Calculation of the Pressure Distribution for a Prescribed Shape of Profile . . . . .	75	10.4.1 Appearance of Shock Waves . . . . .	107
8.2.1 Velocity Distribution on a Thin Profile; Vortex Distribution . . . . .	75	10.4.2 Similarity Rules . . . . .	108
8.2.2 Velocity Distribution on a Symmetrical Profile; Source Distribution and Additional Vortex Distribution . . . . .	76	10.5 Supersonic Flow . . . . .	111
8.2.3 Velocity Distribution on an Unsymmetrical Profile of Finite Thickness and Small Camber . . . . .	76	10.5.1 The Flow Field . . . . .	111
8.2.4 Simple Formulas for Practical Calculation . . . . .	78	10.5.2 The Pressure Distribution in Supersonic Flow . . . . .	112
8.2.5 Forces and Moments . . . . .	79	10.5.3 Approximate Formulas for the Forces on an Arbitrary Profile . . . . .	113
8.3 Calculation of the Profile Shape for a Prescribed Velocity Distribution . . . . .	80	10.5.4 Approximate Formulas for Special Profiles, and Comparison with Wind-tunnel Measurements . . . . .	113
8.3.1 Thin Profiles . . . . .	81	10.5.5 Exact Solution for the Flat Plate . . . . .	114
8.3.2 Symmetrical Profile at Zero Incidence . . . . .	81	10.6 References . . . . .	116
8.3.3 Unsymmetrical Profile at Incidence . . . . .	82		
8.4 Remarks on the Rigorous Methods of Conformal Mapping . . . . .	83	<b>11 Tables</b>	
8.4.1 Older Solutions of the Second Main Problem . . . . .	83	11.1 Collection of Geometrical and Aerodynamic Data . . . . .	120
8.4.2 Iteration without Intermediate Mapping . . . . .	84	11.2 Ordinates, Slopes, and Velocity Distributions of Camber Lines . . . . .	138
8.5 References . . . . .	85	11.3 Profile Co-ordinates . . . . .	141
<b>9 The Theory of Wing Profiles III</b>		11.4 Ordinates and Velocity Distributions (from Potential Theory) of NACA Profiles . . . . .	160
Viscous Flow . . . . .	87	11.5 Measured Force and Moment Coefficients . . . . .	162
9.1 Influence of Reynolds Number on Pressure Distribution and Lift . . . . .	87	11.6 Profiles with High-lift Devices . . . . .	176
9.2 Calculation of Boundary Layers . . . . .	88	11.7 Coefficients for the Determination of Theoretical Lift and Drag Coefficients . . . . .	193
9.2.1 Introductory Remarks . . . . .	88	11.8 Coefficients for Determining the Velocity Distribution (Given the Co-ordinates) . . . . .	194
9.2.2 Basic Equations. Momentum and Energy Theorems . . . . .	89	11.9 Coefficients for Determining the Co-ordinates (Given the Velocities) . . . . .	196
9.2.3 TRUCKENBRODT's Approximate Procedure . . . . .	90		
9.2.4 Effect of Compressibility . . . . .	92		
9.3 Results of Stability Calculations and Calculation of the Critical Reynolds Number . . . . .	93	<b>12 Catalogue of Theoretical and Experimental Results</b>	
9.3.1 The Critical Reynolds Number . . . . .	93	12.1 Pressure Distributions of Camber Lines . . . . .	198
		12.2 Pressure Distributions of Symmetrical Profiles . . . . .	199
		12.3 Pressure Distributions of Cambered Profiles . . . . .	210
		12.4 Measured Pressure Distributions . . . . .	222
		12.4.1 For Incompressible Flow . . . . .	222
		12.4.2 For Compressible Flow . . . . .	228
		12.5 Polars . . . . .	237
		12.5.1 For Incompressible Flow . . . . .	237
		12.5.2 For Compressible Flow . . . . .	256
		12.5.3 With Cavitation . . . . .	267
		List of Symbols . . . . .	275
		Indexes . . . . .	277

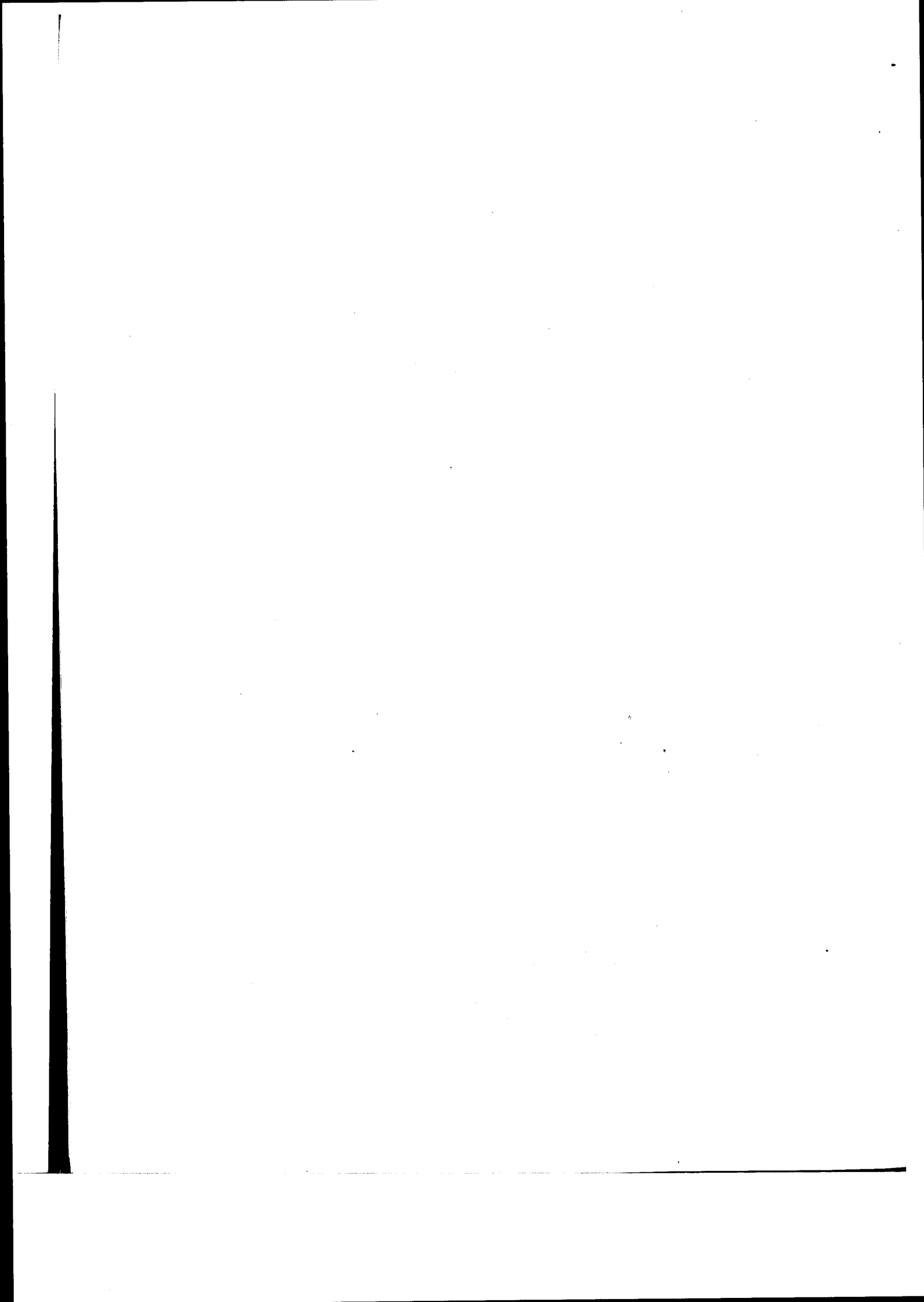
## **FOREWORD**

During the last fifty years fluid dynamics has become indispensable in the solution of industrial problems, particularly those associated with aviation. Technology has advanced so rapidly that, to meet its demands, research on a gigantic scale is necessary. A regrettable consequence of this is that advances in the field of fluid dynamics have become too numerous for one person to be able to survey them. There is therefore a pressing need for surveys of the various branches, so that a reader can obtain a view of the

whole subject and can be informed on the questions of greatest importance. Unfortunately, little has been accomplished in this direction; the chief reason is that few workers have a real mastery of their field. Consequently, this book is most welcome, since it provides a clear and comprehensive survey of the subject of wing profiles. It is highly desirable that similar books should be written on other subjects.

Göttingen,  
*October, 1956*

**ALBERT BETZ**



## PREFACE TO THE ENGLISH EDITION

Dr. Riegels's book was written with the needs of German workers in mind, yet it should appeal to a much wider circle of readers. Our knowledge of a scientific subject is never complete, but further advances in the subject of wing profiles are likely to be small-scale; therefore, a book that surveys all the main theories and discusses many of the experimental investigations should be most valuable. Not the least useful part of the book is the large amount of tabular and graphical information on the geometrical and aerodynamic characteristics of profiles.

In times when slenderness is such a desirable attribute of wings, and supersonic speeds are commonplace, there is

a tendency to think of low-speed, two-dimensional flow as an outdated topic. It is forgotten that the subject is still of importance: it is continually required in the design of ship propellers, turbines, and compressors; and it is still of use for a wide variety of aircraft, ranging from gliders to model aeroplanes.

I wish to thank many of my colleagues at the Royal Aircraft Establishment (not all of them German-born) for their ready help. It is a pleasure to express my gratitude to Mrs. W. T. Lord for performing the secretarial work so competently.

Farnborough,  
*February, 1960*

D. G. RANDALL

## ABBREVIATIONS

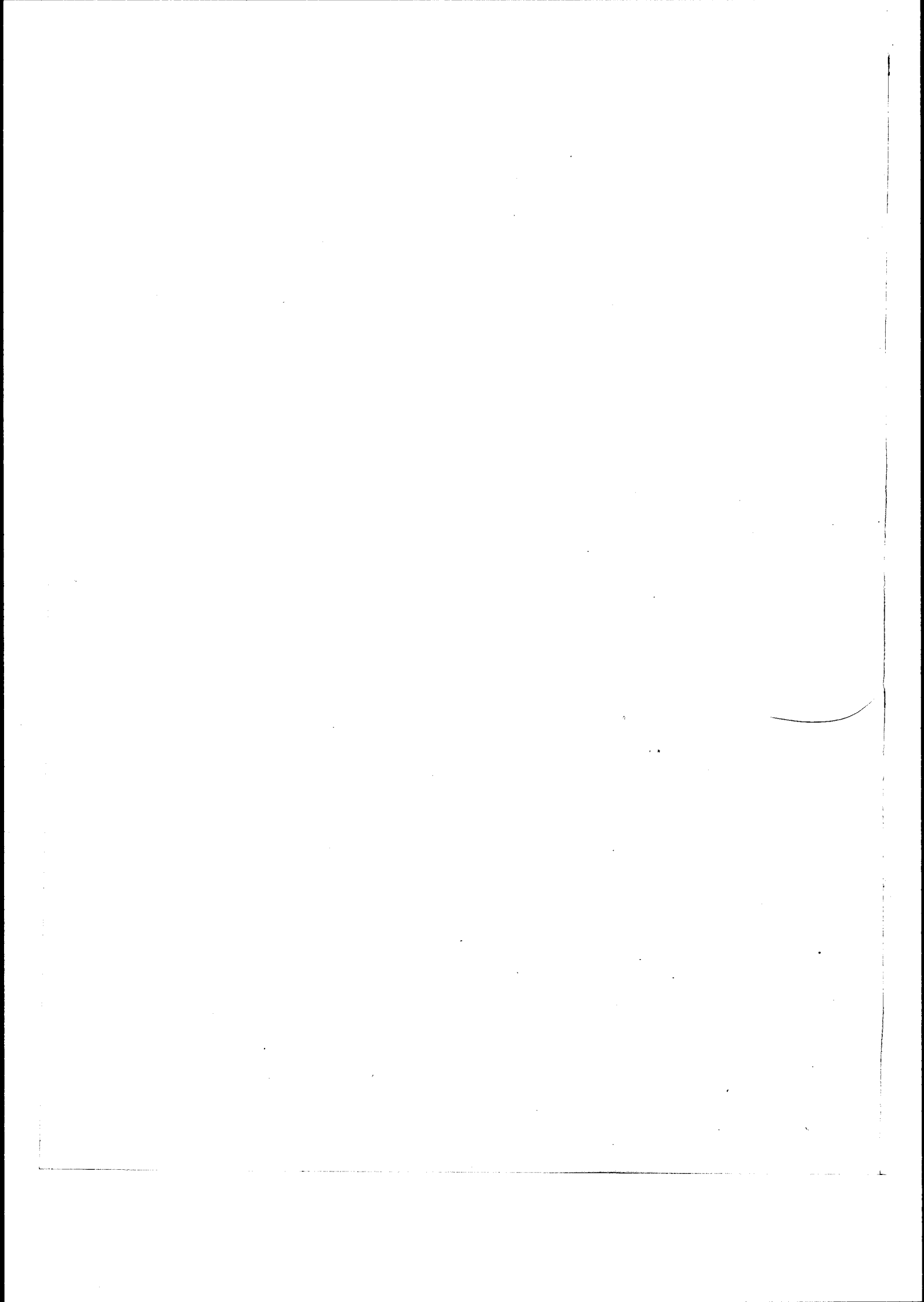
AVA	Aerodynamische Versuchsanstalt Göttingen. In references to reports (often unpublished) the first two figures denote the year when the report appeared; for example, 41/A/15 means Report A/15, produced 1941.	UM	"Deutsche Luftfahrtforschung" ("Forschungsbericht"). Investigations and Communications in the ZWB Series "Deutsche Luftfahrtforschung" ("Untersuchungen und Mitteilungen").
KWI, MPI	Kaiser-Wilhelm-Institut; from 1947, Max Planck-Institut für Strömungsforschung, Göttingen.	ZFM	Zeitschrift für Flugtechnik und Motor-Luftschiff-Fahrt (Oldenbourg, Munich).
Gö. Mon.	Monographs on Progress in German Aeronautical Research since 1939, Göttingen (1946). General Editor: A. Betz. Unpublished. Obtainable from the AVA on payment of appropriate charge.	Lufo	Zeitschrift für Luftfahrtforschung (Oldenbourg, Munich).
DAL	Deutsche Akademie der Luftfahrtforschung.	DVL	Deutsche Versuchsanstalt für Luftfahrt.
LGL	Lilienthalgesellschaft für Luftfahrtforschung.	NACA	National Advisory Committee for Aero-nautics, Washington.
Jb.dDL	Jahrbuch der deutschen Luftfahrtforschung (Oldenbourg, Munich).	R or TR or Rep	} NACA Technical Report.
ZWB	Zentrale für Wissenschaftliches Berichtwesen des Generalluftzeugmeisters.	N or TN	NACA Technical Note.
TB	ZWB Technical Reports ("Technische Berichte").	WR	NACA Wartime Report.
FB	ZWB Research Reports, in the Series	RM	NACA Research Memorandum.
		ARC	Aeronautical Research Council, Ministry of Aviation.
		R & M	Reports and Memoranda, ARC.
		CP	Current Paper, ARC.

## NOTES ON THE REFERENCES

1. The year is given in parentheses.
2. The references at the end of each chapter are arranged alphabetically (according to the names of the authors). Where an author has several works referred to, these are arranged in the order in which they appeared.
3. If an author is referred to in the text, this usually means that a corresponding reference occurs in the list at the end of the chapter. If several works of one author are mentioned, the year of publication is added when the titles do not give sufficient indication.

### *Special Acknowledgment*

Figures 3.20, 3.21, 3.22, 12.51a, 12.60, 12.75, 12.103, and the tables for the profile Gö 625 at  $R = 2 \cdot 10^4$  and  $R = 6 \cdot 3 \cdot 10^4$  have (by kind permission of the publishers) been taken from the book by F. W. SCHMITZ, "Aerodynamik des Flugmodells" (second, enlarged edition), 160 pages, 92 figures, 5 tables, price 13 DM (Carl Lange, Duisburg).



# I. NOMENCLATURE. GEOMETRY. SURVEY

## 1.1 Definitions. Scope of Book

Every body moving through a fluid is subjected to a force. Of particular importance are those bodies for which the component of force opposite to the direction of motion is small compared with the component of force normal to the direction of motion. Bodies with this property are called "wings" if the dimension in one direction, the "thickness", is substantially smaller than the dimensions in two directions normal to each other and to the first direction, the "chord" and the "span"; the direction of the chord is approximately that of the flow at infinity, the "free stream". A section normal to the span is called a "wing profile"—briefly, a "profile". We shall be mainly concerned with two-dimensional flow about a profile—in others words, with flow about a wing of infinite span. The wing is assumed to be moving with a constant speed  $V$ ; if we use a system of co-ordinates fixed with respect to the wing, the speed of the fluid at infinity is assumed to be  $V$ .

## 1.2 Characteristic Geometrical Quantities

### 1.2.1 Thickness Distribution and Camber Line

The ordinates of the profile are measured from some suitable axis, the  $x$ -axis. It is usual to regard the profile as formed by superposition of a "thickness distribution"  $y^{(t)}(x)$ , symmetrical about the  $x$ -axis, on a "camber line"  $y^{(c)}(x)$ . The camber line, sometimes called "mean line" or "skeleton line", has been defined in two ways. The older

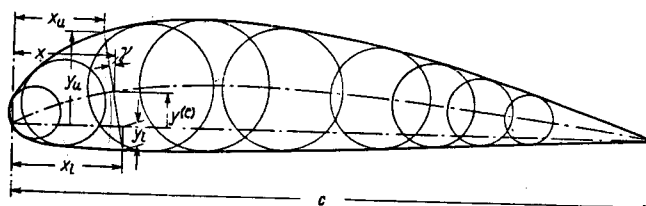


Fig. 1.1. General definition of the camber line

definition assumes that the complete profile is given; the camber line is then the line joining the centres of inscribed circles (Figure 1.1). The second definition assumes that the two parts of the profile are separately given; the complete profile is then formed by measuring the ordinates of the thickness distribution from the camber line in a direction normal to this line. These two definitions are approximately equivalent.† Using the second definition, we obtain for the

† On the difference between the two definitions see BAUSCH.

ordinates of the upper or "suction" side (suffix  $u$ ) and the lower or "pressure" side (suffix  $l$ )

$$x_u = x - y^{(t)} \sin \gamma, \quad y_u = y^{(c)} + y^{(t)} \cos \gamma, \\ x_l = x + y^{(t)} \sin \gamma, \quad y_l = y^{(c)} - y^{(t)} \cos \gamma, \quad (1.1)$$

where  $\tan \gamma = dy^{(c)}/dx$ . This is the method used for the design of NACA profiles; it is the most usual one nowadays. Simple addition and subtraction of the camber line and thickness distribution are usually sufficient for slightly cambered profiles (small  $\gamma$ ):

$$x_u \approx x, \quad y_u \approx y^{(c)} + y^{(t)}, \\ x_l \approx x, \quad y_l \approx y^{(c)} - y^{(t)} \quad (1.2)$$

The co-ordinates  $x$  and  $y$  are generally divided by the chord,  $c$ , of the profile, the origin of co-ordinates lying at the leading edge. In addition to the co-ordinate system  $(x, y)$  a second one  $(\xi, y)$  is often employed, in which the origin

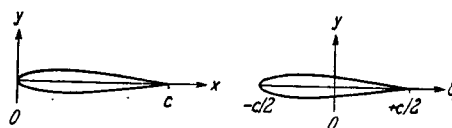


Fig. 1.2. Usual co-ordinate systems

lies at  $x = c/2$ ,  $y = 0$  and the co-ordinates are divided by  $c/2$  instead of by  $c$  (see Figure 1.2). The following relation holds between these two systems†:

$$\xi = x - \frac{c}{2}, \quad \text{or} \quad \frac{\xi}{c/2} = 2 \frac{x}{c} - 1 \quad (1.3)$$

The  $x$ -axis is defined as the straight line joining the ends of the camber line, and so it is possible that a few points in the region of the nose of a cambered profile have a value of  $x$  less than 0, or a value of  $\xi$  less than  $-(c/2)$ ; usually this occurs only when the camber is large. To avoid it we use the longest line joining two points of the profile as reference axis in the theory of Chapters 7 and 8; this axis is obtained from the axis used above (the chord of the camber line) by rotation through a small angle  $\alpha_R$ ; in Table 11.1 this angle is given for some common profiles. The chord of

† The experimenter prefers to work in the region  $0 \leq x \leq c$ : the theorist, to make use of certain symmetrical properties of the formulas, prefers  $-(c/2) \leq \xi \leq (c/2)$ . Both definitions are used in this book; when no confusion is possible,  $c$  is occasionally set equal to 1, or (to avoid the decimal point) to 100.

the pressure side or the tangent at the trailing edge on the pressure side have been used as reference axes for the ordinates when the profile has large camber. For symmetrical profiles (or for thickness distributions) the axis of symmetry is always used as the reference axis.

### 1.2.2 Parameters

For fixing the geometrical form with the help of a few data, the following parameters are suitable.

(a) For the camber line (Figure 1.3):

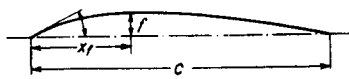


Fig. 1.3. Geometrical parameters of the camber line

1. the ratio of the maximum camber,  $f$ , to the chord,  $c$ —briefly, the “maximum camber”,  $f/c$ ;

2. the position of maximum camber,  $x_f$ , divided by the chord—briefly, the “position of maximum camber”,  $x_f/c$ .

(b) For the thickness distribution (Figure 1.4):

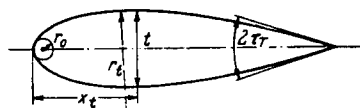


Fig. 1.4. Geometrical parameters of the thickness distribution

1. the ratio of the maximum thickness,  $t$ , to the chord—briefly, the “thickness ratio”,  $t/c$ ;

2. the position of maximum thickness,  $x_t$ , divided by the chord—briefly, the “position of maximum thickness”,  $x_t/c$ ;

3. the nose radius, referred to the chord,

$$\frac{r_0}{c} = \lim_{x \rightarrow 0} \left\{ -\frac{1}{c} \frac{(dy^{(t)})^3}{d^2y^{(t)}/dx^2} \right\}; \quad (1.4)$$

4. the slope at the trailing edge,  $\tan \tau_T = -dy^{(t)}/dx$  at  $x = c$ . In special cases it is useful to know:

5. the leading edge coefficient, †

$$\tan \tau_L = \lim_{x \rightarrow 0} \left( \frac{dy^{(t)}}{dx} - \sqrt{\frac{r_0}{2x}} \right); \quad (1.5)$$

6. the radius of curvature at the maximum thickness, referred to the chord,

$$\frac{r_1}{c} = \frac{1}{c} \frac{1}{d^2y^{(t)}/dx^2} \text{ at } x = x_t. \quad (1.6)$$

The parameters  $f/c$  and  $t/c$  are generally regarded as scale factors of an affine transformation. To have the remaining parameters in a form that remains constant

† This quantity, which by its definition is limited to the thickness distribution, is positive or negative when the nose is respectively hyperbolic or elliptic.

when the scale factors change, the following characteristic combinations of parameters are frequently used; they are designated by the quantity that is made dimensionless.

$$(a) \text{Nose radius: } \rho_0 = \frac{r_0 c}{t^2}. \quad (1.7)$$

$$(b) \text{Slope at the trailing edge: } \varepsilon_T = \frac{\tan \tau_T}{t/c}. \quad (1.8)$$

$$(c) \text{Leading edge coefficient: } \varepsilon_L = \frac{\tan \tau_L}{t/c}. \quad (1.9)$$

(d) Radius of curvature at the maximum thickness:

$$\rho_1 = \frac{r_1 t}{c^2}. \quad (1.10)$$

If the profile is designed empirically the parameters must be found graphically. To determine the camber line, inscribed circles are drawn and their centres joined† (Figure 1.1); the quantities  $t$  and  $f$  can then be measured. For the determination of the nose radius,  $r_0/c$ , and the leading edge coefficient,  $\tan \tau_L$ , the quantity  $y^{(t)}/\sqrt{x}$  is plotted against  $x$  (Figure 1.5). The slope at the trailing

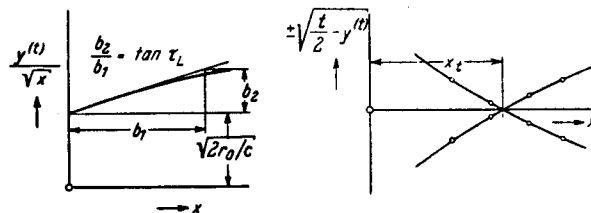


Fig. 1.5. The determination of  $\frac{r_0}{c}$  and  $\tan \tau_L$

Fig. 1.6. The determination of the position of maximum thickness,  $\frac{x_t}{c}$

edge,  $\tan \tau_T$ , can be measured sufficiently accurately if  $y^{(t)}$  is drawn with an enlarged scale near  $x = c$ . The position of maximum thickness,  $x_t$ , is obtained as in Figure 1.6, where the quantity  $\pm \sqrt{\frac{t}{2} - y^{(t)}}$  is plotted against  $x$ . When  $x_t$  has been thus found, the radius of curvature at the maximum thickness,  $r_1/c$ , is obtained by plotting  $\frac{(x - x_t)^2}{(t/2) - y^{(t)}}$  against  $x$  (Figure 1.7).

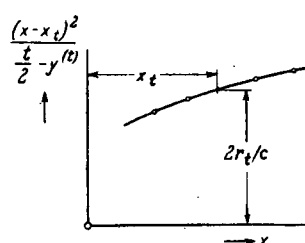


Fig. 1.7. The determination of the radius of curvature at the maximum thickness,  $r_1$

In the construction of profiles by the NACA method it is useful to know the initial slope of the camber line, because the centre of the circle of curvature at the nose is assumed

† For a refined method see BAUSCH.

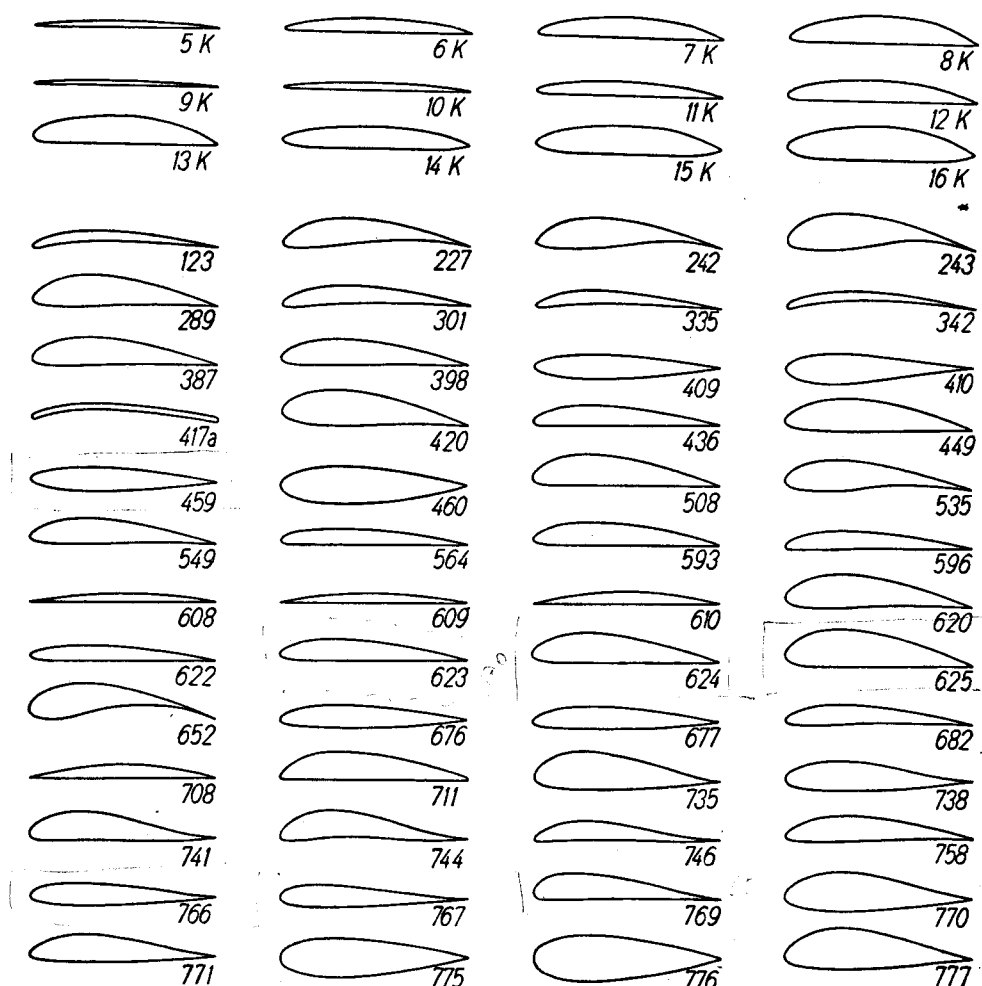


Fig. 1.8. Survey of some Göttingen profiles

to lie on this line; for NACA profiles it is usual to give the initial slope of the camber line in addition to the nose radius; for a certain class of camber lines, with infinite slope at the leading edge, it is further agreed to give the slope at  $x/c = 0.005$ , and to use this for constructing the profile nose.

### 1.2.3 Introduction of the Parametric Angle

In theoretical work it is convenient to introduce a parametric angle,  $\varphi$ , in place of  $x$  by the relationship

$$x = \frac{c}{2} + \frac{c}{2} \cos \varphi, \text{ or } \xi = \frac{c}{2} \cos \varphi \quad (1.11)$$

(see Chapter 7). Any profile can be represented by a Fourier series

$$\frac{y}{c/2} = \sum_{v=0}^{\infty} (a_v \cos v\varphi + b_v \sin v\varphi), \quad (1.12)$$

$c$  being the greatest chord of the profile; the cosine series represents the camber line, and the sine series represents the thickness distribution.

We end this section by showing how the nose radius is determined from the representation of  $y$  as a function of  $\varphi$ . If the profile is not pointed at the nose it can be described in the region of the nose by an equation of the form

$$y = b\sqrt{x} + \dots; \text{ hence, } y' = \frac{b}{2}x^{-1/2} \text{ and } y'' = -\frac{b}{4}x^{-3/2},$$

so that  $\frac{r_0}{c} = \frac{b^2}{2}$  or  $b = \sqrt{2\frac{r_0}{c}}$ . If  $y$  is now plotted against  $\varphi$  in the neighbourhood of  $\varphi = \pi$ , the slope of this curve is  $\frac{1}{c} \frac{dy}{d\varphi} = \frac{dy}{dx} \frac{dx}{cd\varphi} = -\frac{b}{2}$  when  $\varphi = \pi$ ; since this slope is proportional to the constant  $b$ , it is a measure of the nose radius.

## 1.3 Experimentally Investigated Families of Profiles

### 1.3.1 Göttingen Profiles

"Göttingen" profiles are numbered approximately in the order in which they were tested. Figure 1.8 is a survey of the profiles described here; in general, the few profiles have been preferred which form systematic groups with common characteristics. To these belong the following.

- (a) The symmetrical profiles: Gö 409, 410, 459, 460.

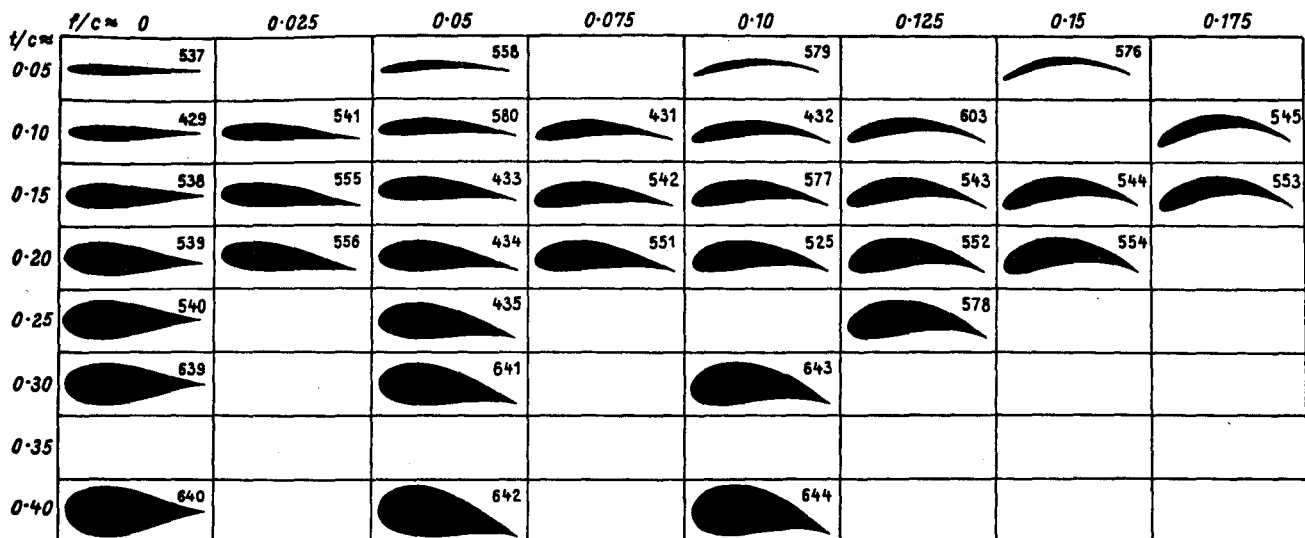


Fig. 1.9. Survey of measured Joukowsky profiles

- (b) The profiles whose pressure side is predominantly straight: Gö 436, 508, 564, 593; the series Gö 622, 623, 624, 625 (with thickness ratios  $t/c = 0.08, 0.12, 0.16, 0.20$ ).

- (c) Profiles which are segments of circles.

1. With sharp nose and trailing edge: Gö 608, 609, 610, 708 (ratio of radius of circular arc to chord is 2.8, 2.45, 1.9, 1.75, so that  $f/c = 0.045, 0.051, 0.066, 0.071$ ), and Gö 1K, 2K, 4K (with  $f/c = 0.0385, 0.0735, 0.1475$ ).
2. With nose and trailing edge rounded: Gö 5K, 6K, 7K, 8K, an affine series with thickness ratios  $t/c = 0.037, 0.075, 0.110, 0.1485$ ; Gö 9K, 10K, 11K, 12K, 13K, an affine series with  $t/c = 0.0245, 0.0385, 0.0745, 0.1110, 0.1480$ ; Gö 14K, 15K, 16K, an affine series with  $t/c = 0.12, 0.15, 0.1815$ . (The K which follows the numbers signifies that measurements were carried out on these profiles in the presence of cavitation.)

- (d) The American profiles: M6, identical with Gö 677; M12, identical with Gö 676.

- (e) The Joukowsky profiles (Figure 1.9), which are shown here because of their extraordinarily large maximum cambers and thickness ratios.

The remaining profiles are mostly without systematic behaviour, but, because of their special properties, they have proved to be of use for certain purposes. The ordinates of the profiles are collected together in Table 11.3.

### 1.3.2 Four-figure NACA Profiles

Figure 1.10 is a survey of typical profiles of this kind; their designation is descriptive of the profile geometry, and the figures have the following meaning [R460].

*The first figure:* the maximum camber as a percentage of the chord.

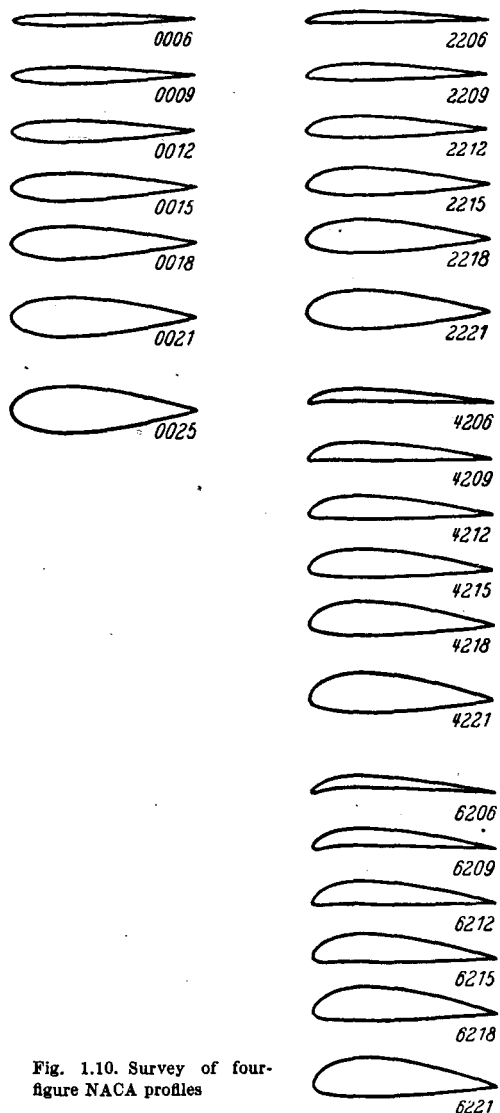


Fig. 1.10. Survey of four-figure NACA profiles

*The second figure:* the position of maximum camber in tenths of the chord.

*The third and fourth figures:* the maximum thickness as a percentage of the chord.

**EXAMPLE:** the profile NACA 4412 has a maximum camber of 4% at 40% of the chord, and a maximum thickness of 12%.

*Thickness Distribution:* Type D<sub>1</sub> of Section 7.3; for this type the position of maximum thickness lies at 30% of the chord.

*Camber Line:* Type S<sub>2</sub> of Section 7.2; the first two numbers, together with the preceding NACA, define the general behaviour of the camber line (in the example: NACA 44). Table 11.2 gives ordinates and aerodynamic characteristics of the camber lines NACA 62 to 65; those of the camber lines NACA 42 to 45 and NACA 22 to 25 can be obtained from those of NACA 62 to 65 by affinely reducing, with factors 4/6 and 2/6 respectively.

### 1.3.3 Five-figure NACA Profiles

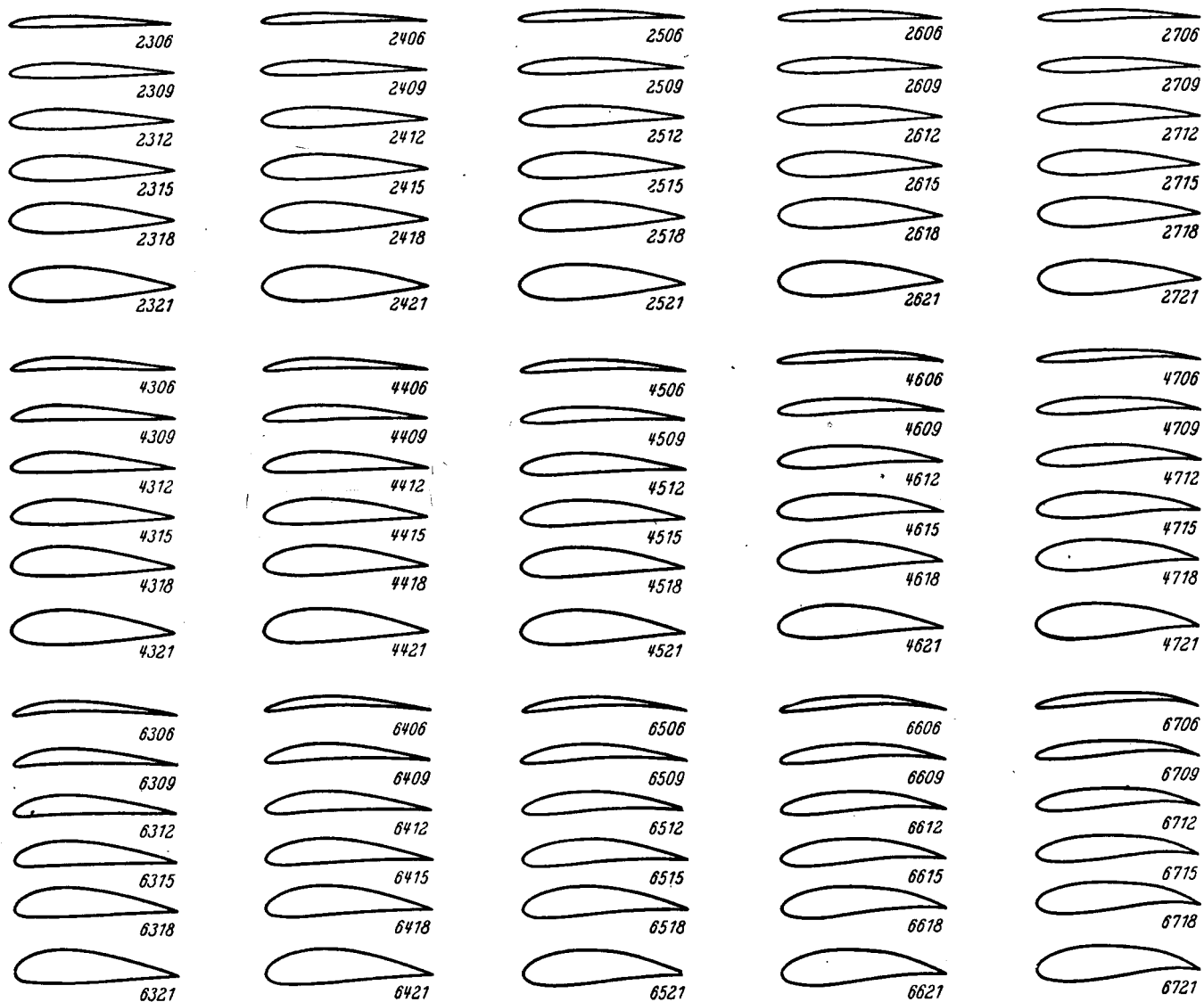
These profiles differ from the four-figure series by having a camber line with a smaller value of the position of maximum camber [R537]. In the designation of these profiles the first figure denotes an aerodynamic property, and the last four figures again denote geometrical properties. For the profiles of the series beginning with 2 the figures have the following meaning.

*The first figure:* 20/3 of the "lift coefficient at the ideal angle of incidence,  $C_L^*$ " (see Section 3.1).

*The second and third figures:* twice the value of the position of maximum camber as a percentage of the chord.

*The fourth and fifth figures:* the maximum thickness as a percentage of the chord.

**EXAMPLE:** the profile NACA 23018 has a  $C_L^*$  of 0.3, its maximum camber lies at 15% of the chord, and it has a maximum thickness of 18%.



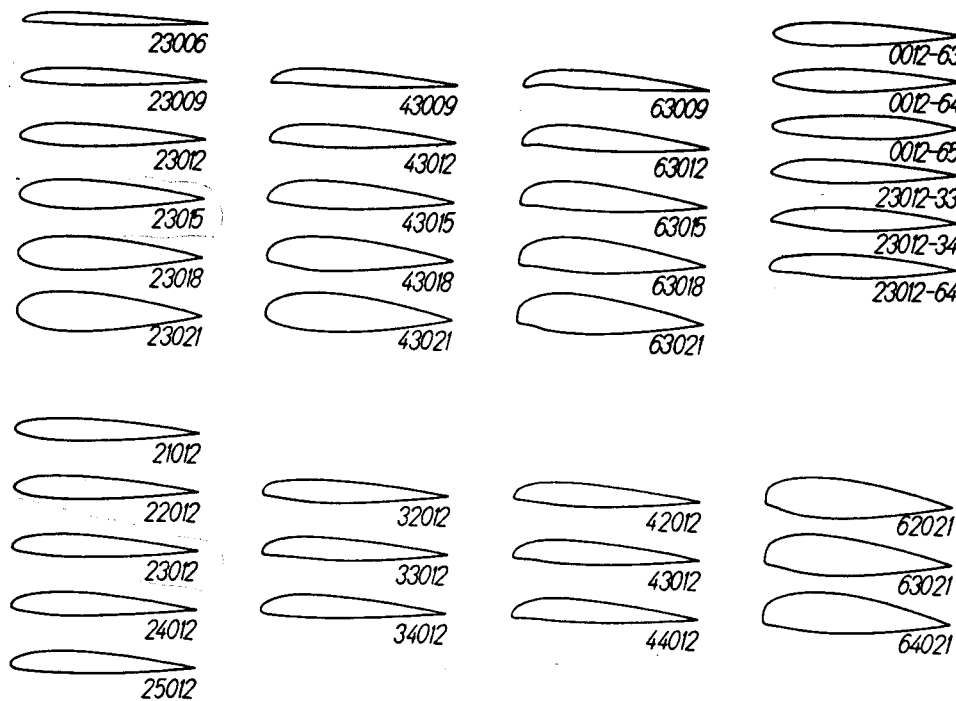


Fig. 1.11. Survey of five-figure NACA profiles

*Thickness Distribution:* Type D<sub>1</sub> of Section 7.3.

*Camber Line:* Type S<sub>4</sub> of Section 7.2.

The following small table gives the geometrical parameters of the camber lines of this series.

Camber line	210	220	230	240	250
Maximum camber, $f/c =$	0.0111	0.0154	0.0184	0.0208	0.0226
Position of maximum camber, $x_f/c =$	0.05	0.10	0.15	0.20	0.25

The ordinates and the aerodynamic characteristics are given in Table 11.2; Figure 12.2 shows the shapes and the pressure distributions. Modifications to this series for other  $C_L^*$  are made by affine transformation of the ordinates of the camber line; examples of such modifications are the profiles whose first numbers are 3, 4 and 6 (the corresponding  $C_L^*$  being 0.45, 0.6, and 0.9). A survey of these profiles is given in Figure 1.11.

The employment of a different camber line is indicated by the third figure: if a 1 stands in this position the camber line of Type S<sub>3</sub> (with fixed centre of pressure) has been used (see Section 7.2).

### 1.3.4 First Extension of the Four-figure and Five-figure NACA Series

Occasionally the extensions affect the camber line, but mostly they affect the thickness distribution. Some of the four-figure profiles have camber lines with a point of inflection, so that systematic variations of the pitching

moment at zero lift can be investigated; to this group belong, for example, the profiles 2R<sub>1</sub>12 and 2R<sub>2</sub>12 [R460].

The first modifications to the thickness distribution affect only the nose radius, and they are indicated by an appended capital letter: *T* (smaller nose radius, more pointed shape); or *B* (larger nose radius, bluffer shape). In the later modifications the position of maximum thickness is also systematically varied [R492]. For both the four-figure and five-figure profiles these modifications are described by the addition of two figures following a short horizontal dash; in the designation of such profiles the figures have the following meaning.

*The first figure after the dash:* a measure of the nose radius. In detail:

- 0, zero radius of curvature (pointed nose);
- 3, one-quarter of the normal radius of curvature;
- 6, normal radius of curvature;
- 9, three or more times the normal radius of curvature; the "normal" radius of curvature is that belonging to the thickness distribution D<sub>1</sub>,  $r_0/c = 1.1(t/c)^2$ .

*The second figure after the dash:* the position of maximum thickness in tenths of the chord.

EXAMPLE: the profile 0012—34 is symmetrical, it has 12% thickness ratio, its nose radius is one quarter of the normal radius, and its position of maximum thickness lies at 40% of the chord.

*Thickness Distribution:* Type D<sub>2</sub>.

### 1.3.5 Extension of the NACA Series by the DVL

The first extension involves changes in the thickness distribution similar to those of Section 1.3.4, but the gradations in the variations of nose radius and position of maximum thickness are refined. The following have been investigated.

- (a) Normal nose radius,  $\rho_0 = r_0 c/t^2 = 1.1$ .
- $\frac{3}{4}$ -normal nose radius,  $= 0.825$ .
- $\frac{1}{2}$ -normal nose radius,  $= 0.55$ .
- $\frac{1}{4}$ -normal nose radius,  $= 0.275$ .
- (b) Position of maximum thickness:  $x_t/c = 0.35, 0.40, 0.45, 0.50$ .

The second extension involves, in addition, a change in  $\tau_T$  (the angle at the trailing edge) and in the corresponding parameter  $\epsilon_T = (\tan \tau_T)/(t/c)$ .

*Thickness Distribution:* Type D<sub>2</sub>. *Camber Line:* Mostly Type S<sub>2</sub>.

**EXAMPLE:** the profile 1 35 12—0.825 40 0.5 has a camber line with maximum camber  $f = 0.01c$ , and

position of maximum camber,  $x_f$ , equal to 0.35c; it has a thickness distribution with maximum thickness  $t = 0.12c$ , the nose radius is  $\frac{3}{4}$ -normal, the position of maximum thickness,  $x_t$ , is equal to 0.4c, and the slope at the trailing edge is half the normal value.

The method of designation is purely geometrical and, as the example has shown, the series of figures gives immediately the parameters necessary for the description of the profile geometry (see Section 1.2). Figure 1.12 gives a survey of these profiles; for the ordinates see Table 11.3, for the aerodynamic coefficients see Table 11.1, and for the pressure distributions see Chapter 12.

### 1.3.6 Extensions of the NACA Series with regard to the Pressure Distribution. Laminar Profiles

#### 1.3.6.1 Series 1 to 6

The modern NACA profiles (see Figure 1.13) are recognisable by the altered arrangements of figures in the designations. Camber lines and thickness distributions are so

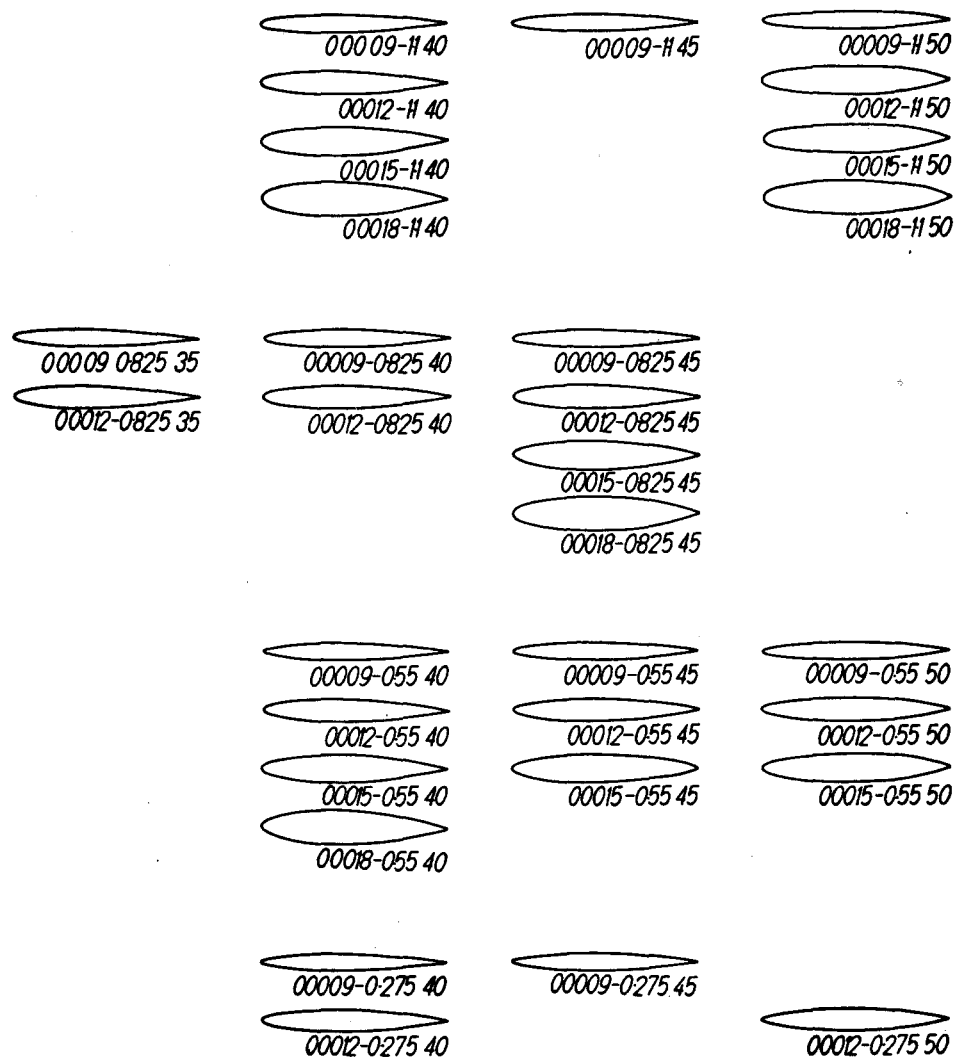


Fig. 1.12. Survey of profiles of the DVL series

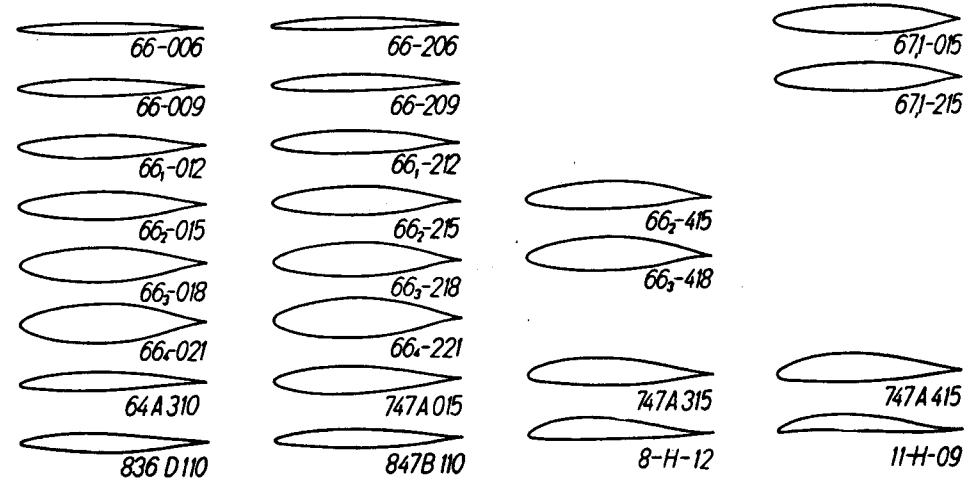
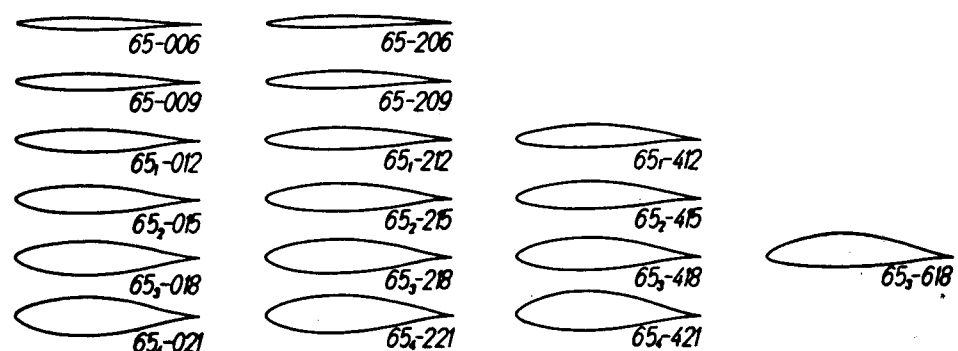
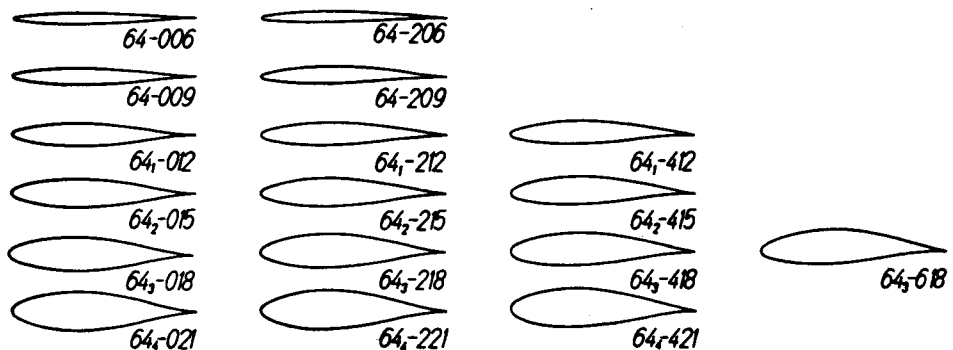
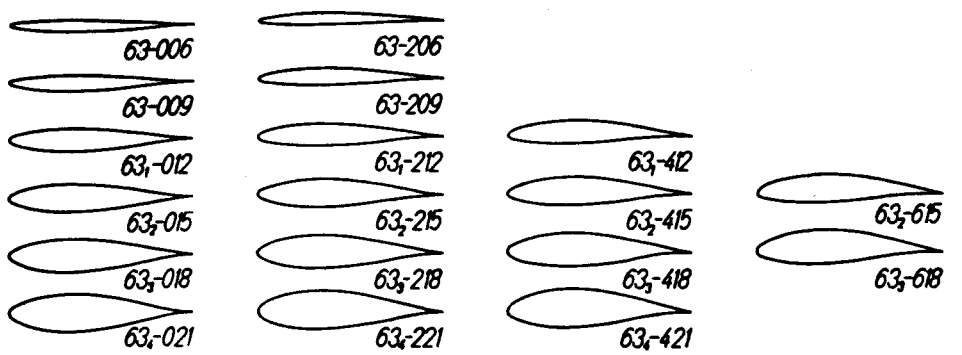


Fig. 1.13. Survey of modern  
NACA profile series

designed that they have a prescribed pressure distribution at a certain value of  $C_L$ .

This mode of procedure is suited to a study of the behaviour of the boundary layer; it is particularly helpful in the problem of reducing the drag of profiles, especially at large Reynolds numbers; in addition, it facilitates the design of profiles suitable for high speeds. The figures have the following meaning.

*The first figure:* this characterises a definite series of profiles—1, 2, 3, 4, 5, or 6; usually the prescribed pressure distributions of each series have a common fundamental property.

*The second figure:* the position of minimum pressure in tenths of the chord.

*The first figure after the dash:* the value of  $C_L^*$  in tenths; hence, a measure of the amount of camber.

*The second and third figures after the dash:* the thickness ratio.

**EXAMPLE:** the profile 64—208 belongs to the "NACA 6-series", the thickness distribution has minimum pressure at 40% of the chord,  $C_L^*$  (the lift coefficient at the ideal angle of incidence) is 0·2, and the maximum thickness is 8%.

*Thickness Distribution:* Calculated theoretically from the prescribed pressure distribution.

*Camber Line:* Type S<sub>5</sub>.

In shape and in pressure distribution the profiles of the 1-series are similar in character to those of the DVL series described in Section 1.3.5. The profile series which begin with 2, 3, 4, 5 [L345] are no longer in use since the 6-series profiles have better properties [R824].

Extra numbers or letters are frequently added to the basic arrangements if a more detailed designation is required.

(a) The thickness distributions of the 6-series are generally combined with camber lines that have either constant pressure over the whole chord (camber line of Type S<sub>5</sub> in Section 7.2) or constant pressure up to a certain point  $x_a$  of the chord (the point where the minimum pressure for the thickness distribution occurs, or a point lying further back) after which the pressure decreases linearly (camber line of Type S<sub>6</sub>). When the pressure distribution has the latter behaviour it is described by adding "a = . . ." to the profile designation; the number to be inserted is the value of  $x_a/c$ . If no such addition to the profile designation exists this usually means that Type S<sub>5</sub> has been used.

(b) An index after the second figure gives the extent of the range of  $C_L$  (in tenths) for which the smooth, symmetrical profile is of laminar character (that is, for which it has extremely small drag).

**EXAMPLE:** the profile 64<sub>3</sub>—018 belongs to the 6-series, the minimum pressure occurs at 40% of the chord, the profile is of laminar character for a range of  $C_L$  of extent  $\Delta C_L = 0\cdot3$ , it is symmetrical, and its thickness ratio is 18%.

(c) A figure following a comma has approximately the same significance. It gives the extent of the range of  $C_L$  (in tenths) for which a favourable pressure gradient exists on both sides of the profile; the profiles differ only trivially from those of (b).

**EXAMPLE:** the profile 64<sub>3</sub>—418 a = 0·6 belongs to the 6-series, the thickness distribution has minimum pressure at 40% of the chord, the pressure distribution is favourable in a range of  $C_L$  of extent  $\Delta C_L = 0\cdot3$ ,  $C_L$  at the ideal angle of incidence ( $C_L^*$ ) is 0·4, the thickness ratio is 18%, and the camber line is Type S<sub>6</sub> with  $a = 0\cdot6$ .

(d) Changes in the thickness ratio are usually made by affine transformation of a profile that already exists in the thickness distribution series; they are indicated by the addition of the thickness ratio of the latter profile in brackets.

**EXAMPLE:** the profiles 64(318)—419 and 64<sub>(318)</sub>—419 belong to the 6-series, they have their pressure minimum at 40% of the chord, the pressure distribution is favourable (that is, the profiles are of laminar character) in a range of  $C_L$  of extent  $\Delta C_L = 0\cdot3$ ,  $C_L^*$  is 0·4, the thickness ratio is 19%, and the profiles are obtained by affine transformation of profiles of thickness ratio 18%.

(e) Employment of several camber lines is denoted by an addition which gives details of all the components.

**EXAMPLE:** the profile 64<sub>3</sub>—418  $\{a = 0\cdot6 \quad C_L^* = 0\cdot3\}$   $\{a = 1\cdot0 \quad C_L^* = 0\cdot1\}$  has the same thickness distribution as Example (c); its camber line is formed by the addition of two camber lines, one of Type S<sub>6</sub> (with  $C_L^*$  equal to 0·3) and one of Type S<sub>5</sub> (with  $C_L^*$  equal to 0·1).

(f) Changes to the rear part of the profile are denoted by the use of capital letters in place of the dash.

**EXAMPLE:** the profile 64<sub>3</sub> A 018 differs from that of Example (b) by the contour's being straight for the last 20% of the chord.

### 1.3.6.2 Series 7 and 8

The profiles of the 7-series differ from those of the series just discussed by the possibility of a larger laminar region on the pressure side. The last three figures of the designation have the same significance as in the profiles of the 6-series; the two figures after the "7" give the positions

of minimum pressure on the suction and pressure sides. The capital letter placed between these two groups of figures distinguishes the actual combination of thickness distribution and camber line which possesses the properties expressed by the figures; another possible combination of thickness distribution and camber line with the same properties would require a different capital letter. The camber line of such a profile is usually produced by addition of several basic camber lines.

Up till now only a few profiles of the 7-series to which this method of designation has been applied are known: for example,

$$\text{NACA } 747 \text{ A } 315 \left\{ \begin{array}{ll} a = 0.4 & C_L^* = 0.763 \\ a = 0.7 & C_L^* = -0.463 \end{array} \right\}$$

and

$$\text{NACA } 747 \text{ A } 415 \left\{ \begin{array}{ll} a = 0.4 & C_L^* = 0.763 \\ a = 0.7 & C_L^* = -0.463 \\ a = 1.0 & C_L^* = 0.1 \end{array} \right\}$$

The basic thickness distribution NACA 747 A 015 has minimum pressure at 40% of the chord on pressure and suction sides; the cambered profiles built up on it have minimum pressures at 40% on the suction side and at 70% on the pressure side. Some profiles of the 8-series have been described and are designated by the letters A, B, C, D [R947]; various superpositions of thickness distributions and camber lines are used; in other respects the figures have the same meaning as in the 7-series.

## 1.4 Theoretically Developed Families of Profiles

### 1.4.1 Joukowsky Profiles and Generalisations

The best-known theoretical families of profiles are those of JOUKOWSKY and KÁRMÁN-TREFFFTZ; VON KÁRMÁN and BURGERS (see Section 1.5.1) and SCHRENK (see Section 1.5.3) have given excellent descriptions of these families, so that we can confine ourselves to a few remarks. As is well-known the profiles are derived by applying the Joukowsky transformation,

$$z = \zeta + \frac{a^2}{\zeta}, \quad (1.13)$$

to a circle, which is eccentrically placed with respect to the circle  $\zeta = ae\bar{\varphi}$  and touches this circle; the first circle has a radius of  $a(1 + \varepsilon_1)$ , a little greater than  $a$ . These profiles have a cusped trailing edge (trailing edge angle equal to zero), and their maximum thickness lies usually at a distance from the nose of from 23% to 27% of the chord. Variation in the thickness of the profile is caused by a small displacement of the centre of the transformed circle in the direction of the abscissa; camber (the camber line being a circular arc) is obtained by a small displacement of the centre in the direction of the ordinate. A rearward

displacement of the position of maximum thickness, and hence a generalisation of this type of profile, is obtained (following BETZ) by enlarging the radius of the eccentrically placed circle to  $R = a(1 + \varepsilon_1 + \varepsilon_2)$ . The new circle does not touch the circle  $\zeta = ae\bar{\varphi}$  and, as a result, the trailing edge is not cusped but rounded. For vanishing camber the circle corresponding to  $\varepsilon_1 = 0$  transforms into an ellipse (with maximum thickness at 50% of the chord!). SCHLICHTING-ULRICH have performed the calculation for symmetrical profiles; for the shape of the profile they obtain

$$\frac{\xi}{a} = (k \cos \bar{\varphi} - \varepsilon_1) \left( 1 + \frac{1}{N} \right), \quad (1.14)$$

$$\frac{\eta}{a} = k \sin \bar{\varphi} \left( 1 - \frac{1}{N} \right), \quad (1.15)$$

where  $k = 1 + \varepsilon_1 + \varepsilon_2$  and  $N = k^2 + \varepsilon_1^2 - 2\varepsilon_1 k \cos \bar{\varphi}$ . With  $a$  as unit of length, the profile chord is obtained from

$$\left( \frac{\xi}{a} \right)_{\bar{\varphi}=0} - \left( \frac{\xi}{a} \right)_{\bar{\varphi}=\pi} = \pi,$$

and is given by

$$\frac{c}{a} = 2k + \frac{1}{k - \varepsilon_1} + \frac{1}{k + \varepsilon_1}. \quad (1.16)$$

Figure 1.14 shows the connection between  $\varepsilon_1$  and  $\varepsilon_2$  and the thickness ratio and position of maximum thickness.

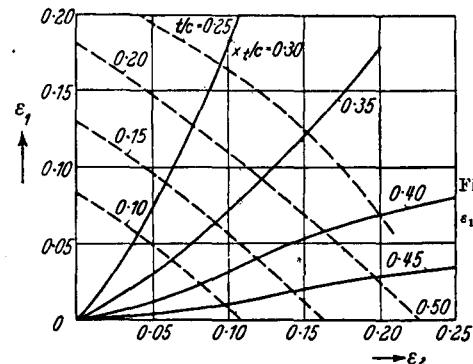


Fig. 1.14. Relation of  $\varepsilon_1$  and  $\varepsilon_2$  to  $\frac{t}{c}$  and  $\frac{\xi_t}{a}$

Numerically, the position of maximum thickness (at which  $\bar{\varphi} = \bar{\varphi}_1$ ) is determined from

$$\frac{d\eta}{d\varphi} = 0 = \cos \bar{\varphi}_1 [(N(\bar{\varphi}_1))^2 - k^2 - \varepsilon_1^2] + 2\varepsilon_1 k. \quad (1.17)$$

The thickness ratio,  $t/c$ , can be obtained from Equations (1.15) and (1.16); from Equations (1.14) and (1.16).

$$\frac{x_t}{c} = k + \varepsilon_1 + \frac{1}{(k + \varepsilon_1)} + \left( \frac{\xi}{a} \right)_{\bar{\varphi}=\bar{\varphi}_1}. \quad (1.18)$$

In addition to this generalisation, which affects the thickness distribution and the shape near the trailing edge, an extension to other camber lines has been undertaken: Joukowsky profiles with camber lines which, instead of being circular arcs have points of inflection, can be designed

and calculated (SCHMIDT); they do not have the disadvantage of rapid movement of the centre of pressure, a disadvantage to which the simple Joukowsky profiles are subject because the position of maximum camber lies so far back.

#### 1.4.2 Kármán-Treffitz and Betz-Keune Profiles

The Kármán-Treffitz profiles differ from the Joukowsky profiles by having a finite angle at the trailing edge; they are derived by the same process as the Joukowsky profiles, but the transformation to be applied is

$$\ln \frac{z - ka}{z + ka} = k \ln \frac{\zeta - a}{\zeta + a} , \quad (1.19)$$

where  $k = 2 - (\tau/\pi)$ . The form of this equation has led BETZ and KEUNE to a very simple construction for the profile shape and the velocity distribution. If the field of a source-sink distribution is drawn and the equipotentials and streamlines suitably numbered, then the values of potential,  $\Phi$ , and stream-function,  $\Psi$ , can be read off from this network—in particular, the quantity

$$\Phi + i\Psi = C \ln [(\zeta - a)/(\zeta + a)] ; \quad (1.20)$$

the constant  $C$  depends only on the manner of numbering. To be able to use the same source-sink network for both sides of Equation (1.19), we write  $\zeta^* = k\zeta$ ; then,

$$\begin{aligned} C \ln \frac{z - ka}{z + ka} &= \Phi_s + i\Psi_s = \\ &= k\Phi_\zeta + ik\Psi_\zeta = kC \ln \frac{\zeta^* - ka}{\zeta^* + ka} . \end{aligned} \quad (1.21)$$

This means that if the source-sink network is regarded as a system of curvilinear co-ordinates, and the co-ordinates  $(\Phi, \Psi)$  of a point  $P_1$  on the circle  $C_1$  are read off (see Figure 1.15), then  $P$ , the point on the profile corresponding to  $P_1$ , has the curvilinear co-ordinates  $(k\Phi, k\Psi)$  in the same network. We see that the manner of numbering is of no importance since the constant  $C$  drops out.

For once we anticipate the results of Chapter 7: the determination of the velocity distribution still requires

$$\left| \frac{dz}{d\zeta} \right| = k^2 \frac{|z + ka|}{|\zeta^* + ka|} \frac{|z - ka|}{|\zeta^* - ka|} . \quad (1.22)$$

The various quantities appearing here can be measured from the drawing (see Figure 1.15) so that (allowing for the change in velocity at infinity) the velocity at the point  $P$  of the profile becomes

$$\frac{w}{V} = \frac{2h}{k^2 R} \frac{NP_1}{NP} \frac{TP_1}{TP} . \quad (1.23)$$

Here,  $h$  is the perpendicular distance of  $P_1$  from the line drawn through  $T$  parallel to the free-stream direction, and  $R = MT$  is the radius of the circle through  $P_1$  and  $T$ . The lift coefficient is given by

$$C_L = \frac{8\pi}{k} \frac{R}{c} \sin(\alpha + \beta_0) , \quad (1.24)$$

where  $\beta_0$  is equal to the angle  $MTN$ , and  $c$  denotes the profile chord. On this basis the same authors have obtained a generalisation of this profile, the camber line having a point of inflexion. To obtain a point of inflection the value of  $\Psi'$  must be decreased near the trailing edge and must be

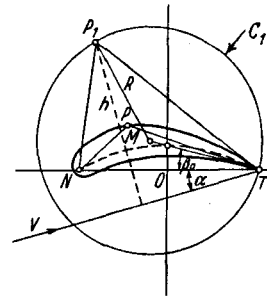


Fig. 1.15. Construction of the Kármán-Treffitz profiles. The intersection of the free-stream direction (shown in the figure) with the transformed circle gives the position of the stagnation point on this circle

increased near the nose; in addition, the function to be superimposed must be regular outside the circle  $\zeta = ae^{i\varphi}$  and must vanish at infinity. The doublet flow has just these properties: the complex potential of a suitably orientated doublet is purely imaginary,  $\pm i\mu$ , at the points  $\zeta^* = \pm ka$ ; by addition of this potential only the stream function is increased or decreased (by an amount  $\mu$ ). This superposition then leads to a generalised mapping function,

$$\ln \frac{z - ka}{z + ka} = k \ln \frac{\zeta^* - ka}{\zeta^* + ka} + i\mu \frac{ka}{\zeta^*} . \quad (1.25)$$

Profile shape and velocity distribution can be constructed in a way similar to that described for the Kármán-Treffitz profiles. Investigation of the profile properties shows that the profile has a fixed centre of pressure if  $\mu$  is chosen so that

$$\mu \approx 4\beta_0 \frac{k(k^2 - 1)}{1 + 2k^2} . \quad (1.26)$$

If, instead of one singular point near the nose, several singular points are assumed to exist in the interior of the profile, then (following von MISES) a large number of special classes of profiles can be obtained in addition to the Joukowsky and Kármán-Treffitz profiles and their generalisations; the number of free parameters is increased, and a diversity of profile shapes results.

### 1.4.3 The Hyperbola Family

We shall now refer to a special family of profiles introduced by PIERCY, PIPER, and PRESTON, and treated in Germany by RINGLEB. The principle of generation of this family is that the inversion of a branch of a hyperbola with respect to a circle whose centre is the focus lying outside the branch (or a point near to this) leads to contours having the form of profiles. As we see from Figure 1.16, two

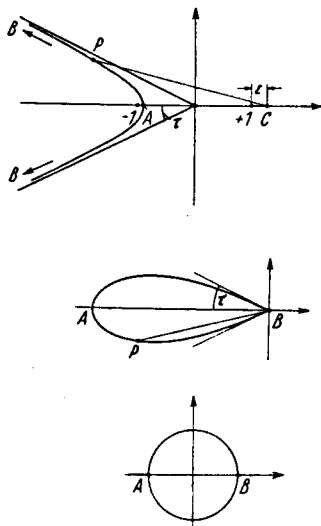
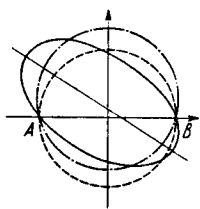


Fig. 1.16. Formation of the symmetrical hyperbola profiles

parameters are initially at our disposal: the trailing edge angle of the profile, which is identical with the angle between the asymptotes of the hyperbola; and the profile thickness, which is given by the distance  $\epsilon$  of the centre of inversion,  $C$ , from the outer focus of the hyperbola. The position of maximum thickness and the nose radius depend on the choice of trailing edge angle and maximum thickness. The profile shape can be further varied if curves

Fig. 1.17. Generation of camber and of a point of inflection in the hyperbola profiles



deviating slightly from the hyperbola are subjected to this inversion process. The calculation of the velocity distribution is performed by conformal mapping of the exterior of the profile into the exterior of the unit circle; this is possible by a chain of intermediate conformal mappings.

Starting from the plane containing the circle it is possible to choose two more profile parameters, the maximum camber and the position of a point of inflection in the camber line, by the following modifications. If, instead of mapping a circle containing two symmetrically

placed singular points  $A$  and  $B$ , we map one that passes through these points, we obtain profiles whose camber lines are circular arcs; as usual the upward displacement of the centre of the circle serves as a measure of the camber. We can obtain a point of inflection in the camber lines, and thereby more favourable pitching-moment behaviour, if, instead of transforming a circle, we transform an ellipse passing through the two points  $A$  and  $B$  (Figure 1.17); as a measure for the amount of inflection we can use the angle that this ellipse makes with the circle at the point  $B$  (corresponding to the trailing edge).

### 1.4.4 Remarks on Further Families of Profiles

A simple approximation to the hyperbola profiles just described is designated as Type D<sub>5</sub> in Section 7.3.2 (following LOCK-PRESTON). The EC and EQ profiles, which are built up from several parts and have algebraic equations, are also treated there.

Modern development of profiles tends to start from a prescribed pressure or velocity distribution; the shape of the profile is then determined by means of a theoretical procedure (see Section 8.3).

## 1.5 References

### 1.5.1 Books

- ABBOTT, J. H. and A. E. v. DOENHOFF: Theory of Wing Sections. McGraw Hill 1949.
- BETZ, A.: Applied Airfoil Theory; in Durand, Aerodynamic Theory, Vol IV, Berlin 1934.
- Konforme Abbildung. Berlin 1948.
- and R. SEIFERTH: Untersuchung von Flugzeugmodellen im Windkanal. Handb. d. Experimental-Physik, Bd. IV, 2, Leipzig 1932.
- DONOVAN, A. F. and H. R. LAWRENCE: Aerodynamic Components of Aircraft at High Speeds (Section A, Chapter 1). Oxford 1957.
- GLAUERT, H.: The Elements of Aerofoil and Airscrew Theory. C.U.P. 1948.
- HOERNER, S.: Aerodynamic Drag. Dayton, Ohio, 1951.
- HOWARTH, L.: Modern Developments in Fluid Dynamics, High Speed Flow. Vols. I and II, Oxford 1953.
- KÁRMÁN, T. v. and J. M. BURGERS: General Aerodynamic Theory—Perfect Fluids; in Durand, Aerodynamic Theory, Vol. II, Berlin 1934.
- OSWATITSCH, K.: Translated by Kuerti, G.: Gas Dynamics. Academic Press Inc. 1956.
- PRANDTL, L. and A. BETZ: Ergebnisse der Aerodynamischen Versuchsanstalt, I—IV. Lfg., München 1921—1932.
- Vier Abhandlungen zur Hydro- und Aerodynamik. Götingen 1927.
- PRANDTL, L.: Führer durch die Strömungslehre. 3. Auflage, Braunschweig 1949.
- SAUER, R.: Einführung in die theoretische Gasdynamik. 2. Auflage, Berlin 1951.
- SCHLICHTING, H.: Grenzschichttheorie. Karlsruhe 1958 and London 1960 (English translation by J. Kestin).
- SCHMITZ, F. W.: Aerodynamik des Flugmodells. 2. Aufl., Duisburg 1952.

### 1.5.2 Comprehensive Reports

- ABBOT, I. H., A. E. v. DOENHOFF and L. S. STIVERS: Summary of Airfoil Data. NACA Rep. No. 824 (1945).
- BEAVAN, J. A., R. F. SARGENT, R. J. NORTH and P. M. BURROWS: Measurements of Maximum Lift on 26 Aerofoil Sections at High Mach Number. R & M No. 2678 (1948).
- BUSEMANN, A.: Aerodynamische Flügelgestaltung. Der Einfluß der Machschen Zahl, Jahrb. 1941 dDL I, S. 1—7.
- CAHILL, J. F.: Summary of Section Data on Trailing Edge High Lift Devices. NACA RM L8D09 or NACA Rep. 938 (1949).
- FERRI, A.: Completed Tabulation in the United States of Tests on 24 Airfoils at High Mach Numbers. (Derived from interrupted work at Guidonia, Italy, in the 1.31 by 1.74 foot High Speed Tunnel.) NACA ACR No. L5E21, (1945) (Wartime Rep. No. L143).
- GÖTHERT, B.: Hochgeschwindigkeitsmessungen an symmetrischen Profilen mit verschiedenen Dickenverhältnissen im DVL-Hochgeschwindigkeitskanal und Vergleich mit Untersuchungen in anderen Windkanälen. FB 1505/1—5 und FB 1506 (1959).
- Hochgeschwindigkeitsmessungen an Profilen gleicher Dickenverteilung mit verschiedener Krümmung im DVL-Hochgeschwindigkeits-Windkanal. FB 1910/1 bis 6 (1943).
  - Widerstandsanstieg bei Profilen im Bereich hoher Unterschallgeschwindigkeiten. UM 1167 (1944) und Techn. Berichte (1944).
- HILTON, W. F.: An Experimental Analysis of the Forces on 18 Aerofoils at High Speeds. R & M No. 2058 (1946).
- JACOBS, E. N., K. E. WARD and R. M. PINKERTON: The Characteristics of 78 Related Airfoil Section from Tests in the Variable Density Wind-Tunnel. NACA Rep. No. 460 (1933).
- JACOBS, E. N. and R. M. PINKERTON: Tests in the Variable Density Wind-Tunnel of Related Airfoils Having the Maximum Camber Unusually Far Forward. NACA Rep. No. 537 (1935).
- JACOBS, E. N. and A. SHERMAN: Airfoil Section Characteristics as Affected by Variations of the Reynolds Number. NACA Rep. No. 586 (1937).
- JACOBS, E. N., R. M. PINKERTON and H. GREENBERG: Tests of Related Forward-Camber Airfoils in the Variable-Density Wind-Tunnel. NACA Rep. No. 610 (1937).
- JACOBS, E. N., and I. H. ABBOT: Airfoil Section Data Obtained in the NACA Variable Density Tunnel as Affected by Support Interference and Other Corrections. NACA Rep. No. 669 (1939).
- JACOBS, E. N.: Preliminary Report on Laminar-Flow Airfoils and New Methods Adopted for Airfoil and Boundary-Layer Investigations. NACA-WR L-345 (1939).
- KNACKSTEDT: Prüfung und Sichtung der bisher vorliegenden Ergebnisse bei Strömungen mit hohen Geschwindigkeiten. FB 1147 (1939).
- KÖSTER, H.: Zusammenstellung von Ergebnissen von Messungen an Luftschaubenprofilen in ausländischen Windkanälen. UM 1241 (1944).
- KRÜGER, W.: Hochauftrieb. UM 3025 (1943).
- LOFTIN jr., L. K. and H. A. SMITH: Aerodynamic Characteristics of 15 NACA Airfoil Sections at seven Reynolds Numbers from  $0 \cdot 7 \cdot 10^6$  to  $9 \cdot 10^6$ . NACA TN 1945 (1949).
- LOFTIN jr., L. K. and H. A. SMITH: Two-Dimensional Aerodynamic Characteristics of 34 Miscellaneous Airfoil Sections. NACA RM L8L08 (1949).
- and W. J. BURSNALL: The Effects of Variations in Reynolds Number Between  $3 \cdot 10^6$  and  $25 \cdot 10^6$  upon the Aerodynamic Characteristics of a Number of NACA 6-series Airfoil Sections. NACA Rep. 964 (1950).
- MUNK, M. and E. HÜCKEL: Systematische Messungen an Flügelprofilen. Techn. Ber. d. Inspektion d. Fliegertruppen, Bd. I (1917), S. 148—163.
- MUNK, M. and C. POHLHAUSEN: Messungen an einfachen Flügelprofilen. Techn. Ber. d. Inspektion d. Fliegertruppen, Bd. I (1917), S. 204—218.
- MUNK, M.: Weitere Messungen an Flügelprofilen. Techn. Ber. d. Inspektion d. Fliegertruppen, Bd. I (1917), S. 204—218.
- MUNK, M. and E. HÜCKEL: Weitere Göttinger Flügelprofiluntersuchungen. Techn. Ber. d. Inspektion d. Fliegertruppen, Bd. II (1918), S. 407—450.
- PANKHURST, R. C.: NPL-Aerofoil-Catalogue. C.P. 81 (1952).
- PINKERTON, R. M. and H. GREENBERG: Aerodynamic Characteristics of a Large Number of Airfoils Tested in the Variable-Density Wind Tunnel. NACA Rep. No. 628 (1938).
- QUINN, J. H. jr.: Summary of Drag Characteristics of Practical Construction Wing Sections. NACA Rep. No. 910.
- STACK, J. and A. E. v. DOENHOFF: Tests of 16 Related Airfoils at High Speeds. NACA Rep. No. 492 (1934).
- TOLLMIEN, W.: Grenzschichten. Gö. Mon. B (1946).
- Kompressible Strömung. Gö. Mon. C (1946).
- WENZINGER, C. J. and F. M. RÓGALLO: Résumé of Airfoil Data on Slats and Flaps. NACA TN 690 (1939).
- YOUNG, A. D.: A Review of Some Stalling Research. R & M No. 2609 (1942).

### 1.5.3 Specialised Reports

- BAUSCH, K.: Strenges Verfahren der Skeletlinienbestimmung für Profile unbekannter Verwölbung. Techn. Berichte 11 (1944), S. 11—15.
- BETZ, A.: Eine Verallgemeinerung der Joukowskyschen Flügelabbildung. ZFM (1924), S. 100.
- BETZ, A. and F. KEUNE: Verallgemeinerte Karman-Treffitz-Profile. Lufo 13 (1936) 336.
- DOUGLAS, O.: A Series of Low Drag Aerofoils Embodying a New Camber Line. R & M No. 2494 (1947).
- DUNCAN, W. J.: Aerofoils with Many Parameters. Aircraft Engineering 11.383 (1939).
- GINZEL, J.: Krümmungseigenschaften von Profilen. Lufo 14 (193.), S. 573—576.
- GOLDSTEIN, S.: A Theory of Aerofoils of Small Thickness. CP 68—70 (1945).
- GROTH: Modification of the NACA-System of Profile Enumeration for Profiles with Small Trailing Edge Angles. Min. Airc. Prod., Völkenrode-Rep. No. AGD 1003 (1945).
- HELMBOLD, H. B. and F. KEUNE: Beiträge zur Profilforschung, Teil I, II. Jufo (1943), S. 77—96.
- KÁRMÁN, Th. v. and E. TREFFTZ: Profilströmung um gegebene Tragflächenquerschnitte. ZFM9 (1918), S. 111.
- KOSCHMIEDER, F. and A. WALZ: Vorschläge zu einer Profilsystematik. FB 1691 (1943).
- LEHMANN and F. ZEUNERT: Beitrag zur Profilforschung. UM 7603 (1944).
- LIGHTHILL, M. J.: A New Method of Two-dimensional Aerodynamic Design. R & M No. 2112 (1945).
- LOCK, C. N. H. and J. H. PRESTON: The New Type of Aerofoil Section, Aircraft Engineering 11 (1939), p. 151.
- PANKHURST, R. C.: Equations to Given Aerofoil Sections "Clark Y" and RAF 6. R & M No. 2130 (1944).
- PEARCY, H. H. and J. A. BEAVAN: Force and Pressure Coefficients up to Mach Number 0·87 on the Goldstein Roof Top Section 1442/1547. R & M No. 2346 (1946).
- PIERCY, N. A. V., R. W. PIPER and J. H. PRESTON: A New Family of Wing Profiles. Phil. Mag. 24 (1937), p. 425.
- PIERCY, N. A. V., R. W. PIPER and L. G. WHITEHEAD: The New Transformed Wing Sections. Aircraft Engineering (1938), pp. 339—343.

- PIPER, R. W.: Extensions of the New Family of Wing Profiles. Phil. Mag. Ser. 7, Vol. 24 (1937), p. 1114.
- RINGLEB, F.: Beiträge zur Theorie der Tragflügelprofile. FB 1496 und Jahrb. dDL I, S. 133—140.
- ROGERS, E. W. E.: Observations on a Thin Cambered Aerofoil Beyond the Critical Mach Number. R & M No. 2432 (1950).
- ROSSNER, G.: Über eine Klasse von theoretischen Profilen mit vier frei wählbaren geometrischen Parametern. Jahrb. 1942 dDL, S. I 142/59.
- SCHLICHTING, H. and A. ULRICH: Zur Berechnung des Um- schlages laminar/turbulent. LGL-Bericht S 10, S. 75—135 und Jahrb. 1942 dDL I, S. 8.
- SCHMIDT, W.: Entwurf, Auftrieb, Moment und Druckverteilung eines Joukowsky-S-Profiles, Jahrb. 1939 dDL I, S. 50 bis 54.
- SCHRENK, O.: Theoretisches über Joukowsky-Profile. Ergebnisse AVA III, S. 13—16.
- SQUIRE, H. B.: A Family of Camber Lines for Subsonic Applications. C.P. 437 (1959).
- STACK, J.: Tests of Airfoils Designed to Delay the Compressibility Burble. NACA TN No. 976 (1944).
- Staff of H. S. T.: Measurements of Force Coefficients on Aerofoil EC 1240 in the High Speed Tunnel at the NPL. R & M No. 2246 (1940).
- TANNER, L. H.: Curves Suitable for Families of Aerofoils with Variable Maximum Thickness Position, Nose Radius, Camber and Nose Droop. C.P. 358 (1957).
- TREFFITZ, E.: Graphische Konstruktion Joukowskyscher Tragflächen. ZFM 4 (1913), S. 130.

## 2. ON EXPERIMENTAL METHODS. WIND TUNNELS AND CORRECTIONS

### 2.1. Some Details of Wind Tunnels used for Profile Measurements

#### 2.1.1 Göttingen Wind-tunnels

##### 2.1.1.1 2 m × 2 m Wind-tunnel of the MVA

*First Operated:* 1908. Rebuilt in 1918; in operation again in 1920.

*Cross-section:* quadratic, 1.96 m × 1.96 m, closed-throat test-section; from 1920, octagonal open-jet with diameter of 1.2 m; from 1934, elliptical open-jet with axes 1.06 m and 1.5 m.

*Contraction Ratio:* at first 1:1; from 1920, 1:3.3; from 1934, 1:3.

*Maximum Speed:* 10 m/sec; with nozzle (from 1920) 30 m/sec.

*Velocity Variation:* (deviation from the mean value of the velocity in the test section)  $\approx \pm 1\%$ .

*Turbulence Factor:*  $\approx 1.7$  (before 1920).

*Balance:* 3 or 4 component balance, description in [AVA II].

*Models:* rectangular wings; span  $b = 1.00$  m or 1.20 m, chord  $c = 0.20$  m.

*Corrections:*† the measured values are converted to  $A = \infty$  by formulas for the additional angle of incidence and the additional drag ( $bc$  in  $m^2$ ).

$$\alpha = \tilde{\alpha} - (20.9c/b - 2.2bc)C_L \quad (\alpha \text{ in degrees}),$$

$C_D = \tilde{C}_D - (0.33c/b - 0.038bc)C_L^2$ , which contain jet-boundary corrections and corrections for the lift distribution on the rectangular wing (see Section 2.3).

##### 2.1.1.2 2.25 m Wind-tunnel of the AVA

*First Operated:* 1917.

*Test Section:* circular cross-section of diameter 2.25 m; length, 3.4 m; open jet.

*Contraction Ratio:* 1:4.85.

*Maximum Speed:* 58 m/sec; in continuous running, 50 m/sec.

† See Sections 2.3.1 and 2.3.2.

*Degree of Turbulence:*  $\approx 0.0024$ . *Turbulence Factor:*  $\approx 1.16$ .

*Balance:* 3 and 6 component beam-balance; description in [AVA I, II].

*Models:* 0.2 m × 1 m rectangular wings; wing-tips usually blunt.

*Corrections:* jet-boundary corrections (given in [AVA I—IV]); conversion of the measured values to  $A = \infty$ , with allowance for the lift distribution on the wing, by the formulas

$$\alpha = \tilde{\alpha} - 4.18C_L \quad (\alpha \text{ in degrees}),$$

$$C_D = \tilde{C}_D - 0.066C_L^2$$

##### 2.1.1.3 4.7 m × 7 m Wind-tunnel of the AVA

*First Operated:* 1936.

*Test Section:* elliptical cross-section (minor axis 4.7 m, major axis 7.0 m); open jet, 8.5 m length; can be used at pressures of from 0.25 to 4 atmospheres.

*Contraction Ratio:* 1:3.

*Maximum Speed:*

Pressure	20-minute bursts	Continuous running
1 atmosphere	59 m/sec	55 m/sec
4 atmospheres	38 m/sec	35 m/sec
0.25 atmospheres	96 m/sec	88 m/sec

*Degree of Turbulence:*  $\approx 0.003$ .

*Turbulence Factor:*  $\approx 1.26$  (1944), 1.4 (1940).

*Balance:* 6-component counterpoise balance, operated by remote control. Description by KLEIN.

*Models:* rectangular wings,  $b = 4.0$  m and  $c = 0.8$  m; wing-tips blunt, and with tip-fairings of various types; maximum chord for wings with end-plates, 2–3 m.

*Corrections:* conversion of measured values to  $A = \infty$ , with allowance for the lift distribution on the wing, by the formulas

$$\alpha = \tilde{\alpha} - 4.18C_L \quad (\alpha \text{ in degrees}),$$

$$C_D = \tilde{C}_D - 0.066C_L^2.$$

Jet-boundary correction is also required. The  $4\text{ m} \times 5.4\text{ m}$  wind-tunnel of the AVA is identical with the one just described, except that it has a smaller nozzle.

*Test Section:* elliptical cross-section (minor axis 4 m, major axis 5.4 m); open jet, 7.5 m length.

*Contraction Ratio:* 1:4.5.

*Maximum Speed:*

Pressure	20-minute bursts	Continuous running
1 atmosphere	74 m/sec	66 m/sec
4 atmospheres	48 m/sec	42 m/sec
0.25 atmospheres	117 m/sec	104 m/sec

*Degree of Turbulence:*  $\approx 0.0026$ . *Turbulence Factor:*  $\approx 1.21$ .

*Models:* normal rectangular wings,  $b = 3$  m,  $c = 0.6$  m.

#### 2.1.1.4 Cavitation Tunnel

*First Operated:* 1927.

*Cross-section:* rectangular,  $0.06\text{ m} \times 0.161\text{ m}$ , closed-throat test-section. Fluid used in experiments: water.

*Maximum Speed:* 8 m/sec.

*Balance:* spring balance.

*Models:* rectangular wings mounted on a revolving plate, flush with the tunnel wall.

*Corrections:* to allow for the effect of the walls, static pressure and kinetic pressure are measured in a section at a distance of about three times the chord in front of the wing; these measurements, together with Bernoulli's equation and the equation of continuity, are used to convert the results for the flow about the profile and cavitation layer to free fluid. In addition, a deduction in the angle of incidence must be made, because of the influence of the horizontal walls on the flow round the profile; this deduction is proportional to  $C_L$ , and is given by

$$\Delta\alpha = \frac{\pi}{96} \left(\frac{c}{H}\right)^2 C_L$$

( $c$  = wing chord,  $H$  = tunnel height).

#### 2.1.2 Wind Tunnels of the DVL

##### 2.1.2.1 5 m $\times$ 7 m Wind Tunnel

*First Operated:* end of 1934.

*Test Section:* elliptical cross-section (minor axis 5 m, major axis 7 m); open jet of length 9 m.

*Contraction Ratio:* 1:4.

*Maximum Speed:* 65 m/sec.

*Velocity Variation:* about 1.5%; on the major axis of the elliptical cross-section about 0.5%.

*Direction Variation:*  $\pm 0.5^\circ$  on the jet axis.

*Turbulence Factor:*  $\approx 1.1$ .

*Balance:* 6-component counterpoise balance operated by remote control, with data-recording apparatus; described by KRAMER.

*Models:* normal wings,  $0.8\text{ m} \times 4.0\text{ m}$ . Welded steel skeleton with plaster surface (10 mm thick), polished. Wing-tips rounded.

*Corrections:* jet-boundary correction and conversion to  $A = \infty$ .

#### 2.1.2.2 2.7 m High-speed Wind-tunnel

*First Operated:* 1939.

*Test Section:* circular cross-section of 2.7 m diameter, and length of 2.7 m; closed-throat test-section.

*Contraction Ratio:* 1:7.2.

*Maximum Speed:* without models  $M = 0.93$ ; with models ( $c = 500$  mm)  $M \approx 0.86$ .

*Turbulence Factor:*  $\approx 1.04$ .

*Balance:* 3-component counterpoise balance operated by remote control; experimental results (including pressure) given on paper tape.

*Models:* made from light alloy, either with 0.1 mm layer of plaster and lacquer (ground to required degree of fineness and polished) or with a simple metallic surface.

*Corrections:* (1) correction of free-stream velocity for constraint due to model; (2) correction for additional constraint due to wake; (3) jet-boundary correction (see GÖTHERT).

#### 2.1.3 Wind Tunnels of the NACA

##### 2.1.3.1 Variable-density Wind-tunnel (VDT)

*First Operated:* built 1923; rebuilt 1928 after destruction by fire.

*Test Section:* circular cross-section of 5 ft diameter; closed-throat test-section; excess pressure up to 21 atmospheres [R416].

*Maximum Speed:* 72 ft/sec.

*Velocity Variation:*  $\pm 0.5\%$ .

*Direction Variation:* less than  $\pm 0.25^\circ$ .

*Turbulence Factor:* 2.64 [R558].

*Balance:* built 1929; 3-component balance for lift, drag, and pitching moment.

*Models:* normal rectangular wings,  $A = 6$  (5 in  $\times$  30 in). Made from Dural or steel, to accuracy of 0.001 inches; highly polished.

*Corrections:* (1) conversion to free air; (2) conversion to infinite aspect-ratio, with allowance for the lift distribution on the wing; (3) support interference (on drag and pitching moment); (4) allowance for the flow at the tips of the rectangular wing ( $\sim$  = value for model of finite span),

$$C_{L \max} = 1.07 \tilde{C}_{L \max}.$$

$$\frac{dC_L}{d\alpha} = 0.96 \frac{\tilde{d}C_L}{d\alpha}$$

$$\alpha = \tilde{\alpha} + 0.39 \tilde{C}_L \quad (\alpha \text{ in degrees}),$$

$$C_D = \tilde{C}_D + 0.0016 \tilde{C}_L^2 - 0.0001(t-6), \quad (t \geq 6)$$

where  $t$  is the maximum thickness of the wing as a percentage of the chord; (5) the adjustment to effective Reynolds number requires a correction of the drag coefficients and maximum lift coefficients. For wings with flaps deflected a further approximate correction is required. See [R586, 669].

### 2.1.3.2 Full-scale Wind-tunnel (FST)

*First Operated:* spring 1931.

*Test Section:* nozzle with parallel upper and lower walls and semicircular side-walls; cross-section 30 ft  $\times$  60 ft; open jet [R459].

*Contraction Ratio:* 1:4.9.

*Maximum Speed:* 174 ft/sec.

*Turbulence Factor:* 1.1.

*Degree of Turbulence:*  $\approx 0.003$  [R558].

*Balance:* 6-component balance for three forces and three moments; printing device gives simultaneous recording of all quantities.

*Models:*  $A = 6$  (6 ft  $\times$  36 ft to 8 ft  $\times$  48 ft). Made of metal coated with aluminium skin (0.064 in thick) and lacquered. Wing-tips blunt; later, rounded semicircularly. Mounted on stings.

*Corrections:* (1) jet-boundary and constraint correction (slight change of Reynolds number with angle of incidence); (2) support interference (on the drag); (3) for direction of jet (measurement in normal position and reversed position). Conversion of the corrected value from  $A = 6$  to  $A = \infty$  by the formulas

$$\alpha = \tilde{\alpha} - 3.58 C_L \quad (\alpha \text{ in degrees}),$$

$$C_D = \tilde{C}_D - 0.056 C_L^2.$$

### 2.1.3.3 Langley Two-dimensional Low-turbulence Tunnel (LTT)

*First Operated:* 1941.

*Test Section:* closed-throat tunnel, rectangular cross-section, of 3 ft width and 7.5 ft height [R824].

*Contraction Ratio:* 1:20.

*Maximum Speed:* 230 ft/sec.

*Degree of Turbulence:*  $\approx 0.0003$ .

*Balance:* for moments only. Lift obtained from the pressures on the roof and floor of the tunnel. Drag from measurement of momentum loss.

*Models:* wooden models, mostly with chord of 2 ft; for small  $C_L$ , also with chord of 8 ft.

*Corrections:* wall effect, and constraint correction [R824].

### 2.1.3.4 Langley Two-dimensional Low-turbulence Pressure Tunnel (TDT)

*First Operated:* 1941.

*Test Section:* closed-throat tunnel with rectangular cross-section (3 ft width and 7.5 ft height). Pressure: variable, from 1 to 10 atmospheres [N1283].

*Contraction Ratio:* 1:17.6.

*Maximum Speed:* 440 ft/sec at 1 atmosphere;

330 ft/sec at 3 atmospheres;

230 ft/sec at 10 atmospheres.

*Degree of Turbulence:* increasing with speed, from  $\approx 0.0002$  to  $0.001$  [R940].

*Balance:* for moments only. Lift obtained from the pressures on the roof and floor of the tunnel. Drag from measurement of momentum loss.

*Models:* normal models made from wood; chord of 2 ft. Laminar profiles: 8 ft chord, for small values of the lift. Reynolds number in usual experiments:  $9.10^6$ . Maximum Reynolds number:  $60.10^6$ .

**Corrections:** wall effect and constraint correction [R824].

#### 2.1.3.5 1 ft × 3½ ft High-speed Tunnel, Ames Laboratory

**First Operated:** 1944.

**Test Section:** closed-throat tunnel with rectangular cross-section of 1 ft × 3½ ft. [R832, R947.]

**Maximum Speed:**  $M = 0.9$ .

**Models:** 6 in chord. Manufactured from aluminium alloy.

**Balance:** none. Lift obtained from the pressures on the roof and floor. Drag from measurement of momentum loss.

#### 2.1.4 British Wind-tunnels

##### 2.1.4.1 CAT Compressed Air Tunnel (NPL)

**First Operated:** 1932.

**Test Section:** pressurised tunnel,  $p \leq 25$  atmospheres. Open, circular section; closed return-circuit. Nozzle diameter, 6 ft.

**Contraction Ratio:** 1:3·6.

**Maximum Speed:** 88 ft/sec.

**Turbulence Factor:** 2·1.

**Models:** rectangular wings, 8 in × 48 in; manufactured from aluminium, polished surface.

**Corrections:** jet-boundary and constraint correction, and correction for support interference on the drag. For conversion to  $A = \infty$ , with allowance for the rectangular shape of the wing, the formulas to be used are

$$\alpha = \tilde{\alpha} - 3.55C_L \quad (\alpha \text{ in degrees}), \\ C_D = \tilde{C}_D - 0.0555C_L^2.$$

##### 2.1.4.2 20 in × 8 in High-speed Tunnel (NPL)

**First Operated:** 1941.

**Test Section:** closed-throat tunnel with rectangular cross-section of 20 in × 8 in, and length of 64 in; provided with movable side-walls. Running time: 20 minutes. [R & M 2005, 2067.]

**Maximum Speed:**  $M = 0.94$ .

**Models:** 5 in chord.

#### 2.1.5 Some Other Wind-tunnels

##### 2.1.5.1 Large Wind-tunnel of the Aerodynamic Institute of the ETH in Zürich

**First Operated:** 1936.

**Test Section:** open-jet or closed-throat; rectangular cross-section with chamfered corners, 3·00 m wide and 2·10 m high. Adjustable diffusor.

**Contraction Ratio:** 1:3·25.

**Maximum Speed:** for intermittent running (20 min), 90 m/sec.

**Degree of Turbulence:**  $\approx 0.004$ .

**Balance:** 6-component balance; forces are measured singly; balance arranged to rotate with model.

**Models:** rectangular wings, 0·25 m × 1·50 m; manufactured from wood.

#### 2.1.5.2 High-speed Wind-tunnel in Guidonia

**First Operated:** 1939.

**Test Section:** open-jet between plane walls. Rectangular cross-section of 0·4 m × 0·54 m. Pressure in the test section: variable, from 0·1 to 1 atmosphere.

**Speed:**  $0.4 < M < 2.9$ .

**Models:** wings of 0·04 or 0·05 m chord, spanning the tunnel.

#### 2.2 On the Turbulence of Wind Tunnels

##### 2.2.1 Degree of Turbulence and Scale of Turbulence

Deviations from the mean velocity occur to some extent in the test sections of all wind tunnels; these deviations (the disturbance velocities  $u'$ ,  $v'$ ,  $w'$ , in the three co-ordinate directions) exhibit large fluctuations. To obtain a measure for these we define a *degree of turbulence*,  $T$ , of the wind tunnel; this is the ratio of the mean disturbance velocity to the mean flow velocity,  $V$ , so that

$$T = \frac{1}{V} \sqrt{\frac{1}{3} (\bar{u'^2} + \bar{v'^2} + \bar{w'^2})} ; \quad (2.1)$$

here,  $\bar{u'^2}$  is the square of the disturbance velocity in the axial direction averaged over a time interval  $t$ , so that

$$\bar{u'^2} = \frac{1}{t} \int_0^t u'^2 dt. \quad (2.2)$$

$\bar{v'^2}$  and  $\bar{w'^2}$  are the corresponding quantities in the two co-ordinate directions normal to the axis. In the consideration of wind-tunnel turbulence the last two quantities are often assumed to be of the same order of magnitude as the first; therefore,  $T$  can be taken as  $\sqrt{\bar{u'^2}}/V$ .

Direct measurement of the degree of turbulence has become usual only in recent times; the mean value of the disturbance velocity is determined from the cooling of one hot wire. Suppose we use two hot wires to measure the disturbance velocities  $u'_1$  and  $u'_2$  at two points in a cross-section, and vary the distance ( $y$ ) between them; we can then obtain a correlation coefficient from such measurements,

$$F(y) = \frac{u'_1 \cdot u'_2}{\sqrt{u'^2_1} \sqrt{u'^2_2}}. \quad (2.3)$$

By integration we obtain a length called the *scale of turbulence*:

$$L = \int_0^\infty F(y) \cdot dy. \quad (2.4)$$

$L$  can be regarded as a measure of the size of eddies; together with the degree of turbulence, it characterises the state of turbulence in the wind tunnel.

### 2.2.2 The Critical Reynolds Number for Turbulence

As a means of comparing the turbulence of various wind-tunnels PRANDTL has suggested the use of the critical Reynolds number of the sphere; this is the Reynolds number at which a sudden sharp drop in the drag coefficient,  $C_D$ , occurs, the drop being caused by a change in the type of flow in the boundary layer; as the turbulence of the air in the tunnel increases, the Reynolds number at which the drop occurs becomes smaller. To define this number more exactly, DRYDEN and KUETHE choose as critical Reynolds number that at which a  $C_D$  of 0.3 is reached. HOERNER, in his measurements, uses the fact that an equally sudden

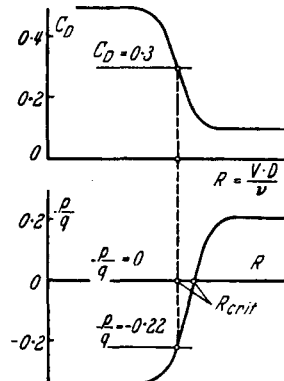


Fig. 2.1. Definition of the critical Reynolds number for a sphere

rise in pressure,  $p$ , on the rear part of the sphere (very close to where the sting is attached) is associated with the sudden drop in  $C_D$ ; this is another easily determined quantity that can be used to define the critical Reynolds number. To obtain approximately the same value of  $R_{crit}$  as given by  $C_D = 0.3$ ,  $p/q$  ( $q$  being the kinetic pressure,  $\frac{1}{2}\rho V^2$ ) is plotted against  $R$  and the value of  $R$  corresponding to  $p/q = -0.22$  read off. The latter value is the one recommended by PLATT: HOERNER suggests that  $p/q$  be taken as zero; this leads to larger values for the critical Reynolds number (see Figure 2.1).

### 2.2.3 The Turbulence Factor

To be able to compare the turbulence of wind tunnels PLATT introduces a characteristic quantity, the *turbulence*

factor (t.f.), defined by the ratio

$$\text{t.f.} = \frac{R_{crit.} \text{ in free air}}{R_{crit.} \text{ in the wind tunnel}}.$$

For "R<sub>crit.</sub> in free air" he uses the value  $3.85 \cdot 10^5$  (obtained from flight measurements, and corresponding to  $p/q = -0.22$ ); for the denominator he uses a mean value obtained from a number of measurements on spheres. If we now suppose that, to a first approximation, the critical Reynolds number varies inversely with the turbulence, we can use the turbulence factor to convert the experimental results for profiles in various wind-tunnels to an "effective Reynolds number" (corresponding to free air with very low turbulence); the conversion formula is

$$R_{eff.} = (\text{t.f.}) R, \quad (2.5)$$

where  $R = Vc/\nu$ . This procedure has proved fairly successful for the maximum lift coefficient (that is, for predicting the onset of separation); it has not proved successful for other profile properties (in particular, not for the drag).

### 2.2.4 Influence of the Diameter of the Sphere. More Exact Definition of the Turbulence Factor

Modern wind-tunnels possess very small turbulence (the values of  $R_{crit.}$  lie between  $3 \cdot 10^5$  and  $4 \cdot 10^5$ ); so it is not

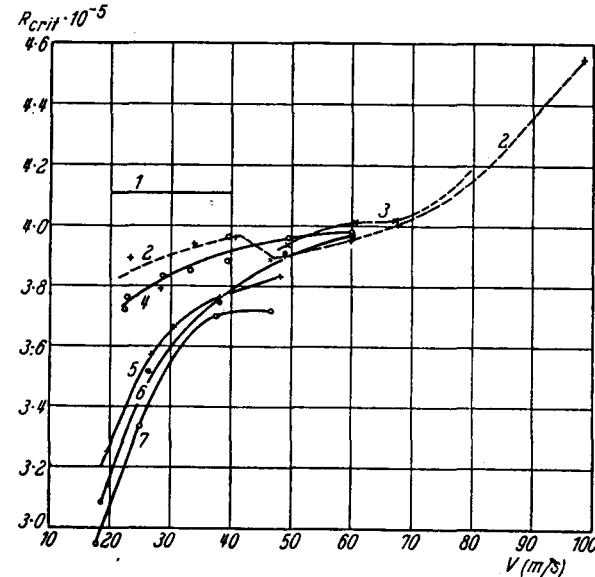


Fig. 2.2. Measurement of  $R_{crit.}$  (defined by  $\frac{p}{q} = 0$ ) plotted against velocity.

- |                                 |                                |
|---------------------------------|--------------------------------|
| (1) Free air.                   | (4) 1.3 m tunnel;              |
| (2) to (7) In AVA wind-tunnels: | (5) 2.25 m tunnel;             |
| (2) low-turbulence wind-        | (6) 4 m $\times$ 5.4 m tunnel; |
| tunnel;                         |                                |
| (3) 0.36 m Eiffel-tunnel;       | (7) 4.7 m $\times$ 7 m tunnel. |
|                                 | (SEIFERTH)                     |

sufficient simply to utilise mean values from a number of measurements on one sphere, because the value of

$R_{crit}$  depends on the diameter,  $D$ , of the sphere, and on the speed,  $V$ . This fact has been known for some time; it is verified by measurements on spheres, which SEIFERTH performed in five Göttingen wind-tunnels in 1943/44. In

SEIFERTH proposes that, to characterise the turbulence, the value of  $R_{crit}$  corresponding to a definite diameter of the sphere, about 22 cm, be chosen; as the measurements show, this suggestion leads to a well-defined parameter.

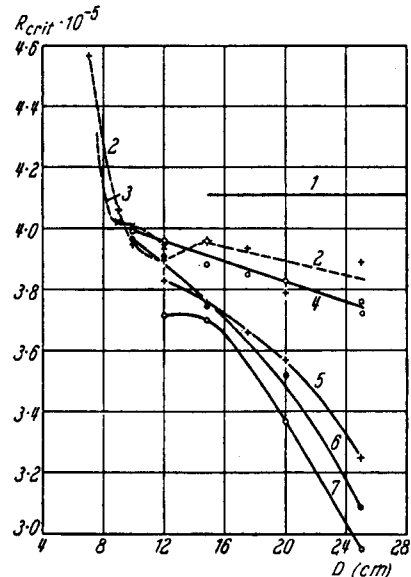
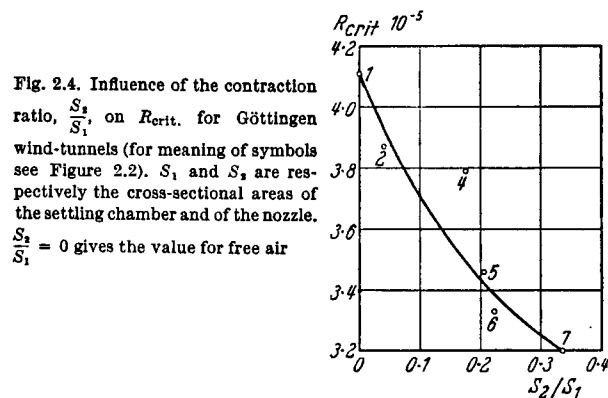


Fig. 2.3. The measurements of Figure 2.2 plotted against diameter of sphere. (SEIFERTH)

these measurements the pressure,  $p$ , on the rear part of the sphere is measured, and the criterion  $p/q = 0$  used to determine  $R_{crit}$ . For the critical Reynolds number in free air a mean value of  $4.11 \cdot 10^5$  (corresponding to  $p/q = 0$ ) is taken; this is derived from the measurements of HOERNER and PLATT (after obviously erroneous measurements have been rejected). The dependence of  $R_{crit}$  on the speed,  $V$ ,



and on the diameter of the sphere,  $D$ , is reproduced† in Figures 2.2 and 2.3. On the basis of these measurements

† In the computation of these experimental values  $\nu$  has been taken as a constant, equal to  $0.15 \cdot 10^{-4} \text{ m}^2/\text{sec}$ . F. W. SCHMITZ has made further measurements on the spheres, and has shown that corrections are required to allow for the influence on  $\nu$  of the temperature at the measured point.

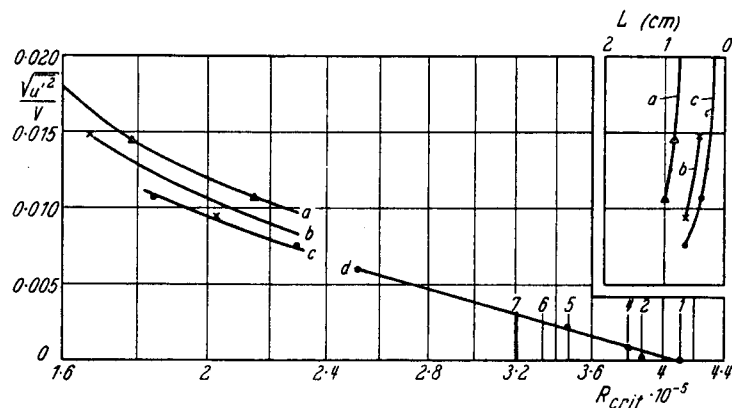


Fig. 2.5. Degree and scale of turbulence (shown respectively left and top right), from measurements made behind grids with the following mesh-widths: (a) 2.45 cm; (b) 1.27 cm; (c) 0.64 cm. Curve shown bottom right: wind-tunnel measurements (for meaning of symbols see Figure 2.2). Point (d), at the left end: from measurements made behind a grid in the 1.3 m tunnel (number 4); the right end is the value for free air

The method is possible only for test sections in which a sphere of this diameter does not occupy too large a part of the cross-section; it cannot be applied to small wind-tunnels.

In Figure 2.4  $R_{crit}$  thus determined is plotted against the contraction ratio,  $S_2/S_1$ , of some wind-tunnels†; it is seen that this ratio has a decisive influence on the turbulence of the wind tunnels.

## 2.2.5 Comparison Between Hot-wire and Sphere Measurements

DRYDEN has carried out hot-wire measurements behind grids in the presence of strong turbulence, and compared his results with measurements on a sphere of 21.5 cm diameter (see Figure 2.5); the dependence on mesh size, which is present in the Figure, disappears if  $\frac{\sqrt{u'^2}}{V} (D)^{1/5}$ , instead of  $\frac{\sqrt{u'^2}}{V}$ , is plotted against  $R_{crit}$ .

The quantity  $L$  increases as the degree of turbulence,  $T$ , decreases, reaching values up to 1 cm. Hot-wire measurements made at Göttingen for the determination of the degree of turbulence of the wind tunnels gave the following results:

for the 2.25 m tunnel  $\sqrt{u'^2}/V \approx 0.0024$ ;

for the 1.3 m tunnel ‡  $\approx 0.0009$ ;

for the low-turbulence tunnel §  $\approx 0.0002$ .

†  $S_2$  is the cross-sectional area of the nozzle,  $S_1$  that of the settling chamber.

‡ Since dismantled.

§ See the footnote in Section 2.3.1.

These values are in good agreement with the points obtained by DRYDEN; in Figure 2.5 a curve (lower right-hand side) is drawn through them, and this curve can be easily extrapolated to pass through the point corresponding to free air; in this way a connection between hot-wire and sphere measurements is demonstrated (see SEIFERTH).

### 2.3 General Remarks on Experimental Investigations

#### 2.3.1 On Profile Measurements in Wind Tunnels

At first, weighing was the only method of importance for the experimental determination of force and moments (see BETZ-SEIFERTH). Nearly all the 3 and 6 component balances of the most important wind-tunnels have been exhaustively described; in Section 2.1 a reference is given to the appropriate place in the literature for the description of each tunnel, and the type of balance is stated. In general, the measurements have been carried out upon rectangular wings of aspect ratio  $A = b^2/S = 5$  or 6. With the help of known formulas for the conversion of wind-tunnel measurements from one aspect ratio to another [AVA II], the measured values of forces and moments can be converted to  $A = \infty$ , which corresponds to a wing of infinite span; the conversion formulas have been derived on the assumption of a constant lift coefficient,  $C_L$ . The formulas are:

(a) for the angle of incidence (in radians),

$$\alpha = \tilde{\alpha} - \frac{C_L}{\pi A} (1 + \tau_1); \quad (2.6a)$$

(b) for the drag coefficient,

$$C_D = \tilde{C}_D - \frac{C_L^2}{\pi A} (1 + \tau_2); \quad (2.6b)$$

here,  $\tilde{\alpha}$  and  $\tilde{C}_D$  denote values measured at an aspect ratio  $A$ . In this form the correction formulas (originally derived for an elliptical distribution of lift) contain factors,  $(1 + \tau_1)$  and  $(1 + \tau_2)$ , which allow for the actual lift-distribution. The following table for rectangular wings is taken from GLAUERT; it is assumed that  $\frac{dC_L}{d\alpha}$  has its theoretical value of  $2\pi$ .

$A$	4	5	6	7	8	9	10
$\tau_1$	0.122	0.145	0.163	0.183	0.201	0.216	0.228
$\tau_2$	0.026	0.037	0.046	0.055	0.064	0.072	0.080

The increased accuracy of weighing and the close approach to uniform flow in modern wind-tunnels mean that variations in the details of model manufacture, in the quality of the model surface, in the type of suspension used, and in the shape of the wing-tips, now produce detectable effects. As a result, the profile drag (that is, the part of the drag due to friction) is no longer obtained by weighing followed by subtraction of the vortex drag, but

is found directly by measurement of the momentum lost in the wake. The theoretical foundations of this method have been given by BETZ, B. M. JONES, G. I. TAYLOR, and (for high speeds) by GÖTHERT: the practical applications are described by MUTTRAY, DOETSCH, SILVERSTEIN and KATZOFF, GOETT, and others (see the references of Section 2.4).

In later times, wind-tunnels intended for profile measurements have been built by the NACA and at Göttingen; in these tunnels the wings are placed between plane walls in an attempt to produce two-dimensional flow. Disturbances caused by the apparatus for measuring forces are largely avoided in the American wind-tunnels LTT and TDT by determining the lift from an integration of the pressures on the floor and on the roof of the wind tunnel; only the moments are still measured by weighing.

#### 2.3.2 On Wind-tunnel Corrections

Because of the finite dimensions of the stream of air, the lift measured in a wind tunnel differs from that measured in air of infinite extent. In an open-jet tunnel the lift is smaller: in a closed-throat tunnel the lift is greater (assuming that the angle of incidence remains unchanged). However, following a proposal of PRANDTL, it is more useful not to apply the necessary correction to the lift, but rather to correct the angle of incidence and the drag coefficient at constant  $C_L$  (the procedure that is used in the conversion from one aspect ratio to another).

The most important correction, a correction for the induced downwash on the wing, depends on the lift coefficient ( $C_L$ ), on the ratio of wing area ( $S$ ) to the cross-sectional area of the jet ( $S_0$ ), and on a factor that allows for the influence both of the shape of the cross-section and of the wing span. The latter factor is written  $\delta_a$  in the correction for the angle of incidence, and  $\delta_D$  in the correction for the drag; many authors have calculated it (under the assumptions of potential theory), and the most diverse cross-sectional shapes and spans have been considered. RIEGELS has given a comprehensive summary of such results for incompressible flow, in which other kinds of correction are also considered (camber corrections, constraint corrections, etc.); LUDWIEG is engaged on a supplement, a corresponding summary for compressible flows.

To show the order of magnitude of the correction first mentioned, we give the values for the circular jet (worked

† A two-dimensional low-turbulence wind-tunnel was built at Reyershausen near Göttingen during the war; the test cross-section was  $1.5 \text{ m} \times 3 \text{ m}$ , and the speed was  $90 \text{ m/sec}$ . Measurements concerning its velocity distribution and state of turbulence were made, but it was then dismantled without having served its purpose—the carrying out of profile measurements. This tunnel (with a smaller test-section) has since been rebuilt in Göttingen; the degree of turbulence is small ( $0.0004$ ), the cross-section is  $0.35 \text{ m} \times 1.50 \text{ m}$ , and the speed is  $40 \text{ m/sec}$ ; it was first operated in 1955.

out by PRANDTL); in terms of the wing span,  $b$ , and the jet diameter,  $D$ , there results

$$\delta = 1 + \frac{3}{16} \left( \frac{b}{D} \right)^4 + \frac{5}{64} \left( \frac{b}{D} \right)^8 + \dots; \quad (2.7)$$

the correction for angle of incidence is

$$\Delta \alpha = -\delta \frac{C_L}{8} \frac{S}{S_0}, \quad (2.8)$$

and for the drag

$$\Delta C_D = -\delta \frac{C_L^2}{8} \frac{S}{S_0}. \quad (2.9)$$

For normal profiles of 1 m span and with  $A$  equal to 5, in the Göttingen 2.25 m wind-tunnel, the angle of incidence and the drag coefficient corrected for jet-boundary effects are given by

$$\alpha = \alpha_M - 0.36 C_L \quad (\alpha \text{ in degrees}),$$

$$C_D = C_{D_M} - 0.00635 C_L^2;$$

the uncorrected, measured values are designated by the suffix  $M$ . For normal profiles (0.6 m  $\times$  3 m) in the elliptic jet of the Göttingen 4 m  $\times$  5.4 m wind-tunnel,

$$\alpha = \alpha_M - 0.64 C_L \quad (\alpha \text{ in degrees}),$$

$$C_D = C_{D_M} - 0.0112 C_L^2.$$

Further corrections may be necessary because of support interference (see Section 2.3.3).

### 2.3.3 Influences of Wing-tips and Supports

All the earlier profile measurements made by the AVA and by the NACA have been carried out on wings with blunt tips, but measurements in the DVL wind-tunnel show that considerable differences in the experimental values arise, depending on whether the wings are blunt at

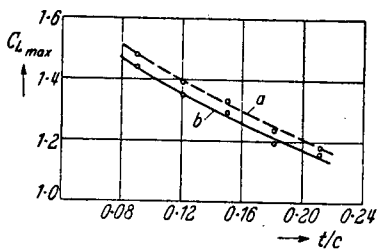


Fig. 2.6. Values of  $C_{L_{max}}$  for the profile-series NACA 24 with: (a) blunt tips; (b) rounded tips. Wind tunnel: DVL 5 m  $\times$  7 m. Effective Reynolds-number: approximately  $3 \cdot 10^6$ .

the tips or are rounded (that is, fitted with tip-fairings). These measurements have been carried out at a Reynolds number of  $2.7 \cdot 10^6$ ; for this reason the drag coefficients are smaller than previous results. In Figure 2.6  $C_{L_{max}}$ , for the NACA profiles 2409 to 2421, is plotted against thickness; this example shows how the thickness changes the effect of rounded tips. The tip-fairings employed here are of the

usual type; at each point of the chord they have a radius equal to half the local thickness. Neither kind of tip is entirely satisfactory: because of the complicated vortex formation, wings that are blunt at the tips give too large values for the measured drag coefficient (when the lift coefficient is close to zero); on the other hand, too large values in the upper range of  $C_L$  are found when "normal" tip-fairings are used.

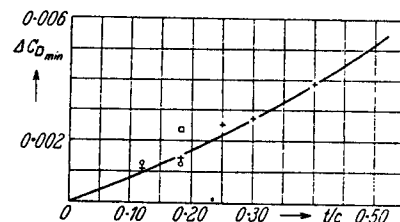


Fig. 2.7. Drag correction for interference from model support in the VDT (from [R669])

From measurements in the 4 m  $\times$  5.4 m tunnel of the AVA, REGENSCHETT is able to show that both these disadvantages can be overcome to a certain extent by using a particular type of tip-fairing. This tip-fairing is of the same form as the normal one up to the position of maximum thickness; from this point on it is elliptic (the minor semi-axis being half the local thickness, and the major semi-axis being half the maximum thickness). Measurements of the drag of wings with such tip-fairings are fairly close to the true values (Figure 12.74).

The means of suspension of the wing automatically introduces errors; this can be seen, for example, from the measurements of momentum loss shown in Figure 4.8. JACOBS and ABBOTT [R669] give corrections that should be applied to the drag to allow for support interference. They are applicable to the measurements made in the NACA variable-density wind-tunnel from 1931 to 1939, and are reproduced in Figure 2.7.

### 2.3.4 Influence of Turbulence in the Air

In Section 2.2 the problem of turbulence in wind tunnels has been very thoroughly treated, because the state of turbulence of the air-stream has a decisive influence on the formation of the boundary layer; this in turn affects the drag and, above all, the maximum lift. When measurements made on models are applied to free air of low turbulence it is, therefore, essential to take the origin of the measurements into account. Both the American VDT and the first 2 m  $\times$  2 m tunnel of the Göttingen Institute for Model Tests have a particularly high degree of turbulence; consequently, the maximum lift coefficients measured in these tunnels are not usually attained in free air, and the measurements should not be applied to free-flight models (even if the Reynolds numbers seem to lie in the correct range); instead, later measurements made in low-turbulence wind-tunnels should be applied. The results of SCHMITZ are of interest here.

Attention is drawn to a source of errors of a special kind which has up till now received little attention; sometimes it can exert a considerable influence upon the measured maximum lift since it causes a change in the state of the boundary layer. Suppose that the wires used to measure the drag component, which are fastened to points on the leading edge of the wing, do not both run parallel to the free-stream direction to two points in front of the wing, but are brought together in V-form to a single point; the effect is the same as if a "turbulence wire" were stretched in front of the wing, parallel to the leading edge; as a result there is transition of the laminar boundary layer to a turbulent one, and an apparent increase in the values of  $C_{L_{\max}}$ . The measurements on some Göttingen profiles (from Profile 456 to Profile 592, but there are exceptions) have been made in the presence of such a V-shaped wire-suspension, and therefore require certain corrections; this is particularly true of the  $C_{L_{\max}}$  results.

#### 2.4 References

- ACKERET, J.: Experimentelle und theoretische Untersuchungen über Hohlraumbildung (Kavitation) im Wasser. Techn. Mech. und Thermodynamik 1 (1930), S. 1—22 u. 63—72.
- Das Institut für Aerodynamik des neuen Maschinenlaboratoriums der E.T.H. Mitt. Inst. für Aerodynamik, Zürich, Nr. 8 (1943).
- BETZ, A.: Eine Methode zur direkten Bestimmung des Profilwiderstandes. ZFM (1925).
- and R. SEIFERTH: Untersuchung von Flugzeugmodellen im Windkanal. Handb. d. Experimental-Physik, Bd. IV, 2 (1932).
- DOENHOFF, A. E. v. and F. T. ABBOTT jr.: The Langley Two-dimensional Low-turbulence Pressure Tunnel. NACA TN No. 1283 (1947).
- DOETSCH, H.: Profilwiderstandsmessungen im großen Windkanal der DVL. Lufo 14 (1937), S. 173.
- DRYDEN, H. L. and A. M. KUETHE: Effect of Turbulence in Wind-Tunnel Measurements. NACA Rep. 342 (1930).
- DRYDEN, H. L., C. B. SCHUBAUER, W. C. MOCK, Jr. and H. K. SKRAMSTAD: Measurements of Intensity and Scale of Wind-Tunnel Turbulence and their Relation to the Critical Reynolds Number of Spheres. NACA Rep. 581 (1937).
- DRYDEN, H. L. and L. H. ABBOTT: The Design of Low Turbulence Windtunnels. NACA TN 1755 (1948) und R 940 (1949).
- FAGE, A.: Experiments on a Sphere at Critical Reynolds Numbers. R & M No. 1766 (1936).
- FERRI, A.: La Galleria Ultrasonora di Guidonia. Atti di Guidonia No. 15, (1939) and Aircraft Engineering 12 (1940), p. 302—305.
- Influenza del Numero di Reynolds ai Grandi Numeri di Mach. Atti di Guidonia No. 67—69 (1942).
- DE FRANCE, S. I.: The NACA Full-Scale Wind-Tunnel. NACA Rep. 459 (1933).
- GLAERT, H.: see Section 1.5.1.
- GOETT, H. I.: Experimental Investigations of the Momentum Method for Determining Profile Drag. NACA Rep. 660 (1938).
- GÖTHERT, B.: Widerstandsbestimmung bei hohen Unterschallgeschwindigkeiten aus Impulsverlustmessungen. Jb. 1941 dDL I, S. 148.
- GÖTHERT, B.: Windkanalkorrekturen bei hohen Unterschallgeschwindigkeiten. LGL-Bericht 127 (1940), S. 114 und Jahrb. 1941 dDL, S. I 684/691.
- HOERNER, S.: Versuche mit Kugeln betreffend Kennzahl, Turbulenz und Oberflächenbeschaffenheit. Lufo 12 (1935), 42 bis 54.
- Aerodynamic Drag, Dayton, Ohio, 1951.
- JACOBS, E. N. and J. H. ABBOTT: The NACA Variable-density Wind Tunnel. NACA Rep. 416 (1932).
- JONES, B. M.: The Measurement of Profile Drag by the Pitot-Traverse Method. R & M No. 1688 (1936).
- KLEIN, M.: Windkanalwaagen. Mon. D<sub>2</sub> 1.1.
- KRAMER, M.: Der 5 × 7 m-Windkanal der DVL. Lufo 12 (1935), S. 181—187.
- Elektrisch gesteuerte Laufgewichtswaage für hohe Meßgenauigkeit und Fernaufzeichnung der Meßwerte, Z. VDI 80 (1936), S. 141.
- LOCK, C. N. H., W. F. HILTON and S. GOLDSTEIN: Determination of Profile Drag at High Speeds by a Pitot Traverse Method. R & M No. 1971 (1940).
- LUDWIG, H.: Windkanalkorrekturen bei kompressibler Strömung. Mon. D<sub>3</sub> 4.2 (1946).
- MATT, H.: Aufbau und Strahleigenschaften des DVL-Hochgeschwindigkeitswindkanals. LGL-Bericht 127 (1940) und Mon. D<sub>1</sub> 2.1.
- Einfluß verschiedener Windkanalaufhängungen auf die aerodynamischen Beiwerte von Flügeln, LGL-Bericht 156 (1942).
- PLATT, R. C.: Turbulence Factors of NACA Wind-Tunnels as Determined by Sphere Tests. NACA Rep. 558 (1936).
- PRANDTL, L.: Der Luftwiderstand von Kugeln. Nachrichten der Gesellschaft der Wissenschaften, Math.-Phys.-Klasse 1914.
- Die Bedeutung von Modellversuchen für die Luftschiffahrt und Flugtechnik und die Einrichtungen für solche Versuche in Göttingen. Z. VDI 1909, S. 1711.
- Tragflügeltheorie II. Mitt. Nachr. d. Kgl. Ges. d. Wiss. Göttingen, Math.-Phys. Kl. 1919, S. 107—137. Wiederabdruck in: Vier Abhandlungen zur Hydrodynamik und Aerodynamik, Göttingen 1927.
- REGENSCHEIT, B.: Untersuchungen über den Einfluß der Randkappenform auf die Tragflügelmeßergebnisse. Techn. Ber. d. ZWB. Bd. 11 (1944), S. 113.
- RIEGELS, F.: Windkanalkorrekturen bei inkompressibler Strömung. Mon. D<sub>3</sub> 4.1 (1946).
- SEIFERTH, R.: Messung der Kanalturbulenz und ihr Zusammenhang mit der Hitzdrahtmessung. Mon. D<sub>1</sub> 4.2 (1946).
- SCHLICHTING, H.: Einfluß der Turbulenz und der Reynoldschen Zahl auf die Tragflügeleigenschaften. Ringbuch der Luftfahrttechnik I A 1 (1937).
- SCHMITZ, F. W.: Zur Aerodynamik der kleinen Reynolds-Zahlen. Jahrb. 1953 der WGL, S. 149—165.
- SCHUBAUER, G. B. and H. L. DRYDEN: The Effect of Turbulence on the Drag of Flat Plates. NACA Rep. 546 (1935).
- SILVERSTEIN, A.: Scale Effect on Clark Y Airfoil Characteristics from NACA Full-Scale Wind-Tunnel Tests. NACA Rep. 502 (1934).
- TAYLOR, G. I.: The Determination of Drag by the Pitot-Traverse Method. R & M No. 1808 (1937).
- WEINIG, F.: Berechnung der Profilbeiwerte aus den Beiwerten des Modellflügels. FB 1666 (1942).
- WINTER, H.: Überdruckkanal der Aerodynamischen Versuchsanstalt Göttingen. Jb. 1937 dDL und Luftwissen 3 (1936), S. 237.
- ZOBEL, TH.: Fortschritte in der optischen Strömungsmessung. FB 1934 (1944) und DAL Nr. 5008/44.

### 3. FORCE AND MOMENT COEFFICIENTS

#### 3.1 Characteristic Aerodynamic Quantities

The force on a moving wing is proportional to the area,  $S$ , of the wing (or, in the two-dimensional case we are considering, to the chord,  $c$ , of the profile) and to the kinetic pressure,  $q = (\rho/2)V^2$  (where  $\rho$  is the density of the fluid). Consequently, it is usual to give the *drag*,  $D$ , and the *lift*,  $L$ , in the form of dimensionless coefficients:

$$C_D = \frac{D}{qS}, \quad C_L = \frac{L}{qS}; \quad (3.1)$$

in wind tunnels these coefficients are measured for various values of the angle of incidence,  $\alpha$  (the angle made by the profile with the free-stream direction).

For symmetrical profiles the axis of symmetry is always used in the definition of angle of incidence, but various possibilities exist for cambered profiles (see Section 1.2.1). From the aerodynamic point of view the following angles of incidence are of particular interest:

- (a) the angle of incidence at zero lift,  $\alpha_{L=0}$ , or, more briefly,  $\alpha_0$ ;
- (b) the ideal angle of incidence,  $\alpha^*$ ; this is the angle of incidence (for cambered profiles) at which the flow does not turn abruptly round the leading or trailing edges of the camber line, but attaches smoothly and leaves smoothly; in theoretical work  $\alpha^*$  is sometimes called the "design angle of incidence"†. For further remarks see Sections 8.2.1.2 and 8.2.5.

According to theory, a simple relation exists between lift coefficient and angle of incidence,

$$C_L = \frac{dC_L}{d\alpha} \sin(\alpha - \alpha_0). \quad (3.2)$$

Experimental results confirm this equation for small angles of incidence, in which range the relationship is linear, being

$$C_L = \frac{dC_L}{d\alpha} (\alpha - \alpha_0). \quad (3.3)$$

Because of viscous effects the constant value for the lift-curve slope,  $\frac{dC_L}{d\alpha}$ , is less than the theoretical value. It is not possible to find a similar simple theoretical relation for the drag coefficient,  $C_D$ .

† The German expression for  $\alpha^*$  is "der Anstellwinkel des stoßfreien Eintritts", "the angle of incidence of shock-free attachment".

Drag and lift are to be regarded as components of the total force,  $R = \sqrt{L^2 + D^2}$ , in the direction of the free stream and normal to this direction respectively (see Figure 3.1). If the total force is resolved in the direction of the

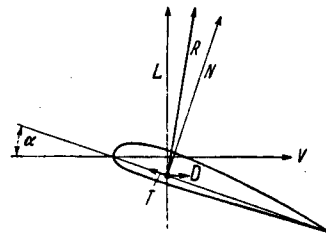


Fig. 3.1. Resolution of total aerodynamic force ( $R$ ) into drag ( $D$ ) and lift ( $L$ ), or into tangential and normal forces (respectively  $N$  and  $T$ )

chord and in a direction normal to the chord the respective components are called the *tangential force* ( $T$ ) and the *normal force* ( $N$ ), and the respective coefficients are written as

$$C_T = \frac{T}{qS}, \quad C_N = \frac{N}{qS}. \quad (3.4)$$

If  $\alpha$  is the angle between the direction fixed with respect to the profile and the direction of the free stream, then the formulas connecting the coefficients are

$$\begin{aligned} C_T &= -C_L \sin \alpha + C_D \cos \alpha \\ C_N &= C_L \cos \alpha + C_D \sin \alpha \end{aligned} \quad (3.5)$$

for small values of  $\alpha$  these become

$$\left. \begin{aligned} C_T &\approx C_D - \alpha C_L \\ C_N &\approx C_L + \alpha C_D \end{aligned} \right\} \quad (3.6)$$

In addition to these forces we are interested in the *pitching moment* of the total force with respect to a fixed point of the profile—for example, the leading edge (suffix  $l$ ); we write

$$(M)_l = (C_m)_l q S c; \quad (3.7)$$

it is taken to be positive if its effect is to increase the angle of incidence. The total force,  $R$  (resulting from the lift,  $L$ , and the drag,  $D$ ), cuts the line chosen as reference axis in a point at a distance  $h$  from the leading edge; the reference axis is a line fixed with respect to the profile, examples being the chord and the free-stream direction at zero lift.

Hence, we can write

$$(M)_l = -h(L \cos \alpha + D \sin \alpha) = -hN. \quad (3.8)$$

The point (at a distance  $h$  from the leading edge) that is the intersection of the profile chord and the line of action of the total force is called the *centre of pressure* of the profile; its position is given by

$$\frac{h}{c} = -\frac{(C_m)_l}{C_N}. \quad (3.9)$$

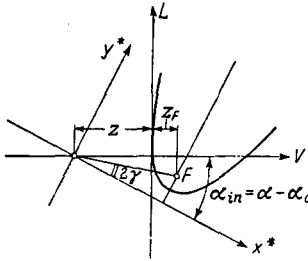
In general, this value varies considerably with the angle of incidence,  $\alpha$ ; but for a symmetrical profile (that is, for a profile with a straight camber line) the centre of pressure lies at one quarter of the chord from the leading edge, a theoretical result which is well confirmed by experiment (see Equation 8.44 and Figures 3.19 to 3.23).

According to theory a simple relation exists between the moment coefficient and the angle of incidence:

$$(C_m)_l = \frac{1}{2} \left( \frac{dC_m}{d\alpha} \right)_l \sin 2(\alpha - \alpha_0 - \gamma); \quad (3.10)$$

here,  $\gamma$  is an angle shown in Figure 3.2; its significance appears in the following discussion.

Fig. 3.2. Definition of  $\gamma$  and  $z$



*Additional theory.* In inviscid flow  $D = 0$ ; since the lift is then normal to the free-stream direction,  $M = -hL$ . The angle of incidence is now measured from the free-stream direction at zero lift and, since  $D = 0$ , it is written with the suffix "in" (inviscid flow). Then  $C_L = \frac{dC_L}{d\alpha_{in}} \sin \alpha_{in}$  and  $(C_m)_l = \frac{1}{2} \left( \frac{dC_m}{d\alpha_{in}} \right)_l \times$

$\sin 2(\alpha_{in} - \gamma)$ ; for the arm of the moment (the perpendicular distance,  $z$ , of the line of action of the lift from the point to which the moment is referred) we find

$$z = -c \frac{(C_m)_l}{C_L} = -\frac{c}{2} \frac{\left( \frac{dC_m}{d\alpha_{in}} \right)_l}{\left( \frac{dC_L}{d\alpha_{in}} \right)} \times \frac{\sin 2(\alpha_{in} - \gamma)}{\sin \alpha_{in}}.$$

Choose co-ordinates  $x^*$  and  $y^*$  with origin at the point to which the moment is referred; let the  $x^*$  axis be parallel to the free-stream direction at zero lift, and the  $y^*$  axis be normal to this direction. The line of action of the lift cuts the  $x^*$  axis at the point  $h = z/\cos \alpha_{in}$ , and the equation of this line is

$$x^* + y^* \tan \alpha_{in} = \frac{z}{\cos \alpha_{in}};$$

$\tan \alpha_{in}$  ( $k$ , say) occurs as a parameter here. The family of lines of action  $F(x^*, y^*, k) = 0$  has an envelope whose equation is found by eliminating  $k$  between  $F = 0$  and  $\frac{\partial F}{\partial k} = 0$ . The

equation of the envelope is

$$\left[ x^* + c \frac{\left( \frac{dC_m}{d\alpha} \right)_l \cos 2\gamma}{\left( \frac{dC_L}{d\alpha} \right)} \right]^2 = -2c \frac{\left( \frac{dC_m}{d\alpha} \right)_l \sin 2\gamma}{\left( \frac{dC_L}{d\alpha} \right)} \left[ y^* + \frac{c}{2} \frac{\left( \frac{dC_m}{d\alpha} \right)_l \sin 2\gamma}{\left( \frac{dC_L}{d\alpha} \right)} \right];$$

the envelope is called the *metacentric parabola*. Its axis is parallel to the  $y^*$  axis; its apex,  $A$ , lies at

$$x_A^* = -c \frac{\left( \frac{dC_m}{d\alpha} \right)_l}{\left( \frac{dC_L}{d\alpha} \right)} \cos 2\gamma, \quad y_A^* = -\frac{c}{2} \frac{\left( \frac{dC_m}{d\alpha} \right)_l}{\left( \frac{dC_L}{d\alpha} \right)} \sin 2\gamma;$$

and its focus,  $F$ , at

$$x_F^* = -c \frac{\left( \frac{dC_m}{d\alpha} \right)_l}{\left( \frac{dC_L}{d\alpha} \right)} \cos 2\gamma, \quad y_F^* = -c \frac{\left( \frac{dC_m}{d\alpha} \right)_l}{\left( \frac{dC_L}{d\alpha} \right)} \sin 2\gamma.$$

We see that the distance between the focus and the point to which the moment is referred is

$$c \frac{\left( \frac{dC_m}{d\alpha} \right)_l}{\left( \frac{dC_L}{d\alpha} \right)},$$

and that the straight line joining these two points is inclined at an angle  $2\gamma$  to the free-stream direction at zero lift.

If we now refer the moment of the lift force to the focus of the lift parabola we obtain for the arm

$$z_F = -\frac{c}{2} \frac{\left( \frac{dC_m}{d\alpha} \right)_l \sin 2\gamma}{\left( \frac{dC_L}{d\alpha} \right) \sin \alpha_{in}},$$

and for the moment coefficient referred to  $F$

$$(C_m)_F = \frac{1}{2} \left( \frac{dC_m}{d\alpha} \right)_l \sin 2\gamma;$$

$(C_m)_F$  is, therefore, independent of angle of incidence.

The method by which the behaviour of the moment has been obtained is strictly valid for inviscid flow only; but the assumptions made concern only the dependence of  $C_L$  and  $(C_m)_l$  on  $\alpha_{in}$ . According to measurement,  $C_L$  and  $(C_m)_l$  differ from the theoretical values; therefore, the focus almost always lies at a point different from that just determined, and the moment with respect to this point is not exactly constant. Nevertheless, even in viscous flow, a point exists referred to which the moment is approximately independent of angle of incidence; this is true for every profile in a certain (sometimes very limited) range of  $C_L$ . The point is called the *aerodynamic centre* (a.c.) of the profile or, sometimes, the *neutral point* of the profile; it corresponds to the focus of the lift parabola in

inviscid flow, and in general lies very close to the point on the chord which is at a distance of one quarter of the chord from the leading edge.

If the moment is measured with respect to some point  $(x, y)$  then the position of the aerodynamic centre (suffix  $a$ ) can be obtained from the relation

$$(C_m)_a = C_m + \frac{(x_a - x)}{c} C_N - \frac{(y_a - y)}{c} C_T. \quad (3.11)$$

If the dependence of  $C_m$ ,  $C_L$ , and  $C_D$  on  $\alpha$  is known, then the required values  $(x_a, y_a)$ , and  $(C_m)_a$ , can be obtained by using this equation three times: when  $C_L = 0$ ; when  $C_L$  is close to its maximum; and when  $C_L$  lies somewhere between these two values†. From its definition  $(C_m)_a$  should be approximately constant over the whole range of angle of incidence (up to separation).

### 3.2 Review of Experimental Results

#### 3.2.1 Angle of Incidence Ranging from $0^\circ$ to $360^\circ$

A knowledge of the forces and moments occurring at all possible angles of incidence is highly desirable (for example, in problems concerning helicopters and variable-pitch propellers). In Figure 12.105a measurements for the profile NACA 0012 between plane walls are reproduced; these give an indication of the forces and moments to be expected at other free-stream conditions.

In addition, measurements on rectangular wings of aspect ratio 5 are shown in Figures 12.51b, 12.61, and 12.72b; the profiles are flat and cambered plates, and the

#### 3.2.2 Normal Range of Angle of Incidence

Extensive investigations of profiles have been carried out in the wind tunnel of the old Göttingen Institute for Model Tests (MVA); the results are published in the "Technical Reports" of the first world war (see Section 1.5.2). The Reynolds number is usually about  $7 \cdot 10^4$  and, although these old measurements have long ceased to have any value for the aircraft constructor, they have great interest today precisely because of the small Reynolds number. For example, they are useful in estimating the characteristics of free-flight models and for determining the best possible setting of turbine blades. Some of the experimental results for such profiles are reproduced in the Tables of Section 11.5 and in the Figures of Section 12.5.1; before they are used the remarks in Section 2.3.4 should be noted.

After the 2.25 m tunnel of the AVA at Göttingen had been put into operation measurements on profiles were made exclusively in this tunnel, mostly at Reynolds numbers of about  $4 \cdot 10^5$ . Since 1937 measurements have also been carried out at higher Reynolds numbers in the large wind-tunnel of the AVA; in extreme cases the value  $R = 7 \cdot 10^6$  has been reached. Details of a selection of the profiles investigated in these tunnels are included in this book; the ordinates are given in the Tables of Section 11.3, and the measured force and moment coefficients in the Tables of Section 11.5. In the original publications the reference point for the moment is the leading edge or, more accurately, the point of the profile chord which lies

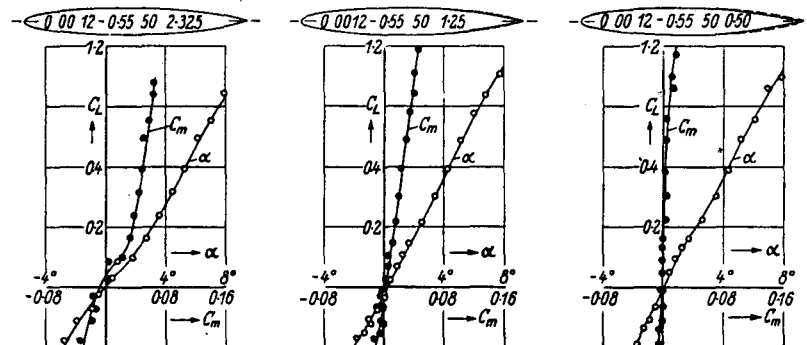


Fig. 3.3 Influence of trailing edge angle on  $C_L(\alpha)$  and  $C_L(C_m)$ . Wind tunnel: DVL 2.7 m

two profiles Gö 420 and Gö 623. Although the assumption of two-dimensional flow made elsewhere in this book does not hold here and a conversion to  $A = \infty$  would have little meaning, these measurements should be regarded as a welcome addition to our knowledge.

† Instead of the three values of  $C_L$  proposed here the NACA (see [R537]) determine the aerodynamic centre and the corresponding moment by using Equation (3.11) twice (when  $C_L = 0$ ; and when  $C_L = C_{L_2}$ ,  $C_{L_2}$  being close to  $C_{L_{\max}}$ ) and by making  $\frac{dC_m}{dC_L}$  have the measured value at  $C_L = 0$ .

on the perpendicular from the leading edge (the coefficient,  $(C_m)_l$ , is positive when the tendency is to decrease the angle of incidence!); for the profiles Gö 758 and beyond, the reference point lies at one quarter of the chord from the leading edge (the coefficient,  $C_m$ , is positive when the tendency is to increase the angle of incidence); the latter definition is here used throughout (that is, for the older profiles as well). In the figures and tables, jet-boundary corrections have been applied, and the conversion to  $A = \infty$  has been performed with allowance for the effect of the lift distribution on the wing (see Section 2.3).

The Göttingen profile Gö 398 (with its maximum thickness at 30% of the chord) has proved particularly favourable (this profile is approximately the same as the Clark Y profile); its thickness distribution is, therefore, the basis of the extensive systematic measurements made by the NACA in the VDT (see Section 7.3.2, Type D<sub>1</sub>). These measurements, carried out at the high effective Reynolds number of  $8 \cdot 10^6$  [R460], have led to a number of standard profiles (in particular, the 24 and 230 series) with distinctive properties. Although later measurements in low-turbulence wind-tunnels of the DVL and the NACA reveal a number

After verification of the properties of the NACA 24 and 230 series by measurements in the 5 m  $\times$  7 m wind-tunnel of the DVL (DOETSCH), an extensive programme was carried out in this tunnel to determine the effect of changes in the thickness distribution (in particular, the effect of varying the nose radius and the position of maximum thickness); the results of these measurements can be found in the collection of data of Table 11.1 and also in Table 11.5. The investigations, carried out at a Reynolds number of  $2 \cdot 7 \cdot 10^6$ , demonstrate the favourable influence on the drag both of a rearward displacement of the maximum thickness

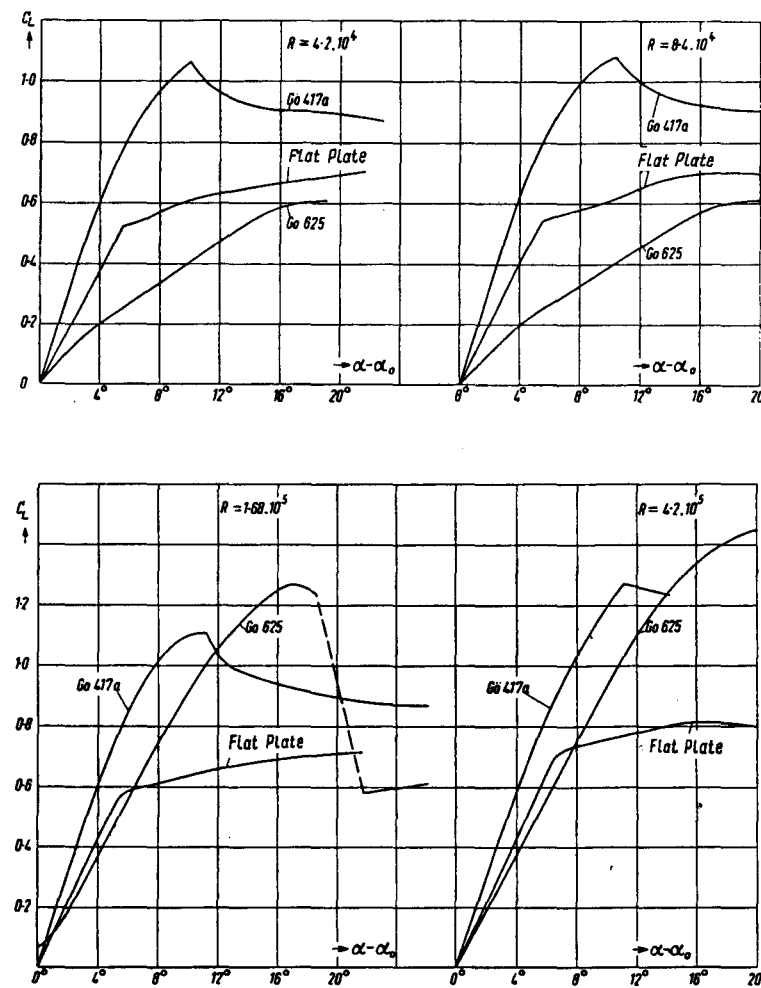


Fig. 3.4a, b. Dependence of lift coefficient on Reynolds number, for typical profiles (SCHMITZ). Wind tunnel: Cologne

of deficiencies in these results, such a systematic investigation gives considerable insight into the influences of thickness, camber, and position of maximum camber. The deficiencies are removed to a certain extent by the application of corrections (in particular, for the maximum lift ( $C_{L_{\max}}$ ) and the minimum drag ( $C_{D_{\min}}$ ) [R669]) and by new measurements in low-turbulence wind-tunnels [R 824]. Because of the existence of later measurements, we do not reproduce the old experimental results, but simply refer to the literature.

from the normal value of 30% of the chord and of a decrease in nose radius from the normal value  $r_0/c = 1 \cdot 1 (t/c)^2$ ; it is found possible to obtain significant laminar effects (that is, to keep the boundary layer laminar longer than is usual with "normal" profiles). Unfortunately, undesirable changes frequently occur in the lift-curve slope and in the behaviour of the moment; they are caused by the unfavourable movement of the transition point on profiles of this type. These changes are eliminated only when the trailing edge angle is made smaller (Figure

3.3). The resulting profile (or, better, pressure distribution) is close to that which the NACA take as a basis in a systematic investigation, carried out at about the same time in the low-turbulence wind-tunnels LTT and TDT; the pressure distributions were prescribed and the corresponding profiles designed by theoretical methods. At high Reynolds numbers the drags are lower than those of the earlier profiles, and the remaining profile properties are also satisfactory. The results of these later measurements are given in the Figures of Chapter 12 and in Table 11.1. The Reynolds numbers for the measurements are  $3 \cdot 10^6$ ,  $6 \cdot 10^6$ , and  $9 \cdot 10^6$ ; each profile is measured with and without a split-flap deflection of  $60^\circ$  [R824]. Some models have been investigated at Reynolds numbers of from  $0 \cdot 7 \cdot 10^6$  upwards [N1945, R964], the high value of  $5 \cdot 10^7$  being reached. Most models have been measured both with a smooth surface and with "standard roughness" (see Section 4.1.3).

### 3.3 Behaviour of the Lift

#### 3.3.1 Lift-curve Slope

The theoretical value for the lift-curve slope of the flat plate is  $\frac{dC_L}{da} = 2\pi$ , if  $a$  is measured in radians, or  $\frac{dC_L}{da} = 0.11$  if  $a$  is measured in degrees. We introduce an efficiency factor,  $\eta$ , by the relation

$$\frac{dC_L}{da} = 2\pi\eta. \quad (3.12)$$

For the Göttingen flat-plate measurements (Figure 3.4b), the value  $\eta = 1$  is very nearly reached, but the measured value becomes smaller as the Reynolds number decreases, and falls to  $\eta = 0.84$  when  $R = 4.2 \cdot 10^4$ .

The behaviour of  $\eta$  for the cambered plate is anomalous (Figures 3.4a and b): although  $\eta$  increases theoretically by a factor of only  $[1 + k(\frac{f}{c})^2]$ , if  $\frac{f}{c}$  is small, the measurements on, for example, Gö 417a for  $C_L < 0.6$ , give the high value†  $\eta \approx 1.38$ , corresponding to  $\frac{dC_L}{da} = 2.8\pi$ ; this value is almost independent of Reynolds number from  $R = 4.2 \cdot 10^4$  up to  $R = 4.2 \cdot 10^5$ . For  $C_L > 0.6$ ,  $\eta$  certainly decreases with increasing  $C_L$  and is soon less than 1.

The usual profiles of finite thickness, with maximum thickness at about 30% of the chord, have a poor value of  $\eta$  in the sub-critical region, but  $\eta$  increases with the Reynolds number and reaches values of about 0.9 in the supercritical region, at a Reynolds number of  $4 \cdot 10^5$ . At Reynolds numbers of the order of  $10^6$ , and with not too large a thickness ratio,  $\eta$  becomes almost equal to 1. For a constant Reynolds number (say,  $R = 6 \cdot 10^6$ ) a fall is detectable

† This high value results from separation on the pressure side, the expected suction not being realised.

with increasing thickness ratio (to  $\eta = 0.9$  when  $\frac{t}{c} = 0.23$ ) (Figure 3.5). According to potential theory the value of  $\frac{dC_L}{da}$  should become larger than  $2\pi$  as the thickness increases (see Section 8.2.5), but the relatively thick boundary layer causes  $\eta$  to decrease as the thickness increases.

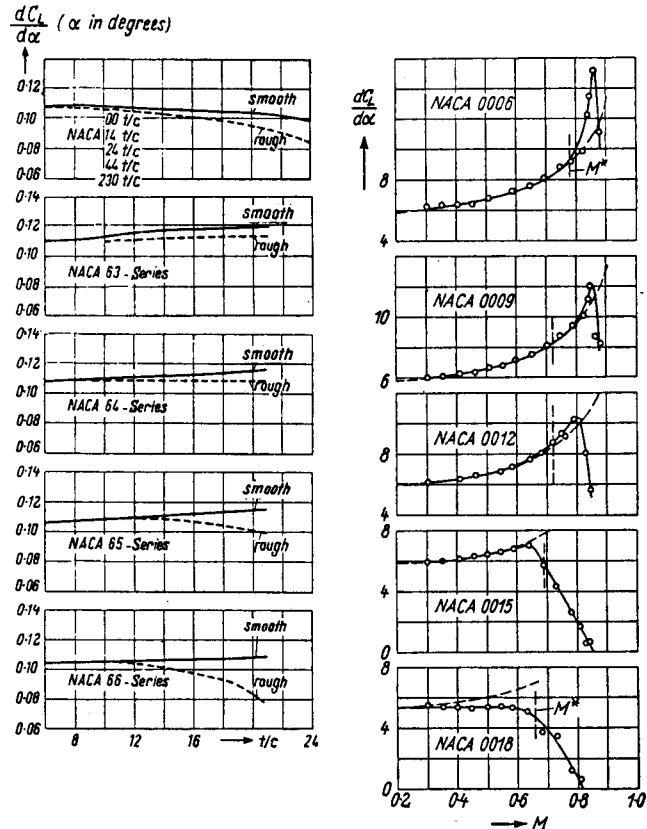


Fig. 3.5.  $\frac{dC_L}{da}$  ( $a$  in degrees) as a function of thickness ratio, for various profile series. Wind tunnel: LTT. Reynolds number:  $6 \cdot 10^6$

Fig. 3.6. Influence of Mach number on  $\frac{dC_L}{da}$ , for symmetrical NACA profiles. Wind tunnel: DVL 2.7 m

The later profiles with small nose radius and maximum thickness lying further back display a somewhat different behaviour; because of the favourable pressure distribution the boundary layer remains very thin even in the turbulent region; turbulent separation does not occur until near the trailing edge, so that the influence of viscosity is considerably smaller. At Reynolds numbers above  $6 \cdot 10^6$ , therefore,  $\eta$  continues to increase with thickness and reaches values up to about 1.07. However, if the rear part of the profile bulges too much (large trailing edge angle), as in profiles investigated by the DVL and in those of the NACA 1-series, the unfavourable pressure distribution causes a thicker boundary layer, and hence a decrease in  $\eta$ ; for such profiles an increase in camber leads to improvement.

In general, the factor  $\eta$  decreases considerably with Reynolds number at high  $C_L$  values, the cause being the

large increase in boundary layer thickness. The influence of "standard roughness" of the surface (see Section 4.1.3) on the lift-curve slope is shown in Figure 3.5.

From the Prandtl-Glauert rule (see Section 10.3)  $\frac{dC_L}{d\alpha}$  increases with Mach number as  $\frac{1}{\sqrt{1 - M^2}}$ ; this is well confirmed for profiles of small and moderate thickness, until the critical Mach number is reached, but considerable deviations occur at higher Mach numbers and  $C_L$  values (Figures 3.6 and 3.7). As the Mach number increases there

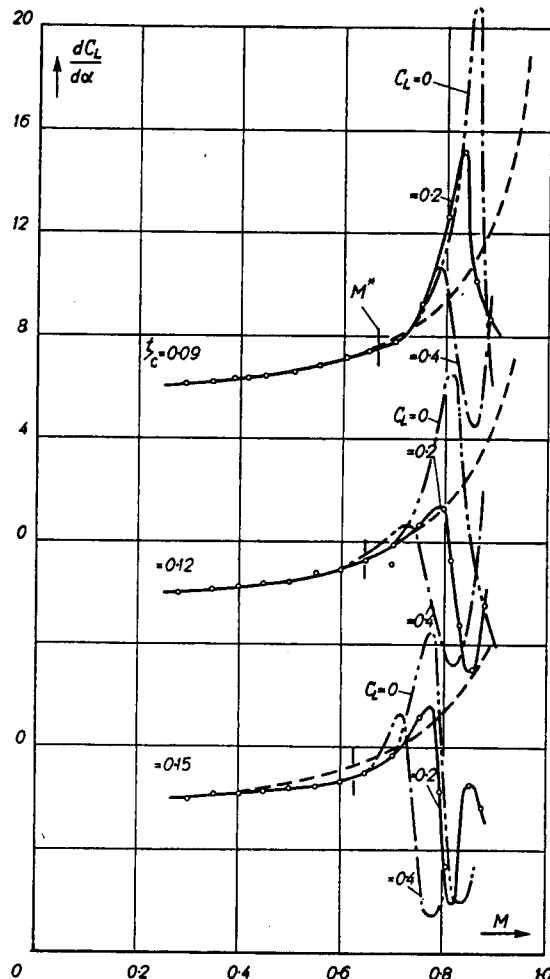


Fig. 3.7. Influence of Mach number on  $\frac{dC_L}{d\alpha}$ , for the NACA 230-series. Wind tunnel: DVL 2.7 m

is initially a considerable rise, then a fall, and finally another rise. As the camber is increased, the measured values of  $\frac{dC_L}{d\alpha}$  cease to show the theoretical increase with Mach number, and  $C_L$  no longer behaves linearly with  $\alpha$ . The initial large increase in  $\frac{dC_L}{d\alpha}$ , which occurs when the critical Mach number is exceeded, is predicted by more accurate theory, but the changes occurring as the Mach

number increases still further are caused by the appearance of shocks and their interaction with the boundary layer.

When the Mach number is greater than unity, but not large compared with unity then, if the flow is wholly supersonic and the angle of incidence is small, a linear behaviour is again observed; according to a well-confirmed theory  $\frac{dC_L}{d\alpha}$  then takes the value  $\frac{4}{(M^2 - 1)^{1/2}}$  (see Section 10.5.3).

### 3.3.2 Angle of Zero Lift

The angle of zero lift for the flat plate is independent of Reynolds number but, for a cambered plate, a small decrease with increasing Reynolds number is detectable (Figure 3.8); the effect of Reynolds number is most

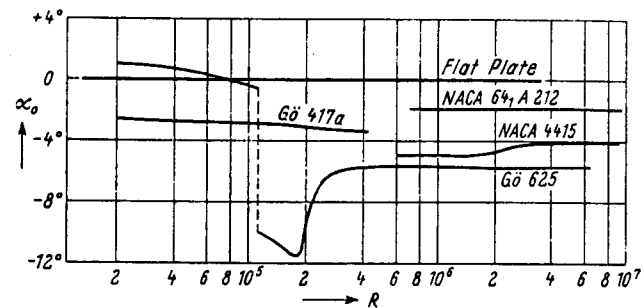


Fig. 3.8. Angle of incidence at zero lift, as a function of Reynolds number

marked on cambered, thick profiles.  $\alpha_0$  is always relatively small for sub-critical Reynolds numbers, but it jumps to a large negative value when the critical Reynolds number is

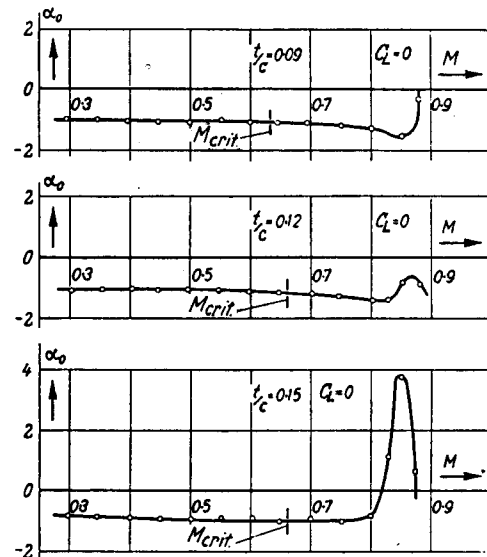


Fig. 3.9. Angle of incidence for zero lift, as a function of Mach number (for the 230-series)

exceeded (that is, when there is transition to turbulent flow in the boundary layer); it then rises with increasing Reynolds number to an almost constant value. This value

is essentially dependent only on the camber for medium and high Reynolds numbers; it is almost completely independent of the profile thickness (see Table 11.1). Deviations from the theoretical angle of zero lift usually lie between  $\pm 10\%$ , the actual amount depending on the type of camber line; for the camber line which has a constant velocity deviations of  $-25\%$  are found.

The angle of zero lift does not change rapidly with Mach number until shocks appear; the change then depends very much on the profile shape. The behaviour with increasing Mach number is usually as follows: there is a small decrease in  $\alpha_0$ , until a Mach number of about 0.8 is reached; the decrease is then usually followed by a sudden, large rise. For the NACA 230-series (Figure 3.9) only a small dependence on Mach number is detectable until far beyond the critical Mach number. When the Mach number is greater than 0.8 the large changes already mentioned appear, and they increase with thickness. Figure 3.10 is a comparison of the variation of angle of zero lift with Mach number for three profiles of various shapes [R947];

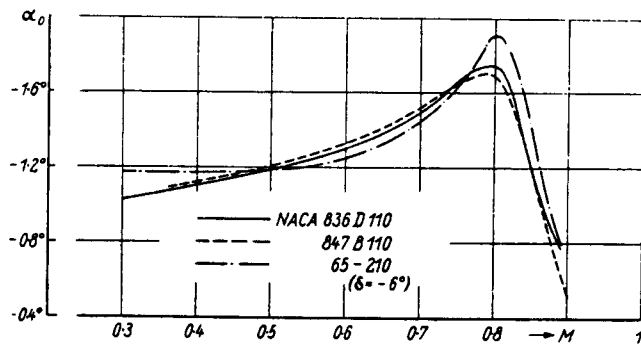


Fig. 3.10.  $\alpha_0(M)$  for some modern profiles.

with a flap deflection of  $-6^\circ$ , the profile having a fairly large  $C_L^*$  shows approximately the same variation as the other two profiles with no flap deflection.

For a fixed, supersonic Mach number the angle of zero lift decreases as the square of the thickness ratio; this is shown in Section 10.5.4 for the profile whose suction side is a circular arc and whose pressure side is straight.  $\alpha_0$  increases with Mach number in supersonic flow.

### 3.3.3 Effect of Increase in Mach Number on the Relation between Lift and Angle of Incidence

Because of the large irregularities as sonic speed is approached (from below), diagrams of the behaviour of either angle of incidence for constant  $C_L$  or  $C_L$  for constant angle of incidence are frequently used in addition to diagrams for  $\frac{dC_L}{d\alpha}$  and  $\alpha_0$ . An example of the first type of diagram is given in Figure 3.11; according to the Prandtl-Glauert rule the curves of  $\alpha$  against  $M$  should be ellipses, and these are also drawn in the diagram; the ellipses have zero slope when  $M = 0$ , and infinite slope at  $\alpha = 0, M = 1$ .

By a combination of suitable thickness and camber distributions, it is possible to design profiles for which  $C_L^*$

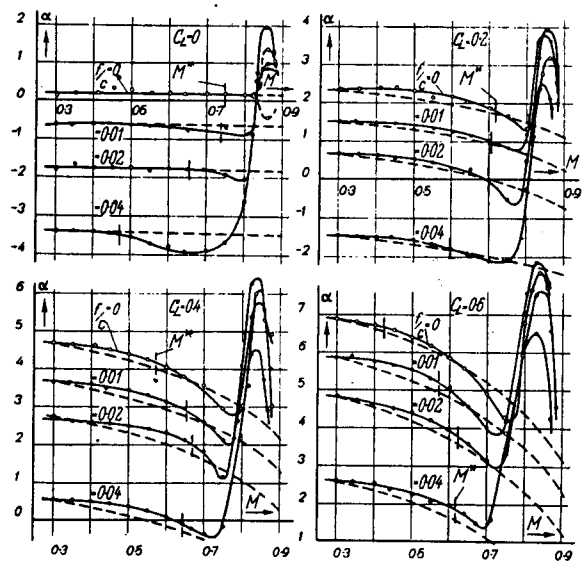


Fig. 3.11.  $\alpha$  plotted against  $M$  at constant  $C_L$ . Profile series: z 3512 - 0.55 40 (with various values of maximum camber). Dashed lines: Prandtl-Glauert rule

remains almost constant as the Mach number increases, up to a value of  $M$  between 0.85 and 0.9 (NACA 836D110 and 847B110).

### 3.4 Maximum Lift

There is generally a considerable variation of maximum lift with Reynolds number. Figure 3.12 shows a small selection from the large amount of material in Table 11.1.

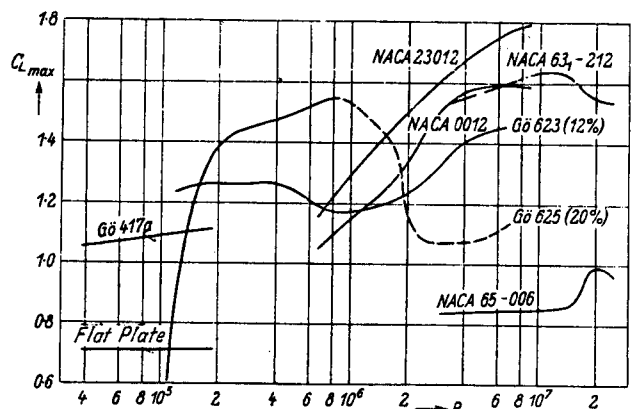


Fig. 3.12. Maximum lift as a function of Reynolds number, for selected profiles

For sub-critical flow only very small lifts are reached throughout (the cambered plate forming an exception); after the critical Reynolds number is passed,  $C_{L_{max}}$  increases very rapidly at first; when the super-critical state is reached its growth is again slow, and this behaviour often continues up to high Reynolds numbers, but is

sometimes disturbed by a temporary fall. In general, the maximum lift increases with camber.

For a fixed Reynolds number  $C_{L_{\max}}$ , when plotted against thickness, shows pronounced maxima, the position of these maxima depending on the profile series being investigated; for profiles whose maximum thickness lies at about 30% of the chord they are usually close to  $\frac{t}{c} = 0.12$ . If the maximum thickness lies further back, the maxima occur at higher values of the thickness ratio ( $\frac{t}{c} = 0.16$ ); for the NACA 66-series  $C_{L_{\max}}$  has a high, constant value in the range of  $\frac{t}{c}$  from 0.15 to 0.21, provided that the Reynolds number is high (9.10<sup>6</sup>).

The influence of nose radius on the maximum lift is quite large (see Figure 5.2). For the DVL series ( $R = 2.7 \cdot 10^6$ )  $C_{L_{\max}}$ , with normal thickness ratios of 12% and 15%, shows the following behaviour as the nose radius is decreased: from the normal value of nose radius down to one half this value there is a slight fall; but, when the nose radius has become one quarter the normal value,  $C_{L_{\max}}$  has sunk to almost one half of its initial value.

Other factors affect the behaviour of  $C_{L_{\max}}$ : both the state of turbulence of the air and the quality of the surface have a decisive influence (see Sections 2.3.4 and 4.1).

### 3.5 Profile Drag

#### 3.5.1 Incompressible Flow. Minimum Drag

The minimum drag of a profile occurs at vanishing lift ( $C_L = 0$ ) for symmetrical profiles and, generally, at the ideal angle of incidence for cambered profiles (that is, when  $C_L = C_L^*$ ). Figure 3.13 gives a survey of experimental

values in the Reynolds-number range  $R = 2 \cdot 10^4$  to  $R = 6 \cdot 10^7$ . The drag of the flat plate is wholly skin-friction drag and agrees with theoretical predictions: on the other hand, the cambered plate (in a super-critical stream) is almost completely independent of Reynolds number at  $\alpha = 0$  (that is, the drag is predominantly form drag). For cambered profiles of finite thickness both types of drag occur, and a strong dependence on Reynolds number becomes apparent.  $C_{D_{\min}}$  is very high in sub-critical flow because the contribution of the form drag is high; when the critical Reynolds number is exceeded the drag falls suddenly, because the boundary layer is no longer laminar when it separates; the region of separated flow is then considerably smaller, since the turbulent boundary layer remains attached for longer. Therefore, a turbulent boundary layer is desirable in this region of Reynolds number (usually beyond  $R = 10^5$ ); the effect is to reduce the drag, because flow that would otherwise have separated stays attached, and so the form drag contribution is reduced. For normal profile shapes transition of the boundary layer usually occurs in the first third of the profile chord; this is true of the four-figure NACA profiles (shown together with Göttingen profiles in Figure 3.13) in the range of Reynolds number between  $10^5$  and  $10^6$ . With increasing Reynolds number the skin-friction drag becomes more important. A glance at the theoretical curves for the flat plate (Figure 9.15) shows that large reductions in drag are obtainable at higher Reynolds numbers, if it is possible to increase the length of laminar boundary layer (that is, to displace rearwards the point of transition). With a suitable pressure distribution or profile shape it is possible to achieve these reductions, as measurements in all wind-tunnels of sufficiently low turbulence have shown. In Figure 3.13 are also plotted the drag coefficients of some

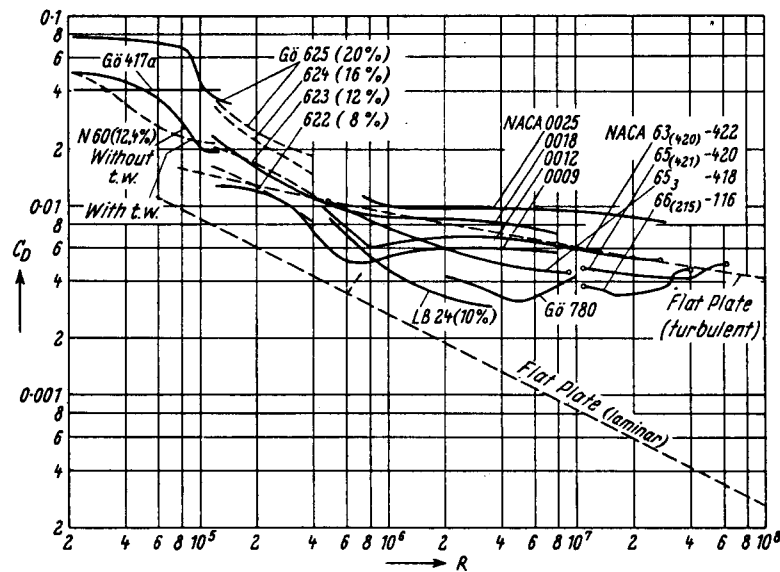


Fig. 3.13. Minimum drag coefficient as a function of Reynolds number for some profiles (tw, turbulent wire; LB 24, Japanese profile)

characteristic profiles for which the point of transition has been displaced rearwards to 60% of the chord. It must be emphasised that these profiles, though favourable at high Reynolds numbers, may have higher drag coefficients at low Reynolds numbers than profiles with a maximum thickness at 30% of the chord; this is because the large pressure-rise behind the minimum pressure gives rise to laminar separation, and so produces an increase in the form drag.

The behaviour of the drag coefficient as a function of thickness and camber, at constant Reynolds number, is of interest. Measurements carried out at a Reynolds number of  $4 \cdot 10^5$  on Joukowsky profiles lead to the approximate formula

$$C_{D\min.} = 0.0046 + 0.044 \frac{t}{c} + \\ + 0.48 \left( \frac{f}{c} \right)^3 \text{ for } R = 4 \cdot 10^5;$$

this has been derived by a careful study of the results in the region  $\frac{t}{c} < 0.25$ ,  $\frac{f}{c} < 0.11$ . We see that the drag coefficient increases as the first power of the thickness ratio, but as the third power of the camber. Corresponding approximate formulas for other profiles and Reynolds numbers can be easily derived from Table 11.1. This table shows that, at a Reynolds number of  $6 \cdot 10^6$ , the approximately linear rise with thickness ratio is still valid. For the four and five figure NACA profiles we have, approximately,

$$C_{D\min.} = 0.0038 + 0.016 \frac{t}{c} \text{ for } R = 6 \cdot 10^6, \frac{t}{c} < 0.15;$$

and for the NACA 66-series we have

$$C_{D\min.} = 0.0026 + 0.007 \frac{t}{c} \text{ for } R = 6 \cdot 10^6, \frac{t}{c} < 0.15.$$

With increasing thickness ratio, terms of higher order appear and these soon become dominant. For example, HOERNER (see Section 1.5.1) gives the following formula:

$$\frac{C_{D\min.}}{(C_D) \text{ flat plate}} = 1 + 2 \frac{t}{c} + 60 \left( \frac{t}{c} \right)^4,$$

which is derived from older measurements for  $3 \cdot 10^6 \leq R \leq 8 \cdot 10^6$  and  $\frac{t}{c} < 0.5$ .

The measured NACA profiles have small camber, and a dependence of drag on camber is barely detectable. When the position of maximum thickness is moved back, a decrease in drag is noticed; as the Reynolds number is increased this decrease is initially more pronounced, but at very high Reynolds numbers (from  $2 \cdot 10^7$  to  $5 \cdot 10^7$ ) instability of the boundary layer leads to transition and the drag again increases.

### 3.5.2 Incompressible Flow. Dependence on Lift Coefficient

Figure 12.66 and Tables 11.5 contain measured polars for Joukowsky profiles at  $R = 4 \cdot 10^5$ . An important feature (which is true of all profiles) is that the effect of camber, provided it is small, consists simply in a shift of the whole polar to a higher value of  $C_L$ ; more radical changes in the shape of the polar occur only when the camber is large (above 10%); these become more noticeable with increasing thickness.

There is no basic change in this behaviour at higher Reynolds numbers. For laminar profiles, the region of minimum drag is shifted in the same way.

The point of transition moves forward suddenly when  $C_L$  exceeds a certain value, and so the laminar region is generally sharply delimited; for example, almost all measurements on the profiles of the NACA 6-series show this. The width of the region increases considerably with thickness; in particular, its upper limit moves to higher

$C_L$  values. For thickness ratios  $\frac{t}{c} \leq 0.12$ , the width of the  $C_L$  region with minimum drag is usually less than  $\Delta C_L = 0.1$ . The measurements show clearly that this region becomes smaller as the Reynolds number increases; this is confirmed by an investigation of the profile NACA 65(421)-420 carried out up to very high Reynolds numbers (up to  $R = 35 \cdot 10^6$ ) [R824]. Once the laminar region has ended, a steep rise in the drag occurs (usually very soon), an effect that becomes more noticeable as the Reynolds number is increased. It is interesting that exactly the opposite behaviour is observed with the usual four and five figure NACA profiles (with maximum thickness at 30% of the chord): the drag decreases with increasing Reynolds number at the higher  $C_L$  values. If we were to examine the range of  $C_L$  in which the drag is small, we would find that, in contrast to the laminar profiles, these profiles show a broadening of the region with increasing Reynolds number. If the position of maximum thickness is moved still further forward, the drag coefficient remains approximately constant up to very high  $C_L$  values (see, for example, the profile Gō 769, Figure 12.88).

### 3.5.3 Compressible Flow

The behaviour of the drag, as the free-stream speed increases and approaches the speed of sound, is of particular importance. The diagrams in Figures 3.14 to 3.18 show the characteristic behaviour of  $C_D$  with Mach number for three profile series. In the first the position of maximum thickness is normal (at 30% of the chord), and in the second the position of maximum thickness is varied (in both these series the profiles are symmetrical); the third is a series of cambered profiles with maximum thickness at 40% of the chord. Each figure corresponds either to a constant value of  $C_L$  or to a constant value of  $\alpha$ . Further results for the NACA series 1, 6, and 8 are contained in the figures of

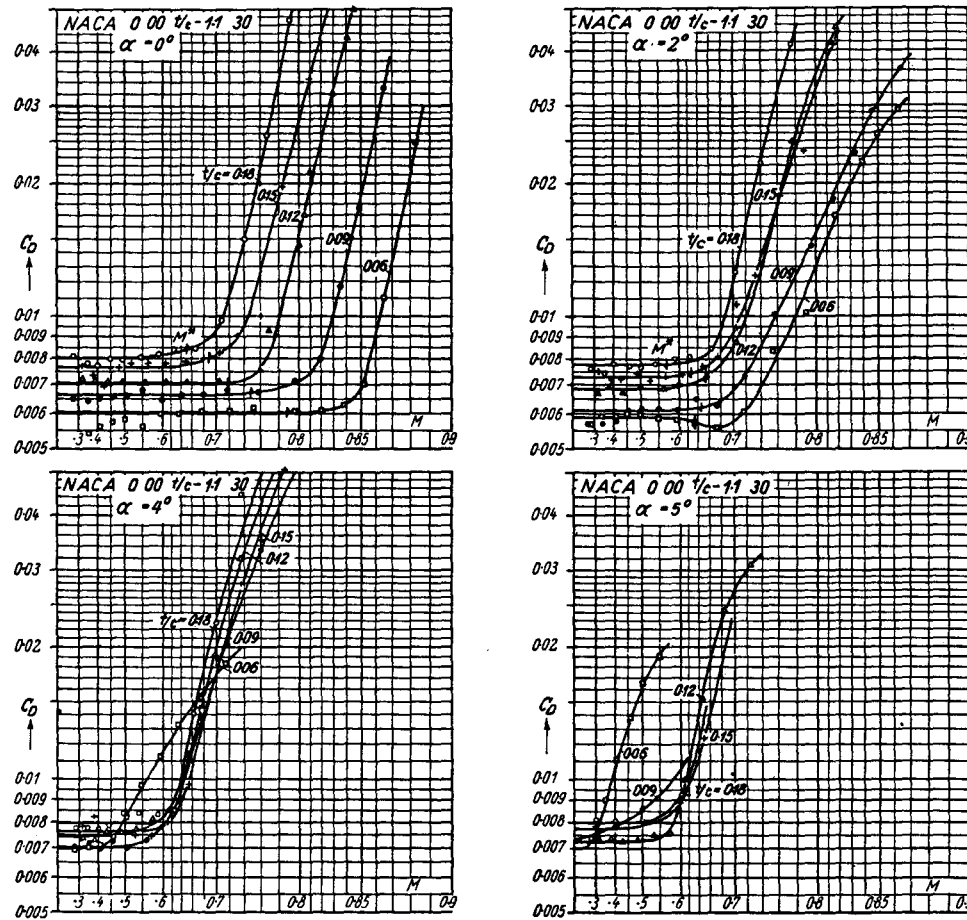


Fig. 3.14. Drag coefficient as a function of Mach number for various combinations of angle of incidence and thickness ratio (maximum thickness at 30% of the chord). Wind tunnel: DVL 2.7 m

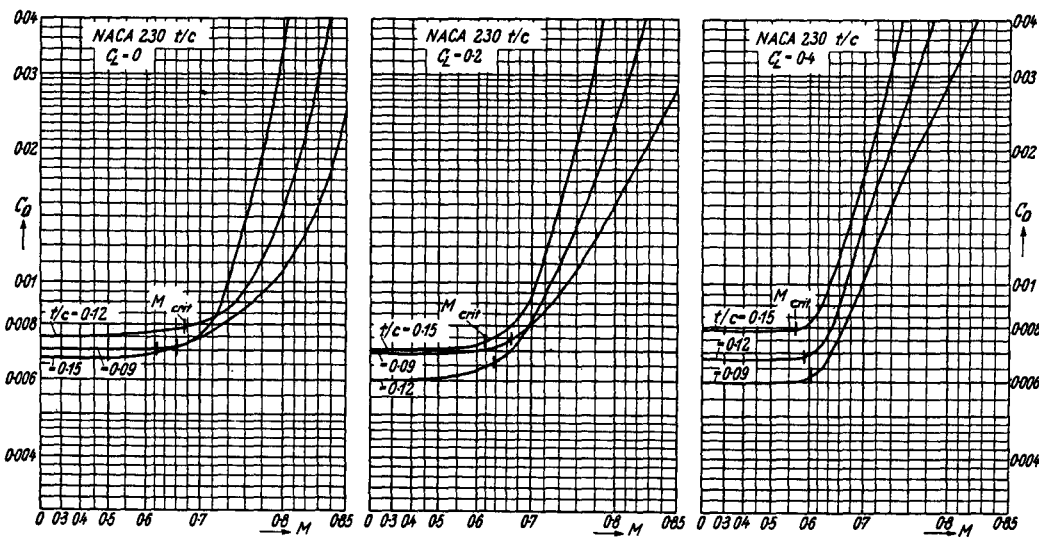


Fig. 3.15. As above, but for the 230-series at various values of  $C_L$  (DVL)

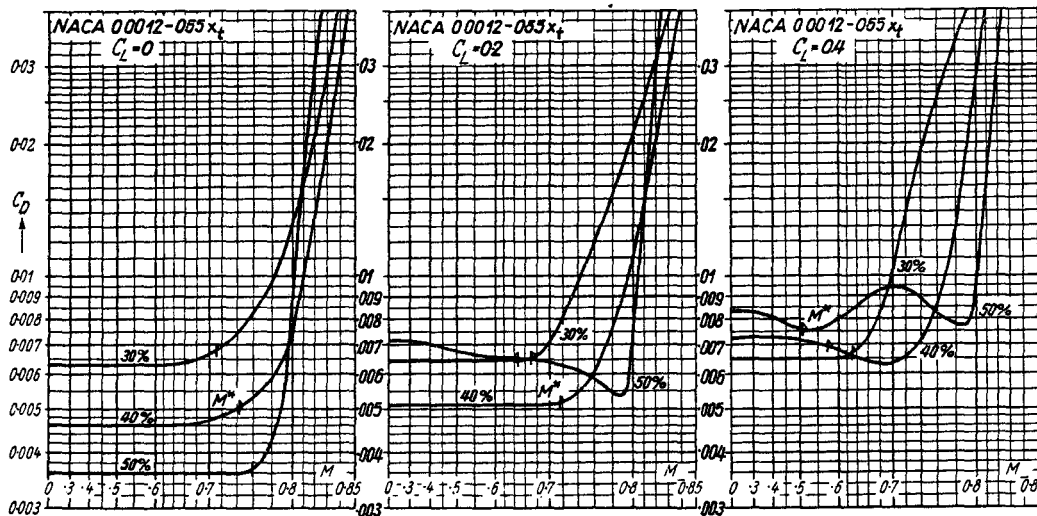


Fig. 3.16 a-c

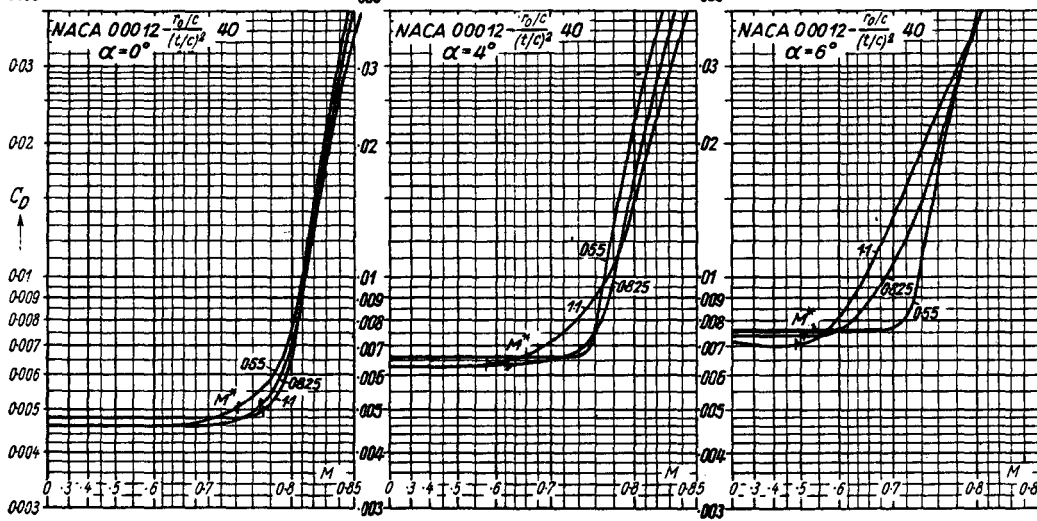


Fig. 3.17 a-c

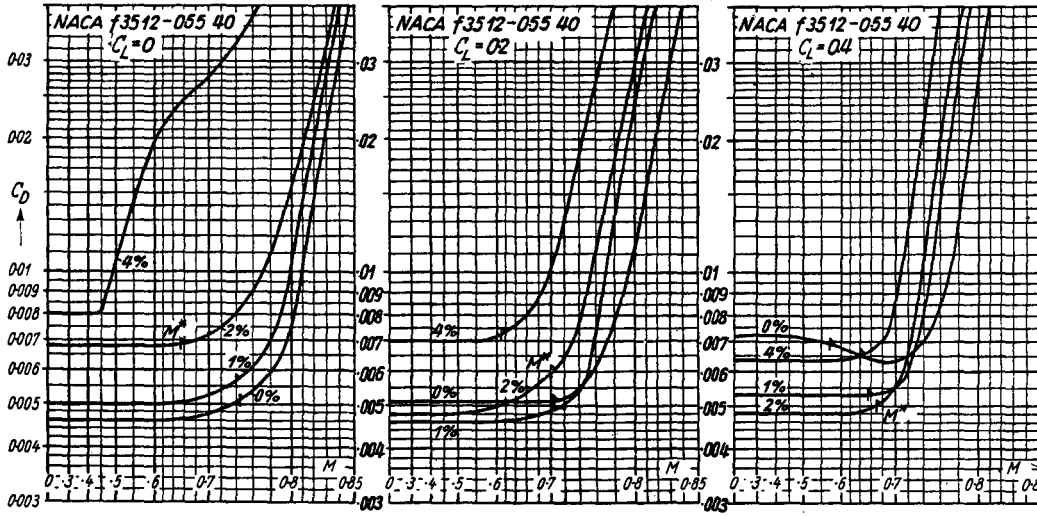


Fig. 3.18 a-c

Fig. 3.16. As above, but for various positions of maximum thickness (see Equation (1.7))

Fig. 3.17. As above, but for various values of nose radius

Fig. 3.18. As above, but for various cambers, with half-normal nose radius and maximum thickness at 40% of the chord

Chapter 12. For profiles with normal position of maximum thickness, the sharp rise in drag usually begins soon after the critical Mach number is exceeded; this Mach number becomes higher as the thickness decreases, because the disturbance velocities are smaller. For profiles whose maximum thickness lies further back, the critical Mach number can often be considerably exceeded without a consequent rise in drag. For the first class of profiles the Mach number at which the drag rise begins becomes lower as the angle of incidence (or  $C_L$ ) increases; but, if the thickness lies further back and the nose radius is suitably chosen, the Mach number at which the rise begins is practically the same for a small  $C_L$  as for a fairly high  $C_L$ . The reason is that the shocks on a profile of the latter class interact with a boundary layer which is thin and usually subjected to a favourable pressure gradient, so that it is not likely to separate (see Section 10.4.1).

### 3.6 Moment Coefficient, Centre of Pressure, and Aerodynamic Centre

#### 3.6.1 Incompressible Flow

At a fixed, not too small, Reynolds number the moment coefficient at  $\alpha = \alpha_0$ ,  $C_{m_0}$ , is proportional to the camber. At a Reynolds number of  $6 \cdot 10^6$  the four and five figure NACA profiles show a very slight increase of  $C_{m_0}$  with thickness, but the  $C_{m_0}$  values of the 6-series are practically independent of thickness and position of maximum thickness.

For symmetrical profiles the aerodynamic centre usually lies at  $0.25c$ , but on the cambered four and five figure profiles it moves forward as the thickness increases (for example, at  $R = 6 \cdot 10^6$ , to about  $0.23c$  when  $\frac{t}{c} = 0.24$ ).

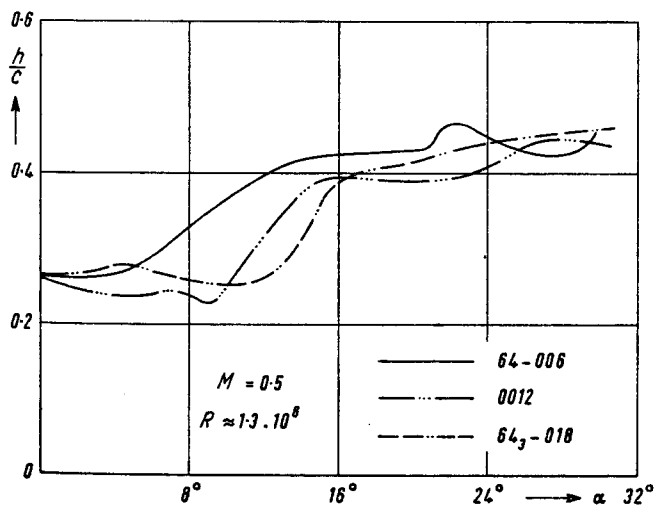


Fig. 3.19. Position of centre of pressure of NACA profiles

In contrast, the NACA profiles of the 6-series show a rearward movement to a value of between  $0.27c$  and  $0.28c$  when  $\frac{t}{c} = 0.21$ ; this movement becomes smaller as the

position of maximum thickness moves rearward (see Table 11.1).

Figure 3.19 shows the position of the centre of pressure on some symmetrical profiles at high angles of incidence [N3241]. For small Reynolds numbers, Figures 3.20 to 3.23 show measured positions of centre of pressure; we see

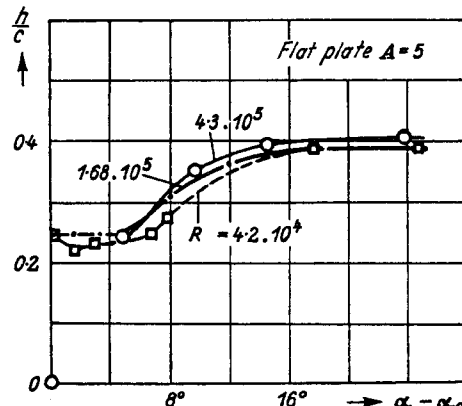


Fig. 3.20. Movement of centre of pressure at various Reynolds numbers, for the flat plate. Wind tunnel: Cologne (SCHMITZ)

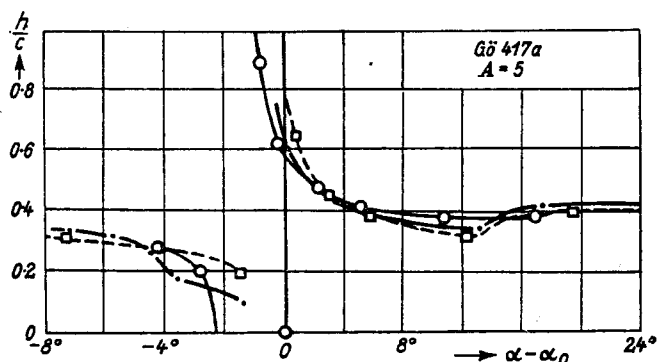


Fig. 3.21. As above, but for the cambered plate Go 417a (SCHMITZ)

that for flat and cambered plates the Reynolds number influence remains small, but that for profiles with thickness a considerable influence is apparent. At higher Reynolds numbers the influence of Reynolds number usually becomes insignificant.

#### 3.6.2 Compressible Flow

The influence of Mach number on  $\frac{dC_m}{dC_L}$  is shown in Figures 3.24 and 3.25; at first the coefficients increase slightly with Mach number, and then there is a fall. For some profiles the initial increase of  $\frac{dC_m}{dC_L}$  is considerable, but, after the critical Mach number is exceeded, the fall is all the greater. This fall is sometimes followed by a further rise. The position of aerodynamic centre should theoretically be independent of Mach number. Nevertheless, a slight forward displacement of the aerodynamic centre is observed, corresponding to the initial increase in  $\frac{dC_m}{dC_L}$ . The

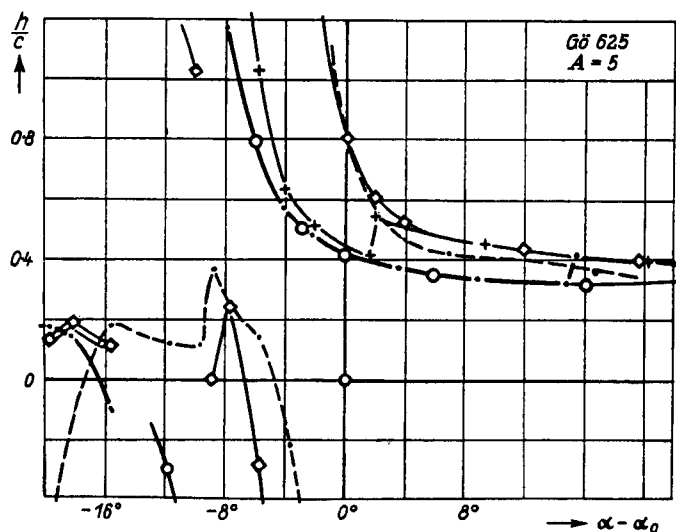


Fig. 3.22. As above, but for the profile Go 625 (SCHMITZ)

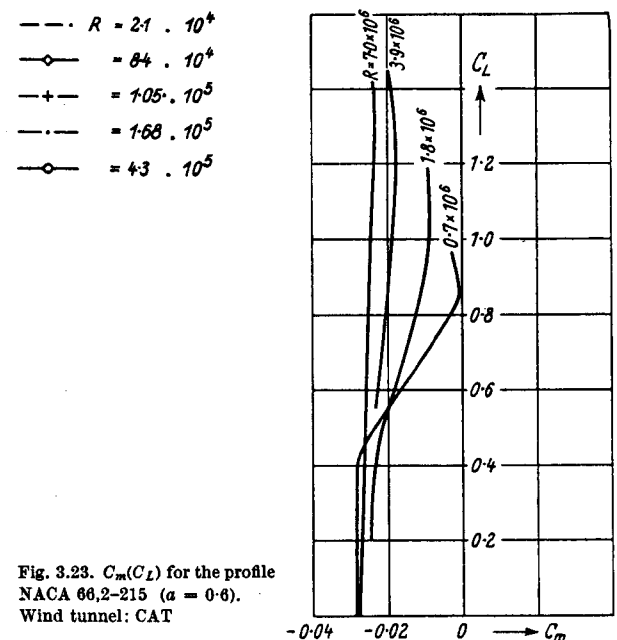
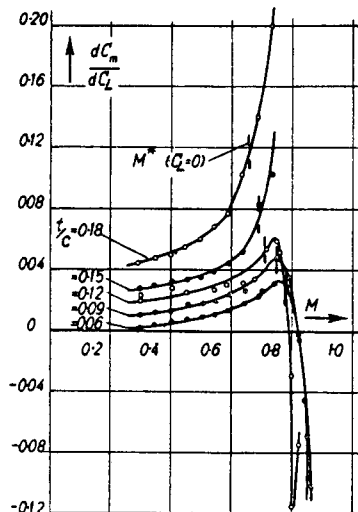
Fig. 3.23.  $C_m(C_L)$  for the profile NACA 66,2-215 ( $\alpha = 0.6$ ). Wind tunnel: CAT

Fig. 3.24. Position of aerodynamic centre as a function of Mach number, for the symmetrical NACA series. Wind tunnel: DVL 2.7 m

explanation lies in the development of the boundary layer: because of the increasing Mach number, this is subjected to a pressure distribution similar to that of a thicker profile, and the result is a forward movement of the aerodynamic centre. If the Mach number is so high that shocks occur, the movement of the shocks along the chord determines whether the aerodynamic centre moves forwards or backwards, as an examination of the appropriate pressure distributions confirms. From Figure 3.25 we see that this forward and backward movement of the aerodynamic centre is different for each profile and for each  $C_L$  value, so that general remarks are not possible; in a particular case all that can be done is to use the behaviour of the moment for a suitable profile which has been experimentally investigated (see, for example, Figures 12.133 ff).

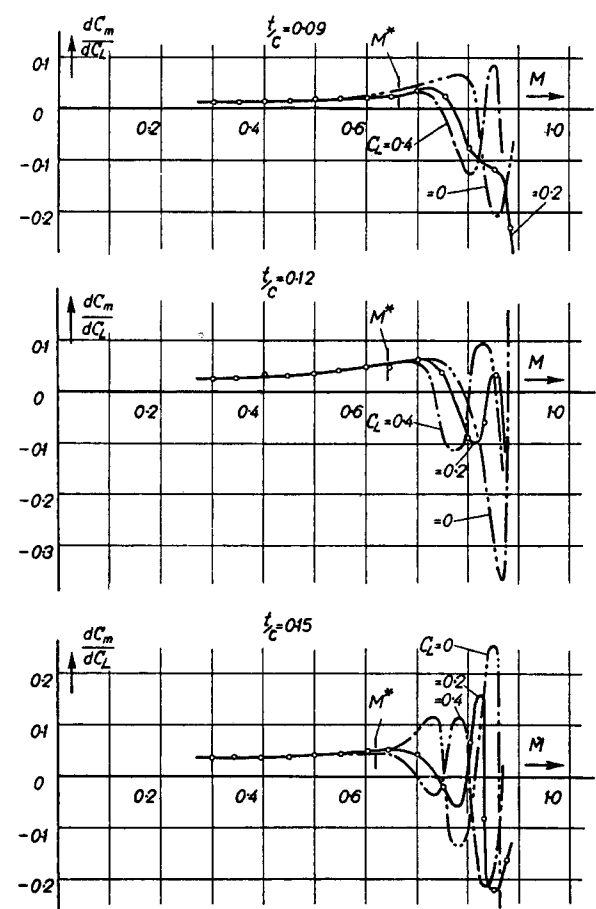


Fig. 3.25. As above, but for the 230-series

### 3.7 References

#### 3.7.1 Incompressible Flow

- BREFORD, M.: Messungen am Originalflügel des Baumusters P 51 "Mustang". FB 1224/2 (1943).
- and K. VOLZ: Messungen an zwei Laminarprofilen bei hohen Reynoldszahlen. UM 2100 (1944).
- BUSSMANN, K.: Experimentelle und theoretische Untersuchungen an Laminarprofilen. FB 1709/1 (1942).
- Messungen am Laminarprofil P 51 "Mustang". FB 1724 (1943).
- CLEARY, H. E.: The Effects of Reynolds Number on the Application of NACA 16-Airfoil Characteristics to Propeller Design. NACA TN 2591 (1952).
- CRITZOS, C. C., H. H. HEYSON and R. W. BOSWINKLE jr.: Aerodynamic Characteristics of NACA 0012 Airfoil Section at Angles of Attack from 0° to 180°. NACA TN 3361 (1955).
- DOENHOFF, A. E. v. and N. TETERVIN: Investigation of the Variation of Lift Coefficient with Reynolds Number at a Moderate Angle of Attack on a Low-drag Airfoil. NACA CB, 1942 (Wartime Rep. No. L-661).
- DOETSCH, H. and M. KRAMER: Profilwiderstandsmessungen im großen Windkanal der DVL. Jahrb, 1937 dDL I, S. 59 und Lufo 14 (1937) S. 173.
- Systematische Profiluntersuchungen im großen Windkanal der DVL. Lufo 14 (1937) S. 480.
- DOETSCH, H. and A. PASCHKE: Druckverteilungsmessungen und Wägungen an den Profilen NACA 23009, 23012 und 23018 ohne und mit Spreizklappe im 5 × 7 m-Windkanal der DVL. FB 1095 (1939).
- DOETSCH, H.: Untersuchungen an einigen Profilen mit gerinem Widerstand im Bereich kleiner  $c_a$ -Werte. Jahrb. 1940 dDL I, S. 54—57.
- Versuche an Tragflügelprofilen des North-American "Mustang". FB 1712/1 und 2 (1943).
- Bericht über das Fachgebiet Profile vor dem Sonderausschuß "Windkanäle". UM 1190 (1944).
- FAGE, A. and W. S. WALKER: Experiments on Laminar-flow Aerofoil EQH 1260 in the William Froude National Tank and the 13 ft. × 9 ft. and the 9 ft. × 7 ft. Windtunnel at the N.P.L. R & M No. 2165 (1942).
- FRANKE, A. and F. WEINIG: Der neutrale Momentenbezugspunkt. Lufo 14 (1937), S. 486.
- GOETT, H. J. and W. K. BULLIVANT: Tests of NACA 0009, 0012 and 0018 Airfoils in the Full Scale Tunnel. NACA Rep. 647 (1939).
- HOLSTEIN, H. and A. DONEIS: Messungen an einem Laminarprofil mit extremer Rücklage des Druckminimums. FB 1522 (1941).
- Messungen zur Laminarhaltung der Reibungsschicht an einem Tragflügel mit Profil NACA 0012—64. FB 1654 (1942).
- and A. DONEIS: Messungen an vier aus der Ellipse entstandenen Laminarprofilen verschiedener Wölbung. FB 1716 (1942).
- JACOBS, E. N. and W. E. CLAY: Characteristics of the NACA 23012 Airfoil from Tests in the Full-Scale and Variable-Density Tunnels. NACA Rep. 530 (1935).
- and R. M. PINKERTON: Tests of NACA Airfoils in the Variable-Density Wind Tunnel, Series 230. NACA TN No. 576 (1936).
- and A. SHERMAN: Airfoil Section Characteristics as affected by Variations of the Reynolds Number. NACA Rep. 586 (1937).
- JACOBS, E. N. and R. V. RHODE: Airfoil Section Characteristics as Applied to the Prediction of Air Forces and their Distribution on Wings. NACA Rep. 631 (1938).
- Preliminary Report on Laminar Flow Airfoils and New Methods Adopted for Airfoil and Boundary Layer Investigations. NACA ACR, 1939 (Wartime Rep. L-345).
- JONES, R. and D. H. WILLIAMS: The Profile Drag of Aerofoils at High Reynolds Numbers in the Compressed Air-Tunnel. R & M No. 1804 (1937).
- KELLY, I. A.: Effects of Modifications to the Leading-Edge Region on the Stalling Characteristics of the NACA 631—012 Airfoil Section. NACA TN 2228 (1950).
- KOSIN, R. and W. LEHMANN: Ein Beitrag zur Entwicklung von Profilen für hohe Flugzeuggeschwindigkeiten. Jahrb. 1941 dDL I, S. 11—17.
- KRAEMER, K.: Untersuchung eines Tragflügelprofils im Windkanal bei unter- und überkritischen Reynoldszahlen. AVA-Bericht 58—01 (1958).
- KUMBRUCH, H.: Mitteilungen aus der Göttinger Modellversuchsanstalt für Aerodynamik. III. Folge. 1. Ähnlichkeitsversuche an Flügelprofilen. ZFM 10 (1919), S. 93—109.
- LIPPISCH, A.: Profile für Flugmodelle. Thermik 4. Jahrg. (1951) M 54 und M 73.
- LOFTIN jr. and K. S. COHEN: Aerodynamic Characteristics of a Number of Modified NACA Four-Digit-Series Airfoil Sections. NACA TN 1591 (1948).
- Theoretical and Experimental Data for a Number of NACA 6A-Series Airfoil Sections. NACA Rep. 903 (1948).
- and W. I. BURSNALL: The Effects of Variations in Reynolds Number between  $3 \cdot 0 \times 10^6$  and  $25 \cdot 0 \times 10^6$  upon the Aerodynamic Characteristics of a Number of NACA 6-Series Airfoil Sections. NACA Rep. 964 (1950).
- Aerodynamic Section Characteristics at High Angles of Attack. NACA TN 3241 (1954).
- LÖSSL, E. v.: Profilwiderstandsverminderung durch künstlichen Druckanstieg im Umschlaggebiet. Techn. Ber. ZWB (1943) S. 211—212 u. S. 367—368.
- MCCULLOUGH, G. B. and W. M. HAIRE: Low-Speed Characteristics of Four Cambered 10-Percent-Thick NACA Airfoil Sections. NACA TN 2177 (1950).
- MUESMANN, G.: Messungen und Grenzschichtbeobachtungen an affin verdickten Gebläseprofilen in Abhängigkeit von der Reynoldszahl. ZFW 7 (1959), S. 253—264.
- MUTTRAY, H.: Über die Abhängigkeit des Profilwiderstandes vom Auftrieb. Lufo, S. 165—173.
- Zuschrift zu dem Bericht von H. Doetsch: Profilwiderstandsmessungen im großen Windkanal der DVL. Lufo 14 (1937), S. 371/2.
- NAUMANN, N.: Messungen eines Profils im Anstellwinkelbereich 0 bis 360°. Jahrb. 1940 dDL I, S. 51—53.
- NOVOTNY and BERGEN: Windkanalmessungen an drei Rechteckflügeln. Dreikomponentenmessungen an Profilen von 21, 22 und 25% Dicke und Untersuchung über den Einfluß von Störkörpern auf der Flügelausgeseite. AVA 43/W/07.
- PETERSON, R. F.: The Boundary-Layer and Stalling Characteristics of the NACA 64A010 Airfoil Section. NACA TN 2235 (1950).
- QUICK, A. W.: Einige Bemerkungen über Laminarprofile und über das Verhalten der laminaren Grenzschicht unter dem Einfluß von Störkörpern. Nachtrag zum LGL-Bericht 141.
- RELF, E. F., R. JONES and A. H. BELL: Tests of Six Aerofoil Sections at Various Reynolds Numbers in the Compressed Air-tunnel. R & M No. 1706 (1936).
- SALTER, C., C. J. MILES and R. OWEN: Tests on a Glas II Wing without Suction in the Compressed Air Tunnel. R & M No. 2540 (1948).
- SCHLICHTING, H. and K. BUSSMANN: Messungen an Laminarprofilen. LGL 149, S. 17—20.

- SCHMITZ, F. W.: Zur Aerodynamik der kleinen Reynoldsschen Zahlen. Jahrb. 1953 d. WGL. Braunschweig 1954.
- SERBY, I. E., M. B. MORGAN and E. R. COPPER: Flight Test on the Profile Drag of 14% and 25% Thick Wings. R & M 1826 (1937).
- SILVERSTEIN, A.: Scale Effect on Clark Y Airfoil Characteristics from NACA Wind-Tunnel Tests. NACA Rep. 502 (1934).
- and I. V. BECKER: Determination of Boundary-Layer Transition on Three Symmetrical Airfoils in the NACA Full-Scale Wind Tunnel. NACA Rep. 637 (1939).
- SMITH, H. A. and R. F. SCHÄFER: Aerodynamic Characteristics at Reynolds Numbers of  $3 \cdot 10^6$  and  $6 \cdot 10^6$  of three Airfoil Sections Formed by Cutting off Various Amounts from the Rear Portion of the NACA 0012 Airfoil Section. NACA TN 2074 (1950).
- SWATY, F.: Untersuchungen über die Beeinflussung der Beizahlen des Profils NACA 0018 durch Kürzungen an der Profilhinterkante. FB 1349 und Jahrb. 1940 dDL I, S. 58—61.
- WALZ, A.: Messungen an zwei 13,6% dicken Profilen mit kleinem Hinterkantenwinkel im großen AVA-Kanal. UM 3092 (1944).
- WILLIAMS, D. H. and A. F. BROWN: Experiments on an Elliptic Cylinder in the Compressed Air Tunnel. R & M No. 1817 (1937).
- YOUNG, A. D.: A Review of Some Stalling Research. R & M No. 2609 (1951).
- gleich mit Ergebnissen in mittleren Windkanälen der DVL. FB 1329 (1940).
- Profilmessungen im DVL-Hochgeschwindigkeits-Windkanal an symmetrischen NACA-Profilen mit verschiedenen Dickenverhältnissen. FB 1490 (1941).
- Druckverteilungsschaubilder und Impulsverlustschaubilder für das Profil NACA 00018—1, 1—30. FB 1505.
- Profilmessungen im DVL-Hochgeschwindigkeits-Windkanal. LGL 156 (1942).
- Hochgeschwindigkeitsmessungen an einem Flügel sehr kleiner Abmessungen im DVL-Hochgeschwindigkeits-Windkanal. LGL 156 (1942).
- GÖTHERT, B.: Hochgeschwindigkeitsmessungen am Heinkel-Profil 0 00 12—0,715 36,6 im DVL-Hochgeschwindigkeits-Windkanal. DVL-Bericht J 900/6 (1942).
- Hochgeschwindigkeitsmessungen am Messerschmitt-Profil Me 23513—1,130 im DVL-Hochgeschwindigkeits-Windkanal, DVL-Bericht J 900/17 (1942).
- Profilmessungen bei hohen Unterschallgeschwindigkeiten. UM 1229/1 und 2 (1944).
- Hochgeschwindigkeitsmessungen am Profil Me 1 25 12—0,825 40. UM 1234/1, 2 (1944).
- Hochgeschwindigkeitsmessungen an Profilen der Reihe NACA 230 mit verschiedenen Dickenverhältnissen (9, 12, 15%). UM 1259/1 bis 3 und UM 1260/1 bis 3 (1944).
- Hochgeschwindigkeitsmessungen am Mustang-Profil 1,6 50 13,6—0,825 39. UM 1282/1 (1944).
- Hochgeschwindigkeitsmessungen an Luftschraubenprofilen der RAF-Reihe mit verschiedenen Dickenverhältnissen (6 und 9%). UM 1321/1 a und 1b (1944).
- GRAHAM, D. J.: High Speed Tests of an Airfoil Section Cambered to have Critical Mach Numbers Higher than those Attainable with a Uniform-load Mean Line. NACA TN 1396 (1947).
- G. E. NITZBERG and R. T. OLSON: A Systematic Investigation of Pressure Distributions at High Speeds over Five Representative NACA Low-Drag and Conventional Airfoil Sections. NACA Rep. 832 (1945).
- The Development of Cambered Airfoil Sections having Favourable Lift Characteristics at Supercritical Mach Numbers. NACA Rep. 947 (1949).
- HAMILTON, W. T. and W. H. NELSON: Summary Report on the High-Speed Characteristics of Six Model Wings having NACA 65-Series Sections. NACA Rep. 877 (1947).
- HELMBOLD, H. B.: Einige Ergebnisse aus der aerodynamischen Industrie-Forschung. DAL (1942).
- Physikalische Erscheinungen in der kompressiblen Unterschallströmung. LGL 156 (1942), S. 170/174.
- Flügelprofile bei hohen Geschwindigkeiten. UM 2502 (1944).
- HOERNER, S.: Einfluß der Kompressibilität auf den Widerstand. UM 7810 (1944).
- HOLDER, D. W., A. CHINEREK and R. I. NORTH: Pressure Measurements in a Supersonic Tunnel on a Two-Dimensional Aerofoil of RAE 104 Section. CP 62 (1951).
- KNAPPE, O.: Schnellkanalversuche an einem symmetrischen Klappenflügel. Jahrb. 1941 dDL I, S. 96—100.
- Schnellkanalversuche an Profilen und Flugzeugmodellen und ihre flugtechnische Auswertung. LGL 156 (1942), S. 128—132.
- MAKI, R. L. and L. W. HUNTON: An Investigation at Subsonic Speeds of Several Modifications to the Leading-Edge Region of the NACA 64A010 Airfoil Section Designed to Increase Maximum Lift. NACA TN 3871 (1956).
- NAUMANN, A.: Messungen am Profil 23008—64 und 23012—64 im kompressiblen Unterschallbereich. Bericht d. Aerodynamischen Instituts d. TH. Aachen.
- NITZBERG, G. E. and S. M. CRANDALL: A Comparative Examination

### 3.7.2 Compressible Flow

- ACKERET, J., F. FELDMANN and N. ROTT: Untersuchungen an Verdichtungsstößen und Grenzschichten in schnell bewegten Gasen. Mitt. ETH Zürich Nr. 10 (1946).
- BEAVAN, J. A. and G. A. M. HYDE: Compressibility Increase of Lift and Moment on EC 1250 for Low Speed  $C_L = 0 \cdot 17$ . R & M No. 2055 (1942).
- BUSEMANN, A.: Profilmessungen bei Geschwindigkeiten nahe der Schallgeschwindigkeit. Jahrb. b. WGL 1928, S. 95.
- and O. WALCHNER: Profileigenschaften bei Überschallgeschwindigkeit. Forschung auf dem Gebiete des Ingenieurwesens 4 (1933), S. 87.
- BRYSON jr., A. E.: An Experimental Investigation of Transonic Flow past Two-Dimensional Wedge and Circular-Arc Sections using a Mach-Zehnder Interferometer. NACA TN 2560 (1951).
- FERRI, A.: Aluni Resultati Experimentali. Atti di Guidonia Nr. 17 (1939).
- FRÖSSEL, W.: Experimentelle Untersuchungen der kompressiblen Strömung an und in der Nähe einer gewölbten Wand. UM 6608, 6611, 6622 (1944) und Mitt. d. MPI für Strömungsforschung Nr. 4 (1951).
- FURLONG, G. Ch. and J. E. FITZPATRICK: Effects of Mach Number and Reynolds Number on the Maximum Lift Coefficient of a Wing of NACA 230-series Airfoil Sections. NACA MR No. L6F04 (1946) and TN No. 1299.
- GAULT, D. E.: Correlation of Low Speed Airfoil-Section Stalling Characteristics with Reynolds Number and Airfoil Geometry. NACA TN 3963 (1957).
- GOLDSTEIN, S., W. F. HAMILTON and C. F. COWDREY: Tests of a New Aerofoil in the H.S.T. at the N.P.L. R & M No. 2246 (1940).
- GÖTHERT, B.: Messungen am Profil NACA 0015—64 im Hochgeschwindigkeits-Windkanal der DVL. FB 1247 (1940).
- Messungen am Profil NACA 0015—64 mit verschiedenen Tiefen im DVL-Hochgeschwindigkeits-Windkanal und Ver-

- tion of Some Measurements of Airfoil Section Lift and Drag at Supercritical Speeds. NACA TN 2825 (1952).
- PEARCEY, H. H. and J. A. BEAVAN: Profile Drag Measurements at Compressibility Speeds on three Aerofoils having Spanwise Wires or Grooves. R & M No. 2252 (1943).
- Force and Pressure Coefficients up to Mach Number 0.87 on the Goldstein Roof Top Section 1442/1547. R & M 2346 (1946).
- ROGERS, E. W. E.: Observations on a Thin Cambered Aerofoil Beyond the Critical Mach Number. R & M No. 2432 (1950).
- STACK, J. and A. E. v. DOENHOFF: Tests of 16 Related Airfoils at High Speeds. NACA Rep. 492 (1934).
- STACK, J., W. F. LINDSAY and R. E. LITTEL: The Compressibility Burble and the Effects of Compressibility on Pressures and Forces Acting on an Airfoil. NACA Rep. 646 (1938).
- STACK, J. and W. F. LINDSAY: Tests of N-85, N-86 and N-87 Airfoil Sections in the 11-inch High Speed Wind-Tunnel. NACA TN 665 (1938).
- STACK, J.: Tests of Airfoils Designed to Delay the Compressibility Burble. NACA Rep. 763 (1943).
- STAFF OF H. S. T.: Measurements of Force Coefficients on Aerofoil EC 1240 in the High Speed Tunnel at the N.P.L. R & M No. 2246 (1940).
- STIVERS, Louis S. jr.: Effects of Subsonic Mach Number on the Forces and Pressure Distributions on four NACA 64A—Airfoil Sections at Angles of Attack as High as 28°. NACA TN 3162 (1954).
- SUMMERS, I. L. and S. L. TREON: The Effects of Amount and Type of Camber on the Variation with Mach Number of the Aerodynamic Characteristics of a 10-Percent-Thick NACA 64 A-Series Airfoil Section. NAC TN 2096 (1950).
- ZALOVCIK, I. A. and E. P. LUKE: Some Flight Measurements of Pressure-Distribution and Boundary-Layer Characteristics in the Presence of Shock. NACA RM L8C22 (1948).

## 4. SPECIAL PROBLEMS

### 4.1 Influence of Quality of Surface

#### 4.1.1 Older Results

The quality of the surface has a large effect on the profile properties. From an old AVA measurement (Figure 12.63), at the relatively small Reynolds number of  $6 \cdot 3 \cdot 10^5$ , we can see the main effects caused by a surface which is not smooth: a considerable increase in drag; and, usually, a decrease in maximum lift. The roughening for this measurement was rather coarse: it was produced by a wire net of 0.5 mm gauge, with 38 square meshes in a length of 10 cm; the net was soldered on to a wing of sheet metal, the profile being Gö 449. According to this measurement the suction side is very sensitive to roughness; this is generally true, the nose of the profile being particularly sensitive. Figure 4.1 illustrates the effects of various amounts of coarse roughness on the suction side for the profile NACA 0012 at a Reynolds number of  $5 \cdot 10^6$ . The same behaviour occurs at higher Reynolds numbers, as will be shown.

#### 4.1.2 Surface Roughness

DOETSCH has investigated the effect of the roughness caused by paint on some industrially manufactured wings; the profiles are mostly those of the NACA 24-series, and the range of span is fairly large. DOETSCH obtains the following result: an increase in drag over that of an ideal smooth wing is found in the Reynolds number range of  $4 \cdot 10^6$  to  $10^7$ . A Ju 288 wing shows an increase of 46%, an He 177 wing 60%, an Me 109B wing 50%, and an FW 190 wing 33%; the wings are all painted with camouflage paint, and no priming has been used; the average height of roughness is about 0.019 mm (Ju 288), 0.014 mm (He 179), and 0.007 mm (FW 190). Figure 4.2 shows the results from the measurement of momentum loss along the span of the FW 190 wing. A Mustang wing (including armament), measured at the same time, gives an increase in sectional drag of 41% over the ideal smooth value; the latter value is actually obtained over large parts of the span, and is very small,  $C_D$  being 0.0044. The effect of various kinds of surface at high Reynolds numbers can be clearly seen from Figure 4.3. Further information on the effects of surface roughness has been obtained from flat-plate measurements (see Section 4.1.5).

#### 4.1.3 Standard Roughness

We have already mentioned that roughness near the profile nose is especially harmful. An example at  $R =$

$26 \cdot 10^6$  (Figure 4.4) shows how the effect of roughness varies with the place on the chord at which it occurs. Figure 4.5 shows the influence of the height of the roughness when this occurs at the nose; in this experiment there is only a strip of granular roughness along the leading edge. When such a strip (made from a carborundum layer of a certain grain size) is placed at a certain point of the chord, this is practically equivalent to making this point the point of transition (certainly for the Reynolds numbers of most interest today). The flow past profiles with roughness over the whole surface obeys the laws of turbulent flow over a rough wall, and so the aerodynamic characteristics do not change with increasing Reynolds number; however, profiles with rough strips on an otherwise smooth surface show a continual decrease of the drag with increasing Reynolds number (Figure 4.6). The "standard roughness" applied at the nose consists of a carborundum layer with a grain size of 0.28 mm, which covers between 5 and 10% of the surface in the region  $0 \leq x \leq 0.08c$ , on the suction and the pressure sides. To investigate the effect of such roughness in modern NACA measurements (where it is used to control transition), the profile characteristics have been measured in the LTT, usually at a Reynolds number of  $6 \cdot 10^6$ , both with a smooth surface and with standard roughness at the nose; the chord of the rectangular wings used in these measurements is 2 ft. Results of this kind can be found in the figures of Chapter 12. It is not difficult to see from these measurements that roughness, at first sight seemingly insignificant, can completely counteract any

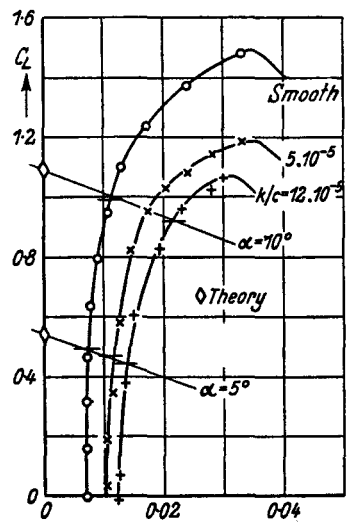


Fig. 4.1. NACA 0012 with various amounts of coarse roughness on the suction side. Reynolds number:  $5 \cdot 10^6$

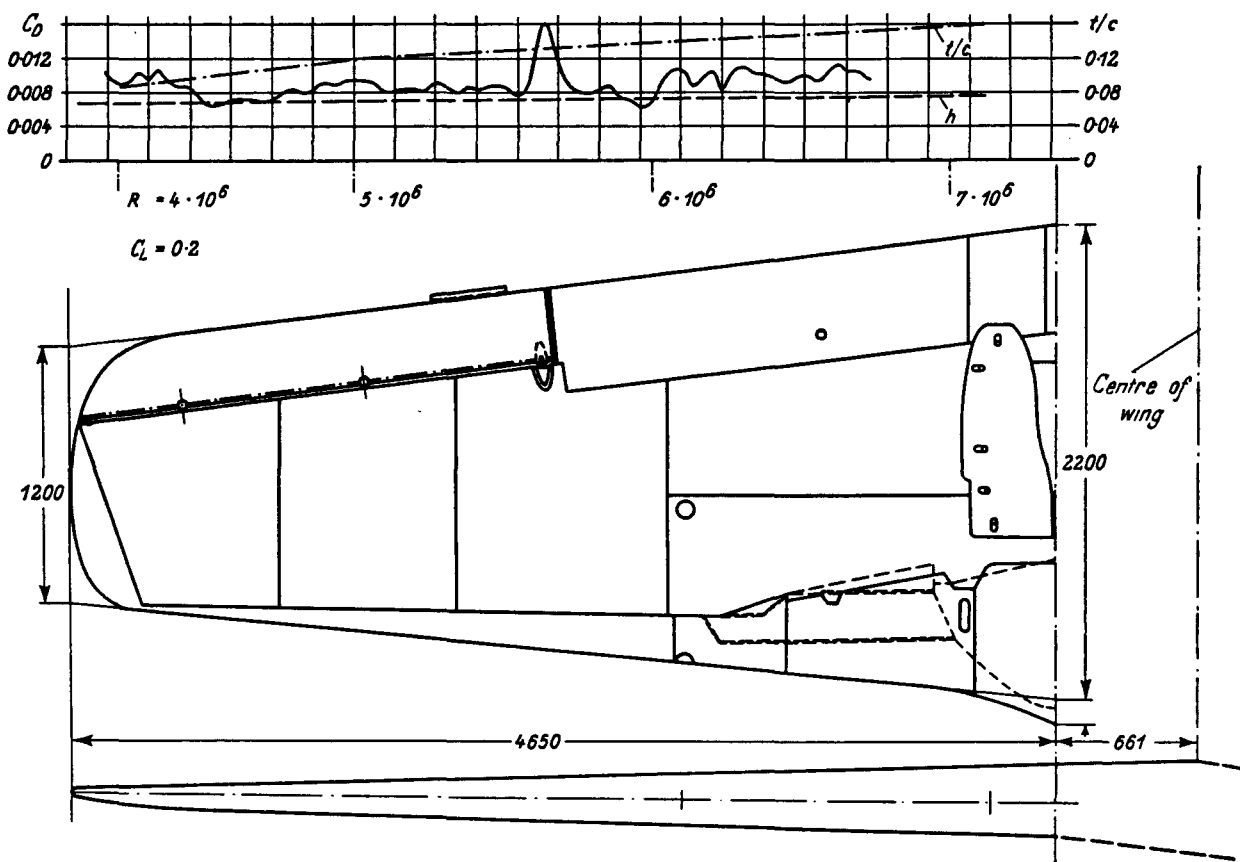


Fig. 4.2. Distribution of thickness and sectional drag coefficient of an actual FW 190 wing with camouflage paint but without priming.  
Roughness height:  $h_{max.} = 0.006$  to  $0.008$  mm. Profiles: NACA 24-series. Wind tunnel: DVL 5 m  $\times$  7 m

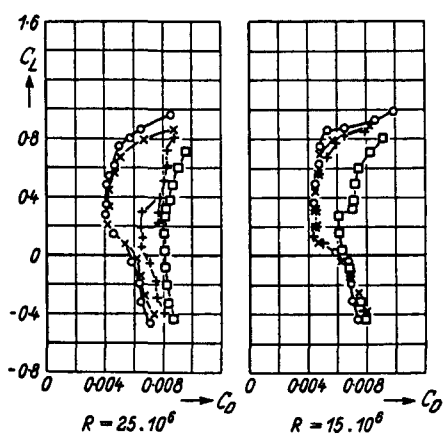


Fig. 4.3. Drag of the profile 65(421)-420,  $a = 1$ , for  $R = 15 \cdot 10^6$  (right) and  $25 \cdot 10^6$  (left). Wing chord: 1.54 m. Wind tunnel: TDT.  $\square$ : production model with camouflage paint, not finished.  $\times$ : production model with camouflage paint, highly polished.  $+$ : camouflage paint, not finished.  $\circ$ : primed, lacquered, polished aerodynamically smooth

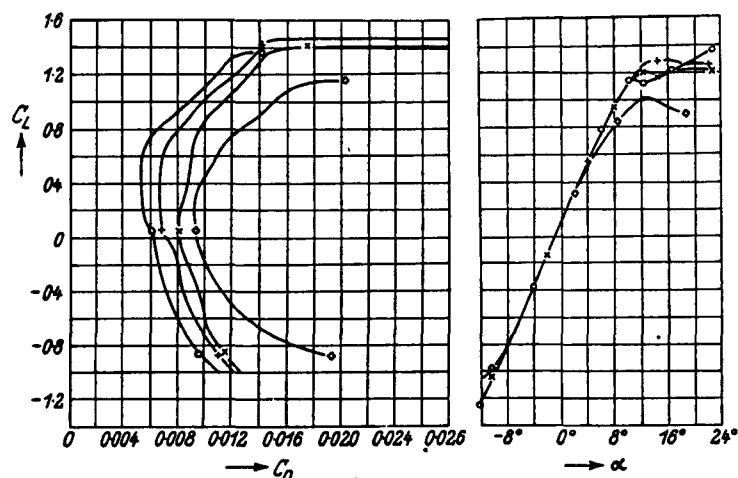


Fig. 4.4. Polars for the profile 63(422)-422, for various positions of roughness. Strips of roughness at  $\frac{x}{c} = 0.3$  (+);  $0.2$  ( $\times$ );  $0-0.05$  ( $\diamond$ ); smooth ( $\circ$ ). Wind tunnel: TDT. Reynolds number:  $26 \cdot 10^6$ . Chord: 0.915 m

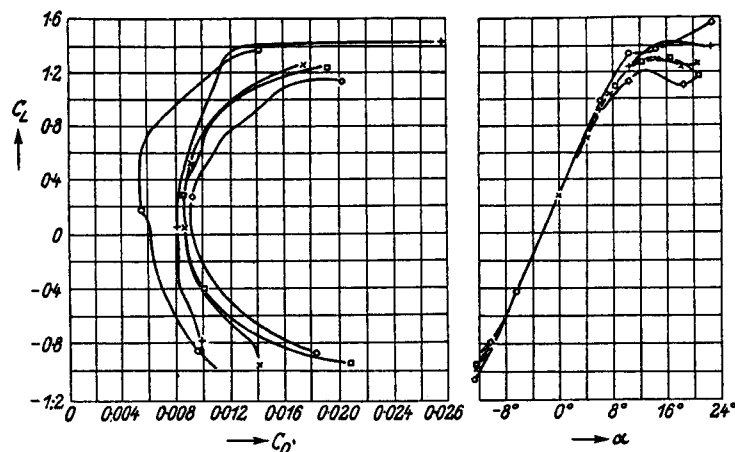


Fig. 4.5. Polars for the profile 63(422)-422, with various types of roughness at the nose. Smooth (○); shellac (+). Size of grain: 0.051 mm (×); 0.0102 mm (□); 0.028 mm (◊). Reynolds number:  $26 \cdot 10^6$ . Chord 0.915 m. Wind tunnel: TDT

favourable influence that the profile shape has on the drag; as the lift coefficient increases, roughness certainly leads to considerably increased drags; and the maximum lift generally suffers a large reduction. The lift-curve slope of a profile with standard roughness decreases with increasing thickness (Figure 3.5), and sometimes the angle of zero lift and the moment are noticeably influenced as well. Drag measurements on wings in their original construction, with various types of nose, confirm the above experimental results (Figure 4.7).

#### 4.1.4 Isolated Disturbances

Isolated disturbances on a surface on which laminar flow exists produce transition of the boundary layer in a region which extends rearwards; the region is conical at first, with an angle of 14° to 18°, but then broadens more

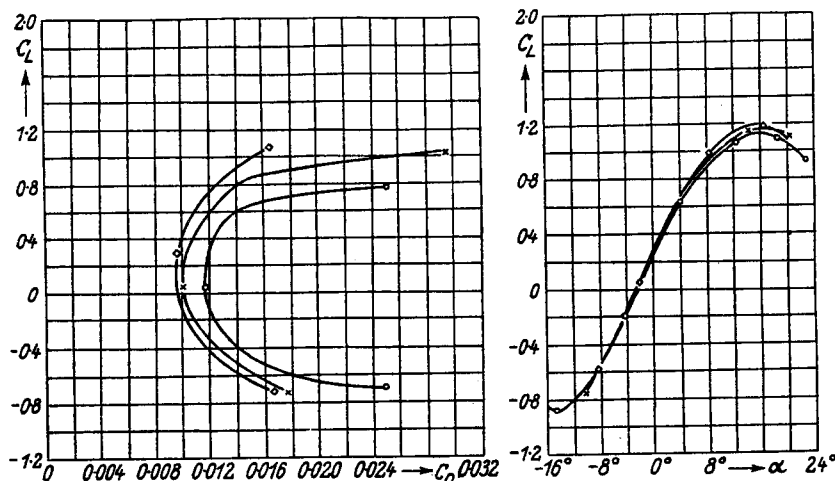


Fig. 4.6. Polars for the profile 63(422)-422 (modified), with standard roughness at the nose. Reynolds number:  $6 \cdot 10^6$  (○);  $14 \cdot 10^6$  (×);  $26 \cdot 10^6$  (◊). Wind tunnel: TDT. Chord: 0.915 m

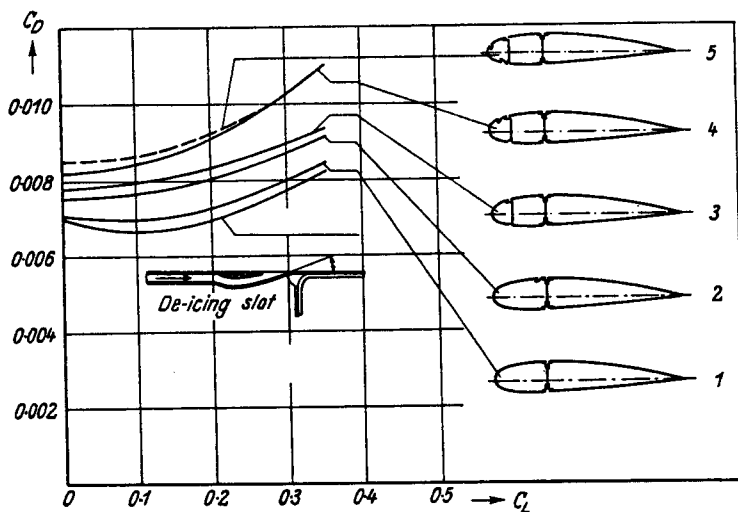


Fig. 4.7. Actual FW wing with smoothly polished metal-surface (without paint). Profile: NACA 2415. Reynolds number:  $10 \cdot 4 \cdot 10^6$ . Wind tunnel: DVL 5 m × 7 m. (1) Front spar (FS) at 30% of the chord. (2) FS at 30% of the chord; de-icing slot (DS) at 27% of the chord, on the suction side. (3) FS at 10% of the profile chord. (4) FS at 10% of the chord; DS at 4% of the chord, on the suction side. (5) FS at 10% of the chord; DS at 2% of the chord on the suction side and 8% of the chord on the pressure side

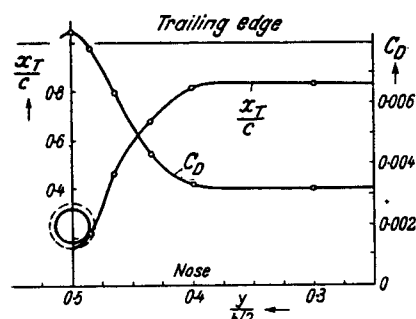


Fig. 4.8. Sectional drag coefficient and position of point of transition, in the vicinity of an isolated disturbance (suspension wire). Wind tunnel: 5 m × 7 m DVL. Reynolds number:  $2 \cdot 7 \cdot 10^6$

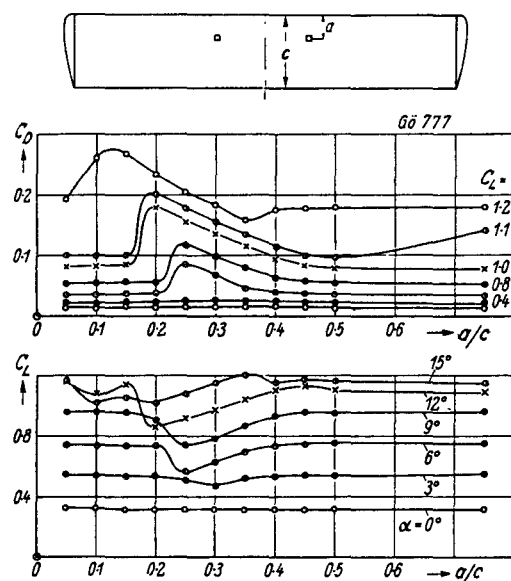


Fig. 4.9. Effect of coarse, isolated disturbances (two small plates, 22 mm square) at various distances from the nose. Profile: GÖ 777. Chord: 0.6 m. Wind tunnel: 4 m × 5.4 m AVA. Reynolds number:  $2.3 \cdot 10^6$  (see also Figure 12.91)

rapidly. Figure 4.8 shows how the drag changes in the neighbourhood of such a point; in this case the disturbance is produced by the suspension wire of the model. Figure 4.9 shows an example of the influence of isolated disturbances on the lift and drag coefficients at various angles of incidence.

Naturally, there is particular interest in the question what additional drag is to be expected from the very varied isolated disturbances occurring in practice in an already turbulent boundary layer. Among many measurements which have been made in attempts to answer this question, the systematic investigations of WIEGHARDT and TILLMANN are particularly worth mentioning, because they permit a direct application to isolated roughness elements on an arbitrary profile in the region where the boundary layer is turbulent. A coefficient for the additional drag,  $\Delta C_D = \frac{\Delta D}{\bar{q}S}$ , has been introduced, where  $S$  is the maximum cross-sectional area (normal to the flow direction) of the protuberance causing the disturbance, and  $\bar{q}$  is the average kinetic pressure over the height,  $k$ , of the protuberance, so that

$$\bar{q} = \frac{1}{k} \int_0^k \frac{\rho}{2} [u(y)]^2 dy;$$

$u(y)$  is the velocity distribution in the boundary layer on a flat plate (see Section 9.2). If the disturbances are caused not by protuberances but by indentations, then  $\bar{q}$  is the average of the kinetic pressure at the outer edge of the boundary layer and  $S$  is the plan area of the indentation. The ratio of the height of the protuberance (or depth of the indentation) to the boundary layer thickness at the disturbance is very important in determining the effect of the disturbance; the investigations of WIEGHARDT and TILLMANN have an advantage over others, since this quantity is considered in every case.

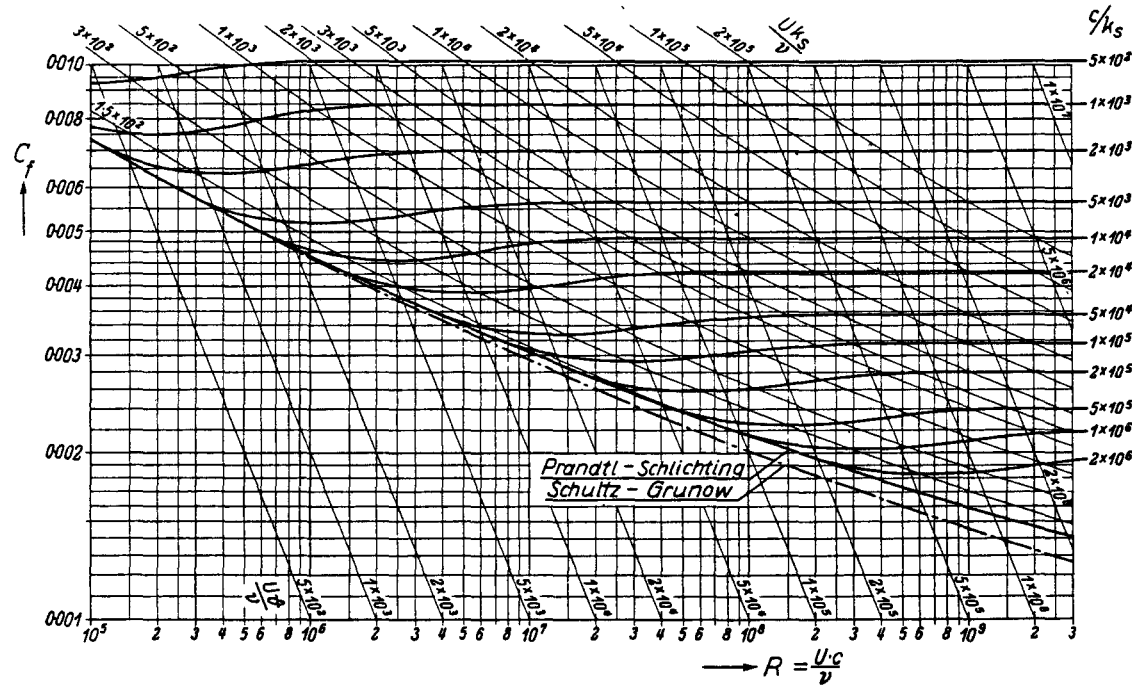


Fig. 4.10. Skin-friction drag of rough plates.  $k_s$ , height of roughness (sand);  $t^*$ , momentum thickness;  $C_f$ , drag coefficient for one side of plate

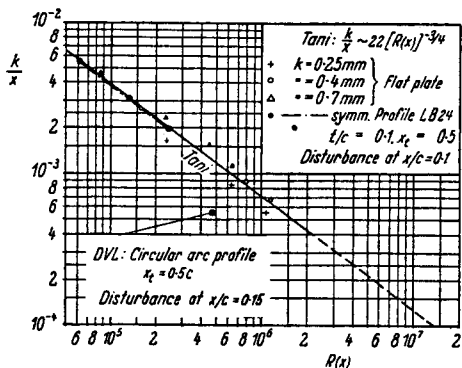


Fig. 4.11. Critical disturbance height, referred to length of boundary layer;  $R = \frac{Vx}{v}$ . Flat plate and symmetrical profile ( $\bullet$ )

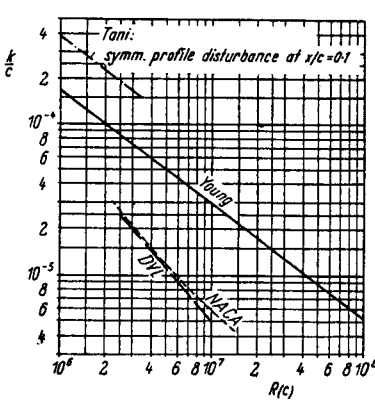


Fig. 4.12. Critical disturbance height referred to chord;  $R = \frac{Vc}{v}$ . Disturbance in front third of a 15% thick profile

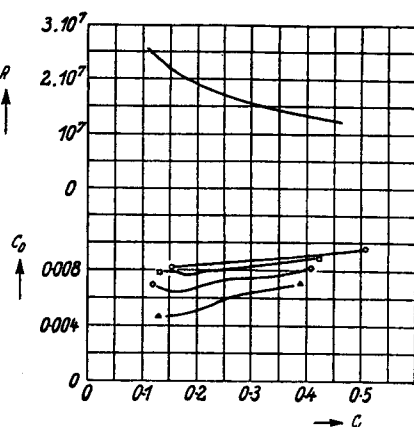


Fig. 4.13. Flight measurements for various qualities of surface. Profile: NACA 66 (215) - 1 (14-5).  $\circ$ : factory made, with camouflage paint.  $\square$ : smoothed.  $\diamond$ : waviness reduced.  $\triangle$ : visible waves filled up, surface waxed. [R 824]

#### 4.1.5 Permissible Size of Grain and Critical Height of Roughness

We now investigate the effect of surface roughness on the skin-friction drag of flat plates. Figure 4.10 (from measurements by PRANDTL and SCHLICHTING) shows that the skin-friction drag of the plate deviates from the curve corresponding to a smooth surface, and becomes constant from a certain Reynolds number onwards, this number depending on the grain size. From this it follows that, at a given Reynolds number, the skin-friction drag of a plate with a rough surface is the same as that of a smooth plate, provided that the grain size is below a certain permissible value; in other words, the surface can be regarded as "aerodynamically smooth" if the grain size is below a permissible value. According to SCHLICHTING the permissible grain size is given approximately by

$$k_{\text{perm.}} \leq 100 \frac{v}{V}, \quad \text{or} \quad \frac{k_{\text{perm.}}}{c} \leq \frac{100}{R};$$

these results come from measurements on flat plates but, to a first approximation, similar results are found for profiles with finite thickness.

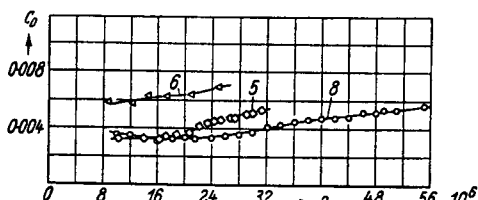


Fig. 4.14. Drag coefficient of wings with various types of waviness (see Figure 4.15).

Model 5: NACA 66 (215)-116  $\left\{ a = 1.0; C_L = 0.2 \atop a = 0.6; C_L = -0.1 \right\}$  at  $C_L = 0.1$ .

Model 6: NACA 66 (215)-116 at  $C_L = 0.15$ .

Model 8: NACA 66 (2x15)-116 at  $C_L = 0.1$

The relationships are rather more favourable if the boundary layer is not turbulent; we then speak of a critical roughness height, and understand by this the roughness height that just induces transition. Some examples of the behaviour of this quantity with Reynolds

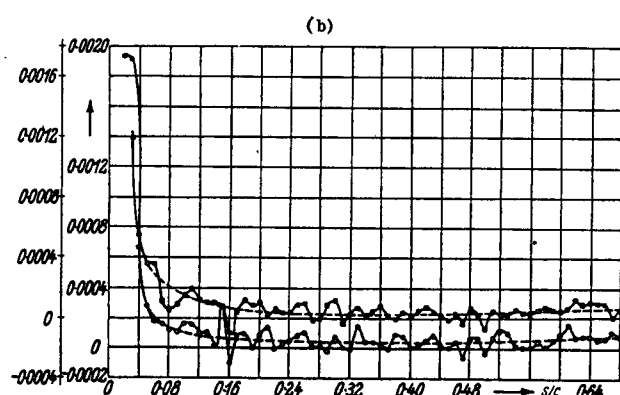
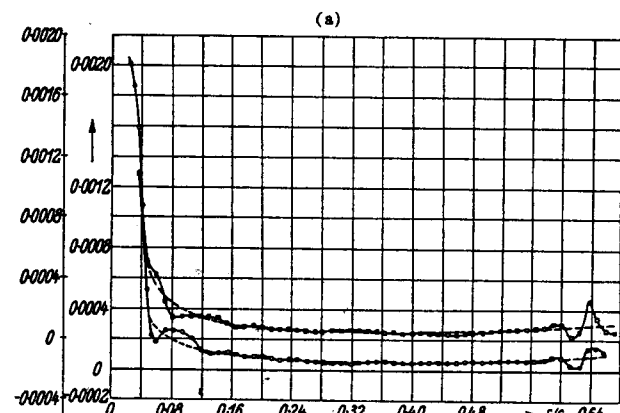


Fig. 4.15. Deviations,  $\frac{\Delta y}{c}$ , from the design profile shape, on an actual wing.  
(a) Model 5: waviness at the profile nose on both sides. (b) Model 6: considerable waviness over the whole chord [R910]. Dashed curves: design values of the pressure side (upper curve) and the suction side (lower curve)

number are shown in Figures 4.11 and 4.12; the measurements have been made on isolated disturbances ([R824 (Figure 19)]; DOETSCH; YOUNG; TANI). New measurements and calculations by TANI and DRYDEN give the ratio of roughness height to the displacement thickness at the disturbance; they confirm that, for profiles with a favourable pressure gradient, there is approximately the same dependence on the critical Reynolds number as for the flat plate.

#### 4.1.6 Waviness

Free-flight measurements on a modern profile (Figure 4.13) show that the effect of flight roughness is sometimes insignificant compared with the effect of surface waviness. Figure 4.14 shows the behaviour of  $C_D$  with Reynolds number for profiles with various types of waviness (see Figure 4.15): model 8 is largely free from waviness; in the

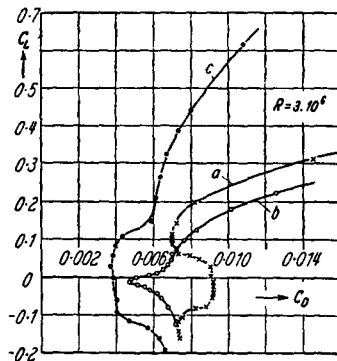


Fig. 4.16. Drag coefficient as a function of  $C_L$ : (a) with a discontinuity in curvature that causes a large disturbance; (b) with a discontinuity in curvature that does not cause a large disturbance; (c) without discontinuity in curvature (DOETSCH)

neighbourhood of the nose of model 5 and, especially, of model 6, considerable waviness exists, which leads to an increase in the drag.

Similar effects (changes in the pressure distribution, which lead to premature transition) can also occur when a profile has a discontinuity in curvature at a certain point (see DOETSCH). From Section 7.3.3 we see that the velocity distribution possesses a point of inflection and that a relatively large variation of the velocity occurs in the region of this point. Figure 4.16 shows that this behaviour can lead to transition. By rounding off the nose of a circular arc profile ( $\frac{t}{c} = 0.1$ ) with another circular arc, of radius 0.01c (the two parts having the same slope at the join), a discontinuity in curvature is obtained; the radius of curvature changes from  $\frac{r_I}{c} = 0.01$  to  $\frac{r_{II}}{c} = 2.6$ . The behaviour of polar (a) shows that the expected forward movement of the point of transition (the existence of which is confirmed by direct measurement) produces a considerable increase in drag. Polar (b) corresponds to a smaller nose radius, and hence to a still greater discontinuity in curvature; the influence of this is masked to a certain extent by the sharp drop in pressure at the nose. Only a

parabolic nose with continuous curvature at the join causes the behaviour expected of a laminar profile: small drag for small lift-coefficients, as in polar (c).

Profiles with a discontinuity in curvature are very sensitive to changes in Reynolds number, because of the large influence of the discontinuity on the onset of transition.

#### 4.2 Problems of High Speed in Liquid Media: Cavitation

In an incompressible medium the pressure falls when the free-stream speed increases; the smallest pressure that can occur in a liquid is the vapour pressure of the liquid (if we ignore the possibility of delay in boiling). When the liquid boils, cavities filled with vapour occur; this phenomenon, known as "cavitation", occurs on ship propellers when in rapid motion, and also in water turbines; decreased efficiency and, sometimes, corrosive effects are associated with it. In the flow about a profile the smallest pressures occur on the surface and so, if cavitation occurs, it starts from the surface; the flow separates from the profile and forms a free surface (of constant pressure), which encloses the region of cavitation. This region extends to various distances in the direction of flow; it ends in a turbulent mixing region of liquid and vapour, where a sudden increase in pressure takes place.

The state of cavitation is characterised by the "cavitation number",

$$\sigma = \frac{p - p_v}{q};$$

in particular, this characterises the magnitude of the cavitation region.  $p$  is the pressure in the undisturbed flow,  $p_v$  is the vapour pressure of the liquid (dependent on the temperature), and  $q$  is the kinetic pressure of the undisturbed flow. The cavitation number is defined more accurately if, instead of  $p_v$ , the actual pressure in the region of cavitation ( $p_c$ ) is introduced.  $p_c$  is the same as  $p_v$  only for liquids in which no gas is present; for liquids with gas present (for example, water containing air)  $p_c$  is greater than  $p_v$  (REICHARDT).

If we wish to avoid cavitation on profiles we must be familiar with the manner of its formation and with its effect on the profile polars at various cavitation-numbers. Measurements on profiles with normal position of maximum thickness show that the lift falls with decreasing cavitation number. It is found that shapes whose maximum thickness lies further forward are unfavourable because of the high minimum pressure and the consequent premature occurrence of cavitation. Profiles with a uniform pressure distribution are favourable; the circular segment profile (whose maximum thickness occurs at half the chord) has a pressure distribution of approximately this type.

Measurements of forces on profiles show three typical forms of cavitation (see Figure 4.17).

1. cavitation on the suction side which starts from the leading edge—this occurs if the front stagnation point lies on the pressure side, so that the flow accelerates round the nose from the pressure side and the point of minimum pressure lies very far forward;
2. cavitation which starts approximately from the position of maximum thickness when the profile is at the ideal angle of incidence or when the front stagnation point lies on the suction side;
3. cavitation on the pressure side which starts from the leading edge—this occurs if the front stagnation point lies on the suction side, so that the flow accelerates round the nose from the suction side.

Measurements by WALCHNER of lift and drag coefficients of circular segment profiles at various cavitation-numbers are reproduced in Figures 12.150 to 12.152. The points are not experimental points, but have been obtained by

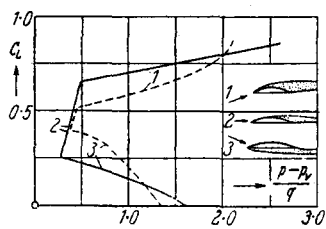


Fig. 4.17. Dependence of lift coefficient,  $C_L$ , on the cavitation number, for three different types of cavitation:

- (1) suction-side cavitation starting from the leading edge;
  - (2) suction-side cavitation starting from about half-chord;
  - (3) pressure-side cavitation starting from the leading edge.
- start of cavitation on circular segment profile.  
— — start of cavitation on improved profile

averaging the experimental values; points corresponding to the same angle of incidence are designated by the same symbol. The figures show that considerable falls in lift are associated with a decrease in cavitation number. From the appended diagrams we can see how the extent of the cavitation region depends on angle of incidence and cavitation number. Further measurements have been made on circular segment profiles with suitable rounding of the leading and trailing edges (from which the profiles Gö 5K to 16K have been derived); these measurements show that such rounding can considerably increase the region free from cavitation (Figures 12.153 ff). For the original circular segment profiles, cavitation is unavoidable if  $\sigma < 5 \frac{t}{c}$ ; the smallest cavitation number compatible with

flow free from cavitation is given by  $\sigma \approx 4 \frac{t}{c}$  for profiles

5K to 13K and by  $\sigma \approx 3 \frac{t}{c}$  for profiles 14K to 16K. At small cavitation numbers the diminution of the pressure-side cavitation is also noteworthy; it has almost completely vanished for the profiles Gö 14K to 16K (intended to be used on propeller hubs) in the range of positive lift.

A theoretical treatment of cavitation is difficult, but the following results have been obtained. For completely developed cavitation on the suction side BETZ found that the shape of the suction side (hence, in general, the profile thickness) is unimportant. For profiles with a flat pressure-side the theory gives

$$C_L = \frac{\pi}{2} \alpha + \frac{p - p_v}{q};$$

the first term is the lift coefficient (according to KIRCHHOFF's theory) of a flat plate at a small angle of incidence,  $\alpha$ , the flow having separated; the second term allows for the fact that the dominant pressure on the suction side is not that of the undisturbed flow, but the vapour pressure, which is smaller than the undisturbed pressure. If we take the skin-friction drag ( $C_f$ ) into account, the drag coefficient becomes

$$C_D = \alpha C_L + C_f.$$

Measurements confirm these theoretical estimates only if the whole suction side is covered by a cavitation layer; otherwise, the profile properties are worse than the theoretical predictions.

If cavitation starts from the middle of the suction side (a phenomenon that can occur simultaneously with cavitation on the pressure side) there is a similarity rule for profiles of different thickness ratios (HELMBOLD); thickness ratio, angle of incidence, and cavitation number must be small quantities whose squares are negligible. The rule states that the same condition of cavitation exists on two similar profiles of thickness ratios  $\tau_1$  and  $\tau_2$  if the respective angles of incidence and cavitation number are proportional to  $\tau_1$  and  $\tau_2$ ; this follows because, under the stated conditions, the disturbance pressures vary linearly with thickness ratio. For the lift coefficient,  $C_L$ , it follows that, at the same cavitation number, the values of  $C_L$  for two similar profiles of different thickness ratios  $\tau_1$  and  $\tau_2$  are proportional to  $\tau_1$  and  $\tau_2$  respectively; accordingly, with a suitable plotting, a collapse of experimental results for profiles of different thickness ratios but of similar shape can be obtained. As the experimental results show (Figures 12.162 to 12.164), the rule is well confirmed.

## 4.3 References

### 4.3.1 Quality of Surface

ABBOTT, T. F. and H. R. TURNER: The Effects of Roughness at High Reynolds Numbers on the Lift and Drag Characteristics of Three Thick Airfoils. NACA ACR No. L4H21 (1944) WR L—46.

ALLEN, H. J.: Notes on the Effect of Surface Distortion on the Drag and Critical Mach Number of Airfoils. NACA ACR No. 3129 (1943).

- BRASLOW, A. L.: Investigation of Effects of Various Camouflage Paints and Painting Procedures on the Drag Characteristics of an NACA 65(421)-420  $a = 1.0$  Airfoil Section. NACA CB No. L4G17, 1944 (WR L-141).
- and E. C. KNOX: Simplified Method for Determination of Critical Height of Distributed Roughness Particles for Boundary-Layer-Transition of Mach Numbers from 0 to 5. NACA TN 4363 (1958).
- DOENHOFF, A. E. and E. A. HORTON: A Low-Speed Experimental Investigation of the Effect of a Sandpaper Type of Roughness on Boundary-Layer-Transition. NACA Rep. 1349 (1958).
- DOETSCH, H.: Einige Versuche über den Einfluß von Oberflächenstörungen auf die Profileigenschaften insbesondere auf den Profilwiderstand im Schnellflug. Jahrb. 1939 dDL I, S. 88 und LGL 117.
- Profilwiderstandsmessungen an Modellflügeln in serienmäßiger Glattblechbauweise. FB 1731 (1943).
- Versuche an zwei Modellflügeln in Blechbauweise mit Laminaprofilen. FB 1855 (1943).
- Über den Einfluß von Oberflächenstörungen auf den Widerstand der Tragflügel. UM 1233 (1944), LGL-Bericht 176/I und 179a (1944).
- DRYDEN, H. L.: Review of Published Data on the Effect of Roughness on Transition from Laminar to Turbulent Flow. J. Aer. Sci. 20 (1953), pp. 477/482.
- GÖTHERT, B.: Einfluß von Einzelrauhigkeiten auf den Widerstand von Tragflügelprofilen. UM 1480 (1945).
- GRAY, V. H. and U. W. GLAHN: Aerodynamic Effects Caused by Icing of an Unswept NACA 65A004 Airfoil. NACA TN 4155 (1958).
- HOERNER, S.: Einfluß der Oberflächenrauhigkeit auf die aerodynamischen Eigenschaften der Luftfahrtzeuge. Ringbuch der deutschen Luftfahrtforschung, Teil IA (1937) 9.
- HOLSTEIN, H.: Versuche an einer parallel angestromten ebenen Platte über den Rauhigkeitseinfluß auf den Umschlag laminar/turbulent. UM 3110 (1944).
- HOOKER, R. W.: The Aerodynamic Characteristics of Airfoils as Affected by Surface Roughness. NACA TN 457 (1933).
- HOOD, M. J.: The Effects of some Common Surface Irregularities on Wing Drag. NACA TN No. 695, 1939.
- JONES, R. and D. H. WILLIAMS: The Effect of Surface Roughness on the Characteristics of the Aerofoils NACA 0012 and RAF 34. R & M 1708 (1936).
- KRAEMER, K.: Die Wirkung von Stolperdrähten auf den Grenzschichtumschlag. Jahrb. 1959 d. Wiss. Ges. Luftf.
- KRETT, P.: Profilwiderstandsmessungen an rauen Flächen. FB 1456 (1941).
- and A. WANNER: Profilwiderstandsmessungen an Gleitflugzeugen. FB 1212 (1940) und Jahrb. 1941 dDL., S. I 111/19.
- LOFTIN, L. K.: Effects of Specific Types of Surface Roughness on Boundary-layer Transition. NACA ACR L5J29a (1945) WR L-48.
- PRANDTL, L. and A. BETZ: Ergebnisse der Aerodynamischen Versuchsanstalt zu Göttingen. R. Oldenbourg. München, III. Lieferung (1927).
- PRANDTL, L. and H. SCHLICHTING: Das Widerstandsgesetz rauer Platten. Werft, Reederei, Hafen 15 (1934).
- RUNKEL: Profilwiderstand- und Grenzschichtmessung an einem NACA 23012-Profil bei glattem und rauhem Anstrich. UM 3507 (1943).
- SCHERBARTH, K.: Grenzschichtmessungen hinter einer punktförmigen Störung in laminarer Strömung. Jahrb. 1942 dDL I, S. 51—52.
- SCHLICHTING, H.: Experimentelle Untersuchungen zum Rauhigkeitsproblem. Ing.-Arch. 7 (1936), S 1.
- Grenzschichttheorie, Verlag Braun 1951 and London 1955 (English translation).
- TANI, J., R. HAMA and S. MITUSSI: On the Permissible Roughness in the Laminar Boundary Layer. Rep. Aer. Res. Inst. Tokyo No. 199 (1940).
- On the Effect of a Single Roughness Element on Boundary-layer Transition. Rep. Inst. Sci. Techn. Tokyo 8 (1954), p. 125/133.
- TILLMANN, W.: Neue Widerstandsmessungen an Oberflächenstörungen in der turbulenten Reibungsschicht. Forschungshefte f. Schiffstechnik 1 (1953), S. 81—88.
- WIEGHARDT, K.: Zum Reibungswiderstand rauher Platten. UM 6612 (1944).
- Erhöhung des turbulenten Reibungswiderstandes durch Oberflächenstörungen. Forschungs-Heft f. Schiffstechnik 1 (1953), S. 65—81.
- WILLIAMS, D. H. and A. F. BROWN: Tests on RAF 34 Negative at Incidences and of the Effect of Surface Roughness on RAF 34 with Split Flap in the Compressed Air-tunnel. R & M No. 1772 (1937).
- YOUNG, A. D.: Surface Finish and Performance. Aircr. Eng., Sept. 1939.
- ZALOVCIK, J. A.: Profile-Drag Coefficients of Conventional and Low-Drag Airfoils as Obtained in Flight. NACA—ACR No. L4E31 (1944) WR L-139.

#### 4.3.2 Cavitation

- BETZ, A.: Einfluß der Kavitation auf die Leistung von Schiffs-schrauben. Verh. 3. Int. Kongr. Techn. Mech., Stockholm, Teil 1, S. 411. Stockholm 1931.
- HELMBOLD, H. B.: Erörterungsbeitrag über Kavitation. Hydro-mechanische Probleme des Schiffsantriebes, Hamburg (1932), S. 338.
- MARTYRER, E.: Kraftmessungen an Widerstandskörpern und Flügelprofilen im Wasserstrom bei Kavitation. Hydro-mechanische Probleme des Schiffsantriebes, Hamburgische Schiffsbau-Versuchsanstalt, 1932, S. 268.
- NUMACHI, F.: Profilmessungen bei Kavitation. 1. Mitt.: Kraftmessungen an vier Profilen bei Hohlsog. VDI-Forschung 11 (1940), S. 303.
- 3. Mitt.: Kraftmessung an Spaltflügelprofilen bei Kavitation, Werft, Reederei, Hafen 22 (1941), S. 295.
- Summary Report on the Research of Cavitation Phenomena Obtained Hitherto by our Institute. Rep. Inst. High Speed Mech. Tohoku Univ. 4 (1954), p. 159/171.
- REICHARDT, H.: Kavitationskanäle. Göttinger Monographie, Teil D<sub>1</sub> 3.2 (1946).
- WALCHNER, O.: Profilmessungen bei Kavitation. Hydromechanische Probleme des Schiffsantriebes, Hamburgische Schiffsbau-Versuchsanstalt, 1932, S. 256.
- Bericht über Profilmessungen bei Kavitation. Nicht veröffentlichter Bericht des KWI, Göttingen 1934.

## 5. PROFILES WITH FLAPS

### 5.1 Survey

The simplest method of increasing the maximum lift of a profile is to increase the profile camber by deflection of a flap. The possible ways of fitting a flap on to a profile are numerous, and the effects on the profile properties are extraordinarily varied. The principal arrangements are:

1. plain flaps;
2. split flaps;
3. slotted and double-slotted flaps;
4. nose flaps;

In addition, the most diverse combinations of these arrangements are used. Since the representation of the experimental results in diagrams would take too much space, the reader is referred to Table 11.6 (a survey of the results) and, for more detail, to the literature (see Section 5.6). The influence of Reynolds number can be estimated from the table, but hardly any profiles with flaps have been investigated over a large Reynolds number range. Some brief remarks about the results† follow.

### 5.2 Plain Flaps

The maximum lift depends essentially upon the ratio of the flap chord,  $c_\eta$ , to the profile chord,  $c$ , as well as upon the flap deflection,  $\eta$ . Ratios  $c_\eta/c$  that lie in the range 0.2 to 0.25 are favourable when  $\eta$  is about 60°; the increased maximum lift rises with thickness. For laminar profiles the range of  $C_L$  in which the drag is small can be displaced to higher  $C_L$  values by small flap-deflections (a small camber has the same effect). As with all flaps it is essential that the unavoidable gap between wing and flap be kept as small as possible; otherwise losses in lift cannot be avoided (see Figure 5.1). The increase in the moment coefficient ( $\Delta C_m$ ) is proportional to the increase in the lift coefficient ( $\Delta C_L$ ), and is in fair agreement with the theoretical value; the normal forces and hinge moments also agree well with theoretical predictions (see [R634]). Section 12.4 contains some pressure distributions on wings with flaps.

### 5.3 Split Flaps

With a split flap the suction side of the profile remains unaltered, but on the pressure side a downward flap-deflection is possible at the rear. The effect is similar to that of a plain flap, but considerably more marked.  $C_{L_{\max}}$ .

† The published experimental results are usually for wings of finite span, and only in rare cases for two-dimensional flow.

increases with thickness ratio, but so do the flap deflection and the size of flap required to produce the prescribed maximum value of  $C_L$ . An additional camber is, more effective on thin profiles than on thick ones. The shape of the front part of the profile has an important effect on the efficiency of a split flap; this can be seen from Figure 5.2,

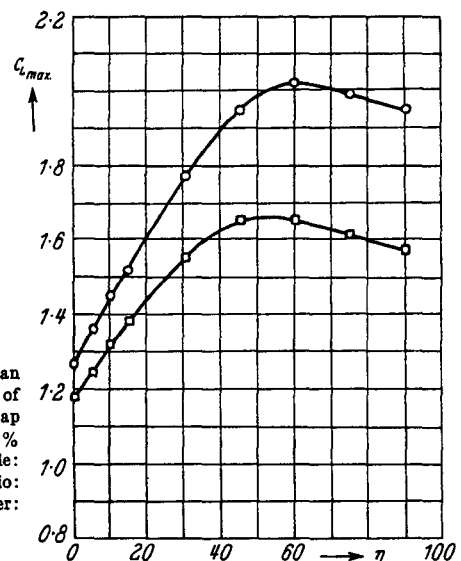


Fig. 5.1. Effect of an "insignificant" gap of 0.0032  $c$  at a plain flap (flap chord being 20% of wing chord). Profile: Clark Y. Aspect ratio: 6. Reynolds number:  $0.61 \cdot 10^6$ . [R938]

in which are plotted the results of a large number of  $C_{L_{\max}}$  measurements on profiles with split flaps, for various values of thickness, position of maximum thickness, and nose radius; the results are plotted against the parameter  $\frac{t}{2c} \sqrt{\frac{r_0}{x_t}}$ .

Table 11.6 and many diagrams of Chapter 12 contain further numerical results. The theoretical behaviour of the moment is not so easily predicted as for plain flaps.

### 5.4 Slotted Flaps

A still higher lift-coefficient can be obtained by the use of a slotted flap, but the geometrical shape of the slot must be carefully considered if the desired increase is to be realised; for this reason it is difficult to give definite rules for the best position of the flap. Sharp edges at the beginning of the slot are to be avoided as much as possible on thick profiles, but thin profiles are less sensitive in this respect. If the suction side is bent round at the trailing edge in the

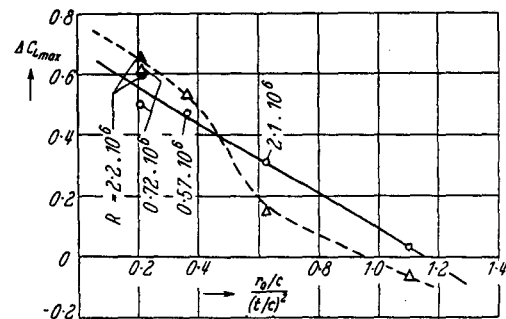
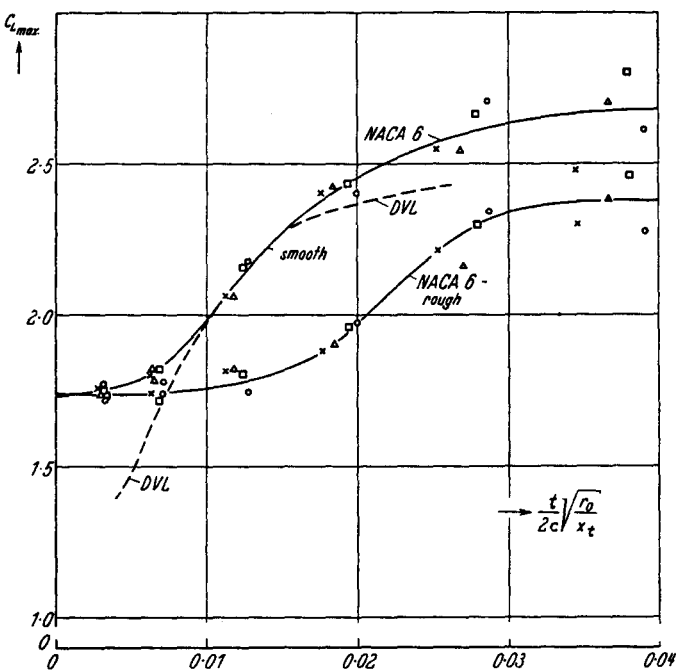


Fig. 5.3. Increase in  $C_{L_{\max}}$  from nose flap on various profiles, as a function of the nose radius (see Equation (1.7)). (○) without split flap. (Δ) with split flap;  $\frac{c_{\eta}}{c} = 0.2$ ;  $\eta = 60^\circ$ . [FB1948]

Fig. 5.2. Split-flap measurements for the NACA 6-series (full line,  $\frac{t}{c} = 0.06$  to  $0.21$ ), and the DVL series (dashed line,  $\frac{t}{c} = 0.09$  to  $0.18$ ,  $\frac{x_t}{c} = 0.3$  to  $0.5$ ). Meaning of symbols: (○) 63-series; (□) 64-series; (Δ) 65-series; (×) 66-series

direction of the upper side of the flap, there is often a favourable effect. Numerous results for wings with slotted flaps are shown in Table 11.6. The use of a double-slotted flap can produce a further increase in maximum lift-coefficient, but this is realised in practice only at the expense of a considerable increase in constructional weight.

### 5.5 Nose Flaps and Slats

Profiles with small nose-radius have very small maximum lift. W. KRÜGER recommends the use of a nose flap to

improve the value of  $C_{L_{\max}}$ ; with a suitable arrangement an increase in maximum lift coefficient,  $\Delta C_{L_{\max}}$ , of between 0.6 and 0.7 is obtained. The additional use of a split flap then produces a further increase, so that in the most favourable case  $C_{L_{\max}}$  is increased from 0.7 (without flaps) to 2.2 (with nose flap and split flap). According to the existing measurements the most favourable angle between nose flap and wing chord is about  $130^\circ$ . With decreasing flap-chord, and especially with increasing nose radius (see Equation (1.7)), the effect diminishes (see Figure 5.3). The

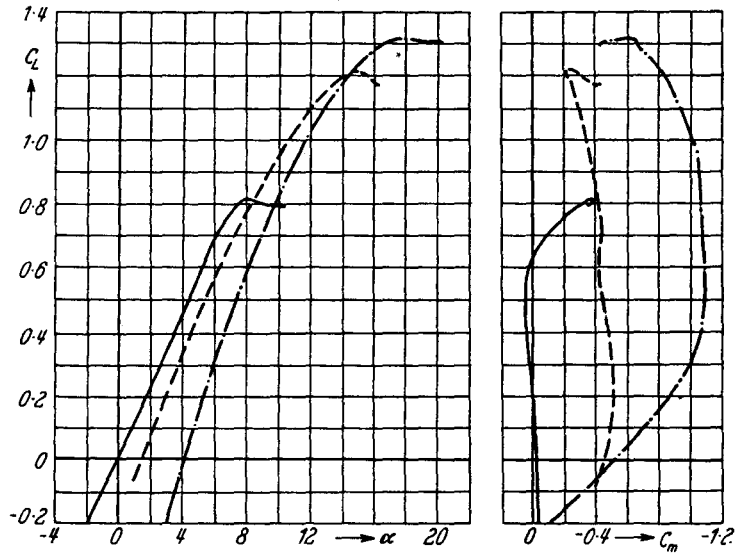
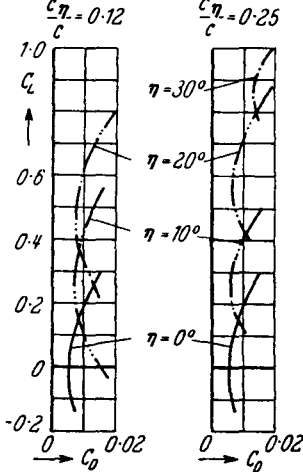


Fig. 5.4. Characteristics of a double-wedge profile ( $\frac{t}{c} = 0.0423$ ; wedge angle =  $5.1^\circ$ ; circular arc faired in from  $0.425 < \frac{x}{c} < 0.575$ ) with nose flaps of chords  $\frac{c_{\eta}}{c} = 0.12$  and  $0.25$ . — with no deflection,  $\eta = 0^\circ$ . - - - with deflection,  $\eta = 30^\circ$  ( $\frac{c_{\eta}}{c} = 0.12$ ). - - - with deflection,  $\eta = 30^\circ$  ( $\frac{c_{\eta}}{c} = 0.25$ ). [N2018]. Reynolds number:  $5.8 \cdot 10^6$ . Mach number: 0.17

remaining aerodynamic coefficients change less than, for example, when a split flap is used. This flap arrangement is of importance for the take-off of aircraft having supersonic profiles (with pointed noses); Figure 5.4 shows the aerodynamic coefficients of such a profile.

For profiles with normal nose radius, retractable slats can be recommended as a means of increasing  $C_{L_{max}}$ . Measurements on a profile, NACA 23012, equipped with them [L-261] show that  $\Delta C_{L_{max}} = 0.5$  and that the corresponding angle of incidence is increased by between eight and ten degrees; for further experimental results see Table 11.6.

## 5.6 References

- ABBOTT, I. H. and H. GREENBERG: Tests in the Variable-Density Wind-Tunnel of the NACA 23012 Airfoil with Plain and Split Flaps. NACA Rep. 661 (1939).
- ABBOTT, I. H.: Lift and Drag Characteristics of a Low-Drag Airfoil with Slotted Flap Submitted by Curtiss-Wright Corporation. NACA MR, Dec. 2, 1941.
- and H. R. TURNER jr.: Lift and Drag Tests of Three Airfoil Models with Fowler Flaps Submitted by Consolidated Aircraft Corporation. NACA MR, Dec. 29, 1941.
- Tests of Four Models Representing Intermediate Sections of the XB-33 Airplane Including Sections with Slotted Flap and Ailerons. NACA MR, June 4, 1942.
- AMES, MILTON B., jr.: Wind-Tunnel Investigation of Two Airfoils with 25-Percent-Chord Gwinn and Plain Flaps. NACA, TN 763, 1940.
- BOGDONOFF, S. M.: Tests of Two Models Representing Intermediate Inboard and Outboard Wing Sections of the XB-36 Airplane. NACA MR, Jan. 7, 1943.
- Wind-Tunnel Investigation of a Low-Drag Airfoil Section with a Double Slotted Flap. NACA ACR 2130 (1943).
- BRASLOW, A. L. and L. K. LOFTIN, jr.: Two-Dimensional Wind-Tunnel Investigation of an Approximately 14-Percent Thick NACA 66-Series-Type Airfoil Section with a Double Slotted Flap. NACA TN 1110, 1946.
- BRYANT, L. W., A. S. HALLIDAY and A. S. BATSON: Two-Dimensional Control Characteristics. R & M No. 2730.
- CAHILL, J. F.: Aerodynamic Tests of an NACA 66 (215)-116,  $a = 0.6$  Airfoil with a 0.25 c Slotted Flap for the Fleetwings XA-39 Airplane. NACA MR L4K21, 1944.
- Aerodynamic Data for a Wing Section of the Republic XF-12 Airplane Equipped with a Double Slotted Flap. NACA L6A08a, 1946 (Wartime Rep. L-544).
- Two-Dimensional Wind-Tunnel Investigation of Four Types of High Lift Flap on NACA 65—210 Airfoil Section. NACA TN 1191, 1947.
- and ST. RACISZ: Wind-Tunnel Development of Optimum Double-Slotted-Flap Configurations for Seven Thin NACA Airfoil Sections. NACA RM L7B17 1947.
- Wind-Tunnel Investigation of Seven Thin NACA Airfoil Sections to Determine Optimum Double-Slotted-Flap configurations. NACA TN 1545, 1948.
- W. J. UNDERWOOD, R. J. NUBER and G. A. CHEESMAN: Aerodynamic Forces and Loadings on Symmetrical Circular Arc Airfoils with Plain Leading-Edge and Plain Trailing-Edge Flaps. NACA Rep. 1146 (1953).
- CHEERS, E., W. S. WALKER and C. R. TAYLOR: Two-Dimensional Tests on a 15% Thick Symmetrical Roof-Top Aerofoil with 20% Plain Flap in the N.P.L. 13 ft.  $\times$  9 ft. Wind-Tunnel. R & M No. 2412 (1946).
- CRANE, R. M. and R. W. HOLTZCLAW: Wind-Tunnel Investigation of the Effects of Profile Modification and Tabs on the Characteristics of Ailerons on a Low-Drag Airfoil. NACA Rep. 803 (1944).
- CUNNING, R. W., N. GREGORY and W. S. WALKER: An Investigation of the Use of an Auxiliary Slot to Reestablish Laminar Flow on Low-Drag Airfoils. R & M No. 2742 (1950).
- DAVIDSON, J. M.: The Jet Flap. J. Roy. Aeron. Soc. 60 (1956), pp. 25—50.
- DOETSCH, H. and M. KRAMER: Der Maximalauftrieb der Profilreihe NACA 24 mit Spreizklappe, Oberflächenrauhigkeit und Stördraht, FB 642.
- DOETSCH, H. and G. KÖNIG: Untersuchung an einem Normalflügel NACA 1242 mit Spaltruder und verschiedenen Spaltformen. FB 762.
- and A. PASCHKE, Druckverteilungsmessungen und Wägungen an den Profilen NACA 23009, 23012 und 23018 ohne und mit Spreizklappe. FB 1095 (1939).
- DUSCHIK, F.: Wind-Tunnel Investigations of an NACA 23021 Airfoil with Two Arrangements of a 40-Percent-Chord Slotted Flap. NACA TN 728, 1939.
- FISCHEL, J. and J. M. RIEBE: Wind-Tunnel Investigation of an NACA 23021 Airfoil with a 0.32-Airfoil-Chord Double Slotted Flap. NACA ARR L4J05 (1944) WR L-7.
- FULLMER, F. J., jr.: Wind-Tunnel Investigation of NACA 66 (215)-216, 66, 1—212, and 65<sub>1</sub>—212 Airfoils with 0.20-Airfoil-Chord Split Flaps. NACA CB L4G10 (1944). WR L-140.
- Two-Dimensional Wind-Tunnel Investigation of the NACA 64<sub>1</sub>—012 Airfoil Equipped with two Types of Leading Edge Flap. NACA TN 1277 (1947).
- GAMBUCI, B. J.: Section Characteristics of the NACA 0006 Airfoil with Leading Edge and Trailing-Edge Flaps. NACA TN 3797 (1956).
- GLAUERT, H.: Theoretical Relationships for an Airfoil with Hinged Flap. R & M No. 1095 (1927).
- GÖTHERT, B.: Ruderwirkung bei hohen Unterschallgeschwindigkeiten. LGL 156 (1942), S. 51.
- Unterbrecherwirkung bei hohen Unterschallgeschwindigkeiten. LGL 156 (1942), S. 64.
- GÖTHERT, R.: Systematische Untersuchungen an Flügeln mit Klappen und Hilfsklappen. Jahrb. 1940 dDL I, S. 278/307.
- HANDLEY PAGE: Aeron. Journal (1921), p. 270.
- HARRIS, TH. A.: Wind-Tunnel Investigation of an NACA 23012 Airfoil with Two Arrangements of a Wide-Chord Slotted Flap. NACA TN 715 (1939).
- and P. E. PURSER: Wind-Tunnel Investigation of an NACA 23012 Airfoil with Two Sizes of Balanced Split Flap. NACA ACR, Nov. 1940.
- and R. S. SWANSON: Wind-Tunnel Tests of an NACA 23021 Airfoil Equipped with a Slotted Extensible and a Plain Extensible Flap. NACA TN 782 (1940).
- and J. G. LOWRY: Pressure Distribution over an NACA 23021 Airfoil with a Slotted and a Split Flap. NACA Rep. 718 (1941).
- and I. G. RECANT: Wind-Tunnel Investigation of NACA 23012, and 23030 Airfoils Equipped with 40-Percent-Chord Double Slotted Flaps. NACA Rep. 723 (1941).
- and J. G. LOWRY: Pressure Distribution over an NACA 23012 Airfoil with a Fixed Slot and a Slotted Flap. NACA Rep. 732 (1942).
- HILTON, W. F. and A. E. KNOWLER: Lift, Drag and Pitching Moment Coefficients on an EC 1240 Tailplane-Elevator at High Speeds. R & M No. 2227 (1943).

- HOLTZCLAW, R. W. and Y. WEISMANN: Wind-Tunnel Investigation of the Effects of Slot Shape and Flap Locations on the Characteristics of Low-Drag Airfoils Equipped with a 0-25-Chord Slotted Flap. NACA WR A-80 (1944).
- v. HOLST, E.: Der rotierende Flügel als Mittel zur Hochauftriebserzeugung. Jahrb. (1941) dDL I, S. 372.
- JACOBS, E. N. and R. M. PINKERTON: Pressure Distribution over a Symmetrical Airfoil Section with Trailing Edge Flap. NACA Rep. 360 (1930).
- JACOBS, E. N.: Tapered Wings, Tip Stalling, and Preliminary Results from Tests of the Stall-Control Flap. NACA ACR, Nov. 1937.
- KÖSTER, H.: Messungen am Profil 0 00 12—0,55 45 mit Spreiz- und Nasenspreizklappe. UM 1317 (1944).
- Untersuchungen am Profil NACA 0 00 12—0,55 45 mit Nasenspreizklappe. UM 1363 (1944).
- KNAPPE, O.: Schnellkanalversuche an einem symmetrischen Klappenflügel. Jahrb. (1941) dDL I, S. 96/100.
- Schnellkanalversuche an Profilen und Flugzeugmodellen und ihre flugtechnische Auswertung. LGL 156 (1942), S. 128/132.
- KRAMER, M.: Steigflugklappen. FB 1576 (1942).
- KRÜGER, W.: Über eine neue Möglichkeit der Steigerung des Höchstauftriebes von Hochgeschwindigkeitsprofilen. UM 3049 (1943).
- Systematische Windkanalmessungen an einem Laminarflügel mit Nasenklappe. FB 1948 (1944).
- Windkanalmessungen an einem abgeänderten Mustang-Profil mit Nasenklappe. Kraft- und Druckverteilungsmessungen. UM 3153 (1944).
- KÜCHEMANN, D.: Dreikomponentenmessungen an einem Flügel mit rotierendem Hilfsflügel. FB 1513 (1944).
- Auftrieb und Widerstand eines rotierenden Flügels. FB 1651 (1942).
- LEMME, H. G.: Kraftmessungen und Druckverteilungen an einem Flügel mit Knicknase, Vorflügel, Wölbungs- und Spreizklappe. FB 1676 (1942).
- Kraftmessungen und Druckverteilungsmessungen an einem Rechteckflügel mit Spaltknicknase, Wölbungs- und Spreizklappe oder Rollklappe. FB 1676/2 (1943).
- Kraftmessungen und Druckverteilungsmessungen an einem Rechteckflügel mit Doppelknicknase. FB 1676/3 (1944).
- LOFTIN, L. K., jr. and F. J. RICE jr.: Two-Dimensional Wind-Tunnel Investigation of Two NACA Low-Drag Airfoil Sections Equipped with Slotted Flaps and a Plain NACA Low-Drag Airfoil Section for XF6U-1 Airplane. NACA MR L5L11, (1946).
- LOWRY, J. G.: Wind-Tunnel Investigation of an NACA 23012 Airfoil with Several Arrangements of Slotted Flap with Extended Lips. NACA TN 808 (1941).
- NONWEILER, T.: Maximum Lift Data for Symmetrical Wings. Aircr. Eng. XXVII (1955) No. 311, p. 2.
- Flaps, Slots and other High-lift Aids. Aircr. Eng. XXVII (1955) No. 311, p. 2.
- The Design of Wing Sections, Aircr. Eng., July 1956.
- NOYES, R. W.: Wind-Tunnel Tests of a Wing with a Trailing Edge Auxiliary Airfoil Used as a Flap. NACA TN 524 (1935).
- NUBER, R. J. and F. J. RICE jr.: Lift Tests of a 0-1536 c Thick Douglas Airfoil Section of NACA 7-Series Type Equipped with a Lateral-Control Device for Use with a Fullspan Double-Slotted Flap on the C-74 Airplane. NACA MR L5C24a (1945).
- PETRIKAT, K.: Untersuchungen an festen und selbsttätig öffnenden Flügeln. Jahrb. 1940 dDL I, S. 248—264.
- PLATT, R. C.: Aerodynamic Characteristics of a Wing with Fowler Flaps Including Flap Loads, Downwash, and Calculated Effect on Take-off. NACA Rep. 534 (1935).
- Aerodynamic Characteristics of Wings with Cambered External-Airfoil Flaps, Including Lateral Control with a Full-Span Flap. NACA Rep. 541 (1935).
- and I. H. ABBOTT: Aerodynamic Characteristics of NACA 23012 and 23021 Airfoils with 20-Percent-Chord External-Airfoil Flaps of NACA 23012 Section.. NACA Rep. 573 (1936).
- and J. A. SHORTAL: Wind-Tunnel Investigation of Wings with Ordinary Ailerons and Full-Span External Airfoil Flaps. NACA Rep. 603 (1937).
- PURSER, P. E., J. M. RIEBE: Wind-Tunnel Investigation of an NACA 23012 Airfoil with a 0-30-Airfoil-Chord Double Slotted Flap. NACA ARR 3L10 (1943) WR L-469.
- PURSER, P. E. and H. S. JOHNSON: Effect of Trailing Edge Modification on Pitching-Moment Characteristics of Airfoils. NACA CB L4I30, (1944) WR L-664.
- QUINN, J. H. jr.: Tests of the NACA 64<sub>1</sub> A212 Airfoil Section with a Slat, a Double Slotted Flap, and Boundary-Layer Control by Suction. NACA TN 1293 (1947).
- RACISZ, ST. F.: Investigation of NACA 65<sub>(112)</sub>A111 (Approx.) Airfoil with 0-35-Chord Slotted Flap at Reynolds Numbers up to 25 Millions. NACA TN 1463 (1947).
- RECAN, I. G.: Wind-Tunnel Investigation of an NACA 23030 Airfoil with Various Arrangements of Slotted Flaps. NACA TN 755 (1940).
- REGENSCHEIT, B.: Versuche an einem Flügel mit einem Rotor. FB 826.
- ROGALLO, F. M. and B. S. SPANO: Wind-Tunnel Investigation of an NACA 23012 Airfoil with 30-Percent-Chord Venetian-Blind Flaps. NACA Rep. 742 (1942).
- ROSE, L. M. and I. M. ALTMANN: Low-Speed Investigation of a Thin, Faired, Double-Wedge Airfoil Section with Nose-Flaps of Various Chords. NACA TN 2018 (1950).
- ROSE, L. M. and I. M. ALTMANN: Low-Speed Investigation of a Thin, Faired, Double-Wedge Airfoil Section with Nose Flap. NACA TN 2172 (1950).
- SCHILLER, M.: Windkanaluntersuchungen an einem Flügel mit Klappenflügeln und Vorflügel. FB 543.
- SCHRENK, O.: Kritischer Überblick über Auslandsuntersuchungen zur Hochauftriebserzeugung. Jb. 1939 dDL I, S. 79.
- SCHULDENFREI, M. J.: Wind-Tunnel Investigation of an NACA 23012 Airfoil with a Handley Page Slot and Two Flap Arrangements. NACA ARR, Febr. 1942 WR L-261.
- SEIFERTH, R.: Neuere Messungen an Hochauftriebsflügeln. Jahrb. 1939 dDL I, S. 84—87.
- SHAW, R. A.: Changes in Control Characteristics with Changes in Flow Pattern at High Subsonic Speeds: Tests on an EC 1250 Aerofoil with 25% Concave Flap. R & M No. 2436 (1949).
- SHERMAN, A. and T. A. HARRIS: The Effect of Equal Pressure Fixed Slots on the Characteristics of a Clark Y-Airfoil. NACA TN 507 (1934).
- SILVERSTEIN, A., S. KATZOFF and J. HOOTMAN: Comparative Flight and Full-Scale Wind-Tunnel Measurements of the Maximum Lift of an Airplane. NACA Rep. 618 (1938).
- SIVELLS, I. C. and S. H. SPOONER: Investigation in the Langley 19-Foot Pressure Tunnel of Two Wings of NACA 65-210 and 64-210 Airfoil Sections with Various Type Flaps. NACA Rep. 642 (1949).
- STAUFER: Windkanalmessungen an einem Flügel mit Doppel-spaltklappe. Jahrb. 1940 dDL I, S. 245.

| Cap. 60

- SWANSON, R. S. and M. J. SCHULDENFREI: Wind-Tunnel Investigation of an NACA 23012 Airfoil with Two Sizes of Balanced Split Flaps. NACA ACR, Febr. 1941.
- UNDERWOOD, W. J. and F. T. ABBOTT jr.: Tests of NACA 66-2-116,  $a = 0.6$  Airfoil Section Fitted with Pressure Balanced and Slotted Flaps for the Wing of the XP-63 Airplane. NACA MR, May 23, 1942.
- VISCONTI, F.: Wind-Tunnel Investigation of Air Loads over a Double Slotted Flap on the NACA 65 (216)-215,  $a = 0.8$  Airfoil Section. NACA RM L7A30 (1947).
- WALZ, A.: Messungen am Laminarprofil 2315 BIS mit Absaugung in der Nähe der Profilnase ohne und mit Nasenspreizklappe. UM 3195 (1944).
- Messungen über die Querruderwirksamkeit an einem 15% dicken Profil mit 60% Dickenrücklage und kleinem Hinterkantenwinkel. UM 3121 (1944).
- WEICK, F. E. and TH. A. HARRIS: The Aerodynamic Characteristics of a Model Wing Having a Split Flap Deflected Downward and Moved to the Rear. NACA TN 422 (1932).
- WEICK, F. E. and J. A. SHORTAL: The Effect of Multiple Fixed Slots and a Trailing Edge Flap on the Lift and Drag of a Clark Y Airfoil. NACA Rep. 427 (1932).
- WEICK, F. E. and M. J. BAMBER: Wind-Tunnel Tests of a Clark Y Wing with a Narrow-Auxiliary Airfoil in Different Positions. NACA Rep. 428 (1932).
- WEICK, F. E. and C. R. PLATT: Wind-Tunnel Tests on a Model Wing with Fowler Flap and Specially Developed Leading Edge Slot. NACA TN 459 (1933).
- WEICK, F. E. and R. SANDERS: Wind-Tunnel Tests on Combinations of a Wing with Fixed Auxiliary Airfoils Having Various Chords and Profiles. NACA Rep. 472 (1933).
- WENZINGER, C. J.: Wind-Tunnel Investigation of Ordinary and Split Flaps on Airfoils of Different Profile. NACA Rep. 554 (1936).
- Pressure Distribution over an Airfoil Section with a Flap and Tab. NACA Rep. 574 (1936).
- Wind-Tunnel Tests of a Clark Y Wing Having Split Flaps with Gaps. NACA TN 650 (1938).
- Pressure Distribution over an NACA 23012 Airfoil with an NACA 23012 External-Airfoil Flap. NACA Rep. 614 (1938).
- and W. B. ANDERSON: Pressure Distribution over Airfoils with Fowler Flaps. NACA Rep. 620 (1938).
- and J. B. DELANO: Pressure Distribution over an NACA 23012 Airfoil with a Slotted and a Plain Flap. NACA Rep. 633 (1938).
- and TH. A. HARRIS: A Wind-Tunnel Investigation of an NACA 23012 Airfoil with Various Arrangements of Slotted Flaps. NACA Rep. 664 (1939).
- Wind-Tunnel Investigation of an NACA 23021 Airfoil with Various Arrangements of Slotted Flaps. NACA Rep. 667 (1939).
- Wind-Tunnel Investigation of NACA 23012, 23021 and 23030 Airfoils with Various Sizes of Split Flap. NACA Rep. 668 (1939).
- Wind-Tunnel Investigations of an NACA 23021 Airfoil with Various Arrangements of Slotted Flaps. NACA Rep. 677 (1939).
- and W. E. GAUVAIN: Wind-Tunnel Investigation of an NACA 23012 Airfoil with a Slotted Flap and Three Types of Auxiliary Flap. NACA Rep. 679 (1939).
- and B. S. SPANO: Wind-Tunnel Investigation of an NACA 23012 Airfoil with Various Arrangements of Venetian-Blind Flaps. NACA Rep. 689 (1940).
- WILLIAMS, D. H., A. F. BROWN and E. SMYTH: Tests of Airfoils RAF 69 and RAF 89, with and without Split Flaps, in the Compressed Air-Tunnel. R & M No. 1717 (1936).
- WILLIAMS, D. H. and A. F. BROWN: Tests of RAF 34 at Negative Incidences and of the Effect of Surface Roughness of RAF 34 with Split Flap in the Compressed Air Tunnel. R & M No. 1772 (1937).
- WYSOCKI: Windkanaluntersuchungen an Flügeln mit Klappen, Vorflügeln und Bremsen. FB 1655 (1942).

## 6. BOUNDARY LAYER CONTROL

### 6.1 Suction as a Means of Increasing the Lift

Only a limited increase in lift can be obtained by arrangements of flaps; to gain a further increase, the distribution of energy in the boundary layer must be controlled by suitable means. This can be done by sucking away the fluid in the boundary layer near the wall (this fluid is deficient in energy) or by blowing out air in the direction of flow—that is, by bringing in additional energy (see Section 6.2). It is customary to use a dimensionless coefficient for  $Q$ , the amount sucked away or blown out, called the *volume-flow-rate coefficient*,

$$c_Q = Q/Vs \quad (6.1)$$

(where  $S$  is the area of the part of the wing surface affected). For the required suction or blowing pressure,  $p_s$ , the coefficient

$$(C_p)_s = \frac{p_s}{\frac{\rho}{2} V^2} \quad (6.2)$$

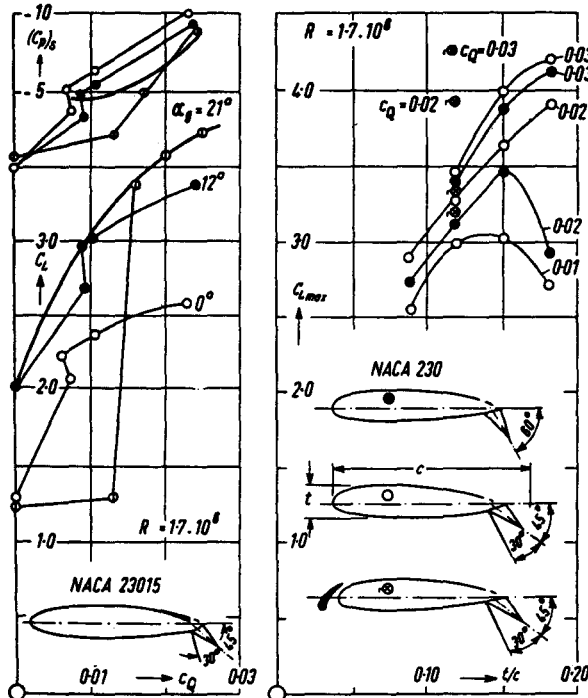


Fig. 6.1. Suction behind a flap, on profiles with hinged and split flaps ( $\alpha_g$  = geometrical angle of incidence). (AVA)

Fig. 6.2.  $C_{L_{\max}}$  as a function of profile thickness, for various volume-flow-rate coefficients. (AVA)

is used (negative when the pressure is less than the free-stream pressure).

The older experiments on boundary-layer suction (by BETZ, ACKERET, and SCHRENK) were concerned with the generation of high lift, in conformity with the state of aircraft development at that time. For practical application it seemed advantageous to use a wing with a flap and apply suction at the flap; this arrangement has been more accurately investigated by SCHRENK and REGENSCHEIT, and they obtain better results by sucking through two slots, one slot lying in front of and the other behind the flap (Figure 6.1). In this way maximum lift coefficients,  $C_{L_{\max}}$ , greater than 3.5 are obtained, and the volume-flow-rate coefficient has a practical value ( $c_Q < 0.02$ ). The suction aircraft of the AVA (AF1 and AF2) have been tested in flight by STÜPER; an increase in  $C_{L_{\max}}$  of about 1.5 is obtained (from  $C_{L_{\max}} = 2.6$  without suction to  $C_{L_{\max}} = 4.1$  with suction); suction is applied at a flap, the value of  $c_Q$  being 0.02.

From Figure 6.1 it is seen that the behaviour of  $C_{L_{\max}}$  with increasing  $c_Q$  is usually as follows: at first there is a sharp rise in  $C_{L_{\max}}$ , up to a value of about 3; a relatively small increase follows, despite the application of a large amount of suction. From theoretical calculations of the point of separation of the turbulent boundary layer it is found that, in the range of  $c_Q$  corresponding to the steep rise in  $C_{L_{\max}}$ , there is no danger of separation before the point at which suction is applied (that is, before the flap); consequently, in this range the only purpose of suction is to guide the flow past the flap and to keep the flow attached despite the adverse pressure gradient existing on the suction side of the flap. In the range of  $c_Q$  corresponding to the shallow rise in  $C_{L_{\max}}$  (that is, for values of  $C_{L_{\max}}$  greater than 3), the adverse pressure gradient on the front part of the profile is so great that a danger of separation exists before the point at which suction is applied; with suction, separation is prevented by a reduction in the pressure gradient on the front part of the profile, the reduction being produced by the sink effect of the suction; the reduction in the pressure gradient has a noticeable effect only at large values of  $c_Q$ , so that small increases in  $C_{L_{\max}}$  require a relatively large amount of suction.

The influence of profile thickness has been investigated by REGENSCHEIT for the profile series NACA 230 at a Reynolds number of  $1.7 \cdot 10^6$  (Figure 6.2). If the volume-flow-rate coefficient is kept constant,  $C_{L_{\max}}$  at first

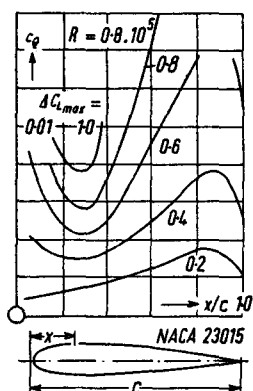


Fig. 6.3. Influence of position of suction slot on the  $c_Q$  necessary for a certain increase in  $C_{L_{\max}}$ . Profile: NACA 23015

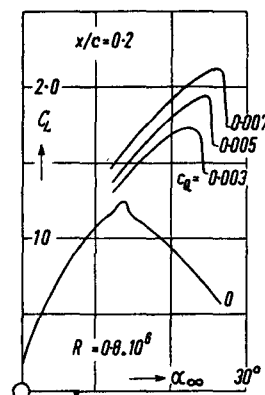


Fig. 6.4.  $C_{L_{\max}}$  corresponding to the most favourable position of suction slot. Profile: NACA 23015

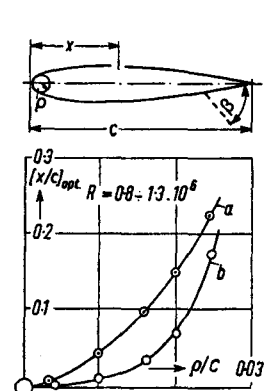


Fig. 6.5. Influence of nose radius  $r$  (see Equation (1.7)) on the most favourable position of suction slot (with split flap):  
(a) for increasing  $C_{L_{\max}}$ ;  
(b) for increasing  $\alpha C_{L_{\max}}$ .

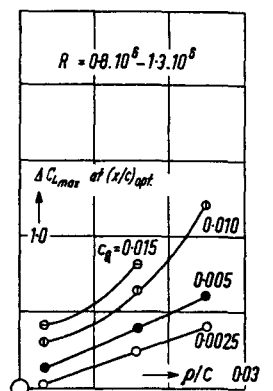


Fig. 6.6. Influence of nose radius  $r$  on the increase in  $C_{L_{\max}}$ , when the suction slot is at the most favourable position (no flap-deflection)

increases with thickness ratio; it reaches its greatest value at a definite thickness ratio (dependent on  $c_Q$ ). Profiles without suction behave similarly. For the still practical value  $c_Q = 0.02$ , the favourable thickness ratio lies between 0.15 and 0.20. WALZ has investigated theoretically and experimentally the influence of the position of a single suction slot; the profiles have a split flap but no plain flap; the results are shown in Figures 6.3 to 6.6. From these investigations and from further measurements by REGENSCHEIT and EHLERS it appears that there are two places on the profile where suction is most advantageously applied. One of these favourable positions lies at the point where, at the required value of  $C_{L_{\max}}$ , separation would occur in the absence of suction; separation is prevented by removing from the boundary layer fluid which is deficient in energy. According to a proposal of WALZ, for the practical

application of this result on profiles with a flap there must be a further suction slot in either the middle or the forward part of the profile so that the behaviour of  $C_{L_{\max}}$  with  $c_Q$  can be improved near  $C_{L_{\max}} = 3.0$ . Using the first of these arrangements QUINN has been able to increase the lift of a wing with a double-slotted flap from  $C_{L_{\max}} = 3.5$  to  $C_{L_{\max}} = 3.68$  when  $c_Q = 0.024$ , and to  $C_{L_{\max}} = 4.16$  when  $c_Q = 0.04$ .

According to REGENSCHEIT, the other favourable position for a suction slot is the trailing edge of the profile. Removal of portions of the boundary layer is then of no importance; the change in the flow is caused only by the sink effect of the suction, and can therefore be treated by potential theory. Figures 6.7 and 6.8 come from theoretical calculations by EHLERS for the flat plate; they show the

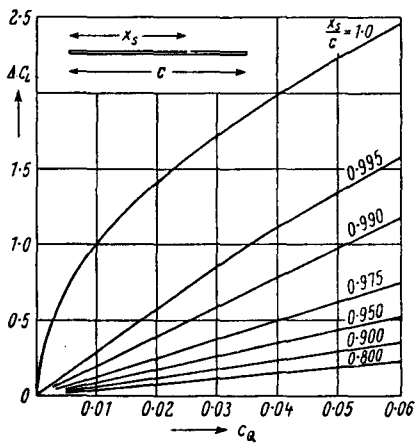


Fig. 6.7. Influence of position of suction slot on the increase in lift obtained for a given volume-flow-rate coefficient. Flat plate (theoretical)

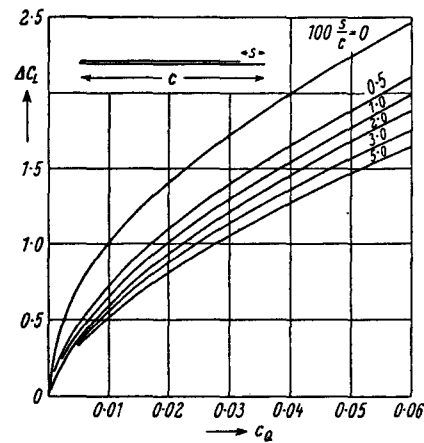


Fig. 6.8. Influence of width of suction slot, for suction at the trailing edge. Flat plate (theoretical)

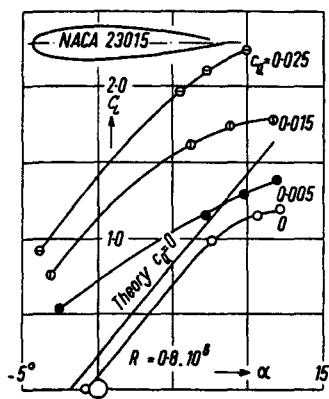


Fig. 6.9.  $C_L$  plotted against  $\alpha$  for various  $c_Q$ , for suction at the trailing edge

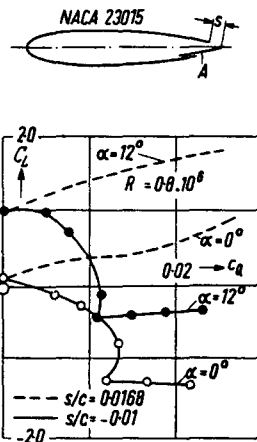


Fig. 6.10. Control by suction at the trailing edge

very large effectiveness of a suction slot at the trailing edge with small values of  $c_Q$ . These calculations and the experimental investigations of REGENSCHEIT confirm that suction at the trailing edge, with a suitable shape of slot, can produce an increase in the lift, no change in the angle of incidence being required;  $\Delta C_L$  is of the order of 1 (see Figures 6.9 and 6.10). The particular advantage of this system is that a value of  $C_{L_{max}}$  can easily be reached at which the pressure gradient on the front of the profile would have led to separation in the absence of suction;

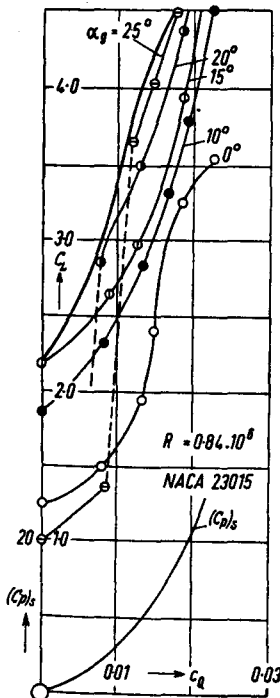
hence, it seems that trailing edge suction is particularly suitable for control purposes, a possibility that has been investigated by THWAITES.

These investigations demonstrate the rather small influence of the shape and width of the suction slot on the effectiveness of suction, apart from trailing edge suction. No systematic measurements on the influence of Reynolds number exist; it might be expected that the required amounts of suction and power decreases as the Reynolds number increased (because of the decrease in boundary layer thickness), but this has not been confirmed by the American measurements made up till now.

## 6.2 Blowing as a Means of Increasing the Lift

Following older, more tentative experiments, SCHWIER has investigated an arrangement for blowing, which is fitted to a profile with a slotted flap; air is blown out over the flap through a slot at the trailing edge. The results are equally as good as and sometimes better than those obtained with the corresponding arrangement using suction and a plain flap (Figures 6.11 and 6.12).

However, the measurements for small values of the volume-flow-rate coefficient usually show only a tiny change in lift (assuming the angle of incidence is kept constant). The lift increases rapidly with  $c_Q$  only if  $c_Q$  is large (greater than 0.01); this is because the air blown out has a favourable effect on the outer flow only if it has approximately the same speed as the flow. Clearly, the



Figs. 6.11 and 6.12. Blowing behind a flap, on profiles with a hinged flap ( $\alpha_g$  = geometrical angle of incidence). (AVA)

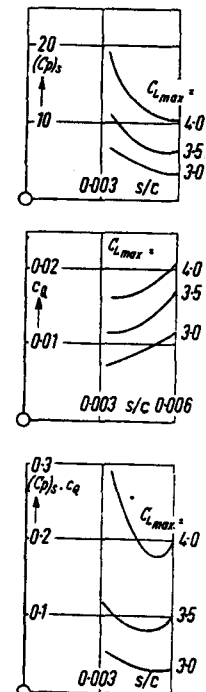
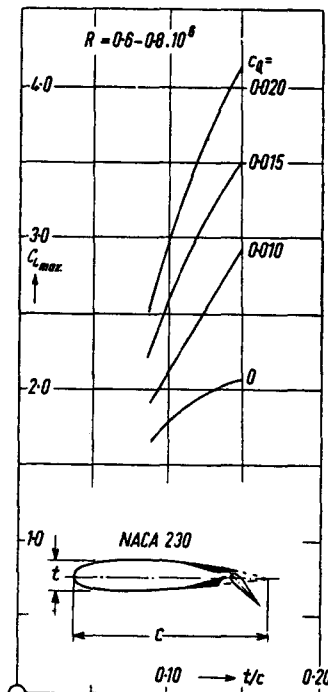


Fig. 6.13. Influence of width of blowing slot

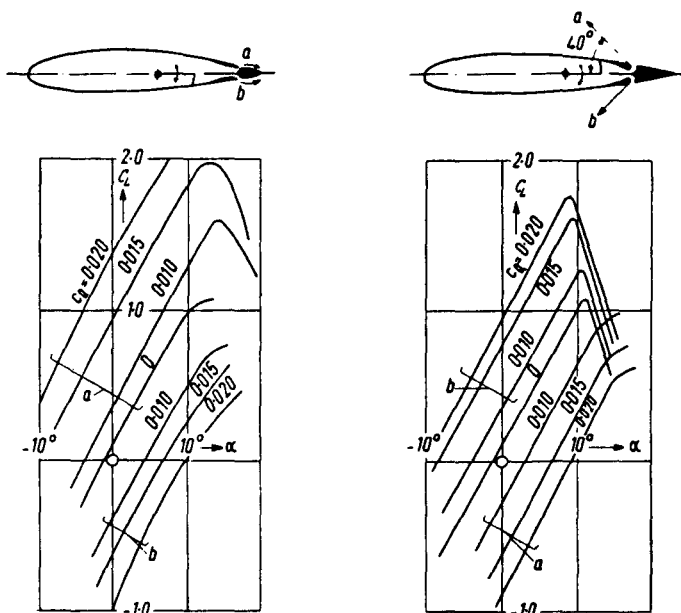


Fig. 6.14. Control by blowing over a rounded trailing edge. Blowing can be performed on either the suction side (a) or the pressure side (b). (AVA)

Fig. 6.15. Control by blowing against the flow direction. Blowing can be performed on either the suction side (a) or the pressure side (b). (AVA)

value of  $c_Q$  required to produce a certain increase in  $C_{L_{\max}}$  becomes smaller as the width of the slot decreases (that is, as the blowing speed increases). In contrast to suction the value of  $c_Q$  required to produce a certain increase in lift is always dependent on the width of the slot: the narrower the slot, the more effective the blowing; however, the required pressure and power ( $(C_p)_s c_Q$ ) increase (see Figure 6.13).

Another form of blowing that results in an increase in  $C_{L_{\max}}$ , but which does not directly influence the boundary layer, is the blowing of a jet of air out of the profile on the pressure side (a proposal of BETZ). This produces an effect similar to that of a split flap [UM 3192]; the necessary value of  $c_Q$  is relatively high (Figures 6.14 and 6.15).

### 6.3 Suction as a Means of Reducing Drag

#### 6.3.1 Keeping the Boundary Layer Laminar

Suction is frequently used to keep the boundary layer laminar; the present state of the theory on this subject is described in Chapter 9. Theoretical work usually assumes continuous suction, which can be easily visualised physically; it is of great practical interest, being theoretically the most efficient form of suction. With continuous suction (for example, on a flat plate) gains in performance of 50% and more are possible, the gains being particularly large at high Reynolds numbers.

To reduce the technical difficulties, suction through a number of slots has been tried as a means of keeping the boundary layer laminar. It has even been found possible to make the boundary layer stay laminar by a special design of profile, which leads to a pressure distribution favourable right to the trailing edge (with the exception of the slot itself); this is illustrated in Figure 6.16 (GOLDSTEIN). HOLSTEIN and, independently, ACKERET, RAS, and PFENNINGER were the first to demonstrate that gains in performance can be realised which are of practical value, but that the number and position of the simultaneously operated suction slots must be carefully chosen. Some of these results are quoted in Table 6.1.

Table 6.1. Measurements by HOLSTEIN on the Kármán-Trefftz Profile 0015, with Suction to Keep the Boundary Layer Laminar;  $R = 1 \cdot 6 \cdot 10^6$

$C_L$	Without suction. $10^3 C_D$	With suction at $(C_P)_{\min}$ . (see Equation (6.6a))				Percentage reduction.
		$u$ , upper; $l$ , lower.	$10^3 C_D$	$10^4 c_Q$	$10^3 C_P$	
		Open slot at $x/c =$				
0	6.75	0.4u	5.40	3.3	5.85	20 13
0	6.75	0.4u 0.4l	4.23	5.9	4.94	37 27
0	6.75	0.4u 0.6u	5.12	5.9	5.84	24 13
0.09	7.85	0.3u 0.5u 0.7u	4.95	11.8	6.30	37 20
0.09	7.85	0.4l 0.6l	6.70	4.4	7.10	15 10
0.23	7.35	0.2u 0.4u 0.6u	4.52	9.4	5.64	38 23
0.23	7.35	0.4l 0.6l	6.34	4.0	6.70	14 9

In all these tests a result of fundamental significance is obtained: it is possible to increase the length of laminar boundary layer by suction only if the suction slot lies in

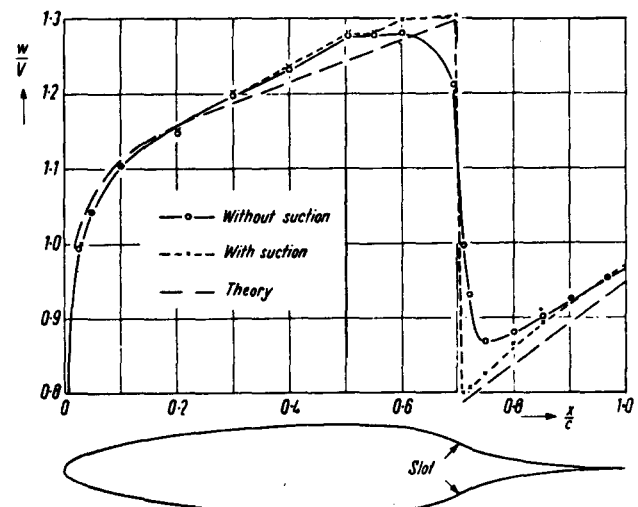


Fig. 6.16. Profile with a suction slot, the pressure rise being displaced rearwards to the slot; designed by GOLDSTEIN

the original laminar boundary layer (it is then certainly possible, even with an adverse pressure gradient). Once the boundary layer has become turbulent it seems impossible to bring it back to a laminar state by suction (in agreement with older measurements by GERBER). Investigations on the effect of the number of suction slots and the distances between them lead to the important result that, as the Reynolds number increases, so also does the number of suction slots necessary to achieve worthwhile gains. The exhaustive measurements show that considerable reductions can be obtained with relatively small amounts of suction if the number of slots is sufficiently large (see also Figure 6.17).

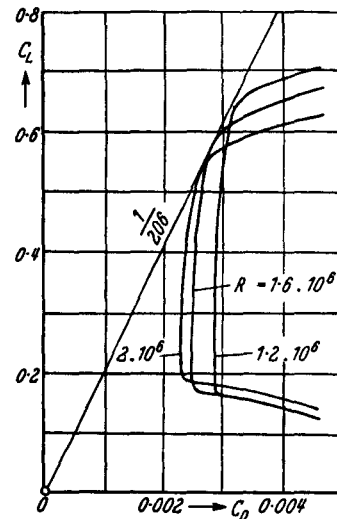
In the present stage of technology the manufacture of a wing with a large number of suction slots (or, better still, the realisation of continuous suction) would be extraordinarily difficult; however, the large gains in performance predicted by theory for continuous suction provide a strong stimulus to look for solutions of this technical problem. Some progress has already been made: of particular interest are successful experiments (RASPET) with a specially designed sailplane; and, above all, the results obtained by BRASLOW and others [R1025] on a wing with a porous surface made from sintered bronze (Figure 6.18).

Suction applied to the boundary layer at higher Mach numbers is of particular importance; this is confirmed by one of the first experiments in this field, carried out by REGENSCHEIT; the results are shown in Figure 6.19.

### 6.3.2 Control of the Turbulent Boundary Layer

The technical difficulties of an attempt to reduce the drag by controlling a turbulent boundary layer are expected to be smaller than in an attempt to reduce the

Fig. 6.17.  $C_L$  plotted against  $C_{D,\text{tot}}$  (which includes power consumed in turbine) at several Reynolds numbers, for a laminar suction profile designed by Pfenniger. Profile with 12 slots on the suction side and 10 on the pressure side.  $\frac{t}{c} = 0.105$ ;  $f_c = 0.019$ ;  $q_s = 1.04$  (see Equation (1.7)); no coordinates available. Total  $c_q$  in all cases less than 0.0016. Wind tunnel: Zurich



drag by keeping the boundary layer laminar. We can obtain either a reduction in the form drag by sucking away the boundary layer in the region of the trailing edge, or a reduction in the turbulent skin-friction drag by blowing away the more slowly moving air (following a proposal by BETZ). The latter case has yet to be investigated, but results exist for the former one.

In the region behind a suction slot the thinning of the boundary layer (when this is not kept laminar) always increases the skin-friction drag and decreases the form drag; the nearer the suction slot is to the trailing edge, the less is the disadvantage of the increased skin-friction drag; the gains in performance are expected to be largest if the suction slot can be placed at the trailing edge. Measurements by WALZ [FB 1611] on the profile NACA 23015 at the small Reynolds number of  $0.8 \cdot 10^6$  show a gain in performance of about 7% for an arrangement in which the

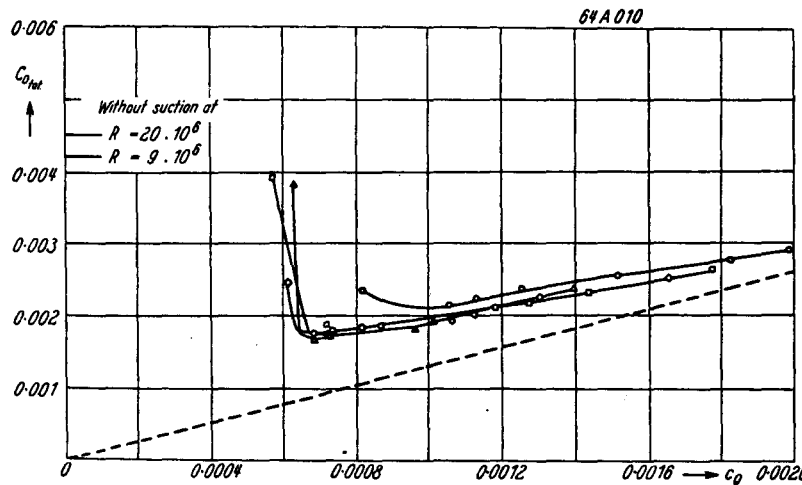


Fig. 6.18. Drag of the profile NACA 64A010 with porous surface, at  $C_L = 0$ , as a function of volume-flow-rate coefficient,  $c_q$ . Wind tunnel: TDT. Reynolds number:  $5.9 \cdot 10^6$  ( $\circ$ );  $12 \cdot 10^6$  ( $\square$ );  $18.8 \cdot 10^6$  ( $\diamond$ ). Full line is total drag. Dashed line is portion of drag arising from suction;  $(C_D)_s = 1.32$

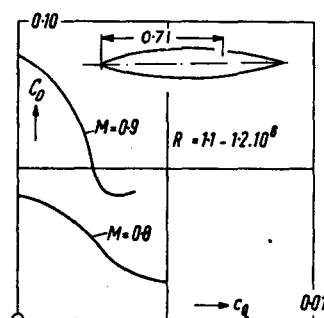


Fig. 6.19. Reduction in drag of profile by suction at higher Mach numbers. Profile: circular arc with rounded leading edge. Reynolds number:  $1.1 \cdot 10^6$  to  $1.2 \cdot 10^6$ . (AVA)

suction slot is at approximately 95% of the chord ( $C_L \approx 0$ ). REGENSCHEIT [FB 1550] has carried out other measurements, at  $R = 2.2 \cdot 10^6$ , with an arrangement in which a suction slot is placed exactly at the trailing edge, the opening of the slot lying on the suction side (Figure 6.20).

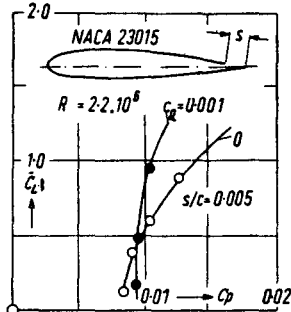


Fig. 6.20. Improvement of polars by suction at the trailing edge.  
 $C_{D_{\text{tot}}} = C_D + c_Q[1 - (C_p)_s]$

In contrast to the results of WALZ a gain in performance occurs only for values of  $C_L$  greater than 0.4; at  $C_L = 1$  it amounts to roughly 25% (referred to  $C_D$ ). The arrangement of the suction slot at the trailing edge has the great advantage that an increase in  $C_{L_{\max}}$  can be achieved at take-off and landing with the same suction slot.

Although the control of the turbulent boundary layer as a method for drag reduction still seems problematic at low lift coefficients, it is undoubtedly of considerable importance at larger values of  $C_L$ , and so is suitable for improving polars. The suction is particularly effective if the slot is placed immediately behind the nose (or the suction peak), and is supported by an independent slot in the middle of the wing; this is demonstrated in Figure 6.21.

#### 6.4 Pressure and Power Requirements for Boundary Layer Control

In a report on suction measurements it is customary to give the requisite suction pressure,  $p_s$ , in a dimensionless form by referring it to the kinetic pressure  $q$  according to Equation (6.2);  $p_s$  is the pressure necessary to draw the sucked air into the interior of the wing. The separate portions of  $p_s$  are the static pressure,  $p$ , in the outside flow at the point of suction (in general, lower than the free stream pressure), and the loss in pressure,  $p_l$ , caused when the sucked air is drawn through the slot into the interior of the wing. Hence, we have

$$(C_p)_s = \frac{p_s}{q} = \frac{p}{q} + \frac{p_l}{q}. \quad (6.2a)$$

The sucked air moves into the interior of the wing with a small speed, because of the generally large cross-section of the interior; hence, the "slot loss" is approximately equal to the kinetic pressure formed with the speed in the slot,

$$v_l = c_Q \frac{V}{ks/c},$$

and can be written as

$$\frac{p_l}{q} = \left( \frac{v_l}{V} \right)^2 = \frac{c_Q^2}{(ks/c)^2}. \quad (6.3)$$

The factor  $k$  ( $0 \leq k \leq 1$ ) appears in this expression because the width of the slot,  $s$ , is not wholly effective; the loss in efficiency is caused by separation at the sharp edges of the entrance; in the suction measurements carried out in Göttingen  $k$  is usually between 0.3 and 0.5.

If the sucked air is blown out in the free-stream direction with a velocity  $v_b$ , then the power,  $P_s$ , required for the suction is given by

$$\begin{aligned} P_s &= -Q p_s + Q \frac{\rho}{2} v_b^2 \\ &= c_Q \left[ \left( \frac{v_b}{V} \right)^2 - (C_p)_s \right] \frac{\rho}{2} V^3 S. \end{aligned} \quad (6.4)$$

To decide whether suction, when it is used to reduce drag, does result in a saving of power, we must consider the sum of the power required to overcome the drag,  $VD = C_D \frac{\rho}{2} V^3 S$ , and the power required for the suction; the sum is

$$P = \left\{ C_D + c_Q \left[ \left( \frac{v_b}{V} \right)^2 - (C_p)_s \right] \right\} \frac{\rho}{2} V^3 S. \quad (6.5)$$

We now introduce the power-consumption coefficient,  $C_P$ ; this is defined by

$$C_D + c_Q \left[ \left( \frac{v_b}{V} \right)^2 - (C_p)_s \right] = C_P. \quad (6.6)$$

It can be verified that  $C_P$  has a minimum when  $v_b = V$  (see SCHRENK), so that

$$(C_P)_{\min.} = C_D + c_Q[1 - (C_p)_s]. \quad (6.6a)$$

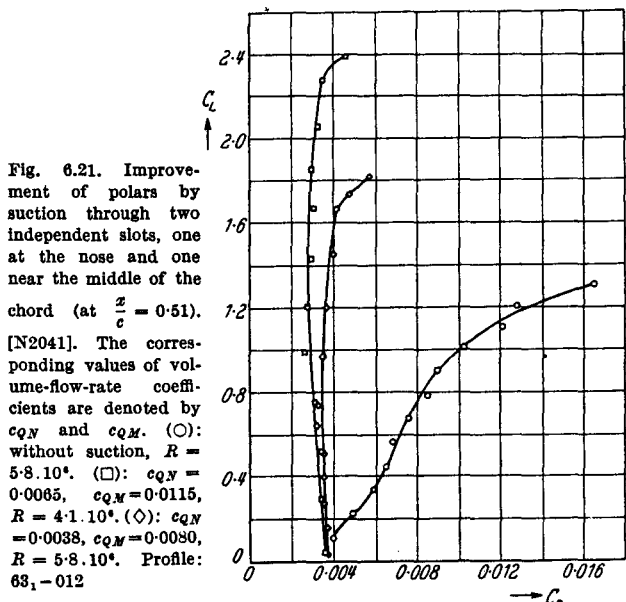


Fig. 6.21. Improvement of polars by suction through two independent slots, one at the nose and one near the middle of the chord (at  $\frac{x}{c} = 0.51$ ).

[N2041]. The corresponding values of volume-flow-rate coefficients are denoted by  $c_{Q,N}$  and  $c_{Q,M}$ . (O): without suction,  $R = 5.8 \cdot 10^6$ . (□):  $c_{Q,N} = 0.0085$ ,  $c_{Q,M} = 0.0115$ ,  $R = 4.1 \cdot 10^6$ . (◊):  $c_{Q,N} = 0.0038$ ,  $c_{Q,M} = 0.0080$ ,  $R = 5.8 \cdot 10^6$ . Profile: 63-012

In the analysis of drag measurements for profiles with boundary layer control it is usually assumed that  $C_p$  has this minimum value; it is occasionally referred to as the total drag coefficient ( $C_{D_{tot}}$ ).

In the practical application of boundary layer control to an aircraft, additional losses (increasing rapidly with  $c_Q$ ) arise in the ducting and the pump; these pipe losses can be essentially greater than the power required to suck the air into the interior of the wing (particularly for large values of  $c_Q$ ). When values of  $(C_p)_s$  obtained from wind-tunnel measurements are used in calculations, the calculations have meaning only if  $c_Q$  is very small (for example, when the suction is used to reduce drag). For further estimates of the pressure and power requirements on an aircraft with boundary layer control the reader is referred to the exhaustive work of KRÜGER.

## 6.5 References

- ACKERET, J.: Grenzschichtabsaugung. Z. VDI 35 (1926) 1153.  
 — M. RAS and W. PENNINGER: Verhinderung des Turbulentewerdens einer Reibungsschicht durch Absaugung. Naturw. (1941), S. 622.
- BAMBER, M. J.: Wind-Tunnel Tests on Airfoil Boundary Layer Control Using a Backward-opening Slot. NACA Rep. No. 385 (1931).
- BEAVAN, J. A.: Note on Reynolds and Mach Number Effects on the Pressure Distribution on the Tail of EC 1250. R & M No. 2252 (1943).
- BETZ, A.: Die Wirkungsweise von unterteilten Flügelprofilen. Berichte und Abhandlungen der WGL (1922), Heft 6.
- Beeinflussung der Reibungsschicht und ihre praktische Verwertung. Schriften der Deutschen Akademie der Luftfahrtforschung, Heft 49 (1941).
- Neue Ergebnisse der Auftriebsbeeinflussung von Flügeln. DAL 1047 (1942).
- BRASLOW, A. L., D. L. BURROWS, N. TETERVIN and F. VISCONTI: Exp. and Theoret. Studies of Area Suction for the Control of the Laminar Boundary Layer on an NACA 64A010 Airfoil. NACA Rep. 1025 (1951).
- CHEERS, F. and O. DOUGLAS: Tests on a Glauert Nose-suction Aerofoil in the N.P.L. 4-ft. No. 2 Wind-Tunnel. R & M No. 2356 (1947).
- CHEERS, F., W. G. RAYMER and O. DOUGLAS: Tests on a 'Lighthill' Nose-suction Aerofoil in the N.P.L. 4-ft. No. 2 Wind-Tunnel. R & M No. 2355 (1951).
- DANNENBERG, R. and WEIBERG, J.: Effect of Type of Porous Surface and Suction Velocity Distribution on Characteristics of a 10.5% thick Airfoil with Distributed Suction over the Nose. NACA TN 3093 (1953).
- DOENHOFF, A. E. v. and LOFTIN, L. K.: Present Status of Research on Boundary-Layer Control. J. Aeron. Sci. 16 (1949), p. 729.
- EHLERS, F. and W. SCHWIER: Blasversuche an einem Flügel mit Spaltklappe. FB 1247 (1940).
- EHLERS, F.: Über die Änderung des Auftriebes und der Druckverteilung an Absaugeflügeln durch Senkenwirkung. AVA-Bericht 45/W/15 (1945).
- GAINER, TH. G.: Low-Speed Wind-Tunnel Investigation to Determine the Aerodynamic Characteristics of a Rectangular Wing Equipped with a Full-Span and an Inboard Half-Span Jet-Augmented Flap Deflected 55°. NASA MEMO 1-27-59L (1959).
- GERBER, A.: Untersuchungen über Grenzschichtabsaugung. Mitteilungen aus dem Institut für Aerodynamik der E.T.H. Zürich Nr. 6 (1938).
- GLAUERT, M. B.: The Design of Suction Aerofoils with a Very Large  $C_L$ -range. R & M No. 2111 (1945).
- W. S. WALKER and W. G. RAYMER: Wind-Tunnel Tests on Thick Suction Aerofoil with a Single Slot. R & M No. 2646 (1947).
- GOLDSTEIN, S.: Low-drag and Suction Airfoils. J. Aeron. Sci., 15 (1948), pp. 189—214.
- GREGORY, N. and W. S. WALKER: Further Wind-Tunnel Tests on a 36% Symmetrical Suction Aerofoil with a Movable Flap. R & M No. 2287 (1946).
- GREGORY, N., W. S. WALKER and W. G. RAYMER: Wind-Tunnel Tests on the 30% Symmetrical Griffith Aerofoil with Ejection of Air at the Slots. R & M No. 2475 (1946).
- GREGORY, N.: Note on Sir Geoffrey Taylor's Criterion for the Rate of Boundary Layer Suction at a Velocity Discontinuity. R & M No. 2496 (1947).
- Further Observations on the Boundary Layer Theory of Suction Aerofoils. R & M No. 2577 (1948).
- Addendum to ARC 10-854 (Tests on Glas II). ARC 11797.
- W. S. WALKER and A. N. DEVEREUX: Wind-Tunnel Tests on the 30% Symmetrical Griffith Aerofoil with Distributed Suction over the Nose. R & M No. 2647 (1948).
- and A. R. CURTIS: A Comparison of Three Thick, Symmetrical, Multi-slot Suction Aerofoils. C. P. 20 (1950).
- R. C. PANKHURST and W. S. WALKER: Wind-Tunnel Tests on the Prevention of Boundary-layer Separation by Distributed Suction at the Rear of a Thick Aerofoil. R & M No. 2788 (1950).
- and W. S. WALKER: Wind-Tunnel Tests on the NACA 63 A 009 Aerofoil with Distributed Suction over the Nose. R & M No. 2900 (1955).
- HOLSTEIN, H.: Auftriebsmessungen an einem Flügel mit Absaugung durch Düsenwirkung. FB 1253 (1940).
- HOLSTEIN, H.: Messung zur Laminarhaltung der Grenzschicht durch Absaugung an einem Tragflügel. LGL S 10 (1941), S. 17—27.
- HOLSTEIN, H. and A. DONEIS: Messungen an einem Laminarprofil mit extremer Rücklage des Druckminimums. FB 1522 (1941).
- Messungen zur Laminarhaltung der Reibungsschicht durch Absaugen an einem Tragflügel mit dem Profil NACA 0012—64. FB 1654 (1942).
- HORTON, E. A., S. F. RACISZ and N. I. PARADISO: Investigation of Boundary-Layer Control to Improve the Lift and Drag Characteristics of the NACA 65<sub>2</sub>—415 Airfoil Section with Double-Slotting and Plain Flaps. NACA TN 2149 (1950).
- KNIGHT, M. and M. J. BAMBER: Wind-tunnel Tests on Airfoil Boundary Layer Control Using a Backward Opening Slot. NACA TN No. 323 (1929).
- KRÜGER, H.: Über den Einfluß der Absaugung auf die Lage der Umschlagstelle an Tragflügelprofilen. Ing.-Arch., 19. Bd. (1951), S. 384—387.
- KRÜGER, W.: Rechnerische und experimentelle Untersuchung zur Frage des Förderleistungsbedarfes von Flugzeugen mit Grenzschichtbeeinflussung. FB 1618 (1942).
- Windkanalmessungen am Absaugeklappenflügel 23012 mit Vorflügel. FB 1623 (1942).

- LACHMANN, G. V.: Boundary Layer Control. *J. Roy. Aero. Soc.* 59 (1955), pp. 163—198 und Jahrb. 1953 d. Wiss. Ges. Luftf., S. 132—143.
- Grenzschichtsteuerung in der Praxis. *Z. Flugwiss.* 4 (1956), S. 9—14.
- LIGHTHILL, M. J.: A Theoretical Discussion of Wings with Leading Edge Suction. *R & M No.* 2162 (1945).
- LOFTIN, L. K. and D. L. BURROWS: Investigations Relating to the Extension of Laminar Flow by Means of Boundary-Layer Suction through Slots. NACA TN 1961 (1949).
- MCCULLOUGH, G. B. and D. E. GAULT: An Experimental Investigation of the NACA 63<sub>1</sub>—012 Airfoil Section with Leading-Edge and Midchord Suction Slots. NACA TN 2041 (1950).
- PANKHURST, R. C., W. G. RAYMER and A. N. DEVEREUX: Wind-Tunnel Tests of the Stalling Properties of an 8% Thick Symmetrical Section with Uniformly Distributed Nose Suction. *R & M No.* 2666 (1946).
- PANKHURST, R. C. and N. GREGORY: Power Requirements for Distributed Suction for Increasing Maximum Lift. *C. P.* 82 (1948).
- PEARCEY, H. H. and E. W. E. ROGERS: The Effect of Compressibility on the Performance of a Griffith Aerofoil. *R & M No.* 2511 (1946).
- PFENNINGER, W.: Untersuchungen über Reibungsverminde rungen an Tragflügeln, insbesondere mit Hilfe von Grenzschichtabsaugung. Mitteilg. a. d. Inst. f. Aerodynamik E.T.H. Zürich Nr. 13 (1946).
- Experiments on a Laminar Suction Airfoil of 17 Percent Thickness. *Journ. Aeron. Sci.* 16 (1949), pp. 227—236.
- PRESTON, J. H.: The Boundary Layer Flow over a Permeable Surface through which Suction is Applied. *R & M No.* 2244.
- W. S. WALKER and C. R. TAYLOR: The Effect on Drag of the Ejection of Air from Backward Facing Slots on a 16·2% Griffith Aerofoil. *R & M No.* 2108 (1946).
- PRETSCH, J.: Die Leistungsersparnis durch Grenzschichtabsaugung beim Schleppen einer ebenen Platte. *UM* 3048 (1943).
- Umschlagbeginn und Absaugung. *Jahrb.* 1942 I, S. 1/7.
- QUINN, J. H. jr.: Tests of the NACA 65<sub>3</sub>-018 Airfoil Section with Boundary-layer Control by Suction. NACA CB No. L4H10 (1944) WR L-209.
- Wind-Tunnel Investigation of Boundary-layer Control by Suction on the NACA 65<sub>3</sub>-418,  $a = 1.0$  Airfoil Section with a 0·29 Airfoil-chord Double Slotted Flap. NACA TN No. 1071, 1946.
- Tests of the NACA 64<sub>1</sub>A212 Airfoil Section with a Slat, a Double Slotted Flap, and Boundary-layer Control by Suction. NACA TN No. 1293, 1947.
- RASPET, A.: Boundary-layer Studies on a Sailplane. *Aer. Eng. Rev.* 11 (1952) 52.
- REGENSCHEIT, B.: Hochauftriebsversuche mit Absaugeklappenflügeln. Bericht A 64 der LGL (1938).
- and O. SCHRENK: Versuche mit Absaugeflügeln verschiedener Profilwölbung und Wölbungslage. FB 1061 (1939).
- Systematische Untersuchungen von Absaugeklappenflügeln. Messungen an den Profilen 23015, 23018, 6215 g, 6218 g. FB 1221 (1940).
- Versuche zur Widerstandsverringerung eines Flügels bei hoher Machscher Zahl durch Absaugung der hinter dem Gebiet unstetiger Verdichtung abgelösten Grenzschicht. FB 1424 (1941).
- Messungen mit und ohne Knicknase an einem Absaugeklappenflügel NACA 23015. FB 1312 (1941).
- Versuche zur Verringerung des Tragflügelwiderstandes durch Hinterkantenabsaugung. FB 1550 (1942).
- Untersuchungen an einem Flügel mit Hinterkantenabsaugung. FB 1594 (1942).
- Absaugeklappenflügel 23009: FB 1555; 23012: FB 1543; 23015: FB 1591; 23018: FB 1639 (1942).
- Versuche zur Verringerung des Tragflügelwiderstandes durch selbsttätige Absaugung. FB 1673 (1942).
- Versuche an einem Flügel mit einer Klappe geringer Tiefe und selbsttätiger Absaugung. UM 3053 (1943).
- Versuche über eine neue strömungstechnische Steuerung. UM 3104 (1944).
- Messungen am Absaugeklappenflügel NACA 23015 mit 10 und 15% Klappentiefe. FB 1763 (1943)—und 43015: FB 1763/2 (1944).
- Eine neue Anwendung der Absaugung zur Steigerung des Auftriebes eines Tragflügels. FB 1474 (1941).
- Absaugung in der Flugtechnik. Jahrbuch 1952 der Wissenschaftlichen Gesellschaft für Luftfahrt, Braunschweig 1953.
- RICHARDS, E. J., W. S. WALKER and R. J. GREENING: An Aerofoil Designed to give Laminar Flow over the Whole Surface with Boundary Layer Suction. *R & M No.* 2263 (1943).
- RICHARDS, E. J.: Tests on a Griffith Aerofoil in the 13 ft. × 9 ft. Wind-Tunnel. Part I—Wind-Tunnel Technique and Interim Note. *R & M No.* 2148 (1944).
- RICHARDS, E. J., W. S. WALKER and J. R. GREENING: 13 ft. × 9 ft. Wind-Tunnel Tests on a Griffith Aerofoil. Part II — Effect of Concavity on Drag. *R & M No.* 2148 (1944).
- and W. S. WALKER: 13 ft. × 9 ft. Wind-Tunnel Tests on a Griffith Aerofoil. Part III—The Effect of Wide Slots and of Premature Transition to Turbulence. *R & M No.* 2148 (1944).
- 13 ft. × 9 ft. Wind-Tunnel Tests on a Griffith Aerofoil Part IV—Lift, Drag, Pitching Moments and Velocity Distributions. *R & M No.* 2148 (1944).
- W. S. WALKER and C. R. TAYLOR: Wind-Tunnel Tests on a 30% Suction Wing (Replacing 8473). *R & M No.* 2149 (1945).
- and C. H. BURGE: An Aerofoil Designed to Give Laminar Flow over the Whole Surface with Boundary-Layer-Suction. *R & M No.* 2263 (1949).
- REID, E. G. and M. J. BAMBER: Preliminary Investigation on Boundary Layer Control by Means of Suction and Pressure with the U.S.A. 27 Airfoil. NACA TN No. 286 (1928).
- SCHLICHTING, H.: Die Grenzschicht an der ebenen Platte mit Absaugen und Ausblasen. *Lufo* 19 (1940), S. 293.
- Die Grenzschicht mit Absaugung und Ausblasen. *Lufo* 19 (1942), S. 179.
- Berechnung der laminaren Grenzschicht mit Absaugung. LGL 141 (1941), S. 14—17 und DLG. Arch. 16 (1948), S. 201.
- and K. BUSSMANN: Exakte Lösungen für die laminare Grenzschicht mit Absaugung und Ausblasen. Schriften d. DAL Bd. 7B (1943), Heft 2, S. 25—69.
- SCHRENK, O.: Tragflügel mit Grenzschichtabsaugung. *Lufo* 2 (1928), S. 49 und 5 (1931), S. 634.
- Versuche mit Absaugeflügeln. *Lufo* 9 (1935), S. 10.
- and F. EHLERS: Spaltklappenflügel mit Absaugung an der Hinterkante des Hauptflügels. FB 1064 (1938).
- Grenzschichtabsaugung. *Luftwissen* 7 (1940), S. 409.
- SCHWARTZBERG, M. A. and A. L. BRASLOW: Experimental Study of the Effects of Finite Surface Disturbances and Angle of Attack on the Laminar Boundary Layer of an NACA 64 A 010 Airfoil with Area Suction. NACA TN 2796 (1952).
- SCHWIER, W.: Fremde Arbeiten über Absaugung und Ausblasen. LGL A 64 (1938).
- Versuche zur Auftriebssteigerung durch Ausblasen von Luft an einem symmetrischen Profil mit Wölbungsklappe großer

- Tiefe. FB 1462 (1941).
- Auftriebsänderung durch Ausblasen von Luft. FB 1481 (1941).
- Absaugeversuche an einem Flügel mit einem Querruder geringer Tiefe. FB 1579 (1941).
- Ausblaseversuche zur Auftriebssteigerung an einem Flügel von 9% Dicke mit Vorflügel und Klappe. FB 1622 (1942).
- Versuche zur Auftriebssteigerung durch Ausblasen von Luft an einem Profil von 12% Dicke mit verschiedenen Klappenformen. FB 1658 (1942).
- Versuche über Widerstandsänderungen eines Tragflügels beim Ausblasen von erwärmer Luft. FB 1783 (1943).
- Blasversuche zur Auftriebssteigerung am Profil 23015 mit verschiedenen Klappenformen. FB 1865 (1943).
- Änderung von Auftrieb und Widerstand eines Tragflügels bei Luftaustritt auf der Flügelausgeseite. UM 3064 (1943).
- Auftriebsänderung durch einen auf der Flügeldruckseite ausgeblassener Luftstrahl. UM 3192 (1944).
- SPENCE, D. A.: The Lift Coefficient of a Thin Jet Flapped Wing. Proc. Roy. Soc. London A 238 (1956), pp. 46—68 and J. Aeron. Sci. 23 (1956), pp. 92—94.
- STÜPER, J.: Messungen und Flugerfahrungen an zwei Absaugeflugzeugen. FB 1821 (1942).
- THWAITES, B.: A Theoretical Discussion of High-Lift Aerofoils with Leading-edge Porous Suction. R & M No. 2242 (1946).
- On the Design of Aerofoils for which the Lift is Independent of the Incidence. R & M No. 2612 (1947).
- The Production of Lift Independently of Incidence. J. Roy. Aer. Soc. 52 (1948), pp. 117/24.
- ULRICH, A.: Theoretische Untersuchungen über die Widerstandersparnis durch Laminarerhaltung mit Absaugung. Schriften d. DAL 8B (1944) Heft 2.
- WALZ, A.: Messungen zur Erhöhung der Überziehsicherheit durch Absaugung im vorderen Profilteil (Messungen am Profil 0012 und zusammenfassende Auswertung früherer Messungen). AVA-Bericht 45/W/14 (1945).
- Theoretisches zur Absaugung der Reibungsschicht. FB 1775 (1943).
- Versuche mit Reibungsschichtabsaugung an einem Flügelprofil NACA 23015 bei verschiedenen Lagen des Absaugeschlitzes längs Flügeltiefe. FB 1611 (1942).
- WIEGHARDT, K.: Über das Ausblasen von Warmluft für Enteiser. KWI-Bericht (1943).
- WILLIAMS, J.: Some Investigations of the Stalling Properties of Some Thin Nose-suction Aerofoils. R & M No. 2693 (1952).
- Some Improvements in the Design of Thick Suction Aerofoils. C.P. 31 (1950).
- An Analysis of Aerodynamic Data on Blowing over Trailing Edge Flaps for Increasing Lift. C. P. No. 209 (1955).

## 7. THE THEORY OF WING PROFILES I

### Profile Shape and Pressure Distribution in Inviscid Incompressible Flow

#### 7.1 General Remarks

The velocity distribution on the surface of a profile is primarily determined by the distribution of curvature. In inviscid incompressible flow the velocities can theoretically be found for an arbitrary contour (see Section 8.2). If the flow is not initially regarded as inviscid, the velocity distribution can often be calculated theoretically (see Section 9.1) by correcting for viscous effects, although the necessary calculations are more lengthy. A calculation is always possible if the flow has not separated from the profile; it can frequently be carried out even if this requirement is not met.

Suppose the speed of the free stream is  $V$  and its pressure is  $p_\infty$ ; let the speed at a point on the profile contour be  $w$  and the pressure there be  $p$ . The pressure coefficient,  $C_p$ , is defined as the difference between the pressure on the profile and the free-stream pressure ( $\Delta p$ ) divided by the kinetic pressure  $q$ , where  $q = \frac{1}{2}\rho V^2$ ; it is given by Bernoulli's equation as

$$C_p = \frac{\Delta p}{q} = \frac{p - p_\infty}{q} = 1 - \left( \frac{w}{V} \right)^2. \quad (7.1)$$

The corresponding relationship for compressible flow is derived in Section 10.2.

Direct measurements of the pressure distribution, made by small pressure holes bored in the profile surface, show that the theoretical distribution is accurate enough for practical purposes, provided that the influence of viscosity has been allowed for (see Section 9.1). The theoretical values for inviscid flow provide a good basis for comparison of profiles; at small angles of incidence or for small lift coefficients, they are usually quantitatively satisfactory as well.

The pressure distributions given in Chapter 12 can be divided into three classes:

- (A) pressure distributions calculated on potential theory for inviscid incompressible flow, which agree approximately with experiment only at small lift coefficients and for moderately thick profiles;
- (B) pressure distributions calculated theoretically, with an allowance for the effect of viscosity, which agree well with experiment except in a region at the rear of

the profile, the length of this region being a small percentage of the chord;

- (C) experimental pressure distributions.

The velocity or pressure distributions for camber lines given in Section 7.2 and Chapters 11 and 12 are of type (A); those for thickness distributions in symmetrical flow ( $\alpha = 0$ ) given in Section 7.3 are also of type (A); those for symmetrical profiles at incidence or for cambered profiles in Chapter 12 are mostly of type (B). For a comparison between theory and experiment see Figure 12.27. Theoretical pressure distributions on profiles with flaps are much more difficult to obtain, because of the occurrence of separation; experimental results, type (C), have usually been chosen for these. Figures 12.35 and 12.36 compare theoretical and experimental pressure distributions on profiles with flaps at small and large lift coefficients, with and without separation.

In compressible flow at subsonic speed the pressures increase by a factor  $\frac{1}{\sqrt{1 - M^2}}$ , to a first approximation; they vary more rapidly as the speed of sound is approached, and if this is locally exceeded significant deviations from the simple rule are observed (see Section 10.3); the pressure distribution is also considerably altered, a feature that is treated in more detail in Section 10.4. In Chapter 12, pressure distributions at these Mach numbers are experimental results from wind tunnels (that is, of type (C)). If the free-stream speed is sufficiently greater than the speed of sound then the pressure distributions can again be determined theoretically with good accuracy, except for a small region on the upper side of the profile near the trailing edge (see Figures 12.48 and 12.49).

### 7.2 Camber Line and Velocity Distribution

We first consider inviscid incompressible flow. In the theoretical results of this and the next two sections the upper and lower signs refer to the upper and lower sides of the profile respectively.

#### 7.2.1 Simple Special Cases

If the free-stream speed is  $V$  then, from Section 8.2.1.2, we find for the local speed,  $w$ :

(a) on the surface of a flat plate at an angle of incidence  $\alpha$ ,

$$\frac{w}{V} = \cos \alpha \pm \sin \alpha \sqrt{\frac{c-x}{x}} \quad (0 \leq x \leq c); \quad (7.2)$$

if the angle of incidence is small,

$$\frac{w}{V} = 1 \pm \alpha \sqrt{\frac{c-x}{x}}; \quad (7.3)$$

(b) on a circular arc of small camber  $f$ , whose contour is given by the equation

$$\frac{y}{c} = 4 \frac{f}{c} \frac{x}{c} \left(1 - \frac{x}{c}\right) \quad (0 \leq x \leq c), \quad (7.4)$$

at the ideal angle of incidence,

$$\frac{w}{V} = 1 \pm 8 \frac{f}{c} \sqrt{\frac{x}{c} \left(1 - \frac{x}{c}\right)}; \quad (7.5)$$

(c) on a profile with a point of inflexion, whose contour is given by the equation

$$y = -\frac{8}{5} h \frac{x}{c} \left(1 - \frac{x}{c}\right) \left(1 - 2 \frac{x}{c}\right) \quad (7.6)$$

(where  $h$  is assumed small), at the ideal angle of incidence,

$$\frac{w}{V} = 1 \mp \frac{24}{5} \frac{h}{c} \left(1 - 2 \frac{x}{c}\right) \sqrt{\frac{x}{c} \left(1 - \frac{x}{c}\right)}. \quad (7.7)$$

## 7.2.2 Various Types of Camber Line

Some common camber lines are now described, and, where possible, the corresponding velocity distributions are given.

Of the two purely geometrical parameters, maximum camber ( $f/c$ ) and position of maximum camber ( $x_f/c$ ), the first is usually regarded as an affine scale-factor. For further parameters, aerodynamic quantities are generally used: the lift coefficient at the ideal angle of incidence,  $C_L^*$ —the “design  $C_L$ ” (see Sections 3.1 and 8.2.1.2); and the moment coefficient referred to a point fixed with respect to the profile—for example, the aerodynamic centre (Section 3.1). Other important quantities are the ideal angle of incidence,  $\alpha^*$ , and the angle of incidence at which the lift vanishes,  $\alpha_0$ .

*Type S<sub>1</sub>:* Birnbaum-Glauert camber lines.

The special cases (a) to (c) of Section 7.2.1 are known as the Birnbaum-Glauert basic distributions. Other camber lines can be derived from these by linear superposition. We can easily obtain further special camber lines from the following series (which does not include a term containing the angle of incidence):

$$\frac{2y(c)}{c} = (1 - \xi^2) \sum_{n=1}^{\infty} s_n \xi^{n-1},$$

$$\text{where } \xi = \frac{2x}{c} - 1. \quad (7.8)$$

HELMBOLD and KEUNE have systematically investigated such camber lines. With the notation employed here and with retention of the first three terms only, this camber line may be written

$$\begin{aligned} \frac{y(c)}{c} &= 4 \frac{f}{c} \frac{x}{c} \left(1 - \frac{x}{c}\right) \left(1 + l_1 \frac{x}{c} + l_2 \left(\frac{x}{c}\right)^2\right) \\ 0 \leq \frac{x}{c} &\leq 1. \end{aligned} \quad (7.9)$$

From Section 8.2.1 the velocity distribution is given by

$$\begin{aligned} \frac{w}{V} &= 1 \pm 8 \frac{f}{c} \sqrt{\frac{x}{c} \left(1 - \frac{x}{c}\right)} \times \\ &\quad \times \left(d_0 + d_1 \frac{x}{c} + d_2 \left(\frac{x}{c}\right)^2\right), \end{aligned} \quad (7.10)$$

$$\begin{aligned} \text{where } d_0 &= 1 - \frac{1}{4} l_1, \\ d_1 &= \frac{3}{2} l_1 - \frac{1}{2} l_2, \\ d_2 &= 2 l_2. \end{aligned}$$

From Section 8.2.5 we obtain for the angle of incidence at zero lift,  $\alpha_0$ , the ideal angle of incidence,  $\alpha^*$ , and the moment coefficient at  $C_L = 0$ ,  $C_{m_0}$ :

$$\alpha_0 = -2 \frac{f}{c} \left(1 + \frac{3}{4} l_1 + \frac{5}{8} l_2\right); \quad (7.11)$$

$$\alpha^* = -\frac{f}{2c} (l_1 + l_2); \quad (7.12)$$

$$C_{m_0} = -\pi \frac{f}{c} \left(1 + \frac{7}{8} l_1 + \frac{3}{4} l_2\right). \quad (7.13)$$

Type S<sub>2</sub>: a well-known camber line, that of the four-figure NACA profiles, which consists of two parabolic arcs having continuous slope at their join;

$$\left. \begin{aligned} \frac{y(c)}{c} &= \frac{f}{c} \frac{1}{x_1^2} \left( 2x_1 \frac{x}{c} - \left( \frac{x}{c} \right)^2 \right) \\ \text{for } 0 \leq \frac{x}{c} \leq x_1, \\ \frac{y(c)}{c} &= \frac{f}{c} \frac{1}{(1-x_1)^2} \left[ (1-2x_1) + 2x_1 \frac{x}{c} - \right. \\ &\quad \left. - \left( \frac{x}{c} \right)^2 \right] \quad \text{for } x_1 \leq \frac{x}{c} \leq 1, \\ \text{with } x_1 &= x_f/c. \end{aligned} \right\} (7.14)$$

The corresponding velocity distribution is

$$\frac{w}{V} = \frac{f}{c} \frac{\cos \alpha \left( \sin \varphi - \frac{1}{\pi} J \right) + \sin \alpha (1 - \cos \varphi)}{\sin \varphi \sqrt{1 + 16 \frac{(\cos \varphi_1 - \cos \varphi)^2}{(1 \pm \cos \varphi_1)^4}}}; \quad (7.15)$$

where the positive sign is to be taken for  $\varphi_1 \leq \varphi \leq (2\pi - \varphi_1)$  and the negative sign for  $-\varphi_1 \leq \varphi \leq \varphi_1$ , and

$$\begin{aligned} J &= -4(1+t_1^2)^2 \frac{t^2}{1+t^2} \left\{ \frac{1-t_1^2}{t_1^3} + \right. \\ &\quad \left. + \frac{(1-t_1^2)(t_1^2-t^2)}{t t_1^4 (1+t^2)} \ln \left| \frac{t_1+t}{t_1-t} \right| + \right. \\ &\quad \left. + \left[ \frac{2(1-t_1^2)(1+t_1^2)}{t_1^4} \tan^{-1} t_1 + \pi \right] \times \right. \\ &\quad \left. \times \left[ \frac{1}{2} - \frac{1}{1+t_1^2} + \frac{1}{1+t^2} \right] \right\}. \end{aligned}$$

Here,

$$t = \tan \frac{\varphi}{2}, \quad \frac{c}{2}(1 + \cos \varphi) = x,$$

$$t_1 = \tan \frac{\varphi_1}{2}, \quad \frac{c}{2}(1 + \cos \varphi_1) = x_1. \quad (7.16)$$

(I am indebted to Dr. G. JUNGCLAUS for the derivation of Equations (7.15), (7.18), and (7.41).) The velocity distributions corresponding to positions of maximum camber  $x_f/c = 0.2, 0.3, 0.4, 0.5, 0.6$ , and  $0.7$  are given in Figure 12.1 and in Table 11.2; the maximum camber,  $f$ , is equal to  $0.06c$ . Results for smaller values of the maximum camber can be obtained by affinely reducing the velocities in proportion to the maximum camber. A discontinuity in curvature exists at the point where the two parabolas join.

Type S<sub>3</sub>: consists of two cubics, which are joined together without a discontinuity in curvature,

$$\left. \begin{aligned} \frac{y(c)}{c} &= \frac{1}{6} k_1 \left[ \left( \frac{x}{c} - x_1 \right)^3 - \frac{k_2}{k_1} (1-x_1)^3 \frac{x}{c} + \right. \\ &\quad \left. + \left( 1 - \frac{x}{c} \right) x_1^3 \right] \quad \text{for } 0 \leq \frac{x}{c} \leq x_1, \\ \frac{y(c)}{c} &= \frac{1}{6} k_1 \left[ \frac{k_2}{k_1} \left( \frac{x}{c} - x_1 \right)^3 - \frac{k_2}{k_1} (1-x_1)^3 \frac{x}{c} + \right. \\ &\quad \left. + \left( 1 - \frac{x}{c} \right) x_1^3 \right] \quad \text{for } x_1 \leq \frac{x}{c} \leq 1 \end{aligned} \right\} (7.17)$$

$k_1, k_2$ , and  $\varphi$  are chosen so that a prescribed value for  $C_L^*$  results and  $(C_m)_a = 0$ . Hence, camber lines of this type have a fixed centre of pressure. The numerical values of the constants are:

Table 7.1

$x_f$	0.10	0.15	0.20	0.25
$x_1$	0.13	0.217	0.318	0.441
$C_L^*/(f/c)$	19	14.3	12.6	11
$k_1/C_L^*$	173.3	52.62	21.73	10.64
$k_2/k_1$	7.64	67.70	303	1355

The velocity distribution is

$$\frac{w}{V} = \frac{\cos \alpha \left( \sin \varphi - \frac{1}{\pi} J^* \right) - \sin \alpha (1 - \cos \varphi)}{\sin \varphi \sqrt{1 + \frac{1}{64} [6b(\cos \varphi - \cos \varphi_1)^2 - a(1 - \cos \varphi_1) - (1 + \cos \varphi_1)^3]^2}}; \quad (7.18)$$

where  $a = k_2/k_1$ , and

$$\begin{aligned} b &= 1 \quad \text{for } \varphi_1 \leq \varphi \leq 2\pi - \varphi_1, \\ b &= a \quad \text{for } -\varphi_1 \leq \varphi \leq \varphi_1. \end{aligned}$$

The abbreviations are defined by Equation (7.16);  $J^*$  is given by

$$\begin{aligned} J^* = & -\frac{6t}{(1+t_1^2)^2} \left\{ \left( \frac{3}{8}\beta_1 + \frac{1}{2}\beta_2 + \beta_3 \right) \pi - \right. \\ & - (1-a) \left[ \frac{\frac{1}{2}\beta_1 t_1}{(1+t_1^2)^2} + \frac{\left(\frac{3}{4}\beta_1 + \beta_2\right)t_1}{1+t_1^2} + \right. \\ & \left. \left. + \left(\frac{3}{4}\beta_1 + \beta_2 + 2\beta_3\right) \tan^{-1} t_1 + \right. \right. \\ & \left. \left. + \beta_4 \ln \left| \frac{t_1-t}{t_1+t} \right| \right] \right\} \\ & - 2\pi(1-x)[x_1^3 + a(1-x_1^3)], \end{aligned}$$

where

$$\beta_1 = -\frac{t}{1+t^2}(1+t_1^2)^2,$$

$$\beta_2 = \frac{t}{(1+t^2)^2}(1+t_1^2)^2(1-t_1^2+2t^2),$$

$$\beta_3 = -\frac{t}{(1+t^2)^3}(t^2-t_1^2)^2, \quad \beta_4 = \frac{(t^2-t_1^2)^2}{(1+t^2)^3}.$$

*Type S<sub>4</sub>*: this is another well-known NACA camber line (Figure 12.2). The front part consists of a cubic with a monotonically increasing radius of curvature; this is joined to a straight line, which forms the rear part. The ordinates are given by the equations

$$\frac{y^{(c)}}{c} = \frac{1}{6}k_1 \left[ \left( \frac{x}{c} \right)^3 - 3x_1 \left( \frac{x}{c} \right)^2 + x_1^2(3-x_1) \left( \frac{x}{c} \right) \right]$$

for  $0 \leq \frac{x}{c} \leq x_1$ ,

$$\frac{y^{(c)}}{c} = \frac{1}{6}k_1 x_1^3 \left( 1 - \frac{x}{c} \right) \text{ for } x_1 \leq \frac{x}{c} \leq 1. \quad (7.19)$$

Here,  $x = x_1$  is a point lying a little behind the position of maximum camber,  $x = x_f$ ; the relation between  $x_1$  and  $x_f$

is  $x_f = x_1 \left( 1 - \sqrt{\frac{x_1}{3}} \right)$ .  $k_1$  (and hence  $f$ ) is usually chosen so that a prescribed value of  $C_L^*$  results. The numerical values are

Table 7.2

$x_f$	0.05	0.10	0.15	0.20	0.25
$x_1$	0.058	0.1280	0.2025	0.2900	0.3910
$C_L^*/(f/c)$	26.9	19.6	16.4	14.5	11.3
$k_1/C_L^*$	1205	172.1	53.2	22.13	10.77

The velocity distribution comes from Equation (7.18), if  $a$  is put equal to zero.

*Type S<sub>5</sub>*: this has a special analytical representation, and possesses the property that the pressure distribution is constant over the whole chord. If the prescribed velocity distribution is written in the form

$$\frac{w}{V} = 1 \pm \frac{C_L^*}{4}, \quad (7.20)$$

the equation of the camber line is

$$\begin{aligned} \frac{y^{(c)}}{c} = & -\frac{C_L^*}{4\pi} \left[ \left( 1 - \frac{x}{c} \right) \ln \left( 1 - \frac{x}{c} \right) + \right. \\ & \left. + \frac{x}{c} \ln \frac{x}{c} \right]. \quad (7.21) \end{aligned}$$

*Type S<sub>6</sub>*: the pressure distribution is constant up to a certain point of the chord,  $x = ac$ ; it decreases linearly until it becomes zero at a point given by  $x = bc$ , and it then remains zero up to the trailing edge [L-345]. The velocity distribution may be written

$$\frac{w}{V} = \begin{cases} 1 \pm \frac{1}{2} \frac{C_L^*}{a+b}, & 0 \leq \frac{x}{c} \leq a, \\ 1 \pm \frac{1}{2} \frac{b-(x/c)}{b^2-a^2} C_L^*, & a \leq \frac{x}{c} \leq b, \\ 1, & b \leq \frac{x}{c} \leq 1. \end{cases} \quad (7.22)$$

The equation of the camber line is

$$\begin{aligned} \frac{y^{(c)}}{c} = & \frac{C_L^*}{2\pi(a+b)} \left\{ \frac{1}{b-a} \left[ \frac{1}{2} \left( a - \frac{x}{c} \right)^2 \times \right. \right. \\ & \times \ln \left| a - \frac{x}{c} \right| - \frac{1}{2} \left( b - \frac{x}{c} \right)^2 \ln \left| b - \frac{x}{c} \right| + \\ & \left. \left. + \frac{1}{4} \left( b - \frac{x}{c} \right)^2 - \frac{1}{4} \left( a - \frac{x}{c} \right)^2 \right] - \right. \\ & \left. - \frac{x}{c} \ln \frac{x}{c} + g - h \frac{x}{c} \right\}; \quad (7.23) \end{aligned}$$

where

$$g = -\frac{1}{b-a} \left[ a^2 \left( \frac{1}{2} \ln a - \frac{1}{4} \right) - b^2 \left( \frac{1}{2} \ln b - \frac{1}{4} \right) \right],$$

$$h = +\frac{1}{b-a} \left[ \frac{1}{2} (1-a)^2 \ln (1-a) - \frac{1}{2} (1-b)^2 \ln (1-b) + \frac{1}{4} (1-b)^2 - \frac{1}{4} (1-a)^2 \right] + g.$$

The ideal angle of incidence,  $\alpha^*$ , is given by

$$\alpha^* = \frac{C_L^* h}{2\pi(a+b)}. \quad (7.24)$$

The camber lines for which  $b = 1$  are the most popular at the present time; the formulas then simplify; for  $b = 1$ ,  $a = 1$ , they reduce to those of Type S<sub>5</sub>. Table 11.2 gives numerical values for  $b = 1$  and  $a = 0, 0.1, 0.2, 0.3, 0.4, 0.5, 0.6, 0.7, 0.8, 0.9$ , and 1; Figure 12.2 shows some examples.

Type S<sub>7</sub>: this camber line has the equation

$$\frac{y(c)}{c} = m \sum_{\nu=1}^{\nu} a_{\nu} \left[ 1 - \frac{x}{c} - \left( 1 - \frac{x}{c} \right)^{\nu} \right]. \quad (7.25)$$

If the terms beyond  $\nu = 5$  are ignored, the velocity distribution is (from Section 8.2.1.2)

$$\frac{w}{V} = 1 \pm m \sqrt{\frac{x}{c} \left( 1 - \frac{x}{c} \right)} \left[ c_0 + c_1 \left( 1 - \frac{x}{c} \right) + c_2 \left( 1 - \frac{x}{c} \right)^2 + c_3 \left( 1 - \frac{x}{c} \right)^3 \right]; \quad (7.26)$$

where

$$c_0 = 2a_3 + \frac{3}{2}a_3 + \frac{3}{2}a_4 + \frac{25}{16}a_5,$$

$$c_1 = 3a_3 + 2a_4 + \frac{15}{8}a_5,$$

$$c_2 = 4a_4 + \frac{5}{2}a_5, \\ c_3 = 5a_5.$$

For the angle of incidence at zero lift,  $\alpha_0$ , the ideal angle of incidence,  $\alpha^*$ , and the moment coefficient (referred to the leading edge) at  $C_L = 0$ ,  $(C_m)_l$ , there results

$$a_0 = \frac{1}{2}a_2 + \frac{5}{8}a_3 + \frac{11}{16}a_4 + \frac{93}{128}a_5,$$

$$\alpha^* = \frac{1}{8}a_3 + \frac{1}{4}a_4 + \frac{39}{250}a_5,$$

$$(C_m)_l = -\pi \left( \frac{1}{4}a_2 + \frac{9}{32}a_3 + \frac{9}{32}a_4 + \frac{35}{128}a_5 \right).$$

*Special Case:* if we put  $a_{\nu} = 1$ ,  $\nu = (n+1)$ , and  $m = \frac{c}{f} \frac{(1+n)}{n \left( 1 - \frac{x_f}{c} \right)}$ , the separate terms of the equation lead

to camber lines identical with those given by KAWALSKI. These are characterised by the fact that all derivatives higher than the first vanish at the trailing edge. If we write  $2x/c = 1 + \cos \varphi$ , the velocity distribution becomes

$$\begin{aligned} \frac{w}{V} = 1 &\pm 2 \frac{c}{f} \frac{(n+1)}{\left( 1 - \frac{x_f}{c} \right)} \frac{1 \cdot 3 \cdot 5 \dots (2n-1)}{2 \cdot 4 \cdot 6 \dots 2n} \times \\ &\times \left[ -\sin \varphi + \frac{(n-1)}{(n+2)} \sin 2\varphi - \right. \\ &- \frac{(n-1)(n-2)}{(n+2)(n+3)} \sin 3\varphi + \\ &\left. + \frac{(n-1)(n-2)(n-3)}{(n+2)(n+3)(n+4)} \sin 4\varphi - \dots \right]. \end{aligned} \quad (7.27)$$

Table 7.3 gives characteristic aerodynamic quantities for some values of  $n$ .

Table 7.3

$n =$	3	4	5	6	7
$x_f/c$	0.370	0.3313	0.3012	0.2770	0.257
$C_L^*(f/c)$	12.46	12.84	13.29	13.72	14.15
$(C_m)_l/(f/c)$	-1.870	-1.605	-1.423	-1.288	-1.180
$\alpha^*/(f/c)$	1.454	1.357	1.296	1.249	1.212

Figure 12.1 gives the ordinates and velocity distributions for  $n = 3, 4, 5, 6, 7$ .

Type S<sub>8</sub>: the flat plate with a point of discontinuity. The equation of this camber line is

$$\begin{aligned}\frac{y(c)}{c} &= \lambda(1-x_1) \frac{x}{c} \text{ for } 0 \leq \frac{x}{c} \leq x_1, \\ &= \lambda x_1 \left(1 - \frac{x}{c}\right) \text{ for } x_1 \leq \frac{x}{c} \leq 1;\end{aligned}\quad (7.28)$$

where  $\lambda$  is a function of  $x_1$  (the position of the discontinuity) and of the jump in local angle of incidence,  $\eta$  (flap deflection).  $\lambda$  is given by

$$\lambda = \frac{\sqrt{1 + 4x_1(1-x_1)\tan^2\eta} - 1}{2x_1(1-x_1)\tan\eta} \quad (\text{for } |\eta| \ll \pi/2, \lambda \approx \eta). \quad (7.29)$$

From Equation (8.21) the velocity distribution is

$$\begin{aligned}\frac{w}{V} &= F(\lambda, x_1) \left[ \cos\alpha \left\{ 1 - \frac{\lambda}{\pi} (-\varphi_1 t + \ln \left| \frac{t_1 - t}{t_1 + t} \right| + \right. \right. \\ &\quad \left. \left. + \pi(1-x_1)t \right\} + t \sin\alpha \right],\end{aligned}\quad (7.30)$$

where  $\varphi_1$ ,  $t$ , and  $t_1$  have been defined by Equation (7.16).  $t > 0$  for the upper side and  $t < 0$  for the lower side;  $t_1$  is always greater than zero. The function  $F(\lambda, x_1)$  is given by

$$\begin{aligned}F(\lambda, x_1) &= \frac{1}{\sqrt{1 + \lambda^2(1-x_1)^2}} \text{ for } 0 \leq \frac{x}{c} \leq x_1 \\ &= \frac{1}{\sqrt{1 + \lambda^2 x_1^2}} \text{ for } x_1 \leq \frac{x}{c} \leq 1 \\ &\quad (\text{for } |\eta| \ll \pi/2 \quad F = 1).\end{aligned}$$

\*Equation 7.34

$$\begin{aligned}\frac{w}{V} &= \frac{\sqrt{(1+\tau^2)^2 - 4\tau^2\bar{x}^2}}{1+\tau^2} \left( 1 + \frac{2}{\pi} \sin^{-1} \frac{2\tau}{1+\tau^2} \right) - \\ &\quad - \frac{1}{\pi} \frac{2\tau\bar{x}}{1+\tau^2} \ln \frac{(1+\bar{x})[(1+\tau^2)^2 - 4\tau^2\bar{x} + (1-\tau^2)\sqrt{(1+\tau^2)^2 - 4\tau^2\bar{x}^2}]}{(1-\bar{x})[(1+\tau^2)^2 + 4\tau^2\bar{x} + (1-\tau^2)\sqrt{(1+\tau^2)^2 - 4\tau^2\bar{x}^2}]}\end{aligned}\quad (7.34)$$

### 7.3 Thickness Distribution and Velocity Distribution

#### 7.3.1 Simple Special Cases

(a) The ellipse of thickness ratio  $t/c$  is given by

$$x = \frac{c}{2} + \frac{c}{2} \cos\varphi, \quad y = \frac{t}{2} \sin\varphi; \quad (7.31)$$

the velocity distribution is

$$\frac{w}{V} = \left(1 + \frac{t}{c}\right) \frac{\cos\alpha \sin\varphi + \sin\alpha(1 - \cos\varphi)}{\sqrt{\sin^2\varphi + \left(\frac{t}{c}\right)^2 \cos^2\varphi}}. \quad (7.32)$$

(b) The symmetrical circular arc section of thickness ratio  $t/c = \tau$  is given by

$$\begin{aligned}\frac{2y}{c} &= -\frac{1-\tau^2}{2\tau} + \frac{1}{2\tau} \sqrt{(1+\tau^2)^2 - 4\tau^2\bar{x}^2}, \\ \text{where } \bar{x} &= \frac{2x}{c} - 1;\end{aligned}\quad \left.\right\} \quad (7.33)$$

at  $\alpha = 0$  it has the velocity distribution

Equation 7.34 \*

For small thickness ratios the circular arcs can be replaced by parabolic arcs:

$$x = \frac{c}{2} + \frac{c}{2} \cos\varphi, \quad y = \pm \frac{t}{2} (1 - \cos^2\varphi). \quad (7.35)$$

The velocity distribution can be derived either from Equation (7.35) or by linearising Equation (7.34); it has the simple form

$$\frac{w}{V} = 1 + \frac{4\tau}{\pi} \left[ 1 + \left( \frac{x}{c} - \frac{1}{2} \right) \ln \frac{c-x}{x} \right]. \quad (7.36)$$

Infinitely large velocities are predicted at the leading and trailing edges when linearised theory is used to determine the flow over a circular arc section (uncambered and at zero incidence); the singularities are of the form  $\log \zeta$ , and for practical purposes they become unimportant at a very small distance from the points of infinite velocity.

- (c) The contour of the symmetrical Joukowsky profile has the approximate equation

$$x = \frac{c}{2} (1 + \cos \varphi), \quad y = \frac{\epsilon}{2} \sin \varphi (1 - \cos \varphi); \quad (7.37)$$

the velocity distribution is

Equation 7.38 \*

when  $\epsilon = 0$  this reduces to the velocity distribution for the flat plate. Results obtained by using this approximate equation are in very good agreement with the exact values; the velocity distribution shows small deviations from that calculated by means of exact conformal mapping (see below) if the thickness ratio is too large ( $t/c > 0.2$ ); this is primarily because the linearised equation for the body, Equation (7.37), is no longer in good agreement with the exact equation.

The parametric representation for the shape of the symmetrical generalised Joukowsky profile (Equations (1.14) and (1.15)) comes from exact conformal transformation: the velocity distribution for zero angle of incidence is

$$\frac{w}{V} = 2 \sin \bar{\varphi} \frac{N(\bar{\varphi})}{\sqrt{(N-1)^2 + 4k^2 \sin^2 \bar{\varphi}}}; \quad (7.39)$$

for the meaning of the symbols see Section 1.4.1.

\*Equation 7.38

$$\frac{w}{V} = \frac{\cos \alpha \left[ \left( 1 + \frac{\epsilon}{c} \right) \sin \varphi - \frac{\epsilon}{c} \sin 2\varphi \right] + \sin \alpha (1 - \cos \varphi) \left( 1 - 2 \frac{\epsilon}{c} \cos \varphi \right)}{\sqrt{\sin^2 \varphi + \frac{\epsilon^2}{c^2} (\cos \varphi - \cos 2\varphi)^2}}; \quad (7.38)$$

### 7.3.2 More General Thickness Distributions†

Type  $D_1$ : the NACA standard profile, of which the ordinates (Table 11.3) are given by

$$\begin{aligned} y^{(t)} = & \pm 5t (0.2969 \sqrt{x} - 0.1260x - 0.3516x^2 + \\ & + 0.2843x^3 - 0.1015x^4) \\ = & \pm t (a_0 \sqrt{x} + a_1 x + a_2 x^2 + a_3 x^3 + a_4 x^4), \end{aligned} \quad (7.40)$$

and the geometrical parameters by

$$\frac{x_t}{c} = 0.3, \quad \rho_1 = 0.27, \quad \rho_0 = 1.1, \quad \epsilon_L = -1.26.$$

It has the following velocity distribution when  $\alpha = 0$ :

$$\frac{w}{V} = \frac{1 + A}{\sqrt{1 + \frac{1}{4} B^2}}, \quad (7.41)$$

where

$$\begin{aligned} A = & \frac{1}{\pi} \left\{ \frac{a_0}{2\sqrt{x}} \ln \frac{1+\sqrt{x}}{1-\sqrt{x}} - a_1 \ln \frac{1-x}{x} - \right. \\ & - 2a_2 \left( 1 + x \ln \frac{1-x}{x} \right) - \\ & - 3a_3 \left( \frac{1}{2} + x + x^2 \ln \frac{1-x}{x} \right) - \\ & \left. - 4a_4 \left( \frac{1}{3} + \frac{1}{2}x + x^2 + x^3 \ln \frac{1-x}{x} \right) \right\}, \end{aligned}$$

$$\text{and } B = \frac{a_0}{\sqrt{x}} + 2a_1 + 4a_2 x + 6a_3 x^2 + 8a_4 x^3.$$

† For simplicity  $c$  is set equal to unity in this section;  $x$  and  $x_t$  represent  $\frac{x}{c}$  and  $\frac{x_t}{c}$  respectively.

**Type D<sub>2</sub>:** profiles with various positions of maximum thickness can be obtained by joining two curves together (without a discontinuity in curvature); the equation of such a profile is

$$\left. \begin{aligned} y_t &= \pm 5t(a_0\sqrt{x} + a_1x + a_2x^2 + a_3x^3) \quad 0 \leq x \leq x_t \\ &= \pm 5t[0.002 + d_1(1-x) + d_2 \times \\ &\quad \times (1-x)^2 + d_3(1-x)^3] \quad x_t \leq x \leq 1. \end{aligned} \right\} \quad (7.42)$$

The slope at the trailing edge,  $\varepsilon_T$ , is related to the position of maximum thickness,  $x_t$ , by the equation

$$\varepsilon_T \approx \frac{2.24 - 5.42x_t + 12.3x_t^2}{1 - 0.878x_t}.$$

The parameters of this thickness distribution are given in Table 7.4; the coefficients in Equation (7.42) can be obtained in terms of the parameters; they are given by

$$a_0 = \frac{1}{5}\sqrt{2\rho_0}, \quad d_1 = 10\varepsilon_L, \quad \rho_1 = \frac{1}{5} \frac{(1-x_t)^2}{0.588 - 2d_1(1-x_t)},$$

$$a_1 = 10\varepsilon_L,$$

$$2a_1x_t = 0.6 - \frac{3}{4}\sqrt{2\rho_0x_t} - \frac{x_t^2}{5\rho_1},$$

$$a_2x_t^2 = -0.3 + \frac{1}{4}\sqrt{2\rho_0x_t} + \frac{x_t^2}{5\rho_1},$$

$$2a_3x_t^3 = 0.2 - 0.15\sqrt{2\rho_0x_t} - \frac{x_t^2}{5\rho_1},$$

$$d_2(1-x_t)^2 = 0.294 - 2d_1(1-x_t),$$

$$d_3(1-x_t)^3 = -0.196 + d_1(1-x_t).$$

Table 7.4

$n$	$\rho_0$	$x_t = 0.2$	$0.3$	$0.4$	$0.5$	$0.6$
0	0	$\varepsilon_T = 2.00$	2.34	3.15	4.65	7.00
3	0.275	$a_1 = 0.4776$	0.3766	0.3428	0.4064	1.1428
6	1.1	$\varepsilon_L = 14.5812$	9.2034	6.333	4.7696	4.4750
9	3.3	$\rho_1 = 8.3625$	4.1259	1.9357	0.8366	0.8843
		$d_1 = 2.1438$	-0.9516	-2.4616	-3.0964	-2.7063
		$d_2 = -6.97$	-8.38	-8.90	-8.86	-7.97

**Type D<sub>3</sub>:** the symmetrical profile

$$y = t\sqrt{x}(1-x)(1+a_1x+a_2x^2+a_3x^3+a_4x^4+a_5x^5) \quad (0 \leq x \leq 1). \quad (7.43)$$

The slope is given by

$$\begin{aligned} y' &= \frac{t}{2} \frac{1}{\sqrt{x}} [1 + 3(a_1 - 1)x + 5(a_2 - a_1)x^2 \\ &\quad + 7(a_3 - a_2)x^3 + 9(a_4 - a_3)x^4 \\ &\quad + 11(a_5 - a_4)x^5 - 13a_5x^6]. \end{aligned} \quad (7.44)$$

When  $\alpha = 0$  the velocity distribution is

$$\frac{w}{V} = \left[ \frac{y'}{\pi c} \ln \frac{1+\sqrt{x}}{1-\sqrt{x}} - \frac{t}{\pi c} (c_0 + c_1x + c_2x^2 + \right. \\ \left. + c_3x^3 + c_4x^4 + c_5x^5) \right] \frac{1}{\sqrt{1+y'^2}}, \quad (7.45)$$

where

$$\begin{aligned} c_0 &= -3 + \frac{4}{3}a_1 + \frac{4}{15}a_2 + \frac{4}{35}a_3 + \frac{4}{63}a_4 + \frac{4}{99}a_5, \\ c_1 &= -5a_1 + \frac{8}{3}a_2 + \frac{8}{15}a_3 + \frac{8}{35}a_4 + \frac{8}{63}a_5, \\ c_2 &= -7a_2 + 4a_3 + \frac{4}{5}a_4 + \frac{12}{35}a_5, \\ c_3 &= -9a_3 + \frac{16}{3}a_4 + \frac{16}{15}a_5, \\ c_4 &= -11a_4 + \frac{20}{3}a_5, \\ c_5 &= -13a_5. \end{aligned}$$

If  $a_3$ ,  $a_4$ , and  $a_5$  are zero then, when the profile is at an angle of incidence  $\alpha$ ,

$$\begin{aligned} \frac{w}{V} &= \frac{1}{\sqrt{1+y'^2}} \left\{ \cos \alpha \left( 1 + \frac{y'}{\pi} \ln \frac{1+\sqrt{x}}{1-\sqrt{x}} - \right. \right. \\ &\quad \left. \left. - \frac{t}{\pi} (c_0 + c_1x + c_2x^2) \pm \sin \alpha \sqrt{\frac{1-x}{x}} \times \right. \right. \\ &\quad \times \left[ 1 + \frac{1}{\pi} \left( y' + \frac{y}{4x(1-x)} \right) \ln \frac{1+\sqrt{x}}{1-\sqrt{x}} - \right. \\ &\quad \left. \left. - \frac{t}{\pi} (c_0' + c_1'x + c_2'x^2) \right] \right\}; \end{aligned} \quad (7.46)$$

where

$$c_0 = -3 + \frac{4}{3}a_1 + \frac{4}{15}a_2, \quad c_0' = -3 + \frac{11}{6}a_1 + \frac{13}{30}a_2,$$

$$c_1 = -5a_1 + \frac{8}{3}a_2, \quad c_1' = -5a_1 + \frac{19}{6}a_2,$$

$$c_2 = -7a_2, \quad c_2' = -7a_2.$$

Type D<sub>4</sub>: the symmetrical profile

$$y^{(t)} = a \frac{x(1-x)}{1+bx} \text{ with } a = \frac{t}{2x_t^2}; \quad b = \frac{1-2x_t}{x_t^2}. \quad (7.47)$$

The position of maximum thickness is variable (it depends on  $b$ ), the contour has no point of inflection, and the slopes at the leading and trailing edges are finite. When  $\alpha = 0$  the velocity distribution is

$$\frac{w}{V} = \frac{1}{\sqrt{1+y'^2}} \left\{ 1 + \frac{1}{\pi} \frac{a}{(1+bx)^2} \left[ 1 + \frac{1+b}{b} \times \right. \right. \\ \left. \left. \times \ln(1+b) + (1-2x-bx^2) \ln \frac{x}{1-x} + bx \right] \right\}. \quad (7.48)$$

Finally, we give some other thickness distributions, for which the velocity distributions have been calculated but for which no simple algebraic formulas exist.

Type D<sub>5</sub>: a simple approximation for the contour of the hyperbola profile (see Section 1.4.3) is

$$y^{(t)} = k(1-x)\sqrt{(1+b)x-bx^2}. \quad (7.49)$$

Type D<sub>6</sub>: profiles designated EC or EQ (R & M No. 4726, No. 4978) are constructed by joining two curves together. The front part of the profile is an ellipse and the rear part is either a cubic (EC) or a quartic (EQ). The formulas for the two curves are

$$y^{(t)} = \sqrt{Ax-Bx^2} \quad 0 \leq x \leq x_1, \quad (7.50) \\ = b_0 + b_1x + b_2x^2 + b_3x^3 + b_4x^4 \quad x_1 \leq x \leq 1,$$

in which  $b_4 = 0$  for EC profiles.

Profiles designated EQH or ECH are composed of three curves; the rear part is a hyperbola. The formulas are

$$y^{(t)} = \begin{cases} \sqrt{Ax-Bx^2} & 0 \leq x \leq x_1, \\ = b_0 + b_1x + b_2x^2 + b_3x^3 + b_4x^4 & x_1 \leq x \leq x_2, \\ = \sqrt{C(1-x)+D(1-x)^2} & x_2 \leq x \leq 1, \end{cases} \quad \dots (7.51)$$

in which  $b_4 = 0$  for ECH profiles.

The camber lines with which these thickness distributions are usually combined are those of Equation (7.9) with  $l_2 = 0$ .

### 7.3.3 Influence of a Sudden Change in Curvature of the Profile Contour

Engineers and designers often approximate a curve of high order by simple curves (for example, straight lines or parabolas); they usually ensure that the change from one curve to another occurs so that the function and its first derivative are continuous, but higher derivatives are frequently not made continuous. Profiles are occasionally designed by joining curves together in this manner. For example, DOETSCH has investigated a symmetrical circular arc section the front part of which is replaced by a parabola; the curvature is made continuous at the join, but the third derivative is not continuous, so that the curvature has a "kink". The camber line of the four-figure NACA profiles provides another example (see Section 7.2.2). It is composed of two parabolas; at the join the curvature is not continuous, so that the curvature has a "jump". The questions arise, what effects such discontinuities have on the velocity and pressure distributions, and how the resultant changes in these distributions affect the boundary layer. These questions have been investigated many times and the answers are now clear. It is shown below that a jump in the curvature leads to a point of inflection in the velocity distribution, the slope at the point of inflection being infinite; and even a kink in the curvature manifests itself in a slight concavity in the pressure distribution. The latter behaviour has been confirmed both theoretically and experimentally for the symmetrical circular arc section with a parabolic nose (see Figure 12.3).

Let us consider a jump in curvature, at which the radius of curvature changes from  $R_1$  to  $R_2$ ; let the  $x$  axis lie along the tangent at the point of discontinuity, and assume that, in the neighbourhood of this point, the contour is given by

$$\left. \begin{aligned} y &= \frac{x^2}{2R_1} + a_3 x^3 + a_4 x^4 + \dots \quad (x < 0), \\ y &= \frac{x^2}{2R_2} + a_3 x^3 + a_4 x^4 + \dots \quad (x > 0). \end{aligned} \right\} \quad (7.52)$$

By an approximate calculation BETZ has been able to show that the velocity in the neighbourhood of such a point may be written in the form

$$\frac{w}{W_0} = 1 + \frac{1}{\pi} \left( 1 - \frac{R_1}{R_2} \right) \frac{x}{R_1} \ln \frac{x}{R_1} + F(x); \quad (7.53)$$

where  $W_0$  is the velocity at  $x = 0$ , and  $F(x)$  is a regular function that can be determined only when the exact shape of the contour is known. A point of inflection exists at  $x = 0$ , the slope being infinite there.

*Special Case:* a semi-infinite body with a semi-circular nose. The equation of the body is

$$\left. \begin{aligned} y &= \sqrt{1 - x_0^2} \quad \text{for } -1 \leq x_0 \leq 0, \\ y &= 1 \quad \text{for } x_0 \geq 0, \end{aligned} \right\} \quad (7.54)$$

$x$  being measured from the join; the velocity distribution, calculated by the method of Section 8.2.2, is

$$\left. \begin{aligned} \frac{W}{V} &= \frac{3}{2} \sqrt{1 - x^2} - \frac{x}{\pi} \ln \frac{1 + \sqrt{1 - x^2}}{|x|} \\ &\quad \text{for } -1 \leq x \leq 0, \\ &= \frac{3}{2} - \frac{x}{\pi \sqrt{1 - x^2}} \ln \frac{1 + \sqrt{1 - x^2}}{x} \\ &\quad \text{for } 0 \leq x \leq 1, \\ &= \frac{3}{2} + \frac{x}{\pi \sqrt{x^2 - 1}} \left( \sin^{-1} \frac{1}{x} - \frac{\pi}{2} \right) \\ &\quad \text{for } 1 \leq x \leq \infty. \end{aligned} \right\} \quad (7.55)$$

Figure 12.4 shows that the pressure distribution has a point of inflection at  $x = 0$ , the slope being infinite there.

Similar results are obtained by exact conformal mapping of special profiles with a prescribed behaviour of curvature. Examples are: profiles consisting of three circular arcs; and profiles consisting of two semi-circles joined by two parallel straight lines. The latter have been investigated by SCHMIEDEN; his results are reproduced in Figure 12.5.

The boundary layer often reacts very strongly to sudden rises in pressure, and the preceding example suggests that contours formed from a combination of curves should be

used with caution; this is especially true if, as a result of its previous development, the boundary layer at the join is expected to be sensitive to pressure rises.

We must emphasise that the point of inflection (with infinite slope) in the velocity distribution occurs only on the contour itself; at an arbitrarily small distance from the wall no singularity of this nature exists. To investigate this, BETZ has considered the simple example represented in Figure 7.1. Far away from the singular point the velocity,  $V$ , is parallel to the straight section of the wall; on the circular arcs of radius  $+R$  and  $-R$  the velocity is respectively greater and smaller than  $V$ ; it is equal to  $V$  at  $x = 0$  for reasons of symmetry. At a point  $(x, y)$  near the wall,

$$\begin{aligned} \frac{R\pi}{s} \ln \left| \frac{w}{V} \right| &\approx \frac{R\pi}{s} \left( \left| \frac{w}{V} \right| - 1 \right) = \\ &= x \ln \frac{\sqrt{(s+x)^2 + y^2} \sqrt{(s-x)^2 + y^2}}{x^2 + y^2} - \\ &- \frac{s}{2} \ln \frac{(s-x)^2 + y^2}{(s+x)^2 + y^2} + \\ &+ y \left( \tan^{-1} \frac{s+x}{y} - \tan^{-1} \frac{s-x}{y} - 2 \tan^{-1} \frac{x}{y} \right). \end{aligned} \quad \dots \quad (7.56)$$

the symbols are explained in the figure. The behaviour of the velocity is shown for various values of the distance from the wall. Although the point of inflection and the infinite slope do not appear to be dangerous, since the

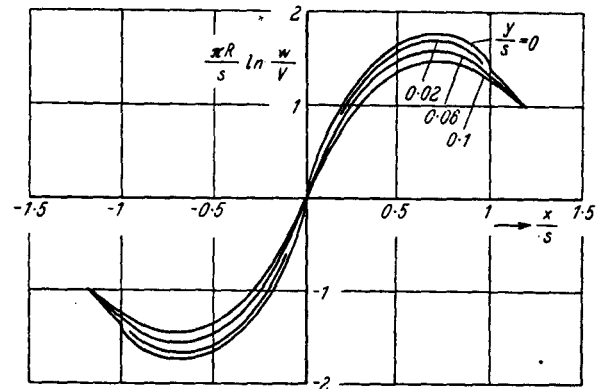
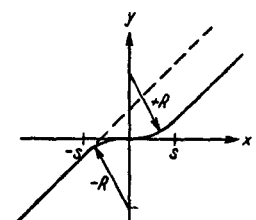


Fig. 7.1. Behaviour of the velocity distribution in the neighbourhood of a discontinuity of curvature according to potential theory (BETZ)



slope is finite at an arbitrarily small distance from the wall, the total fluctuation of the velocity in the neighbourhood of such a point is considerable. It is advisable not to expose sensitive boundary layers to such fluctuations.

#### 7.4 Cambered Profiles

For small camber, camber lines and thickness distributions can be additively superimposed: the corresponding velocity-distributions can then also be additively superimposed, to a good approximation. Even if the cambered profiles have not been constructed by simple superposition, the velocity distributions can still be thus determined provided that co-ordinates with the longest chord as abscissa are used in the calculation (as required in the theoretical treatment in Section 8.2.3). Theoretical pressure distributions on some profiles, with allowance for viscous effects, are given in Figures 12.7 ff, for various lift coefficients; these distributions have been calculated by the method described in Section 9.1. In Section 12.4 experimental pressure distributions are reproduced, in which the influence of various arrangements of flaps can be examined. The regions of separated flow are prominent; they are recognisable by the pressure's becoming suddenly constant.

#### 7.5 References

- ALLEN, H. J.: Calculation of the Chordwise Load Distribution over Airfoil Sections with Plain, Split or Serially Hinged Trailing Edge Flaps. NACA Rep. 634 (1938).
- BETZ, A.: Verlauf der Strömungsgeschwindigkeit in der Nachbarschaft einer Wand im Fall einer unstetigen Krümmungsänderung. Lufo 19 (1942), S. 129—131.
- DOETSCH, H. and A. PASCHKE: Druckverteilungsmessungen und Wägungen an den Profilen NACA 23009, 23012 und 23018 ohne und mit Spreizklappe im 5 × 7 m-Windkanal der DVL. FB 1095 (1939).
- DOETSCH, H.: Untersuchungen an einigen Profilen mit geringem Widerstand im Bereich kleiner  $c_a$ -Werte. Jahrb. 1940 dDL I, S. 54—57.
- FLÜGGE-LOTZ, J. and F. KEUNE: Druckverteilungen an Kármán-Treffitz-Profilen bei hohen Auftriebsziffern. Jahrb. 1938 dDL I, S. 39.
- FLÜGGE-LOTZ, J. and I. GINZEL: Die ebene Strömung um ein geknicktes Profil mit Spalt. Jahrb. 1939 dDL, I S. 55/66.
- GLAUERT, H.: A Theory of Thin Aerofoils. R & M No. 910 (1924).
- Theoretical Relationships for an Aerofoil with Hinged Flap. R & M No. 1095 (1927).
- HARRIS, A. TH. and G. J. LOWRY: Pressure Distribution over an NACA 23012 Airfoil with a Fixed Slot and a Slotted Flap. NACA Rep. 732 (1942).
- HELMBOLD, H. B. and F. KEUNE: Beiträge zur Profilforschung II, III. Lufo 20 (1943), S. 82.
- JACOBS, E. N.: Preliminary Report on Laminar Flow Airfoils and New Methods Adopted for Airfoil and Boundary Layer Investigation. NACA-WR 345 (1939).
- N. EASTMAN and R. M. PINKERTON: Pressure Distribution over a Symmetrical Airfoil Section with Trailing Edge Flap. NACA Rep. 360 (1930).
- KAWALKI, K. H.: Theoretische Untersuchungen von Schnellflugprofilen, die aus Ellipsenprofilen entwickelt sind. FB 1224/1 und 2 (1940).
- KOCHANOWSKY, W.: Zur Berechnung der Druckverteilung über den Umfang beliebig geformter Flügelschnitte. Jahrb. 1937 dDL I, S. 58.
- Weitere Ergebnisse von Druckverteilungsrechnungen über den Umfang beliebig geformter Flügelschnitte. Jahrb. 1938 dDL I, S. 82.
- KOPPENFELS, W. v.: Ebene Potentialströmung längs einer glatten Wand mit stückweise stetiger Krümmung. Lufo 17 (1940), S. 189—195.
- LEHMANN and F. ZEUNERT: Beiträge zur Profilforschung. UM 7603 (1944).
- LEMME, H. G.: Kraftmessungen und Druckverteilungsmessungen an einem Rechteckflügel mit Spalt-Knicknase, Wölbungs- und Spreizklappe oder Rollklappe. FB 1676/2 (1943).
- Kraftmessungen und Druckverteilungsmessungen an einem Rechteckflügel mit Doppel-Knicknase. FB 1676/3 (1944).
- PANKHURST, R. C. and H. B. SQUIRE: Calculated Pressure Distributions for the RAE 100—104 Aerofoil Sections. C.P. 80 (1950).
- PATTERSON, E. W. and A. L. BRASLOW: Ordinates and Theoretical Pressure-Distribution Data for NACA 6- and 6A-Series Airfoil Sections with Thicknesses from 2 to 21 and from 2 to 15 per cent Chord, Respectively. NACA TN 4322 (1958).
- PIERCY, N. A. V., R. W. PIPER and L. G. WHITEHEAD: The New Transformed Wing Sections. Aircraft Engineering 10 (1938), p. 339.
- PIPER, R. W.: Extensions of the New Family of Wing Profiles. Phil. Mag. Ser. 7 (1937), p. 1114.
- PINKERTON, R. M.: Calculated and Measured Pressure Distributions over the Midspan Section of the NACA 4412 Airfoil. NACA Rep. No. 563 (1936).
- The Variation with Reynolds Number of Pressure Distribution over an Airfoil Section. NACA Rep. No. 613 (1937).
- RIEGELS, F. and J. LISE: Druckverteilungskatalog. FB 1884 (1944).
- RIEGELS, F.: Umströmungsproblem bei inkompressiblen Potentialströmungen I, II. Ing. Arch. 16 (1948), S. 373, 17 (1949), S. 94 und Berichtigung 18 (1950), S. 321.
- ROSSNER, G.: Über eine Klasse von theoretischen Profilen mit vier frei wählbaren geometrischen Parametern. Jahrb. 1942 dDL I, S. 142.
- SCHLICHTING, H. and A. ULRICH: Zur Berechnung des Umlaufschlages laminar/turbulent. Jahrb. 1942 dDL I, S. 8—35.
- SCHMIDT, W.: Entwurf, Auftrieb, Moment und Druckverteilung eines Joukowsky-S-Profiles. Jahrb. 1939 dDL I, S. 50—54.
- SCHMIEDEN, S.: Die konforme Abbildung von Tragflügeln mit Krümmungssingularitäten. Jahrb. 1942 dDL I, S. 106—10.
- SCHRENK, O.: Druck- und Geschwindigkeitsverteilung längs der Flügeltiefe für verschiedene Flugzustände. Ringbuch der Luftfahrttechnik, I A 11 (1938).
- and A. WALZ: Theoretische Verfahren zur Berechnung von Druck- und Geschwindigkeitsverteilungen. Jahrb. 1939 dDL I, S. 29.
- THWAITES, B.: A Method of Aerofoil Design. I, II R & M No. 2166 und 2167 (1945).
- A New Family of Low Drag Wings with Improved  $C_L$ -ranges. R & M No. 2292 (1945).
- WALZ, A.: Übertragung gemessener Druckverteilungen auf beliebige Anstellwinkel. Lufo 16 (1939), S. 121—128.
- Potentialtheoretisch gerechnete Druckverteilungen dünner symmetrischer Profile mit heruntergeklappter Nase und Auftriebsklappe. FB 1170 (1940).

- WANNER, A. and P. KRETZ: Druckverteilungs- und Profilwiderstandsmessungen im Flug an den Profilen NACA 23012 und Gö 549. Jahrb. 1941 dDL I, S. 111—119.
- WENZINGER, C. J.: Pressure Distribution over an Airfoil Section with a Flap and Tab. NACA Rep. No. 574 (1936).
- Pressure Distribution over an NACA 23012 Airfoil with an NACA 23012 External-Airfoil Flap. NACA Rep. No. 614 (1938).
- and B. J. DELANO: Pressure Distribution over an NACA 23012 Airfoil with a Slotted and a Plain Flap. NACA Rep. No. 633 (1938).

## 8. THE THEORY OF WING PROFILES II

### Numerical Methods

#### 8.1 The Flow Field

Two-dimensional incompressible flow about a profile can be treated as potential flow throughout most of the field; the only exceptions are small regions very close to the profile in which viscous effects dominate (see Section 9.2). It is therefore possible to determine most of the flow field theoretically, so that experiments are necessary only in special cases (for example, when the effect of large regions of separated flow is to be investigated). If we continue to ignore changes in density, the inviscid flow about a profile at normal speeds (those compared with which the speed of sound,  $a$ , is very large) is governed by the equations of continuity

$$\operatorname{div} \mathbf{w} = 0, \quad (8.1)$$

and irrotationality

$$\operatorname{curl} \mathbf{w} = 0. \quad (8.2)$$

A velocity potential,  $\Phi$ , and a stream function,  $\Psi$ , can be introduced by means of the equations

$$\frac{\partial \Phi}{\partial x} = \frac{\partial \Psi}{\partial y} = w_x, \quad \frac{\partial \Phi}{\partial y} = -\frac{\partial \Psi}{\partial x} = w_y, \quad (8.3)$$

where  $w_x$  and  $w_y$  are the components of  $\mathbf{w}$ . It follows that both  $\Phi$  and  $\Psi$  satisfy Laplace's equation:

$$\nabla^2 \Phi = 0; \quad \nabla^2 \Psi = 0. \quad (8.4)$$

This differential equation has been treated by the most diverse mathematical methods. If an accurate knowledge of the flow in the immediate neighbourhood of the profile is required, the method of conformal transformation is the most appropriate one. The flow at larger distances is more easily determined if the profile is replaced by source and vortex distributions, or simply by isolated singularities (sources and sinks, and vortices).

The former method has remained limited to special profile families. The method of TREFFITZ for the construction of Joukowsky profiles has become well-known; in an extension of this RUDEN describes a graphical procedure (later simplified by PÉRÈS) for the determination of the velocity vector at an arbitrary point,  $P$ , of the flow field. The construction requires no auxiliary lines, the magnitude of the velocity being determined from the following quantities (the notation is that of Figure 1.15): the distance  $PO$  of  $P$ , the point being considered, from  $O$ , the origin; the distance  $PM$  between  $P$  and  $M$ , the centre of the transformed circle; the distance  $PN$  between  $P$  and  $N$ , the singular point near the nose; and the distance  $PS$  between  $P$  and  $S$ , the front stagnation point on the transformed circle. We find that

$$\frac{w}{V} = \frac{(PO)^2 \cdot (PS)}{(PM)^2 \cdot (PN)}. \quad (8.5)$$

The direction of this velocity makes an angle  $\vartheta$  with the free-stream direction, where

$$\vartheta = \angle NPS + 2 \angle MPO. \quad (8.6)$$

SCHRENK and WALZ have extended the graphical method of RUDEN to Kármán-Treffitz and Betz-Keune profiles; the effect of a change in profile shape can be found from their results. The advantage of all these methods is that they can be used to determine the whole flow field, including the immediate neighbourhood of the profile.

If we are interested only in the flow at some distance from the profile we can obtain information much more quickly by placing sources, sinks, and vortices along the chord, and determining the flow field from these singularities. At very large distances isolated singularities usually suffice; at distances of from a quarter or a half of the profile chord to about four times the profile chord, it is more accurate to place suitable distributions of sources, sinks, and vortices along the chord. For profiles of zero thickness vortex distributions alone are sufficient. WEINIG has calculated the fields of the vortex distributions for the flat plate at incidence, for profiles whose camber line is a circular arc, and for profiles whose camber line has a point of inflection. The theory uses the function  $\log(w_x + iw_y) = \log w - iv$ : for profiles with small camber this has the advantage that both  $\log w$  and  $v$  (the angle made by the

free-stream direction with the tangent to the profile) are usually small, so that  $\log w = \log(1 + \Delta w) \approx \Delta w$  gives the disturbance velocity directly; here, the disturbance velocity is the deviation from the free-stream velocity divided by the magnitude of this velocity. KEUNE (1938) has constructed similar fields, in which, as usual, the complex velocity ( $w_x + iw_y$ ) is used.

For profiles of finite thickness PISTOLESI and KEUNE have developed simple methods of calculation that use source and sink distributions in addition to vortex distributions. KEUNE's method involves the construction of networks representing the flow fields of certain basic distributions (as in the method for thin profiles); these are immediately applicable to other cases. PISTOLESI chooses the same form for both the vortex distribution and the source and sink distribution:

$$\begin{aligned} \gamma &= V \left( a_0 \cos \frac{\theta}{2} + \sum_1^{\infty} a_n \sin n\theta \right), \quad \frac{x}{c} = -\cos \theta; \\ q &= V \left( b_0 \cos \frac{\theta}{2} + \sum_1^{\infty} b_n \sin n\theta \right), \quad \frac{x}{c} = -\cos \theta. \end{aligned} \quad (8.7)$$

He considers a combination of the two distributions,  $\gamma + iq$ ; by using complex variable notation for the velocity components, he arrives at the simple result

$$\begin{aligned} \frac{2w_x}{V} &= -a_0 \frac{\sin \theta_1}{\cosh \theta_2 - \cos \theta_1} + \\ &+ b_0 \left( 1 - \frac{\sinh \theta_2}{\cosh \theta_2 - \cos \theta_1} \right) - \\ &- \sum_1^{\infty} (a_n \sin n\theta_1 + b_n \cos n\theta_1) \cdot e^{-n\theta_1}, \end{aligned} \quad (8.8)$$

$$\begin{aligned} \frac{2w_y}{V} &= a_0 \left( 1 - \frac{\sinh \theta_2}{\cosh \theta_2 - \cos \theta_1} \right) + \\ &+ b_0 \frac{\sin \theta_1}{\cosh \theta_2 - \cos \theta_1} - \\ &- \sum_1^{\infty} (a_n \cos n\theta_1 - b_n \sin n\theta_1) \cdot e^{-n\theta_1}. \end{aligned} \quad (8.9)$$

$\theta_1$  and  $\theta_2$  can be determined from  $d_1$  and  $d_2$ , where  $d_1$  and  $d_2$  are respectively the distances of  $P$ , the point being considered, from  $L$  (leading edge) and  $T$  (trailing edge), the end points of the line of singularities that replaces the profile; the relations are

$$d_2 - d_1 = 2c \cos \theta_1, \quad d_2 + d_1 = 2c \cosh \theta_2. \quad (8.10)$$

Methods involving the use of singularities are simple, but unfortunately they do not give the velocity distribution on an arbitrary profile to the required accuracy. BIRNBAUM and GLAUERT were able to solve this problem only for the special case of a "thin" profile: later, RIEGELS gave a suitable solution for profiles of finite thickness; the results of this extended theory are presented in Section 8.2.

## 8.2 Calculation of the Pressure Distribution for a Prescribed Shape of Profile†

### 8.2.1 Velocity Distribution on a Thin Profile; Vortex Distribution

#### 8.2.1.1 Vortex Distribution on a Straight Line of Length $c$

Suppose vortices are distributed along the  $x$  axis from  $x = 0$  to  $x = c$ . This vortex distribution,  $\gamma(x)$ , induces velocities,  $w_y$ , normal to the  $x$  axis; if  $w_y$  is positive when its direction is upwards, then

$$w_y = \frac{1}{2\pi} \int_0^c \frac{\gamma(x')}{x' - x} dx'. \quad (8.11)$$

When the normal velocity is prescribed this is an integral equation for the circulation  $\gamma(x)$ . If in place of  $x$  we introduce a parametric angle,  $\varphi$ , by the relation

$$x = \frac{c}{2} (1 + \cos \varphi), \quad (8.12)$$

the required vortex distribution can be shown to be

$$\gamma(\varphi) = \frac{1}{\sin \varphi} \frac{1}{\pi} \int_0^{2\pi} w_y \sin \varphi' \left( \cot \frac{\varphi' - \varphi}{2} - \right. \\ \left. - \cot \frac{\varphi'}{2} \right) d\varphi'; \quad (8.13)$$

the second term in the brackets ensures that at  $x = c$  (that is, at  $\varphi = 0$ ) the Kutta condition is satisfied, so that  $\gamma = 0$  there. Corresponding solutions in  $x$  have also been given. If the Kutta condition is not satisfied (that is, if  $\gamma(x)$  tends to infinity both when  $x$  approaches  $c$  as well as when  $x$  approaches 0) then

$$\gamma(x) = -\frac{2}{\pi \sqrt{x(c-x)}} \int_0^c \frac{w_y(x') \sqrt{x'(c-x')}}{x'-x} dx'; \quad (8.14)$$

† "The second main problem of profile theory."

if the vortex strength vanishes at  $x = c$ , we have

$$\gamma(x) = -\frac{2}{\pi} \sqrt{\frac{c-x}{x}} \int_0^c w_y(x') \sqrt{\frac{x'}{c-x'}} \frac{dx'}{x'-x}, \quad (8.15)$$

which corresponds to Equation (8.13).

### 8.2.1.2 Flat and Cambered Plates (Camber Lines)

We can obtain the flow past camber lines (bodies of zero thickness) in a simple way by superimposing a parallel flow (of speed  $V$ ) on the flow produced by a vortex distribution. The vortices are distributed along a straight line having the direction of the parallel flow; but, if we suppose that the parallel flow makes a small angle  $\alpha$  with the  $x$  axis, it is sufficiently accurate to regard the vortices as distributed along this axis. Suppose that the chord lies along the  $x$  axis, and that  $w_y$  is the normal component of the velocity induced on the  $x$  axis by the vortex distribution. The surface boundary condition may be written

$$\frac{w_y + V \sin \alpha}{V \cos \alpha} = \frac{dy^{(c)}}{dx}. \quad (8.16)$$

If  $\alpha$  is small this may be linearised to

$$\frac{w_y}{V} + \alpha = \frac{dy^{(c)}}{dx}, \quad (8.17)$$

where  $y^{(c)}$  denotes the ordinate of the plate at station  $x$ . For the flat plate that coincides with the part of the  $x$  axis lying between  $x = 0$  and  $x = c$ ,  $\frac{dy^{(c)}}{dx} = 0$ , so that  $w_y = -\alpha V$ ; from this, with the help of Equation (8.13), we obtain the familiar expression for the distribution of circulation along a flat plate,

$$\begin{aligned} \gamma_t &= 2 V \alpha \frac{1 - \cos \varphi}{\sin \varphi} = 2 V \alpha \tan \frac{\varphi}{2} = \\ &= 2 V \alpha \sqrt{\frac{c-x}{x}}. \end{aligned} \quad (8.18)$$

From Equations (8.17) and (8.12) we find that, for plates of small camber at zero incidence,

$$\begin{aligned} w_y &= V \frac{dy^{(c)}}{dx} = V \frac{dy^{(c)}}{d\varphi} \frac{d\varphi}{dx} \\ &= -\frac{2 V}{c} \frac{1}{\sin \varphi} \frac{dy^{(c)}}{d\varphi}. \end{aligned} \quad (8.19)$$

From this, with the help of Equation (8.13), we can derive the distribution of circulation along an arbitrarily cambered plate,

$$\begin{aligned} \gamma_c &= -\frac{4 V}{c \sin \varphi} \frac{1}{2\pi} \int_0^{2\pi} \frac{dy^{(c)}}{d\varphi'} \left( \cot \frac{\varphi' - \varphi}{2} - \right. \\ &\quad \left. - \cot \frac{\varphi'}{2} \right) d\varphi'. \end{aligned} \quad (8.20)$$

No assumption at all about the vortex strength at the leading edge has been made in the derivation of this equation. In general, infinitely large velocities occur at the leading edge; by superimposing a term containing angle of incidence (see Equation (8.18)) it is always possible to make the vortex strength zero at the leading edge; the angle of incidence necessary to do this is called the "ideal" angle of incidence (see Section 3.1).

Because the camber has been assumed small the corresponding velocity distribution along the chord can be obtained by linear superposition; it is

$$w = V \pm \gamma_t/2 \pm \gamma_c/2; \quad (8.21)$$

the upper and lower signs refer respectively to the upper and lower sides of the plate.

### 8.2.2 Velocity Distribution on a Symmetrical Profile; Source Distribution and Additional Vortex Distribution

Consider a symmetrical profile whose contour,  $y = y^{(t)}(x)$ , makes a small angle almost everywhere with the  $x$  axis. Suppose the flow is symmetrical, with a free-stream speed of  $V \cos \alpha$ . The profile can be replaced by a distribution of sources along the  $x$  axis,  $q_s(x)$ , where

$$q_s(x) = 2 V \cos \alpha \frac{dy^{(t)}}{dx}; \quad (8.22)$$

this source distribution induces a velocity  $w_{xs}$  along the  $x$  axis, where

$$w_{xs} = -\frac{1}{2\pi} \int_0^c \frac{q_s(x')}{x'-x} dx'. \quad (8.23)$$

The approximation is not satisfactory if the angle between the  $x$  axis and the tangent to the profile is large; in particular, it breaks down at the nose of the profile. We

can circumvent this difficulty by resolving along the body contour the sum of the free-stream velocity and the disturbance velocity in the  $x$  direction; we find that

$$w = (V \cos \alpha + w_{xs}) \frac{1}{\sqrt{1 + (dy/dx)^2}} . \quad (8.24)$$

It has been proved that the velocity distribution thus obtained agrees with that obtained by exact conformal mapping, when the latter is expanded in powers of a thickness parameter and the linear terms only are retained (RIEGELS).

If the flow is not symmetrical ( $\alpha \neq 0$ ) further consideration is necessary, since a free-stream velocity component  $V \sin \alpha$  appears in the boundary conditions. The surface boundary condition requires that the flow direction at each point of the profile coincide with the slope of the contour, and so we must distribute additional singularities along the  $x$  axis, in order to induce an additional downwash,  $\Delta w_y$ ; this downwash must compound with the tangential velocity from the vortex distribution ( $\gamma_t$ ) of the flat plate to give a resultant velocity having the direction of the profile contour. Here it must be remembered that the downwash induced by the vortex distribution of the flat plate is constant only along the  $x$  axis, and that its magnitude changes as the distance,  $y$ , from the  $x$  axis increases. The conditions can be fulfilled by means of an additional vortex distribution along the  $x$  axis,  $\gamma_v$ , which induces a correction velocity of just the right amount;  $\gamma_v$  is given by

\* Equation 8.27

$$\frac{w}{V} = \frac{1}{\sqrt{1 + \left[ \frac{dy^{(t)}}{dx} \right]^2}} \left[ \cos \alpha \left\{ 1 - \frac{1}{\pi} \int_0^c \frac{dy^{(t)}}{dx'} \frac{dx'}{x' - x} \right\} \pm \right. \\ \left. \pm \sin \alpha \sqrt{\frac{c - x}{x}} \left\{ 1 - \frac{1}{\pi} \int_0^c \left( \frac{dy^{(t)}}{dx'} - \frac{y^{(t)}}{2x'(c - x')} \right) \frac{dx'}{x' - x} \right\} \right] . \quad (8.27)$$

\*\* Equation 8.27a

$$\frac{w}{V} = \frac{1}{\sqrt{\sin^2 \varphi + \frac{4}{c^2} \left( \frac{dy^{(t)}}{d\varphi} \right)^2}} \left[ \cos \alpha \left\{ \sin \varphi - \frac{2}{c} \frac{1}{2\pi} \int_0^{2\pi} \frac{dy^{(t)}}{d\varphi'} \cot \frac{\varphi' - \varphi}{2} d\varphi' \right\} + \right. \\ \left. + \sin \alpha (1 - \cos \varphi) \left\{ 1 - \frac{2}{c \sin \varphi} \frac{1}{2\pi} \int_0^{2\pi} \left( \frac{dy^{(t)}}{d\varphi'} + \frac{y^{(t)}}{\sin \varphi'} \right) \cot \frac{\varphi' - \varphi}{2} d\varphi' \right\} \right] . \quad (8.27a)$$

$$\gamma_v = -\frac{2}{\pi} V \sin \alpha \sqrt{\frac{c - x}{x}} \\ \int_0^c \left( \frac{dy^{(t)}}{dx'} - \frac{y^{(t)}}{2x'(c - x')} \right) \frac{dx'}{x' - x} . \quad (8.25)$$

Equations (8.18), (8.22), and (8.25) give the source and vortex distributions that replace a symmetrical profile at an angle of incidence  $\alpha$ . The contributions to the velocity from these distributions are as follows:

$$w_{xt} = \pm (\gamma_t/2); \quad w_{xs} \text{ from Equation (8.23)}; \\ w_{xv} = \pm (\gamma_v/2). \quad (8.26)$$

If the velocity on the  $x$  axis is resolved along the profile contour and the tangential component of the free-stream velocity is added to the above contributions, there results for the velocity:

Equation 8.27 \*

In terms of  $\varphi$  this equation is

Equation 8.27a \*\*

### 8.2.3 Velocity Distribution on an Unsymmetrical Profile of Finite Thickness and Small Camber

The technique that we used in the previous section for the determination of the influence of angle of incidence can

obviously be applied to bodies whose mean line is not straight. If, however, we consider only profiles with small camber (in practice, the camber of most profiles is small), the contribution of the additional term proportional to  $\sin \alpha$  can be neglected. Unsymmetrical body shapes  $y = y(x)$  (more exactly:  $y = y_u(x)$  for the upper surface, and  $y = y_l(x)$  for the lower surface) can be regarded as having been formed by a superposition of symmetrical profile shapes  $y^{(t)}$  on cambered plates  $y^{(c)}$ :

$$y = y^{(c)} \pm y^{(t)} = \frac{y_u + y_l}{2} \pm \frac{y_u - y_l}{2}; \quad (8.28)$$

or, in terms of  $\varphi$ ,

$$y(\varphi) = \frac{y(\varphi) + y(-\varphi)}{2} + \frac{y(\varphi) - y(-\varphi)}{2}.$$

In the calculation of the corresponding velocity contributions along the  $x$  axis a contribution due to the camber,  $w_{xc} = \pm \frac{1}{2} \gamma_c$ , where  $\gamma_c$  is given by Equation (8.20), must be added to those listed in Equation (8.26). It is now possible to write down an equation corresponding to Equation (8.28), in which both  $y^{(t)}$  and the ordinate,  $y$ , of the cambered, thick profile appear:

Equation 8.29 \*

#### 8.2.4 Simpler Formulas for Practical Calculation

In the further development of these fundamental parts of the theory it is convenient to write  $y$  as a Fourier series:

$$\frac{y}{c/2} = \sum (a_n \cos n\varphi + b_n \sin n\varphi). \quad (8.30)$$

The cosine series represents the camber distribution, and the sine series the thickness distribution. We can easily

\*Equation 8.29

$$\begin{aligned} \frac{w}{V} &= \frac{1}{\sqrt{\sin^2 \varphi + \frac{4}{c^2} \left( \frac{dy}{d\varphi} \right)^2}} \left[ \cos \alpha \left\{ \sin \varphi - \frac{2}{c} \frac{1}{2\pi} \int_0^{2\pi} \frac{dy}{d\varphi'} \left( \cot \frac{\varphi' - \varphi}{2} - \cot \frac{\varphi'}{2} \right) d\varphi' \right\} + \right. \\ &\quad \left. + \sin \alpha (1 - \cos \varphi) \left\{ 1 - \frac{2}{c \sin \varphi} \frac{1}{2\pi} \int_0^{2\pi} \left( \frac{dy^{(t)}}{d\varphi'} + \frac{y^{(t)}}{\sin \varphi'} \right) \cot \frac{\varphi' - \varphi}{2} d\varphi' \right\} \right]. \end{aligned} \quad (8.29)$$

\*\*Equation 8.34

$$\frac{w}{V} = \frac{\{ \cos \alpha (\sin \varphi + \sum_1^\infty \nu a_\nu \cos \nu \varphi + \sum_1^\infty \nu b_\nu \sin \nu \varphi - \sum_1^\infty \nu a_\nu) + \sin \alpha (1 - \cos \varphi) (1 + \sum_0^\infty \beta_\mu \cos \mu \varphi) \}}{\sqrt{\sin^2 \varphi + (\sum \nu b_\nu \cos \nu \varphi - \sum \nu a_\nu \sin \nu \varphi)^2}}; \quad (8.34)$$

where  $\beta_0 = \sum_1^\infty \nu b_\nu$ ,  $\beta_\mu = 2 \sum_{-\mu}^\infty [(2\nu + \mu - 1) b_{2\nu+\mu-1} + 2 \nu b_{2\nu+\mu}]$ .

show that, if  $b_\nu = 0$ , the usual theory of thin profiles results: using Equation (8.30) with Equation (8.29) we find that, for small  $\frac{dy}{d\varphi}$ ,

$$\frac{w}{V} = 1 + \sum \nu a_\nu \frac{\cos \nu \varphi - 1}{\sin \varphi} + \alpha \tan \frac{\varphi}{2}, \quad (8.31)$$

this being the expression familiar from the theory of thin profiles (see DURAND II, p. 41). The term that is singular at the leading edge can be written separately if we split the series up into its even and odd terms; we find that

$$\begin{aligned} \frac{w}{V} &= 1 + \sum_1^\infty 2\nu a_{2\nu} \frac{\cos 2\nu \varphi - 1}{\sin \varphi} + \\ &\quad + \sum_1^\infty (2\nu - 1) a_{2\nu-1} \frac{\cos (2\nu - 1)\varphi - \cos \varphi}{\sin \varphi} + \\ &\quad + (\alpha - \alpha^*) \tan \frac{\varphi}{2}, \end{aligned} \quad (8.32)$$

where  $\alpha^*$ , the ideal angle of incidence, is given by

$$\alpha^* = \sum_1^\infty (2\nu - 1) a_{2\nu-1}. \quad (8.33)$$

For bodies of finite thickness ( $b_\nu \neq 0$ ) Equations (8.30) and (8.29), after some manipulation, lead to

Equation 8.34 \*\*

For an exact calculation from this equation the contour must be given in the form of a Fourier series. This can be avoided by using a suitable approximate procedure: if we are given the ordinates at certain fixed values of  $x$  we can replace the Fourier series by a finite series whose terms consist of products of the ordinates with certain fixed coefficients; the fixed values of  $x$  are given by †

$$x_n = \frac{1}{2} \left( 1 + \cos \frac{\pi n}{N} \right). \quad (8.35)$$

The velocity distribution is

$$\frac{w(x_n)}{V} = \frac{1}{\sqrt{c_n + (dy/d\varphi)^2}} [C \cos \alpha \pm D \sin \alpha]; \quad (8.36)$$

where

$$C = |a_n| + \sum_{m=1}^{N-1} A_{mn} \times 2y_m^{(t)} \pm \sum_{m=1}^{N-1} S_{mn} \times 2y_m^{(c)},$$

$$D = |b_n| + \sum_{m=1}^{N-1} H_{mn} \times 2y_m^{(c)}.$$

The upper and lower signs refer to the upper and lower sides of the profile respectively.  $\frac{dy}{d\varphi}$  denotes the slope of the profile with respect to the parametric angle; we can easily obtain this by plotting  $y$  against  $\varphi$  or  $n$ ; it is important only near the nose.  $2N$  is the total number of fixed points at which the ordinates  $y_m$  (on the suction side) and  $y_{2N-m}$  (on the pressure side) are prescribed;  $y_m^{(t)}$  and  $y_m^{(c)}$  are given by

$$2y_m^{(t)} = y_m - y_{2N-m}, \quad 2y_m^{(c)} = y_m + y_{2N-m}.$$

$a_n$ ,  $c_n$ ,  $A_{mn}$ ,  $S_{mn}$ , and  $H_{mn}$  are fixed coefficients, which can be tabulated for arbitrary values of  $N$ ; they are given in Table 11.8 for  $N = 12$ . If we wish to shorten the labour of calculation, we can calculate the values at the points  $n = 2, 4, 6, \dots$  and introduce the intermediate points (those in the series  $n = 1, 3, 5, \dots$ ) after, if necessary.

### 8.2.5 Forces and Moments

To determine the force and moment exerted on the body we require the vortex distribution along the  $x$  axis in Fourier form. Let the numerator of the right-hand side of Equation (8.34) be denoted by  $F(\varphi)$ ; then the vortex

† For practical reasons  $x$  and  $y$  are here referred to a chord of unity ( $c = 1$ ).

distribution (the difference between the velocities  $w\sqrt{1+y^2}$  on the upper and lower sides of the axis) is

$$\gamma(\varphi) = V \left\{ \frac{F(\varphi)}{\sin \varphi} - \frac{F(2\pi-\varphi)}{\sin(2\pi-\varphi)} \right\} \\ = V \frac{F(\varphi) + F(2\pi-\varphi)}{\sin \varphi}, \quad (0 \leq \varphi \leq \pi)$$

or

$$\gamma(\varphi) = \frac{2V}{\sin \varphi} \left\{ \cos \alpha \left[ \sum_{v=1}^{\infty} v a_v (\cos v\varphi - 1) \right] + \right. \\ \left. + \sin \alpha (1 - \cos \varphi) \left( 1 + \sum_{\mu=0}^{\infty} \beta_{\mu} \cos \mu \varphi \right) \right\}. \quad (8.37)$$

An integration along the chord gives the force normal to the free-stream direction:

$$L = \rho V \int_0^c \gamma(x) dx = \rho V \int_0^{\pi} \gamma(\varphi) \sin \varphi d\varphi;$$

its coefficient is

$$C_L = \frac{L}{\frac{\rho}{2} V^2 c} = 2\pi \left[ - \sum_{v=1}^{\infty} v a_v + \alpha \left( 1 + \sum_{v=1}^{\infty} b_{2v-1} \right) \right]. \quad (8.38)$$

The following formulas are obtained by the use of an approximate procedure (TRUCKENBRODT): the lift-curve slope is given by

$$\frac{dC_L}{d\alpha} = 2\pi \left( 1 + \frac{2}{\pi} \int_0^{\pi} \frac{y^{(t)}(\varphi)}{\sin \varphi} d\varphi \right)$$

$$= 2\pi \left( 1 + \sum_{v=1}^{\infty} b_{2v+1} \right)$$

$$= 2\pi \left( 1 + \sum_{v=1}^{N-1} A_{2v} \times 2y_m^{(t)} \right); \quad (8.39)$$

the angle of incidence at zero lift by

$$\begin{aligned}\alpha_0 &= -\frac{2}{\pi} \int_0^\pi \frac{y^{(c)}(\varphi)}{\sin \varphi} d\varphi = \sum_1^\infty \nu a_\nu, \\ &= \sum_1^{N-1} B_m \times 2y_m^{(c)};\end{aligned}\quad (8.40)$$

and, from the theory of thin profiles ( $y^{(t)} = 0$ ), the ideal angle of incidence by

$$\begin{aligned}\alpha^* &= -\frac{2}{\pi} \int_0^\pi \frac{\cos \varphi}{\sin^2 \varphi} y^{(c)}(\varphi) d\varphi \\ &= \sum_1^\infty (2\nu - 1) a_{2\nu-1} = \sum_1^{N-1} E_m \times 2y_m^{(c)};\end{aligned}\quad (8.41)$$

the corresponding lift coefficient is

$$\begin{aligned}C_L^* &= 2\pi(\alpha^* - \alpha_0) = 4 \int_0^\pi \frac{y^{(c)}(\varphi)}{\sin^2 \varphi} d\varphi \\ &= -4\pi \sum_1^\infty \nu a_{2\nu} = \sum_1^{N-1} F_m \times 2y_m^{(c)}.\end{aligned}\quad (8.42)$$

When calculating the moment we must remember that the source distribution, as well as the vortex distribution, makes a contribution. If we refer the moment to the point  $x = 0$ , then the contribution from the source distribution has the value

$$A(M)_l = \rho V \sin \alpha \int_0^c q(x) x dx;$$

so that, for the total moment referred to the point  $x = 0$ , we have

$$\begin{aligned}(M)_l &= -\rho V \int_0^c [q(x) - \alpha q(x)] x dx \\ &= -\rho V \frac{c^2}{4} \left[ \int_0^\pi \gamma(\varphi) (1 + \cos \varphi) \sin \varphi d\varphi - \right. \\ &\quad \left. - \alpha \int_0^\pi q(\varphi) \cos \varphi \sin \varphi d\varphi \right],\end{aligned}$$

$$\text{where } q(\varphi) = -\frac{2V}{\sin \varphi} \sum_1^\infty \nu b_\nu \cos \nu \varphi;$$

the positive sense of the moment is clockwise, if the flow is assumed to come from the left; the coefficient is

$$(C_m)_l = \frac{(M)_l}{\frac{\rho}{2} V^2 c^2} =$$

$$\frac{\pi}{2} \left[ -a_1 + 2 \sum_1^\infty \nu a_\nu - a \left( 1 + 2b_1 + 2 \sum_1^\infty b_{2\nu} \right) \right]. \quad (8.43)$$

$\frac{d(C_m)_l}{dC_L}$  can be written in the form

$$\frac{d(C_m)_l}{dC_L} = -\frac{1}{4} \left( 1 + \frac{2}{\pi} \int_0^\pi \frac{1 + 2 \cos \varphi - 2 \cos 2\varphi}{\sin \varphi} y^{(t)}(\varphi) d\varphi \right)$$

$$\begin{aligned}&= -\frac{1}{4} \left( 1 + b_1 + 2 \sum_1^\infty b_{2\nu} - \sum_1^\infty b_{2\nu+1} \right) \\ &= -\frac{1}{4} \left( 1 + \sum_1^{N-1} C_m \times 2y_m^{(t)} \right).\end{aligned}\quad (8.44)$$

The moment at zero lift is

$$\begin{aligned}Cm_0 &= -\int_0^\pi \frac{2 \cos \varphi - \cos 2\varphi}{1 - \cos \varphi} y^{(c)}(\varphi) d\varphi = \frac{\pi}{2} \sum_2^\infty \nu a_\nu, \\ &= \sum_1^{N-1} D_m \times 2y_m^{(c)}.\end{aligned}\quad (8.45)$$

Numerical values of  $A_m$ ,  $B_m$ , etc are given in Table 11.7.

### 8.3 Calculation of the Profile Shape for a Prescribed Velocity Distribution†

The problem described in the title has been solved approximately by RIEGELS (1943) on the same basis as in the preceding sections: by use of the method of singularities. The process is based on relations that are the converse of those derived in the previous section. A convenient

† "The first main problem of profile theory."

approximate method has been given by TRUCKENBRODT. We shall describe only the results necessary for practical application.

### 8.3.1 Thin Profiles

Suppose the velocities on the upper and lower sides of the chord are different from one another at each point, but that they satisfy the relation  $w = V \pm w_1$ , where the upper and lower signs refer to the upper and lower sides respectively; this corresponds to the camber line of a profile at a certain angle of incidence,  $\alpha$ . For the flow to leave the trailing edge smoothly  $w_1$  must vanish there. We can regard the distribution of  $w_1$  as induced by a vortex distribution assumed to lie along the chord. From the condition that the normal velocity vanish on the camber line we obtain the following formula for the slope of the camber line,  $\frac{dy^{(c)}}{dx}$ , by using Equations (8.11), (8.17), and (8.21).

$$\frac{dy^{(c)}}{dx} = \alpha - \frac{1}{\pi} \int_0^c \frac{w_1(x')}{V} \frac{dx'}{x - x'} ; \quad (8.46)$$

here,  $y^{(c)}$  denotes the ordinate of the camber line, and  $\alpha$  the angle of incidence (both being measured from the chord). Let  $g^{(c)}$  denote the prescribed velocity distribution, so that

$$g^{(c)} = \frac{w_1}{V} = \pm \left( \frac{w}{V} - 1 \right); \quad (8.47)$$

if  $g_m$  represents the value of  $g$  at the point  $x_m$ , then the local angle of incidence of the camber line,  $\alpha^{(c)}$ , is given by the following finite series:

$$\alpha^{(c)} = \sum_{m=1}^{N-1} d_m g_m + d_N \lim_{\varphi \rightarrow \pi} (g \sin \varphi); \quad (8.48)$$

the ordinate of the camber line at the point  $x_n$  is

$$\frac{y_n^{(c)}}{c} = \sum_{m=1}^{N-1} d_m g_m + d_N \lim_{\varphi \rightarrow \pi} (g \sin \varphi). \quad (8.49)$$

The fixed coefficients  $d_m$  and  $d_N$  are given in Table 11.9a.

### 8.3.2 Symmetrical Profile at Zero Incidence

Suppose the velocities on the upper and lower sides of the chord are the same at each point; this corresponds to a

symmetrical profile,  $y^{(t)}$ , at zero incidence, the direction of its chord coinciding with the free-stream direction. Such a velocity distribution can be written  $w = V + w_2$ , where  $w_2$  denotes the disturbance velocity associated with the thickness distribution. A stagnation point occurs at the leading edge of the profile (that is,  $w$  must vanish there). We can think of the distribution of  $w_2$  as induced by a source distribution assumed to lie along the chord; since the normal velocity on the surface of the profile must be zero, Equation (8.24) represents an integral equation for the slope of the upper side.

This equation becomes

$$\begin{aligned} \frac{dy^{(t)}}{dx} = & - \frac{1}{\pi} \int_0^c \left[ \frac{w}{V} \sqrt{1 + \left( \frac{dy^{(t)}}{dx'} \right)^2} - 1 \right] \times \\ & \times \sqrt{\frac{x'(c-x')}{x(c-x)}} \frac{dx'}{x-x'} . \end{aligned} \quad (8.50)$$

By an approximate procedure the solution can be obtained as a finite series (if we approximate the distribution of  $w$  by a finite series). If  $y^{(t)}$  is written in the form

$$y^{(t)} = \frac{c}{2} \sum_1 b_n \sin n\varphi, \quad (8.51)$$

this ensures that the profile is closed at both the leading ( $\varphi = \pi$ ) and trailing ( $\varphi = 0$ ) edges. After some manipulation we obtain

$$\bar{y}_n' = \frac{1}{c} \frac{dy^{(t)}}{d\varphi} = \sum_{m=1}^{N-1} a_{mn} f_m. \quad (8.52)$$

The quantity  $f_m$  is the value of  $f$ , the velocity function, at the point  $x = x_m$ ;  $f$  is given by

$$f = \kappa \frac{w}{V} - 1, \quad \text{where } \kappa = \sqrt{1 + \left( \frac{dy}{dx} \right)^2}. \quad (8.53)$$

The factor  $\kappa$  is important only at points of large curvature (at the profile nose); elsewhere it is negligible.

For the  $p^{\text{th}}$  stage of the approximate procedure we have

$$f_m^{(p)} = \kappa_m^{(p)} f_m^{(o)} + \kappa_m^{(p)} - 1; \quad (8.54)$$

$$\text{where } \kappa_m^{(p)} = \sqrt{1 + \left( \frac{\bar{y}_m'^{(p-1)}}{a_m} \right)^2},$$

$$\text{and } f_m^{(o)} = \left( \frac{w}{V} \right)_m - 1.$$

$a_m$  and  $a_{mn}$  are constants; they are given in Table 11.9b for  $N = 12$ . In the execution of the iterative procedure it is an advantage if  $a_{mn}$  vanishes whenever  $(m - n)$  is even. To calculate the zero approximation, we put  $\kappa_m^{(0)} = 1$ , so that  $f_m$  can be immediately obtained from the prescribed velocity distribution. The values are then inserted into Equation (8.52), and the profile slope,  $\bar{y}_n^{(0)}$ , is determined at the points  $n = 1, 3, \dots$ . With the help of Equations (8.54) and (8.53) the values of  $f_m^{(1)}$  for the same points are easily calculated, and these are inserted into Equation (8.52); this gives the first approximation,  $\bar{y}_n^{(1)}$ , at the points  $n = 2, 4, \dots$ . The succeeding approximations are obtained similarly. In order that the approximation should converge rapidly, it is advisable to calculate values at the leading edge ( $y_N$ ) and at the trailing edge ( $y_0$ ). Once the behaviour of  $\bar{y}'(\varphi)$  is known the desired profile ordinates can be obtained by an integration with respect to  $\varphi$ .

In addition to this iterative solution we can also derive a solution from the Fourier representation, which allows an immediate calculation of the profile ordinates; we obtain

$$\frac{y^{(t)}}{c} = \frac{1}{4\pi} \int_0^\pi f(\varphi') \sin \varphi' \ln \frac{1 - \cos(\varphi + \varphi')}{1 - \cos(\varphi - \varphi')} d\varphi'. \quad (8.55)$$

For numerical evaluation this solution can be replaced by the following finite series:

$$y_n^{(t)} = \frac{y^{(t)}}{c} = \sum_{m=1}^{N-1} b_{mn} f_m; \quad (8.56)$$

TRUCKENBRODT has given the coefficients  $b_{mn}$  for  $N = 12$ .

### 8.3.3 Unsymmetrical Profile at Incidence

Suppose the velocities on the upper and lower sides of the chord are different at each point; we can then write

$$w = V \pm w_1 + w_2 \pm \alpha w_3. \quad (8.57)$$

The additional velocity component  $\alpha w_3$  arises if the body of finite thickness is at an angle of incidence  $\alpha$ . If the velocity distribution on the upper surface is denoted by  $w_u$  and that on the lower surface by  $w_l$ , then

$$V + w_2 = \frac{w_u + w_l}{2}, \quad w_1 + \alpha w_3 = \frac{w_u - w_l}{2}. \quad (8.58)$$

To convert the velocity on the surface to that in the direction of the chord we must multiply the former by a factor  $\kappa$ , where  $\kappa = \sqrt{1 + (dy/dx)^2}$ . The factor is of importance only at points where the profile curvature is large; it is the thickness distribution that produces such points, and hence the influence of the camber line can be neglected at such points, so that  $y$  may be replaced by  $y^{(t)}$ . With this simplification the thickness distribution can be calculated immediately, if the velocity distribution in Section 8.3.2,  $w$ , is put equal to  $\frac{1}{2}(w_u + w_l)$ ;  $f$  is then given by

$$f = \frac{\kappa}{2} \frac{w_u + w_l}{V} - 1.$$

The iteration procedure described in Section 8.3.2 gives the profile slope as a function of  $\varphi$ ; the ordinates  $\bar{y}^{(t)}$  of the thickness distribution are then obtained by integration. We suppose first that  $w_3$ , which depends only on the thickness distribution, is known; the shape of the camber line and the local angle of incidence can then be calculated as described in Section 8.3.1. There the required velocity distribution is denoted by  $w_1$ ; for  $w_1$  we must now write

$$w_1 = \sqrt{1 + \left(\frac{dy}{dx}\right)^2} \left[ \frac{1}{2} (w_u - w_l) - \alpha w_3 \right]; \quad (8.59)$$

so that Equation (8.47) becomes

$$g = \frac{\kappa}{2} \frac{w_u - w_l}{V} + \Delta g, \quad (8.60)$$

where

$$\Delta g = -\alpha \kappa \frac{w_3}{V}. \quad (8.61)$$

We first put  $\Delta g = 0$ ; then, carrying out the calculation described in Section 8.3.1, we find that

$$g = \frac{\kappa}{2} \frac{w_u - w_l}{V},$$

or

$$\lim_{\varphi \rightarrow \pi} (g \sin \varphi) = \left[ \frac{w_u - w_l}{V} \left| \frac{1}{c} \frac{dy^{(t)}}{d\varphi} \right| \cdot \right]_{\varphi=\pi}; \quad (8.62)$$

here, the factor  $\kappa$  is taken from the calculation for the thickness distribution. From Equations (8.48) and (8.49) we can obtain the local angle of incidence,  $\alpha^{(c)}$ , and the ordinates,  $y^{(c)}$ , of the camber line. The previously neglected velocity component  $w_3$  is determined by using Equation (8.27); TRUCKENBRODT has shown that the influence

this term, which is produced by the incidence of the thickness distribution, can be considered simply as an additional change in the camber line; the corresponding change in the local angle of incidence is found to be

$$\Delta\alpha = -\alpha \lim_{\varphi \rightarrow \pi} \left( \frac{y^{(t)}}{c} \tan \frac{\varphi}{2} \right) = \left[ \alpha \frac{2}{c} \frac{dy^{(t)}}{d\varphi} \right]_{\varphi=\pi}. \quad (8.63)$$

The total local angle of incidence,  $\alpha$ , obtained from the sum  $\alpha = \alpha^{(c)} + \Delta\alpha$ , is

$$\alpha = \frac{\alpha^{(c)}}{\left[ 1 - \frac{2}{c} \frac{dy^{(t)}}{d\varphi} \right]_{\varphi=\pi}} = \frac{\alpha^{(c)}}{1 - \bar{y}_N^{(t)}}. \quad (8.64)$$

We find that the change in the ordinates of the camber line is

$$\Delta y^{(c)} = -\alpha(1 - \cos \varphi) \left( \frac{y^{(t)}}{\sin \varphi} + \left[ \frac{dy^{(t)}}{d\varphi} \right]_{\varphi=\pi} \right); \quad (8.65)$$

and, at the points  $n = \frac{\varphi}{\pi} N$ , we have

$$\Delta y_n^{(c)} = -\alpha (p_n \bar{y}_n^{(t)} + q_n \bar{y}_N^{(t)}), \quad (8.66)$$

where the constants,  $p_n$  and  $q_n$ , have been calculated for  $N = 12$ , and are given in Table 11.9c. The three parts,  $y^{(t)}$ ,  $y^{(c)}$ , and  $\Delta y^{(c)}$ , must be combined to give the required ordinates:

$$y = y^{(t)} \pm y^{(c)} \pm \Delta y^{(c)}. \quad (8.67)$$

## 8.4 Remarks on the Rigorous Methods of Conformal Mapping

### 8.4.1 Older Solutions of the Second Main Problem

Mathematical methods for the conformal mapping of the exterior of a given profile (lying in the  $z$  plane) into the exterior of the unit circle (lying in the  $\zeta$  plane) are based on the mapping function

$$z = \zeta + c_0 + \frac{c_1}{\zeta} + \frac{c_2}{\zeta^2} + \frac{c_3}{\zeta^3} + \dots \quad (8.68)$$

("Riemann's Mapping Theorem"). In the familiar procedures of VON KÁRMÁN and TREFFTZ, MÜLLER, HÖHN-DORF, and THEODORSEN, the given profile is mapped into an approximately circular figure by using a known mapping function (for example, that of the Joukowski transformation or that of the Kármán-Trefftz transformation); this figure is then transformed by another procedure

into a circle. Almost all the authors do the second stage by an iterative procedure, in which the imaginary part of an analytic function is determined from a knowledge of the real part. Both MÜLLER and VON KÁRMÁN and TREFFTZ use the convenient method of harmonic analysis for this; the reader is referred to DURAND for a description of the process (by VON KÁRMÁN and BURGERS). THEODORSEN and GARRICK determine the imaginary part, without using harmonic analysis, by direct evaluation of the Poisson integral

$$\varepsilon(\bar{\varphi}) = -\frac{1}{2\pi} \int_0^{2\pi} \Psi(\bar{\varphi}') \cot \frac{\bar{\varphi}' - \bar{\varphi}}{2} d\bar{\varphi}'. \quad (8.69)$$

Here  $\varepsilon = \bar{\varphi} - \Theta$ ; it is the angular difference between the vectors of two points connected by the mapping function, one on the approximately circular figure ( $\zeta'$ , with angular coordinate  $\Theta$ ), and one on the circle ( $\zeta$ , with angular coordinate  $\bar{\varphi}$ ); this is illustrated in Figure 8.1.  $\zeta'$  and  $\log |\zeta'| = \Psi$  are known functions of the angle  $\Theta$ , since  $\zeta'$  is the distance from the point chosen as centre of the circle to the point on the approximately circular figure, and so  $\zeta'$  can be obtained graphically. If we write  $\bar{\varphi}' \approx \Theta$  and use  $\Psi(\Theta)$  as the distribution function in Equation (8.69), we can find a first approximation,  $\varepsilon^{(1)}$ ; from this we obtain an improved value of  $\bar{\varphi}$ ,  $\bar{\varphi}^{(1)} = \Theta + \varepsilon^{(1)}$ ;  $\varepsilon^{(2)}$  is formed from  $\Psi(\bar{\varphi}^{(1)})$  in the same way, and an iteration procedure carried out until successive approximations cease to differ significantly.

The idea sketched here has been used by the authors as a method of calculation. In an extension by WALZ it is made the basis of a graphical procedure, by which even irregular contours (for example, profiles with flaps and dead-water regions) can be mapped into a circle; the graphical aids are used mainly in the construction of the approximately circular figure and in the evaluation of the Poisson integral.

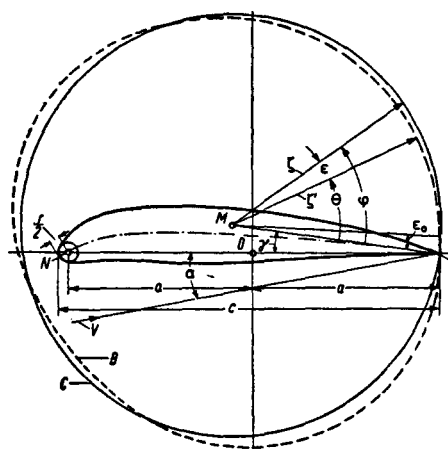


Fig. 8.1. Mapping the approximately circular figure into the circle ( $C$ )

BETZ and KEUNE treat the first problem with the help of a network based on the source-sink flow field; the second problem is solved with the aid of a suitably numbered network. For normal profiles the iteration converges rapidly, and only a few steps are necessary†. In the determination of the velocity distribution the derivative of the mapping function is required; this can be obtained in terms of distances between certain points, as described in Section 8.1.

We end this brief description of other procedures that use potential theory by referring to some later work. RINGLEB and ROSSNER have been able to represent more general types of profiles by a combination of known mapping functions; the significance of the methods used can be easily understood intuitively. THEODORSEN, GOLDSTEIN, LIGHTHILL, THWAITES, and others have succeeded in obtaining solutions of the first and second main problems in a different way: they have treated the mapping problem analytically; there is then little need for intuitive assumptions about the form of certain functions, but the mathematical analysis cannot be described as simple.

#### 8.4.2 Iteration without Intermediate Mapping

The procedure of Theodorsen requires the evaluation of a Poisson integral; such an integral frequently occurs in boundary value problems concerning a circle. Graphical methods are not always the most accurate of procedures; and a direct calculation of the integral is often both inaccurate and inconvenient because of the singular points. For these reasons WITTICH approximates the distribution function by a trigonometric polynomial, and determines the coefficients by considering the integrand at certain fixed values of  $\bar{\varphi}$ ; by this method the integral is approximated in the sense of the method of least squares (Gauss).

Instead of the integral

$$-\frac{1}{2\pi} \int_0^{2\pi} f(\bar{\varphi}') \cot \frac{\bar{\varphi}' - \bar{\varphi}}{2} d\bar{\varphi}' = h(\bar{\varphi}), \quad (8.70)$$

we obtain a finite series,

$$\begin{aligned} h(\bar{\varphi}_n) &= \left\{ \pm \sum_{m=0}^N a_{mn} s_m - \sum_{m=0}^N \beta_{mn} d_m \right\}; \\ h(\bar{\varphi}_{2N-n}) &= \end{aligned} \quad (8.71)$$

where

$$s_m = f(\bar{\varphi}_m) + f(\bar{\varphi}_{2N-m}), \quad d_m = f(\bar{\varphi}_m) - f(\bar{\varphi}_{2N-m}).$$

† WITTICH has investigated the basic question of the convergence of the Theodorsen procedure; he finds that, in general, it is assured provided that the approximately circular figure is stellar (that is, its radius vector is a one-valued function of the polar angle) and that the maximum value of  $|d\Psi/d\Theta|$  is less than approximately 1/12.

Here,  $\bar{\varphi}_m = \frac{\pi m}{N}$  ( $m = 0, 1, \dots, 2N$ );  $a_{mn}$  and  $\beta_{mn}$  are constants that can be calculated once and for all,

$$\begin{aligned} a_{mn} &= \left\{ \frac{1 - (-1)^{m+n}}{4N} \times \right. \\ \beta_{mn} &= \left. \times \left( \cot \frac{\pi(m+n)}{2N} \pm \cot \frac{\pi(m-n)}{2N} \right) \right\}; \quad (8.72) \end{aligned}$$

$2N$  is the number of values of  $\varphi$ .

WITTICH realises that, with the help of this representation, the function that maps the profile into the circle can be obtained by iteration from a simple initial approximation, and that an intermediate mapping into an approximately circular figure is unnecessary. This idea leads him to a representation of the mapping in the form of an integral equation for  $x(\bar{\varphi})$ ,

$$x(\bar{\varphi}) = a_0 + 2a \cos \bar{\varphi} - 2b \sin \bar{\varphi} - \frac{1}{2\pi} \int_0^{2\pi} f(x(\bar{\varphi})) \cot \frac{\bar{\varphi}' - \bar{\varphi}}{2} d\bar{\varphi}'; \quad (8.73)$$

this equation is a relationship between the co-ordinates of the profile,  $x$  and  $y (=f(x))$ , and the angle  $\bar{\varphi}$ . The constants,  $a_0$ ,  $2a$ , and  $2b$  are determined from the chosen normalisation of the profile; if the longest chord is chosen as the  $x$  axis, we can make the point on the circle for which  $\bar{\varphi} = 0$  go into the trailing edge ( $x = 1$ ), and another point on the circle,  $\bar{\varphi} = \bar{\varphi}^*$ , go into the leading edge ( $x = 0$ ). These conditions can be written:

$$x(0) = 1, \left( \frac{dx}{d\bar{\varphi}} \right)_{\bar{\varphi}=0} = 0; \quad x(\bar{\varphi}^*) = 0, \left( \frac{dx}{d\bar{\varphi}} \right)_{\bar{\varphi}=\bar{\varphi}^*} = 0.$$

The solution of the above integral equation, Equation (8.73), is obtained by the following iteration procedure. As a first approximation we take  $x_0 = \frac{1}{2}(1 + \cos \bar{\varphi})$ ; we find that

$$h_1(\bar{\varphi}) = -\frac{1}{2\pi} \int_0^{2\pi} y_0(\bar{\varphi}') \cot \frac{\bar{\varphi}' - \bar{\varphi}}{2} d\bar{\varphi}',$$

where  $y_0 = f(x_0)$ ; we determine the constants and so obtain the second approximation,

$$x_1 = a_0^{(1)} + 2a^{(1)} \cos \bar{\varphi} - 2b^{(1)} \sin \bar{\varphi} + h_1(\bar{\varphi}); \quad (8.74)$$

with  $y_1 = f_1(x)$  we obtain the third approximation,  $x_2$ , in the same way. For the calculation of the Poisson integral  $h_v(\bar{\varphi})$  we use WITTICH's finite series. Numerical calculations

show that the sequence converges fairly well. For thick and uncambered profiles the convergence of the process can be improved by using the following procedure from  $x_2$  onwards: we write  $\bar{x}_2 = \frac{x_1 + x_2}{2}$  and, from this, determine

$x_3$ ; we then write  $\bar{x}_3 = \frac{\bar{x}_2 + x_3}{2}$  and, from this, determine

$x_4$ ; and so on. A procedure due to IMAI (proposed at about the same time) differs only in minor details; Tables 11.4 contain velocity distributions that have been calculated by IMAI, KAJI, and UMEDA, with the help of this method.

If we restrict ourselves to symmetrical profiles, the determination of the constants is greatly simplified; it can be reduced to the solution of the two linear equations

$$a_0 + 2a + h(0) = 1, \quad a_0 - 2a + h(\pi) = 0.$$

In this case the original idea of RIEGELS-WITTICH (to determine the mapping constants by iteration, without using the preceding integral representation) is easily carried out; this has been shown by RINGLEB.

## 8.5 References

- ALLEN, H. J.: A Simplified Method for the Calculation of Airfoil Pressure Distribution. NACA TN 708 (1939).
- General Theory of Airfoil Section Having Arbitrary Shape or Pressure Distribution. NACA ACR No. 3G29 (1943).
- BETZ, A.: Änderung der Profilform zur Erzielung einer vorgegebenen Änderung der Druckverteilung. Lufo 11 (1934), S. 1.
- and F. KEUNE: Verallgemeinerte Kármán-Trefftz-Profile. Lufo Bd. 13 (1936), S. 336.
- CURTIS, A. R.: Note on the Application of Thwaites' Numerical Method for the Design of Cambered Sections. R & M No. 2665 (1949).
- EPPLER, R.: Die Berechnung von Tragflügelprofilen aus der Druckverteilung. Ing. Arch. 23 (1955), 436—452.
- Laminarprofile für Segelflugzeuge. ZfW 3 (1955), 345—353.
- FLÜGGE-LOTZ, J. and I. GINZEL: Die ebene Strömung um ein geknicktes Profil mit Spalt. Jahrb. 1939 dDL I, S. 55—66.
- GARRICK, I. E.: Determination of the Theoretical Velocity Distribution for Twenty Airfoils. NACA TN 465.
- GLAUERT, H.: Theoretical Relationships for an Aerofoil with Hinged Flap. R & M No. 1095 (1927).
- GLAUERT, M. B.: The Application of the Exact Method of Aerofoil Design. R & M No. 2683 (1947).
- GOLDSTEIN, S.: A Theory of Aerofoils of Small Thickness. Parts I—III, C.P. 68, 69, 70 (1942).
- Approximate Two-Dimensional Aerofoil Theory, Parts IV—VI, C.P. 71—73 (1945).
- GRAHAM, O. D.: A Modification to Thin Airfoil Section Theory. NACA TN 2298 (1951).
- HELMBOLD, H. B. and F. KEUNE: Beiträge zur Profilforschung III—VI. Lufo 20 (1943), S. 152—170, 192—206.
- HÖHNDRÖF, F.: Verfahren zur Berechnung des Auftriebes gegebener Tragflächenprofile. ZAMM 6 (1926), S. 265.
- IMAI, J., J. KAJI and K. UMEDA: Mapping Functions of the NACA-Airfoils into the Unit Circle. Journ. Fac. Sci. Hokkaidō Univ. Ser. II, Vol. III, No. 8 (1950).
- JAECKEL, K.: Das Geschwindigkeitsfeld eines beliebigen dünnen und schwach gewölbten Tragflügelprofils. Lufo 16 (1939), S. 209.
- Eine Formel für die von einem dünnen Tragflügelprofil induzierten Geschwindigkeiten in Punkten, die auf der verlängerten Sehne liegen. Lufo 16 (1939), S. 53.
- Auswertung der Ackermann-Birnbaumschen Integralgleichung mit Hilfe einer Interpolationsformel. Z. f. Flugwiss. 3 (1955), S. 46/48.
- KÁRMÁN, T. v. and E. TREFFTZ: Profilströmung um gegebene Tragflächenquerschnitte. ZfM 9 (1918), S. 111.
- KAWALKI, K. H.: Profile geringster Übergeschwindigkeit bei vorgegebenen Auftriebsbewertungen. LGL-Bericht 156, S. 163 bis 169.
- Theoretische Untersuchungen von Schnellprofilen, die aus Ellipsenprofilen entwickelt sind. FB 1224/1 und 2 (1940).
- KEUNE, F.: Auftrieb einer geknickten ebenen Platte. Lufo 13 (1936), S. 85—87.
- Momente und Ruderauftrieb einer geknickten ebenen Platte. Lufo 14 (1937), S. 558.
- KEUNE, F.: Die ebene Potentialströmung um allgemeine dicke Tragflügelprofile. Jahrb. 1938 dDL I, S. 3.
- Theoretische Profilformen mit weitgehend freier Wahl der Dickenverteilung und der Skelettformen. Jahrb. 1940 dDL I, S. 36—40.
- Aerodynamische Berechnung systematischer Flügelprofile. Jahrb. 1943 dDL I A 024 in Techn. Ber. 11 (1944), Heft 1.
- KOCHANOWSKI: Anwendung der Druckverteilungsrechnung auf die Ermittlung der Unterdruckspitzen und den Einfluß des Hochbiegens der Profilvorderkante. Jahrb. 1940 dDL I, S. 72 bis 80.
- KRÜGER, H.: Zur Geschwindigkeitsbestimmung an gewölbten, dünnen Profilen in allgemeiner Potentialströmung. MPI-Bericht 52/B/12.
- LEHMANN and F. ZEUNERT: Beitrag zur Profilforschung. UM 7603 (1944).
- LIGHTHILL, M. J.: A New Method of Two-Dimensional Aerodynamic Design. R & M No. 2112 (1945).
- LOCK, C. N. H. and J. H. PRESTON: The New Type of Aerofoil Section. Aircraft Engineering Vol. 11 (1939), p. 151.
- MÄGLER, K. W.: Die Berechnung eines Tragflügelprofils mit vorgeschriebener Druckverteilung. Jb. 1938 dDL I, S. 46.
- MENZEL-ROGNER, H.: Das Geschwindigkeitsfeld in der Umgebung eines Leitwerkprofils endlicher Dicke verschwindenden Spalts. Lufo 17 (1940), S. 11—16.
- MISES, R. v.: Zur Theorie des Tragflächenauftriebes. ZFM 8 (1917), S. 11 and 157 sowie 11 (1920), S. 68 und 87.
- MÜLLER, W.: Ebene Potentialströmung mit Zirkulation. ZAMM 3 (1923), S. 117.
- Zur Konstruktion von Tragflächenprofilen, ZAMM 4 (1924), S. 213.
- MUNK, M. M.: Elements of the Wing Section Theory and of the Wing Theory. NACA Rep. 191 (1924).
- The Determination of the Angles of Attack of Zero Lift and Zero Moment, Based on Munk's Integrals. NACA TN 122, (1923).
- NAIMANN, I.: Numerical Evaluation of the Integral Occurring in the Theodorsen Arbitrary Airfoil Potential Theory. NACA ARR No. L4D27a, April 1944 (Wartime Rep. No. L-136).
- Numerical Evaluation by Harmonic Analysis of the Function of the Theodorsen Arbitrary Potential Theory. NACA ARR No. L5H18, Sept. 1945 (Wartime Rep. No. L-153).
- PANKHURST, R. C.: A Method for the Rapid Evaluation of Glauert's Expressions for the Angle of Zero Lift and the Moment at Zero Lift. R & M No. 1914 (1944).

- PÉRÈS, J.: Bemerkungen zum Rudenverfahren für die Bestimmung der Geschwindigkeit im Felde eines Joukowsky-Profil. Ing.-Arch. 10 (1939), S. 46.
- PIERCY, N. A. V., R. W. PIPER and J. H. PRESTON: A New Family of Wing Profiles. Phil. Mag. 24 (1937), pp. 425 and 1114.
- PIERCY, N. A. V., R. W. PIPER and L. G. WHITEHEAD: The New Transformed Wing Sections. Aircraft Engineering, Vol. 10 (1938), p. 339.
- PINKERTON, R. M.: Analytical Determination of the Load on a Trailing Edge Flap. NACA TN No. 353, (1930).
- Calculated and Measured Pressure Distribution over the Midspan Section of the NACA 4412 Airfoil NACA TR 563 (1936).
- PIPER, R. W.: Extensions of the New Family of Wing Profiles. Phil. Mag. Ser. 7, v. 24 (1937), p. 1114.
- PISTOLESI, E.: Sulla Teoria delle Ali Sottili. Acta Pont. Acad. Scient. I (1937), S. 57—72.
- RIEGELS, F. and H. WITTICH: Zur Berechnung der Druckverteilung von Profilen. Jb. 1942 dDL I, S. 120—132.
- Zur konformen Abbildung beliebiger Profile auf den Kreis und Bestimmung der Druckverteilung in inkompressibler Strömung. AVA 42/A/20 (1942).
- RIEGELS, F.: Über die Berechnung der Druckverteilung von Profilen. Techn. Ber. 10 (1943), S. 13.
- Russische Laminarprofile. UM 3040, 3067, 3159 (1943/44).
  - Profile mit vorgegebener Druckverteilung. UM 3019 (1943) und ZAMM 24 (1944), 273.
  - Bemerkung über den Ersatz von Profilen endlicher Dicke durch Singularitäten auf der Achse. AVA-Bericht 45/A/23 (1945) (Betz-Festschrift).
  - Das Umströmungsproblem bei inkompressiblen Potentialströmungen (I. Mitt.) Ing.-Arch. 16 (1948), S. 373—376.
  - Das Umströmungsproblem bei inkompressiblen Potentialströmungen (II. Mitt.) Ing.-Arch. 17 (1949), S. 94—106 und Berichtigung Ing.-Arch. 18 (1950), S. 329.
- RINGLEB, F.: Beiträge zur Theorie der Tragflügelprofile. FB 1496 oder Jahrb. 1942 dDL I, S. 133—140.
- Iterationsverfahren zur Bestimmung der Geschwindigkeitsverteilung eines Tragflügelprofils. Vorabdruck Jahrb. 1943 dDL.
- ROSSNER, G.: Systematische theoretische Untersuchungen über den Einfluß von Gestalt und Umrißkontur eines Tragflügelprofiles auf den Verlauf der zugehörigen Druckverteilung. FB 1893 (1940).
- Über eine Klasse von theoretischen Profilen mit vier frei-wählbaren geometrischen Parametern. Jahrb. 1942 dDL I, S. 142—159.
- RUDEN, P.: Ein graphisch-rechnerisches Verfahren zur Bestimmung des Geschwindigkeitsvektors im Strömungsfeld eines Joukowsky-Profil. Ing.-Arch. 7 (1936), S. 71—80.
- SCHRENK, O.: Druck- und Geschwindigkeitsverteilung längs der Flügeltiefe für verschiedene Flugzustände. Ringb. d. Luftfahrttechnik (1938) I A 11.
- and A. WALZ: Theoretische Verfahren zur Berechnung von Druck- und Geschwindigkeitsverteilungen. Jahrb. 1939 dDL I, S. 29—49.
  - STRASSL, H.: Die ebene Potentialströmung um ein Flügelprofil mit Vorflügel. Jahrb. 1939 dDL I, S. 67—71.
  - TANI, I. and S. MITUSSI: Contributions to the Design of Airfoils Suitable for High Speeds. Rep. 198 Aer. Res. Inst. Tokyo XV (1940), pp. 399—415.
  - THEODORSEN, TH.: Theory of Wing Sections of Arbitrary Shape. NACA Rep. No. 411, (1932).
  - and I. E. GARRICK: General Potential Theory of Arbitrary Wing Sections. NACA Rep. No. 452, 1933.
  - Airfoil Contour Modification Based on  $\epsilon$ -Curve Method of Calculating Pressure Distribution. NACA ARR No. LAG05, 1944 (Wartime Rep. No. L-135).
  - THWAITES, B.: A Method of Airfoil Design. Part I—Symmetrical Airfoils. R & M No. 2166 (1945).
  - A Method of Airfoil Design. Part II—Cambered Airfoils. R & M No. 2167 (1945).
  - A New Family of Low Drag Wings with Improved  $C_L$ -ranges. R & M No. 2292 (1945).
  - On the Design of Aerofoils for which the Lift is Independent of the Incidence. R & M No. 2612 (1952).
  - TIMANN, R.: The Direct and the Inverse Problem of Airfoil Theory. A Method to Obtain Numerical Solutions. NLL-Rep. F 16 (1951).
  - TRUCKENBRODT, E.: Ergänzungen zu F. RIEGELS: Das Umströmungsproblem bei inkompressibler Potentialströmung. Ing.-Arch. 18 (1950), S. 324—329.
    - Die Berechnung der Profilform bei vorgegebener Geschwindigkeitsverteilung. Ing.-Arch. 19 (1951), S. 365—377.  - WALZ, A.: Übertragung gemessener Druckverteilungen auf beliebige Anstellwinkel. Lufo 16 (1939), S. 121—128.
    - Ermittlung symmetrischer Profilformen mit kleinstmöglicher Übergeschwindigkeit bei vorgegebenem Schlankheitsgrad. FB 1051 (1939).
    - Zur Anwendung des Druckverteilungsrechenverfahrens von Theodorsen-Pinkerton. UM 3160 (1944).  - WEINIG, F.: Beitrag zur Theorie des Schlitzflügels. Lufo 12 (1935), S. 149—154.
  - WEINIG, F.: Übertragung der Druckverteilung eines Tragflügelprofils bei einem bestimmten auf einen beliebigen Anstellwinkel. Werft, Reederei, Hafen 94 (1931), S. 115.
    - Die Abhängigkeit der Geschwindigkeit und Druckverteilung an einem Tragflügelprofil vom Anstellwinkel. Werft, Reederei, Hafen 96 (1933), S. 127.
    - Geschwindigkeit und Richtung der Strömung um ein Tragflügelprofil. Lufo 12 (1935), S. 222—228.
    - Die Strömungsverhältnisse im Felde dünner schwachgewölbter Tragflügelprofile. ZAMM 18 (1938), S. 107.  - WITTICH, H.: Bemerkung zur Druckverteilungsrechnung nach Theodorsen-Garrick. Jahrb. 1941 dDL I, S. 52—57.
    - Zur näherungsweisen Berechnung der Geschwindigkeit um Tragflächenquerschnitte. UM 3145 (1944).

## 9. THE THEORY OF WING PROFILES III

### Viscous Flow

#### 9.1 Influence of Reynolds Number on Pressure Distribution and Lift

It is easily confirmed that, if the flow has not separated, pressure distributions obtained by potential theory agree well with measurements at small values of  $C_L$  (apart from the immediate neighbourhood of the trailing edge). At higher values of  $C_L$  systematic deviations occur; a familiar result is that the measured lift-curve slope is less than the value predicted by potential theory (Figure 9.1). A

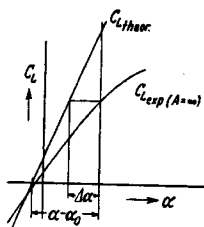


Fig. 9.1. Definition of  $\Delta\alpha$

calculation using potential theory leads to larger peak suctions and  $C_L$  values than are measured, provided that the angle of incidence is the same as in the experiment: the same calculation carried out for a smaller angle of incidence, such that the theoretical value of  $C_L$  is the same as the experimental value, produces peak suctions that are too small. Provided that the value of  $C_L$  is not too high, the fact that the boundary layer thickens rapidly near the trailing edge (so that the potential flow is displaced outwards) is responsible for only a small part of the discrepancy. Usually a more important cause is that the Kutta condition, that the flow leave the trailing edge smoothly, is not fulfilled, and so a change in the circulation occurs. BETZ has therefore proposed that the rear stagnation point should be moved a small distance from the trailing edge and be placed on the suction side of the profile. PINKERTON has successfully extended this proposal by assuming that the slope of the profile changes in a way dependent on the local state of the boundary layer; the distortion corresponds to a reduction in local camber (that is, to a decrease in the local angle of incidence). The distribution along the chord of the change is arbitrarily assumed to have the form  $\frac{\Delta\alpha}{2}(1 + \cos\varphi)$ , since the approximate behaviour only is required;  $\Delta\alpha$  is the amount by which the angle of incidence must be changed to produce the experimental value of  $C_L$ .

(see Figure 9.1). Because  $\alpha$  is a small angle we can obtain a linearised representation for the corrected pressure distribution,

$$\left( \frac{\Delta p}{q} \right)_{\text{corr.}} = \frac{\Delta p}{q} \pm \Delta\alpha \frac{w}{V} \times \left[ \frac{1 - x_*}{\sqrt{F}} + 2x_*(D \mp C \sin\alpha) \mp 2a_* \frac{w}{V} \right] \quad \dots (9.1)$$

The derivation of this equation is based on the theory of Section 8.2;  $\frac{\Delta p}{q}$  and  $\frac{w}{V}$  are respectively the pressure and velocity distributions at the angle of incidence of the experiment,  $\alpha$ , determined according to Equation (8.36); the meanings of the double sign and of the remaining quantities (including  $F = c_n + \left(\frac{dy}{dx}\right)^2$ ) have already been explained. The correction term,  $\Delta\alpha$  (dependent on Reynolds number), is a function of  $C_L$  and can be taken from an experiment on the profile being considered; if no such experiment is at our disposal we can either estimate the behaviour of  $C_L(\alpha)$  from the results of a similar profile or try to derive an approximation from the calculated boundary layer thickness near the trailing edge.

Figure 12.27 illustrates the agreement to be expected between theory and experiment when a slide rule and graphical aids are used; attached flow is assumed. We usually find that large discrepancies between theory and experiment occur only in the neighbourhood of the trailing edge (approximately, between  $\frac{x}{c} = 0.9$  and  $\frac{x}{c} = 1$ ); they arise mainly from the assumption that the rear stagnation point lies at the trailing edge, this being only approximately true.

We have seen that the influence of Reynolds number on the pressure distribution is small, if the flow is attached. Figure 12.38 shows that important changes occur if separation of the boundary layer takes place (for example, at a sufficiently high angle of incidence); the pressure distribution is then strongly influenced by the appearance of regions of separated flow. A remarkable feature is that the variation of pressure along the whole chord is altered; as the Reynolds number decreases, the theoretically high suction peaks are considerably reduced and finally disappear almost completely. Consequently, at small Rey-

nolds numbers and high angles of incidence the pressure distribution shows the typically constant behaviour that corresponds to separation; at sufficiently high Reynolds numbers vestiges of the theoretical suction peaks occur in the immediate neighbourhood of the nose.

## 9.2 Calculation of Boundary Layers

### 9.2.1 Introductory Remarks

From the previous section the influence of the boundary layer on the pressure distribution can be crudely estimated. We now give a more detailed description of the results of modern boundary layer theory: we show how to determine the remaining profile characteristics (a theoretical determination is often to be preferred to wind-tunnel measurements); and we indicate the value of the results for the aircraft constructor.

The boundary layer is the generally very thin layer on the profile in which the velocity changes from its value in the outer, potential flow to zero; the boundary layer can show laminar or turbulent character. For an estimate of its thickness ( $\delta$ ) it is tempting to use the following simple formulas, which apply to the flat plate (that is, to constant pressure in the outer flow): in the laminar case we have

$$\delta \approx 5x \left( \frac{Vx}{\nu} \right)^{-1/4}; \quad (9.2)$$

and in the turbulent case

$$\delta \approx 0.37x \left( \frac{Vx}{\nu} \right)^{-1/6}; \quad (9.3)$$

where  $x$  denotes the length of the boundary layer. These are not sufficient to make an accurate forecast of the boundary layer development on a profile; the reason is the strong dependence of the velocity distribution in the boundary layer on the pressure distribution in the outer flow.

In general, the velocity profile  $u(y)$  is concave towards the axis in a favourable pressure gradient; if the pressure begins to rise, a point of inflexion soon appears in the velocity profile, and this becomes convex near the wall (see Figure 9.2 for the laminar case). At the wall the slope of the velocity,  $\frac{du}{dy}$ , and the skin friction,  $\tau = \mu \frac{du}{dy}$ , decrease as the outside pressure increases, and finally become zero ("laminar separation"). However, according to TOLLMIEN, velocity profiles with a point of inflexion are unstable—that is, small disturbances can be amplified to such an extent that transition from a laminar to a turbulent boundary layer takes place. The velocity profile is also strongly influenced when air is sucked in or blown

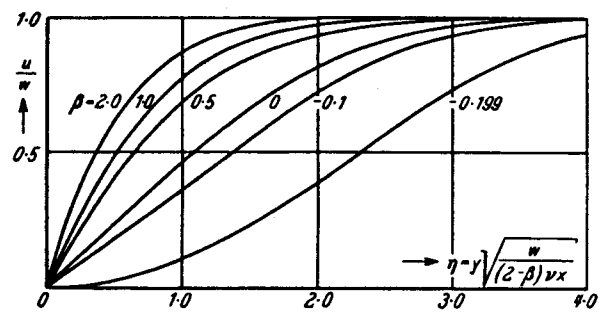


Fig. 9.2. Influence of various pressure gradients: velocity distribution in the boundary layer for potential flows  $w \sim x^m$ .  $\beta = \frac{2m}{(1+m)}$  is a measure of the pressure gradient.  $\beta = 0$ : flat plate.  $\beta = -0.199$ : separation. (HARTREE)

out along the surface (see Figure 9.3). Suction has a stabilising effect on the velocity profile, similar to that of a fall in the outside pressure: on the other hand, blowing has a destabilising effect, similar to that of a rise in the outside pressure (see Section 9.3.1).

The solution of Prandtl's boundary layer equations for an arbitrary pressure distribution has been attempted in various ways. Among others, PRANDTL, GÖRTLER, and MANGLER have sought exact solutions of the differential equations; more details of these and other procedures can be found in the exhaustive works of TOLLMIEN (see Section 1.5.2) and SCHLICHTING (see Section 1.5.1). Before any of these procedures had been devised, the methods of von KÁRMÁN and POHLHAUSEN were of great importance; these methods use the momentum theorem as a starting-point for a theoretical calculation. There is an inevitable loss in accuracy, because the velocity profiles in the boundary layer are assumed to be a one-parameter family of curves; familiar choices are the boundary layer profiles calculated by HARTREE for the special potential flows

$w \sim x^{(\frac{\beta}{2-\beta})}$  ( $x$  being the arc length of the contour), and the polynomial distributions used by POHLHAUSEN to represent an arbitrary velocity distribution along the

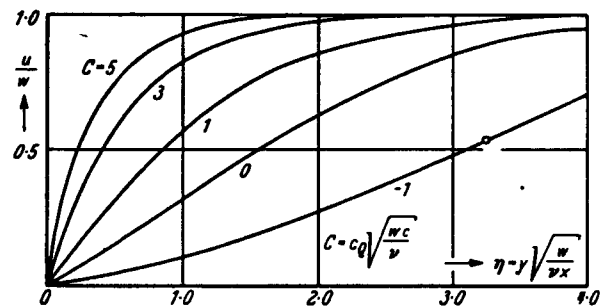


Fig. 9.3. Influence of suction, for the flat plate; suction velocity given by  $v_s = -\frac{C}{2} \sqrt{\frac{vw}{x}}$ . Figure shows velocity distribution in the boundary layer for various suction-parameters  $C = c_0 \sqrt{R}$ .  $C < 0$ : blowing.  $C = 0$ : Blasius.  $C > 0$ : suction. (SCHLICHTING-BUSSMANN)

contour

$$\frac{u}{w} = a_1\eta + a_2\eta^2 + a_3\eta^3 + a_4\eta^4, \quad \left( \eta = \frac{y}{\delta} \right). \quad (9.4)$$

The corresponding boundary layer quantities are given in Tables 9.1 and 9.2.

Table 9.1

Characteristic boundary layer quantities for potential flows of the form  $w \sim x^m$ ,  $m = \frac{\beta}{2 - \beta}$  (HABTREE)

$\beta$	$\frac{w'\delta^2}{v}$	$\frac{\tau_0\delta}{\mu w}$	$\frac{\delta^*}{\delta}$
-0.1988	-0.0682	0	4.038
-0.190	-0.0632	0.0496	3.480
-0.180	-0.0580	0.0730	3.296
-0.160	-0.0488	0.1053	3.091
-0.140	-0.0407	0.1290	2.963
-0.10	-0.0266	0.1644	2.797
0	0	0.2204	2.591
0.1	0.0190	0.2556	2.481
0.2	0.0333	0.2802	2.412
0.5	0.0811	0.3241	2.307
1.0	0.0864	0.3602	2.217
2.0	0.1063	0.3891	2.157
$\infty$	0.142	0.435	2.07

Table 9.2

Characteristic boundary layer quantities for arbitrary potential flows  $w = w(x)$ ;  $\lambda = (dw/dx) \delta^2/v$  (POHLHAUSEN)

$\lambda$	$\frac{w'\delta^2}{v}$	$\frac{\tau_0\delta}{\mu w}$	$\frac{\delta^*}{\delta}$
-12	-0.1587	0	3.800
-10	-0.1369	0.039	3.276
-8	-0.1130	0.079	3.084
-5	-0.0720	0.140	2.847
-3	-0.0429	0.179	2.716
-1	-0.0140	0.217	2.604
0	0	0.235	2.554
1	0.0135	0.252	2.508
5	0.0599	0.310	2.361
7.052	0.0770	0.332	2.308
10	0.0920	0.351	2.260
12	0.0940	0.356	2.250

Essential simplifications in and improvements to the original methods of calculation have been achieved by transformation of the governing differential equation and choice of suitable parameters. The latest procedures, following WIEGHARDT, employ an energy theorem for the boundary layer, in addition to the momentum theorem; we shall discuss these in the next section.

Hence, the problem of determining the laminar boundary layer for an arbitrary pressure distribution (that is, for an arbitrary wing and angle of incidence) can for

practical purposes be considered as solved; nowadays a laminar boundary layer calculation can be performed with speed and ease.

The theory of the turbulent boundary layer has not yet reached the stage where the development of the boundary layer can always be successfully forecast, and it is still necessary to make use of experimental material. However, great improvements have been made in recent years, allowing a uniform treatment of the laminar and turbulent cases; we now consider these new results†.

### 9.2.2 Basic Equations. Momentum and Energy Theorems

In this section  $x$  and  $y$  denote the co-ordinates respectively parallel and normal to the body surface;  $u$  and  $v$  are the velocity components inside the boundary layer in the  $x$  and  $y$  directions respectively. The general problem is to calculate the velocity components  $u$  and  $v$  (for  $0 \leq y \leq \delta$ ) by solving Prandtl's differential equations

$$u \frac{\partial u}{\partial x} + v \frac{\partial u}{\partial y} = - \frac{1}{\rho} \frac{dp}{dx} + \frac{1}{\rho} \frac{\partial \tau}{\partial y},$$

$$\frac{1}{\rho} \frac{dp}{dx} = - w \frac{dw}{dx}, \quad (9.5)$$

together with the equation of continuity

$$\frac{\partial u}{\partial x} + \frac{\partial v}{\partial y} = 0. \quad (9.6)$$

The boundary conditions are:  $u = 0$ ,  $v = v_0$ ,  $\tau = \tau_0$ , at  $y = 0$ ; and  $u = w$ ,  $\tau = 0$ , at  $y = \delta$ . In general, exact solutions of these equations are obtained only by laborious procedures. Fortunately, approximate solutions are usually satisfactory for practical purposes; the complete detailed solution is not of great importance, only certain integrated quantities being of interest; integral theorems (for example, the momentum and energy theorems) suffice for the determination of these quantities.

For the formulation of these theorems we introduce various integrals (the integration being from the profile surface to the outside flow):

(a) "Displacement thickness",

$$\delta^* = \int_0^\delta \left( 1 - \frac{u}{w} \right) dy; \quad (9.7)$$

† K. KRAEMER has developed a convenient boundary layer slide-rule for carrying out the procedures described.

(b) "Momentum thickness",

$$\vartheta = \int_0^\delta \frac{u}{w} \left(1 - \frac{u}{w}\right) dy; \quad (9.8)$$

(c) "Energy thickness",

$$\bar{\delta} = \int_0^\delta \frac{u}{w} \left[1 - \left(\frac{u}{w}\right)^2\right] dy; \quad (9.9)$$

(d) "Work done against shearing stress",

$$\frac{D + T}{\rho w^3} = \int_0^\delta \frac{\tau}{\rho w^2} \frac{\partial}{\partial y} \left(\frac{u}{w}\right) dy. \quad (9.10)$$

Using these quantities, we can derive the following theorems:

I. Momentum theorem (VON KÁRMÁN, POHLHAUSEN),

$$\frac{1}{w^2} \frac{d}{dx} (w^2 \vartheta) + \frac{\delta^*}{w} \frac{dw}{dx} = \frac{\tau}{\rho w^2}; \quad (9.11)$$

II. Energy theorem (WIEGHARDT, ROTT),

$$\frac{1}{w^3} \frac{d}{dx} (w^3 \bar{\delta}) = 2 \frac{D + T}{\rho w^3}. \quad (9.12)$$

The right-hand side of Equation (9.12) requires clarification. For the laminar boundary layer the work done against shearing stress is simply equal to the dissipation,  $D$  (that is, the energy converted into heat); for the turbulent boundary layer the work done against shearing stress contains a further contribution; this is the turbulent energy produced per unit time, and is written  $T$ ; it is usually so small that it need not be taken into account in the determination of approximate solutions.

### 9.2.3 TRUCKENBRODT's Approximate Procedure

We introduce the ratios  $H = \frac{\delta^*}{\vartheta}$  and  $\bar{H} = \frac{\delta}{\vartheta}$ , replace  $\delta$  in Equation (9.12) by  $\bar{H}\vartheta$ , and from this equation subtract Equation (9.11) multiplied by  $\bar{H}$ ; the result is

$$\vartheta \frac{d\bar{H}}{dx} = (\bar{H} - 1) \bar{H} \frac{\vartheta}{w} \frac{dw}{dx} + 2 \frac{D + T}{\rho w^3} - \bar{H} \frac{\tau_0}{\rho w^2} \dots (9.13)$$

TRUCKENBRODT shows that  $\frac{\tau_0}{\rho w^2}$  and  $\frac{D + T}{\rho w^3}$  can be ex-

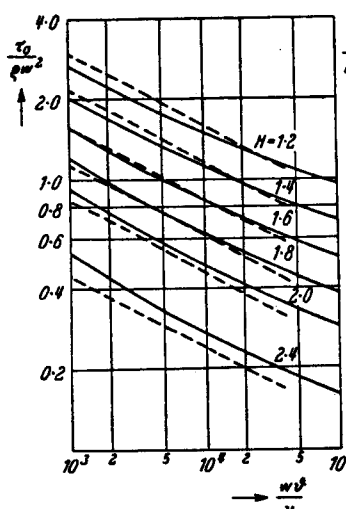


Fig. 9.4. Turbulent skin-friction.  
(Full line: Rotta. Dashed line:  
LUDWIEG-TILLMAN)

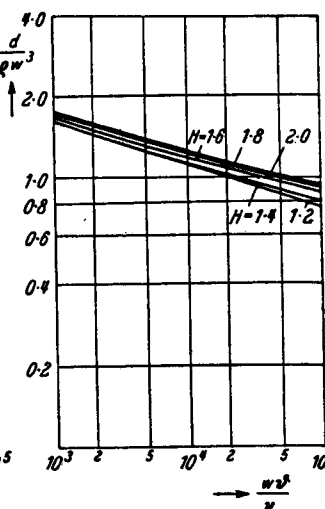


Fig. 9.5. Turbulent dissipation.  
(ROTTA)

pressed as functions of  $\frac{wv^2}{\nu}$  (a Reynolds number based on the momentum thickness) and  $H$  (see Figures 9.4 and 9.5). In addition, a fixed relationship exists between  $\bar{H}$  and  $H$ , if it is assumed that the velocity distributions in the boundary layer form a one-parameter family (Figure 9.6). Equations (9.12) and (9.13) then represent two equations for the two unknowns  $\vartheta$  and  $\bar{H}$ ; the first of these is to be obtained from the energy theorem, Equation (9.12), the second from Equation (9.13).

We now describe TRUCKENBRODT's approximate procedure, which is applicable to an arbitrary profile; the derivation and details are omitted. In practice the velocity distribution on the profile,  $w(x)$ , and the Reynolds number

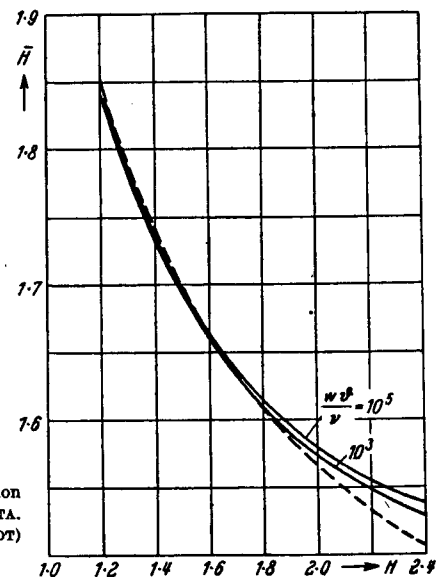


Fig. 9.6.  $\bar{H}$  as a function  
of  $\bar{H}$ . (Full line: Rotta.  
Dashed line: WIEGHARDT)

based on the chord,  $\frac{V_c}{\nu}$ , are prescribed; we wish to know the development of the laminar and turbulent boundary layers (that is, the behaviour of the momentum thickness,  $\vartheta(x)$ , and the form parameter,  $H(x)$ ). The formulas for the laminar and the turbulent boundary layers are placed side by side.

First,  $\vartheta(x)$  is easily obtained from

$$\frac{\vartheta(x)}{c} = \frac{A_l^{1/2}}{\left(\frac{w}{V}\right)^3}; \quad \left| \frac{\vartheta(x)}{c} = \frac{A_t^{6/7}}{\left(\frac{w}{V}\right)^3}; \quad (9.14)\right.$$

in these equations

$$A_l(x) = c_1 + \left( \frac{C_{fl}}{2} \right)^2 \int_{x_1/c}^{x/c} \left( \frac{w}{V} \right)^5 d\left(\frac{x}{c}\right), \quad A_t(x) = c_1 + \left( \frac{C_{ft}}{2} \right)^{7/6} \int_{x_1/c}^{x/c} \left( \frac{w}{V} \right)^{10/3} d\left(\frac{x}{c}\right),$$

where

$$C_{fl} = 1.328 \left( \frac{V_c}{\nu} \right)^{-1/2}, \quad C_{ft} = 0.0306 \left( \frac{V_c}{\nu} \right)^{-1/7},$$

(Blasius) (Falkner)

and  $c_1 = 0$  if the boundary layer starts from the point  $x_1 = 0$ ; if we are given that  $w = w_1$  and  $\vartheta = \vartheta_1$  at the point  $x = x_1$ , then

laminar	turbulent
$c_1 = \left[ \left( \frac{w_1}{V} \right)^3 \cdot \frac{\vartheta_1}{c} \right]^2;$	$c_1 = \left[ \left( \frac{w_1}{V} \right)^3 \frac{\vartheta_1}{c} \right]^{7/6};$

for a turbulent boundary layer we sometimes have to take  $c_1$  from a previous laminar boundary layer calculation. We obtain  $L$ , a parameter characterising the velocity profiles, by using the auxiliary variable

$A_l^{6.5}$ (for decreasing pressure),	$\xi = A_t,$
$\xi =$	
$A_l^8$ (for increasing pressure),	

defined in terms of the functions  $A_l(x)$  or  $A_t(x)$ , which have already been calculated; the required expression for  $L$  is

$$L = \frac{\xi_1}{\xi} L_1 + \ln \frac{w(\xi)}{w_1} + \frac{1}{\xi} \int_{\xi_1}^{\xi} \left[ b(\xi') - \ln \frac{w(\xi')}{w_1} \right] d\xi', \quad (9.15)$$

where

$$b = 0. \quad \left| \quad b = 0.07 \log \frac{w\vartheta}{\nu} - 0.23. \right.$$

The corresponding form parameter,  $H$ , and (in the laminar case) the skin-friction coefficient,  $\frac{\tau_0 \vartheta}{\mu w}$ , can be read off from Figure 9.7. In the turbulent case, the skin-friction coefficient can be found subsequently from the values obtained for  $H$  and  $\frac{w\vartheta}{\nu}$ , as described by either LUDWIEG and TILLMANN or ROTTA (Figure 9.4 and Section 9.4.3).

#### Initial Values

(a) A boundary-layer calculation is usually started at the stagnation point (so that  $x_1 = 0$ ); at this point  $w = cx$  where  $c = \left( \frac{dw}{dx} \right)_{x=0}$ . For the laminar boundary layer the following initial values are then valid:

$$\sqrt{\frac{c}{\nu}} \vartheta_0 = 0.271; \quad L_0 = 0.0260; \quad H_0 = 2.25.$$

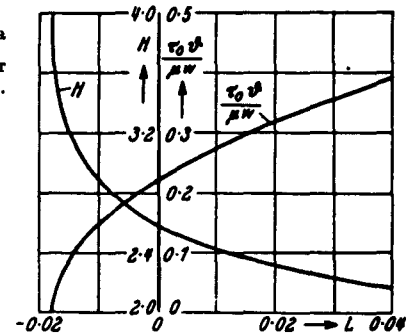
(b) After a certain distance the boundary layer changes from the laminar to the turbulent state. This happens in a region of transition, in which the behaviour of  $\vartheta(x)$  and  $H(x)$  changes; the latter quantity decreases from a high value (about 2.6 for the flat plate) to a smaller value (between 1.2 and 1.4 for the flat plate). The phenomenon of transition is still not well understood. As an approximation we assume that transition takes place at a certain point (suffix  $T$ ), and we write

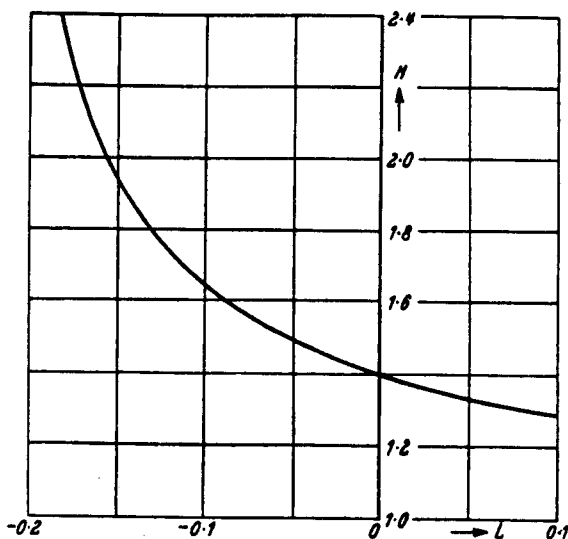
$$\vartheta_t(x_T) = \vartheta_l(x_T), \quad H_t(x_T) = H_l(x_T) - \Delta H, \quad (9.16)$$

where for  $\Delta H$  we use values corresponding to the flat plate ( $\Delta H = 1.2, 1.32, 1.38$ , when  $\frac{w\vartheta}{\nu} = 10^3, 10^4, 10^5$ , respectively);  $L(x_T)$  is read off from Figures 9.7 and 9.8 and is then placed in Equation (9.15), where it is written as  $L_1$ .

Separation occurs in a laminar boundary layer when  $\tau_0 = 0$ ; that is, when  $H = 4.038$  and  $L = -0.318$ .

Fig. 9.7.  $H$  and  $\frac{\tau_0 \vartheta}{\mu w}$  as a function of the parameter  $L$ , for laminar flow. (TRUCKENBRODT)



Fig. 9.8.  $H$  as a function of  $L$ , for turbulent flow. (TRUCKENBRODT)

According to recent work (Figure 9.4)  $\tau_0$  in a turbulent boundary layer does decrease as  $H$  increases, but it never vanishes completely; as an approximation TRUCKENBRODT and also DOENHOFF and TETERVIN take the smallest value of  $H$  at which separation begins to be 1.8 and the largest value to be 2.4. The corresponding values of  $L$  are -0.13 and -0.18.

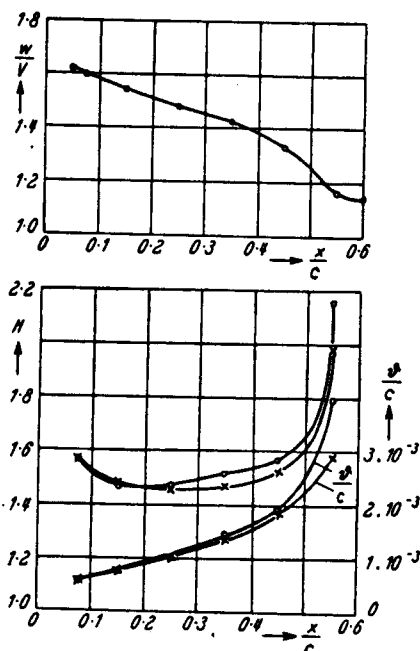
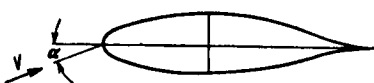
Fig. 9.9. Comparison of a NACA experiment ( $\circ$ ) with a theoretical boundary layer calculation as described in Section 9.2.3

Figure 9.9 gives a comparison between results from this method and from a NACA experiment [R772] on the profile NACA 65 (216)-222.

#### 9.2.4 Effect of Compressibility

An allowance for the effect of compressibility on the boundary layer leads to a considerable complication in the theoretical methods and solutions, because not only the velocity profile but also the density (or temperature) profile is unknown. Nevertheless, there already exists a large number of theoretical results for the flat plate (with constant pressure) and for boundary layers in favourable and unfavourable pressure gradients.

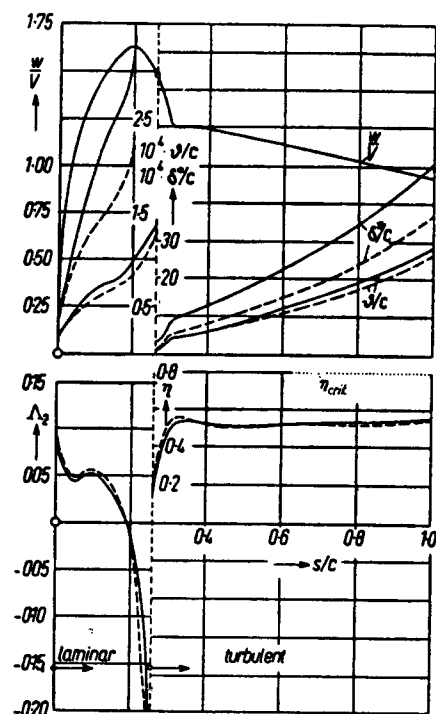


Fig. 9.10. Example of a boundary layer calculation for compressible flow,  $M = 0.7$ . Dashed line: incompressible calculation for the same pressure distribution.  $A_2 = \frac{w' \theta^2}{v}$ : Pohlhausen parameter. Danger of separation when  $\eta \approx 0.8$ ,  $\eta$  being Gruschwitz parameter. Reynolds number:  $4 \cdot 10^6$ . Profile: 23009.  $\alpha = 1.47^\circ$ .  $C_L = 0.34$ . (WALZ)

An attempt to determine the effect of compressibility meets still greater difficulties when the boundary layer is turbulent, since the approximations made for the density profile in a laminar boundary layer are not valid in a turbulent boundary layer. To obtain a first estimate WALZ introduces an average density, which is dependent on the Mach number and the velocity of the outer flow but not on the velocity profile of the boundary layer. Figure 9.10 shows results for boundary layers on the profile NACA 23009 at a Mach number of 0.7, which have been obtained by this method; also shown is a calculation performed for the same pressure distribution on the assumption that the

flow is incompressible. We see that there is little change in the quantities  $\vartheta$  and  $\eta$  ( $\eta$  is a boundary layer parameter introduced by GRUSCHWITZ and used in the calculation); on the other hand, the displacement thickness,  $\delta^*$ , increases considerably with Mach number.

We conclude this section by mentioning the later work of COPE, LEVY, MANGLER, MOORE, VAN DRIEST, WILSON, and YOUNG.

### 9.3 Results of Stability Calculations and Calculation of the Critical Reynolds Number

#### 9.3.1 The Critical Reynolds Number

No satisfactory answer has yet been given to the question where the position of the point of transition from a laminar to a turbulent boundary layer is. Considerable progress has been achieved by using the theory of small disturbances, which was developed by TOLLMIEN and considerably extended by SCHLICHTING and PRETSCH. According to this theory, the reason for transition is that the laminar boundary layer becomes unstable to small disturbances at a sufficiently high Reynolds number. Under certain conditions these small disturbances can be amplified; when they become sufficiently large they cause transition to the turbulent state. The original small disturbances arise in practice from surface roughness, or from isolated roughnesses such as rivet-heads or small pieces of metal; they also come from turbulence in the air (for example, in a wind tunnel). We shall discuss only the results of the theory, which has been experimentally confirmed by SCHUBAUER and SKRAMSTAD.

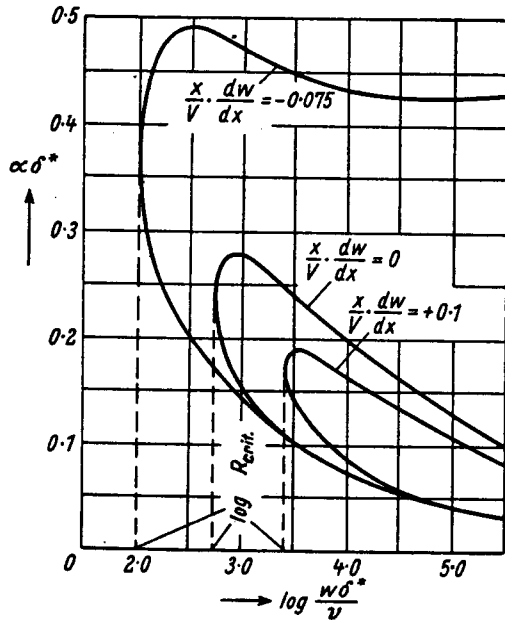


Fig. 9.11. Result of a stability calculation for the boundary layer in a potential flow  $w = V + \frac{dw}{dx}x$ . Instability inside, stability outside, the region enclosed by thick line.  $R_{\text{crit.}} = \left(\frac{w\delta^*}{\nu}\right)_{\text{crit.}}$ , the "critical Reynolds number".

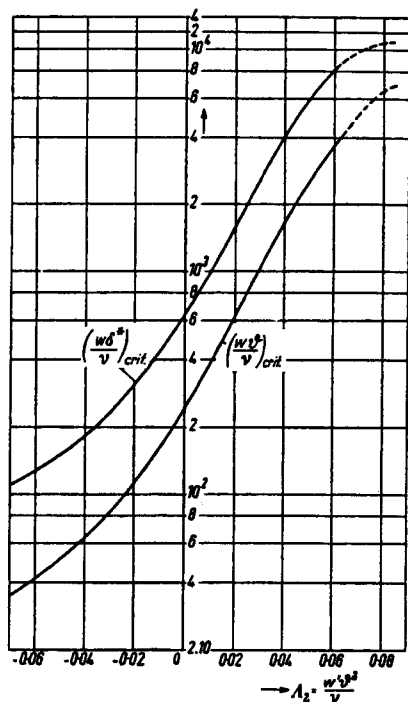


Fig. 9.12. The critical Reynolds numbers  $\left(\frac{w\delta^*}{\nu}\right)_{\text{crit.}}$  and  $\left(\frac{w\delta^*}{\nu}\right)^2_{\text{crit.}}$  for the Pohlhausen class of profiles, as a function of pressure gradient (more accurately, of the form parameter,  $A_2 = \frac{\partial^2 w}{\nu^2 dx^2}$ )

The extensive calculations lead to diagrams in which  $\alpha\delta^*$  is plotted against  $\log(w\delta^*/\nu)$  (see Figure 9.11). Here,  $\alpha = \frac{2\pi}{\lambda}$ , where  $\lambda$  is the wave length of the disturbance superimposed on the potential flow; hence, apart from a factor of  $2\pi$ ,  $\alpha\delta^*$  is the reciprocal of the disturbance wave length referred to  $\delta^*$ , the displacement thickness;

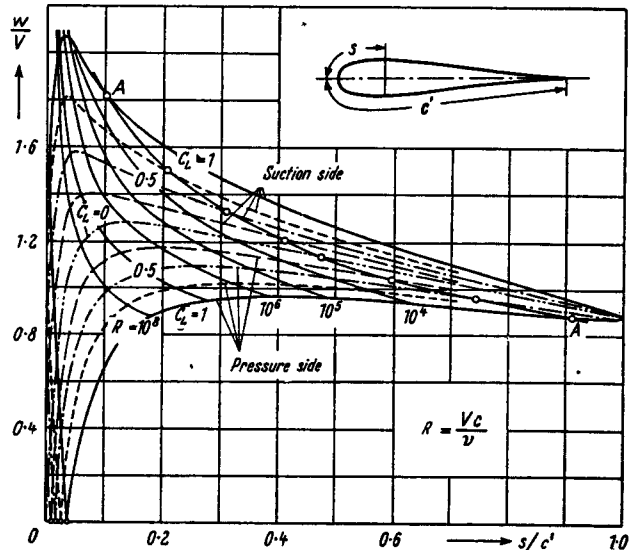


Fig. 9.13. Position of the point of instability on a Joukowsky profile ( $\frac{t}{c} = 0.15$ ), for various values of lift coefficient and Reynolds number. (SCHLICHTING-ULRICH). A: position of laminar separation

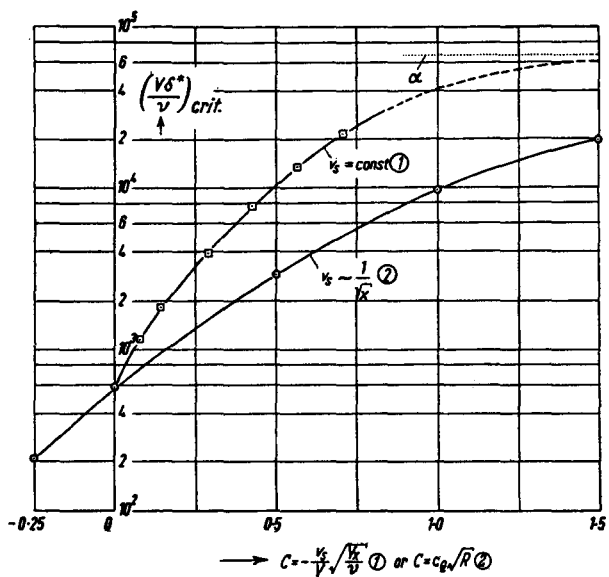


Fig. 9.14. The critical Reynolds number,  $\left(\frac{w\delta^*}{v}\right)_{\text{crit.}}$ , for the flat plate with suction or blowing, as a function of the coefficient  $c_0\sqrt{R}$  or  $-\frac{v_0}{\sqrt{x}}\sqrt{\frac{Vx}{v}}$ . The suction velocity behaves as either  $v_s \sim \frac{1}{\sqrt{x}}$  or  $v_s = \text{const.}$   $\alpha$  corresponds to the asymptotic suction profile

$\frac{w\delta^*}{v}$  is a Reynolds number formed with the local velocity,  $w$ , and the displacement thickness. The curves shown in the figure are the boundaries between the regions of stability and instability: points inside the boundary correspond to an unstable state; those outside to a stable state. The lowest Reynolds number at which instability can occur is denoted by  $R_{\text{crit.}}$ , and is called the critical Reynolds number. The authors mentioned above have investigated the stability of various boundary layer profiles in favourable and unfavourable pressure gradients, the profiles

being characterised by the parameter  $\frac{\partial^2 dw}{\partial x^2}$ . Figure 9.12 shows the critical Reynolds numbers  $\left(\frac{w\delta^*}{v}\right)_{\text{crit.}}$  obtained from stability calculations on the boundary layer profiles of Pohlhausen; compared with these, the numerical values for the Hartree class of profiles show only trifling differences. For an arbitrary pressure distribution we need only perform a boundary layer calculation as described in Section 9.2.4; the stability or instability of the boundary layer can then be determined with the help of Figure 9.12. Figure 9.13 shows the results of such a calculation.

Investigation of the stability of boundary layers when suction or blowing is used leads to the remarkable result that suction (like decreasing pressure) stabilises the boundary layer, whereas blowing (like increasing pressure) has a destabilising effect. In Figure 9.14 the critical Reynolds number is plotted against the coefficient  $C = c_0\sqrt{R}$  for the flat plate: we see that the critical Reynolds number can be approximately 100 times higher than its value when no suction is used†; consequently, the effect of an adverse pressure gradient can be removed by using suction with a small value of the volume-flow-rate coefficient (see Figures 9.12 and 9.14). We can obtain a fairly detailed picture of the behaviour of the critical Reynolds number,  $\left(\frac{w\delta^*}{v}\right)_{\text{crit.}}$ ,

if we plot this quantity against the ratio  $\frac{\delta^*}{\theta}$  (see Figure 9.15)

† The results obtained by different workers contain small deviations; these are due to the various form parameters used and also to the approximations made in the extensive theoretical calculations. For the asymptotic suction profile, which appears on the flat plate with uniform suction at a sufficiently large distance from the leading edge, the following values of  $R_{\text{crit.}}$  have been obtained: 70,000 according to ULRICH; 55,200 according to PRETSCH; and (most recently) 58,000 according to WUEST.

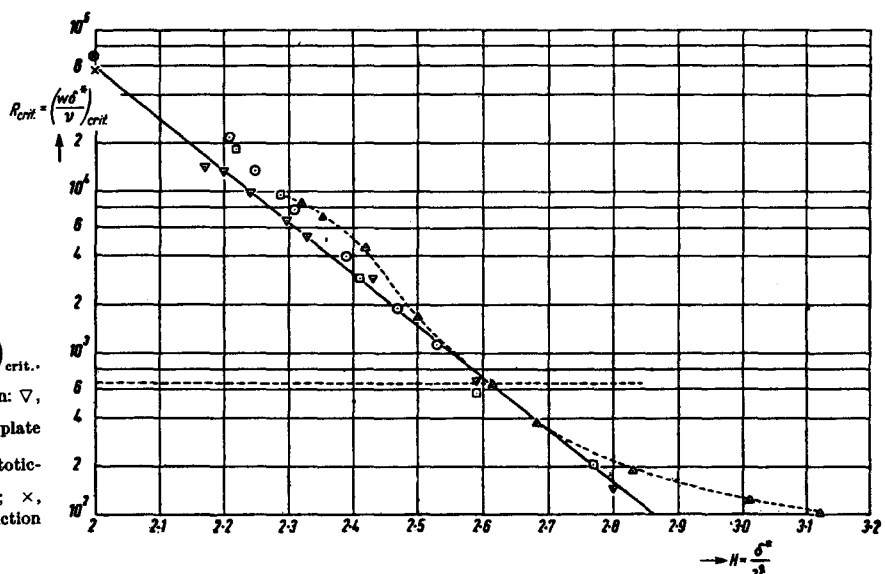


Fig. 9.15. The critical Reynolds number,  $\left(\frac{w\delta^*}{v}\right)_{\text{crit.}}$ , as a function of the parameter  $H - \frac{\delta^*}{\theta}$ . Without suction:  $\nabla$ , Hartree profiles;  $\Delta$ , Pohlhausen profiles. Flat plate with suction:  $\circ$ ,  $v_s = \text{const.}$ ;  $\square$ ,  $v_s \sim \frac{1}{\sqrt{x}}$ . Asymptotic-suction profile:  $\oplus$ , according to SCHLICHTING;  $\times$ , according to PRETSCH. --- flat plate without suction

for either a pressure gradient in the absence of suction (and blowing) or constant pressure with suction (or blowing). The results lie approximately on a single curve, so it can be presumed that this curve is valid for any combination of suction (or blowing) and pressure fall (or rise).

### 9.3.2 Amplification and Transition

The critical Reynolds number is not the only quantity that determines whether transition from the laminar to the turbulent state occurs; the amount by which disturbances are amplified is also of decisive importance. This is characterised by the parameter  $\beta_i \delta^*/w$  (the logarithmic increment of the amplification of the amplitude). This quantity has been calculated by SCHLICHTING

number  $\frac{w\delta^*}{v}$  and the pressure gradient (characterised by  $\beta$  or by a similar parameter). Whether the region of instability is reached depends on the wave length of the disturbance as well as on the Reynolds number; for disturbances of very small wave length† the region is not reached, so that if the boundary layer separates it does so when it is still laminar; for disturbances of large wave length, on the other hand, the amplification is usually very great in an unfavourable pressure gradient, and this can lead to transition; it is conceivable that transition can occur even when the amplification is relatively small and a favourable pressure gradient exists over large parts of the chord. The solution of the problem of transition is still incomplete, because it is not yet possible to state what amplification is necessary to cause transition.

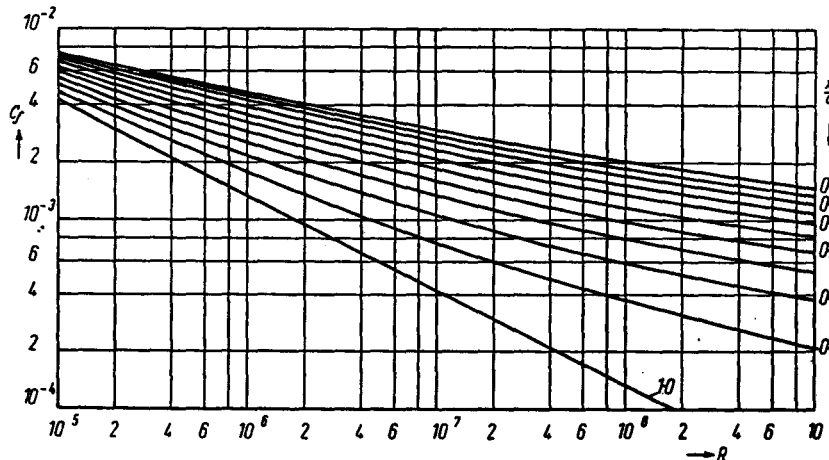


Fig. 9.16. Skin-friction drag coefficient of the flat plate, wetted on one side, as a function of Reynolds number for various values of the (chosen) position of transition point. The momentum thickness is assumed continuous at the transition point

for the flat plate, and by PRETSCH for boundary layers in favourable and unfavourable pressure gradients. The essential result of PRETSCH's work is that in the unstable region the amplification in the boundary layer is considerably larger in an unfavourable pressure gradient than on the flat plate or in a favourable pressure gradient. The following example illustrates this: for a Hartree profile (see Table 9.1) with  $\beta = 1$  (corresponding to a favourable pressure gradient) the maximum value of the amplification is given by  $\left(\frac{\beta_i \delta^*}{w}\right)_{\max} = 7.3 \cdot 10^{-4}$ ; for the flat plate ( $\beta = 0$ ) the value is  $3.45 \cdot 10^{-3}$ ; for  $\beta = -0.1$  (corresponding to an unfavourable pressure gradient) the value is  $1.55 \cdot 10^{-2}$ ; finally, for the separation profile ( $\beta = -0.1988$ ) the value is as high as  $8 \cdot 10^{-2}$ . In addition, the curves of constant amplification (constant  $\frac{\beta_i \delta^*}{w}$ ) for various pressure gradients (characterised by  $\beta$ ) have been calculated for the whole unstable region of the disturbances; consequently, it is possible to predict theoretically the amplification of disturbances along the whole of a profile for an arbitrary pressure distribution; all that is required is to determine at each point on the profile the Reynolds

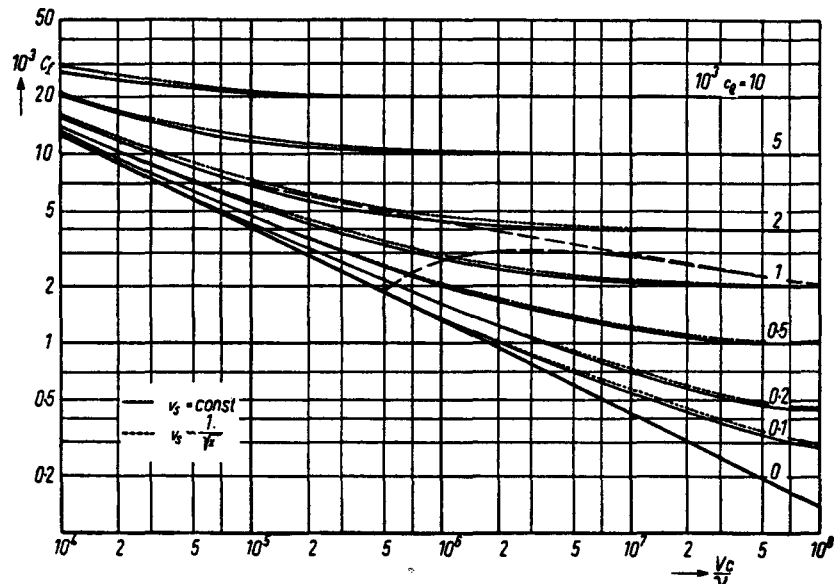
### 9.3.3 Keeping the Boundary Layer Laminar at Higher Reynolds Numbers

It is shown in Section 9.4.2 that a large reduction in drag can be obtained if the boundary layer is kept laminar at higher Reynolds numbers; for this it is necessary to displace the point of transition rearwards from its position on normal profiles (which is a point somewhere on the first third of the chord); this is clearly true both for the flat plate and for a wing profile. Whether it is at all possible to keep the boundary layer laminar in this way can be easily decided by a stability calculation. We might think that the stability of the boundary layer can be controlled by a suitable choice of pressure distribution (that is, by a suitable shape of profile); however, stability calculations for a large number of profiles with systematically varied pressure distributions show that, for a prescribed minimum pressure (in effect, for a prescribed maximum thickness), it is almost impossible by purely geometrical means to keep the boundary layer stable over a large part of the chord,

† For example:  $\lambda < 35\delta^*$  when  $\beta = 1$ ;  $\lambda < 21\delta^*$  when  $\beta = 0$ ;  $\lambda < 11\delta^*$  when  $\beta = -0.1$ ; and  $\lambda < 6\delta^*$  when  $\beta = -0.1988$  (separation profile).

if the Reynolds number is above a certain value. For profiles with a thickness ratio between 10% and 12% this limit lies at about  $R = 10^7$ ; for thicker profiles it is higher. We therefore presume that many of the laminar effects measured in the American low-turbulence wind-tunnels at still higher Reynolds numbers occur at points that lie in the unstable region; consequently the smallest disturbance can lead to transition, and this has actually been found (sensitivity to finger marks; and other observations). This explains why in the profile measurements in German wind-tunnels all the characteristics of a laminar boundary layer disappear as the Reynolds number approaches  $10^7$ , in spite of favourable pressure distributions and very smooth surfaces; the turbulence of the jet in the wind tunnel is sufficient to cause transition of the unstable boundary layer.

Fig. 9.17. Skin-friction drag coefficient of the flat plate with suction as a function of Reynolds number, for various types of suction velocity and various volume-flow-rate coefficients  $c_Q$  (without consideration of the stability of the boundary layer)



On the other hand, if suction is applied to the boundary layer it is possible to keep the laminar boundary layer stable even at higher Reynolds numbers, provided that the volume-flow-rate coefficient is above a certain minimum value,  $(c_Q)_{\text{crit.}}$ ; this is shown by calculations for the flat plate, described in Section 9.4.2.

#### 9.4 Calculation of the Profile Drag

##### 9.4.1 Preliminary Remarks

On the basis of potential theory and boundary layer theory (as described in Chapters 8 and 9), and with some simplifying assumptions, it is possible to calculate approximately the most important aerodynamic characteristics of an arbitrary wing profile at a given Reynolds number. This statement is not true if there is a region of separated flow; but otherwise it is possible to solve many problems in a time which is short compared with the time required for wind-tunnel experiments.

##### 9.4.2 Drag of the Flat Plate with and without Boundary Layer Control

The flat plate is often used to provide a crude estimate for the skin-friction drag of profiles as a function of Reynolds number; this is because the skin-friction drag of the flat plate is a minimum value. It is usual to consider the skin-friction drag coefficient of one side of the plate. For a laminar boundary layer,

$$(C_f)_{\text{lamin.}} = \frac{\int_0^x \tau_0 dx}{\frac{\rho}{2} V^2 x} = \frac{2\vartheta(x)}{x} = 1.328 \left( \frac{x}{c} R \right)^{-1/2}; \quad (9.17)$$

for a turbulent boundary layer when  $R < 10^7$ ,

$$(C_f)_{\text{turb.}} = \frac{2\vartheta(x)}{x} = 0.074 \left( \frac{x}{c} R \right)^{-1/5}; \quad (9.18)$$

and for a turbulent boundary layer when  $R > 10^7$  (from measurements by SCHULTZ-GRUNOW),

$$(C_f)_{\text{turb.}} = \frac{0.417}{\left[ \log \left( \frac{x}{c} R \right) - 0.407 \right]^{2.64}}. \quad (9.19)$$

Figure 9.16 shows drag coefficients for a flat plate of length  $c$ , worked out by means of these formulas; the curves correspond to various positions of the point of transition, and it has been assumed that at this point the momentum thicknesses of the laminar and turbulent boundary layers join together continuously.

When boundary layer control is applied, the formulas for the drag change; they depend on the volume-flow-rate coefficient,  $c_Q$ , and on the variation of suction along the chord. Figures 9.17 and 9.18 show results for continuous suction (when  $v_s \sim \frac{1}{\sqrt{x}}$ ), and for uniform suction (when  $v_s = \text{const.}$ ). The smallest value of  $c_Q$  necessary to keep the boundary layer laminar depends upon the variation of

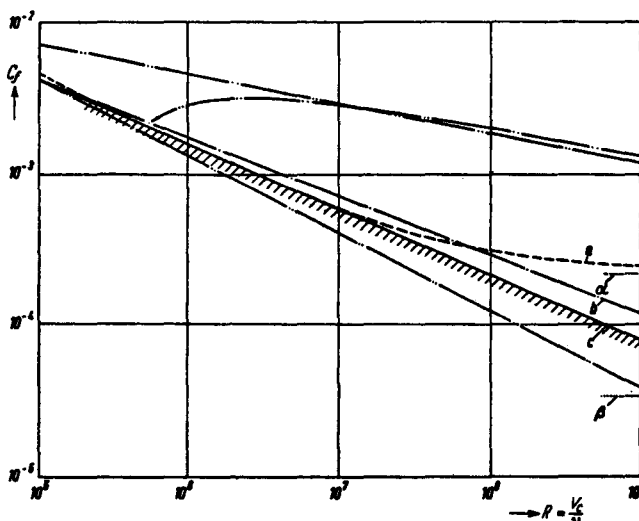


Fig. 9.18. Skin-friction drag coefficient of the flat plate with suction, as a function of Reynolds number,  $R = \frac{V_c}{v}$ . The figure shows the minimum value attainable when the stability of the boundary layer has been considered, for various types of suction velocity. These types are: (a)  $v_s = \text{const.}$ ; (b)  $v_s \sim \frac{1}{\sqrt{x}}$ , with a coefficient such that the critical Reynolds number is nowhere exceeded; (c) with optimum distribution of suction velocity, as shown in Figure 9.19. Asymptotic values for Reynolds number:  $\alpha = 2.35 \cdot 10^{-4}$  for a;  $\beta = 3.62 \cdot 10^{-4}$  for b and c.

suction<sup>†</sup>. BETZ considers the question what distribution of suction along a flat plate is necessary for the greatest gain in power to be obtained (that is, for there to be a minimum value of the sum of the power required to overcome the drag and the power required by the suction). Such a distribution is clearly obtained if at each point of the plate a boundary layer profile exists whose Reynolds number  $(\frac{V\delta^*}{v})$  lies just below the critical Reynolds number; using results obtained for the flat plate, PRETSCH has calculated this distribution of suction velocity (Figure 9.19). The drag coefficient corresponding to this "optimum suction" is plotted in Figure 9.18, together with the minimum drag coefficients when the distribution of suction is  $v_s = \text{const.}$  and when it is  $v_s \sim \frac{1}{\sqrt{x}}$ ; the volume-flow-rate

<sup>†</sup> When  $v_s \sim \frac{1}{\sqrt{x}}$  the value of  $c_D$  is between  $1.1 \cdot 10^{-4}$  and  $2.8 \cdot 10^{-4}$ ; when  $v_s = \text{const.}$  it is  $1.18 \cdot 10^{-4}$  (according to PRETSCH).

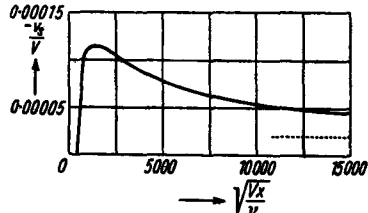


Fig. 9.19. Optimum distribution of suction velocity for the flat plate; this distribution results in the boundary layer profile's just being stable everywhere

coefficient for the last two distributions is chosen so that the critical Reynolds number is never exceeded. In the Reynolds number range  $10^7 < R < 10^8$  the drag is in all three cases reduced to between 70% and 90% of the turbulent drag of a flat plate without suction. To exploit this reduction in drag it is necessary to keep the boundary layer laminar over the whole of the chord: in the United States, experiments are in progress to achieve this aim by the realization of continuous suction; in England, special profiles have been developed in attempts to solve the problem by means of suction slots (see Section 6.3.1).

#### 9.4.3 Drag of an Arbitrary Profile

What is probably the most accurate empirical formula for the local drag coefficient of a profile comes from measurements made by LUDWIEG and TILLMANN on a flat plate in favourable and unfavourable pressure gradients. The formula is

$$C_f = 0.246 \cdot 10^{-0.678H} \left( \frac{w\vartheta}{v} \right)^{-0.288H}; \quad (9.20)$$

to use it we require a knowledge only of the momentum thickness,  $\vartheta$ , and the form parameter,  $H$ , of the boundary layer profile; the exact behaviour along the contour is seldom required.

Two approximate methods have been widely used for making a quick calculation of the drag of a profile in the absence of separation; both require a determination of the boundary layer thickness at the trailing edge of the wing. The first method (SQUIRE and YOUNG) applies the momentum theorem to the wake; the resulting approximate formula is

$$C_D = \frac{2\vartheta_{te}}{c} \left( \frac{w_{te}}{V} \right)^{3.2}. \quad (9.21)$$

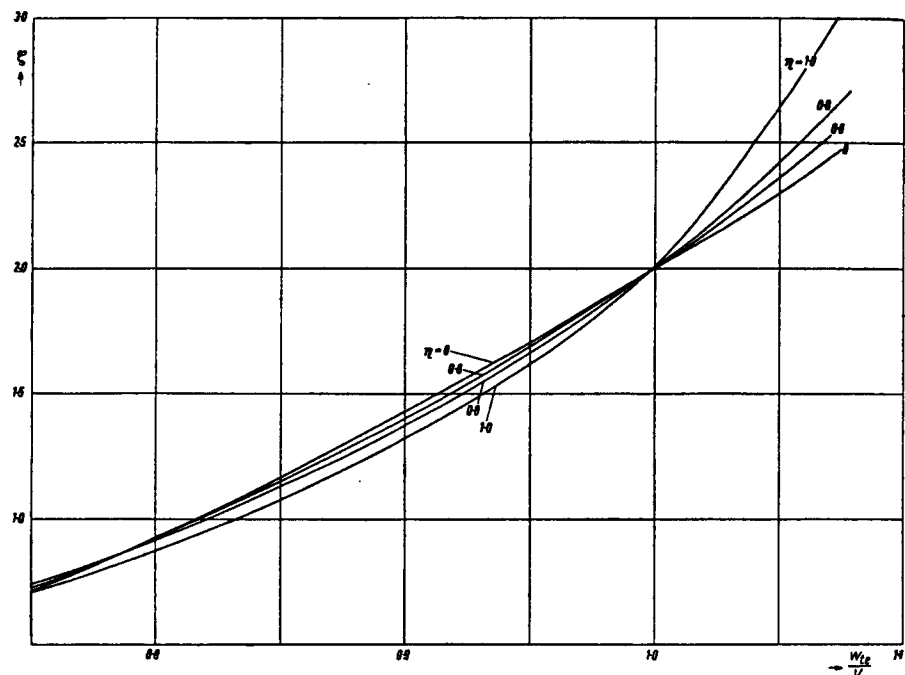
The second method determines the profile drag by addition of the skin-friction and form drags; the latter is estimated from the variation of displacement thickness in the wake with the outside pressure, so that the form of the turbulent velocity profile at the trailing edge must be considered. According to PRETSCH and WALZ the drag coefficient is given by

$$C_D = \left( \frac{\vartheta}{c} \right)_u \zeta_u + \left( \frac{\vartheta}{c} \right)_l \zeta_l; \quad (9.22)$$

the indices  $u$  and  $l$  refer respectively to the upper and lower sides of the profile; the function  $\zeta \left( \frac{w_{te}}{V} \right)$  is shown in Figure 9.20.

A difficulty arises if we start from a velocity distribution calculated from potential theory; at the trailing edge the theory predicts a value of zero for  $\frac{w_{te}}{V}$  and an infinite value for  $\frac{\vartheta_{te}}{c}$ ; consequently, the value of  $C_D$  is indeterminate. We

Fig. 9.20. Function used in calculation of the profile drag, according to PRETSCH



can avoid this difficulty by using the theoretical velocity distribution up to about 90% of the chord, and then extrapolating the velocity (in a way based on measured velocity distributions) to a value at the trailing edge,  $\frac{w_{te}}{V}$ , different from zero—usually between 0.75 and 1.0.

$C_D$  varies but little with  $\frac{w_{te}}{V}$  in this range, because  $\vartheta$

usually varies in the opposite way to  $\frac{w}{V}$ ; the physical explanation of this is that in the region of the trailing edge kinetic energy is transformed into pressure energy with hardly any loss, because the dissipative effect of viscosity is less marked in a thick boundary layer.

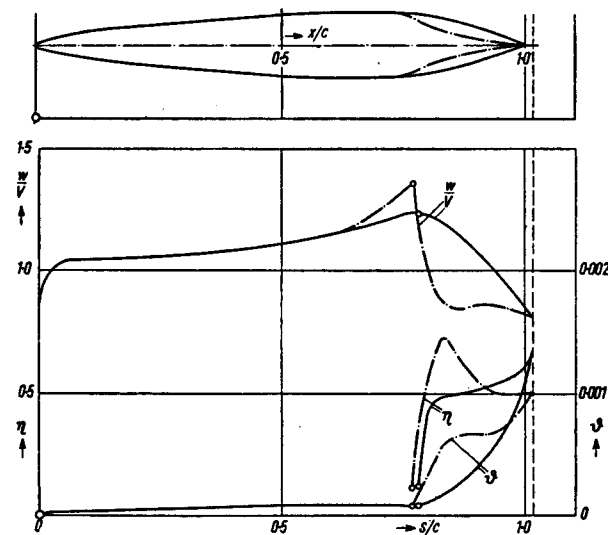


Fig. 9.21. Effect of a suitable shaping near the trailing edge on the velocity distribution, momentum thickness, and form parameter;  $C_L = 0$ . (WALZ)

To avoid the boundary layer calculation required by Equations (9.21) and (9.22) HELMBOLD and SCHLICHTING have introduced approximate formulas for  $\vartheta$  (see p. 467 of the reference in Section 1.5.1); only the velocity distribution of the profile still appears in their formula. SCHLICHTING's formula for the drag coefficient of one side of the profile is

$$C_D = \frac{0.074}{R^{1/5}} \left\{ \int_{x_T/c}^1 \left( \frac{w}{V} \right)^4 d \left( \frac{x}{c} \right) + C \right\}^{0.8}; \quad (9.23)$$

$x_T$ , the position of the point of transition is assumed known;  $R$  is written for  $\frac{Vc}{\nu}$ , and

$$C = \frac{1}{0.0160} \left( \frac{\vartheta_T}{c} \right)^{5/4} R^{1/4} \left( \frac{w_T}{V} \right)^{4.25};$$

$\vartheta_T$ , the value of the momentum thickness at the point of transition, is obtained from

$$\frac{w_T \vartheta_T^2}{\nu} = \frac{0.470}{w_T^5} \int_{z=0}^{x_T} w^5 dx.$$

The approximate formula used for the momentum thickness differs from that given in Equation (9.14), but the differences in the results (at least for small values of  $C_L$ ) are small.

Recently TRUCKENBRODT has made a further step in the simplification of the drag calculation. On the assumption of a slender profile with small disturbance velocities he derives a simple approximate formula; the only quantities required are the profile ordinates,  $y_m$  (at fixed points  $x_m$ ),

Table 9.3

Constants in the drag formula, Equation (9.24)

 $N = 12$ 

$x_T = z_n$	0	0-0670		0-25		0-50		0-75		1-00		
$n$	12	10		8		6		4		0		
	$P_n$	$Q_n$	$P_n$	$Q_n$	$P_n$	$Q_n$	$P_n$	$Q_n$	$P_n$	$Q_n$	$P_n$	$Q_n$
	0	1-0000	0-2588	0-8423	0-5000	0-7814	0-7071	0-5521	0-8860	0-3047	1-6099	0
$m$	$z_m$	$P_{mn}$	$Q_{mn}$	$P_{mn}$								
1	0-9830	0	1-8399	-0-0078	1-8606	-0-0187	1-9280	-0-0402	2-0675	-0-1020	2-3655	1-6099
3	0-8536	0	0-6734	-0-0284	0-6887	-0-0715	0-7442	-0-1726	0-8977	-0-7217	1-6914	0-5893
5	0-6294	0	0-4930	-0-0736	0-5199	-0-2107	0-6390	-0-8735	1-3239	1-1480	-0-7840	0-4314
7	0-3706	0	0-4930	-0-2314	0-5671	-1-1257	1-1838	1-4835	-0-7795	0-6197	-0-1467	0-4314
9	0-1465	0	0-6734	-1-6333	1-1696	2-4285	-0-7442	1-0059	-0-1540	0-7217	-0-0498	0-5893
11	0-0170	0	1-8399	8-1995	-0-5914	3-3963	-0-1051	2-3168	-0-0358	1-8697	-0-0130	1-6099

and the drag coefficients of the flat plate,  $C_{fl}$  and  $C_{ft}$  (for smooth and rough surfaces). For symmetrical profiles the formula is

$$\frac{C_D}{2} = C_{fl} \left( P_n + \sum_{m=1}^{N-1} P_{mn} 2 y_m^{(t)} \right) + \\ + C_{ft} \left( Q_n + \sum_{m=1}^{N-1} Q_{mn} 2 y_m^{(t)} \right); \quad (9.24)$$

the constants are given in Table 9.3.

A particular difficulty in the calculation of the profile drag is the uncertainty in the predicted position of the "point of transition",  $x_T$ . If we assume an aerodynamically smooth wing then, for a prescribed velocity distribution, we can at least determine numerically a region in which the point of transition is expected to lie: the rearward limit of this region is the point at which the laminar boundary layer separates; the forward limit is the point at which the critical Reynolds number is reached (according to the theory of small disturbances). For small Reynolds numbers the second point usually lies near the point of minimum pressure, so that we can simplify the calculations by defining the point of minimum pressure as the forward limit for the point of transition. If the maximum thickness lies far back and the Reynolds number is high, the point at which the critical Reynolds number is reached can lie in front of the point of minimum pressure; nevertheless, the boundary layer is strongly stable when the pressure is falling, and so transition would not usually be expected to take place before the point of minimum pressure. The results of calculations using the first of the theoretical positions are plotted in Figure 12.109.

Figure 9.21 clarifies the question whether it is possible to reduce the portion of the drag that arises from the turbulent boundary layer; in general, this contribution is dominant.

For this we must try to thicken the turbulent boundary layer in the first part of its length, since there the shear stress at the wall is usually high; in doing this we must avoid increasing the

momentum thickness of the boundary layer at the trailing edge. WALZ has made some calculations of the boundary layer quantities and of  $C_D$  for a 13.6% thick profile with maximum thickness at 70% of the chord. These show that, with a suitable shaping of the rear part of the profile (the contour must change from convex to concave), a reduction in the value of  $C_D$  can be obtained; it is assumed that the shaping does not change the position of the point of transition, and that the rise in pressure is not so great that the turbulent boundary layer separates. A remarkable result of WALZ's calculations is that the percentage reduction in  $C_D$  thus produced increases with Reynolds number: for example, suitable shaping of one profile produces a reduction in  $C_D$  of 6.5% at a Reynolds number of  $1 \cdot 10^6$ , and of about 25% at a Reynolds number of  $30 \cdot 10^6$ .

The calculations show further that, with this shaping of the rear part (which results in a small trailing edge angle,  $\tau$ ), the danger of separation in the region of the trailing edge is reduced (cf. the behaviour of the form parameter of the turbulent boundary layer in Figure 9.21). Therefore, the flow in this region can be subjected to a further rise in pressure (for example, by a control deflection) without the occurrence of separation; this improvement in the behaviour of the boundary layer is probably the reason why a control is more effective when the trailing edge angle is small.

As a result of these theoretical calculations the following conclusion can be drawn: if the flow has to overcome a certain pressure rise, then both the drag and the danger of separation are reduced by displacing the main part of this pressure rise to the region in which the boundary layer is still thin; this measure becomes more effective as the Reynolds number increases. The numerous American measurements on the laminar profiles of the NACA 6-series confirm these theoretical results; further, the behaviour of the pressure on ordinary profiles when  $C_L$  is near  $C_{L_{max}}$  is in conformity with these ideas.

## 9.5 Calculation of Polars

### 9.5.1 Calculation of the Maximum Lift

The attainment of maximum lift coincides with the occurrence of separation on the suction side. Usually this begins at the trailing edge of the profile, and it generally moves quickly forwards as the angle of incidence is increased (more quickly for thin profiles than for thick ones). If the profile has a pointed nose, separation can also begin on the front part of the profile. In both cases it

appears that, at the Reynolds numbers reached in flight, the boundary layer is turbulent when it separates. Numerical procedures exist with which we can determine approximately whether a particular pressure distribution will cause separation; hence, if we have theoretical pressure distributions calculated for a number of values of  $C_L$ , we can find an approximate value for  $C_{L_{\max}}$ .

In carrying out such a calculation we have to overcome a difficulty similar to that met in the determination of the drag: a theoretical calculation of the pressure predicts stagnation pressure at the trailing edge, which is contrary to reality; if we calculate the turbulent boundary layer for such a pressure distribution, we find that, since separation occurs before the trailing edge even when  $C_L = 0$ , we are unable to obtain a value for  $C_{L_{\max}}$ . A simple assumption enables us to proceed further: we use the theoretical pressure distribution up to a point (say,  $\frac{x}{c} = 0.90$ ) before which the deviations of theory from experiment are small; we then suppose that  $C_{L_{\max}}$  has been reached if, from the calculation, the flow separates at or before  $\frac{x}{c} = 0.9$ . In the range of  $C_L$  near  $C_{L_{\max}}$  a small change in angle of incidence causes a large movement of the separation point; therefore, fixing  $C_{L_{\max}}$  by this criterion is not unduly arbitrary. As in the calculation of  $C_D$ , a further difficulty is the uncertainty of the position of the point of transition, and we are forced to make plausible assumptions about the position of this point. As described in Section 9.4 we can determine a section of the chord in which the point of transition lies; in the calculation of  $C_{L_{\max}}$  this section is small because there is usually a large rise in pressure; it follows that the effect of an uncertainty in the position of the point of transition is usually not large.

A further difficulty arises if, following PINKERTON, we calculate the pressure distribution with an approximate allowance for the influence of the boundary layer (for the estimation of this influence see Section 9.1); the apparent reduction in camber caused by the boundary layer is considered, but not its displacement effect. At large values of  $C_L$  this displacement effect can become noticeable even

before the point  $\frac{x}{c} = 0.9$ , and the pressure rise over the rear part then becomes less marked; consequently, the value of  $C_{L_{\max}}$  obtained from a pressure distribution calculated by PINKERTON's method may be too small if the displacement effect has not been taken into account. However, in the calculation of the pressure distribution it is possible to allow for the displacement of the potential flow away from the profile surface (by an amount equal to the displacement thickness of the boundary layer,  $\delta^*$ ); WALZ has calculated three examples and finds that, compared with calculations ignoring the displacement

effect, the danger of separation is reduced (by roughly the same amount in each example).

These simplifying ideas allow us to determine the value of  $C_{L_{\max}}$  and to predict the complete behaviour of  $C_L(\alpha)$ .

### 9.5.2 Behaviour of the Pitching Moment

Once the pressure distribution has been found there are no basic difficulties in the calculation of the moment coefficient; if the leading edge is the point of reference, then

$$(C_m)_t = \int_0^1 \frac{\Delta p}{q} \frac{x}{c} d\left(\frac{x}{c}\right).$$

The small deviations of the theoretical from the experimental pressure distribution near the trailing edge can produce relatively large discrepancies between the theoretical and experimental behaviour of the moment; this is because the local forces acting near the trailing edge are further from the reference point than those acting at other points. An extrapolation of the theoretical distribution from a certain point to the trailing edge (as described in Section 9.4.3) removes this difficulty. A more exact consideration of the influence of viscosity appears to be necessary in other respects, even though the discrepancies are seldom so large that the result of a theoretical calculation must be regarded as unsatisfactory.

## 9.6 References

- ALLEN, H. J.: Calculation of the Chordwise Load Distribution over Airfoil Sections with Plain, Split or Serially Hinged Trailing Edge Flaps. NACA Rep. 634 (1938).
- BREBNER, G. G. and J. A. BAGLEY: Pressure and Boundary-layer Measurements on a Two-Dimensional Wing at Low Speed. R & M No. 2886 (1956).
- BURSNALL, W. J. and L. K. LOFTIN jr.: Experimental Investigation of Localized Regions of Laminar Boundary Layer Separation. NACA TN 2338 (1951).
- BUSSMANN, K.: Die laminare Reibungsschicht an Joukowsky-Profilen. FB 1632 (1942).
- CHARTERS, A. C.: Transition between Laminar and Turbulent Flow by Transverse Contamination. NACA TN 891 (1943).
- COLES, D.: Measurement of Turbulent Friction on a Smooth Flat Plate in Supersonic Flow. J. Aer. Sci. 21 (1954), pp. 433-448.
- COPE, W. F.: Notes and Graphs for Boundary Layer Calculations in Compressible Flow. CP 89 (1952).
- CRABTREE, L. F.: The Formation of Regions of Separated Flow on Wing Surfaces. R & M No. 3122 (1959).
- DOENHOFF, A. E. v.: A Method of Rapidly Estimating the Position of the Laminar Separation Point. NACA TN 671 (1938).
- and N. TETERVIN: Determination of General Relations for the Behaviour of Turbulent Boundary Layers. NACA ACR. No. 3G13 (1943) and Rep. 772 (1943).
- DONALDSON, C. du P. and R. H. LANGE: Study of the Pressure Rise across Shock Waves Required to Separate Laminar and Turbulent Boundary Layers. NACA TN 2770 (1952).

- DRIEST, E. R. van: Turbulent Boundary Layer in Compressible Fluids. *J. Aer. Sci.* 18 (1951), p. 145.
- Calculation of the Stability of the Laminar Boundary Layer in a Compressible Fluid on a Flat Plate with Heat Transfer. *J. Aer. Sci.* 19 (1952), pp. 801—812.
- FERRARI, C.: Velocity and Temperature Distribution Through the Laminar Boundary Layer in Supersonic Flow. *J. Aeron. Sci.* 19 (1952), pp. 39—47.
- GADD, E. and B. S. STRATFORD: Flow in the Laminar Boundary Layer near Separation. *R & M No. 3002* (1957).
- GARNER, H. C.: The Development of Turbulent Boundary Layers. *R & M No. 2133* (1944).
- GÖRTLER, H.: Weiterentwicklung eines Grenzschichtprofils bei gegebenem Druckverlauf. *Z. angew. Math. Mech.* 19 (1939), S. 129—140.
- Ein Differenzenverfahren zur Berechnung laminarer Grenzschichten. *UM 6615* (1944) und *Ing. Arch.* 16 (1948), S. 173.
- GRUSCHWITZ, E.: Die turbulente Reibungsschicht in ebener Strömung bei Druckabfall und Druckanstieg. *Ing. Arch.* 11 (1931), S. 321—346.
- HARTREE, D. R.: On an Equation Occurring in Falkner and Skan's Approximate Treatment of the Equations of the Boundary Layer. *Proc. Cambr. Phil. Soc.* 33 II (1937), p. 233.
- HELBOLD, H. B.: Zur Berechnung des Profilwiderstandes. *Ing. Arch.* 17 (1949), S. 273.
- HOŁSTEIN, H. and T. BOHLEN: Ein einfaches Verfahren zur Berechnung laminarer Reibungsschichten, die dem Näherungsansatz von K. Pohlhausen genügen. *LGL S 10* (1941), S. 5—16.
- HOOD, M. J. and M. E. GAYDOS: Effects of Propellers and of Vibration on the Extent of Laminar Flow on the NACA 27—212 Airfoil. *NACA ACR* (1939), (Wartime Rep. No. L-784).
- JUNGCLAUS, G.: Druckverteilungen angestellter ebener Platten mit Totwassereinfluß. *ZfW* 4 (1956).
- KÁRMÁN, T. v.: Über laminare und turbulente Reibung. *Z. angew. Math. Mech.* Bd. 1 (1921) H. 4, S. 233—252.
- and C. B. MILLIKAN: On the Theory of Laminar Boundary Layers Involving Separation. *NACA Rep. No. 504*, (1934).
- and H. S. TSIEN: Boundary Layer in Compressible Fluids. *J. Aeron. Sci.*, Vol. 5 (1938), p. 227.
- KAYE, J.: Survey of Friction Coefficient, Recovery Factors, and Heat Transfer Coefficient for Supersonic Flow. *J. Aer. Sci.* 21 (1954), pp. 117—129.
- KELLY, J. A.: Effects of Modification to the Leading-Edge Region on the Stalling Characteristics of the NACA 63—012 Airfoil Section. *NACA TN 2228* (1950).
- KRAEMER, K.: Praktische Berechnung von Grenzschichten. *VDI-Luftfahrttechnik* 2 (1956), S. 8—13.
- LEES, L.: The Stability of a Laminar Boundary in a Compressible Fluid. *NACA TN 1115* (1946).
- LEVY, S.: Effect of Large Temperature Changes (including Viscous Heating) upon Laminar Boundary Layers with Variable Free-Stream Velocity. *J. Aer. Sci.* 21 (1954), pp. 459—474.
- LIEPMANN, H. W.: The Interaction Between Boundary Layer and Shock Waves in Transonic Flow. *J. Aeron. Sci.*, Vol. 13 (1946), pp. 623—637.
- LUDWIG, H. and W. TILLMANN: Untersuchungen über die Wandschubspannung turbulenten Reibungsschichten. *Ing. Arch.* 17 (1949), 288.
- MANGLER, K. W.: Die allgemeine Lösung der Prandtlischen Grenzschichtgleichungen. *LGL-Bericht 141* (1941), S. 3—7.
- Ein Verfahren zur Berechnung der laminaren Grenzschicht mit beliebiger Druckverteilung und Wärmeübertragung für alle Machzahlen. *ZfW* 4 (1956), S. 63/66.
- MICKLEY, H. S. and R. S. DAVIS: Momentum Transfer for Flow over a Flat Plate with Blowing. *NACA TN 4017* (1957).
- MOORE, L. L.: A Solution of the Laminar Boundary Layer Equations for a Compressible Fluid with Variable Properties, Including Dissociation. *J. Aer. Sci.* 19 (1952), pp. 505—518.
- NITZBERG, G. E.: A Concise Theoretical Method for Profile-drag Calculation. *NACA ACR No. 4B05* (1944).
- PETERSON, R. F.: The Boundary Layer and Stalling Characteristic of the NACA 64A010 Airfoil Section. *NACA TN 2235* (1950).
- PINKERTON, R. M.: Calculated and Measured Pressure Distribution Over the Midspan Section of the NACA 4412 Airfoil. *NACA Rep. 563* (1936).
- The Variation with Reynolds Number of Pressure Distribution over an Airfoil Section. *NACA Rep. 613* (1937).
- POHLHAUSEN, K.: Zur näherungsweisen Integration der Differentialgleichung der laminaren Reibungsschicht. *ZAMM* 1 (1921) 235.
- PRANDTL, L.: Zur Berechnung der Grenzschichten. *Z. angew. Math. Mech.* 18 (1938), S. 77—82.
- PRETSCH, J.: Zur theoretischen Berechnung des Profilwiderstandes. *Jb. dDL* I, S. 60.
- Die Stabilität einer ebenen Laminarströmung bei Druckgefälle und Druckanstieg. *Jb.* 1941 *dDL* I, S. 58.
- Umschlagbeginn und Absaugung. *Jb.* 1942 *dDL* I, S. 1—7.
- Die Anfachung instabiler Störungen in einer laminaren Reibungsschicht. *Jb.* 1942 *dDL* I, S. 54.
- Die Leistungersparnis durch Grenzschichtabsaugung beim Schleppen einer ebenen Platte. *UM 3048* (1943).
- RIEGELS, F.: Über die Berechnung der Druckverteilung von Profilen. *Techn. Ber. d. ZWB* 10 (1943), 13—20.
- and J. LIESE: Über den Einfluß der Druckverteilung eines Tragflügelprofils auf Lage und Wanderung der Stabilitätsgrenze für die Reibungsschicht mit Reynoldschen Zahlen. *UM 3202* (1945).
- RIEGELS, F. W.: Neuere Ergebnisse zur Profiltheorie. *ZfW* 4 (1956), S. 61/63.
- RINGLEB, F.: Computation of the Laminar Boundary Layer with Suction. *J. Aeron. Sci.* 19 (1952), pp. 48—54.
- ROTTA, J.: Näherungsverfahren zur Berechnung turbulenten Grenzschichten unter Benutzung des Energiesatzes. *Mitt. MPI Strömungsforschung Nr. 8* (1953).
- SCHLICHTING, H.: Amplitudenverteilung und Energiebilanz der kleinen Störungen bei der Plattenströmung. *Nachr. Ges. Wiss. Göttingen, Math.-Phys. Klasse, Fachgr. I*, 1 (1935), S. 47.
- Über die theoretische Berechnung der kritischen Re-Zahl einer Reibungsschicht in beschleunigter und verzögter Strömung. *Jb.* 1940 *dDL* I, S. 97.
- Berechnung der laminaren Grenzschicht mit Absaugung. *LGL 141*, S. 14—17.
- and A. ULRICH: Zur Berechnung des Umschlages laminar/turbulent. *LGL S 10*, S. 75—135 und *Jb.* 1942 *dDL* I, S. 8.
- and K. BUSSMANN: Exakte Lösungen für die laminare Grenzschicht mit Absaugung und Ausblasen. *Schriften d. DAL* (1943) Bd. 7 B, Heft 2, S. 25—69.
- Ein Näherungsverfahren zur Berechnung der laminaren Reibungsschicht mit Absaugung. *Ing. Arch.* 16 (1948) H. 3 und 4.
- SCHOLZ, N.: Über eine rationelle Berechnung des Strömungswiderstandes schlanker Körper mit beliebig rauher Oberfläche. *Jb. d. Schiffbautechn. Ges.* Bd. 45 (1951).
- SCHUBAUER, G. B.: Air Flow in the Boundary Layer of an Elliptical Cylinder. *NACA Rep. No. 652* (1939).
- and H. K. SKRAMSTAD: Laminar Boundary Layer Oscillations and Transition on a Flat Plate. *NACA ACR 1943* (Wartime Rep. No. 8) und *NACA Rep. 909* (1947).

- SCHULTZ-GRUNOW, F.: Neues Reibungswiderstandsgesetz für glatte Platten. *Luftfahrtforschung* 17 (1940), S. 293.
- SILVERSTEIN, A. and J. V. BECKER: Determination of Boundary Layer Transition on three Symmetrical Airfoils in the NACA Full-Scale Wind Tunnel. *NACA Rep. No. 637* (1939).
- SPENCE, D. A.: Prediction of the Characteristics of Two-Dimensional Airfoils. *J. Aer. Sci.* 21 (1945), pp. 577—587.
- SQUIRE, H. B. and A. D. YOUNG: The Calculation of the Profile Drag of Aerofoils. *R & M No. 1838* (1938).
- TEREVIN, N.: A Method for the Rapid Estimation of Turbulent Boundary Layer Thickness for Calculating Profile Drag. *NACA ACR No. L4G14* (1944), (Wartime Rep. No. L-16).
- TOLLMIEN, W.: Ein allgemeines Kriterium der Instabilität laminarer Geschwindigkeitsverteilungen. *Nachr. Ges. Wiss. Göttingen, Math. Phys. Kl. I*, 1 (1935), S. 79.
- TRUCKENBRODT, E.: Ein Quadraturverfahren zur Berechnung der laminaren und turbulenten Grenzschicht bei ebener und rotationssymmetrischer Strömung. *Ing. Arch.* 20 (1952), S. 212.
- Die Berechnung des Profilwiderstandes aus der vorgegebenen Profilform. *Ing. Arch.* 21 (1953), S. 176—186.
- ULRICH, A.: Theoretische Untersuchungen über die Widerstandsersparnis durch Laminarhaltung mit Absaugung. *Schriften der DAL 8 B* (1944) Heft 2.
- WALZ, A.: Potentialtheoretisch gerechnete Druckverteilungen dünner symmetrischer Profile mit heruntergeklappter Nase und Auftriebsklappe. *FB 1170* (1940).
- Berechnung der Druckverteilung von Klappenprofilen mit Totwasser. *Jahrb. 1940 dDL I*, S. 265—277.
- WALZ, A.: Näherungsverfahren zur Berechnung der laminaren und turbulenten Reibungsschicht (mit Anhang: Berechnung von  $c_{d_{\max}}$  und  $c_{w_p}$ ). *UM 3060* (1943).
- Zur theoretischen Berechnung des Höchstaustrittsbeiwertes von Tragflügelprofilen ohne und mit Auftriebsklappen. *FB 1769* (1943).
- Einige Beispiele zur theoretischen Berechnung der Polare eines Tragflügelprofils. *FB 1848* (1943).
- Theoretisches zur Absaugung der Reibungsschicht. *FB 1775* (1943).
- Theoretische Rechnung zum Einfluß des Hinterkantenwinkels auf Höchstaustritt und Profilwiderstand. *UM 3116* (1944).
- Theoretische Widerstandsberechnung an einem Laminarprofil mit verschiedenen Schwanzteileformen. *UM 3131* (1944).
- Zur näherungsweisen Berechnung laminarer und turbulenter Reibungsschichten mit Berücksichtigung der Kompressibilität. *AVA-Bericht 45/W/16* (1945).
- Näherungstheorie für kompressible turbulente Grenzschichten. *ZAMM-Sonderheft 1956* (Tagung des Fachauschusses für Strömungsforschung, Göttingen 1955).
- WIEGHARDT, K.: Über einen Energiesatz zur Berechnung laminarer Grenzschichten. *Ing. Arch.* 16 (1938), S. 231.
- Zur Berechnung ebener und drehsymmetrische Grenzschichten mit kontinuierlicher Absaugung. *Ing. Arch.* 22 (1954), S. 368/77.
- WILSON, R. E.: Turbulent Boundary Layer Characteristics at Supersonic Speeds—Theory and Experiment. *J. Aer. Sci.* 17 (1950), pp. 585—594.
- WORTMANN, F. X.: Ein Beitrag zum Entwurf von Laminarprofilen für Segelflugzeuge und Hubschrauber. *ZfW. 3* (1955), S. 333—345.
- WUEST, H.: Näherungsweise Berechnung und Stabilitätsverhalten von laminaren Grenzschichten mit Absaugung durch Einzelschlitz. *Ing. Arch.* 21 (1953), S. 90—103.
- YOUNG, A. D.: The Calculation of the Profile Drag of Aerofoils and Bodies of Revolution at Supersonic Speeds. *WGL-Jb.* 1953, pp. 66—75.
- YOUNG, G. B. W. and E. JANSEN: The Compressible Boundary Layer. *J. Aer. Sci.* 19 (1952), pp. 229—236 and p. 288.
- ZATT, J. A.: Revised Methods for Routine Calculations of Laminar and Turbulent Boundary Layers of Two-Dimensional Incompressible Flows. *NLL Rep. F 79* (1951).
- Pressure Distributions with Viscosity Corrections for Airfoils with Flaps. *NLL Rep. F. 88* (1951).
- The Calculation of the Point of Turbulent Boundary Layer Separation on an NACA 0018 Profile and the Determination of the Optimum Angle of Incidence. *NLL Rep. F. 89* (1951).
- ZALOVCIK, J. A. and E. P. LUKE: Some Flight Measurements of Pressure Distribution and Boundary Layer Characteristics in the Presence of Shock. *NACA RM No. L8C22.* (1948).

## 10. THE THEORY OF WING PROFILES IV

### Compressible Flow

#### 10.1 General Remarks

If the density,  $\rho$ , of the medium is no longer constant then, in place of the simple equation of continuity (Equation 8.1), a more complicated equation holds:

$$\operatorname{div}(\rho \mathbf{w}) = 0. \quad (10.1)$$

Let  $u$  and  $v$  denote the components of the velocity vector  $\mathbf{w}$  in the  $x$  and  $y$  directions respectively; it is then possible to obtain the following differential equation,

$$(a^2 - u^2) \frac{\partial u}{\partial x} + (a^2 - v^2) \frac{\partial v}{\partial y} - uv \left( \frac{\partial v}{\partial x} + \frac{\partial u}{\partial y} \right) = 0 \quad \dots (10.2)$$

(a non-linear equation);  $\rho$  and  $a^2$  are functions of the magnitude of the velocity,  $|\mathbf{w}| = w$ . If the flow is assumed to be irrotational we can introduce a velocity potential,  $\Phi$ , so

that  $u = \frac{\partial \Phi}{\partial x}$  and  $v = \frac{\partial \Phi}{\partial y}$ ; we obtain the familiar equation

$$\left(1 - \frac{u^2}{a^2}\right) \Phi_{xx} - 2 \frac{uv}{a^2} \Phi_{xy} + \left(1 - \frac{v^2}{a^2}\right) \Phi_{yy} = 0 \quad \dots (10.3)$$

the suffixes  $x$  and  $y$  denoting differentiation with respect to  $x$  and  $y$ . Our knowledge of mixed, non-linear, partial differential equations is limited, and it is almost impossible to obtain solutions of Equation (10.3), which satisfy boundary conditions on a profile, which yield numerical results, and which are valid in both subsonic and supersonic regions; nevertheless, an inspection of the relevant literature (see Sections 1.5.1 and 1.5.2) shows that progress has been made during recent years.

#### 10.2 Relation between Speed and Pressure

For compressible flows the relationship between speed and pressure is the general Bernoulli equation, which takes into account the variation in density:

$$\frac{w^2}{2} + \int_{p_0}^p \frac{dp}{\rho} = \text{const.} \quad (10.4)$$

If we assume that speed is "converted" into pressure adiabatically, and vice versa, in the whole flow field (with

the exception of points where shock waves occur), Bernoulli's equation can be integrated to give

$$w^2 = \frac{2\gamma}{\gamma-1} \frac{p_0}{\rho_0} \left[ 1 - \left( \frac{p}{p_0} \right)^{\frac{\gamma-1}{\gamma}} \right]; \quad (10.5)$$

$\gamma = \frac{c_p}{c_v}$  is the ratio of the specific heats of the gas at constant pressure and at constant volume;  $p_0$  and  $\rho_0$  denote respectively the pressure and density of the gas when brought to rest (the "stagnation" or "reservoir" pressure and the "stagnation" or "reservoir" density). For reference quantities we choose the free-stream speed,  $V$  (the "speed at infinity"), and the corresponding pressure,  $p_\infty$ , and density,  $\rho_\infty$ ; if we write  $M_\infty = \frac{V}{a_\infty}$ , the Mach number of the free stream†, then the previous equation can be written

$$\frac{p}{p_\infty} = \left\{ 1 - \frac{\gamma-1}{2} M_\infty^2 \left[ \left( \frac{w}{V} \right)^2 - 1 \right] \right\}^{\frac{\gamma}{\gamma-1}}. \quad (10.6)$$

We now introduce the kinetic pressure,  $q$ , where

$$q = \frac{\rho_\infty V^2}{2} = \frac{\gamma}{2} p_\infty M_\infty^2; \quad (10.7)$$

and we find for the pressure coefficient,

$$C_p = \frac{\Delta p}{\frac{\rho_\infty}{2} V^2} = \frac{p - p_\infty}{q} \\ = \frac{2}{\gamma M_\infty^2} \left\{ \left[ 1 - \frac{(\gamma-1)}{2} M_\infty^2 \left( \frac{w^2}{V^2} - 1 \right) \right]^{\frac{\gamma}{\gamma-1}} - 1 \right\}. \quad (10.8)$$

In terms of the local speed of sound,  $a$ , and the local Mach number,  $M = \frac{w}{a}$ , this equation is

$$C_p = \frac{2}{\gamma M_\infty^2} \left\{ \left[ \frac{1 + \frac{(\gamma-1)}{2} M_\infty^2}{1 + \frac{(\gamma-1)}{2} M^2} \right]^{\frac{\gamma-1}{\gamma}} - 1 \right\}. \quad (10.9)$$

† In this section we distinguish between  $a_\infty$ , the speed of sound corresponding to free-stream conditions, and  $a$ , the local speed of sound; there is a corresponding distinction between  $V$  and  $w$ . For simplicity, we write  $M$  instead of  $M_\infty$  in Chapters 3 and 12.

The nomogram of Figure 10.1 displays in a convenient manner the relation between pressure and speed given by this equation, and also the relation for the absolute pressure ratio. The pressure coefficient when  $M = 1$  (the critical pressure coefficient) varies with the free-stream Mach number, and can easily be obtained from this nomogram; the values of this pressure coefficient are shown in the relevant diagrams of Chapter 12. The nomogram, which can be used to obtain other quantities, has been designed by MULTHOFF.

### 10.3 Subsonic Flow

#### 10.3.1 The Prandtl-Glauert Rule

Since the solution of the general problem is very difficult, PRANDTL reduces it to a linear one by assuming that the local velocity differs from the free-stream velocity only by a small amount, in both magnitude and direction; profiles with small thickness ratios and pointed noses are a class of bodies for which this assumption is valid. With this assumption Equation (10.3) can be reduced to the simpler equation

$$(1 - M_\infty^2) \Phi_{zz} + \Phi_{yy} = 0, \quad (10.10)$$

where  $M_\infty = \frac{V}{a_\infty}$  denotes the ratio of the free-stream speed,

$V$ , to the free-stream speed of sound,  $a_\infty$ . Equation (10.10) is of elliptic type if  $M_\infty < 1$  (subsonic flow) and of hyperbolic type if  $M_\infty > 1$  (supersonic flow); with the latter type of equation stationary waves are possible. If  $M_\infty < 1$  we can reduce the solution of Equation (10.10) to the determination of the field of an incompressible flow, by an affine distortion in the  $y$  direction with the factor  $\sqrt{1 - M_\infty^2}$ ; the equation then becomes the familiar Laplace equation. Further investigation yields the simple result that the pressure coefficients in compressible flow (suffix  $c$ ) are greater than those in incompressible flow

(suffix  $i$ ) by a factor  $\frac{1}{\sqrt{1 - M_\infty^2}}$  — the “Prandtl-Glauert rule”.

For example, Figure 10.2 shows the increase in the minimum value of the pressure coefficient for the symmetrical NACA profiles with various thicknesses, the angle of incidence being zero; both theoretical and experimental results are shown. The increase becomes more marked as the Mach number rises; more will be said about this later. The rule certainly cannot be used if the local Mach number becomes greater than unity, and strictly the deviations of the local velocity from the free-stream velocity should always be small compared with  $V$ . It follows immediately that the rule should be applied only to thin, pointed profiles at small angles of incidence; fortunately, comparison with wind-tunnel measurements (Figure 3.6) shows that its

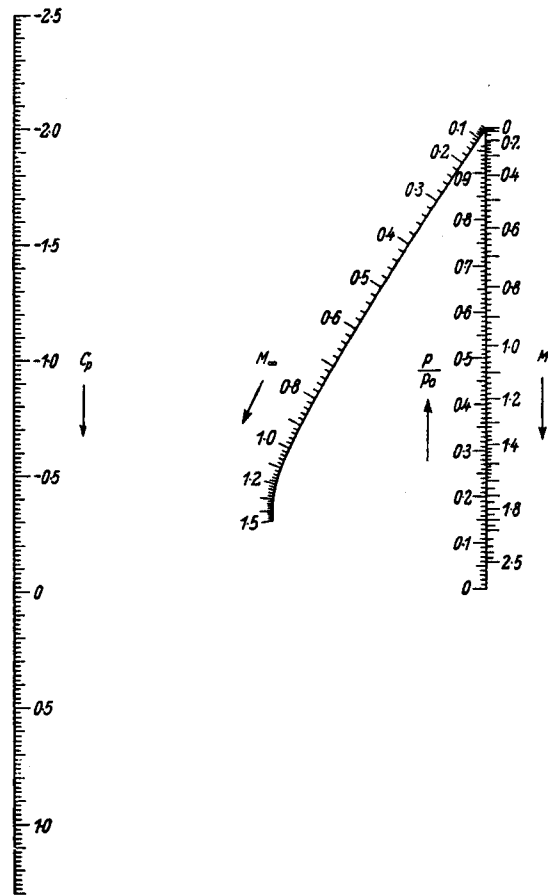


Fig. 10.1. Nomogram for pressures and Mach numbers in adiabatic flow.  $M$  = local Mach number;  $M_\infty$  = free-stream Mach number;  $p_0$  = stagnation pressure (reservoir pressure);  $p_\infty$  = free-stream static pressure;  $p = p_\infty + \Delta p$  = local static pressure;  $q = \frac{\rho_\infty V^2}{2}$  = kinetic pressure;  $C_p = \frac{\Delta p}{q}$

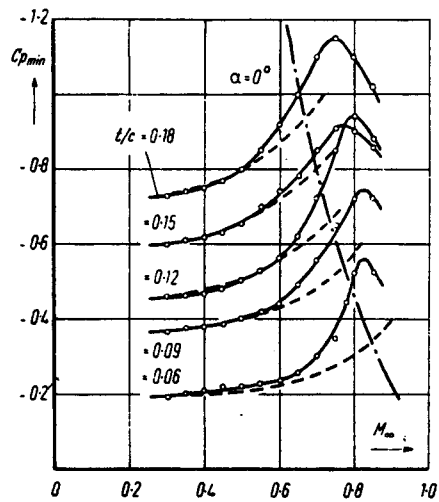


Fig. 10.2. Minimum pressure coefficients plotted against Mach number, for symmetrical NACA profiles at  $\alpha = 0^\circ$ . Points: experimental values. Dashed line: Prandtl-Glauert rule. Chain-dotted line: sonic conditions

application to normal, not too thick, profiles at not too high Mach numbers gives results which are generally of practical use, especially if an integral of the pressure distribution (for example, the lift) is required; the experimental results then show agreement, up to quite high Mach numbers, with the Prandtl-Glauert rule written in the form

$$(C_L)_c = (C_L)_t \frac{1}{\sqrt{1 - M_\infty^2}} . \quad (10.11)$$

The highest Mach number at which the rule can be used depends on the thickness of the profile (roughly,  $M_\infty = 0.8$  if  $\frac{t}{c} = 0.06$ , and  $M_\infty = 0.06$  if  $\frac{t}{c} = 0.15$ ). A corresponding formula is valid for the moment of the profile:

$$(C_m)_c = (C_m)_t \frac{1}{\sqrt{1 - M_\infty^2}} . \quad (10.12)$$

### 10.3.2 Higher Approximations

To a first approximation the stream function satisfies the equation

$$\Psi_{xx} (1 - M_\infty^2) + \Psi_{yy} = 0, \quad (10.13)$$

which is identical with Equation (10.10). If the neglected terms are re-introduced and placed on the right-hand side and the first approximation to  $\Psi$  is inserted in them, the equation for the second approximation is

$$\Psi_{xx} (1 - M_\infty^2) + \Psi_{yy} = f(x, y). \quad (10.14)$$

BUSEMANN introduces a parameter,  $t'$ , which is a measure of the maximum thickness or camber, and he expands the right-hand side in terms of this parameter. The transformation  $\xi = x$ ,  $\eta = y\sqrt{1 - M_\infty^2}$ , then leads to the following differential equation, from which an improvement on the Prandtl-Glauert rule can be obtained:

$$\Psi_{\xi\xi} + \Psi_{\eta\eta} = F(\xi, \eta). \quad (10.15)$$

Only terms up to order  $t'^2$  are considered in the second approximation; higher approximations are obtained by the retention of higher powers of  $t'$  on the right-hand side. HANTZSCHE and WENDT have been able to calculate typical special cases on this basis: for example, they find for the thin circular arc profile

$$\begin{aligned} \frac{C_L}{4} &= \mu \frac{f}{c} + 2 \left( \frac{f}{c} \right)^3 \times \\ &\times \left\{ \left( \frac{25}{12} \mu^7 + \frac{1}{12} \mu^5 - \frac{5}{12} \mu^3 - \frac{13}{12} \mu \right) M_\infty^2 \right. \\ &\left. + (\gamma - 1) \left( \frac{25}{12} \mu^7 + \frac{1}{3} \mu^5 - \frac{1}{4} \mu^3 \right) M_\infty^4 \right\} \dots (10.16) \end{aligned}$$

where  $\mu = \frac{1}{\sqrt{1 - M_\infty^2}}$ ; and for the symmetrical Joukowski profile at a small angle of incidence, they find

$$\begin{aligned} \left( \frac{dC_L}{da} \right)_c / \left( \frac{dC_L}{da} \right)_t &= \left\{ \mu + \frac{4}{9} \sqrt{3} \frac{t}{c} \times \right. \\ &\times \left. \left( 1 - \mu + \mu^2 M_\infty^2 + \frac{\gamma + 1}{4} M_\infty^4 \mu^4 \right) \right\} \quad (10.17) \end{aligned}$$

(see Figure 10.3).

We have still to mention the well-known, older method of JANSEN-RAYLEIGH, which uses a similar iteration principle, but in which the right-hand side is expanded in powers of the Mach number (instead of the thickness); usually the equation for the potential is considered. The application of this method to profiles is limited, since too many terms are required at higher Mach numbers.

The differential equation becomes linear if we change the independent variables from the two spatial co-ordinates to

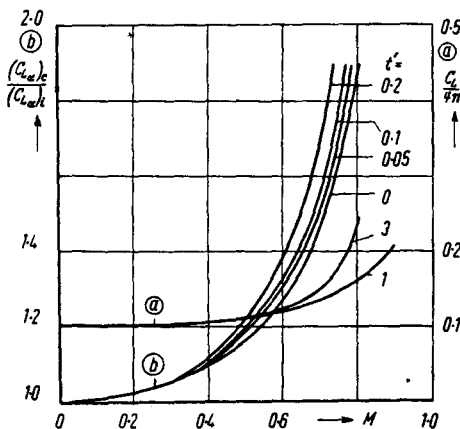


Fig. 10.3. Lift in compressible flow.

- (a) For the circular arc,  $\frac{f}{c} = 0.1$ : (1), Prandtl-Glauert rule; (3), HANTZSCHE and WENDT.
- (b) For Joukowski profiles of various thicknesses: (0) Prandtl-Glauert rule; and HANTZSCHE and WENDT ( $t' = 0.05, 0.1, 0.2$ )

the magnitude of the velocity,  $w$ , and the direction of the velocity,  $\theta$ . According to VON KÁRMÁN (1941) the equation for the stream function is

$$\frac{(1 - M^2)}{\rho^2} \frac{\partial^2 \Psi}{\partial \theta^2} + \left( \frac{w}{\rho} \frac{\partial}{\partial w} \right)^2 \Psi = 0. \quad (10.18)$$

Particular solutions of this equation can be obtained in which the local speed of flow considerably exceeds the local speed of sound; the reader is referred to the literature for further details. CHAPLYGIN succeeds in simplifying Equation (10.18) by assuming that  $\frac{(1 - M^2)}{\rho^2}$  is constant; this assumption means that, instead of the adiabatic relation between pressure,  $p$ , and specific volume,  $\frac{1}{\rho}$ , a linear relation

$$p = \text{const} - \frac{a_0^2 \rho_0^2}{\rho} \quad (10.19)$$

exists; this straight line is made to touch the adiabatic at a certain point. CHAPLYGIN requires that the linear relation should best approximate the adiabatic at the point  $(p_0, \rho_0)$  corresponding to stagnation conditions, from which he determines the value of the constant in Equation (10.19); on the other hand, VON KÁRMÁN and TSIEN (1939) require that the linear relation should best approximate the adiabatic at the point  $(p_\infty, \rho_\infty)$  corresponding to free-stream conditions, and this leads to a different value of the constant; the Kármán-Tsien approximation is more suited to the conditions of flow about a profile. From their simplified form of Equation (10.18) VON KÁRMÁN and TSIEN derive simple approximate formulas for the velocity,  $w_c$ , and the pressure,  $p_c$ , of the compressible flow in terms of the corresponding quantities in incompressible flow,  $w_i$  and  $p_i$ . If we write

$$\beta = \sqrt{1 - M_\infty^2}, \quad \lambda = \frac{1 - \beta}{1 + \beta},$$

$$\frac{\Delta p}{q} = \frac{p - p_\infty}{\frac{\rho_\infty}{2} V^2},$$

the formula for the velocity is

$$\left( \frac{w}{V} \right)_c = \left( \frac{w}{V} \right)_i \frac{(1 - \lambda)}{\left\{ 1 - \lambda \left( \frac{w_i}{V} \right)^2 \right\}}, \quad (10.20)$$

and that for the pressure is

$$\left( \frac{\Delta p}{q} \right)_c = \frac{(\Delta p/q)_i}{\beta + \left( \frac{1 - \beta}{2} \right) (\Delta p/q)_i}; \quad (10.21)$$

these formulas are superior to the Prandtl-Glauert approximation.

The  $\sqrt{\rho}$  method of KRAHN (1942) differs from all the familiar methods. From the outset, no attempt is made to fulfil simultaneously the conditions of continuity and irrotationality. An empirical formula is used,

$$w = w_i \sqrt{\frac{\rho_\infty}{\rho}};$$

$\rho$  and  $w$  are respectively the local density and speed;  $\rho_\infty$  and  $V$  are respectively the free-stream density and speed. For moderate values of the pressure coefficient this approximation is quite satisfactory. An improvement can be obtained in the following way: we insert this approximation in the differential equations of compressible flow ( $\text{div} \frac{\rho}{\rho_\infty} \mathbf{w} = 0$  and  $\text{curl} \mathbf{w} = 0$ ); on the right-hand side certain expressions appear that can be regarded as a source field in the first equation and as a vortex field in the second equation; a detailed discussion shows that the fields of these sources and vortices tend to cancel—particularly on the profile contour; the reader is referred to the thorough investigation of BETZ and KRAHN for the theory of the second approximation, which considers the effect of the remaining vortex and source fields. Ellipses, the ratio of whose axes is 0, 0·2, 0·4, 0·6, 0·8, and 1, and some common profiles (for example, NACA 0009, 0020, 0030, 23012) have been treated. KRAHN has given an empirical correction term to the Prandtl-Glauert rule, which is based on the formula for the minimum pressure coefficient,  $\left( \frac{\Delta p}{q} \right)_{c, \min.}$  on the ellipse (derived from the second approximation); this formula contains the maximum disturbance velocity in the incompressible flow  $(w_i)_{t, \max.}$ , and is particularly easy to handle; it is

$$\left( \frac{\Delta p}{q} \right)_{c, \min.} = \left\{ \frac{1}{\sqrt{1 - M_\infty^2}} + \frac{(w_i)_{t, \max.} - V}{V} \times \left( \frac{1}{\sqrt{1 - M_\infty^2}} - 1 \right) \right\} \left( \frac{\Delta p}{q} \right)_{t, \min.}. \quad (10.22)$$

Because this formula is so simple KRAHN proposes that it should be used for the calculation of the pressure distribution on profiles;  $(w_i)_{t, \max.}$  is to be replaced by the local incompressible velocity on the profile. Simple relations for the forces produced can no longer be given.

## 10.4 Mixed Subsonic and Supersonic Flows

### 10.4.1 Appearance of Shock Waves

At a sufficiently high Mach number a finite region of supersonic flow forms on the profile; Figure 10.4 gives a schematic representation of this.

The theory of mixed subsonic and supersonic flow is still in its early stages, and most of our knowledge has been derived from experimental results. The schlieren and interferometer photographs of Figure 10.5 show how the flow field in the vicinity of the profile alters with increasing Mach number. The transition from the supersonic region

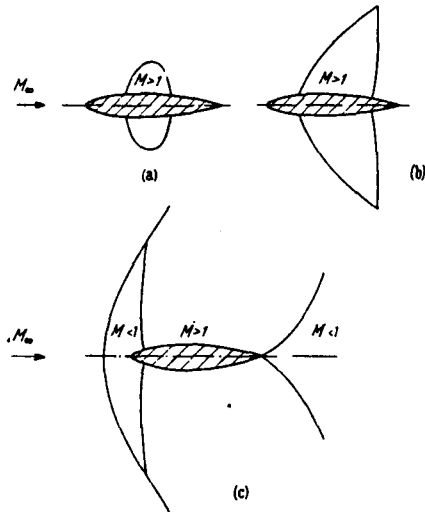


Fig. 10.4. Subsonic flows with local supersonic region (a—without, b—with, shock wave), and supersonic flow with local subsonic region (c)

to the region downstream, in which the flow is again subsonic, usually takes place through a shock wave; and the appearance of a shock on the profile results in a discontinuous behaviour of the pressure distribution (a sudden rise in pressure). If the angle of incidence remains constant while the Mach number increases, the supersonic region becomes larger and the shock wave moves rearwards along the chord; BETZ has determined the position of the shock from the requirement that the energy losses in the shock must be equal to the pressure drag.

The pictures show that, as the speed of sound is approached, the appearance of shock waves considerably alters the behaviour of the flow, making it more complicated; this statement is true both for subsonic flows with local supersonic regions and for supersonic flows with local subsonic regions. The latter occur when normal profiles are placed in a supersonic free stream; a subsonic region (usually small) appears around the stagnation point, and the transition from supersonic velocity to subsonic velocity occurs through a shock wave lying at a short distance in front of the profile; this shock wave is of infinite extent, and is called the "bow wave" (see Figure

10.4c). The cases illustrated in Figures 10.4a and 10.4b (local supersonic regions) have received the most extensive treatment. Whether supersonic regions and shock waves occur and, if they do, where they appear, are questions whose answers depend not only on the free-stream Mach number but also on the shape of the profile and on the angle of incidence. Figures 12.40 to 12.47 show pressure distributions for symmetrical and cambered profiles with various values of maximum thickness and camber. On the whole, the pressure rises resulting from shock waves measured in American wind-tunnels seem to appear less suddenly than those measured elsewhere; this more gradual transition is probably to be explained by the occurrence of unsteady processes (fluctuations in the position of the shock waves).

In a consideration of the quality of a profile it is important to know whether the shock waves (or, more generally, the local supersonic regions) lead to separation of the boundary layer or not. In the supersonic region a fundamental instability can occur between the outer flow and the boundary layer: the rapidly increasing displacement thickness of the boundary layer causes an increase in pressure in the outer flow and this in turn leads to a further increase in the boundary layer thickness. Whether this process actually occurs depends entirely on the state of the boundary layer (hence, in particular on the Reynolds number and the pressure distribution on the profile). The diagrams of pressure distributions already discussed refer to flows with and without boundary layer separation. The presence or absence of separation can be decided from schlieren and interferometer photographs and also from the magnitude of the jumps in pressure and from the measured drag-coefficients (see, for example, Figures 3.14 ff.). For profiles of the normal four-figure NACA series boundary layer separation usually occurs at the measured Reynolds number; the observed shock wave in this case runs obliquely to the direction of flow and causes separation. For local Mach numbers below  $M = 1.2$ , this shock wave bends round into a straight shock as the distance from the profile increases. If the speed of sound is further exceeded ( $M > 1.2$ ), forked shock waves occur; the first oblique shock leads to separation of the flow, so that the rear shock starts from the boundary of a dead-water region (ACKERET, FELDMANN, and ROTT).

Profiles which have a small nose radius and whose position of maximum thickness lies far back behave quite differently: a considerable increase in the speed of sound is frequently observed without the resulting shock wave's leading to separation (see Figures 3.16 and 3.17). The shock wave is straight and is normal to the profile; this can be inferred from the pressure distribution, which corresponds to subsonic conditions downstream of the shock wave (the magnitude of the jump agreeing with the theoretical value for a normal shock). The observed drag coefficients for these profiles do sometimes show the increase caused by separa-

tion of the boundary layer but only when the speed of sound is exceeded by a relatively large amount.

#### 10.4.2 Similarity Rules

According to Sections 10.3.1 and 10.5.2 similar flows at different Mach numbers occur if the thickness ratio is changed by a factor  $\sqrt{1 - M_\infty^2}$  when the free stream is subsonic and by a factor  $\sqrt{M_\infty^2 - 1}$  when the free stream is supersonic. In terms of the local velocity components, the ratio  $\frac{v}{u}$  must change by the factors  $\sqrt{1 - M_\infty^2}$  and  $\sqrt{M_\infty^2 - 1}$  respectively (Prandtl-Glauert and Ackeret rules).

In the transonic range the speed of sound,  $a$ , is of the same order of magnitude as the free-stream speed,  $V$ . We introduce the critical speed,  $a^*$ , where

$$\frac{\gamma + 1}{2} a^{*2} = a^2 + \frac{\gamma - 1}{2} (u^2 + v^2), \quad (10.23)$$

and compare the local velocity component in the  $x$  direction,  $u$ , with the critical speed,  $a^*$ , by forming the disturbance velocity  $u' = u - a^*$  (small in comparison with  $a^*$ ). In Equation (10.2) we then replace  $a^2 - u^2$  by  $-(\gamma + 1) a^* u'$ ,  $a^2 - v^2$  by  $a^{*2}$ , and  $uv$  by  $a^* v$ ; the resulting equation is

$$(\gamma + 1) u' \frac{\partial u'}{\partial x} + v \left( \frac{\partial u'}{\partial y} + \frac{\partial v}{\partial x} \right) - a^* \frac{\partial v}{\partial y} = 0. \quad (10.24)$$

The irrotationality condition is

$$\frac{\partial u'}{\partial y} - \frac{\partial v}{\partial x} = 0. \quad (10.25)$$

In Equation (10.24) the order of magnitude of  $a^*$  is 1, and that of  $u'$  is, say,  $\epsilon$ ; it follows that  $\frac{\partial v}{\partial y} \sim \epsilon^2$ . If we assume that  $v \sim \epsilon^m$  then  $\frac{\partial}{\partial y} \sim \epsilon^{(2-m)}$  and, from Equation (10.25),  $\epsilon^{(3-m)} - \epsilon^m = 0$ , so that  $m = \frac{3}{2}$ ; hence, the middle term of Equation (10.24) is proportional to  $\epsilon^3$ , and can be neglected; consequently, the differential equations characteristic of the transonic range are

$$(y + 1) u' \frac{\partial u'}{\partial x} = a^* \frac{\partial v}{\partial y}, \quad (10.26)$$

$$\frac{\partial u'}{\partial y} = \frac{\partial v}{\partial x}.$$

These differential equations have received considerable attention. VON KÁRMÁN has derived a similarity rule from them, which is of the greatest importance; it states that, when the free-stream Mach number is close to unity, "similar" flows exist about geometrically similar bodies if the parameter

$$\frac{(M_\infty - 1)}{\left[ (\gamma + 1) \frac{t}{c} \right]^{2/3}} \quad (10.27)$$

has the same value; an experimental verification of this similarity rule has been given by MALAVARD (among others).

BÖMELBURG has recently succeeded in removing the restriction that the free-stream Mach number must lie close to unity, and has given a more general similarity rule, containing two parameters; in the subsonic and supersonic regions this passes over into the Prandtl-Glauert and Ackeret rules respectively†. Applied to "similar" states 1 and 2, the rule consists essentially of a "generalised Prandtl-Glauert rule" valid for arbitrary Mach-numbers

$$\frac{(C_p)_2}{(C_p)_1} = \frac{t_2}{t_1} \sqrt{\frac{(M_\infty^2)_1 - 1}{(M_\infty^2)_2 - 1}}, \quad (10.28)$$

but with the requirement that the values of  $M_\infty$  and  $\frac{t}{c}$  satisfy a further condition; this requirement corresponds to a second ("generalised von Kármán") similarity parameter, and may be written

$$\frac{t_2}{t_1} = \frac{F[(M_\infty)_2, \gamma_2]}{F[(M_\infty)_1, \gamma_1]} \quad (M_\infty \neq 1), \quad (10.29)$$

where

$$F = \sqrt{|M_\infty^2 - 1|} \left\{ 1 - \frac{1}{M_\infty} \sqrt{\frac{2}{(\gamma + 1)} \left( 1 + \frac{\gamma - 1}{2} M_\infty^2 \right)} \right\}$$

(see Table 10.1); it becomes more important as the free-stream speed,  $V$ , approaches the speed of sound. If the free-stream speed is approximately equal to the speed of sound we obtain the familiar von Kármán similarity parameter,

$$\frac{|M_\infty - 1|^{3/2}}{(\gamma + 1) \left( \frac{t}{c} \right)} \quad \text{or} \quad \frac{|M_\infty - 1|}{\left[ (\gamma + 1) \frac{t}{c} \right]^{2/3}}, \quad (10.30)$$

† The derivation given here is due to a colleague of mine, E. MARTENSEN, and deviates considerably from BÖMELBURG's.

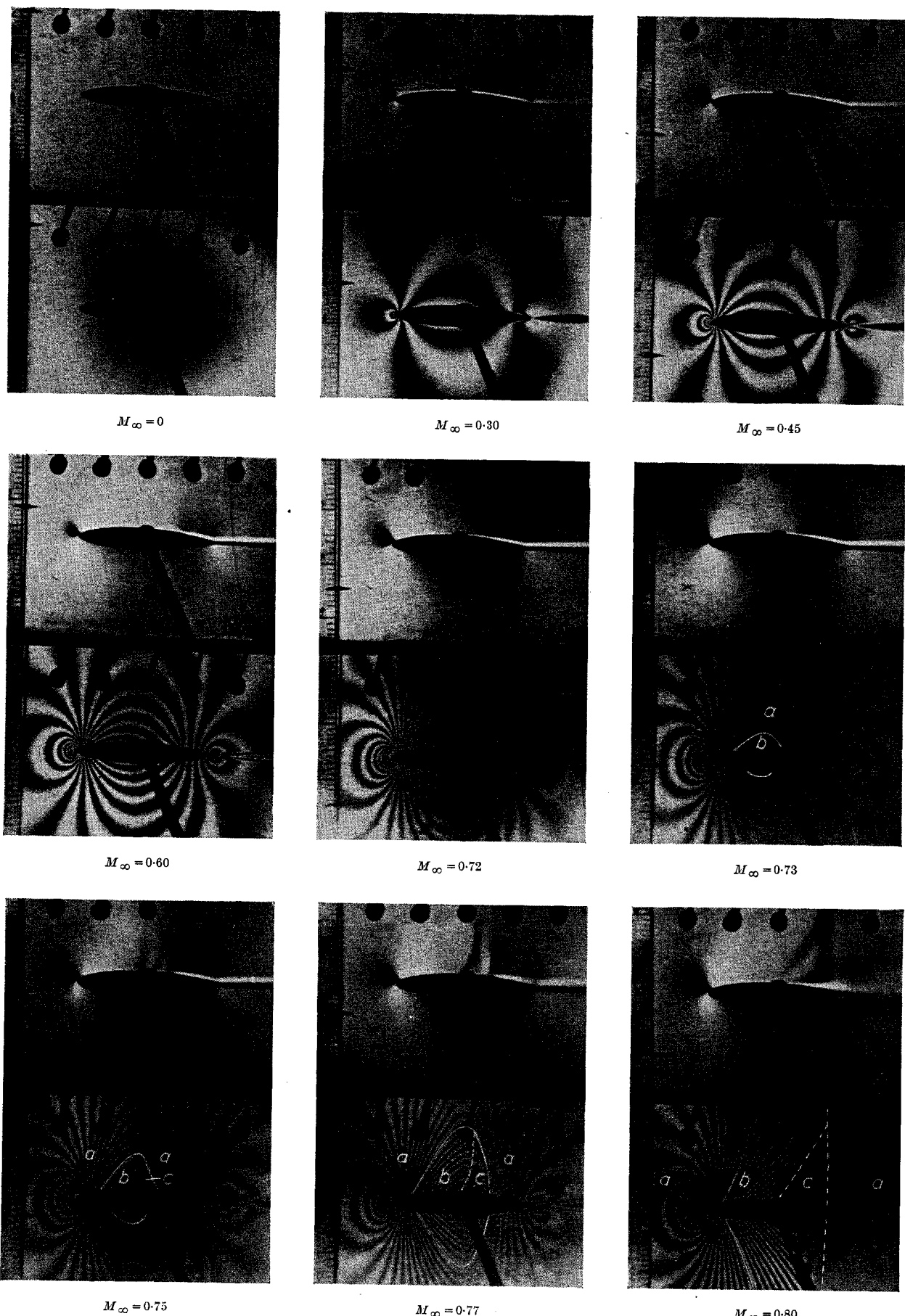


Fig. 10.5. Change in the flow field caused by increasing Mach number. Schlieren and interferometer photographs for the profile NACA 0015-44 (ZOBEL)

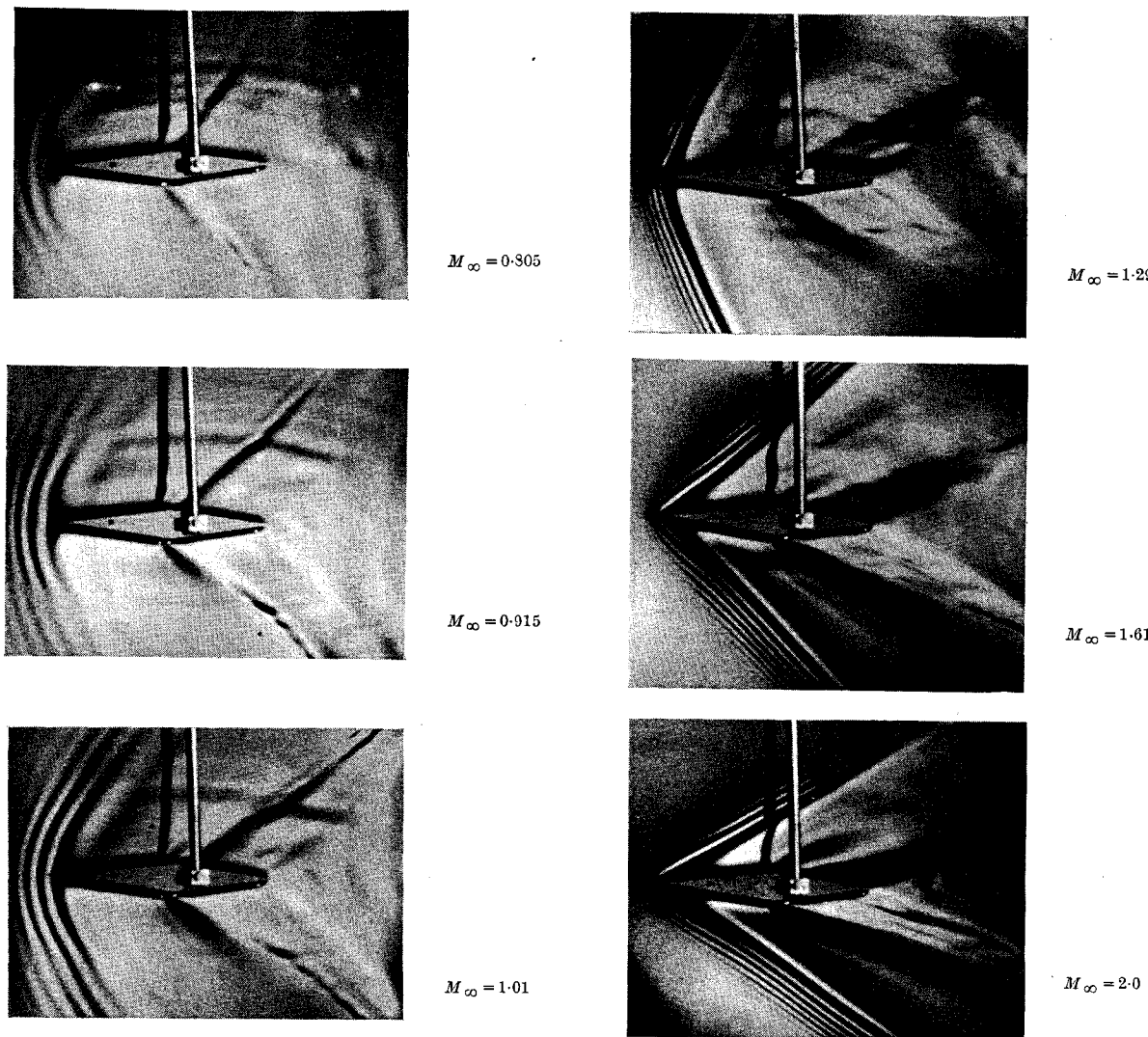


Fig. 10.6. Flow about a symmetrical double wedge, for Mach numbers between 0.8 and 2.0 (BÖMELBURG)

by expanding  $F$  in the region of  $M_\infty = 1$ ; with the help of Equation (10.28) we obtain the following relationship between the pressure coefficients

$$\frac{(C_p)_2}{(C_p)_1} = \left(\frac{t_2}{t_1}\right)^{2/3} \left(\frac{\gamma_1 + 1}{\gamma_2 + 1}\right)^{1/3} \quad (\text{for } M_\infty = 1). \quad (10.31)$$

The additional condition gradually loses significance as the free-stream Mach number moves away from unity; for smaller or larger Mach numbers, Equation (10.28) (the familiar Prandtl-Glauert or Ackeret rule) has unrestricted validity. Corresponding similarity rules are also valid for integrals involving the pressure distribution: for example, for the lift coefficient,  $C_L$ , and for the moment coefficient,  $C_m$ ; in addition,  $\frac{dC_L}{d\alpha}$  behaves as  $\left(\frac{\Delta p}{q}\right)/\left(\frac{t}{c}\right)$ , and  $C_D$  behaves as  $\left(\frac{\Delta p}{q}\right)\left(\frac{t}{c}\right)$ .

## 10.5 Supersonic Flow

### 10.5.1 The Flow Field

If the free-stream speed is supersonic and the profile so shaped that purely supersonic flow occurs, the flow can again be treated by simple theories. Purely supersonic flows had already received extensive theoretical and experimental investigation before the war, and the methods used have since been considerably extended. It is sufficient to give here a short description of the known results for supersonic flow, thereby completing the discussion of

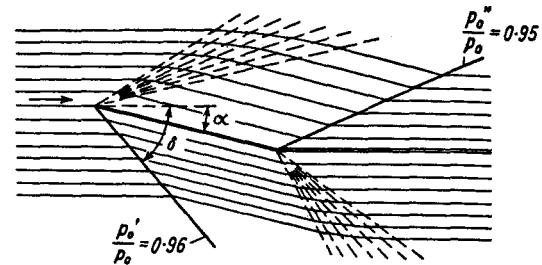


Fig. 10.7. Supersonic flow about a flat plate (BUSEMANN).  $p_0$  = stagnation pressure;  $p_0'$  and  $p_0''$  are the changed stagnation pressures behind the shocks;  $\alpha$  = angle of incidence;  $\delta$  = angle of shock

the relationship between pressure distribution and profile shape begun in Chapter 7; these results come primarily from the work of PRANDTL, MEYER, ACKERET, and BUSEMANN (see PRANDTL's book cited in Section 1.5.1).

Small disturbances propagate with the speed of sound and so stay behind the profile, which is moving with a greater speed; hence the effect of a disturbance of the parallel supersonic flow is confined to a cone-shaped region behind the disturbance, which is called the "Mach cone". The basic character of such a flow can be illustrated by the example of the flat plate. If this is at a positive angle of incidence (see Figure 10.7), the flow expands around the "convex corner" on the upper side of the profile, until it has reached the direction of the plate; it then continues parallel to this: on the other hand, at the "concave corner" on the lower side of the plate, the direction of the flow is changed discontinuously by a shock wave. At the trailing edge of the plate a similar behaviour occurs. On

Table 10.1  
The Function  $F$  (for  $\gamma = 1.4$ )

$M_\infty$	0	1	2	3	4	5	6	7	8	9
0.0	—	90.28	44.64	29.42	21.81	17.24	14.19	12.02	10.38	9.114
0.1	—	8.097	7.265	6.570	5.983	5.479	5.042	4.659	4.321	4.021
0.2	—	3.510	3.291	3.092	2.910	2.743	2.589	2.448	2.316	2.194
0.3	—	1.97491	87572	78284	69561	61356	53623	46325	39426	32896
0.4	—	1.20834	15254	09947	04895	00081	*95489	*91106	*86918	*82914
0.5	—	0.75416	71903	56535	65306	62207	59233	56376	53632	50995
0.6	46022	43677	41421	39250	37161	35151	33216	31353	29560	27835
0.7	26174	24576	23039	21560	20138	18772	17459	16198	14988	13827
0.8	12715	11650	10632	09659	08730	07946	07005	06207	05452	04740
0.9	04070	03443	02859	02319	01824	01375	00975	00628	00339	00119
1.0	+ 0.00000	00117	00328	00597	00913	01265	01650	02063	02501	02962
1.1	03443	03943	04459	04991	05538	06098	06670	07253	07847	08451
1.2	09064	09686	10317	10954	11599	12250	12908	13572	14241	14916
1.3	15595	16279	16967	17660	18356	19056	19759	20466	21175	21888
1.4	22603	23321	24041	24763	25487	26214	26942	27672	28403	29136
1.5	29871	30607	31344	32082	32821	33561	34302	35044	35787	36531
1.6	37275	38020	38765	39511	40267	41004	41751	42498	43246	43994
1.7	44742	45490	46239	46987	47735	48484	49232	49981	50729	51478
1.8	52226	52974	53722	54470	55217	55965	56712	57459	58205	58951
1.9	59698	60443	61189	61934	62679	63423	64167	64911	65654	66397

the upper side the direction of the flow is changed discontinuously by a shock wave, so that it has a direction approximately the same as upstream of the plate: on the lower side a continuous expansion to this direction takes place. The exact direction at the trailing edge is determined by the condition that, behind the trailing edge, the upper and lower flows must be divided by a line (starting from the trailing edge) across which the pressure and the flow direction vary continuously. The energy losses through the upper and lower shock waves differ because of the different velocities in front of them; therefore, above and below the line of separation, the velocities, densities, and temperatures differ from one another; the differences are small if the angle of incidence of the plate is small (and this is usually so), and in the actual flow they soon vanish because of the effect of viscosity. If the angle of incidence and the resulting compression on the pressure side are not so great that subsonic regions occur, then this example illustrates the most important properties of a purely supersonic flow. For small angles of incidence the energy losses through the shock wave are small and the whole flow field can be regarded as homentropic (as can all subsonic flow fields).

If instead of a flat plate we consider a profile, assumed to be pointed at the leading and trailing edges, we can approximate the curved surface by straight lines; at convex corners expansion waves occur, and at concave corners shock waves occur (their strengths being determined by the change in angle). The symmetrical circular arc profile at zero incidence provides a simple example (see Figure 10.8); the changes in flow direction at the leading and trailing edges are such that shock waves occur on the upper and lower sides; the shock waves become less inclined to the free-stream direction as the distance from the profile increases because they are gradually weakened by interaction with the expansion waves that come from the convex profile. At a sufficiently large distance from the profile, the shock waves become indistinguishable from Mach lines; the cosecant of the corresponding "Mach angle" is the ratio of the free-stream speed,  $V$ , to the speed of sound,  $a$ . The losses in stagnation pressure caused by the shock can be obtained from Figure 10.8; because of the relatively small change of flow direction these losses lie within moderate limits.

A further example is given in Figure 10.6, which shows photographs of the flow about a symmetrical double wedge at six different free-stream Mach numbers; they have the character of schlieren photographs, showing the compressed and expanded regions of the flow field very clearly. These results have been obtained by use of the shallow water analogy, and this can be seen by the capillary waves lying in front of the shock waves; these die away with increasing distance in front of the shock; they are not present in an air flow.

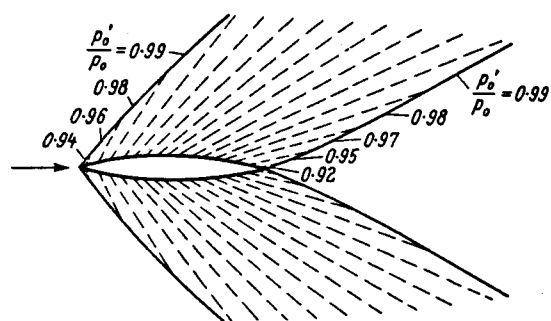


Fig. 10.8. Supersonic flow about a symmetrical circular arc profile (BUSEMANN)

### 10.5.2 The Pressure Distribution in Supersonic Flow

Now that we have become familiar with the behaviour of the flow at supersonic speed, we can consider the pressure forces occurring on a profile. For Prandtl-Meyer flow round a corner (see PRANDTL's book cited in Section 1.5.1), the following relation holds:

$$dp = \frac{\rho w^2}{\sqrt{\left(\frac{w}{a}\right)^2 - 1}} d\beta. \quad (10.32)$$

An approximate solution of this equation (obtained by ACKERET and, later, by BUSEMANN) is applicable to profiles; in this approximation the integral of Equation (10.32), the disturbance pressure at the profile, is written in the form of a power series,

$$\Delta p_{u,l} = (\pm C_1 \beta_{u,l} + C_2 \beta_{u,l}^2 \pm C_3 \beta_{u,l}^3 + \dots) q; \quad (10.33)$$

the first two coefficients are

$$C_1 = \frac{2}{\sqrt{M_\infty^2 - 1}}, \quad C_2 = \frac{(M_\infty^2 - 2)^2 + \gamma M_\infty^4}{2(M_\infty^2 - 1)^2};$$

they are shown as functions of Mach number in Figure 10.9. If the change in flow direction,  $\beta$ , is small, these formulas can be replaced by finite power series in  $\beta$ , the first approximation being as follows:

$$\Delta p_u = -\frac{2\beta_u}{\sqrt{M_\infty^2 - 1}}, \quad \beta_u = a + \beta'_u(x), \quad (10.34)$$

on the suction side; and

$$\Delta p_l = +\frac{2\beta_l}{\sqrt{M_\infty^2 - 1}}, \quad \beta_l = a + \beta'_l(x), \quad (10.35)$$

on the pressure side; the tangent to the profile contour must make a small angle with the free-stream direction if these formulas are to be applicable. This first approxima-

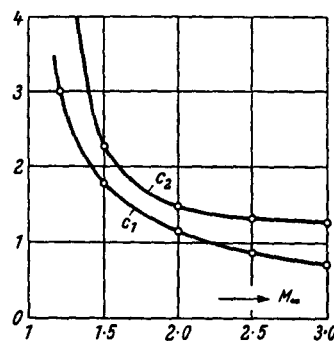


Fig. 10.9.  $C_1$  and  $C_2$  as functions of Mach number

tion gives good results for the flat plate at a small angle of incidence, but for profiles of finite thickness a knowledge of the second approximation is desirable (see Section 10.5.4). If the expansion is taken as far as the third power of  $\beta$ , then the influence of shock waves must be considered; the extension of the method to this degree of approximation is possible† but, when this becomes necessary, graphical methods (not treated here) are preferable‡.

### 10.5.3 Approximate Formulas for the Forces on an Arbitrary Profile

For arbitrary profile shapes an integration of the pressure along the profile chord gives the following results: for the lift,

$$L = \int_0^c (\Delta p_t \cos \beta_t - \Delta p_u \cos \beta_u) ds; \quad (10.36)$$

and for the drag,

$$D = \int_0^c (\Delta p_t \sin \beta_t - \Delta p_u \sin \beta_u) ds. \quad (10.37)$$

For small slopes  $\cos \beta \approx 1$ ,  $\sin \beta \approx \beta$ ; hence, to the first approximation, the lift and drag coefficients become

$$\begin{aligned} C_L &= \frac{4 \alpha}{\sqrt{M_\infty^2 - 1}}, \\ C_D &= 2C_f + \frac{2}{c\sqrt{M_\infty^2 - 1}} \int_0^c (\beta_u'^2 + \beta_t'^2) dx + \\ &\quad + \frac{4 \alpha^2}{\sqrt{M_\infty^2 - 1}}; \end{aligned} \quad (10.38)$$

in the second formula the total coefficient of skin-friction

† The literature on this subject is not free from errors; M. SCHÄFER has given a correct derivation.

‡ An explanation of the method of characteristics, which is used in the graphical construction of supersonic flow fields, can be found in the literature cited in Sections 1.5.1 and 1.5.2 (for example: BUSEMANN, OSWATITSCH, SAUER, TOLLMIEN).

drag,  $2C_f$ , has been included. In the second approximation there appear integrals involving the first, second, and third powers of the local slopes,  $\beta_u'$  and  $\beta_t'$ ; we write  $\beta_u$  and  $\beta_t$  for these integrals, where

$$\begin{aligned} B_{vu} &= \frac{1}{c} \int_0^c (\beta_u')^v dx_u, \\ B_{vt} &= \frac{1}{c} \int_0^c (\beta_t')^v dx_t. \end{aligned} \quad (10.39)$$

The second approximation for the lift coefficient is then

$$C_L = C_1(B_{1t} + B_{1u}) + C_2(B_{2t} - B_{2u}) + \alpha\{2C_1 + 2C_2(B_{1t} - B_{1u})\}; \quad (10.40)$$

and that for the drag coefficient, including the skin-friction drag coefficient, is

$$\begin{aligned} C_D &= 2C_f + C_1(B_{2t} + B_{2u}) + C_2(B_{3t} - B_{3u}) + \\ &\quad + \alpha\{2C_1(B_{1t} + B_{1u}) + 3C_2(B_{2t} - B_{2u})\} + \\ &\quad + \alpha^2\{2C_1 + 3C_2(B_{1t} - B_{1u})\}; \end{aligned} \quad (10.41)$$

here,  $C_1$  and  $C_2$  are the constants introduced in Equation (10.33) and plotted in Figure 10.9.

### 10.5.4 Approximate Formulas for Special Profiles, and Comparison with Wind-tunnel Measurements

The above considerations are easily applied to flat plates and profiles composed of circular arcs. Writing  $f_u$  and  $f_t$  for the absolute values of the maximum ordinates of the suction and pressure sides respectively, we have

$$B_{2u,t} = \frac{16}{3} \left( \frac{f_{u,t}}{c} \right)^2. \quad (10.42)$$

The coefficients  $B_{1u,t}$  and  $B_{3u,t}$  are zero for all profiles that are symmetrical about the  $y$  axis. We have the following special results:

(a) the flat plate (first approximation),

$$C_L = \frac{4 \alpha}{\sqrt{M_\infty^2 - 1}}, \quad C_D = 2C_f + \frac{4 \alpha^2}{\sqrt{M_\infty^2 - 1}}; \quad (10.43)$$

(b) the symmetrical biconvex profile (second approximation),

$$\begin{aligned} C_L &= \frac{4 \alpha}{\sqrt{M_\infty^2 - 1}}, \\ C_D &= 2C_f + \frac{4 \alpha^2}{\sqrt{M_\infty^2 - 1}} + \frac{16}{3} \frac{(t/c)^2}{\sqrt{M_\infty^2 - 1}}; \end{aligned} \quad (10.44)$$

(c) the circular segment profile with straight pressure side (second approximation),

$$C_L = \frac{4\alpha}{\sqrt{M_\infty^2 - 1}} - \frac{16}{3} C_2 (l/c)^2,$$

$$C_D = 2C_f + \frac{32}{3} \left( \frac{t}{c} \right)^2 \frac{1}{\sqrt{M_\infty^2 - 1}} -$$

$$- 16 \left( \frac{t}{c} \right)^2 C_2 \alpha + \frac{4\alpha^2}{\sqrt{M_\infty^2 - 1}}; \quad (10.45)$$

(d) the flat plate with a discontinuity in slope (first approximation),

$$C_L = \frac{4(\alpha + \eta l)}{\sqrt{M_\infty^2 - 1}}, \quad (10.46)$$

where  $l$  is written for  $c_\eta/c$ , the ratio of the chord of the flap to the chord of the profile, and  $\eta$  is the flap deflection; for the moment about an axis at a distance  $hc$  from the nose, we have

$$(C_m)_h = \frac{1}{\sqrt{M_\infty^2 - 1}} [(4h - 2)\alpha + \eta l (4h + 2l - 4)]; \quad (10.47)$$

and for the moment,  $M_\eta = C_\eta \left( \frac{\rho}{2} \right) V^2 c_\eta^2$ , of the flap about its axis of rotation, we have

$$C_\eta = - \frac{2(\alpha + \eta)}{\sqrt{M_\infty^2 - 1}}. \quad (10.48)$$

Following his derivation of the formulas for the symmetrical biconvex profile, A. BUSEMANN considers the smallest attainable value of  $\frac{C_D}{C_L}$  in supersonic flow; he finds that

$$\left( \frac{C_D}{C_L} \right)_{\min.} =$$

$$= \sqrt{\frac{16}{3} \left( \frac{t}{c} \right)^2 + 2C_f \sqrt{M_\infty^2 - 1}}. \quad (10.49)$$

This quantity is plotted against Mach number in Figure 10.10; it is assumed that the skin-friction drag coefficient,  $C_f$ , has the value 0.003; three thickness ratios are considered,  $\frac{t}{c} = 0$ ,  $\frac{t}{c} = 0.02$ , and  $\frac{t}{c} = 0.04$ . From this figure the influences of skin-friction drag and of profile thickness can be separately discerned; small values of  $\left( \frac{C_D}{C_L} \right)_{\min.}$  are to be expected for very small thicknesses.

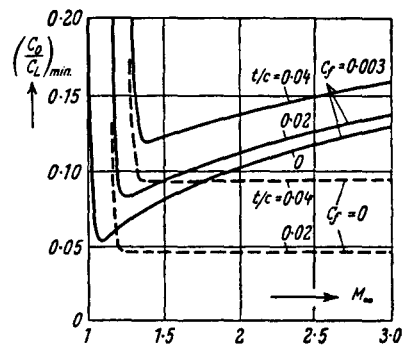


Fig. 10.10. Influence of profile thickness and skin-friction drag on the variation of  $\left( \frac{C_D}{C_L} \right)_{\min.}$  with Mach number (BUSEMANN)

From the above simple formulas we see that the lift of an unsymmetrical circular segment profile has a negative value when the profile is at zero incidence; this has been confirmed by wind-tunnel measurements carried out by BUSEMANN and WALCHNER and, later, by FERRI. Figures 12.147 and 12.148 show some of these wind-tunnel results for the circular segment profile; the theoretical curves (without the skin-friction drag,  $2C_f$ ) are also plotted. A striking feature is the good agreement between experiments (particularly FERRI's) and theory, although the skin-friction drag has been ignored in the theory. Some of the experimental drag coefficients are less than the values predicted from a theory ignoring viscosity; the reason for this seems to be separation of the flow in the vicinity of the trailing edge, remarkable though this may sound. The theoretical pressure distribution of the circular segment profile has falling pressure right to the trailing edge (see Figure 12.48), and so there is little likelihood of separation; however, as a result of the strong shock wave at the trailing edge, a sudden pile-up of boundary layer material occurs; consequently, the boundary layer separates at a short distance in front of the shock, in order to provide the necessary room in the supersonic flow for this material. This leads to the formation of oblique shock waves, which later coalesce with the main shock; at the same time the strong pressure rise at the trailing edge is replaced by several small rises on the profile; the observed reductions in drag result from this breakdown of the theoretical pressure distribution.

### 10.5.5 Exact Solution for the Flat Plate

If we abandon the assumption that the slopes of the profile are small, then, in the integration of Equation (10.32), we cannot assume a linear variation of density,  $\rho$ , speed of sound,  $a$ , and flow speed,  $w$ ; however, the integration can be performed numerically or graphically, without difficulty. The graphical method has been developed to a high degree, particularly in the last ten years, and a neat and quick treatment of fairly strong shock waves can be

Table 10.2 Pressures and Forces on the flat plate at Supersonic Speeds (exact values from EL BADRAWY)

$M_{\infty}$	$c^{\circ}$	$p_{\text{st}}/p_0$	$\delta$	$p_{\text{st}}/p_{\infty}$	$p_{\text{st}}/p_0$	$C_L$	$C_D$	$C_D/C_L$
1.20	1	0.39145	58.75	1.056	0.43527	0.1054	0.0018	0.0175
	2	0.37210	61.10	1.120	0.46187	0.2158	0.0075	0.0349
	3	0.35403	64.37	1.199	0.49444	0.3373	0.0177	0.0524
	3.7	0.35952	68.08	1.277	0.52681	0.4011	0.0259	0.0641
1.40	1	0.29910	46.87	1.051	0.33027	0.0723	0.0013	0.0175
	2	0.28480	48.19	1.104	0.34692	0.1440	0.0050	0.0349
	3	0.27114	49.57	1.159	0.36420	0.2156	0.0113	0.0524
	4	0.25824	51.15	1.219	0.38306	0.2888	0.0202	0.0699
	6	0.23376	54.62	1.353	0.42517	0.4415	0.0464	0.1052
	8	0.21130	59.36	1.527	0.47984	0.6168	0.0867	0.1406
	9.03	0.20050	63.17	1.655	0.52007	0.7321	0.1159	0.1584
	1.60	0.22374	39.67	1.060	0.24939	0.0608	0.0011	0.0175
	2	0.21269	40.73	1.104	0.25978	0.1116	0.0039	0.0349
1.80	3	0.20207	41.82	1.161	0.27300	0.1679	0.0088	0.0624
	4	0.19191	42.93	1.219	0.28679	0.2244	0.0157	0.0699
	6	0.17280	45.36	1.345	0.31637	0.3386	0.0356	0.1051
	8	0.15525	48.04	1.484	0.34938	0.4557	0.0641	0.1406
	10	0.13914	51.14	1.644	0.38685	0.5783	0.1019	0.1762
	12	0.12438	54.89	1.832	0.43101	0.7110	0.1511	0.2125
	14.24	0.11022	61.65	2.143	0.50418	0.9052	0.2532	0.2532
	1	0.16603	34.64	1.064	0.18352	0.0468	0.0008	0.0175
	2	0.15840	35.53	1.110	0.19318	0.0931	0.0033	0.0349
	3	0.14813	36.48	1.170	0.20363	0.1404	0.0074	0.0624
	4	0.14019	37.44	1.230	0.21407	0.1867	0.0131	0.0699
	6	0.12534	39.49	1.382	0.23704	0.2814	0.0296	0.1051
	8	0.11175	41.69	1.605	0.26193	0.3768	0.0630	0.1406
	10	0.09935	44.06	1.661	0.28908	0.4734	0.0834	0.1763
2.00	12	0.08806	46.70	1.835	0.31936	0.6732	0.1218	0.2126
	15	0.07303	51.35	2.139	0.37227	0.7323	0.1962	0.2679
	18	0.06011	58.00	2.551	0.44398	0.9249	0.3005	0.3249
	18.84	0.05788	61.28	2.740	0.47687	1.0045	0.3427	0.3412
	1	0.12076	30.82	1.058	0.13521	0.0404	0.0007	0.0175
	2	0.11401	31.65	1.118	0.14288	0.0807	0.0028	0.0349
	3	0.10757	32.58	1.181	0.15093	0.1211	0.063	0.0523
	4	0.10141	33.40	1.247	0.15937	0.1618	0.0113	0.0699
	6	0.08994	35.24	1.377	0.17726	0.2429	0.0255	0.1051
2.50	8	0.07949	37.22	1.539	0.19668	0.3246	0.0456	0.1406
	10	0.07005	39.32	1.707	0.21815	0.408	0.0719	0.1763
	12	0.06149	41.59	1.889	0.24141	0.4923	0.1046	0.2125
	15	0.05024	45.34	2.195	0.29052	0.6222	0.1667	0.2679
	18	0.04070	49.78	2.655	0.32653	0.7604	0.2471	0.3249
	21	0.03265	55.67	3.014	0.38519	0.9207	0.3534	0.3838
	22.71	0.02886	61.48	3.480	0.44219	1.0659	0.4462	0.4187
	1	0.05296	24.35	1.068	0.06251	0.0373	0.0006	0.0175
	2	0.05113	25.05	1.141	0.06678	0.0611	0.0021	0.0349
	3	0.04772	25.82	1.216	0.07117	0.0914	0.0048	0.0524
	4	0.04450	26.62	1.296	0.07585	0.1221	0.0085	0.0699
	6	0.03857	28.27	1.452	0.08498	0.1826	0.0189	0.1051
	8	0.03455	30.00	1.658	0.09704	0.2416	0.0340	0.1406
	10	0.02859	31.86	1.865	0.10916	0.3098	0.0836	0.1763
	12	0.02445	33.81	2.091	0.12232	0.3738	0.0795	0.2126
	15	0.01917	36.95	2.467	0.14439	0.4723	0.1266	0.2679
	18	0.01484	40.40	2.895	0.16949	0.5742	0.1865	0.3249
	22	0.01035	45.62	2.557	0.20816	0.7162	0.2893	0.4040
5.00	28	0.00575	56.35	4.885	0.28892	0.9659	0.5136	0.5317
	29.67	0.00482	62.65	5.602	0.44220	1.0960	0.6240	0.5895
	3.60	0.00118	14	1.541	0.00291	0.0523	0.0033	0.0627
	6.17	0.00084	16	2.051	0.00388	0.0914	0.0098	0.1076
	10.68	0.00043	20	3.247	0.00614	0.1698	0.0319	0.1879
	16.60	0.00018	26	5.436	0.01027	0.2926	0.0869	0.2972
20.21	20.21	0.00009	30	7.129	0.01347	0.3800	0.1393	0.3666
	26.78	0.00002	38	10.893	0.02059	0.5557	0.2792	0.5024
	31.21	0.000009	44	13.913	0.02629	0.6805	0.4088	0.6000
	36.29	0.000003	52	17.953	0.03392	0.8284	0.6048	0.7301
	41.11	0.000001	66	24.206	0.04575	1.0427	0.9098	0.8726

Table 10.2 continued

$M_\infty$	$\alpha^\circ$	$p_{su}/p_\infty$	$\delta$	$p_{si}/p_\infty$	$p_{si}/p_\infty$	$C_L$	$C_D$	$C_D/C_L$
10.00	3.21		8	2.091		0.0228	0.0013	0.0560
	7.65		12	4.877		0.0614	0.0082	0.1340
	13.31		18	10.981		0.1549	0.0365	0.2356
	18.53		24	19.135		0.2613	0.0877	0.3351
	23.47		30	29.018		0.3828	0.1662	0.4341
	28.17		36	40.164		0.5079	0.2726	0.5366
	32.59		42	52.080		0.6288	0.4017	0.6393
	36.64		48	64.263		0.7488	0.5565	0.7437
	40.18		54	76.213		0.8641	0.7292	0.8441
	42.90		60	87.361		0.9529	0.8862	0.9293
	44.43		67.12	98.713		1.0125	0.9925	0.9803
$\infty$	8.37		10			0.0497	0.0073	0.1471
	16.57		20			0.1873	0.0558	0.2973
	24.50		30			0.3795	0.1731	0.4557
	28.31		35			0.4741	0.2559	0.5386
	32.05		40			0.5843	0.3662	0.6261
	35.55		45			0.6812	0.4846	0.7146
	38.81		50			0.7840	0.6121	0.8042
	41.6		55			0.8735	0.7754	0.8876
	43.9		60			0.9452	0.9123	0.9623
	45.58		67.8			1.0001	1.0204	1.0200

carried out by this process; hence, it is possible to treat flows that are rotational (and, consequently, non-homogeneous). Although the method can be directly applied to wing profiles, the angles of incidence are so small that it is not usually required; the interested reader is referred to the bibliography of Section 10.6.

We now briefly discuss the exact behaviour of the flow quantities for the flat plate in wholly supersonic flow. Some quantitative results† are given in Table 10.2; they have been derived from the exact non-linear equations.

For each free-stream Mach number, the largest angle of incidence considered is the angle for which the Mach number behind the shock on the lower side,  $M_{2l}$ , is unity. The table contains the values of the pressures on the upper

and lower sides (respectively  $p_{2u}$  and  $p_{2l}$ ), the angle of the shock,  $\delta$ , the lift and drag coefficients, and the ratio of these coefficients,  $C_D/C_L$ . The coefficients are formed as follows:

$$C_D = \frac{L}{qc} = \frac{p_{2l} - p_{2u}}{q} \cos \alpha; \quad (10.50)$$

$$C_L = \frac{D}{qc} = \frac{p_{2l} - p_{2u}}{q} \sin \alpha; \quad (10.51)$$

here,  $q = \left(\frac{\gamma}{2}\right) p_\infty M_\infty^2$ .

An example of the differences between the exact solution and the linearised solution (see Equation (10.43)) is given in Table 10.3 (from EL BADRAWY); the index  $l$  refers to the linearised solution.

We note that the differences are considerable at high angles of incidence (particularly at high Mach numbers), the approximate values being too small; for small angles of incidence, which are the rule in practice, the differences are usually of no significance.

## 10.6 References

- ACKERET, J., Luftkräfte an Flügeln, die mit größerer als Schallgeschwindigkeit bewegt werden. ZFM 16 (1925), S. 72–74.
- F. FELDMANN and N. ROTT: Untersuchungen an Verdichtungsstößen und Grenzschichten in schnell bewegten Gasen. Mitt. ETH Zürich Nr. 10 (1946).
- BADRAWY, R. W. EL: Ebene Plattengitter bei Überschallgeschwindigkeit. Mitt. ETH Zürich, Nr. 19 (1952).

Table 10.3  
Comparison of Exact and Linearised Solutions for the Flat Plate

$M_\infty$	$\alpha$	$C_L - (C_L)_l$	$C_L$	$C_D - (C_D)_l$	$C_D$
1.40	1	0.00084	0.07228	0	0.0013
	2	0.00151	0.14399	0	0.0050
	3	0.00163	0.21555	0.0001	0.0113
	4	0.00385	0.28881	0.0002	0.0202
	6	0.01408	0.44152	0.0010	0.0464
	8	0.04690	0.61682	0.0072	0.0867
	9.03	0.08950	0.73209	0.0148	0.1159
	4	0.0005	0.0523	0.0000	0.0033
	6	0.0030	0.0914	0.0010	0.0098
	12	0.0255	0.1698	0.0063	0.0319
	18	0.0696	0.2996	0.0246	0.0869
	24	0.1391	0.3800	0.0341	0.1393
	30	0.1846	0.5557	0.1453	0.2792
	36	0.3972	0.6806	0.2698	0.4088
	41.11	0.4669	0.8284	0.4895	0.6048

† For the meaning of the symbols, see Figure 10.7.

- BEAVAN, J. A. and G. A. M. HYDE: Examples of Pressure Distributions at Compressibility Speeds on EC 1250. R & M No. 2056 (1942).
- Note on Reynolds and Mach Number Effects on the Pressure Distribution on the Tail of EC 1250. R & M No. 2252 (1943).
- BEAVAN, J. A., R. G. FOWLER and G. A. M. HYDE: Pressure and Wake Measurements up to Mach Number 0.85 on an EC 1250 Section with 25 per Cent Control. R & M No. 2065 (1945).
- BEAVAN, J. A. and G. A. M. HYDE: Pressure Distributions at High Speeds on EC 1250. R & M No. 2625 (1947).
- BETZ, A.: Über die Lage des Verdichtungsstoßes bei umströmten Profilen. Vortrag vor der DAL. AVA-Bericht 43/A/31 (1943).
- and E. KRAHN: Berechnung von Unterschallströmungen kompressibler Flüssigkeiten um Profile. Ing. Arch. 17 (1949), S. 403—417.
- BÖMELBURG, H.: Eine Verallgemeinerung des Kármánschen Ähnlichkeitsgesetzes für schallnahe Strömungen. ZfM 3 (1955), S. 313—322.
- BUSEMANN, A.: Aerodynamischer Auftrieb bei Überschallgeschwindigkeiten. Convegno di scienze fisiche, matematiche e naturali. Rom (1936) und Luso 12 (1935), S. 210.
- Gasdynamik. Handbuch der Experimentalphysik. Bd. IV, Teil 1 (1931).
- Der Kompressibilitätseinfluß für dünne wenig gekrümmte Profile bei Überschallgeschwindigkeit. Schriften DAL, H. 18 (1940).
- O. WALCHNER: Profileigenschaften bei Überschallgeschwindigkeit. Forschg. Ing. Wes. 4 (1933), S. 87.
- CHAPMAN, D. R. and R. H. KESTER: Effect of Trailing-Edge Thickness on Lift at Supersonic Velocities. NACA TN 3504 (1955).
- COLLAR, A. R.: Theoretical Forces and Moments on a Thin Aerofoil with Hinged Flaps at Supersonic Speeds. R & M No. 2004 (1943).
- CREAGER, M. O.: Effects of Leading-Edge Blunting on the Local Heat Transfer and Pressure Distributions over Flat Plates in Supersonic Flow. NACA TN 4142 (1957).
- DONALDSON, C. P. and R. H. LANGE: Study of the Pressure Rise across Shock Waves Required to Separate Laminar and Turbulent Boundary-Layers. NACA TN 2770 (1952).
- ERICKSON, W. D.: Study of Pressure Distributions on Simple Sharp-Nosed Models at Mach Numbers from 16 to 18 in Helium Flow. NACA TN 4113 (1957).
- FERRI, A.: Aluni Resultati Experimentali. Atti di Guidonia (1939) Nr. 17.
- GLAUERT, H.: The Effect of Compressibility on the Lift of an Airfoil. R & M No. 1135 (1927).
- GÖTHERT, B.: Ebene und räumliche Strömung bei hohen Unterschallgeschwindigkeiten (ohne und mit Auftrieb). Jb. dDL I (1941), S. 156.
- Berechnung kompressibler ebener Strömung bei hohen Unterschall-Anblasgeschwindigkeiten. UM 1117 (1943).
- Bemerkung über Ausbildung von Verdichtungsstoß an Profilen. LGL 156 (1942), S. 174—183.
- and K. H. KAWALKI: Berechnung kompressibler Strömungen mit örtlichen Überschallfeldern. FB 1794 (1943).
- Die kompressible Strömung um verschiedene ebene Profile in der Nähe der Schallgeschwindigkeit (Beispielrechnungen nach UM 1117). UM 1471 (1945).
- GUDERLEY, G.: The Flow over a Flat Plate with a Small Angle of Attack at Mach Number 1. J. Aer. Sci. 11 (1954), pp. 1—14.
- and H. YOSHIHARA: The Flow over a Wedge Profile at Mach Number 1. J. Aer. Sci. 17 (1950), p. 723.
- HANTZSCHE, W. and K. WENDT: Der Kompressibilitätseinfluß für dünne wenig gekrümmte Profile bei Unterschallgeschwindigkeit. ZAMM 23 (1943), S. 72—85.
- HANTZSCHE, W.: Die Prandtl-Glauertsche Näherung als Grundlage für ein Iterationsverfahren zur Berechnung kompressibler Unterschallströmungen. ZAMM 23 (1943), S. 85.
- HELBOLD, H. B.: Physikalische Erscheinungen in der kompressiblen Unterschallströmung. LGL 156 (1942), S. 170 bis 174.
- JACOBS, E. N.: Methods Employed in America for the Experimental Investigation of Aerodynamic Phenomena at High Speeds. NACA Misc. Paper No. 42 (1936). Paper presented at Volta Meeting in Italy, 1935.
- KAPLAN, C.: Effect of Compressibility at High Subsonic Velocities on the Lifting Force Acting on an Elliptic Cylinder. NACA TN 1118 (1946).
- On Similarity Rules for Transonic Flows. NACA TN 1527 (1948).
- KÁRMÁN, T. v.: Compressibility Effects in Aerodynamics. J. Aer. Sci. 8 (1941), pp. 337—356.
- Supersonic Aerodynamics—Principles and Applications. J. Aer. Sci. 14 (1947), pp. 373/402.
- Similarity Law of Transonic Flow. J. Math. Phys. 26 (1947), p. 182.
- KATZEN, E. D., D. M. KUEHN and W. A. HILL: Investigation of the Effects of Profile Shape on the Aerodynamic and Structural Characteristics of Thin, Two-Dimensional Airfoils at Supersonic Speeds. NACA TN 4039 (1957).
- KNACKSTEDT: Prüfung und Sichtung der bisher vorliegenden Ergebnisse bei Strömungen mit hohen Geschwindigkeiten. FB 1147 (1939).
- KRAHN, E.: Anwendung der Prandtlschen Regel auf dicke Profile. FB 1465 (1941).
- Berechnung von Druckverteilungen an Profilen in ebener Unterschallströmung. LGL-Bericht 156 (1942), S. 185—187.
- Der Kompressibilitätseinfluß nach der Prandtlschen Regel. AVA-Bericht 43/A/20 (1943).
- Ein Korrekturglied zur Prandtlschen Regel. AVA-Bericht 45/A/22 (1954).
- Stationäre Unterschallströmungen. Gö. Mon. C 3 (1946).
- LAMLA, E.: Über die ebene Potentialströmung um ein Profil, das sich konform auf einen Kreis abbilden läßt, im unterkritischen Gebiet. Jb. dDL I (1940), S. 26—35.
- LIGHTHILL, M. J.: Two-Dimensional Subsonic Aerofoil Theory. R & M No. 1929 (1944).
- LOCK, C. N. H.: The Ideal Drag Due to a Shock Wave. R & M No. 2512 (1951).
- LUDWIEG, H.: Ergebnisse der experimentellen Profiluntersuchungen bei hohen Unterschallgeschwindigkeiten. Gö. Mon. E 8 (1946).
- MALAVARD, L.: Étude des Écoulements Transsoniques. Contrôle Experimental des Règles de Similitude. Jahrbuch 1953 der WGL, S. 96—103.
- MEYER, TH.: Über zweidimensionale Bewegungsvorgänge in einem Gas, das mit Überschallgeschwindigkeit strömt. Mitt. Forsch. Arb. VDI (1908) 62.
- OSWATITSCH, K. and K. WIEGHARDT: Theoretische Untersuchungen über stationäre Potentialströmungen und Grenzschichten bei hohen Geschwindigkeiten. LGL S 13 (1942), S. 7—24.
- PUCKETT, A. E.: Supersonic Wave Drag of Thin Airfoils. J. Aer. Sci. 13 (1946), pp. 475—484.
- RICHARDS, E. J.: Theoretical Critical Mach Numbers for NACA 16 Series Aerofoils. R & M No. 2170 (1945).

- RICHTER, G.: Druckverteilungen an Tragflügeln in ebener kompressibler Strömung. LGL-Bericht S 13 (1942), S. 25—29.
- Vergleich von Näherungsverfahren zur Berechnung der Druckverteilung an Profilen bei unterkritischen Machschen Zahlen mit Messungen. LGL-Bericht 156 (1942), S. 183—192.
- Die Stabilität des Verdichtungsstoßes in einer konkaven Ecke. ZAMM (1948), S. 341—345.
- RIEGELS, F. W.: Neuere Ergebnisse zur Profiltheorie. ZfW 4 (1956), S. 61—67.
- RINGLEB, F.: Näherungsverfahren zur Bestimmung der Druckverteilung in adiabatischer Gasströmung. FB 1284 (1940).
- SAENGER, E.: Gaskinetik sehr großer Flughöhen. FB 972 (1938) und Schweizer Archiv, Febr. 1950, S. 43.
- SCHÄFER, M.: Charakteristikenverfahren und Verdichtungsstoße. Gö. Mon. C 4.1 (1946).
- STACK, I.: Compressible Flow in Aeronautics. J. Aer. Sci. (1945), p. 127.
- STEWARTSON, K.: On the Interaction between Shock Waves and Boundary-Layers. Proc. Camb. Phil. Soc. 47 (1951), pp. 545—553.
- THEODORSEN, T.: A Condition on the Initial Shock. NACA TN 1029 (1946).
- TOLLMIEN, W.: Strömungen kompressibler Flüssigkeiten. Gö. Mon. C (1946).
- und H. LUDWIEG: Durchgang durch die Schallgeschwindigkeit. Gö. Mon. C 6 (1946).
- TSIEN, H. S.: Two-dimensional Subsonic Flow of Compressible Fluids. J. Aer. Sci. 6 (1939), pp. 399—407.
- VALENSI, J. and W. PRUDEN: Some Observations on Sharp-Nosed Profiles at Supersonic Speed. R & M No. 2482 (1951).
- VAN DYKE, M. D.: Second Order Subsonic Airfoil Theory Including Edge Effects. NACA Rep. 1274 (1956).
- VINCENTI, W. G. and C. B. WAGONER: Transonic Flow Past a Wedge Profile with Detached Bow Wave - General Analytical Method and Final Calculated Results. NACA TN 2339 (1951).
- ZOBEL, T.: Fortschritte in der optischen Strömungsmessung. FB 1934 (1944) und DAL Nr. 5008/44.

## **11. TABLES**

## 11. TABLES

Table 11.1

Collection of Geometrical and Aerodynamic Data

Designation of profile	$R \cdot 10^{-4}$	$r = \text{with roughness}$ Behaviour of $C_{L_{\max}}$	$C_{L_{\max}} \cdot 10^2$	$a_o^o$	$\frac{dC_L}{da} \cdot 10^2$	$C_L^o \cdot 10^2$	$C_{D_{\min}} \cdot 10^4$	$(C_m)_o \cdot 10^2$	$x_a/c \cdot 10^2$	$y_a/c \cdot 10^2$	$\rho_o \cdot 10^3$	$f/c \cdot 10^2$	$x_t/c \cdot 10^2$	$t/c \cdot 10^2$	$x_s/c \cdot 10^2$	$\epsilon_T \cdot 10^2$	Sources
Gö																	
1 K																	
2 K																	
4 K																	
5 K																	
6 K																	
7 K																	
8 K																	
9 K																	
10 K																	
11 K																	
12 K																	
13 K																	
14 K																	
15 K																	
16 K																	
123	7	127	-37	101	85	0150											TB I
227	7	188	-97	110	65	0270											TB II
242	7	174		116	55	0280											TB II
243	7	150		108	80	0280											TB II
289	14	103	-88	094	55	0260											TB II, E I, E IV
301	168	138	-84	101	55	0100											TB II
335	7	151	-53	103	75	0200											TB II, E I, E IV
342	7	132	-42	108	90	0160											TB II
344	7	097	-17	100	35	0130											TB II
387	840	D	170	-66	097	30	0076	-093	243	040							E I, R 669
398	42		-07	097	64	0116											E I, R 669
810	D	168	-60	094	15	0076	-081	246	010								
409	42		076		093		0082										E I
410	42	A	095	06	101		0101										E I
417 A	4		108	-23	151		0260										E III, Schmitz
		17	111	-27	151		0215										
		42	129	-33	158		0092										
420	42		-09	099	20	0128											
824	D	151	-83	095	18	0104	-084	254	070								E III, R 628
436	7	123	-40	100	65	0150											E I, R 628
		42	121	-53	097		0096										
		805	D	168	-44	098	22	0082	-061	245	050						
449	42		133	-86	094	77	0095										E I, E III
459	42		080	-04	101	23	0081										E I, E IV
460	42		096	-01	084	01	0109										E I, E IV
508	42		142	-77	095		0130										E IV
535	42		155	-85	105		0125										E III
549	42		133	-63	099		0075										E III
564	42		106	-47	091		0084										E IV
570	42		119		063		0255										E III
571	42		138		099		0244										E III
596	42		113	-47	099		0079										E IV
608	42		084	-23	107		0059										E IV
609	42		089	-32	089		0070										E IV
610	42		094	-43	095		0071										E IV
620	42		141	-88	095		0128										E IV
622	12		096	-30	091		0170										Lufo 13, 103 AVA 41/14/29

(Continuation of Table 11.1)

(Continuation of Table 11.1)

Designation of profile	$R \cdot 10^{-4}$	$r = \text{with roughness}$ Behaviour of $C_{L_{\max}}$	$C_{L_{\max}} \cdot 10^4$	$a_0^\circ \cdot 10$	$\frac{dC_L}{da} \cdot 10^4$	$C_D^* \cdot 10^4$	$C_{D_{\min}} \cdot 10^4$	$(C_m)_a \cdot 10^4$	$x_a/c \cdot 10^4$	$y_a/c \cdot 10^4$	$e_0 \cdot 10^4$	$f/c \cdot 10^4$	$x_f/c \cdot 10^4$	$t/c \cdot 10^4$	$x_t/c \cdot 10^4$	$s_T \cdot 10^4$	Sources
<b>Gö</b>	770	240		118	-32	101	47	0075	{ wing-tips not rounded		0750	20	30	15	30	090	AVA 41/14/28
	771	240		123	-29	108	47	0073	wing-tips rounded		0667	40	30	15	30	080	AVA 41/14/28
				118	-30	098	49	0069		0113							
	775	300		102	00	093					1100	00	00	21	30	113	AVA 43/W/7
	776	310		100	-02	085		0124			1100	00	00	25	30	113	AVA 43/W/7
	777	205		144	-48	095	32	0105			0750	60	30	22	30	090	AVA 43/W/7
		310		125	-47	097	52	0097									
	780	80		069	000	104	00	0078			0210	10	50	12	50	185	UM 3040
		200		067	-01	103	09	0042									3056
		350		067	-02	097	12	0031									3159
	793										0224			13-2	60		FB 1522
	794										0238			13-6	70		
	795	38		093				0009			0900	24	44	8	30		
	796	38		115				0010			0900	37	43	12	30		
	797	38		136				0012			0900	51	42	18	30		
	798	38		150				0016			0900	65	41	20	30		
<b>DVL 0 00 06 1-10 30</b>	320			00	108	00	0052				1100	00	00	6	30	113	FB 1490 <sup>7</sup> , FB 1506 <sup>7</sup> )
09 0-275 45	268		062		084		0038			0275			9	45	200	FB 1621, FB 1884	
09 0-55 40	266		067		091		0049			0550			9	40	171	FB 1621, FB 1884	
09 0-55 45	260		076		091		0037			0550			9	45	200	FB 1621, FB 1884	
09 0-55 50	265		069		087		0037			0550			9	50	236	FB 1621, FB 1884	
09 0-825 35	260		110		095		0056			0825			9	35	148	FB 1621, FB 1884	
09 0-825 40	259		107		093		0048			0825			9	40	172	FB 1621, FB 1884	
09 0-82 45	260		073		093		0041			0825			9	45	200	FB 1621, FB 1884	
09 1-10 30	320				105		0064			1100			9	30	113	FB 1490 <sup>7</sup> , FB 1506 <sup>7</sup> )	
09 1-10 40	257		115		096		0048			1100			9	40	172	FB 1621, FB 1884	
09 1-10 45	250		104		092		0038			1100			9	45	200	FB 1621, FB 1884	
09 1-10 50	260		101		103		0052			1100			9	50	236	FB 1621, FB 1884	
12 0-275 40	251		068		082		0050			0275			12	40	172	FB 1621, FB 1884	
12 0-275 50	265		063		086		0039			0275			12	50	236	FB 1621	
12 0-55 40										0550			12	40	172	UM 1167, FB 1621, FB 1884, FB 1910 <sup>7</sup> , AVA 45/W/16, TB 11(1944)	
12 0-55 45	270		111		086		0053			0550			12	45	200	UM 1363, FB 1621, FB 1884	
12 0-55 50	278		112		086		0047			0550			12	50	236	UM 1167	
12 0-55 50	264		098		086		0042			0550			12	50	236	FB 1621, FB 1884, TB 11(1944)	
12 0-825 35	259		121		093		0059			0825			12	35	150	FB 1621, FB 1884	
12 0-825 40	279		126		089		0053			0825			12	40	172	FB 1621, FB 1884	
12 0-825 45	259		122		086		0044			0825			12	45	200	FB 1621, FB 1884	
12 1-10 30	320				108		0072			1100			12	30	113	UM 1167, FB 1490, FB 1503, FB 1506, FB 1884, JB 1937, LGL 127 <sup>7</sup> , AVA 45/W/15	
12 1-10 40	254		126		090		0053			1100			12	40	171	FB 1621, FB 1654, FB 1884	
12 1-10 50	263		122		089		0046			1100			12	50	236	FB 1621, FB 1884	
15 0-55 40	260		105		082		0057			0550			15	40	171	FB 1621, FB 1884	
15 0-55 45	273		112		079		0049			0550			15	45	200	FB 1621, FB 1884	
15 0-65 50	271		113		079		0041			0550			15	50	236	FB 1621, FB 1884	
15 0-825 45	259		113		080		0047			0825			15	45	200	FB 1621, FB 1884	
15 1-10 30	320				105		0076			1100			15	30	113	FB 1490 <sup>7</sup> , FB 1506 <sup>7</sup> )	
15 1-10 40										1100			15	40	172	FB 1884, JB 1937, FB 1505, FB 1227, FB 1329, FB 1621, FB 1884, JB(1941)	

(Continuation of Table 11.1)

Designation of profile	$R \cdot 10^{-4}$	$r = \text{with roughness}$ $\text{Behaviour of } C_{L_{\max}}$	$C_{L_{\max}} \cdot 10^2$	$a_0^\circ \cdot 10$	$\frac{dC_L}{da} \cdot 10^2$	$C_L^* \cdot 10^2$	$C_{D_{\min}} \cdot 10^4$	$(C_m)_a \cdot 10^3$	$x_a/c \cdot 10^2$	$y_a/c \cdot 10^2$	$\rho_0 \cdot 10^4$	$f/c \cdot 10^2$	$x_f/c \cdot 10^2$	$t/c \cdot 10^2$	$x_t/c \cdot 10^2$	$e_T \cdot 10^2$	Sources
DVL 0 00 15 1-10 50	250		115	086		0060					1100			15	50	236	FB 1621, FB 1884
· 18 0-55 40	269		124	080		0073					0550			18	40	172	FB 1621, FB 1884
18 0-55 45	274		101	075		0065					0550			18	45	200	FB 1884
18 0-825 45											0825			18	45	181	FB 1621
18 0-825 45	274		109	078		0056					0825			18	45	181	FB 1884, 1621
18 1-10 30	320			096		0081					1100			18	30	113	FB 1349, FB 1490 <sup>7</sup> , FB 1508 <sup>7</sup> , FB 1506 <sup>7</sup> ) FB 1884, JB (1937), JB (1940), UM 3145
18 1-10 40	263		109	080		0063					1100			18	40	172	FB 1621, FB 1884,
18 1-10 50	259		115	082		0085					1100			18	50	236	FB 1621, FB 1884,
21 1-10 30											1100			21	30	113	FB 1884, JB (1937)
25 0-55 40											0550			25	40	172	FB 1884
25 1-10 30											1100			25	30	113	FB 1884
25 1-10 40											1100			25	40	172	FB 1884
30 1-10 30											1100			30	30	113	FB 1884, UM 3145
1 35 12 0-55 40											0550	10	35	12	40	172	FB 1910 <sup>7</sup> )
2 35 12 0-55 40											0550	20	35	12	40	172	FB 1910 <sup>7</sup> ), AVA 45/W/16
4 35 12 0-55 40											0550	40	35	12	40	172	FB 1910 <sup>7</sup> )
Ma											0825	10	25	12	40		UM 1234 <sup>7</sup> )
K											0098	00	00	10-1	50	198	FB 1621
K	0 00 10-1 -0-098 50	331	067	075		0048					0950	00	00	10-5	48	198	FB 1621
K	0 00 10-5 -0-95 48	322	069	078		0090					0356	00	00	10-7	46	198	FB 1621
K	0 00 10-75-0-356 467	321	067	084		0038					0452	00	00	11	45	198	FB 1621
KP											0356	113	25	10-7	46	198	FB 1621
1-13 25 10-75-0-356 467	307	093	12	082	09	0040					0452	113	25	11	45	198	FB 1621
KE											0452	113	25	11	45	198	FB 1621
KE	0 00 11-4 -0-452 452	322	075	079		0042					0548	00	00	11-4	43	198	FB 1621
KE	1-13 25 11-4 -0-452 452	322	100	079		0046					0548	113	15	11-4	43	198	FB 1621
KE	0 00 11-4 -0-548 434	322	101	085		0046					0548	113	35	11-4	43	198	FB 1621
KE	1-13 15 11-4 -0-548 434	307	122	-10	086	05	0052				0548	113	15	11-4	43	198	FB 1621
KE	1-13 25 11-4 -0-548 434	283	116	-11	084	07	0046				0548	113	25	11-4	43	198	FB 1621
KE	1-13 35 11-4 -0-548 434	303	107	-14	084	14	0046				0548	113	35	11-4	43	198	FB 1621
KE	2 25 11-4 -0-548 434	295	119	--17	084	25	0049				0548	20	25	11-4	43	198	FB 1621
Zürich 11											0890	29	50	9	43	198	Mitt. 13 ETH
Tokio LB 24											0318	00	00	10	50	245	LGL 149 Aer. Res. Tokio Rep. 198
NACA 0003																	
	805	D 158	--29	095	08	0065	-027	243	060	1100	0	—	3	30	113	R 669, R 628	
	810	B 096		095			032	234	-010	1100	0	—	6	30	113		
0006	300	D 084		108		0044	-006	250		1100	0	—	6	30	113	R 824	
	600	D 084		108		0050	0	250									
	600	r D 090		105		0089											
	847	D 091		098		0051	0	243	020								
	900	D 092		103		0052	0	250									
0009	300	A 125		110		0052	0	250		1100	0	—	9	30	113	R 586, 637 R 824	
	600	r D 092		105		0091											
	600	D 131		109		0056	0	250									
	829	A 139		098		0058	0	240	050								
	900	D 131		110		0056	0	250	005								
0012	70	r B 085		083		0129				1100	0	—	12	30	113	R 586, 637, R 660 N 1945	

(Continuation of Table 11.1)

(Continuation of Table 11.1)

(Continuation of Table II.1)

Designation of profile	$R \cdot 10^{-4}$	$C_{L_{max}}$ with roughness Behavior of $C_{L_{max}}$	$a_o^o$	$\frac{dC_L}{da}$	$C_L^*$	$C_{D_{min}}$	$(C_m)_a$	$x_a/c$	$y_a/c$	$e_o$	$f/c$	$x_f/c$	$t/c$	$x_t/c$	$\epsilon_T$	$\cdot 10^4$	Sources
NACA 4421	600	D 142	-39	102	20	0075	-082	236	-010								
	600	D 142	-39	102	20	0075	-082	236	-010								
	821	D 141	-34	089	08	0088	-071	231	-020								R 669
	900	D 148	-39	100	28	0072	-082	238	-009								824
4424	300	D 128	-39	100	21	0088	-080	224	-035	1100	40	40	24	30	113	824	
	600	r D 085	-30	088	10	0132											
	600	D 135	-38	100	21	0080	-080	230	-016								
	900	D 139	-39	100	20	0075	-080	239	-005								
4506	805	D 115	-43	104	42	0087 <sup>1)</sup>	-110	245	-010	1100	40	50	06	30	113	R 460	
4509	824	D 156	-41	103	39	0093 <sup>1)</sup>	-106	247		1100	40	50	09	30	113	460	
4512	845	B 169	-42	097	32	0095 <sup>1)</sup>	-106	239		1100	40	50	12	30	113	460	
4515	814	D 162	-41	101	28	0113 <sup>1)</sup>	-097	241		1100	40	50	15	30	113	460	
4518	826	D 154	-39	096	16	0125 <sup>1)</sup>	-093	236	020	1100	40	50	18	30	113	460	
4521	831	D 146	-34	095	14	0138 <sup>1)</sup>	-082	234	020	1100	40	50	21	30	113	460	
4612	847	B 176	-46	098	30	0099 <sup>1)</sup>	-124	240		1100	40	60	12	30	113	460	
4712	834	A 182	-50	097	30	0104 <sup>1)</sup>	-143	238		1100	40	70	12	30	113	460	
6212	855	A 175	-52	100	55	0101 <sup>1)</sup>	-089	242	040	1100	60	20	12	30	113	460	
6306	813	D 154	-52	105	63	0092 <sup>1)</sup>	-109	254		1100	60	30	06	30	113	460	
6309	821	B 187	-54	104	52	0101 <sup>1)</sup>	-112	244	030	1100	60	30	09	30	113	460	
6312	839	B 186	-55	101	40	0102 <sup>1)</sup>	-111	243	010	1100	60	30	12	30	113	460, R 566	
6315	819	B 155	-54	101	41	0120 <sup>1)</sup>	-105	243	020	1100	60	30	15	30	113	460	
6318	813	D 143	-52	098	30	0130 <sup>1)</sup>	-098	237	010	1100	60	30	18	30	113	460	
6321	829	D 137	-52	096	10	0144 <sup>1)</sup>	-090	235	020	1100	60	30	21	30	113	460	
6406	819	D 143	-56	104	53	0086 <sup>1)</sup>	-129	257		1100	60	40	06	30	113	460	
6409	808	D 168	-59	101	59	0094 <sup>1)</sup>	-133	250	-020	1100	60	40	09	30	113	460	
6412	815	D 187	-57	101	48	0104 <sup>1)</sup>	-133	241	010	1100	60	40	12	30	113	460	
6415	808	D 159	-57	099	39	0120 <sup>1)</sup>	-125	243	-020	1100	60	40	15	30	113	460	
6418	818	D 151	-57	099	28	0132 <sup>1)</sup>	-118	237		1100	60	40	18	30	113	460	
6421	800	D 141	-52	096	17	0148 <sup>1)</sup>	-110	233		1100	60	40	21	30	113	460	
6506	846	D 129	-63	101	63	0093 <sup>1)</sup>	-159	250		1100	60	50	06	30	113	460	
6509	821	D 171	-63	103	51	0100 <sup>1)</sup>	-158	249	-030	1100	60	50	09	30	113	460	
6512	840	D 175	-62	101	44	0108 <sup>1)</sup>	-155	242	-030	1100	60	50	15	30	113	460	
6515	819	D 167	-60	099	40	0127 <sup>1)</sup>	-147	240	-020	1100	60	50	18	30	113	460	
6518	819	D 161	-57	095	29	0141 <sup>1)</sup>	-139	234	-020	1100	60	50	18	30	113	460	
6521	814	D 149	-53	094	10	0154 <sup>1)</sup>	-129	232	030	1100	60	50	21	30	113	460	
6612	868	D 183	-68	099	45	0114 <sup>1)</sup>	-185	233	-020	1100	60	60	12	30	113	460	
6712	853	A 195	-70	097	30	0126 <sup>1)</sup>	-199	238	020	1100	60	70	12	30	113	460, R 586	
21012	837	C 163	-06	099	04	0070	001	235	060	1100	11	5	12	30	113	610	
22012	832	C 172	-09	100	10	0071	-005	237	050	1100	15	10	12	30	113	610	
22112	850	B 184	-08	100	06	0072	-001	240	050	1100	15	10	12	30	113	537	
23006	829	D 117	-12	100	15	0057	-012	240	080	1100	18	15	06	30	113	R 610, 669	
23009	260	A 134	-12	098	19	0076	-061			1100	18	15	09	30	113	FB 1095, FB 1555, JB (1937), AVA 45/W/16, UM 1259 <sup>1)</sup> , R 669	
23012											1100	18	15	12	30	113	FB 1095, FB 1543, FB 1769, FB 1848, JB (1937), UM 3145, UM 3507, UM 1259 <sup>1)</sup> , JB (1941) N 1945
	70	r D 095	-12	080	06	0120											
	70	D 118	-14	099	11	0076	-010	231	152								
	100	r B 100	-14	087	13	0128											
	100	D 130	-13	099	10	0069	-010	230	139								
	150	r B 108	-13	095	12	0123											
	150	B 143	-13	100	11	0065	-010	233	131								
	200	r B 114	-13	097	10	0120											
	200	B 150	-13	095	11	0066	-009	232	098								
	300	B 161	-12	104	13	0063	-013	241	036								
	600	r B 124	-15	103	19	0099											R 824
	600	B 175	-12	105	19	0061	-013	241	036								
	837	A 174	-12	100	08	0080	-008	238	070								R 669
	880	A 179	-14	105	23	0089	-013	247	004								N 1945
23015											1100	18	15	15	30	113	FB 1312, FB 1579, FB 1221, FB 1591, FB 1763, FB 1769, R 824, UM 1259

(Continuation of Table 11.1)

Designation of profile	$R \cdot 10^{-4}$	$r =$ with roughness Behaviour of $C_{L_{max}}$													Sources		
			$C_{L_{max}} \cdot 10^4$	$a_0 \cdot 10^4$	$\frac{dC_L}{da} \cdot 10^4$	$C_L^* \cdot 10^4$	$C_{D_{min}} \cdot 10^4$	$(C_m)_a \cdot 10^4$	$x_a/c \cdot 10^4$	$y_a/c \cdot 10^4$	$e_0 \cdot 10^4$	$f/c \cdot 10^4$	$x_f/c \cdot 10^4$	$t/c \cdot 10^4$	$x_t/c \cdot 10^4$		
NACA 23015	70	r B	097	-13	079	11	0127	-003	241	186						N 1945	
	70	D	131	-11	093	02	0081										
	100	r B	097	-12	091	10	0137										
	100	D	135	-11	095		0071	-005	239	100							
	150	r D	101	-11	092	11	0127	-005	238	062							
	150	D	139	-11	098	10	0070	-005	238	062							
	200	r D	107	-11	098	11	0122										
	200	B	148	-11	099	10	0068	-003	238	054							
	280	B	149	-10	102	12	0070	-006	231	-050						R 824	
	600	r B	119	-11	102	15	0102										
23018	600	D	170	-12	103	09	0062	-005	239	-043						R 669	
	837	A	173	-11	098	10	0067	-008	239	-060						N 1945	
	890	D	172	-10	104	20	0063	-007	243	-021						FB 1095, FB 1221, FB 1611, FB 1639, FB 1769, JB (1937), R 824	
	310	A	141	-10	102		0073	-008	236	019							
	600	r B	105	-10	099	10	0105										
	600	D	159	-12	102	20	0070	-008	241	017						R 824	
	816	B	158	-12	097	08	0074	-006	233	080						R 669	
	890	D	161	-10	102	25	0068	-008	243	007						R 669	
	300	D	129	-10	092	-05	0078		223	072	1100	18	15	21	30	113	
	590	r D	094	-10	093	09	0115									R 668	
23021	590	D	148	-12	102	-10	0074		234	026							
	500	D	148	-12	102		0074									R 669	
	821	B	150	-12	092	07	0080	-005	227	070						R 669	
	890	D	150	-10	102	12	0070		238	-008						R 669	
	300	D	120	-10	100	-10	0082		212	102	1100	18	15	24	30	113	
	590	r D	075	-12	085	08	0123									R 824	
	590	D	130	-11	098	-15	0078		223	065						R 669	
	23030	D	141	-10	100	-10	0071		231	048	1100	18	15	30	30	113	
	23112	A	173	-08	100	08	0074 <sup>1)</sup>	-002	235	080	1100		15	12	30	113	
	24012	C	171	-15	100	08	0072 <sup>1)</sup>	-013	237	060	1100	21	20	12	30	113	
23024	24112	B	167	-09	100	10	0074 <sup>1)</sup>	-019	239	080	1100		20	12	30	113	
	25012	C	167	-16	100	10	0074 <sup>1)</sup>	-009	237	070	1100	23	25	12	30	113	
	25112	B	162	-12	100	08	0074 <sup>1)</sup>	-002	237	070	1100		25	12	30	113	
	32012	A	174	-12	100	15	0075 <sup>1)</sup>	-005	239	060	1100	23	10	12	30	113	
	33012	A	180	-17	099	10	0074 <sup>1)</sup>	-014	240	060	1100	28	15	12	30	113	
	34012	A	180	-21	100	20	0075 <sup>1)</sup>	-022	244	050	1100	31	20	12	30	113	
	42012	A	176	-18	100	20	0078 <sup>1)</sup>	-009	239	060	1100	31	10	12	30	113	
	43009	A	172	-24	100	18	0068 <sup>1)</sup>	-021	242	060	1100	37	15	09	30	113	
	43012	A	184	-23	100	26	0068	-019	240	070	1100	37	15	12	30	113	
	43015	A	176	-23	101	18	0070	-015	238	060	1100	37	15	15	30	113	
43018	43018	C	163	-24	096	16	0078	-013	232	060	1100	37	15	18	30	113	
	43021	A	148	-24	093	10	0108 <sup>1)</sup>	-010	226	070	1100	37	15	21	30	113	
	44012	A	182	-28	098	25	0080 <sup>1)</sup>	-028	245	050	1100	42	15	12	30	113	
	62021	D	152	-31	094	12	0110 <sup>1)</sup>	-006	218	080	1100	48	20	21	30	113	
	63009	A	177	-35	098	57	0081 <sup>1)</sup>	-042	224	070	1100	37	10	09	30	113	
	63012	B	184	-35	100	40	0075	-033	223	130	1100	37	15	12	30	113	
	63015	A	176	-35	098	25	0083 <sup>1)</sup>	-024	234	060	1100	37	15	15	30	113	
	63018	A	163	-34	097	15	0080	-020	229	060	1100	37	15	18	30	113	
	63021	A	148	-36	097	21	0113 <sup>1)</sup>	-018	219	060	1100	37	15	21	30	113	
	64021	A	146	-42	094	13	0115 <sup>1)</sup>	-031	223	080	1100	62	15	21	30	113	
0009-63	787	A	162		098		0068 <sup>1)</sup>		240	060	1100	00	00	9	30	113	
	795	C	156		094		0069 <sup>1)</sup>		235	050						LGL 127 <sup>7)</sup>	
	0012-63										1100	00	00	12	30	113	
	0012-64										1100	00	00	12	40	172	
	0012-65	821	C	136		084		0077 <sup>1)</sup>		215	060	1100	00	00	12	50	236
	0015-64										1100	00	00	12	40	172	
	2209-34	035			-22		15	0100 <sup>1)</sup>	-040			0275	20	20	09	40	172
	2409-34	035			097		15	0100 <sup>1)</sup>	-060			0275	20	40	09	40	172
	4409-34	035			-45		35	0130 <sup>1)</sup>	-110			0275	40	40	09	40	172
	23012-33	853	B	152	-12	097	25	0071 <sup>1)</sup>	-010	243	070	0275	18	15	12	30	113
23012-34	860	C	149	-12	094	13	0072 <sup>1)</sup>	-011	241	040	0275	18	15	12	40	172	
	23012-34	840	A	171	-10	095	10	0072 <sup>1)</sup>	-010	240	040	1100	18	15	12	40	172
	16 006										0489	00	—	6	50	267	
	16 009										0489	00	00	9	50	267	

(Continuation of Table 11.1)

(Continuation of Table 11.1)

Designation of profile	$R \cdot 10^{-4}$	$r = \text{with roughness}$ $\text{Behaviour of } C_{L_{\max}}$	$C_{L_{\max}} \cdot 10^4$	$a_0^\circ$	$\frac{dC_L}{d\alpha} \cdot 10^4$	$C_L^* \cdot 10^4$	$C_{D_{\min}} \cdot 10^4$	$(C_m)_a \cdot 10^4$	$x_a/c \cdot 10^4$	$y_a/c \cdot 10^4$	$\rho_0 \cdot 10^4$	$f/c \cdot 10^4$	$x_f/c \cdot 10^4$	$t/c \cdot 10^4$	$x_t/c \cdot 10^4$	$e_T \cdot 10^4$	Sources
NACA 63 - 210	300	D	141	-14	110	20	0048	-033	264	-031	0770	11	50	10	35	038	R 824
	600	r	102	-10	110	15	0091										
	600	D	151	-13	112	20	0045	-033	261	-037							
	900	D	156	-12	110	20	0045	-033	261	-033							
63 <sub>1</sub> - 212	300	D	152	-20	110	15	0048	-034	264	-046	0755	11	50	12	35	036	R 824
	600	r	119	-20	110	20	0091										
	600	D	159	-18	117	25	0045	-034	263	-034							
	900	D	162	-20	110	25	0045	-034	263	-029							
	1500	D	162	-18	112	15	0051										
	2000	D	155	-18	114		0065										
	2500	D	154	-18	114		0067										
63 <sub>2</sub> - 215	300	D	141	-10	120	15	0058	-031	260	-052	0708	11	50	15	35	035	R 903 824
	600	r	125	-10	112	15	0098										
	600	D	159	-13	118	05	0048	-031	266	-024							
	900	D	161	-12	120	20	0046	-031	267	-020							
63 <sub>3</sub> - 218	290	D	131	-12	120	15	0060	-027	273	-050	0654	11	50	18	35	034	R 824
	600	r	115	-12	110	10	0101										
	600	D	145	-13	118	17	0051	-032	272	-047							
	900	D	150	-12	120	20	0049	-032	271	-042							
63 <sub>4</sub> - 221	300	D	118	-13	110	15	0062	-030	274	004	0601	11	50	21	35	033	R 824
	600	r	103	-13	110	05	0112										
	600	D	131	-13	119	10	0065	-030	270	-017							
	900	D	146	-13	110	20	0053	-030	269	-033							
63 A 210	300	D	158	-30	102	30	0053	-075	271	-095	0742	11	50	10	37	107	R 903 824
63 <sub>1</sub> - 412	600	r	131	-30	100	25	0098				0755	22	50	12	35	036	
	600	D	171	-28	108	38	0048	-075	271	-080							
	900	D	178	-30	100	32	0045	-075	270	-073							
63 <sub>2</sub> - 415	70	r	103	-27	092	06	0118				0708	22	50	15	35	036	R 903 N 1945
	70	D	126	-26	109	16	0077	-063	274	016							
	100	r	108	-25	098	15	0131										
	100	B	130	-28	108	30	0070	-064	271	022							
	150	r	118	-25	100	20	0128										
	150	D	136	-28	112	20	0064	-068	273	-081							
	200	r	119	-25	105	17	0123										
	200	D	141	-28	111	25	0061	-069	273	-069							
	300	D	154	-30	115	35	0055	-071	264	-043							
	600	r	132	-30	113	21	0099										
	600	D	162	-28	118	22	0052	-071	264	-039							
	600	D	167	-30	115	35	0049	-071	262	-036							
63 <sub>3</sub> - 418	300	D	139	-26	118	30	0060	-065	272	-052	0654	22	50	18	35	034	R 824
	600	r	120	-24	110	18	0108										
	600	D	150	-26	118	23	0052	-071	271	-057							
	900	D	158	-26	118	22	0050	-071	272	-051							
63 <sub>4</sub> - 420	310	D	119	-21	101	05	0059	-060	265	-036	0784	22	50	20	35	033	R 824 <sup>b</sup> )
	600	r	109	-21	101	05	0102										
	600	D	133	-21	104	05	0058	-060	264	-049							
	900	D	142	-21	110	05	0055	-060	265	-054							
63 <sub>4</sub> - 420	300	D	120	-25	108	37	0067	-036	264	-025	0784	29	35	20	35	033	R 824
a = 0-3	600	r	104	-25	104	10	0110										
	600	D	122	-25	110	07	0080	-036	264	006							
	900	D	135	-25	108	45	0058	-036	265								
63 <sub>4</sub> - 421	300	D	132	-28	120	20	0067	-057	275	-025	0601	22	50	21	35	033	R 824
	600	r	110	-25	114	20	0112										
	600	D	138	-28	120	25	0056	-057	279	-030							
	900	D	148	-27	120	28	0054	-063	275	-027							
63 <sub>2</sub> - 615	300	D	145	-40	116	25	0058	-110	266	-037	0708	33	50	15	35	035	R 824
	600	r	139	-49	108	30	0102										
	600	D	159	-35	120	42	0052	-110	266	-043							
	900	D	167	-38	120	42	0048	-110	266	-040							
63 <sub>2</sub> - 618	300	D	140	-38	118	22	0060	-098	267	-012	0654	33	50	18	35	034	R 824
	600	r	127	-38	110	24	0107										
	600	D	148	-38	118	28	0053	-098	266	-013							
	900	D	158	-38	118	45	0062	-098	267	-016							
63 <sub>(420)</sub> - 422	600	r	110	-28	105	26	0117				0790	22	50	22	35	033	824
	600	D	130	-31	113	05	0064	-064	269	-068							
	900	D	140	-31	110	12	0060	-064	271	-043							

(Continuation of Table 11.1)



(Continuation of Table 11.1)

Designation of profile	$R \cdot 10^{-4}$	$r = \text{with roughness}$ $\text{Behaviour of } C_{L_{\max}}$													Sources	
			$C_{L_{\max}} \cdot 10^2$	$a_0^o \cdot 10$	$\frac{dC_L}{d\alpha} \cdot 10^3$	$C_L^* \cdot 10^2$	$C_{D_{\min}} \cdot 10^4$	$(C_m)_a \cdot 10^2$	$x_a/c \cdot 10^2$	$y_{a/c} \cdot 10^2$	$e_o \cdot 10^3$	$f/c \cdot 10^3$	$x_f/c \cdot 10^2$	$t/c \cdot 10^2$	$x_t/c \cdot 10^2$	
NACA 64 <sub>2</sub> - 415	100	r D	117	-29	099	18	0136									
	100	B	124	-30	105	10	0071	-067	268	-087						
	150	r B	122	-29	102	20	0123									
	150	D	131	-30	106	10	0062	-068	270	-084						
	200	r B	128	-29	106	16	0123									
	200	D	138	-30	110	40	0061	-069	271	-077						
	310	D	148	-29	114	25	0056	-070	264	-070						
	600	r D	130	-29	110	25	0100									
	600	D	160	-29	115	35	0050	-070	265	-051						
	900	D	164	-29	112	35	0047	-070	264	-040						
64 <sub>3</sub> - 418	70	r D	104	-26	098	15	0125									
	70	D	122	-24	116	30	0093	-062	281	-060	0681	22	50	18		R 824
	100	r D	105	-23	098	20	0146									N 1945
	100	D	125	-27	116	05	0083	-064	277	-064						
	150	r D	109	-22	106	20	0135									
	150	D	129	-27	113	15	0070	-065	279	-077						
	200	r D	111	-23	104	20	0132									
	200	D	131	-28	112	20	0068	-065	279	-084						
	300	D	138	-30	115	35	0060	-064	267	-051						R 824
	600	r D	124	-30	113	25	0107									
64 <sub>4</sub> - 421	600	D	149	-29	116	10	0053	-064	271	-050						
	900	D	158	-30	117	23	0050	-064	273	-049						
	300	D	134	-26	115	10	0062	-065	277	-017	0654	22	50	21		R 824
	600	r D	119	-25	110	20	0112									
	600	D	148	-26	120	10	0055	-065	278	-035						
	900	D	153	-25	115	11	0052	-065	276	-047						
	70	r D	121	-39	098	20	0108				0687	22	50	10	39	N 1945
	70	D	133	-42	102	40	0072	-100	260	-041						
	100	r D	129	-39	099	30	0128									
	100	D	133	-41	106	32	0067	-105	268	-072						R 903
64 A 410	150	r D	133	-39	101	30	0118									
	150	D	140	-40	111	50	0060	-100	271	-048						
	200	r D	134	-41	098	34	0117									
	200	B	145	-40	110	57	0058	-100	271	-063						
	300	D	180	-42	112	37	0050	-105	270	-028						
	600	r D	139	-40	111	44	0096									
	600	D	178	-41	117	50	0046	-105	268	-039						
	900	D	178	-39	117	46	0044	-110	264	003	0681	33	50	18		R 824
	300	D	138	-38	120	40	0058	-076	289	074						
	600	r D	130	-35	112	27	0108									
64 <sub>3</sub> - 618	600	D	150	-38	118	50	0052	-082	275	005						
	900	D	161	-38	120	50	0048	-097	273	-019						
	300	D	138	-38	120	40	0058	-076	289	074	0681	33	50	18		
	600	r D	130	-35	112	27	0108									
64 A 810	600	D	150	-38	118	50	0052	-082	275	005						
	900	D	161	-38	120	50	0048	-097	273	-019						
64 A 910	300	D	081		115		0035	000	250		0667					
	600	D	084		105		0035		256	-014						
	600	r D	092		105		0082									
	900	D	085		115		0035		258	-033						
	1500	D	090		109		0040									
	2000	D	099		110		0044									
	2500	D	100		110		0047									
	300	D	090		110		0044		262	-004	0681					
	600	D	092		107		0088									
	600	r D	106		107		0042		262	-018						
65 - 009	900	D	109		110		0040		264	-034						
	300	D	115		105		0040									
	600	r D	108		112	10	0092									
	600	B	130		110		0040		258	002						
65 - 010	900	B	137		105		0038		261	-012						
	300	B	136		110		0050		263	-024	0669					
	600	r D	103		110		0099									
	600	D	141		111		0042		259							
65 <sub>1</sub> - 012	900	D	142		110		0040		257	014	0694					
	300	D	125		105		0050		270	-007	0605					
	600	r D	108		105		0105									
	600	B	138		110		0044		268	-012						
65 <sub>2</sub> - 015	300	B	136		110		0050									
	600	r D	103		111		0099									
	600	D	141		111		0042		259							
	900	D	142		110		0040		257	014						
65 <sub>2</sub> - 018	300	D	125		105		0050		270	-007	0605					
	600	r D	108		105		0105									
	600	B	138		110		0044		268	-012						



(Continuation of Table 11.1)

Designation of profile	$R \cdot 10^{-4}$	$r = \text{with roughness}$ $\text{Behaviour of } C_{L_{\max}}$	Sources														
			$C_{L_{\max}} \cdot 10^2$	$e_0 \cdot 10$	$\frac{dC_L}{d\alpha} \cdot 10^2$	$C_L^* \cdot 10^2$	$C_{D_{\min}} \cdot 10^4$	$(C_m)_a \cdot 10^2$	$x_a/c \cdot 10^2$	$y_a/c \cdot 10^2$	$e_0 \cdot 10^3$	$f/c \cdot 10^3$	$x_f/c \cdot 10^3$	$t/c \cdot 10^2$	$x_t/c \cdot 10^2$	$e_T \cdot 10^2$	
NACA 65 <sub>s</sub> - 418	300	D	134	-25	110	12	0052	-061	265	-090	0605	022	50	18	40	52 R 824	
	600	r	122	-25	100	12	0106										N 1945
	600	D	150	-25	111	30	0045	-061	263	-059							
	900	D	155	-25	110	35	0044	-061	265	-060							
65 <sub>s</sub> - 418 a = 0.5	290	D	129	-30	110	60	0054	-054	265	-012	0605	030	44	18	40	52 R 824	
	590	r	120	-30	105	30	0120										
	590	D	142	-30	110	35	0047	-056	266	-052							
	890	D	150	-30	110	35	0044	-056	267	-047							
65 <sub>s</sub> - 421	300	D	129	-28	112	08	0054	-067	268	-065	0567	022	50	21	40	51 R 824	
	600	r	120	-25	100	25	0113										
	600	D	140	-28	112	10	0050	-067	272	-046							
	900	D	155	-28	112	25	0045	-067	272	-076							
65 <sub>s</sub> - 421 a = 0.5	300	D	121	-30	110	30	0058	-055	266	-084	0567	022	50	21	40	51 R 824	
	600	r	112	-25	093	15	0119										
	600	D	132	-28	110	12	0050	-055	271	-011							
	890	D	143	-28	110	30	0047	-055	272	-004							
65 <sub>s</sub> - 618	300	D	140	-40	115	45	0055	-104	275	-044	0605	033	50	18	40	52 R 824	
	600	r	130	-40	105	30	0110										
	600	D	154	-41	115	45	0047	-104	274	-035							
	900	D	166	-40	115	50	0042	-104	276	-022							
65 <sub>s</sub> - 618 a = 0.5	300	D	128	-42	105	40	0056	-079	257	-059	0605	045	44	18	40	52 824	
	600	r	120	-42	102	22	0112										
	600	D	142	-42	105	42	0050	-079	264	-008							
	900	D	150	-42	105	42	0048	-079	265	-026							
65 (215) - 114	300	B	142	-07	110	03	0048	-017	261	-020	0670	6	50	14	41	37 824	
	600	r	108	-07	108	08	0098										
	600	D	143	-07	110	10	0042	-022	264	-027							
	900	D	143	-07	110	10	0040	-022	265	-027							
65 (216) - 415	310	D	140	-30	114	47	0052	-057	265	-023	0666	30	44	15	41	35 824	
	600	D	156	-28	114	40	0044	-057	266	-020							
	890	D	162	-30	114	32	0042	-057	267	-031							
65 (216) - 415 a = 0.5	310	D	138	-30	110	25	0055	-080	269	-069							
	600	D	150	-30	110	28	0046	-080	268	-098							
	900	D	159	-30	110	46	0044	-080	266	-086							
65 (421) - 420	310	D	130	-25	116	10	0056	-061	273	-110	0567	22	50	21	41	56 824	
	600	r	112	-21	099	15	0113										
	600	D	144	-25	116	15	0050	-062	272	-070							
	900	D	152	-25	116	26	0045	-063	276	-046							
65 <sub>s</sub> - 618	310	D	138	-41	115	32	0053	-088	279	-020							
	620	r	124	-33	105	23	0109										
	620	D	150	-41	115	42	0044	-100	276	-063							
	900	D	161	-38	116	57	0043	-100	273	-093							
66 - 006	300	D	080	00	100	00	0030	0	255	-027	0619	00	00	6	45	080 R 824	
	600	D	080		100		0030		258	068							
	600	r	081		105		0083										
	900	D	080		100		0032		252								
66 - 008	300	D	082		107		0035		255	063	0654		8	45	079	0824	
66 - 009	300	r	086		107		0090						9	45	078	0824	
	600	D	100		107		0031		258	002							
	900	D	105		107		0030		259	-025							
66 - 010	300	B	122		105		0040	012	259	-008	0662		10	45	077	0824	
66 <sub>s</sub> - 012	300	r	090		109		0094				0661		12	45	075	0824	
	600	B	123		107		0036	-006	259	-004							
	900	D	124		105		0032		258								
66 <sub>s</sub> - 015	300	B	129		102		0046		265	-016	0638		15	45	073	0824	
	600	r	096		100		0100										
	600	B	137		103		0037		265	-011							
	910	D	136		102		0034		265	-006							
66 <sub>s</sub> - 018	300	D	126		100		0048	-006	268	-112	0603		18	45	070	0824	
	590	D	134	03	108		0039	-006	268	-058							
	600	r	104	05	098		0108										
	900	D	133	05	100		0034	-006	264	-027							
66 <sub>s</sub> - 021	300	D	119		100		0052		280	-360	0578		21	45	065	0824	
	600	r	103		075		0120										
	600	D	132		104		0041		275	-235							

(Continuation of Table 11.1)

Designation of profile	$R \cdot 10^{-4}$	$r =$ with roughness	Behaviour of $C_{L_{max}}$	$C_{L_{max}} \cdot 10^2$	$\alpha_0^*$	$\frac{dC_L}{d\alpha} \cdot 10^2$	$C_L^* \cdot 10^2$	$C_D \text{ min} \cdot 10^4$	$(C_m)_a \cdot 10^2$	$x_a/c \cdot 10^2$	$y_a/c \cdot 10^2$	$\theta_0 \cdot 10^2$	$f/c \cdot 10^2$	$x_f/c \cdot 10^2$	$t/c \cdot 10^2$	$x_t/c \cdot 10^2$	$\epsilon_T \cdot 10^2$	Sources
NACA 66 <sub>4</sub> - 021	900	D	138	-15	100	25	0036	-033	257	-024								
66 - 206	300	D	095	-15	110	25	0030	-033	253	-024	0619	11	50	06	45	080	R 824	
600	D	098	-14	108	15	0030	-039	255	-048									
600	r	D	099	-15	105	15	0088											
66 - 209	900	D	100	-15	110	17	0030	-039	257	-017								
300	D	098	-10	110	15	0035	-033	258	-022	0654	11	50	09	45	078	R 824		
600	r	D	098	-10	108	15	0090											
600	D	110	-12	108	17	0032	-033	258	-022									
900	D	118	-10	110	17	0031	-033	257	-013									
66 - 210	300	D	110	-12	108	20	0037	-033	260	-011	0662	11	50	10	45	077	R 824 N 1396	
600	r	D	099	-12	108	15	0092											
600	B	128	-16	110	20	0033	-033	260	-012									
900	B	128	-12	108	20	0030	-033	261	-018									
66 <sub>1</sub> - 212	300	B	130	-14	108	15	0040	-035	255	-037	0661	11	50	12	45	075	R 824	
600	r	D	103	-14	105	15	0093											
600	B	145	-14	102	15	0034	-032	257	-016									
900	D	146	-14	108	15	0032	-032	259	-015									
66 <sub>1</sub> - 212	300	B	130	-12	100	25	0042	-039	255	-025	0620	11	50	12	45	075		
600	B	140	-15	100	20	0033	-039	257	-030									
890	D	137	-12	100	20	0032	-039	259	-031									
66 <sub>4</sub> - 215	300	B	145	-12	100	25	0045	-030	257	-060	0638	11	50	15	45	073	R 824	
600	r	D	110	-12	098	11	0097											
600	D	145	-14	106	25	0035	-030	258	-028									
900	D	150	-12	100	27	0032	-030	260	-020									
66 <sub>2</sub> - 216 a = 0.6	300	D	134	-15	100	05	0045	-050	264	-120	0616	11	50	16	45	072	R 803	
66 <sub>4</sub> - 218	600	r	112	-13	098	14	0108				0603	11	50	18	45	070	R 824	
600	D	143	-16	106	15	0038	-035	261	-085									
900	D	149	-15	100	05	0033	-035	260	-064									
66 <sub>4</sub> - 221	300	D	123	-12	110		0050	-028	266	-006	0578	11	50	21	45	065	R 824	
600	r	B	117	-10	078		0121											
600	D	149	-12	111		0042	-028	260	-018									
900	D	150	-12	110	02	0037	-028	257	088									
66 <sub>2</sub> - 415	70	r	D	103	-27	081	14	0108			0638	22	50	15	45	073	R 824 N 1945	
70	D	115	-27	093	40	0092	-065	253	-022									
100	r	D	115	-23	085	10	0138											
100	D	116	-27	095	35	0070	-065	261	-015									
150	r	D	116	-22	089	10	0133											
150	D	123	-26	099	30	0058	-069	263	023									
200	r	D	115	-22	091	12	0124											
200	B	133	-27	094	25	0052	-070	266	015									
300	D	148	-25	100	30	0044	-072	258	-106									
600	r	D	121	-25	099	30	0105											
600	D	160	-25	107	30	0039	-072	259	-088									
900	D	160	-25	104	35	0036	-072	260	-073									
66 <sub>3</sub> - 418	300	D	140	-28	106	15	0049	-070	266	-134	0603	22	50	18	45	070	R 824	
600	r	D	128	-20	096	10	0109											
600	D	157	-28	110	20	0040	-070	264	-096									
900	D	157	-28	106	35	0037	-070	262	-090									
66 (215) - 016	310	B	132		102	10	0045		263	-045	0615	00	50	16	45	072	R 824	
600	D	136		102	-20	0037		261	-033									
900	D	136		102		0032		260	-022									
66 (215) - 216	290	D	132	-20	100	20	0048	-045	261	-123	0615	11	50	16	45	072	R 824	
600	D	158	-18	100		0039	-045	263	-096									
890	D	152	-20	100	10	0034	-045	262	-076									
66 (215) - 216	300	D	132	-12	104	10	0046	-030	256	-090	0615	15	48	16	45	072	R 824, R 803 <sup>b</sup> )	
a = 0.6	600	D	153	-12	104	25	0039	-030	258	-061								
900	D	148	-12	104	17	0034	-030	257	-043									
66 (215) - 416	310	D	150	-30	104	15	0043	-066	266	-137	0615	22	50	16	45	072	R 824	
600	D	160	-26	112	42	0040	-068	266	-123									
890	D	160	-26	112	30	0036	-070	265	-105									
67 <sub>1</sub> - 015	290	B	143	-12	100	20	0040	-048	237	-046	0677	00	0	15	49	094	R 824	
67 <sub>1</sub> - 215	600	r	D	098	-11	093	20	0104			0677	11	50	15	49	094	R 824	
600	D	147	-18	099	30	0033	-048	248	-065									
747 A 015	300	D	122	-18	110	10	0048	-013	259	066	0686	00	36	15	39	055	R 824	
747 A 315											0686	25	36	15	39		R 824	

(Continuation of Table 11.1)

Designation of profile	$R \cdot 10^{-4}$	$r = \text{with roughness}$ Behaviour of $C_{L_{\max}}$	$C_{L_{\max}} \cdot 10^2$	$a_0^o \cdot 10^3$	$\frac{dC_L}{da} \cdot 10^3$	$C_L^* \cdot 10^3$	$C_{D_{\min}} \cdot 10^4$	$(C_m)_a \cdot 10^3$	$x_a/c \cdot 10^3$	$y_a/c \cdot 10^3$	$\theta_0 \cdot 10^3$	$f/c \cdot 10^3$	$x_f/c \cdot 10^3$	$t/c \cdot 10^3$	$x_t/c \cdot 10^3$	$s_T \cdot 10^2$			Sources	
NACA 747 A 315	600	r	D	110	-16	100	10	0104												
	600	D	138	-16	107	32	0042	-013	281	034										
	900	D	144	-16	110	22	0038	-013	282	012										
747 A 415	300	D	131	-18	105	20	0050	-032	284	-018	0686	31	37	15	39				R 824	
	600	r	D	118	-18	103	20	0104												
	600	D	142	-18	107	35	0042	-032	280	-001										
	900	D	150	-18	105	35	0041	-032	280	-001										
847 B 110																			0693 06	
836 D 110																			0618 05	
8 - H - 12																			0920 35	
11 - H - 09																			0715 45	
CLARK Y - 6 %	835		D	107	-29	-098	15	0055	-038	243	050	1100	19	40	6	30	113	R 628, R 669		
- 8 %	795		D	137	-36	096	14	0060 <sup>1)</sup>	-045	243	060	1100	25	40	8	30	113	R 628		
- 10 %	792		B	168	-45	098	23	0075 <sup>1)</sup>	-059	243	040	1100	31	40	10	30	113	R 628		
- 11.7 %	120			123	-62	096	50	0096 <sup>1)</sup>				1100	36	40	117	30	113	R 502		
	230			128	-57	096	30	0091 <sup>1)</sup>												
	330			133	-56	097	10	0087 <sup>1)</sup>												
	450			145	-55	100	30	0086 <sup>1)</sup>												
	610			146	-54	100	20	0084 <sup>1)</sup>												
	670			151	-53	100	10	0083 <sup>1)</sup>												
	811		D	107	-29	098	15	0059 <sup>1)</sup>	-038	243	050							R 628		
	837		D	168	-50	092	12	0071 <sup>1)</sup>	-069	239	040							R 502		
	960				-54		10	0085 <sup>1)</sup>												
- 14 %	797		D	172	-62	096	15	0090 <sup>1)</sup>	-080	238	060	1100	43	40	14	30	113	R 628		
- 18 %	813		D	148	-76	092	23	0117 <sup>1)</sup>	-098	235	060	1100	55	40	18	30	113	R 628		
- 22 %	794		D	136	-93	088	15	0140 <sup>1)</sup>	-107	232	130	1100	68	40	22	30	113	R 628		
N 22	810		D	172	-54	096	17	0075	-075	244	040	0910	45	40	124	30	074	R 669		
60	810		D	173	-55	097	30	0086	-078	250		0910	30	36	124	30	074	R 628		
85												1000	17	15	09	30	086	N 665		
86												0760	17	15	09	35	107	N 665		
87												0620	17	15	09	40	120	N 665		
RAF 6 - 6 %												1670	30	30	06	30	1280 <sup>4)</sup>	R 463, UM 1321		
6 - 8 %												1250	40	30	08	30	975 <sup>4)</sup>	R 463		
6 - 10 %												1000	50	30	10	30	925 <sup>4)</sup>	R 463		
RAF - C	65			158	-66	085	65	0170				0960	84	30	168	30	602 <sup>4)</sup>	R & M 1771		
	650			151	-65	101	38	0120												
RAF - D	65			139	-57	090	57	0180				0810	64	30	129	30	600 <sup>4)</sup>	R & M 1771		
	650			152	-55	101	70	0120												
RAF - E	65			134	-47	091	60	0140				1080	52	30	103	30	715 <sup>4)</sup>	R & M 1771		
	650			163	-44	105	63	0100												
RAF - F	65			113	-32	097	60	0120				1500	43	30	086	30	1490 <sup>4)</sup>	R & M 1771		
	650			161	-30	105	62	0120												
RAF - 15	851	D	130	-22	096	25	0060	-053	233	100		29	30	064	15	320	R 352			
RAF - 34	805	C	158	-08	098	20	0071 <sup>1)</sup>	-006	246	050	0800	18	30	128	34	115	R & M 1771, R 628			

(Continuation of Table 11.1)

Designation of profile	$f/c$	$x_f/c$	$t/c$	$x_t/c$	Sources
NPL 101 EC 1240	0	—	12	40	R. & M. 2058 <sup>7</sup> , 2246
102 EC 1240/0640	6	40	12	40	R. & M. 2058
103 EC 1240/0658	6	58	12	40	R. & M. 2058
104 EC 1250	0	—	12	60	R. & M. 2058
129 EC 1250/0640	6	40	12	50	R. & M. 2058
130 EC 1250/1050	10	50	12	50	R. & M. 2058
134 EQH 1550	0	—	15	50	R. & M. 2058
135 EQH 1550/1058	10	58	15	50	R. & M. 2058
353 Griffith			16.3	47	R. & M. 2058
355 Griffith			22	45	R. & M. 2108
356 Griffith			30		R. & M. 2511
361 Lighthill			70		R. & M. 2647
362 Lighthill			34		R. & M. 2112
382 GLAS II			31.5		R. & M. 2112
					R. & M. 2683
					R. & M. 2646
					R. & M. 2577
					R. & M. 2540
451 TFA III			34.2		R. & M. 2111
452 TFA			20		R. & M. 2612
453 TFA V			14.7		R. & M. 2612
454 CVA I			9.2		R. & M. 2612
455 CVA II			53.1		R. & M. 2612

## Remarks

As a rule, the values given here are the most modern ones. For the NACA 6-profiles, the values were mainly obtained from graphs and may be in error by a few per cent.

1. These drag coefficients and the  $C_{L_{max}}$  values in these lines still require the correction described in [R669].
2.  $C_m$  is referred to the aerodynamic centre when values for  $x_a$  and  $y_a$  are given; otherwise it is referred to the quarter-chord point.

3. Behaviour of  $C_{L_{max}}$ :



4. Here, the trailing edge is rounded; the radius of the circle of curvature at the trailing edge is  $\rho_T$ , where  $\rho_T = \frac{(r_T/c)}{(t/c)^2} \cdot 10^3$ .  $\rho_T$  is given.
5. Measurements made with flaps deflected.

6. The reference direction is usually the chord according to the NACA definition. For Göttingen profiles it is the tangent at the trailing edge on the pressure side; for symmetrical profiles it is always the line of symmetry.

We now give some typical values for  $\alpha_R$ , the angle (in degrees) between the chord when defined as the longest line joining two points of the profile (the definition in theoretical work) and the chord actually used for the profile.

Profile Gö	436	549	564	596	620	622	623	624	625				
$\alpha_R =$		1.4	2.0	1.3	1.0	3.0	1.4	1.8	2.3	3.2			
Profile Clark Y	6%	8%	10%	11.7%	14%	N85	86	87					
$\alpha_R =$		1.0	1.4	1.7	2.0	2.4	0.1	0.1	0.1				
Profile NACA	2406	2409	2412	2415	2418	2421	4406	4409	4412	4415	4418	4421	
$\alpha_R =$		0	0.1	0.1	0.1	0.2	0.3	.0	0.1	0.2	0.3	0.4	0.6
Profile NACA	6406	6409	6412	6415	6418	6421	23006	23009	23012	23015	23018	23021	
$\alpha_R =$		0.1	0.2	0.3	0.4	0.6	0.8	0.1	0.2	0.3	0.4	0.6	0.9

7. Measurements for various Mach numbers less than 0.9.

Table 11.2

Ordinates, Slopes, and Velocity Distributions of Camber Lines

100 $x/c$	100 $y/c$	$dy/dx$	$\Delta w/V$	100 $y/c$	$dy/dx$	$\Delta w/V$	100 $y/c$	$dy/dx$	$\Delta w/V$	100 $x/c$
<b>NACA 62</b>										
$C_L^* = 0.90; \alpha^* = 2.81^\circ; C_m^* = -0.113$										
0	0	0.60000	0	0	0.40000	0	0	0.30000	0	0
1.25	0.726	0.56250	0.171	0.489	0.38333	0.097	0.369	0.29062	0.064	1.25
2.5	1.406	0.52500	0.258	0.958	0.36667	0.138	0.726	0.28125	0.098	2.5
5.0	2.625	0.45000	0.328	1.833	0.33333	0.197	1.406	0.26250	0.137	5.0
7.5	3.656	0.37500	0.376	2.625	0.30000	0.235	2.039	0.24375	0.167	7.5
10	4.500	0.30000	0.413	3.333	0.26667	0.267	2.625	0.22500	0.187	10
15	5.625	0.15000	0.451	4.500	0.20000	0.305	3.656	0.18750	0.218	15
20	6.000	0	0.383	5.333	0.13333	0.315	4.500	0.15000	0.242	20
25	5.977	—0.0938	0.318	5.833	0.06667	0.308	5.156	0.11250	0.258	25
30	5.906	—0.1875	0.279	6.000	0	0.290	5.625	0.07500	0.260	30
40	5.625	—0.3750	0.238	5.878	—0.02449	0.237	6.000	0	0.250	40
50	5.156	—0.5625	0.211	5.510	—0.4898	0.213	5.833	—0.3333	0.228	50
60	4.500	—0.7500	0.185	4.898	—0.7347	0.191	5.333	—0.6667	0.207	60
70	3.656	—0.9375	0.159	4.041	—0.9796	0.168	4.500	—1.0000	0.188	70
80	2.625	—1.1250	0.131	2.939	—1.2245	0.140	3.333	—1.3333	0.159	80
90	1.406	—1.3125	0.094	1.592	—1.4694	0.102	1.833	—1.6667	0.117	90
95	0.727	—1.4062	0.065	0.827	—1.5918	0.073	0.958	—1.8333	0.084	95
100	0	—1.5000	0	0	—1.7143	0	0	—2.0000	0	100
<b>NACA 65</b>										
$C_L^* = 0.75; \alpha^* = 0^\circ; C_m^* = -0.187$										
0	0	0.24000	0	0	0.59613	0	0	0.39270	0	0
1.25	0.296	0.23400	0.051	0.596	0.36236	0.345	0.442	0.31541	0.206	1.25
2.5	0.585	0.22800	0.074	0.928	0.18504	0.391	0.793	0.24618	0.251	2.5
5.0	1.140	0.21600	0.103	1.114	—0.00018	0.305	1.257	0.13192	0.247	5.0
7.5	1.665	0.20400	0.126	1.087	—0.01175	0.195	1.479	0.04994	0.225	7.5
10	2.160	0.19200	0.143	1.058	—0.01175	0.156	1.535	0.00024	0.200	10
15	3.060	0.16800	0.170	0.999	—0.01175	0.122	1.463	—0.01722	0.154	15
20	3.840	0.14400	0.190	0.940	—0.01175	0.102	1.377	—0.01722	0.116	20
25	4.500	0.12000	0.206	0.881	—0.01175	0.087	1.291	—0.01722	0.095	25
30	5.040	0.09600	0.218	0.823	—0.01175	0.075	1.205	—0.01722	0.082	30
40	5.760	0.04800	0.233	0.705	—0.01175	0.061	1.033	—0.01722	0.063	40
50	6.000	0	0.238	0.588	—0.01175	0.049	0.861	—0.01722	0.051	50
60	5.760	—0.4800	0.233	0.470	—0.01175	0.040	0.689	—0.01722	0.042	60
70	5.040	—0.9600	0.218	0.353	—0.01175	0.032	0.516	—0.01722	0.034	70
80	3.840	—1.4400	0.190	0.235	—0.01175	0.025	0.344	—0.01722	0.025	80
90	2.160	—1.9200	0.143	0.118	—0.01175	0.016	0.172	—0.01722	0.016	90
95	1.140	—2.1600	0.103	0.059	—0.01175	0.011	0.086	—0.01722	0.010	95
100	0	—2.4000	0	0	—0.01175	0	0	—0.01722	0	100
<b>NACA 210</b>										
$C_L^* = 0.30; \alpha^* = 2.09^\circ; C_m^* = -0.006$										
0	0	0.39270	0	0	0.31541	0.206	0	0.206	1.25	0
1.25	0.442	0.31541	0.206	0.793	0.24618	0.251	0.251	0.24618	2.5	0
2.5	0.739	0.24618	0.251	1.257	0.13192	0.247	0.247	0.13192	5.0	0
5.0	1.257	0.13192	0.247	1.479	0.04994	0.225	0.225	0.04994	7.5	0
7.5	1.479	0.04994	0.225	1.535	0.00024	0.200	0.200	0.00024	10	0
10	1.535	0.00024	0.200	1.463	—0.01722	0.154	0.154	—0.01722	15	0
15	1.377	—0.01722	0.154	1.291	—0.01722	0.116	0.116	—0.01722	20	0
20	1.205	—0.01722	0.116	1.205	—0.01722	0.095	0.095	—0.01722	25	0
25	1.120	—0.01722	0.095	1.033	—0.01722	0.063	0.063	—0.01722	30	0
30	1.033	—0.01722	0.063	0.861	—0.01722	0.051	0.051	—0.01722	40	0
40	0.880	—0.01722	0.051	0.689	—0.01722	0.042	0.042	—0.01722	50	0
50	0.609	—0.01722	0.042	0.516	—0.01722	0.034	0.034	—0.01722	60	0
60	0.409	—0.01722	0.034	0.344	—0.01722	0.025	0.025	—0.01722	70	0
70	0.287	—0.01722	0.025	0.172	—0.01722	0.016	0.016	—0.01722	80	0
80	0.188	—0.01722	0.016	0.086	—0.01722	0.010	0.010	—0.01722	90	0
90	0.121	—0.01722	0.010	0.032	—0.01722	0.019	0.019	—0.01722	95	0
95	0.061	—0.01722	0.019	0.016	—0.01722	0.013	0.013	—0.01722	100	0
100	0	—0.01722	0	0	—0.01722	0	0	—0.01722	100	0
<b>NACA 220</b>										
$C_L^* = 0.30; \alpha^* = 1.86^\circ; C_m^* = -0.010$										
0	0	0.39270	0	0	0.31541	0.206	0	0.206	1.25	0
1.25	0.442	0.31541	0.206	0.793	0.24618	0.251	0.251	0.24618	2.5	0
2.5	0.739	0.24618	0.251	1.257	0.13192	0.247	0.247	0.13192	5.0	0
5.0	1.257	0.13192	0.247	1.479	0.04994	0.225	0.225	0.04994	7.5	0
7.5	1.479	0.04994	0.225	1.535	0.00024	0.200	0.200	0.00024	10	0
10	1.535	0.00024	0.200	1.463	—0.01722	0.154	0.154	—0.01722	15	0
15	1.377	—0.01722	0.154	1.291	—0.01722	0.116	0.116	—0.01722	20	0
20	1.205	—0.01722	0.116	1.205	—0.01722	0.095	0.095	—0.01722	25	0
25	1.120	—0.01722	0.095	1.033	—0.01722	0.063	0.063	—0.01722	30	0
30	1.033	—0.01722	0.063	0.861	—0.01722	0.051	0.051	—0.01722	40	0
40	0.880	—0.01722	0.051	0.689	—0.01722	0.042	0.042	—0.01722	50	0
50	0.609	—0.01722	0.042	0.516	—0.01722	0.034	0.034	—0.01722	60	0
60	0.409	—0.01722	0.034	0.344	—0.01722	0.025	0.025	—0.01722	70	0
70	0.287	—0.01722	0.025	0.172	—0.01722	0.016	0.016	—0.01722	80	0
80	0.188	—0.01722	0.016	0.086	—0.01722	0.013	0.013	—0.01722	90	0
90	0.121	—0.01722	0.013	0.032	—0.01722	0.019	0.019	—0.01722	95	0
95	0.061	—0.01722	0.019	0.016	—0.01722	0.013	0.013	—0.01722	100	0
100	0	—0.01722	0	0	—0.01722	0	0	—0.01722	100	0
<b>NACA 230</b>										
$C_L^* = 0.30; \alpha^* = 1.65^\circ; C_m^* = -0.014$										
0	0	0.30508	0	0	0.25233	0	0	0.21472	0	0
1.25	0.357	0.26594	0.132	0.301	0.22877	0.094	0.258	0.19920	0.070	1.25
2.5	0.666	0.22929	0.168	0.572	0.20625	0.123	0.498	0.18416	0.092	2.5
5.0	1.155	0.16347	0.198	1.035	0.16432	0.156	0.922	0.15562	0.119	5.0
7.5	1.492	0.10762	0.213	1.397	0.12653	0.180	1.277	0.12909	0.138	7.5
10	1.701	0.06174	0.215	1.871	0.09290	0.188	1.570	0.10458	0.148	10
15	1.838	—0.0009	0.170	1.991	0.03810	0.169	1.982	0.06162	0.156	15
20	1.767	—0.02203	0.130	2.079	—0.00010	0.142	2.199	—0.02674	0.153	20
25	1.656	—0.02208	0.105	2.018	—0.02160	0.119	2.263	—0.00007	0.137	25
30	1.546	—0.02208	0.090	1.890	—0.02700	0.103	2.212	—0.01880	0.117	30
40	1.325	—0.02208	0.069	1.620	—0.02700	0.076	1.931</			

100 $x/c$	100 $y/c$	$dy/dx$	$\Delta w/V$	100 $y/c$	$dy/dx$	$\Delta w/V$	100 $y/c$	$dy/dx$	$\Delta w/V$	100 $x/c$
<b>NACA <math>a = 0</math></b>										
$C_L^* = 0.10; \alpha^* = -4.56^\circ; C_m^* = -0.083$										
0	0			0			0			0
0.5	0.480	0.75867 <sup>1)</sup>	0.498	0.440	0.73441 <sup>1)</sup>	0.455	0.414	0.69492 <sup>1)</sup>	0.417	0.5
0.75	0.641	0.69212	0.496	0.616	0.67479	0.455	0.581	0.64047	0.417	0.75
1.25	0.964	0.60715	0.494	0.933	0.59896	0.455	0.882	0.57135	0.417	1.25
2.5	1.641	0.48892	0.488	1.608	0.49366	0.455	1.530	0.47592	0.417	2.5
5.0	2.693	0.36561	0.475	2.689	0.38235	0.455	2.583	0.37661	0.417	5.0
7.5	3.507	0.29028	0.463	3.551	0.31067	0.455	3.443	0.31487	0.417	7.5
10	4.161	0.23515	0.450	4.253	0.25057	0.455	4.169	0.26803	0.417	10
15	5.124	0.15508	0.425	5.261	0.16087	0.429	5.317	0.19373	0.417	15
20	5.747	0.09693	0.400	5.905	0.09981	0.404	6.117	0.12405	0.417	20
25	6.114	0.05156	0.375	6.282	0.05281	0.379	6.572	0.06345	0.391	25
30	6.277	0.01482	0.350	6.449	0.01498	0.354	6.777	0.02030	0.365	30
35	6.273	-0.1554	0.325	6.443	-0.1617	0.328	6.789	-0.1418	0.339	35
40	6.130	-0.04086	0.300	6.296	-0.04210	0.303	6.646	-0.04246	0.313	40
45	5.871	-0.06201	0.275	6.029	-0.06373	0.278	6.373	-0.06588	0.287	45
50	5.516	-0.07958	0.250	5.664	-0.08168	0.253	5.994	-0.08522	0.260	50
55	5.081	-0.09395	0.225	5.218	-0.09637	0.227	5.527	-0.10101	0.234	55
60	4.581	-0.10539	0.200	4.706	-0.10806	0.202	4.989	-0.11359	0.208	60
65	4.032	-0.11406	0.175	4.142	-0.11694	0.177	4.396	-0.12317	0.182	65
70	3.445	-0.12003	0.150	3.541	-0.12307	0.152	3.762	-0.12985	0.156	70
75	2.836	-0.12329	0.125	2.916	-0.12644	0.126	3.102	-0.13363	0.130	75
80	2.217	-0.12371	0.100	2.281	-0.12683	0.101	2.431	-0.13440	0.104	80
85	1.604	-0.12099	0.075	1.652	-0.12425	0.076	1.764	-0.13186	0.078	85
90	1.013	-0.11455	0.060	1.045	-0.11781	0.060	1.119	-0.12541	0.052	90
95	0.487	-0.10301	0.255	0.482	-0.10620	0.025	0.518	-0.11361	0.026	95
100	0	-0.07958	0	0	-0.08258	0	0	-0.08941	0	100
<b>NACA <math>a = 0.3</math></b>										
$C_L^* = 1.0; \alpha^* = 3.84^\circ; C_m^* = -0.106$										
0	0			0			0			0
0.5	0.389	0.65536 <sup>1)</sup>	0.385	0.366	0.61759 <sup>1)</sup>	0.357	0.345	0.58195 <sup>1)</sup>	0.333	0.5
0.75	0.548	0.60524	0.385	0.514	0.57105	0.357	0.485	0.53855	0.333	0.75
1.25	0.832	0.54158	0.385	0.784	0.51210	0.357	0.735	0.48360	0.333	1.25
2.5	1.448	0.45399	0.385	1.387	0.43106	0.357	1.295	0.40815	0.333	2.5
5.0	2.458	0.36344	0.385	2.330	0.34764	0.357	2.205	0.33070	0.333	5.0
7.5	3.293	0.30780	0.385	3.131	0.29671	0.357	2.970	0.28385	0.333	7.5
10	4.008	0.26621	0.385	3.824	0.25892	0.357	3.630	0.24890	0.333	10
15	5.172	0.20246	0.385	4.968	0.20185	0.357	4.740	0.19690	0.333	15
20	6.052	0.15068	0.385	5.862	0.15682	0.357	5.620	0.15650	0.333	20
25	6.685	0.10278	0.385	6.546	0.11733	0.357	6.310	0.12180	0.333	25
30	7.072	0.04833	0.385	7.039	0.07988	0.357	6.840	0.09000	0.333	30
35	7.175	-0.02026	0.357	7.343	0.04126	0.357	7.215	0.05930	0.333	35
40	7.074	-0.03710	0.330	7.439	-0.00721	0.357	7.430	0.02800	0.333	40
45	6.816	-0.06492	0.302	7.275	-0.05321	0.327	7.490	-0.00630	0.333	45
50	6.433	-0.08746	0.275	6.929	-0.08380	0.298	7.350	-0.05305	0.333	50
55	5.949	-0.10567	0.247	6.449	-0.10734	0.268	6.965	-0.09765	0.300	55
60	5.383	-0.12014	0.220	5.864	-0.12567	0.238	6.405	-0.12550	0.267	60
65	4.753	-0.13119	0.192	5.199	-0.13962	0.208	5.725	-0.14570	0.233	65
70	4.076	-0.13901	0.165	4.475	-0.14963	0.179	4.955	-0.16015	0.200	70
75	3.368	-0.14365	0.137	3.709	-0.15589	0.149	4.130	-0.18960	0.167	75
80	2.645	-0.14500	0.110	2.922	-0.15837	0.119	3.265	-0.17435	0.133	80
85	1.924	-0.14279	0.082	2.132	-0.15683	0.089	2.395	-0.17415	0.100	85
90	1.224	-0.13638	0.055	1.361	-0.15062	0.060	1.535	-0.18850	0.067	90
95	0.570	-0.12430	0.028	0.636	-0.13816	0.030	0.720	-0.15565	0.033	95
100	0	-0.00007	0	0	-0.11138	0	0	-0.12860	0	100
<b>NACA <math>a = 0.4</math></b>										
$C_L^* = 1.0; \alpha^* = 3.46^\circ; C_m^* = -0.121$										
0	0			0			0			0
0.5	0.389	0.65536 <sup>1)</sup>	0.385	0.366	0.61759 <sup>1)</sup>	0.357	0.345	0.58195 <sup>1)</sup>	0.333	0.5
0.75	0.548	0.60524	0.385	0.514	0.57105	0.357	0.485	0.53855	0.333	0.75
1.25	0.832	0.54158	0.385	0.784	0.51210	0.357	0.735	0.48360	0.333	1.25
2.5	1.448	0.45399	0.385	1.387	0.43106	0.357	1.295	0.40815	0.333	2.5
5.0	2.458	0.36344	0.385	2.330	0.34764	0.357	2.205	0.33070	0.333	5.0
7.5	3.293	0.30780	0.385	3.131	0.29671	0.357	2.970	0.28385	0.333	7.5
10	4.008	0.26621	0.385	3.824	0.25892	0.357	3.630	0.24890	0.333	10
15	5.172	0.20246	0.385	4.968	0.20185	0.357	4.740	0.19690	0.333	15
20	6.052	0.15068	0.385	5.862	0.15682	0.357	5.620	0.15650	0.333	20
25	6.685	0.10278	0.385	6.546	0.11733	0.357	6.310	0.12180	0.333	25
30	7.072	0.04833	0.385	7.039	0.07988	0.357	6.840	0.09000	0.333	30
35	7.175	-0.02026	0.357	7.343	0.04126	0.357	7.215	0.05930	0.333	35
40	7.074	-0.03710	0.330	7.439	-0.00721	0.357	7.430	0.02800	0.333	40
45	6.816	-0.06492	0.302	7.275	-0.05321	0.327	7.490	-0.00630	0.333	45
50	6.433	-0.08746	0.275	6.929	-0.08380	0.298	7.350	-0.05305	0.333	50
55	5.949	-0.10567	0.247	6.449	-0.10734	0.268	6.965	-0.09765	0.300	55
60	5.383	-0.12014	0.220	5.864	-0.12567	0.238	6.405	-0.12550	0.267	60
65	4.753	-0.13119	0.192	5.199	-0.13962	0.208	5.725	-0.14570	0.233	65
70	4.076	-0.13901	0.165	4.475	-0.14963	0.179	4.955	-0.16015	0.200	70
75	3.368	-0.14365	0.137	3.709	-0.15589	0.149	4.130	-0.18960	0.167	75
80	2.645	-0.14500	0.110	2.922	-0.15837	0.119	3.265	-0.17435	0.133	80
85	1.924	-0.14279	0.082	2.132	-0.15683	0.089	2.395	-0.17415	0.100	85
90	1.224	-0.13638	0.055	1.361	-0.15062	0.060	1.535	-0.18850	0.067	90
95	0.570	-0.12430	0.028	0.636	-0.13816	0.030	0.720	-0.15565	0.033	95
100	0	-0.00007	0	0	-0.11138	0	0	-0.12860	0	100
<b>NACA <math>a = 0.5</math></b>										
$C_L^* = 1.0; \alpha^* = 3.04^\circ; C_m^* = -0.139$										
0	0			0			0			0
0.5	0.389	0.65536 <sup>1)</sup>	0.385	0.366	0.61759 <sup>1)</sup>	0.357	0.345	0.58195 <sup>1)</sup>	0.333	0.5
0.75	0.548	0.60524	0.385	0.514	0.57105	0.357	0.485	0.53855	0.333	0.75
1.25	0.832	0.54158	0.385	0.784	0.51210	0.357	0.735	0.48360	0.333	1.25
2.5	1.448	0.45399	0.385	1.387	0.43106	0.357	1.295	0.40815	0.333	2.5
5.0	2.458	0.36344	0.385	2.330	0.34764	0.357	2.205	0.33070	0.333	5.0
7.5	3.293	0.30780	0.385	3.131	0.29671	0.357	2.970	0.28385	0.333</	

100 $x/c$	100 $y/c$	$dy/dx$	$\Delta w/V$	100 $y/c$	$dy/dx$	$\Delta w/V$	100 $y/c$	$dy/dx$	$\Delta w/V$	100 $x/c$	
<b>NACA a = 0·6</b>				<b>NACA a = 0·7</b>				<b>NACA a = 0·8</b>			
$C_L^* = 1·0; \alpha^* = 2·58^\circ; C_m^* = -0·158$				$C_L^* = 1·0; \alpha^* = 2·09^\circ; C_m^* = -0·179$				$C_L^* = 1·0; \alpha^* = 1·54^\circ; C_m^* = -0·202$			
0	0			0			0			0	
0·5	0·325	0·54825 <sup>1)</sup>	0·312	0·305	0·51620 <sup>1)</sup>	0·294	0·287	0·48535 <sup>1)</sup>	0·278	0·5	
0·75	0·455	0·50760	0·312	0·425	0·47795	0·294	0·404	0·44925	0·278	0·75	
1·25	0·695	0·45615	0·312	0·655	0·42960	0·294	0·616	0·40369	0·278	1·25	
2·5	1·220	0·38555	0·312	1·160	0·36325	0·294	1·077	0·34104	0·278	2·5	
5·0	2·080	0·31325	0·312	1·955	0·29545	0·294	1·841	0·27718	0·278	5·0	
7·5	2·805	0·26950	0·312	2·645	0·25450	0·294	2·483	0·23868	0·278	7·5	
10	3·435	0·23730	0·312	3·240	0·22445	0·294	3·043	0·21050	0·278	10	
15	4·495	0·18935	0·312	4·245	0·17995	0·294	3·985	0·16892	0·278	15	
20	5·345	0·15250	0·312	5·060	0·14595	0·294	4·748	0·13734	0·278	20	
25	6·035	0·12125	0·312	5·715	0·11740	0·294	5·367	0·11101	0·278	25	
30	6·570	0·09310	0·312	6·240	0·09200	0·294	5·863	0·08775	0·278	30	
35	6·965	0·06660	0·312	6·635	0·06840	0·294	6·248	0·06634	0·278	35	
40	7·235	0·04060	0·312	6·925	0·04570	0·294	6·528	0·04601	0·278	40	
45	7·370	0·01405	0·312	7·095	0·02315	0·294	6·709	0·02613	0·278	45	
50	7·370	—0·1435	0·312	7·155	0	0·294	6·790	0·00620	0·278	50	
55	7·220	—0·04700	0·312	7·090	—0·02455	0·294	6·770	—0·01433	0·278	55	
60	6·880	—0·09470	0·312	6·900	—0·05185	0·294	6·644	—0·03611	0·278	60	
65	6·275	—0·14015	0·273	6·565	—0·08475	0·294	6·405	—0·06010	0·278	65	
70	5·505	—0·16595	0·234	6·030	—1·36650	0·294	6·037	—0·08790	0·278	70	
75	4·630	—0·18270	0·195	5·205	—1·8510	0·245	5·514	—1·2311	0·278	75	
80	3·695	—0·19225	0·156	4·215	—2·0855	0·196	4·771	—1·8412	0·278	80	
85	2·720	—0·19515	0·117	3·140	—2·1955	0·147	3·683	—2·3921	0·208	85	
90	1·755	—0·19095	0·078	2·035	—2·1960	0·098	2·435	—2·5583	0·139	90	
95	0·825	—0·17790	0·039	0·965	—2·0725	0·049	1·163	—2·4904	0·069	95	
100	0	—0·14550	0	0	—1·6985	0	0	—2·0385	0	100	
<b>NACA a = 0·9</b>				<b>NACA a = 1·0</b>							
$C_L^* = 1·0; \alpha^* = 0·90^\circ; C_m^* = -0·225$				$C_L^* = 1·0; \alpha^* = 0^\circ; C_m^* = -0·250$							
0	0			0						0	
0·5	0·269	0·45482 <sup>1)</sup>	0·263	0·250	0·42120 <sup>1)</sup>	0·250				0·5	
0·75	0·379	0·42064	0·263	0·350	0·38875	0·250				0·75	
1·25	0·577	0·37740	0·263	0·635	0·34770	0·250				1·25	
2·5	1·008	0·31821	0·263	0·930	0·29155	0·250				2·5	
5·0	1·720	0·25786	0·263	1·580	0·23430	0·250				5·0	
7·5	2·318	0·22153	0·263	2·120	0·19995	0·250				7·5	
10	2·835	0·19500	0·263	2·585	0·17485	0·250				10	
15	3·707	0·15595	0·263	3·365	0·13805	0·250				15	
20	4·410	0·12644	0·263	3·980	0·11030	0·250				20	
25	4·980	0·10196	0·263	4·475	0·08745	0·250				25	
30	5·435	0·08047	0·263	4·860	0·06745	0·250				30	
35	5·787	0·06084	0·263	5·150	0·04925	0·250				35	
40	6·045	0·04234	0·263	5·355	0·03225	0·250				40	
45	6·212	0·02447	0·263	5·475	0·01595	0·250				45	
50	6·290	0·00678	0·263	5·615	0	0·250				50	
55	6·279	—0·11111	0·263	5·475	—0·01595	0·250				55	
60	6·178	—0·2965	0·263	5·355	—0·03225	0·250				60	
65	5·981	—0·4938	0·263	5·150	—0·04925	0·250				65	
70	5·681	—0·07103	0·263	4·860	—0·06745	0·250				70	
75	5·265	—0·09583	0·263	4·475	—0·08745	0·250				75	
80	4·714	—0·12605	0·263	3·980	—1·1030	0·250				80	
85	3·987	—0·18727	0·263	3·365	—1·3805	0·250				85	
90	2·984	—0·25204	0·263	2·585	—1·7485	0·250				90	
95	1·503	—0·31463	0·132	1·580	—2·2430	0·250				95	
100	0	—0·26086	0	0						100	

<sup>1</sup> The value of  $dy/dx$  at  $x/c = 0·005$  is given, since  $dy/dx \rightarrow \infty$  as  $x \rightarrow 0$ .

Table 11.3 (a)

### Profile Co-ordinates

$x$	$y_u$	$y_l$	$y_u$	$y_l$	$y_u$	$y_l$	$y_u$	$y_l$	$x$
			<b>Gö 5 K</b>		<b>Gö 6 K</b>		<b>Gö 7 K</b>		<b>Gö 8 K</b>
0	0.533	0.533	1.080	1.080	1.584	1.584	2.138	2.138	0
2.5	1.299	0.174	2.633	0.363	3.861	0.617	5.212	0.698	2.5
5.0	1.669	0.118	3.383	0.240	4.961	0.352	6.697	0.475	5.0
7.5	1.957	0.081	3.968	0.185	5.819	0.242	7.856	0.327	7.5
10	2.216	0.066	4.493	0.113	6.589	0.166	8.895	0.223	10
15	2.627	0.011	5.325	0.023	7.810	0.033	10.644	0.045	15
20	2.942	0	5.963	0	8.745	0	11.806	0	20
30	3.404	0	6.900	0	10.120	0	13.662	0	30
40	3.845	0	7.388	0	10.835	0	14.627	0	40
50	3.700	0	7.500	0	11.000	0	14.850	0	50
60	3.574	0	7.245	0	10.626	0	14.345	0	60
70	3.167	0	6.420	0	9.418	0	12.712	0	70
80	2.501	0	5.070	0	7.438	0	10.039	0	80
90	1.632	0	3.105	0	4.554	0	6.148	0	90
95	0.932	0	1.890	0	2.772	0	3.742	0	95
100	0.111	0.111	0.225	0.225	0.330	0.330	0.446	0.446	100
			<b>Gö 9 K</b>		<b>Gö 10 K</b>		<b>Gö 11 K</b>		<b>Gö 12 K</b>
0	0.578	0.578	0.909	0.909	1.758	1.758	2.620	2.620	0
2.5	1.201	0.142	1.886	0.223	3.651	0.432	5.439	0.644	2.5
5.0	1.441	0.064	2.264	0.085	4.381	0.164	6.527	0.244	5.0
10	1.752	0	2.753	0	5.327	0	7.936	0	10
15	1.977	0	3.107	0	6.012	0	8.958	0	15
20	2.149	0	3.376	0	6.534	0	9.735	0	20
30	2.384	0	3.715	0	7.189	0	10.712	0	30
40	2.435	0	3.827	0	7.405	0	11.033	0	40
50	2.450	0	3.850	0	7.450	0	11.100	0	50
60	2.387	0	3.719	0	7.197	0	10.723	0	60
70	2.102	0	3.303	0	6.392	0	9.624	0	70
80	1.661	0	2.610	0	5.050	0	7.526	0	80
90	1.029	0	1.617	0	3.129	0	4.682	0	90
95	0.639	0	1.005	0	1.944	0	2.897	0	95
100	0.083	0.083	0.131	0.131	0.253	0.253	0.377	0.377	100
			<b>Gö 13 K</b>		<b>Gö 14 K</b>		<b>Gö 15 K</b>		<b>Gö 16 K</b>
0	3.493	3.493	3.996	3.996	4.995	4.995	6.044	6.044	0
2.5	7.252	0.858	6.336	2.196	7.920	2.745	9.583	3.321	2.5
5.0	8.702	0.326	7.332	1.596	9.165	1.995	11.090	2.414	5.0
10	10.582	0	8.664	0.864	10.830	1.080	13.104	1.307	10
15	11.944	0	9.600	0.432	12.000	0.540	14.520	0.653	15
20	12.980	0	10.332	0.192	12.915	0.240	15.627	0.290	20
30	14.282	0	11.340	0	14.175	0	17.152	0	30
40	14.711	0	11.820	0	14.775	0	17.878	0	40
50	14.800	0	12.000	0	15.000	0	18.150	0	50
60	14.297	0	11.664	0	14.580	0	17.642	0	60
70	12.698	0	10.776	0.060	13.470	0.075	16.299	0.091	70
80	10.034	0	9.000	0.264	11.250	0.330	13.613	0.399	80
90	6.216	0	6.540	0.792	8.175	0.990	9.892	1.198	90
95	3.863	0	4.932	1.332	6.165	1.665	7.480	2.014	95
100	0.503	0.503	2.604	2.604	3.255	3.255	3.939	3.939	100
			<b>Gö 123</b>		<b>Gö 227</b>		<b>Gö 242</b>		<b>Gö 243</b>
0	1.0	1.0	2.9	2.9	2.5	2.5	3.9	3.9	0
1.25	2.8	0.1	5.4	1.2	5.4	1.8	8.0	1.9	1.25
2.50	3.6	0.2	6.6	0.6	7.2	1.5	9.8	1.5	2.50
5.00	4.9	0.6	8.6	0.1	9.2	0.9	12.5	0.8	5.00
7.50	5.8	1.1	10.2	0	10.7	0.6	14.3	0.5	7.50
10	6.6	1.6	11.4	0	12.0	0.4	15.7	0.1	10
15	7.7	2.4	13.3	0.2	14.0	0.1	17.6	0	15
20	8.4	2.8	14.6	0.4	15.2	0	18.7	0	20
25	8.8	3.2	15.4	0.8	16.0	0	19.3	0.1	25
30	9.0	3.6	15.8	1.4	16.3	0.2	19.6	0.5	30
40	9.0	3.6	15.8	2.6	16.2	1.3	19.1	1.9	40
50	8.5	3.2	15.0	3.6	15.0	2.7	17.9	3.4	50
60	7.6	2.6	13.0	4.3	13.0	4.2	16.5	4.9	60
70	6.2	2.0	10.6	4.3	10.3	4.9	12.5	5.7	70
80	4.4	1.3	7.5	3.8	7.2	4.3	9.0	5.3	80
90	2.3	0.7	4.1	2.3	3.9	2.6	5.0	3.2	90
100	0.2	0	0.3	0	0.3	0	0.5	0	100



<i>x</i>	<i>y<sub>u</sub></i>	<i>y<sub>l</sub></i>	<i>y<sub>u</sub></i>	<i>y<sub>l</sub></i>	<i>y<sub>u</sub></i>	<i>y<sub>l</sub></i>	<i>y<sub>u</sub></i>	<i>y<sub>l</sub></i>	<i>x</i>
<b>G8 532</b>									
0	2.45	2.45	3.20	3.20	4.30	4.30	3.45	3.45	0
1.25	5.85	1.15	6.05	1.75	8.35	2.30	5.70	1.95	1.25
2.50	7.05	0.80	7.20	1.35	9.75	1.55	6.80	1.60	2.50
5.00	8.55	0.50	8.80	0.95	11.55	0.80	8.45	1.10	5.00
7.50	9.65	0.30	10.05	0.65	12.90	0.50	9.65	0.75	7.50
10	10.55	0.15	11.10	0.50	13.95	0.30	10.70	0.55	10
15	11.60	0	12.40	0.25	15.30	0.05	12.25	0.25	15
20	12.25	0	13.25	0.10	16.05	0	13.20	0.05	20
30	12.75	0.25	13.70	0	16.30	0.25	13.85	0	30
40	12.05	0.65	13.05	0.15	15.35	1.15	13.40	0.10	40
50	10.70	1.05	11.85	0.60	13.75	2.20	12.05	0.30	50
60	9.00	1.35	9.65	1.10	11.65	3.00	10.05	0.55	60
70	7.10	1.50	7.50	1.40	9.22	3.00	7.90	0.65	70
80	4.90	1.35	5.20	1.35	6.55	2.50	5.35	0.55	80
90	2.60	0.80	2.70	0.85	3.55	1.45	2.70	0.30	90
95	1.40	0.45	1.40	0.45	1.90	0.65	1.40	0.15	95
100	0.10	0.10	0	0	0.15	0.15	0	0	100
<b>550</b>									
			<b>564</b>		<b>593</b>		<b>596</b>		
0	4.90	4.90	2.30	2.30	3.00	3.00	1.70	1.70	0
1.25	7.05	3.05	3.90	1.10	5.50	1.80	3.80	0.40	1.25
2.50	8.00	2.25	4.60	0.70	6.50	1.35	4.60	0.15	2.50
5.00	9.35	1.30	5.65	0.25	7.85	0.85	5.80	0.05	5.00
7.50	10.35	0.70	6.30	0.05	8.90	0.55	6.80	0	7.50
10	11.10	0.35	6.85	0	9.75	0.40	7.60	0	10
15	12.30	0	7.50	0	10.95	0.25	8.70	0	15
20	13.05	0.10	7.85	0	11.50	0.15	9.45	0.10	20
30	13.45	0.75	8.20	0	12.00	0.10	10.00	0.25	30
40	13.00	1.20	8.10	0	11.70	0	9.75	0.35	40
50	11.85	1.60	7.60	0	10.85	0	8.80	0.40	50
60	10.20	1.65	6.70	0	9.45	0	7.50	0.35	60
70	8.10	1.60	5.60	0	7.65	0	6.00	0.25	70
80	5.70	1.25	4.05	0	5.50	0	4.15	0.15	80
90	3.10	0.70	2.25	0	3.00	0	2.15	0.10	90
95	1.65	0.40	1.20	0	1.65	0	1.10	0.05	95
100	0	0	0	0	0.00	0	0	0	100
<b>620</b>									
			<b>622</b>		<b>623</b>		<b>624</b>		
0	5.15	5.15	2.40	2.40	3.25	3.25	4.00	4.00	0
1.25	8.30	3.00	3.75	1.45	5.45	1.95	7.15	2.25	1.25
2.50	9.85	2.25	4.50	1.05	6.45	1.60	8.50	1.65	2.50
5.00	11.90	1.40	5.45	0.60	7.90	0.90	10.40	0.95	5.00
7.50	13.35	0.85	6.15	0.35	9.05	0.35	11.75	0.60	7.50
10	14.35	0.50	6.60	0.25	9.90	0.20	12.85	0.40	10
15	16.00	0.10	7.30	0.15	10.95	0.10	14.35	0.15	15
20	16.95	0	7.70	0.05	11.55	0.05	15.30	0.05	20
30	17.70	0.20	8.00	0	12.00	0	16.00	0	30
40	17.30	0.60	7.80	0	11.70	0	15.40	0	40
50	16.00	0.95	7.10	0	10.65	0	14.05	0	50
60	13.95	1.20	6.15	0	9.15	0	12.00	0	60
70	11.10	1.20	5.00	0	7.35	0	9.50	0	70
80	7.80	0.95	3.55	0	5.15	0	6.60	0	80
90	4.10	0.45	1.95	0	2.80	0	3.55	0	90
95	2.10	0.20	1.15	0	1.60	0	2.00	0	95
100	0	0	0.20	0	0.30	0	0.50	0	100
<b>625</b>									
			<b>652</b>		<b>654</b>		<b>676 (M 12)</b>		
0	5.50	5.50	5.80	5.80	3.00	3.00	0	0	0
1.25	9.00	3.30	9.50	2.70	5.60	1.45	1.85	-1.60	1.25
2.50	10.80	2.35	11.00	1.60	7.05	1.10	2.70	-2.15	2.50
5.00	13.30	1.25	13.05	0.60	9.20	0.70	3.95	-2.70	5.00
7.50	14.95	0.75	14.50	0.10	10.75	0.45	4.85	-3.00	7.50
10	16.35	0.40	15.65	0	11.85	0.30	5.50	-3.25	10
15	18.25	0.15	17.20	0.35	13.35	0.10	6.60	-3.50	15
20	19.30	0.10	18.25	1.20	14.20	0.05	7.35	-3.70	20
30	20.00	0	18.85	3.45	14.50	0	7.95	-3.95	30
40	19.05	0	18.45	5.70	13.80	0.20	7.85	-3.95	40
50	17.35	0	17.05	7.25	12.20	0.40	7.25	-3.75	50
60	15.05	0	14.85	7.95	10.25	0.55	6.20	-3.45	60
70	12.10	0	11.90	7.70	7.95	0.55	4.95	-2.95	70
80	8.60	0	8.35	6.30	5.45	0.45	3.40	-2.25	80
90	4.75	0	4.45	3.70	2.85	0.25	1.80	-1.25	90
95	2.75	0	2.35	1.95	1.50	0.15	0.95	-0.70	95
100	0.65	0	0	0	0	0	0.15	-0.15	100

<i>x</i>	<i>y<sub>u</sub></i>	<i>y<sub>l</sub></i>	<i>y<sub>u</sub></i>	<i>y<sub>l</sub></i>	<i>y<sub>u</sub></i>	<i>y<sub>l</sub></i>	<i>y<sub>u</sub></i>	<i>y<sub>l</sub></i>	<i>x</i>
G8 677 (M 6)									
0	0	0	2.50	2.50	7.00	7.00	4.75	4.75	0
1.25	1.80	-1.70	4.55	1.05	10.00	4.50	7.50	2.65	1.25
2.50	2.75	-2.25	5.55	0.60	11.50	3.50	8.80	1.90	2.50
5.00	4.05	-2.75	7.00	0.25	13.50	2.35	10.65	1.05	5.00
7.50	4.90	-3.00	8.05	0.10	15.00	1.65	12.00	0.60	7.50
10	5.65	-3.20	8.90	0	16.10	1.05	12.95	0.30	10
15	6.75	-3.40	10.00	0.05	17.90	0.40	14.35	0.05	15
20	7.50	-3.60	10.65	0.20	19.05	0.10	15.25	0	20
30	8.20	-3.75	11.20	0.55	19.90	0	16.10	0	30
40	8.00	-3.85	10.80	0.75	19.40	0.20	15.90	0	40
50	7.25	-3.80	10.05	0.80	18.10	0.65	14.85	0	50
60	6.05	-3.70	8.65	0.85	16.20	1.25	13.00	0	60
70	4.60	-3.35	6.90	0.75	14.00	2.00	10.60	0	70
80	3.15	-2.75	4.85	0.60	11.60	2.90	7.60	0	80
90	1.65	-1.65	2.55	0.35	9.30	4.30	4.30	0	90
95	0.95	-0.95	1.35	0.15	8.20	5.20	2.50	0	95
100	0.20	-0.20	0	0	7.00	7.00	0.50	0	100
	693		711		735		738		
0	3.60	3.60	1.30	1.30	6.20	6.20	0.600	6.00	0
1.25	5.60	1.95	4.00	0.02	9.75	4.05	0.865	3.80	1.25
2.50	6.55	1.35	5.45	0	11.40	3.10	0.985	2.98	2.50
5.00	7.95	0.70	7.75	0	13.75	1.92	1.133	2.04	5.00
7.50	8.90	0.35	9.55	0	15.45	1.25	1.243	1.45	7.50
10	9.70	0.20	10.95	0	16.80	0.85	1.325	1.00	10
15	10.70	0.05	12.90	0	18.65	0.40	1.444	0.48	15
20	11.45	0	14.02	0	19.72	0.15	1.505	0.20	20
30	12.00	0	14.85	0	20.10	0	1.541	0	30
40	11.85	0	14.60	0	18.95	0.10	1.480	0.10	40
50	11.10	0	13.70	0	16.95	0.30	1.342	0.44	50
60	9.70	0	12.25	0	14.45	0.70	1.155	1.00	60
70	7.85	0	10.40	0	11.55	1.22	0.941	1.72	70
80	5.75	0	8.05	0	8.68	1.98	0.735	2.59	80
90	3.35	0	5.05	0	6.20	3.00	0.570	3.50	90
95	2.00	0.05	3.24	0	5.18	3.65	0.510	4.00	95
100	0.65	0.15	1.40	0	4.45	4.45	0.465	4.65	100
	741		744		746		758		
0	3.75	3.75	2.20	2.20	1.00	1.00	3.45	3.45	0
1.25	6.80	1.60	5.65	0.30	2.95	0.05	5.70	1.95	1.25
2.50	8.15	1.03	7.25	0	4.00	0.05	6.80	1.60	2.50
5.00	10.05	0.48	9.50	0	5.75	0.15	8.45	1.10	5.00
7.50	11.55	0.20	11.25	0.05	7.00	0.30	9.65	0.75	7.50
10	12.65	0.10	12.62	0.20	8.05	0.40	10.40	0.55	10
15	14.28	0	14.53	0.58	9.50	0.65	12.25	0.25	15
20	15.18	0.15	15.58	1.01	10.35	0.85	13.20	0.05	20
30	15.68	0.35	16.05	1.72	10.95	1.20	13.85	0	30
40	14.72	0.30	14.89	1.87	10.25	1.30	13.40	0.10	40
50	12.65	0.05	12.49	1.47	8.60	1.10	12.05	0.30	50
60	10.15	0	9.63	0.80	6.65	0.65	10.05	0.55	60
70	7.45	0	6.83	0.25	4.60	0.15	7.90	0.65	70
80	4.95	0.03	3.95	0	2.75	0	5.35	0.55	80
90	3.00	0.68	1.98	0.15	1.60	0.25	2.70	0.30	90
95	2.33	1.25	1.38	0.50	1.30	0.60	1.40	0.15	95
100	1.90	1.90	1.10	1.10	1.10	1.10	0	0	100
	766		767		769		770		
0	0	0	0	0	3.36	3.36	0	0	0
1.25	2.64	-1.70	2.99	-1.90	6.80	1.13	4.275	-1.750	1.25
2.50	3.60	-2.33	4.00	-2.60	8.35	0.60	5.625	-2.563	2.50
5.00	4.81	-3.03	5.33	-3.48	10.46	0.15	7.688	-3.675	5.00
10	6.28	-3.82	6.72	-4.20	12.70	0	10.550	-4.750	10
15	7.09	-4.19	7.38	-4.44	13.71	0.11	12.413	-5.600	15
20	7.40	-4.43	7.50	-4.50	14.06	0.24	13.675	-6.163	20
25	7.43	-4.58	7.37	-4.52	14.06	0.40		-6.488	25
30	7.28	-4.65	7.05	-4.43	13.75	0.54	14.500	-6.450	40
40	6.54	-4.52	6.09	-4.10	12.55	0.70	13.900	-5.688	50
50	5.67	-4.21	4.98	-3.64	10.85	0.75	12.175	-4.625	60
60	4.53	-3.64	3.90	-3.06	8.75	0.70	9.838	-3.500	70
70	3.46	-2.89	2.94	-2.36	6.55	0.58	7.425	-2.375	80
80	2.37	-2.05	1.97	-1.62	4.36	0.39	4.963	-1.250	90
90	1.19	-1.10	0.97	-0.84	2.19	0.20	2.563	-0.713	95
95	0.61	-0.59	0.50	-0.42	1.10	0.10	1.350	-0.125	100
100	0	0	0	0	0	0	0.138		

<i>x</i>	<i>y<sub>u</sub></i> = - <i>y<sub>l</sub></i>	<i>y<sub>u</sub></i> = - <i>y<sub>l</sub></i>	<i>y<sub>u</sub></i>	<i>y<sub>l</sub></i>	<i>y<sub>u</sub></i>	<i>y<sub>l</sub></i>	<i>y<sub>u</sub></i>	<i>y<sub>l</sub></i>	<i>x</i>
	G6 775	776		777		780		795	
0	0	0	0	0	0	0	2.40	2.40	0
1.25	3.320	3.950	5.267	-1.417	0.0080	-0.0090	3.75	1.30	1.25
2.50	4.580	5.450	6.733	-2.133	0.0127	-0.0130	4.40	0.90	2.50
5.00	8.220	7.400	9.067	-3.017	0.0200	-0.0188	5.30	0.48	5.00
7.50	7.350	8.750	10.880	-3.500	0.0246	-0.0241	5.95	0.24	7.50
10	8.180	9.750	12.370	-3.883	0.0298	-0.0266	6.45	0.15	10
15	9.350	11.133	14.580	-4.483	0.0409	-0.0323	7.15	0	15
20	10.033	11.950	16.016	-4.867	0.0488	-0.0370	7.65	0	20
30	10.500	12.500	16.917	-5.083	0.0611	-0.0443	8.00	0	30
40	10.180	12.080	16.183	-4.917	0.0678	-0.0485	7.90	0	40
50	9.267	11.033	14.167	-4.517	0.0700	-0.0500	7.40	0	50
60	7.983	9.500	11.533	-3.700	0.0650	-0.0488	6.48	0	60
70	2.533	7.630	8.667	-2.783	0.0520	-0.0443	5.25	0	70
80	6.417	5.487	5.833	-1.900	0.0342	-0.0361	3.85	0	80
90	4.600	3.017	2.983	-1.033	0.0175	-0.0215	2.20	0	90
95	1.417	1.683	1.550	-0.833	0.0084	-0.0118	1.30	0.04	95
100	0.217	0.287	0.133	-0.133	0	0	0.40	0.10	100
	796		797		798		801		
0	3.60	3.60	4.80	4.80	6.00	6.00	1.20	1.20	0
1.25	5.62	1.95	7.50	2.60	9.38	3.25	3.80	0.00	1.25
2.50	6.60	1.35	8.80	1.80	11.00	2.25	5.15	0.00	2.50
5.00	7.95	0.72	10.60	0.96	13.25	1.20	6.80	0.20	5.00
7.50	8.92	0.36	11.90	0.48	14.88	0.60	8.00	0.40	7.50
10	9.68	0.22	12.90	0.30	16.12	0.38	8.90	0.60	10
15	10.72	0	14.30	0	17.88	0.10	10.20	1.00	15
20	11.48	0	15.30	0	19.12	0	11.10	1.40	20
30	12.00	0	16.00	0	20.00	0	11.80	2.00	30
40	11.85	0	15.80	0	19.75	0	11.60	2.20	40
50	11.10	0	14.80	0	18.50	0	10.75	2.10	50
60	9.72	0	12.96	0	16.20	0	9.45	1.95	60
70	7.88	0	10.50	0	13.12	0	7.70	1.60	70
80	5.78	0	7.70	0	9.62	0	5.50	1.00	80
90	3.30	0	4.40	0	5.50	0	3.00	0.50	90
95	1.95	0.06	2.60	0.08	3.25	0.10	1.70	0.25	95
100	0.60	0.15	0.80	0.20	1.00	0.25	0.40	0.00	100
	Clark Y		N 60		N 60 R		N 85		
0	3.50	-3.50	3.40	-3.40	3.40	-3.40	0	0	0
1.25	5.45	-1.93	5.60	-1.91	5.60	-1.91	1.77	-1.10	1.25
2.50	6.50	-1.47	6.76	-1.46	6.76	-1.46	2.60	-1.35	2.50
5.00	7.90	-0.93	8.24	-0.96	8.24	-0.96	3.75	-1.62	5.00
7.50	8.85	-0.63	9.33	-0.62	9.33	-0.62	4.53	-1.80	7.50
10	9.60	-0.42	10.14	-0.40	10.14	-0.40	5.07	-1.98	10
15	10.68	-0.15	11.32	-0.15	11.32	-0.15	5.66	-2.36	15
20	11.36	-0.03	11.98	-0.04	11.98	-0.04	6.93	-2.68	20
30	11.70	0	12.41	-0.04	12.41	-0.04	5.94	-3.06	30
40	11.40	0	12.03	-0.22	11.95	-0.14	5.57	-3.14	40
50	10.62	0	11.06	-0.48	10.79	-0.21	5.00	-2.95	50
60	9.15	0	9.55	-0.71	9.18	-0.34	4.25	-2.65	60
70	7.35	0	7.66	-0.78	7.42	-0.54	3.40	-2.17	70
80	5.22	0	5.50	-0.64	5.75	-0.89	2.47	-1.65	80
90	2.80	0	3.04	-0.37	4.28	-1.61	1.47	-1.08	90
95	1.49	0	1.72	-0.19	3.68	-2.13	1.47	-0.95	95
100	0.12	0	0.40	0	3.20	-2.80	0.50	-0.50	100
	N 86		N 87		LB 24		Zü 11		
0	0	0	0	0	0	0	0	0	0
1.25	1.50	-0.85	1.55	-0.73	0.945	-0.945	1.90	-1.15	1.25
2.50	2.35	-1.10	2.28	-0.88	1.417	-1.417	2.85	-1.42	2.50
5.00	3.45	-1.35	3.33	-1.03	1.983	-1.983	5.00		
7.50	4.20	-1.55	4.07	-1.15	2.420	-2.420	7.50		
10	4.83	-1.75	4.62	-1.30	2.790	-2.790	4.19	-1.74	10
15	5.47	-2.07	5.27	-1.72	3.388	-3.388			15
20	5.72	-2.50	5.60	-2.19	3.866	-3.866	5.81	-1.90	20
30	5.87	-3.07	5.85	-2.86	4.533	-4.533	6.80	-1.82	30
40	5.70	-3.25	5.79	-3.21	4.900	-4.900	7.23	-1.66	40
50	5.23	-3.18	5.43	-3.30	5.000	-5.000	7.23	-1.42	50
60	4.50	-2.96	4.81	-3.13	4.900	-4.900	6.92	-1.26	60
70	3.75	-2.50	4.01	-2.74	4.450	-4.450	6.17	-0.95	70
80	2.80	-1.91	2.99	-2.15	3.620	-3.620	4.86	-0.71	80
90	1.88	-1.24	1.79	-1.37	2.180	-2.180	2.88	-0.32	90
100	0.50	-0.50	0.50	-0.50	1.255	-1.255			100

$x$	$y_u = -y_l$	$y_u = -y_l$	$y_u = -y_l$	$y_u = -y_l$	$x$
	DVL 0 00 09—0·825 40	0 00 09—0·55 40	0 00 09—0·55 45	0 00 09—0·55 50	
0·625	0·872	0·752	0·737	0·727	0·625
1·250	1·221	1·061	1·030	1·012	1·250
2·500	1·684	1·499	1·441	1·405	2·500
5·000	2·294	2·109	2·004	1·936	5·000
7·500	2·726	2·561	2·419	2·324	7·500
10	3·064	2·925	2·755	2·638	10
15	3·571	3·484	3·282	3·135	15
20	3·933	3·881	3·682	3·520	20
30	4·366	4·350	4·215	4·070	30
40	4·500	4·500	4·469	4·392	40
50	4·370	4·370	4·468	4·600	50
60	3·987	3·987	4·206	4·376	60
70	3·358	3·358	3·660	3·952	70
80	2·493	2·493	2·808	3·149	80
90	1·401	1·401	1·625	1·888	90
95	0·772	0·773	0·903	1·061	95
100	0·090	0·090	0·090	0·090	100
	0 00 12—1·1 40 NACA 0012—64	0 00 12—0·825 40	0 00 12—0·55 40	0 00 12—0·275 40 NACA 0012—34	
0·625	1·321	1·163	1·003	0·779	0·625
1·250	1·808	1·628	1·414	1·136	1·250
2·500	2·453	2·245	1·998	1·677	2·500
5·000	3·267	3·059	2·812	2·490	5·000
7·500	3·820	3·635	3·414	3·128	7·500
10	4·241	4·085	3·900	3·658	10
15	4·860	4·762	4·645	4·493	15
20	5·297	5·244	5·175	5·098	20
30	5·828	5·821	5·812	5·801	30
40	6·000	6·000	6·000	6·000	40
50	5·827	5·827	5·827	5·827	50
60	5·316	5·316	5·316	5·316	60
70	4·477	4·477	4·477	4·477	70
80	3·324	3·324	3·324	3·324	80
90	1·868	1·868	1·868	1·868	90
95	1·030	1·030	1·030	1·030	95
100	0·120	0·120	0·120	0·120	100
	0 00 12—1·1 50 NACA 0012—65	0 00 15—0·55 40	0 00 15—1·1 50	0 00 18—0·55 40	
0·625	1·297	1·254	1·621	2·121	0·625
1·250	1·762	1·768	2·203	2·998	1·250
2·500	2·364	2·498	2·955	4·218	2·500
5·000	3·101	3·515	3·876	5·121	5·000
7·500	3·589	4·268	4·486	5·850	7·500
10	3·957	4·875	4·946	6·967	10
15	4·503	5·806	5·629	7·762	15
20	4·909	6·468	6·136	8·719	20
30	5·496	7·266	6·870	9·000	30
40	5·864	7·500	7·330	8·740	40
50	6·000	7·284	7·500	7·973	50
60	5·835	6·644	7·294	1·605	60
70	5·269	5·597	6·586	6·716	70
80	4·199	4·156	5·249	4·987	80
90	2·517	2·335	3·146	2·802	90
95	1·415	1·287	1·769	1·545	95
100	0·120	0·150	0·150	0·180	100

$x$	$y_u = -y_l$	$y_u = -y_l$	$x$	$y_u = -y_l$	$x$	$y_u = -y_l$
	<b>0 00 18-1·1 50</b>	<b>0 00 10·75-0·356 46·7</b>	<b>0 00 10·5-0·95 48</b>	<b>0 00 10·1-0·098 50</b>		
0·625	1·946	0·719				
1·250	2·643	1·017	1·047	1·047	0	0
2·500	3·546	1·430	3·208	1·446	2·344	0·541
5·000	4·652	2·034	5·648	1·852	4·687	0·976
7·500	5·334	2·492	9·715	2·432	7·031	1·389
10	5·936	2·877	12·155	2·808	0·375	1·779
15	6·754	3·524	15·409	3·244	15·625	2·710
20	7·363	4·064	21·916	3·967	21·875	3·483
30	8·244	4·865	31·876	4·748	31·250	4·350
40	8·797	5·295	41·437	5·168	40·625	4·868
50	9·000	5·356	51·197	5·228	50·000	5·041
60	8·752	5·049	60·968	4·929	59·375	4·868
70	7·904	4·373	70·718	4·268	68·750	4·350
80	6·298	3·323	80·479	3·244	78·125	3·483
90	3·776	1·897	90·239	1·852	90·622	1·779
95	2·122	1·041	95·120	1·016	95·312	0·976
100	0·180	0·088	100·000	0·086	100·000	0·083

$x$	$y_u = -y_l$	$y_u = -y_l$	$y_u = -y_l$	$y_u = -y_l$	$y_u = -y_l$	$y_u = -y_l$	$y_u = -y_l$	$y_u = -y_l$	$x$
	<b>NACA 0006</b>	<b>0009</b>	<b>0012</b>	<b>0015</b>	<b>0018</b>	<b>0021</b>	<b>0025</b>		
1·25	0·95	1·42	1·89	2·37	2·84	3·31	3·95		1·25
2·50	1·31	1·96	2·62	3·27	3·92	4·58	5·45		2·50
5·00	1·78	2·67	3·66	4·44	5·33	6·22	7·41		5·00
7·50	2·10	3·15	4·20	5·25	6·30	7·35	8·75		7·50
10	2·34	3·61	4·68	5·85	7·02	8·20	9·76		10
15	2·67	4·01	5·34	6·68	8·02	9·35	11·14		15
20	2·87	4·30	5·74	7·17	8·61	10·04	11·95		20
30	3·00	4·50	6·00	7·50	9·00	10·50	12·60		30
40	2·90	4·35	5·80	7·25	8·70	10·16	12·09		40
50	2·65	3·97	5·29	6·62	7·94	9·26	11·03		50
60	2·28	3·42	4·56	5·70	6·84	7·99	9·51		60
70	1·83	2·75	3·66	4·58	5·60	6·41	7·63		70
80	1·31	1·97	2·62	3·28	3·94	4·59	5·46		80
90	0·72	1·09	1·45	1·81	2·17	2·53	3·02		90
95	0·40	0·60	0·81	1·01	1·21	1·41	1·68		95
100	0·06	0·10	0·13	0·16	0·19	0·22	0·26		100
	<b>0030</b>	<b>0012-83</b>	<b>0015-84</b>	<b>0009-34</b>	<b>0009-35</b>	<b>0009-93</b>	<b>16-009</b>		
			<b>00015-1·1 40</b>						
1·25	4·74	1·91	2·287	0·85	0·79	2·12	0·969		1·25
2·50	6·54	2·65	3·067	1·26	1·14	2·74	1·354		2·50
5·00	8·89	3·62	4·083	1·87	1·66	3·40	1·882		5·00
7·50	10·60	4·28	4·767	2·35	2·06	3·76	2·274		7·50
10	11·71	4·76	5·300	2·74	2·40	3·99	2·593		10
15	13·36	5·41	6·083	3·37	2·96	4·25	3·101		15
20	14·34	5·79	6·617	3·82	3·41	4·39	3·498		20
30	15·00	6·00	7·283	4·35	4·03	4·50	4·063		30
40	14·61	5·85	7·500	4·50	4·39	4·38	4·391		40
50	13·24	5·41	7·283	4·37	4·50	4·06	4·500		50
60	11·41	4·72	6·650	3·99	4·38	3·54	4·376		60
70	9·16	3·81	5·600	3·36	3·35	2·86	3·952		70
80	6·56	2·72	4·150	2·49	3·15	2·04	3·149		80
90	3·62	1·48	2·333	1·40	1·89	1·11	1·888		90
95	2·02	0·81	1·283	0·77	1·06	0·61	1·061		95
100	0·31	0·12	0·150	0·09	0·09	0·09	0·090		100

<i>x</i>	$y_u = -y_l$	$y_u = -y_l$	$y_u = -y_l$	$y_u = -y_l$	$y_u = -y_l$	$y_u = -y_l$	$y_u = -y_l$	$y_u = -y_l$	<i>x</i>
	<b>63—006</b>	<b>63—009</b>	<b>63<sub>1</sub>—012</b>	<b>63<sub>2</sub>—015</b>	<b>63<sub>3</sub> A 015</b>	<b>63<sub>3</sub>—018</b>	<b>63<sub>4</sub>—021</b>		
0·50	0·503	0·749	0·985	1·204	1·203	1·404	1·583	0·50	
0·75	0·609	0·906	1·194	1·462	1·448	1·713	1·937	0·75	
1·25	0·771	1·151	1·519	1·878	1·844	2·217	2·627	1·25	
2·50	1·057	1·582	2·102	2·610	2·579	3·104	3·677	2·50	
5·00	1·462	2·186	2·925	3·648	3·618	4·362	5·065	5·00	
7·50	1·766	2·655	3·542	4·427	4·382	5·308	6·182	7·50	
10	2·010	3·024	4·039	5·055	4·997	6·068	7·080	10	
15	2·386	3·591	4·799	6·011	5·942	7·225	8·441	15	
20	2·656	3·997	5·342	6·693	6·619	8·048	9·410	20	
30	2·954	4·442	5·930	7·421	7·384	8·913	10·412	30	
40	2·971	4·447	5·920	7·386	7·435	8·845	10·298	40	
50	2·723	4·056	5·370	6·665	6·558	7·942	9·206	50	
60	2·267	3·358	4·420	5·453	5·820	6·455	7·441	60	
70	1·670	2·458	3·210	3·934	4·468	4·622	5·290	70	
80	1·008	1·471	1·902	2·310	2·991	2·691	3·054	80	
90	0·383	0·550	0·707	0·852	1·512	0·985	1·113	90	
95	0·138	0·196	0·250	0·300	0·772	0·348	0·392	95	
100	0	0	0	0	0·032	0	0	100	
	<b>64—006</b>	<b>64—009</b>	<b>64 A 010</b>	<b>64<sub>1</sub>—012</b>	<b>64<sub>2</sub>—015</b>	<b>64<sub>3</sub>—018</b>	<b>64<sub>4</sub>—021</b>		
0·50	0·494	0·739	0·804	0·978	1·208	1·428	1·646	0·50	
0·75	0·596	0·892	0·969	1·179	1·456	1·720	1·985	0·75	
1·25	0·754	1·128	1·225	1·490	1·842	2·177	2·517	1·25	
2·50	1·024	1·533	1·688	2·035	2·528	3·005	3·485	2·50	
5·00	1·405	2·109	2·327	2·810	3·504	4·186	4·871	5·00	
7·50	1·692	2·543	2·805	3·394	4·240	5·076	5·915	7·50	
10	1·928	2·808	3·199	3·871	4·842	5·803	6·769	10	
15	2·298	3·455	3·813	4·620	5·735	6·942	8·108	15	
20	2·572	3·866	4·272	5·173	6·480	7·782	9·095	20	
30	2·907	4·373	4·837	5·844	7·319	8·789	10·269	30	
40	2·995	4·490	4·995	5·981	7·473	8·952	10·431	40	
50	2·775	4·136	4·684	5·480	6·810	8·114	9·404	50	
60	2·331	3·452	4·021	4·548	5·620	6·658	7·678	60	
70	1·740	2·561	3·127	3·350	4·113	4·842	5·549	70	
80	1·072	1·564	2·103	2·029	2·472	2·888	3·287	80	
90	0·423	0·611	1·062	0·786	0·950	1·101	1·245	90	
95	0·157	0·227	0·541	0·288	0·346	0·400	0·449	95	
100	0	0	0·021	0	0	0	0	100	
	<b>NACA</b>								
	<b>65—006</b>	<b>65 A 006</b>	<b>65 A 008</b>	<b>65 A 010</b>	<b>65<sub>1</sub>—012</b>	<b>65<sub>1</sub> A 012</b>	<b>65<sub>2</sub>—015</b>		
0·50	0·476	0·464	0·615	0·765	0·923	0·913	1·124	0·50	
0·75	0·574	0·563	0·746	0·928	1·109	1·106	1·356	0·75	
1·25	0·717	0·718	0·951	1·183	1·387	1·414	1·702	1·25	
2·50	0·956	0·981	1·303	1·623	1·875	1·942	2·324	2·50	
5·00	1·310	1·313	1·749	2·182	2·606	2·614	3·245	5·00	
7·50	1·589	1·591	2·120	2·650	3·172	3·176	3·959	7·50	
10	1·824	1·824	2·432	3·040	3·647	3·647	4·655	10	
15	2·197	2·194	2·926	3·658	4·402	4·392	5·504	15	
20	2·482	2·474	3·301	4·127	4·975	4·956	6·223	20	
30	2·852	2·842	3·791	4·742	5·716	5·693	7·152	30	
40	2·998	2·998	3·995	4·995	5·997	5·995	7·498	40	
50	2·900	2·925	3·895	4·863	5·757	5·828	7·188	50	
60	2·518	2·602	3·456	4·304	4·943	5·143	6·118	60	
70	1·935	2·087	2·763	3·432	3·743	4·091	4·600	70	
80	1·233	1·437	1·898	2·352	2·345	2·798	2·858	80	
90	0·510	0·727	0·980	1·188	0·947	1·413	1·144	90	
95	0·195	0·370	0·489	0·604	0·356	0·719	0·428	95	
100	0	0·013	0·018	0·021	0	0·025	0	100	

$x$	$y_u = -y_l$	$y_u = -y_l$	$x$						
	<b>65<sub>4</sub>-021</b>	<b>66<sub>4</sub>-006</b>	<b>66<sub>4</sub>-009</b>	<b>66<sub>4</sub>-012</b>	<b>66<sub>4</sub>-015</b>	<b>66<sub>4</sub>-021</b>	<b>66<sub>(215)</sub>-016</b>		
0.50	1.522	0.461	0.687	0.906	1.122	1.525	1.184		0.50
0.75	1.638	0.554	0.824	1.087	1.343	1.804	1.418		0.75
1.25	2.301	0.693	1.030	1.358	1.675	2.240	1.755		1.25
2.50	3.154	0.918	1.368	1.808	2.235	3.045	2.378		2.50
5.00	4.472	1.257	1.880	2.496	3.100	4.289	3.292		5.00
7.50	5.498	1.524	2.233	3.037	3.781	5.233	4.007		7.50
10	6.362	1.752	2.626	3.496	4.358	6.052	4.628		10
15	7.700	2.119	3.178	4.234	5.286	7.369	5.605		15
20	8.720	2.401	3.601	4.801	5.995	8.376	6.362		20
30	10.036	2.782	4.173	5.568	6.956	9.738	7.395		30
40	10.499	2.971	4.457	5.947	7.430	10.407	7.909		40
50	9.952	2.985	4.475	5.965	7.450	10.434	7.957		50
60	8.390	2.815	4.204	5.588	6.059	9.692	7.425		60
70	6.224	2.316	3.428	4.515	5.576	7.610	5.970		70
80	3.800	1.543	2.263	2.944	3.598	4.796	3.849		80
90	1.484	0.665	0.961	1.234	1.489	1.924	1.587		90
95	0.646	0.262	0.374	0.474	0.566	0.717	0.597		95
100	0	0	0	0	0	0	0		100

$x_u$	$y_u$	$x_l$	$y_l$	$x_u$	$y_u$	$x_l$	$y_l$	$x_u$	$y_u$
<b>NACA 1408</b>									
1.189	1.324	1.311	-1.200	1.174	1.639	1.326	-1.515	1.158	1.954
2.418	1.862	2.582	-1.620	2.398	2.297	2.602	-2.055	2.378	2.733
4.896	2.602	5.104	-2.134	4.870	3.194	5.130	-2.726	4.845	3.786
7.386	3.138	7.614	-2.458	7.358	3.837	7.642	-3.157	7.330	4.537
9.883	3.558	10.117	-2.682	9.854	4.338	10.146	-3.462	9.824	5.118
14.989	4.171	15.111	-2.983	14.861	5.062	15.139	-3.844	14.833	5.951
19.904	4.574	20.086	-3.074	19.880	5.531	20.120	-4.031	19.857	6.486
24.926	4.819	25.074	-3.101	24.907	5.809	25.093	-4.091	24.889	6.799
29.950	4.939	30.050	-3.083	29.937	5.940	30.063	-4.064	29.925	6.940
40.000	4.869	40.000	-2.869	40.000	5.836	40.000	-3.836	40.000	6.803
50.020	4.502	49.980	-2.556	50.025	5.385	49.975	-3.439	50.029	6.267
60.034	3.931	59.966	-2.153	60.042	4.692	59.958	-2.914	60.051	5.453
70.041	3.193	69.959	-1.693	70.051	3.804	69.949	-2.304	70.061	4.413
80.039	2.305	79.961	-1.193	80.049	2.741	79.951	-1.629	80.058	3.178
90.027	1.271	89.973	-0.659	90.034	1.513	89.966	-0.901	90.040	1.753
95.018	0.698	94.984	-0.378	95.021	0.832	94.979	-0.512	95.025	0.966
100.000	0.084	100.000	-0.084	100.000	0.105	100.000	-0.105	100.000	0.126

$x_l$	$y_l$
<b>NACA 1410</b>	
1.639	1.326
2.297	2.602
3.194	5.130
4.338	7.642
5.062	10.146
5.385	15.139
5.531	20.120
5.809	25.093
5.940	30.063
5.836	40.000
5.385	49.975
5.692	59.958
5.804	69.949
5.849	79.951
5.113	89.966
4.832	94.979
4.062	100.000
<b>NACA 1412</b>	
1.158	1.954
2.378	2.733
4.845	3.786
5.156	4.537
7.330	4.537
7.670	3.857
10.176	4.242
15.167	4.733
20.143	4.986
25.111	5.081
30.075	5.064
40.000	4.803
49.971	4.321
59.949	3.675
69.939	2.913
79.942	2.066
89.960	1.141
94.975	0.646
100.000	0.126
<b>NACA 847 B 110</b>	
0.792	0.555
0.812	-0.847
1.321	-1.055
2.580	-1.400
5.082	-1.871
7.579	-2.233
10.074	-2.637
15.058	-3.038
20.038	-3.447
25.015	-3.784
29.989	-4.057
39.913	-4.426
49.859	-4.499
59.881	-4.293
69.963	-3.722
75.018	-3.207
80.043	-2.517
85.035	-1.744
90.018	-0.976
95.001	-0.299
100.000	0
<b>NACA 836 D 110</b>	
0.769	0.558
0.812	-0.808
1.204	1.315
1.694	2.564
4.898	2.406
7.406	2.959
9.913	3.422
14.942	4.135
19.977	4.650
30.071	5.204
40.149	5.119
50.139	4.558
60.051	3.709
64.995	3.251
69.941	2.793
74.932	2.325
79.941	1.847
84.964	1.366
89.985	0.885
95.001	0.427
100.000	0
<b>NACA 1408</b>	
1.324	-1.200
2.582	-1.620
5.104	-2.134
7.614	-2.458
10.117	-2.682
15.111	-2.983
20.086	-3.074
25.074	-3.101
30.050	-3.083
40.000	-2.869
50.025	-2.556
60.042	-2.153
70.051	-1.693
80.049	-1.193
90.034	-0.659
100.000	-0.084

<i>x</i>	<i>y<sub>u</sub></i>	<i>y<sub>l</sub></i>	<i>y<sub>u</sub></i>	<i>y<sub>l</sub></i>	<i>y<sub>u</sub></i>	<i>y<sub>l</sub></i>	<i>y<sub>u</sub></i>	<i>y<sub>l</sub></i>	<i>x</i>
NACA 2409									
1.25	1.62	-1.23	2.15	-1.65	2.710	-2.060	3.280	-2.450	1.25
2.50	2.27	-1.66	2.99	-2.27	3.710	-2.860	4.450	-3.440	2.50
5.00	3.20	-2.15	4.13	-3.01	5.070	-3.840	6.030	-4.680	5.00
7.50	3.87	-2.44	4.96	-3.46	6.060	-4.470	7.170	-5.480	7.50
10	4.43	-2.60	5.63	-3.75	6.830	-4.900	8.050	-6.030	10
15	5.25	-2.77	6.61	-4.10	7.970	-5.420	9.340	-6.740	15
20	5.81	-2.79	7.26	-4.23	8.700	-5.660	10.150	-7.090	20
30	6.38	-2.62	7.88	-4.12	9.380	-5.620	10.880	-7.120	30
40	6.35	-2.35	7.80	-3.80	9.250	-5.250	10.710	-6.710	40
50	5.92	-2.02	7.24	-3.34	8.570	-4.670	9.890	-5.990	50
60	5.22	-1.63	6.36	-2.76	7.500	-3.900	8.650	-5.040	60
70	4.27	-1.24	5.18	-2.14	6.100	-3.050	7.020	-3.970	70
80	3.10	-0.85	3.75	-1.50	4.410	-2.150	5.080	-2.800	80
90	1.72	-0.47	2.08	-0.82	2.450	-1.170	2.810	-1.530	90
95	0.94	-0.28	1.14	-0.48	1.340	-0.680	1.650	-0.870	95
100	0.10	-0.10	0.13	-0.13	0.160	-0.160	0.190	-0.190	100
2412									
2415									
2418									
2421									
23006									
23009									
23012									
23015									
23018									
23021									
2209-34									
2409-34									
23012-33									
23012-34									
23012-64									
1.25	1.00	-0.70	1.90	-0.77	1.67	-0.67	2.53	-1.20	1.25
2.50	1.53	-1.00	2.89	-1.15	2.54	-0.90	3.41	-1.61	2.50
5.00	2.39	-1.37	4.34	-1.70	3.80	-1.25	4.59	-2.00	5.00
7.50	3.08	-1.63	5.38	-2.18	4.71	-1.58	5.41	-2.27	7.50
10	3.67	-1.83	6.15	-2.62	5.40	-1.91	6.00	-2.50	10
15	4.61	-2.12	7.08	-3.40	6.34	-2.64	6.70	-3.02	15
20	5.34	-2.31	7.49	-3.98	6.86	-3.35	7.04	-3.55	20
30	6.23	-2.47	7.55	-4.46	7.34	-4.27	7.37	-4.29	30
40	6.50	-2.50	7.11	-4.46	7.33	-4.67	7.32	-4.66	40
50	6.32	-2.42	6.52	-4.30	6.95	-4.71	6.93	-4.70	50
60	5.77	-2.21	5.61	-3.83	6.20	-4.43	6.21	-4.42	60
70	4.87	-1.85	4.48	-3.14	5.16	-3.80	5.17	-3.79	70
80	3.63	-1.37	3.16	-2.26	3.79	-2.87	3.78	-2.86	80
90	2.03	-0.78	1.70	-1.25	2.10	-1.65	2.09	-1.63	90
95	1.09	-0.44	0.93	-0.70	1.15	-0.91	1.15	-0.90	95
100	0.09	-0.09	0.12	-0.12	0.12	-0.12	0.12	-0.12	100

	$x_u$	$y_u$		$x_l$	$y_l$		$x_u$	$y_u$		$x_l$	$y_l$	
<b>NACA 63-209</b>												
0-437	0-796	0-563		-0-696	0-423		0-868	0-577		-0-756		
0-680	0-973	0-820		-0-833	0-684		1-058	0-836		-0-900		
1-170	1-255	1-330		-1-041	1-151		1-367	1-349		-1-125		
2-408	1-765	2-592		-1-393	2-384		1-944	2-616		-1-522		
4-897	2-510	5-103		-1-878	4-869		2-769	5-131		-2-047		
7-394	3-077	7-606		-2-229	7-364		3-400	7-636		-2-428		
9-894	3-539	10-106		-2-605	9-863		3-917	10-137		-2-725		
14-901	4-263	15-099		-2-917	14-869		4-729	15-131		-3-167		
19-912	4-792	20-088		-3-200	19-882		5-328	20-118		-3-468		
24-925	5-169	25-075		-3-379	24-898		5-764	25-102		-3-662		
29-940	5-414	30-060		-3-470	29-916		6-060	30-084		-3-764		
34-956	5-630	35-044		-3-470	34-935		6-219	35-065		-3-771		
39-971	5-518	40-029		-3-378	39-955		6-247	40-045		-3-689		
44-986	5-391	45-014		-3-201	44-975		6-151	45-025		-3-523		
50-000	5-159	50-000		-2-953	49-994		5-943	50-006		-3-283		
60-022	4-429	59-978		-2-287	60-028		5-245	59-972		-2-641		
70-033	3-430	69-967		-1-486	70-052		4-227	69-948		-1-861		
80-032	2-267	79-968		-0-675	80-074		2-974	79-926		-1-104		
90-019	1-067	89-981		-0-033	90-050		1-519	89-950		-0-539		
95-009	0-512	94-991		0-120	95-026		0-769	94-974		-0-279		
100-000	0	100-000		0	100-000		0-021	100-000		-0-021		

	<b>63<sub>1</sub>-212</b>			<b>64 A 210</b>								
0-417	1-032	0-583		-0-932	0-424		0-856	0-576		-0-744		
0-657	1-260	0-843		-1-120	0-865		1-044	0-835		-0-886		
1-145	1-622	1-355		-1-408	1-153		1-342	1-347		-1-100		
2-378	2-284	2-622		-1-912	2-387		1-895	2-613		-1-473		
4-863	3-238	5-137		-2-606	4-874		2-685	5-126		-1-963		
7-358	3-963	7-642		-3-115	7-369		3-288	7-631		-2-316		
9-859	4-554	10-141		-3-520	9-868		3-792	10-132		-2-600		
14-868	5-470	15-132		-4-124	14-874		4-592	15-126		-3-030		
19-882	6-137	20-118		-4-545	19-885		5-200	20-115		-3-340		
24-900	6-606	25-100		-4-816	24-900		5-656	25-100		-3-554		
29-920	6-901	30-080		-4-957	29-917		5-984	30-083		-3-688		
34-941	7-030	35-059		-4-970	34-935		6-192	35-065		-3-744		
39-962	6-991	40-038		-4-849	39-955		6-274	40-045		-3-716		
44-982	6-799	45-018		-4-609	44-975		6-208	45-025		-3-580		
50-000	6-473	50-000		-4-287	49-994		6-014	50-006		-3-354		
60-029	5-491	59-971		-3-349	60-028		5-323	59-972		-2-719		
70-043	4-182	69-957		-2-238	70-054		4-310	69-946		-1-944		
80-042	2-698	79-958		-1-106	80-076		3-037	79-924		-1-167		
90-025	1-224	89-975		-0-190	90-052		1-551	89-948		-0-571		
95-012	0-566	94-988		0-068	95-027		0-785	94-974		-0-295		
100-000	0	100-000		0	100-000		0-021	100-000		-0-021		

	<b>64<sub>1</sub> A 212</b>			<b>65-210</b>								
0-409	1-013	0-591		-0-901	0-435		0-819	0-565		-0-719		
0-648	1-233	0-852		-1-075	0-878		0-999	0-822		-0-859		
1-135	1-580	1-365		-1-338	1-169		1-273	1-331		-1-059		
2-365	2-225	2-635		-1-803	2-408		1-757	2-592		-1-385		
4-849	3-145	5-151		-2-423	4-898		2-491	5-102		-1-859		
7-343	3-846	7-567		-2-874	7-394		3-069	7-606		-2-221		
9-842	4-432	10-158		-3-240	9-894		3-555	10-106		-2-521		
14-849	5-358	15-151		-3-796	14-899		4-338	15-101		-2-992		
19-862	6-060	20-138		-4-200	19-909		4-938	20-091		-3-346		
24-880	6-584	25-120		-4-482	24-921		5-397	25-079		-3-607		
29-900	6-956	30-100		-4-660	29-936		5-732	30-064		-3-788		
34-922	7-189	35-078		-4-741	34-951		5-954	35-049		-3-894		
39-946	7-272	40-054		-4-714	39-968		6-067	40-032		-3-925		
44-970	7-177	45-030		-4-549	44-984		6-058	45-016		-3-868		
49-993	6-935	50-007		-4-275	50-000		5-915	50-000		-3-709		
60-034	6-103	59-966		-3-499	60-027		5-217	59-973		-3-075		
70-064	4-903	69-936		-2-537	70-043		4-128	69-957		-2-184		
80-090	3-433	79-910		-1-563	80-044		2-783	79-956		-1-191		
90-062	1-751	89-938		-0-771	90-028		1-327	89-972		-0-293		
95-032	0-888	94-968		-0-398	95-014		0-622	94-986		0-010		
100-000	0-025	100-000		-0-025	100-000		0	100-000		0		

	$x_u$	$y_u$	$x_l$	$y_l$		$x_u$	$y_u$	$x_l$	$y_l$	
<b>NACA 65<sub>2</sub>-215 (a = 0.5)</b>										
0.370	1.185	0.630	-1.047	0.379	1.168	0.621	-1.038			
0.606	1.445	0.895	-1.251	0.616	1.413	0.884	-1.231			
1.086	1.841	1.414	-1.547	1.101	1.777	1.399	-1.499			
2.311	2.675	2.689	-2.057	2.329	2.466	2.671	-1.973			
4.786	3.679	5.214	-2.797	4.807	3.496	5.193	-2.664			
7.276	4.547	7.724	-3.359	7.298	4.313	7.702	-3.191			
9.774	5.274	10.226	-3.822	9.794	5.019	10.206	-3.645			
14.783	6.448	15.217	-4.552	14.301	6.150	15.199	-4.352			
19.806	7.344	20.194	-5.096	19.818	7.030	20.182	-4.892			
24.835	8.024	25.165	-5.500	29.871	8.245	30.129	-5.617			
29.871	8.519	30.129	-5.783	34.904	8.622	35.096	-5.836			
34.912	8.838	35.088	-5.982	39.910	8.862	40.080	-5.968			
39.958	8.984	40.042	-6.012	44.979	8.969	45.021	-6.021			
45.009	8.925	44.991	-5.929	50.021	8.931	49.979	-5.986			
50.076	8.638	49.924	-5.698	55.069	8.738	54.931	-5.860			
60.154	7.306	59.846	-4.834	60.132	8.336	59.868	-5.684			
70.147	5.589	69.853	-3.607	70.186	6.695	69.814	-4.493			
80.100	3.509	79.900	-2.203	80.139	4.352	79.861	-2.874			
90.039	1.450	89.961	-0.836	90.057	1.838	89.943	-1.136			
95.013	0.572	94.987	-0.284	95.020	0.725	94.980	-0.395			
100.000	0	100.000	0	100.000	0	100.000	0			

	<b>66 (215)-216</b>					<b>67·1-215</b>				
0.401	1.230	0.599	-1.130	0.402	1.213	0.598	-1.113			
0.640	1.484	0.860	-1.344	0.642	1.460	0.858	-1.320			
1.128	1.858	1.372	-1.644	1.128	1.867	1.372	-1.653			
2.362	2.560	2.638	-2.188	2.361	2.577	2.639	-2.205			
4.846	3.604	5.154	-2.972	4.848	3.557	5.152	-2.925			
7.340	4.428	7.660	-3.580	7.344	4.321	7.656	-3.473			
9.838	5.140	10.182	-4.106	9.845	4.947	10.155	-3.913			
14.845	6.276	15.155	-4.930	14.354	5.954	15.148	-4.608			
19.860	7.156	20.140	-5.564	19.869	6.735	20.131	-5.143			
24.879	7.844	25.121	-6.054	24.887	7.348	25.113	-5.558			
29.900	8.366	30.100	-6.422	29.908	7.825	30.092	-5.881			
34.924	8.736	35.076	-6.676	34.930	8.185	35.070	-6.125			
39.949	8.980	40.051	-6.838	39.953	8.430	40.047	-6.288			
44.974	9.092	45.026	-6.902	44.976	8.570	45.024	-6.380			
50.000	9.060	50.000	-6.854	50.000	8.600	50.000	-6.394			
60.048	8.496	59.952	-6.354	60.047	8.302	59.953	-6.160			
70.081	6.941	69.919	-4.997	70.086	7.373	69.914	-5.429			
80.085	4.644	79.915	-3.052	80.100	5.335	79.900	-3.743			
90.055	2.103	89.945	-1.069	90.071	2.537	89.929	-1.503			
95.028	0.913	94.972	-0.281	95.037	1.103	94.963	-0.471			
100.000	0	100.000	0	100.000	0	100.000	0			

	<b>0010 (a = 1, C<sub>L</sub><sup>*</sup> = 0.3)</b>					<b>64 A 310</b>				
1.086	1.731	1.414	-1.409	0.399	0.873	0.601	-0.723			
2.310	2.449	2.690	-1.891	0.638	1.068	0.862	-0.858			
4.792	3.429	5.208	-2.481	1.123	1.379	1.377	-1.057			
7.290	4.130	7.710	-2.858	2.353	1.961	2.647	-1.403			
9.796	4.672	10.204	-3.122	4.837	2.759	5.163	-1.847			
14.816	5.460	15.184	-3.442	7.332	3.436	7.668	-2.164			
19.842	5.973	20.158	-3.585	9.532	3.970	10.168	-2.420			
24.870	6.293	25.130	-3.607	14.842	4.819	15.158	-2.809			
29.899	6.459	30.101	-3.543	19.859	5.484	20.141	-3.076			
39.953	6.443	40.047	-3.231	24.879	5.946	25.121	-3.262			
50.000	6.066	50.000	-2.758	29.902	6.294	30.098	-3.378			
60.037	5.409	59.963	-2.197	34.927	6.513	35.073	-3.423			
70.062	4.512	69.938	-1.594	39.952	6.601	40.048	-3.389			
80.072	3.380	79.928	-0.992	44.977	6.536	45.023	-3.252			
90.063	1.980	89.937	-0.430	50.000	6.334	50.000	-3.030			
95.047	1.144	94.953	-0.196	60.039	5.627	59.961	-2.415			
100.000	0.105	100.000	-0.105	70.063	4.584	69.937	-1.668			
				80.070	3.296	79.930	-0.908			
				90.056	1.836	89.944	-0.286			
				95.038	1.014	94.962	-0.065			
				100.000	0.021	100.000	-0.021			

	$x_u$	$y_u$	$x_l$	$y_l$	
<b>NACA 747 A 315</b>					
	0.229	1.305	0.771	-1.031	
	0.449	1.599	1.051	-1.207	
	0.911	2.065	1.589	-1.473	
	2.109	2.935	2.891	-1.927	
	4.564	4.264	5.436	-2.518	
	7.053	5.286	7.947	-2.952	
	9.558	6.140	10.442	-3.304	
	14.599	7.497	15.401	-3.843	
	19.668	8.503	20.332	-4.247	
	24.758	9.242	25.242	-4.546	
	29.887	9.731	30.133	-4.773	
	40.200	9.962	39.800	-5.020	
	50.447	8.964	49.553	-5.014	
	60.435	7.324	59.565	-4.772	
	70.241	5.384	69.759	-4.110	
	80.073	3.295	79.927	-2.743	
	90.016	1.289	89.984	-1.097	
	95.004	0.481	94.996	-0.405	
	100.000	0	100.000	0	

$x$	$y_u$	$y_l$	$y_u$	$y_l$	$y_u$	$y_l$	$y_u$	$y_l$	$x$
<b>NACA 4406</b>									
1.25	1.25	-0.64	1.81	-1.05	2.44	-1.43	3.07	-1.79	1.25
2.50	1.88	-0.79	2.61	-1.37	3.39	-1.95	4.17	-2.48	2.50
5.00	2.79	-0.82	3.74	-1.65	4.73	-2.49	5.74	-3.27	5.00
7.50	3.53	-0.73	4.64	-1.74	5.76	-2.74	6.91	-3.71	7.50
10	4.15	-0.60	5.37	-1.73	6.59	-2.86	7.84	-3.98	10
15	5.15	-0.25	6.52	-1.55	7.89	-2.88	9.27	-4.18	15
20	5.90	0.12	7.33	-1.30	8.80	-2.74	10.25	-4.15	20
30	6.76	0.74	8.25	-0.76	9.76	-2.26	11.25	-3.75	30
40	6.90	1.10	8.35	-0.35	9.80	-1.80	11.25	-3.25	40
50	6.55	1.24	7.87	-0.07	9.19	-1.40	10.53	-2.72	50
60	5.95	1.27	7.00	0.14	8.14	-1.00	9.30	-2.14	60
70	4.85	1.18	5.76	0.26	6.69	-0.65	7.63	-1.55	70
80	3.56	0.91	4.21	0.26	4.89	-0.39	5.55	-1.03	80
90	1.96	0.49	2.33	0.14	2.71	-0.22	3.08	-0.57	90
95	1.05	0.24	1.26	0.03	1.47	-0.16	1.67	-0.36	95
100	0.06	-0.06	0.09	0.09	0.13	-0.13	0.16	-0.16	100

	<b>4418</b>		<b>4421</b>		<b>43012</b>		<b>4409-34</b>		
1.25	3.76	-2.11	4.45	-2.42	3.55	-0.82	1.17	-0.54	1.25
2.50	5.00	-2.99	5.84	-3.48	4.71	-1.00	1.83	-0.73	2.50
5.00	6.75	-4.06	7.82	-4.78	6.33	-1.06	2.90	-0.90	5.00
7.50	8.06	-4.67	9.24	-5.62	7.42	-1.09	3.80	-0.95	7.50
10	9.11	-5.06	10.35	-6.15	8.20	-1.21	4.58	-0.96	10
15	10.66	-5.49	12.04	-6.75	9.02	-1.66	5.86	-0.90	15
20	11.72	-5.66	13.17	-6.98	9.26	-2.22	6.85	-0.81	20
30	12.76	-5.26	14.27	-6.76	9.10	-2.91	8.11	-0.60	30
40	12.70	-4.70	14.16	-6.16	8.48	-3.15	8.50	-0.50	40
50	11.85	-4.02	13.18	-5.34	7.53	-3.07	8.27	-0.48	50
60	10.44	-3.24	11.60	-4.44	6.35	-2.78	7.58	-0.43	60
70	8.55	-2.45	9.50	-3.35	5.00	-2.32	6.40	-0.35	70
80	6.22	-1.67	6.91	-2.31	3.52	-1.73	4.77	-0.26	80
90	3.46	-0.93	3.85	-1.27	1.90	-1.00	1.41	-0.14	90
95	1.89	-0.55	2.11	-0.74	1.02	-0.58	2.67	-0.18	95
100	0.19	-0.19	0.22	-0.22	0.13	-0.13	0.09	-0.09	100

$x_u$	$y_u$	$x_l$	$y_l$	$x_u$	$y_u$	$x_l$	$y_l$
NACA 63 <sub>2</sub> -415							
0.300	1.287	0.700	-1.087	0.215	1.790	0.785	-1.590
0.625	1.585	0.975	-1.305	0.430	2.196	1.070	-1.916
0.991	2.074	1.509	-1.646	0.887	2.827	1.613	-2.399
2.198	2.964	2.802	-2.220	2.082	3.954	2.918	-3.210
4.660	4.264	5.340	-3.000	4.538	5.557	5.462	-4.293
7.147	5.261	7.853	-3.565	7.024	6.793	7.976	-5.097
9.647	6.077	10.353	-4.009	9.526	7.817	10.474	-5.749
14.669	7.348	15.331	-4.656	14.554	9.424	15.446	-6.732
19.705	8.279	20.295	-5.095	19.603	10.589	20.397	-7.405
24.750	8.941	25.250	-5.361	24.663	11.414	25.337	-7.834
29.800	9.362	30.200	-5.474	29.732	11.895	30.268	-8.007
34.852	9.559	35.148	-5.439	34.803	12.036	35.197	-7.916
39.905	9.527	40.095	-5.243	39.874	11.906	40.126	-7.622
44.955	9.289	45.045	-4.909	44.940	11.556	45.060	-7.176
50.000	8.871	50.000	-4.459	50.000	11.025	50.000	-6.613
60.070	7.595	59.930	-3.311	60.095	9.492	59.905	-5.208
70.106	5.877	69.894	-1.989	70.148	7.438	69.852	-3.550
80.102	3.900	79.898	-0.716	80.150	4.990	79.850	-1.806
90.059	1.884	89.941	-0.184	90.094	2.379	89.906	-0.311
95.028	0.931	94.972	-0.333	95.047	1.131	94.953	-0.133
100.000	0	100.000	0	100.000	0	100.000	0

63 <sub>4</sub> -421				63 (420)-422			
0	0	0	0	0.187	1.959	0.813	-1.759
0.237	1.661	0.763	-1.461	0.398	2.402	1.650	-2.660
0.452	2.054	1.048	-1.774	0.850	3.088	2.959	-3.568
0.902	2.717	1.598	-2.289	2.041	4.312	1.102	-2.122
2.086	3.925	2.914	-3.181	4.492	6.050	5.508	-4.786
4.527	5.675	5.473	-4.411	6.977	7.387	8.023	-5.691
7.007	7.010	7.993	-5.314	9.478	8.496	10.522	-6.428
9.506	8.097	10.494	-6.029	14.509	10.231	15.491	-7.539
14.535	9.774	15.465	-7.082	19.563	11.489	20.437	-8.305
19.555	10.993	20.415	-7.809	24.630	12.377	25.370	-8.797
24.649	11.837	25.351	-8.257	29.705	12.890	30.295	-9.002
29.719	12.352	30.281	-8.464	34.784	13.034	35.216	-8.914
34.793	12.558	35.207	-8.438	39.861	12.883	40.139	-8.599
39.867	12.439	40.133	-8.155	44.934	12.493	45.066	-8.113
44.937	12.044	45.063	-7.664	50.000	11.907	50.000	-7.495
50.000	11.412	50.000	-7.000	60.104	10.227	59.896	-5.943
60.096	9.582	59.904	-5.298	70.163	7.988	69.837	-4.100
70.143	7.232	69.857	-3.344	80.165	5.329	79.935	-2.145
80.135	4.643	79.865	-1.459	90.103	2.613	89.897	-0.445
90.078	2.144	89.922	-0.076	95.051	1.181	94.949	-0.083
100.000	0	100.000	0	100.000	0	100.000	0

64-409				64 A 410			
0.377	0.829	0.623	-0.629	0.350	0.902	0.650	-0.678
0.613	1.021	0.887	-0.741	0.582	1.112	0.918	-0.796
1.095	1.331	1.405	-0.903	1.059	1.451	1.441	-0.969
2.322	1.895	2.678	-1.151	2.276	2.095	2.724	-1.251
4.803	2.732	5.197	-1.468	4.749	3.034	5.251	-1.592
7.297	3.383	7.703	-1.687	7.230	3.865	7.770	-1.919
9.798	3.925	10.202	-1.857	9.737	4.380	10.263	-1.996
14.810	4.796	15.190	-2.104	14.748	5.366	15.252	-2.244
19.830	5.456	20.170	-2.272	19.770	6.126	20.230	-2.406
24.854	5.957	25.146	-2.377	24.800	6.705	25.200	-2.499
29.882	6.315	30.118	-2.427	29.834	7.131	30.166	-2.537
34.912	6.538	35.088	-2.418	34.871	7.414	35.129	-2.518
39.942	6.632	40.058	-2.348	39.910	7.552	40.090	-2.436
44.972	6.554	45.028	-2.174	44.950	7.522	45.050	-2.266
50.000	6.342	50.000	-1.930	49.989	7.344	50.011	-2.024
60.045	5.594	59.955	-1.310	60.057	6.624	59.943	-1.418
70.069	4.504	69.931	-0.616	70.108	5.490	69.892	-0.760
80.069	3.154	79.931	-0.030	80.151	3.967	79.849	-0.229
90.043	1.644	89.957	-0.424	90.104	2.038	89.896	-0.076
95.021	0.658	94.979	-0.406	95.053	1.028	94.947	-0.048
100.000	0	100.000	0	100.000	0.021	100.000	-0.021

	$x_u$	$y_u$		$x_l$	$y_l$		$x_u$	$y_u$		$x_l$	$y_l$	
<b>NACA 64<sub>1</sub>-412</b>												
0.338	1.064		0.662	-0.864		0.299	1.291		0.701	-1.091		
0.569	1.305		0.931	-1.025		0.526	1.579		0.974	-1.299		
1.045	1.690		1.455	-1.262		0.986	2.038		1.504	-1.610		
2.264	2.393		2.736	-1.649		2.207	2.883		2.793	-2.139		
4.738	3.430		5.262	-2.166		4.873	4.121		5.327	-2.857		
7.229	4.231		7.771	-2.535		7.162	5.075		7.838	-3.379		
9.730	4.896		10.270	-2.828		9.662	5.864		10.338	-3.796		
14.745	5.959		15.255	-3.267		14.881	7.122		15.319	-4.430		
19.772	6.780		20.228	-3.576		19.714	8.066		20.286	-4.882		
24.805	7.363		25.195	-3.783		24.756	8.771		25.244	-5.191		
29.842	7.786		30.158	-3.898		29.803	9.260		30.197	-5.372		
34.882	8.037		35.118	-3.917		34.853	9.541		35.147	-5.421		
39.923	8.123		40.077	-3.839		39.904	9.614		40.098	-5.330		
44.963	7.988		45.037	-3.608		44.954	9.414		45.046	-5.034		
50.000	7.686		50.000	-3.274		50.000	9.016		50.000	-4.604		
60.059	6.690		59.941	-2.406		60.072	7.762		59.928	-3.478		
70.090	5.293		69.910	-1.405		70.111	6.055		69.889	-2.187		
80.089	3.619		79.911	-0.435		80.109	4.062		79.891	-0.878		
90.055	1.818		89.945	-0.250		90.066	1.982		89.934	-0.086		
95.027	0.919		94.973	-0.345		95.032	0.976		94.968	-0.288		
100.000	0		100.000	0		100.000	0		100.000	0		

	$x_u$	$y_u$		$x_l$	$y_l$		$x_u$	$y_u$		$x_l$	$y_l$	
<b>64<sub>3</sub>-418</b>												
0.263	1.508		0.737	-1.308		0.313	1.208		0.687	-1.008		
0.486	1.840		1.014	-1.560		0.542	1.480		0.958	-1.200		
0.950	2.370		1.550	-1.942		1.016	1.900		1.484	-1.472		
2.152	3.357		2.848	-2.613		2.231	2.680		2.769	-1.936		
4.609	4.800		5.391	-3.536		4.697	3.863		5.303	-2.599		
7.095	5.908		7.905	-4.212		7.184	4.794		7.816	-3.098		
9.595	6.823		10.405	-4.755		9.682	5.578		10.318	-3.510		
14.617	8.277		15.383	-5.585		14.697	6.842		15.303	-4.150		
19.657	9.366		20.343	-6.182		19.726	7.809		20.274	-4.626		
24.707	10.176		25.293	-6.596		24.764	8.550		25.236	-4.970		
29.763	10.730		30.237	-6.842		29.807	9.093		30.193	-5.205		
34.823	11.037		35.177	-6.917		34.854	9.455		35.148	-5.336		
39.885	11.093		40.115	-6.809		39.903	9.639		40.097	-5.355		
44.945	10.820		45.055	-6.440		44.953	9.617		45.047	-5.237		
50.000	10.320		50.000	-5.908		50.000	9.374		50.000	-4.962		
60.086	8.799		59.914	-4.515		60.079	8.260		59.921	-3.976		
70.131	6.784		69.869	-2.896		70.124	6.542		69.876	-2.654		
80.127	4.477		79.873	-1.293		80.126	4.447		79.874	-1.263		
90.077	2.132		89.923	-0.064		90.080	2.175		89.920	-0.107		
95.037	1.030		94.963	-0.234		95.040	1.058		94.960	-0.206		
100.000	0		100.000	0		100.000	0		100.000	0		

	$x_u$	$y_u$		$x_l$	$y_l$		$x_u$	$y_u$		$x_l$	$y_l$	
<b>65<sub>3</sub>-415 (<math>a = 0.5</math>)</b>												
0.245	1.233		0.755	-0.957		0.278	1.418		0.722	-1.218		
0.484	1.520		1.036	-1.132		0.503	1.729		0.997	-1.449		
0.927	1.965		1.573	-1.377		0.973	2.209		1.527	-1.781		
2.126	2.812		2.874	-1.776		2.181	3.104		2.819	-2.360		
4.674	4.099		5.426	-2.335		4.639	4.481		5.361	-3.217		
7.054	5.122		7.946	-2.746		7.123	5.566		7.877	-3.870		
9.549	5.985		10.451	-3.081		9.619	6.478		10.381	-4.410		
14.668	7.383		15.432	-3.591		14.636	7.942		15.384	-5.250		
19.611	8.459		20.389	-3.963		19.671	9.061		20.329	-5.877		
24.671	9.280		25.329	-4.232		24.716	9.914		25.284	-6.334		
29.743	9.883		30.257	-4.411		29.768	10.536		30.232	-6.648		
34.825	10.280		35.175	-4.508		34.825	10.944		35.175	-6.824		
39.916	10.470		40.084	-4.526		39.884	11.140		40.116	-6.856		
45.019	10.423		44.981	-4.431		44.943	11.091		45.057	-6.711		
50.152	10.106		49.848	-4.226		50.000	10.774		50.000	-6.362		
60.307	8.672		59.693	-3.548		60.094	9.408		59.906	-5.124		
70.294	6.573		69.706	-2.609		70.146	7.368		69.854	-3.480		
80.199	4.157		79.801	-1.545		80.147	4.927		79.853	-1.743		
90.077	1.755		89.923	-0.527		90.092	2.350		89.908	-0.282		
95.027	0.715		94.973	-0.139		95.046	1.120		94.954	-0.144		
100.000	0		100.000	0		100.000	0		100.000	0		

$x_u$	$y_u$	$x_l$	$y_l$	$x_u$	$y_u$	$x_l$	$y_l$
<b>NACA 65<sub>3</sub>-418 (a = 0.5)</b>							
0.197	1.440	0.803	-1.164	0.258	1.537	0.742	-1.337
0.411	1.766	1.089	-1.378	0.482	1.864	1.018	-1.584
0.868	2.271	1.632	-1.683	0.950	2.374	1.550	-1.946
2.057	3.233	2.943	-2.197	2.152	3.353	2.848	-2.614
4.493	4.715	5.507	-2.961	4.603	4.866	5.397	-3.602
6.966	5.891	8.034	-3.515	7.083	6.066	7.917	-4.370
9.459	6.882	10.541	-3.978	9.579	7.060	10.421	-4.992
14.481	8.482	15.619	-4.690	19.634	9.885	20.366	-6.701
19.533	9.709	20.467	-5.213	24.684	10.815	25.316	-7.235
24.604	10.643	25.396	-5.595	29.742	11.494	30.258	-7.606
29.691	11.325	30.309	-5.853	34.805	11.939	35.195	-7.819
34.789	11.770	35.211	-5.998	39.871	12.140	40.129	-7.856
39.899	11.970	40.101	-6.026	44.937	12.056	45.063	-7.676
50.182	11.506	49.818	-5.626	50.000	11.672	50.000	-7.260
60.364	9.820	59.636	-4.696	60.103	10.126	59.897	-5.842
70.347	7.397	69.653	-3.433	70.180	7.861	69.840	-3.973
80.232	4.636	79.768	-2.024	80.159	5.200	79.841	-2.016
90.089	1.930	89.911	-0.702	90.098	2.441	89.902	-0.373
95.030	0.777	94.970	-0.201	95.049	1.150	94.951	-0.114
100.000	0	100.000	0	100.000	0	100.000	0

65 <sub>a</sub> -421 (a = 0.5)				66 <sub>a</sub> -415			
0.155	1.620	0.845	-1.344	0.314	1.206	0.686	-1.006
0.383	1.991	1.137	-1.603	0.544	1.467	0.956	-1.187
0.813	2.553	1.687	-1.965	1.019	1.873	1.481	-1.445
1.992	3.631	3.008	-2.595	2.241	2.592	2.759	-1.848
4.414	5.315	5.586	-3.551	4.711	3.718	5.289	-2.454
6.880	6.651	8.120	-4.275	7.199	4.617	7.801	-2.921
9.371	7.773	10.629	-4.889	9.896	5.381	10.304	-3.313
14.395	9.572	15.605	-5.780	14.709	6.624	15.291	-3.932
19.455	10.951	20.545	-6.455	19.736	7.581	20.264	-4.397
24.538	12.000	25.462	-6.952	24.771	8.329	25.229	-4.749
29.639	12.765	30.361	-7.293	29.812	8.897	30.188	-5.009
34.754	13.258	35.246	-7.486	34.857	9.309	35.143	-5.189
39.882	13.470	40.118	-7.526	39.904	9.571	40.098	-5.287
50.211	12.890	49.789	-7.010	44.962	9.685	45.048	-5.305
60.421	10.942	59.579	-5.818	50.000	9.656	50.000	-5.244
70.398	8.183	69.602	-4.229	60.090	9.100	59.910	-4.816
80.264	5.097	79.736	-2.485	70.150	7.518	69.860	-3.630
90.100	2.095	89.900	-0.867	80.159	5.187	79.841	-2.003
95.034	0.833	94.966	-0.257	90.104	2.519	89.896	-0.451
100.000	0	100.000	0	95.053	1.196	94.947	-0.068
				100.000	0	100.000	0

747 A 415				64 A 610			
0	0	0	0	0	0	0	0
0-183	1-318	0-817	-0-994	0-303	0-930	0-697	-0-630
0-398	1-622	1-102	-1-160	0-530	1-154	0-970	-0-734
0-852	2-106	1-648	-1-406	1-000	1-520	1-500	-0-878
2-041	3-016	2-959	-1-822	2-209	2-221	2-791	-1-105
4-487	4-411	5-513	-2-349	4-676	3-252	5-324	-1-356
6-972	5-488	8-028	-2-730	7-166	4-057	7-834	-1-513
9-476	6-390	10-524	-3-038	9-666	4-733	10-334	-1-631
14-521	7-827	15-479	-3-501	14-685	5-831	15-315	-1-769
19-598	8-897	20-402	-3-845	19-718	6-651	20-282	-1-875
24-698	9-687	25-302	-4-095	24-758	7-285	25-242	-1-915
29-818	10-216	30-182	-4-286	29-804	7-749	30-196	-1-917
34-964	10-497	35-036	-4-411	34-853	8-056	35-147	-1-876
40-176	10-499	39-824	-4-485	39-903	8-207	40-097	-1-781
50-447	9-516	49-553	-4-462	50-000	7-993	50-000	-1-375
60-454	7-859	59-546	-4-235	60-078	7-233	59-922	-0-807
70-273	5-838	69-727	-3-622	70-126	6-040	69-874	-0-208
80-107	3-692	79-893	-2-344	80-139	4-486	79-861	0-290
90-037	1-546	89-963	-0-838	90-111	2-607	89-889	0-495
95-015	0-639	94-985	-0-247	95-075	1-484	94-925	0-412
100-000	0	100-000	0	100-000	0	100-000	0

$x_u$	$y_u$	$y_l$	$y_u$	$y_l$	$y_u$	$y_l$	$y_u$	$y_l$	$x_u$
<b>NACA 64 09</b>									
1.25	2.06	-0.88	2.73	-1.23	4.26	-1.82	5.13	-2.08	1.25
2.50	2.96	-1.11	3.80	-1.64	5.62	-2.59	6.60	-3.04	2.50
5.00	4.30	-1.18	5.36	-1.99	7.53	-3.46	8.65	-4.16	5.00
7.50	5.42	-1.08	6.57	-2.05	8.98	-3.91	10.24	-4.81	7.50
10	6.31	-0.88	7.58	-1.99	10.16	-4.15	11.62	-5.18	10
15	7.78	-0.36	9.18	-1.67	12.02	-4.26	13.44	-5.62	15
20	8.88	-0.17	10.34	-1.25	13.32	-4.07	14.79	-5.49	20
25	9.65	-0.69	11.14	-0.78	14.17	-3.75	15.65	-5.23	25
30	10.13	-1.12	11.65	-0.38	14.64	-3.40	16.15	-4.91	30
40	10.35	-1.65	11.80	-0.20	14.70	-2.70	16.16	-4.16	40
50	9.81	-1.86	11.16	-0.55	13.80	-2.08	15.14	-3.40	50
60	8.78	-1.92	9.95	-0.78	12.24	-1.47	13.44	-2.59	60
70	7.28	-1.76	8.23	-0.85	10.11	-0.94	11.06	-1.83	70
80	5.34	-1.36	6.03	-0.73	7.40	-0.64	8.08	-1.17	80
90	2.95	-0.74	3.33	-0.39	4.12	-0.31	4.51	-0.65	90
95	1.57	-0.35	1.79	-0.16	2.24	-0.23	2.46	-0.42	95
100	0.09	-0.09	0.12	-0.12	0.19	-0.19	0.22	-0.22	100

	$x_u$	$y_u$	$x_l$	$y_l$	$x_u$	$y_u$	$x_l$	$y_l$	
<b>NACA 63<sub>2</sub>-615</b>									
0	0	0	0	0	0.156	1.511	0.844	-1.211	
0	0	0	0	0	0.361	1.878	1.139	-1.458	
0.205	1.317	0.795	-1.017	0.797	2.491	1.703	-1.849		
0.418	1.634	1.082	-1.214	1.965	3.616	3.035	-2.500		
0.866	2.159	1.634	-1.517	4.393	5.268	5.607	-3.372		
2.050	3.129	2.950	-2.013	6.888	6.542	8.132	-3.998		
4.492	4.560	5.608	-2.664	9.387	7.586	10.633	-4.484		
6.973	5.667	8.027	-3.123	14.404	9.219	15.596	-5.181		
9.473	6.578	10.527	-3.476	19.469	10.418	20.531	-5.642		
14.504	8.010	15.496	-3.972	24.549	11.273	25.451	-5.903		
19.558	9.066	20.442	-4.290	29.640	11.822	30.380	-5.990		
24.625	9.830	25.375	-4.460	34.734	12.086	35.266	-5.906		
29.700	10.331	30.300	-4.499	39.829	12.058	40.171	-5.630		
39.857	10.598	40.143	-4.172	44.919	11.787	45.081	-5.197		
50.000	9.974	50.000	-3.356	50.000	11.251	50.000	-4.633		
60.105	8.665	59.895	-2.239	60.125	9.667	59.875	-3.241		
70.159	6.947	69.841	-1.015	70.187	7.534	69.813	-1.702		
80.153	4.693	79.847	-0.083	80.178	5.073	79.822	-0.297		
90.089	2.398	89.911	-0.704	90.103	2.531	89.897	-0.571		
95.042	1.245	94.958	-0.651	95.048	1.293	94.952	-0.603		
100.000	0	100.000	0	100.000	0	100.000	0		

	$x_u$	$y_u$	$x_l$	$y_l$	$x_u$	$y_u$	$x_l$	$y_l$	
<b>64<sub>1</sub>-612</b>									
0.260	1.098	0.740	-0.798	0.150	1.534	0.850	-1.234		
0.482	1.358	1.018	-0.938	0.359	1.885	1.141	-1.485		
0.946	1.780	1.554	-1.138	0.805	2.452	1.695	-1.810		
2.149	2.563	2.851	-1.447	1.982	3.518	3.018	-2.402		
4.609	3.731	5.391	-1.835	4.417	5.093	5.583	-3.197		
7.096	4.642	7.904	-2.098	6.895	6.312	8.105	-3.768		
9.596	5.401	10.404	-2.299	9.395	7.322	10.605	-4.220		
14.619	6.623	15.381	-2.585	14.427	8.937	15.573	-4.899		
19.658	7.550	20.341	-2.774	19.486	10.153	20.514	-5.377		
24.708	8.253	25.292	-2.883	24.560	11.065	25.440	-5.695		
29.764	8.755	30.236	-2.923	29.645	11.698	30.355	-5.866		
34.823	9.065	35.177	-2.885	34.735	12.065	35.265	-5.985		
39.884	9.193	40.116	-2.767	39.827	12.163	40.173	-5.737		
44.945	9.083	45.055	-2.513	44.917	11.915	45.083	-5.345		
50.000	8.789	50.000	-2.171	50.000	11.423	50.000	-4.805		
60.088	7.760	59.912	-1.334	60.129	9.870	59.871	-3.444		
70.135	6.263	69.865	-0.431	70.196	7.754	69.804	-1.922		
80.134	4.413	79.866	-0.363	80.191	5.270	79.809	-0.494		
90.082	2.333	89.918	-0.769	90.115	2.646	89.885	-0.456		
95.040	1.233	94.960	-0.663	95.068	1.344	94.944	-0.552		
100.000	0	100.000	0	100.000	0	100.000	0		

**64<sub>3</sub>-618**

	$x_u$	$y_u$	$x_l$	$y_l$		$x_u$	$y_u$	$x_l$	$y_l$	
<b>NACA 65<sub>3</sub>-618</b>										
0·172	1·446	0·828	—1·146	0·059	1·469	0·941	—1·055			
0·385	1·776	1·115	—1·356	0·256	1·821	1·244	—1·239			
0·839	2·293	1·661	—1·651	0·689	2·375	1·811	—1·493			
2·026	3·268	2·974	—2·152	1·846	3·449	3·154	—1·895			
4·462	4·776	5·638	—2·880	4·248	5·115	5·752	—2·469			
6·936	5·971	8·064	—3·427	6·706	6·448	8·294	—2·884			
9·431	6·978	10·669	—3·876	9·194	7·675	10·806	—3·219			
14·455	8·602	15·645	—4·564	14·225	9·404	15·775	—3·716			
19·506	9·848	20·494	—5·072	19·301	10·815	20·699	—4·071			
24·574	10·803	25·426	—5·433	24·407	11·893	25·593	—4·321			
29·652	11·504	30·348	—5·672	29·537	12·687	30·463	—4·479			
34·738	11·972	35·262	—5·792	34·684	13·209	35·316	—4·651			
39·826	12·210	40·174	—5·784	39·849	13·456	40·151	—4·540			
44·915	12·186	45·085	—5·616	50·273	12·974	49·727	—4·154			
50·000	11·877	50·000	—5·259	60·546	11·090	59·454	—3·404			
60·141	10·479	59·859	—4·053	70·519	8·374	69·481	—2·428			
70·219	8·338	69·781	—2·506	80·347	5·279	79·653	—1·361			
80·220	5·719	79·780	—0·943	90·133	2·233	89·867	—0·391			
90·138	2·863	89·862	—0·239	95·046	0·920	94·954	—0·056			
95·068	1·433	94·932	—0·463	100·000	0	100·000	0			
100·000	0	100·000	0							

	<b>64 A 810 (a = 0·8 mod.)</b>					<b>64 A 910</b>				
0·214	0·976	0·785	—0·526	0·215	0·977	0·785	—0·527			
0·881	1·650	1·619	—0·686	0·884	1·651	1·616	—0·688			
2·064	2·475	2·936	—0·787	2·072	2·470	2·928	—0·796			
4·506	3·716	5·494	—0·832	4·520	3·699	5·480	—0·855			
6·984	4·703	8·016	—0·811	7·003	4·669	7·997	—0·853			
9·479	5·541	10·521	—0·771	9·503	5·487	10·497	—0·834			
14·500	6·902	15·500	—0·658	14·530	6·814	15·470	—0·755			
19·543	7·968	20·457	—0·526	19·578	7·833	20·422	—0·669			
24·601	8·795	25·399	—0·383	24·639	8·620	25·361	—0·565			
29·668	9·420	30·332	—0·232	29·707	9·202	30·293	—0·454			
34·742	9·857	35·258	—0·065	34·780	9·598	35·220	—0·328			
39·820	10·107	40·180	0·123	39·855	9·813	40·145	—0·174			
44·900	10·150	45·100	0·364	44·930	9·822	45·070	0·034			
49·977	10·005	50·023	0·637	50·000	9·648	50·000	0·280			
60·114	9·225	59·886	1·187	60·117	8·839	59·883	0·801			
70·215	7·850	69·785	1·610	70·189	7·495	69·811	1·253			
80·300	5·819	79·700	1·657	80·208	5·675	79·792	1·489			
90·204	3·004	89·796	0·920	90·165	3·376	89·835	1·277			
95·104	1·512	94·896	0·450	95·112	1·951	94·888	0·893			
100·000	0·021	100·000	—0·021	100·000	0	100·000	0			

	<b>8-H-12</b>					<b>11-H-09</b>				
0·147	1·229	0·853	—0·819	0·134	0·983	0·866	—0·301			
0·358	1·520	1·142	—0·946	0·338	1·287	1·162	—0·315			
0·804	2·006	1·696	—1·128	0·785	1·745	1·715	—0·311			
1·980	2·941	3·020	—1·415	2·000	2·680	3·000	—0·238			
4·424	4·312	5·576	—1·736	4·475	3·996	5·625	—0·090			
6·914	5·380	8·086	—1·920	6·988	5·018	8·012	0·036			
9·427	6·263	10·573	—2·059	9·520	5·851	10·480	0·135			
14·497	7·626	15·603	—2·242	14·615	7·112	15·385	0·250			
19·607	8·605	20·393	—2·361	19·728	7·994	20·272	0·278			
24·754	9·243	26·246	—2·417	24·844	8·569	26·156	0·235			
29·969	9·533	30·031	—2·455	29·957	8·890	30·043	0·144			
40·292	9·030	39·708	—2·494	40·217	8·828	39·783	—0·142			
50·390	7·666	49·610	—2·436	50·394	7·721	49·606	—0·613			
60·358	5·846	59·642	—2·290	60·392	5·987	59·608	—0·893			
70·250	3·838	69·750	—2·034	70·295	3·915	69·705	—1·173			
80·118	1·895	79·882	—1·845	80·151	1·843	79·849	—1·271			
90·016	0·343	89·984	—1·051	90·024	0·170	89·976	—1·052			
94·995	0·119	95·005	—0·629	94·995	0·271	95·005	—0·725			
100·000	0	100·000	0	100·000	0	100·000	0			

Table 11.3.(b)

Co-ordinates of R.A.E. 100-104 ( $t/c = 0.10$ )

Crown copyright reserved, reproduced by permission of The Controller, H.M. Stationery Office.

$x$	100 y					$x$	100 y				
	R.A.E. 100	R.A.E. 101	R.A.E. 102	R.A.E. 103	R.A.E. 104		R.A.E. 100	R.A.E. 101	R.A.E. 102	R.A.E. 103	R.A.E. 104
0	0	0	0	0	0	0.35	4.8691	4.9536	4.9992	4.9720	4.9300
0.001	0.4680	0.3905	0.3701	0.3556	0.3441	0.36	4.8369	4.9307	4.9997	4.9841	4.9483
0.002	0.6609	0.5518	0.5231	0.5025	0.4863	0.38	4.7633	4.8728	4.9869	4.9982	4.9775
0.003	0.8083	0.6753	0.6402	0.6151	0.5953	0.4	4.6785	4.8005	4.9534	4.9985	4.9946
0.004	0.9320	0.7792	0.7388	0.7098	0.6870	0.42	4.5834	4.7153	4.8942	4.9848	5.0000
0.005	1.0406	0.8705	0.8254	0.7931	0.7676	0.44	4.4789	4.6183	4.8154	4.9565	4.9937
0.006	1.1383	0.9529	0.9036	0.8682	0.8404	0.45	4.4234	4.5657	4.7699	4.9367	4.9862
0.007	1.2278	1.0285	0.9753	0.9372	0.9072	0.46	4.3657	4.5106	4.7207	4.9128	4.9756
0.0075	1.2700	1.0642	1.0092	0.9698	0.9387	0.48	4.2447	4.3932	4.6124	4.8523	4.9454
0.008	1.3107	1.0987	1.0420	1.0013	0.9692	0.5	4.1163	4.2670	4.4920	4.7715	4.9027
0.009	1.3883	1.1644	1.1044	1.0614	1.0274	0.52	3.9814	4.1329	4.3608	4.6644	4.8468
0.01	1.4613	1.2265	1.1634	1.1181	1.0824	0.54	3.8405	3.9915	4.2201	4.5380	4.7769
0.012	1.5963	1.3416	1.2727	1.2232	1.1842	0.55	3.7680	3.9183	4.1465	4.4689	4.7363
0.0125	1.6281	1.3687	1.2985	1.2480	1.2083	0.56	3.6943	3.8436	4.0709	4.3965	4.6917
0.014	1.7194	1.4469	1.3727	1.3195	1.2776	0.58	3.5432	3.6899	3.9142	4.2423	4.5892
0.016	1.8329	1.5445	1.4655	1.4088	1.3642	0.6	3.3879	3.5310	3.7507	4.0773	4.4650
0.018	1.9387	1.6357	1.5523	1.4924	1.4452	0.62	3.2288	3.3676	3.5813	3.9030	4.3113
0.02	2.0377	1.7215	1.6340	1.5711	1.5215	0.64	3.0665	3.2003	3.4068	3.7206	4.1370
0.025	2.2622	1.9174	1.8205	1.7509	1.6960	0.65	2.9843	3.1154	3.3179	3.6267	4.0438
0.03	2.4605	2.0924	1.9873	1.9118	1.8522	0.66	2.9015	3.0297	3.2279	3.5313	3.9473
0.035	2.6387	2.2513	2.1390	2.0582	1.9945	0.68	2.7343	2.8563	3.0454	3.3362	3.7452
0.04	2.8006	2.3974	2.2786	2.1931	2.1256	0.7	2.5654	2.6807	2.8598	3.1364	3.5331
0.05	3.0861	2.6593	2.5293	2.4357	2.3617	0.72	2.3953	2.5034	2.6720	2.9326	3.3128
0.06	3.3316	2.8898	2.7506	2.6503	2.5709	0.74	2.2245	2.3251	2.4825	2.7260	3.0861
0.07	3.5457	3.0959	2.9491	2.8432	2.7592	0.75	2.1389	2.2357	2.3873	2.6218	2.9708
0.075	3.6429	3.1913	3.0412	2.9328	2.8468	0.76	2.0533	2.1463	2.2920	2.5173	2.8545
0.08	3.7344	3.2822	3.1291	3.0185	2.9307	0.78	1.8822	1.9674	2.1011	2.3074	2.6193
0.09	3.9016	3.4519	3.2937	3.1792	3.0881	0.8	1.7111	1.7886	1.9101	2.0975	2.3819
0.1	4.0505	3.6073	3.4450	3.3273	3.2336	0.82	1.5400	1.6097	1.7191	1.8877	2.1437
0.12	4.3019	3.8820	3.7142	3.5921	3.4945	0.84	1.3689	1.4309	1.5281	1.6780	1.9055
0.14	4.5020	4.1162	3.9463	3.8221	3.7222	0.85	1.2833	1.3414	1.4326	1.5731	1.7864
0.15	4.5859	4.2202	4.0505	3.9258	3.8254	0.86	1.1978	1.2520	1.3371	1.4682	1.6673
0.16	4.6600	4.3163	4.1475	4.0230	3.9224	0.88	1.0267	1.0731	1.1461	1.2585	1.4292
0.18	4.7823	4.4867	4.3219	4.1992	4.0992	0.9	0.8556	0.8943	0.9551	1.0487	1.1910
0.2	4.8737	4.6304	4.4727	4.3536	4.2556	0.92	0.6844	0.7154	0.7641	0.8390	0.9528
0.22	4.9382	4.7496	4.6021	4.4884	4.3936	0.925	0.6417	0.6707	0.7163	0.7865	0.8932
0.24	4.9787	4.8455	4.7117	4.6052	4.5149	0.94	0.5133	0.5366	0.5730	0.6292	0.7146
0.25	4.9908	4.8851	4.7595	4.6574	4.5697	0.95	0.4278	0.4471	0.4775	0.5244	0.5955
0.26	4.9978	4.9190	4.8027	4.7055	4.6208	0.96	0.3422	0.3577	0.3820	0.4195	0.4764
0.28	4.9976	4.9700	4.8761	4.7900	4.7124	0.975	0.2139	0.2236	0.2388	0.2622	0.2977
0.3	4.9799	4.9969	4.9323	4.8597	4.7905	0.98	0.1711	0.1789	0.1910	0.2097	0.2382
0.32	4.9464	4.9956	4.9718	4.9151	4.8556	0.9875	0.1069	0.1118	0.1194	0.1311	0.1489
0.34	4.8983	4.9724	4.9943	4.9565	4.9082	1.0	0	0	0	0	0

**Table 11.4** Ordinates and Velocity Distributions (from Potential Theory) of NACA Profiles  
 $w/V = W_0 \cos \gamma + W_1 \sin \gamma$

100 $x/c$	100 $y/c$	$W_c$	$W_s$	100 $x/c$	100 $y/c$	$W_c$	$W_s$	100 $x/c$	100 $y/c$	$W_c$	$W_s$
<b>23006</b>				<b>23009</b>				<b>23012</b>			
100-000	0	0	0	100-000	0	0	0	100-000	0	0	0
97-335	0-300	0-9677	0-1340	97-250	0-450	0-9550	0-1316	97-115	0-600	0-9370	0-1288
89-740	0-970	1-0018	0-3041	89-420	1-375	0-9987	0-3024	89-065	1-815	0-9956	0-3011
78-220	1-885	1-0271	0-4984	77-670	2-650	1-0364	0-5020	77-125	3-465	1-0463	0-5064
63-990	2-910	1-0536	0-7345	63-295	4-025	1-0723	0-7465	62-665	5-185	1-0919	0-7597
48-515	3-830	1-0807	1-0394	47-840	5-225	1-1106	1-0687	47-170	6-640	1-1391	1-0934
33-345	4-465	1-1134	1-4713	32-760	5-975	1-1523	1-5206	32-185	7-495	1-1911	1-5708
20-000	4-630	1-1815	2-1739	19-555	6-050	1-2080	2-2572	19-145	7-475	1-2555	2-3443
9-830	4-040	1-2176	3-6132	9-540	5-170	1-2606	3-6293	9-250	6-275	1-2913	3-7139
6-070	3-295	1-1819	4-5323	5-840	4-220	1-2064	4-6134	5-590	5-160	1-2391	4-7325
3-180	2-370	1-0790	6-0480	2-980	3-080	1-0942	6-1088	2-820	3-830	1-1067	6-1677
1-160	1-370	0-8964	9-1163	1-030	1-880	0-8908	8-9966	0-935	2-315	0-8509	8-5664
0-135	0-520	0-3267	16-7756	0-085	0-750	0-2840	14-0895	0-030	0-990	0-2480	12-1167
0-120	-0-235	-1-2369	21-7630	0-110	-0-280	-0-9750	16-6788	0-125	-0-330	-0-7683	13-2127
1-270	-0-530	-1-2118	8-7505	1-280	-0-910	-1-1926	8-6556	1-355	-1-270	-1-1433	8-3161
3-840	-0-615	-1-0524	4-7930	3-830	-1-340	-1-0901	4-9804	3-865	-2-040	-1-1200	5-1248
7-795	-0-600	-0-9910	3-2650	7-675	-1-645	-1-0417	3-4404	7-625	-2-625	-1-0855	3-5891
18-995	-1-050	-1-0116	2-0847	18-585	-2-455	-1-0562	2-1805	18-265	-3-825	-1-1023	2-2773
32-780	-1-510	-1-0349	1-4844	32-150	-3-000	-1-0727	1-5408	31-610	-4-490	-1-1129	1-5996
48-170	-1-555	-1-0289	1-0698	47-415	-2-920	-1-0572	1-1007	46-745	-4-295	-1-0856	1-1309
63-800	-1-315	-1-0175	0-7700	63-050	-2-400	-1-0351	0-7844	62-375	-3-520	-1-0550	0-8000
78-125	-0-930	-1-0041	0-5365	77-525	-1-665	-1-0125	0-5419	76-965	-2-435	-1-0210	0-5468
89-710	-0-515	-0-9871	0-3421	89-355	-0-900	-0-9826	0-3413	89-005	-1-325	-0-9818	0-3414
97-330	-0-185	-0-9622	0-1716	97-215	-0-320	-0-9464	0-1695	97-095	-0-465	-0-9295	0-1668
100-000	0	0	0	100-000	0	0	0	100-000	0	0	0
<b>23015</b>				<b>23018</b>				<b>23021</b>			
100-000	0	0	0	100-000	0	0	0	100-000	0	0	0
96-985	0-740	0-9172	0-1262	96-865	0-905	0-9011	0-1239	96-730	1-075	0-8833	0-1211
88-705	2-260	0-9924	0-3003	88-350	2-735	0-9879	0-2988	88-035	3-235	0-9889	0-2987
76-575	4-265	1-0539	0-5103	76-060	5-145	1-0661	0-5181	75-550	5-990	1-0710	0-5179
61-975	6-345	1-1098	0-7724	61-365	7-535	1-1281	0-7850	60-785	8-775	1-1503	0-7997
46-490	8-070	1-1700	1-1234	45-875	9-495	1-1988	1-1509	45-315	10-980	1-2320	1-1817
31-625	9-005	1-2314	1-6245	31-100	10-515	1-2720	1-6776	30-635	12-040	1-3113	1-7281
18-730	8-840	1-2965	2-4217	18-335	10-225	1-3421	2-5063	18-010	11-615	1-3845	2-5829
8-950	7-360	1-3226	3-8058	8-655	8-410	1-3440	3-8663	8-395	9-495	1-3738	3-9466
5-335	6-055	1-2567	4-8026	5-070	6-980	1-2779	4-8878	4-875	7-870	1-2872	4-9092
2-615	4-650	1-1119	6-2024	2-420	5-250	1-0950	6-1048	2-255	5-940	1-0920	6-0735
0-815	2-860	0-8103	8-1713	0-640	3-320	0-7985	7-0541	0-555	3-840	0-7469	7-4927
-0-035	1-205	0-2159	10-6339	-0-100	1-510	0-1926	9-4438	-0-165	1-700	0-1798	8-6366
0-130	-0-360	-0-6448	11-0598	0-145	-0-445	-0-5496	9-4411	0-140	-0-400	-0-4891	8-4623
1-415	-1-645	-1-0766	7-8221	1-420	-1-980	-1-0256	7-4567	1-495	-2-320	-0-9447	6-8896
3-890	-2-750	-1-1398	5-2114	3-930	-3-395	-1-1255	5-1486	3-980	-4-030	-1-1173	5-1211
7-565	-3-625	-1-1283	3-7284	7-545	-4-615	-1-1627	3-8433	7-545	-5-570	-1-1861	3-9235
17-935	-5-200	-1-1506	2-3763	17-655	-6-585	-1-1989	2-4767	17-420	-7-930	-1-2470	2-5787
31-030	-5-955	-1-1507	1-6634	30-590	-7-480	-1-1937	1-7155	30-135	-8-955	-1-2314	1-7712
46-155	-5-665	-1-1140	1-1602	45-460	-7-105	-1-1457	1-1934	44-895	-8-565	-1-1816	1-2318
61-745	-4-670	-1-0769	0-8163	61-090	-5-820	-1-0938	0-8293	60-460	-7-010	-1-1120	0-8438
76-435	-3-220	-1-0290	0-5509	75-890	-4-050	-1-0400	0-5589	75-385	-4-895	-1-0493	0-5624
88-650	-1-765	-0-9814	0-3411	88-290	-2-220	-0-9777	0-3399	87-950	-2-690	-0-9756	0-3396
96-970	-0-610	-0-9131	0-1637	96-855	-0-765	-0-8985	0-1612	96-715	-0-930	-0-8820	0-1586
100-000	0	0	0	100-000	0	0	0	100-000	0	0	0

Table 11.5

## Measured Force and Moment Coefficients

Gö 1 K

Gö 2K

## Gö 4 K

$\alpha \backslash \frac{p - p_v}{q}$	0·0	0·1	0·2	0·3	0·4	0·5	0·6	0·7	0·8	0·9	1·0			
5°	$C_L$ 0·07 $C_D$ 0·046	0·18 0·059	0·29 0·067	0·40 0·072	0·52 0·075	0·62 0·074	0·72 0·070	0·81 0·060	0·88 0·043	0·89 0·040	0·89 0·040			
4°	$C_L$ -0·02 $C_D$ 0·038	0·10 0·051	0·22 0·061	0·35 0·067	0·47 0·069	0·58 0·068	0·70 0·062	0·79 0·053	0·84 0·037	0·85 0·034	0·85 0·034			
3°	$C_L$ -0·04 0·042	0·03 0·049	0·17 0·058	0·30 0·063	0·43 0·063	0·55 0·061	0·66 0·053	0·74 0·043	0·81 0·032	0·81 0·030				
2°	$C_L$ -0·04 0·047	-0·04 0·050	0·11 0·056	0·26 0·059	0·38 0·058	0·51 0·053	0·62 0·045	0·70 0·033	0·74 0·027	0·75 0·026				
1°	$C_L$ -0·04 0·051	-0·05 0·054	0·03 0·054	0·19 0·056	0·34 0·055	0·46 0·049	0·57 0·040	0·65 0·026	0·68 0·022	0·68 0·022				
0°	$C_L$ -0·05 0·057	-0·06 0·059	-0·02 0·054	0·14 0·055	0·29 0·053	0·42 0·047	0·52 0·036	0·60 0·024	0·61 0·020	0·61 0·020				
-1°	$C_L$ -0·06 0·061	-0·06 0·065	-0·06 0·061	0·09 0·055	0·24 0·051	0·37 0·045	0·47 0·034	0·53 0·023	0·54 0·022	0·54 0·022				
-2°	$C_L$ -0·06 0·066	-0·06 0·071	-0·07 0·067	0·03 0·057	0·18 0·051	0·30 0·043	0·40 0·03	0·45 0·025	0·47 0·025	0·47 0·025				
-3°	$C_L$ -0·06 0·070	-0·07 0·074	-0·07 0·074	-0·03 0·065	0·11 0·054	0·23 0·043	0·32 0·035	0·36 0·032	0·38 0·032	0·38 0·032				
-4°	$C_L$ -0·06 0·074	-0·07 0·081	-0·07 0·081	-0·07 0·074	0·03 0·060	0·16 0·047	0·25 0·039	0·28 0·038	0·28 0·038	0·28 0·038				

## Gö 5 K

$\alpha \backslash \frac{p - p_v}{q}$	0·0	0·1	0·2	0·3	0·4	0·5	0·6	0·7	0·8	0·9	1·0	1·1	1·2	1·4	1·6
6°	$C_L$ 0·150 $C_D$ 0·028	0·245 0·036	0·340 0·045	0·440 0·054	0·540 0·063	0·645 0·073	0·750 0·082	0·855 0·089	0·910 0·089	0·890 0·081	0·860 0·072	0·840 0·066	0·825 0·063	0·805 0·059	0·795 0·057
5°	$C_L$ 0·130 $C_D$ 0·023	0·220 0·029	0·320 0·037	0·420 0·044	0·520 0·051	0·615 0·057	0·705 0·062	0·780 0·064	0·790 0·058	0·760 0·050	0·740 0·046	0·725 0·043	0·715 0·041	0·695 0·038	0·685 0·037
4°	$C_L$ 0·105 $C_D$ 0·018	0·200 0·023	0·300 0·028	0·400 0·034	0·500 0·039	0·585 0·043	0·665 0·046	0·700 0·042	0·655 0·032	0·630 0·029	0·615 0·027	0·605 0·026	0·600 0·026	0·590 0·025	0·585 0·024
3°	$C_L$ 0·080 $C_D$ 0·012	0·180 0·016	0·280 0·021	0·380 0·025	0·475 0·028	0·555 0·029	0·555 0·020	0·515 0·017	0·500 0·016	0·490 0·016	0·490 0·016	0·490 0·016	0·490 0·016	0·485 0·016	0·480 0·015
2°	$C_L$ 0·050 $C_D$ 0·008	0·160 0·010	0·265 0·014	0·360 0·017	0·450 0·018	0·450 0·012	0·400 0·011	0·390 0·011	0·385 0·010	0·380 0·010					
1°	$C_L$ 0·020 $C_D$ 0·009	0·130 0·008	0·250 0·008	0·295 0·008											
0°	$C_L$ 0·005 $C_D$ 0·011	0·100 0·008	0·195 0·007												
-1°	$C_L$ -0·005 $C_D$ 0·012	0·050 0·009	0·095 0·008	0·095 0·008											
-2°	$C_L$ -0·010 $C_D$ 0·014	-0·030 0·013	-0·030 0·013	-0·040 0·010	-0·020 0·011	-0·020 0·011	-0·020 0·011	-0·020 0·011	-0·020 0·010	-0·020 0·010	-0·020 0·010				

## Gö 6 K

$\alpha \swarrow \frac{p - p_v}{q}$	0-0	0-1	0-2	0-3	0-4	0-5	0-6	0-7	0-8	0-9	1-0	1-1	1-2	1-4	1-6
6° $C_L$	0-170	0-270	0-365	0-460	0-560	0-655	0-750	0-835	0-915	0-975	0-980	0-955	0-935	0-915	0-905
6° $C_D$	0-026	0-036	0-045	0-054	0-062	0-071	0-077	0-082	0-084	0-082	0-087	0-054	0-046	0-039	0-036
5° $C_L$	0-150	0-250	0-350	0-445	0-540	0-630	0-720	0-800	0-870	0-895	0-860	0-840	0-825	0-810	0-800
5° $C_D$	0-021	0-029	0-036	0-043	0-049	0-054	0-058	0-061	0-058	0-045	0-033	0-029	0-027	0-024	0-023
4° $C_L$	0-120	0-235	0-345	0-445	0-545	0-620	0-695	0-765	0-800	0-780	0-750	0-730	0-725		
4° $C_D$	0-019	0-025	0-030	0-034	0-038	0-041	0-042	0-041	0-027	0-022	0-019	0-018	0-018		
3° $C_L$	0-095	0-220	0-340	0-455	0-570	0-640	0-650								
3° $C_D$	0-019	0-023	0-025	0-027	0-028	0-018	0-013								
2° $C_L$	0-055	0-200	0-335	0-465	0-560	0-585									
2° $C_D$	0-019	0-021	0-021	0-018	0-014	0-011									
1° $C_L$	0-025	0-160	0-305	0-435	0-495										
1° $C_D$	0-019	0-019	0-018	0-014	0-009										
0° $C_L$	0-0	0-110	0-280	0-380	0-405										
0° $C_D$	0-019	0-018	0-015	0-010	0-009										
-1° $C_L$	0-0	0-010	0-200	0-305	0-310										
-1° $C_D$	0-021	0-020	0-014	0-009	0-009										
-2° $C_L$	0-0	0-0	0-130	0-225	0-225										
-2° $C_D$	0-022	0-022	0-016	0-010	0-010										
-3° $C_L$	-0-006	-0-010	0-0	0-095	0-125	0-130	0-135	0-135	0-135	0-135					
-3° $C_D$	0-025	0-024	0-021	0-014	0-012	0-012	0-001	0-011	0-011	0-010					
-4° $C_L$	-0-010	-0-02	-0-045	-0-080	-0-020	0-020	0-035	0-035	0-035	0-035	0-035	0-035	0-035	0-035	0-035
-4° $C_D$	0-028	0-028	0-028	0-027	0-022	0-019	0-018	0-017	0-017	0-016	0-016	0-015	0-015	0-014	

## Gö 7 K

6° $C_L$	0-160	0-280	0-400	0-520	0-640	0-755	0-855	0-925	0-950	0-955	0-955	0-955	0-955	0-955	0-955
6° $C_D$	0-042	0-052	0-061	0-067	0-069	0-066	0-059	0-049	0-039	0-033	0-029	0-027			
5° $C_L$	0-130	0-245	0-365	0-490	0-615	0-740	0-840	0-910	0-940	0-945					
5° $C_D$	0-037	0-045	0-052	0-057	0-059	0-054	0-042	0-030	0-022	0-021					
4° $C_L$	0-095	0-210	0-330	0-455	0-590	0-720	0-815	0-875	0-885						
4° $C_D$	0-032	0-039	0-044	0-049	0-048	0-040	0-029	0-019	0-016						
3° $C_L$	0-050	0-170	0-300	0-430	0-565	0-690	0-780	0-805							
3° $C_D$	0-029	0-035	0-040	0-043	0-039	0-029	0-019	0-016							
2° $C_L$	0-010	0-130	0-265	0-410	0-540	0-660	0-720	0-720							
2° $C_D$	0-029	0-032	0-036	0-038	0-032	0-022	0-015	0-014							
1° $C_L$	-0-010	0-080	0-230	0-375	0-510	0-615	0-635								
1° $C_D$	0-032	0-031	0-033	0-033	0-026	0-016	0-013								
0° $C_L$	-0-010	0-035	0-190	0-335	0-465	0-540	0-545								
0° $C_D$	0-034	0-030	0-031	0-028	0-020	0-013	0-012								
-1° $C_L$	-0-010	-0-015	0-130	0-285	0-410	0-455									
-1° $C_D$	0-036	0-033	0-030	0-026	0-016	0-012									
-2° $C_L$	-0-010	-0-025	0-075	0-225	0-345	0-370									
-2° $C_D$	0-040	0-037	0-031	0-024	0-015	0-012									
-3° $C_L$	-0-015	-0-035	0-020	0-155	0-265	0-285	0-285								
-3° $C_D$	0-043	0-041	0-036	0-025	0-016	0-013	0-012								
-4° $C_L$	-0-020	-0-040	-0-025	0-070	0-150	0-180	0-190	0-195	0-195	0-195	0-195	0-195	0-195	0-195	0-195
-4° $C_D$	0-047	0-047	0-043	0-031	0-022	0-019	0-017	0-016	0-015	0-014	0-014	0-013			
-5° $C_L$	-0-025	-0-040	-0-045	-0-030	0-0	0-045	0-075	0-095	0-100	0-105	0-110	0-110	0-110	0-110	0-110
-5° $C_D$	0-050	0-052	0-052	0-048	0-036	0-032	0-029	0-027	0-025	0-023	0-022	0-021	0-020	0-018	0-018

## Gö 8 K

$\alpha \swarrow \frac{p - p_0}{q}$	0·0	0·1	0·2	0·3	0·4	0·5	0·6	0·7	0·8	0·9	1·0	1·1	1·2	1·4	1·6
4° $C_L$	0·090	0·190	0·315	0·445	0·575	0·700	0·830	0·935	1·00	1·01					
$C_D$	0·054	0·061	0·066	0·069	0·070	0·065	0·056	0·043	0·032	0·031					
3° $C_L$	0·045	0·155	0·275	0·400	0·530	0·660	0·790	0·890	0·930						
$C_D$	0·048	0·055	0·060	0·061	0·060	0·056	0·047	0·033	0·027						
2° $C_L$	0·0	0·100	0·230	0·355	0·485	0·620	0·750	0·835	0·845						
$C_D$	0·047	0·050	0·053	0·054	0·053	0·048	0·037	0·026	0·024						
1° $C_L$	-0·010	0·045	0·165	0·300	0·440	0·570	0·690	0·760	0·765						
$C_D$	0·051	0·048	0·049	0·050	0·048	0·040	0·029	0·021	0·021						
0° $C_L$	-0·010	0·0	0·100	0·250	0·395	0·525	0·635	0·680	0·680						
$C_D$	0·056	0·051	0·048	0·048	0·043	0·034	0·024	0·019	0·019						
-1° $C_L$	-0·015	-0·025	0·0	0·190	0·340	0·475	0·570	0·595							
$C_D$	0·062	0·057	0·052	0·047	0·040	0·030	0·020	0·018							
-2° $C_L$	-0·020	-0·030	-0·035	0·110	0·285	0·420	0·505	0·510							
$C_D$	0·068	0·063	0·058	0·048	0·038	0·026	0·018	0·018							
-3° $C_L$	-0·025	-0·035	-0·045	0·025	0·225	0·355	0·420	0·425							
$C_D$	0·073	0·070	0·066	0·053	0·039	0·024	0·017	0·017							
-4° $C_L$	-0·030	-0·040	-0·055	-0·050	0·140	0·290	0·330	0·335	0·340	0·340					
$C_D$	0·078	0·076	0·073	0·064	0·044	0·026	0·021	0·019	0·017	0·017					
-5° $C_L$	-0·035	-0·045	-0·065	-0·070	0·080	0·190	0·245	0·250	0·255	0·255	0·255	0·255	0·255	0·255	0·255
$C_D$	0·083	0·083	0·082	0·077	0·053	0·035	0·030	0·029	0·028	0·026	0·024	0·023	0·021	0·019	0·018
-6° $C_L$	-0·040	-0·055	-0·070	-0·075	0·0	0·085	0·135	0·160	0·175	0·180	0·180	0·180	0·180	0·180	0·180
$C_D$	0·089	0·091	0·090	0·086	0·065	0·049	0·042	0·039	0·037	0·035	0·034	0·033	0·032	0·029	0·028
-7° $C_L$	-0·050	-0·070	-0·075	-0·070	-0·040	0·0	0·025	0·055	0·080	0·095	0·100	0·100	0·105	0·105	0·105
$C_D$	0·096	0·097	0·096	0·093	0·086	0·070	0·062	0·058	0·055	0·053	0·051	0·049	0·046	0·044	0·057

## Gö 9 K

$\alpha \swarrow \frac{p - p_0}{q}$	0·0	0·1	0·2	0·3	0·4	0·5	0·6	0·7	0·8	0·9	1·0	1·1	1·2	1·4	1·6
5° $C_L$	0·130	0·220	0·315	0·415	0·510	0·610	0·700	0·755	0·745	0·715	0·695	0·680	0·665	0·645	0·635
$C_D$	0·022	0·028	0·035	0·043	0·050	0·057	0·063	0·064	0·060	0·055	0·052	0·050	0·048	0·045	0·044
4° $C_L$	0·110	0·205	0·295	0·390	0·490	0·585	0·655	0·635	0·595	0·565	0·550	0·545	0·540	0·530	0·530
$C_D$	0·016	0·022	0·028	0·034	0·040	0·045	0·048	0·041	0·035	0·033	0·032	0·031	0·030	0·029	0·028
3° $C_L$	0·080	0·180	0·280	0·375	0·475	0·545	0·520	0·470	0·455	0·450	0·445	0·440	0·435	0·435	0·435
$C_D$	0·010	0·016	0·021	0·025	0·028	0·028	0·023	0·020	0·019	0·018	0·018	0·017	0·016	0·016	0·015
2° $C_L$	0·055	0·155	0·255	0·355	0·430	0·360	0·340	0·335	0·335						
$C_D$	0·008	0·011	0·014	0·017	0·016	0·012	0·011	0·010	0·010						
1° $C_L$	0·025	0·125	0·225	0·235											
$C_D$	0·007	0·007	0·007	0·007											
0° $C_L$	0·000	1·100	0·125												
$C_D$	0·007	0·006	0·006												
-1° $C_L$	-0·010	0·020	0·025												
$C_D$	0·008	0·007	0·007												
-2° $C_L$	-0·010	-0·055	-0·155	-0·120	-0·090	-0·085	-0·085	-0·085							
$C_D$	0·010	0·010	0·012	0·010	0·010	0·010	0·010	0·010							

## G6 10 K

$\alpha \swarrow$	$p - p_v$	0·0	0·1	0·2	0·3	0·4	0·5	0·6	0·7	0·8	0·9	1·0	1·1	1·2	1·4	1·6
$a$	$q$															
$6^\circ$	$C_L$	0·160	0·250	0·340	0·440	0·535	0·630	0·720	0·805	0·885	0·910	0·895	0·860	0·845	0·815	0·795
	$C_D$	0·026	0·035	0·043	0·053	0·062	0·071	0·079	0·086	0·091	0·087	0·079	0·072	0·067	0·061	0·057
$5^\circ$	$C_L$	0·135	0·235	0·330	0·425	0·520	0·610	0·695	0·770	0·810	0·760	0·740	0·730	0·725	0·710	0·695
	$C_D$	0·021	0·027	0·035	0·042	0·050	0·056	0·062	0·067	0·063	0·051	0·047	0·045	0·043	0·040	0·037
$4^\circ$	$C_L$	0·110	0·210	0·315	0·415	0·510	0·590	0·660	0·705	0·680	0·640	0·625	0·615	0·610	0·605	0·600
	$C_D$	0·017	0·021	0·026	0·031	0·037	0·042	0·046	0·042	0·034	0·030	0·028	0·027	0·025	0·023	0·021
$3^\circ$	$C_L$	0·080	0·195	0·310	0·420	0·495	0·550	0·580	0·535	0·515	0·505	0·500	0·500	0·500	0·500	0·500
	$C_D$	0·014	0·017	0·019	0·023	0·025	0·027	0·023	0·017	0·016	0·015	0·014	0·013	0·012	0·012	0·012
$2^\circ$	$C_L$	0·055	0·170	0·295	0·395	0·415	0·415									
	$C_D$	0·011	0·013	0·014	0·014	0·009	0·009									
$1^\circ$	$C_L$	0·025	0·140	0·255	0·320											
	$C_D$	0·010	0·011	0·009	0·006											
$0^\circ$	$C_L$	0·000	0·110	0·210												
	$C_D$	0·009	0·009	0·006												
$-1^\circ$	$C_L$	0·000	0·070	0·095												
	$C_D$	0·010	0·008	0·007												
$-2^\circ$	$C_L$	-0·005	-0·035	-0·135	-0·045	-0·020	-0·020	-0·015	-0·015	-0·015	-0·015					
	$C_D$	0·011	0·012	0·013	0·009	0·008	0·008	0·008	0·008	0·008	0·008					

## G6 11 K

$\alpha \swarrow$	$p - p_v$	0·0	0·1	0·2	0·3	0·4	0·5	0·6	0·7	0·8	0·9	1·0	1·1	1·2	1·4	1·6
$a$	$q$															
$6^\circ$	$C_L$	0·170	0·270	0·370	0·470	0·560	0·635	0·700	0·775	0·845	0·915	0·970	0·975	0·955	0·930	0·910
	$C_D$	0·027	0·036	0·045	0·052	0·058	0·064	0·068	0·073	0·077	0·079	0·077	0·065	0·056	0·044	0·036
$5^\circ$	$C_L$	0·140	0·245	0·355	0·460	0·555	0·645	0·720	0·775	0·835	0·885	0·895	0·865	0·845	0·820	0·020
	$C_D$	0·023	0·031	0·039	0·044	0·047	0·049	0·051	0·051	0·050	0·048	0·042	0·033	0·027		
$4^\circ$	$C_L$	0·105	0·220	0·340	0·465	0·580	0·660	0·725	0·765	0·760	0·745					
	$C_D$	0·020	0·027	0·034	0·038	0·037	0·032	0·024	0·018	0·017	0·015					
$3^\circ$	$C_L$	0·075	0·185	0·305	0·435	0·560	0·645	0·675	0·680							
	$C_D$	0·018	0·023	0·029	0·033	0·028	0·016	0·012	0·012							
$2^\circ$	$C_L$	0·040	0·140	0·270	0·400	0·525	0·595	0·600								
	$C_D$	0·016	0·020	0·025	0·024	0·019	0·010	0·010								
$1^\circ$	$C_L$	-0·015	0·100	0·235	0·370	0·500	0·520									
	$C_D$	0·016	0·019	0·021	0·018	0·018	0·010	0·009								
$0^\circ$	$C_L$	-0·015	0·060	0·200	0·345	0·420										
	$C_D$	0·016	0·017	0·017	0·012	0·008										
$-1^\circ$	$C_L$	-0·010	0·025	0·180	0·305	0·310										
	$C_D$	0·017	0·018	0·015	0·009	0·009										
$-2^\circ$	$C_L$	0·000	0·000	0·090	0·215	0·215										
	$C_D$	0·020	0·020	0·016	0·009	0·009										
$-3^\circ$	$C_L$	-0·005	-0·005	-0·005	0·115	0·120										
	$C_D$	0·022	0·023	0·020	0·011	0·011										
$-4^\circ$	$C_L$	-0·010	-0·020	-0·045	-0·075	-0·030	0·015	0·030	0·035	0·040	0·040	0·040	0·040	0·040	0·040	
	$C_D$	0·026	0·027	0·028	0·028	0·022	0·019	0·017	0·016	0·014	0·013	0·012	0·012	0·012	0·012	

$\alpha$	$C_L$	$C_D$	$\alpha$	$C_L$	$C_D$	$\alpha$	$C_L$	$C_D$	$\alpha$	$C_L$	$C_D$	$\alpha$	$C_L$	$C_D$
<b>Gö 12 K</b>			<b>Gö 13 K</b>			<b>Gö 14 K</b>			<b>Gö 15 K</b>			<b>Gö 16 K</b>		
6°	0.965	0.0255	4°	0.970	0.0270	7°	0.825	0.0270	8°	0.880	0.0290	7°	0.905	0.0305
5°	0.910	0.0215	3°	0.905	0.0240	6°	0.775	0.0225	7°	0.845	0.0270	6°	0.915	0.0330
4°	0.865	0.0185	2°	0.835	0.0210	5°	0.735	0.0200	6°	0.830	0.0260	5°	0.910	0.0325
3°	0.835	0.0165	1°	0.765	0.0185	4°	0.715	0.0175	5°	0.825	0.0245	4°	0.865	0.0315
2°	0.770	0.0150	0°	0.670	0.0170	3°	0.715	0.0170	4°	0.820	0.0235	3°	0.795	0.0300
1°	0.675	0.0140	-1°	0.580	0.0165	2°	0.655	0.0165	3°	0.765	0.0220	2°	0.710	0.0275
0°	0.585	0.0135	-2°	0.495	0.0160	1°	0.635	0.0140	2°	0.665	0.0200	1°	0.680	0.0235
-1°	0.465	0.0130	-3°	0.415	0.0155	0°	0.405	0.0115	1°	0.535	0.0175	0°	0.405	0.0185
-2°	0.365	0.0125	-4°	0.325	0.0155	-1°	0.250	0.0100	0°	0.405	0.0150	-1°	0.270	0.0175
-3°	0.275	0.0130	-5°	0.245	0.0155	-2°	0.150	0.0095	-1°	0.290	0.0125	-2°	0.205	0.0175
-4°	0.185	0.0130	-6°	0.180	0.0155	-3°	0.075	0.0095	-2°	0.195	0.0125	-3°	0.145	0.0175
-5°	0.095	0.0145	-7°	0.075	0.0160	-4°	0.005	0.0100	-3°	0.125	0.0125	-4°	0.085	0.0175
						-5°	-0.065	0.0110	-4°	0.050	0.0125	-5°	0.020	0.0175
						-6°	-0.145	0.0130	-5°	-0.010	0.0125	-6°	-0.040	0.0175
						-7°	-0.140	0.0155	-6°	-0.080	0.0135	-7°	-0.105	0.0185

$\alpha$	$C_L$	$100 \cdot C_D$	$-10 \cdot C_m$	$\alpha$	$C_L$	$100 \cdot C_D$	$-10 \cdot C_m$	$\alpha$	$C_L$	$100 \cdot C_D$	$-10 \cdot C_m$
<b>Gö 123: <math>R = 7.2 \cdot 10^4</math></b>				<b>Gö 227: <math>R = 9.6 \cdot 10^4</math></b>				<b>Gö 242: <math>R = 9.6 \cdot 10^4</math></b>			
-8.2	-0.248	9.08	0.089	-11.8	-0.054	13.18	0.530	-9.0	0.016	10.90	0.740
-6.2	-0.236	7.21	0.140	-9.0	0.017	10.00	0.880	-6.8	0.216	3.62	1.730
-4.1	-0.115	5.73		-7.9	0.112	7.30	1.267	-5.8	0.345	3.27	
-3.3	0.094	4.55	0.722	-7.1	0.282	3.30	1.889	-4.8	0.465	2.78	1.890
-2.4	0.278	3.50		-6.0	0.400	2.90		-3.8	0.584	2.75	
-1.4	0.434	2.73	1.156	-4.9	0.512	2.80	1.949	-2.7	0.699	2.92	1.890
-0.4	0.573	2.10		-4.0	0.646	2.70		-1.7	0.819	3.21	
0.7	0.689	1.65	1.135	-2.9	0.748	2.80	1.960	-0.6	0.930	3.22	1.940
1.8	0.793	1.95		-1.9	0.863	2.90		0.4	1.035	3.46	
3.0	0.896	1.54	0.961	-0.8	0.975	3.10	1.979	1.5	1.150	3.64	1.950
4.1	1.015	1.98		1.3	1.196	3.40	1.975	3.6	1.375	4.16	2.020
5.3	1.115	2.08	0.960	3.5	1.404	4.10	2.001	5.9	1.570	4.96	2.170
7.8	1.266	3.42	0.825	5.8	1.585	5.30	1.980	8.2	1.739	6.35	2.240
10.8	1.260	10.69	0.950	8.4	1.679	8.40	1.958				
14.3	1.112	24.00	1.480								
<b>Gö 243: <math>R = 9.6 \cdot 10^4</math></b>				<b>Gö 289: <math>R = 7.2 \cdot 10^4</math></b>				<b>Gö 289: <math>R = 4.2 \cdot 10^5</math></b>			
-12.4	0.104	13.20	0.755	-8.9	-0.013	7.10	0.950	-9.2	0.048	1.65	
-9.6	0.160	10.40	0.827	-6.6	0.182	3.10	1.200	-6.8	0.158	1.49	
-8.5	0.268	5.50		-5.4	0.289	2.80	1.170	-4.6	0.354	1.12	
-7.5	0.376	3.40	1.886	-4.3	0.395	2.70	1.180	-3.6	0.565	1.26	
-6.5	0.523	3.10		-3.1	0.497	2.60	1.070	-0.6	0.780	1.12	
-5.5	0.642	3.00	2.000	-2.0	0.615	2.60	1.110	1.6	0.965	1.45	
-4.5	0.778	2.80		-0.8	0.720	2.80	1.060	3.9	1.160	1.90	
-3.4	0.878	3.10	1.940	0.2	0.830	3.10	1.040	6.1	1.330	2.90	
-2.3	0.990	3.20		1.4	0.931	3.40	1.000	8.9	1.400	5.40	
-1.2	1.100	3.20	1.910	2.6	1.034	3.80	1.030	12.1	1.340	14.80	
0.8	1.333	3.20	1.860	6.6	0.722	14.30	1.060				
3.1	1.500	4.50	1.820	9.3	0.811	18.10	1.060				
7.4	1.180	18.20	1.920	12.4	0.772	25.30	1.180				
10.2	1.220	22.30	1.910								
<b>Gö 301: <math>R = 7.2 \cdot 10^4</math></b>				<b>Gö 335: <math>R = 4.2 \cdot 10^5</math></b>				<b>Gö 417a: <math>R = 4.2 \cdot 10^5</math></b>			
-8.5	-0.165	10.50	0.039	-7.8	-0.258	8.85	0.019	-7.4	-0.203	9.63	-0.13
-5.8	-0.075	7.80	0.467	-5.3	-0.141	5.94	0.419	-4.9	-0.198	7.02	0.15
-4.8	0.078	6.20	0.870	-4.4	-0.025	4.63	0.672	-4.0	-0.100	5.74	0.33
-3.8	0.238	4.60	1.010	-3.4	0.1000	3.43	0.805	-3.1	0.021	4.68	0.55
-2.7	0.375	3.40	1.140	-2.5	0.216	2.17	0.842	-2.2	0.148	3.77	0.81
-1.6	0.497	2.70	1.110	-1.4	0.321	1.32	0.837	-1.6	0.277	3.24	1.03
-0.5	0.611	2.30	1.110	-0.3	0.420	1.18	0.829	-0.7	0.405	2.94	1.17
0.6	0.723	2.00	1.070	0.6	0.523	1.11	0.838	0.1	0.530	2.97	1.25
1.7	0.837	2.10	1.030	1.7	0.623	1.05	0.805	1.0	0.643	2.05	1.28
2.8	0.950	2.10	1.000	2.6	0.724	1.09	0.799	2.0	0.761	1.69	1.28
5.1	1.165	2.70	0.960	4.8	0.916	1.35	0.784	3.8	0.960	1.38	1.31
7.4	1.370	3.70	0.890	7.0	1.080	2.00	0.745	6.0	1.129	1.92	1.41
10.0	1.510	5.90	0.880	9.8	1.143	5.78	0.819	8.1	1.274	3.90	1.25
								11.3	1.241	14.3	1.73

$\alpha$	$C_L$	$100 \cdot C_D$	$-10 \cdot C_m$	$\alpha$	$C_L$	$100 \cdot C_D$	$-10 \cdot C_m$	$\alpha$	$C_L$	$100 \cdot C_D$	$-10 \cdot C_m$
<b>Gö 420: <math>R = 4 \cdot 2 \cdot 10^5</math></b>											
-11.9	-0.216	1.69	-0.969	39.5	0.709	68.00	-4.08	195.8	0.451	31.50	3.82
-00.0	-0.016	1.38	-0.965	49.5	0.651	84.50	-4.66	198.9	0.478	36.20	4.22
-06.1	0.196	1.53	-0.944	59.3	0.636	98.60	-5.17	209.6	0.464	51.30	4.70
-04.6	0.297	1.88	-0.941	69.3	0.376	109.40	-5.57	219.6	0.427	66.20	5.02
-03.1	0.404	2.39	-0.933	79.7	0.186	114.10	-5.85	229.9	0.363	80.70	5.41
-01.7	0.510	3.04	-0.957	89.5	-0.002	113.20	-5.05	240.1	0.260	93.50	5.62
-00.2	0.610	3.76	-0.935	100.1	-0.192	108.00	-6.14	249.5	0.139	102.60	5.69
01.2	0.700	4.56	-0.928	110.1	-0.357	99.50	-6.18	258.4	0.009	105.40	5.55
02.7	0.812	5.66	-0.993	120.6	-0.495	86.30	-6.10	270.0	-0.167	106.40	5.35
04.2	0.892	6.91	-0.957	129.9	-0.574	70.80	-5.83	279.3	-0.299	101.70	5.02
05.6	0.977	7.99	-0.867	139.9	-0.653	53.90	-5.72	290.0	-0.422	91.80	4.45
08.6	1.170	11.60	-1.031	144.7	-0.722	47.20	-5.87	300.2	-0.484	78.80	3.82
11.5	1.280	15.40	-0.992	155.4	-0.589	30.10	-5.59	305.4	-0.493	70.00	3.41
14.5	1.305	20.10	-1.039	160.3	-0.929	20.20	-6.59	310.2	-0.493	62.30	3.04
Values for A = 5; $C_m$ referred to z = 0:											
-00.2	0.618	3.81	-2.41	170.4	-0.549	7.05	-3.14	330.2	-0.346	29.60	1.81
04.7	0.945	7.40	-3.23	175.9	-0.055	4.07	2.30	340.1	-0.294	16.40	0.62
09.4	1.256	12.50	-4.01	179.7	0.219	6.09	2.26	345.0	-0.402	3.35	0.03
14.5	1.355	19.00	-4.28	185.2	0.487	14.20	4.02	349.8	-0.087	1.46	-0.69
19.5	1.246	26.80	-4.24	188.8	0.535	21.50	4.10	364.7	0.251	1.53	-1.50
24.4	1.190	33.90	-4.30	189.8	0.515	23.50	4.03	369.8	0.628	3.61	-2.46
29.6	1.023	43.70	-4.12	194.8	0.453	29.30	3.86				
34.7	0.721	60.20	-3.83								
<b>Gö 436: <math>R = 4 \cdot 2 \cdot 10^5</math></b>											
-7.9	-0.239	3.99	0.705	-8.8	-0.026	1.75	1.142	-6.2	-0.614	2.41	
-5.7	-0.050	1.42	0.759	-6.8	0.173	1.48	1.101	-4.0	-0.412	1.75	
-4.7	0.050	1.28	0.718	-5.7	0.278	1.35	1.069	-2.1	-0.177	1.50	
-3.6	0.150	1.18	0.697	-4.6	0.378	1.36	1.068	-0.1	0.035	1.40	
-2.6	0.246	1.19	0.686	-3.7	0.486	1.22	1.027	1.6	0.298	0.98	
-1.5	0.349	1.09	0.687	-2.5	0.572	1.20	1.030	3.6	0.513	1.68	
-0.5	0.451	1.13	0.691	-1.4	0.666	1.06	0.993	6.0	0.655	1.98	
0.5	0.548	0.96	0.646	-0.5	0.774	0.95	0.999	8.4	0.775	3.18	
1.6	0.647	1.06	0.635	0.5	0.875	1.10	1.001	12.1	0.635	15.14	
2.5	0.751	1.16	0.590	1.5	0.960	1.47	0.981	15.1	0.614	21.38	
4.7	0.945	1.39	0.619	3.8	1.131	2.16	0.932				
6.9	1.120	1.71	0.579	6.2	1.265	3.04	1.078				
9.5	1.204	4.23	0.551	8.9	1.324	6.73	1.293				
<b>Gö 449: <math>R = 4 \cdot 2 \cdot 10^5</math></b>											
-8.8	-0.026	1.75	1.142	-6.2	-0.614	2.41					
-6.8	0.173	1.48	1.101	-4.0	-0.412	1.75					
-5.7	0.278	1.35	1.069	-2.1	-0.177	1.50					
-4.6	0.378	1.36	1.068	-0.1	0.035	1.40					
-3.7	0.486	1.22	1.027	1.6	0.298	0.98					
-2.5	0.572	1.20	1.030	3.6	0.513	1.68					
-1.4	0.666	1.06	0.993	6.0	0.655	1.98					
-0.5	0.774	0.95	0.999	8.4	0.775	3.18					
0.5	0.875	1.10	1.001	12.1	0.635	15.14					
1.6	0.960	1.47	0.981	15.1	0.614	21.38					
4.7	1.131	2.16	0.932								
6.9	1.265	3.04	1.078								
9.5	1.324	6.73	1.293								
<b>Gö 459: <math>R = 1 \cdot 4 \cdot 10^5</math></b>											
-6.2	-0.614	2.41		-6.2	-0.614	2.41					
-4.0	-0.412	1.75		-4.0	-0.407	1.20					
-2.1	-0.177	1.50		-2.1	-0.190	1.10					
-0.1	0.035	1.40		-0.1	0.028	0.94					
1.7	0.242	0.81		1.7	0.242	0.81					
3.8	0.437	0.76		3.8	0.437	0.76					
5.7	0.670	0.88		5.7	0.670	0.88					
7.8	0.850	1.14		7.8	0.850	1.14					
9.8	1.043	1.57		9.8	1.043	1.57					
12.4	1.202	2.17		12.4	1.202	2.17					
<b>Gö 459: <math>R = 1 \cdot 05 \cdot 10^6</math></b>											
-4.0	-0.385	1.09		-4.0	-0.407	1.20					
-2.1	-0.185	1.00		-2.1	-0.190	1.10					
-0.0	0.014	0.79		-0.1	0.028	0.94					
1.8	0.220	0.71		1.7	0.242	0.81					
3.9	0.418	0.76		3.8	0.437	0.76					
5.9	0.620	0.89		5.7	0.670	0.88					
7.9	0.829	1.05		7.8	0.850	1.14					
10.0	1.000	1.43		9.8	1.043	1.57					
14.0	0.835	16.40		12.4	1.202	2.17					
<b>Gö 460: <math>R = 1 \cdot 68 \cdot 10^6</math></b>											
-4.1	-0.368	1.63		-4.1	-0.368	2.11					
-2.2	-0.166	1.51		-6.4	0.110	1.76					
-0.1	0.031	1.45		-5.5	0.217	1.56					
1.8	0.228	1.33		-4.4	0.311	1.62					
3.9	0.424	1.35		-3.3	0.411	1.48					
5.9	0.613	1.51		-2.3	0.513	1.38					
8.1	0.785	1.89		-1.2	0.607	1.36					
10.4	0.930	2.75		-0.3	0.717	1.30					
13.4	0.907	8.27		0.7	0.815	1.31					
16.8	0.876	16.34		1.8	0.917	1.37					
<b>Gö 508: <math>R = 4 \cdot 2 \cdot 10^6</math></b>											
-8.6	-0.086	2.11		-8.6	-0.086	2.11					
-6.4	0.110	1.76		-6.4	0.110	1.76					
-5.5	0.217	1.56		-5.5	0.217	1.56					
-4.4	0.311	1.62		-4.4	0.311	1.62					
-3.3	0.411	1.48		-3.3	0.411	1.48					
-2.3	0.513	1.38		-2.3	0.513	1.38					
-1.2	0.607	1.36		-1.2	0.607	1.36					
-0.3	0.717	1.30		-0.3	0.717	1.30					
0.7	0.815	1.31		0.7	0.815	1.31					
1.8	0.917	1.37		1.8	0.917	1.37					
4.1	1.072	1.87		4.1	1.072	1.87					
6.4	1.225	2.90		6.4	1.225	2.90					
8.9	1.334	5.25		8.9	1.334	5.25					
11.6	1.402	8.63		11.6	1.402	8.63					
14.6	1.412	17.44		14.6	1.412	17.44					

$\alpha$	$C_L$	$100 \cdot C_D$	$-10 \cdot C_m$	$\alpha$	$C_L$	$100 \cdot C_D$	$-10 \cdot C_m$	$\alpha$	$C_L$	$100 \cdot C_D$	$-10 \cdot C_m$
<b>Gö 535: <math>R = 4 \cdot 2 \cdot 10^5</math></b>				<b>Gö 596: <math>R = 4 \cdot 2 \cdot 10^5</math></b>				<b>Gö 608: <math>R = 4 \cdot 2 \cdot 10^5</math></b>			
-8.8	-0.035	1.91	1.224	-10.5	-0.324	11.31	0.137	-6.8	-0.459	7.77	0.047
-6.8	0.179	1.53	1.220	-7.7	-0.274	7.90	0.128	-4.7	-0.288	4.06	0.462
-5.8	0.286	1.43	1.222	-5.6	-0.088	3.77	0.690	-2.8	-5.047	1.70	0.500
-4.7	0.388	1.35	1.196	-3.4	0.115	1.30	0.744	-1.7	0.066	1.18	0.541
-3.7	0.500	1.28	1.192	-1.4	0.318	1.06	0.705	-0.8	0.173	0.83	0.577
-2.7	0.605	1.28	1.167	0.6	0.525	0.79	0.704	0.2	0.285	0.59	0.576
-1.7	0.715	1.27	1.190	2.6	0.739	0.85	0.701	1.3	0.370	0.89	0.523
-0.7	0.820	1.26	1.209	4.7	0.940	1.10	0.683	2.3	0.486	1.36	0.490
0.3	0.925	1.32	1.182	7.0	1.082	1.87	0.616	3.4	0.561	1.96	0.457
1.3	1.025	1.43	1.190	9.8	1.132	4.94	0.624	4.5	0.661	3.02	0.398
3.5	1.211	1.74	1.210	10.8	1.130	6.67	0.671	5.5	0.758	4.74	0.422
5.6	1.390	2.35	1.240	12.8	1.126	10.33	0.740	6.7	0.828	6.38	0.641
8.0	1.630	3.70	1.250					7.4	0.838	8.87	0.800
10.9	1.535	9.07	1.415					8.2	0.838	10.67	0.936
								9.7	0.832	13.23	1.057
<b>Gö 609: <math>R = 4 \cdot 2 \cdot 10^5</math></b>				<b>Gö 610: <math>R = 4 \cdot 2 \cdot 10^5</math></b>				<b>Gö 622: <math>R = 1 \cdot 2 \cdot 10^5</math></b>			
-7.0	-0.425	8.21	0.049	-7.5	-0.319	8.18	0.313	-7.3	-0.386	5.87	
-5.0	-0.209	4.49	0.635	-5.4	-0.121	4.33	0.935	-5.0	-0.216	2.46	
-3.0	0.019	1.92	0.635	-3.3	0.093	1.96	1.120	-3.0	0.002	1.86	
-2.0	0.124	1.28	0.821	-2.2	0.185	1.43	1.048	-1.2	0.068	1.70	
-1.0	0.228	0.90	0.810	-1.2	0.282	1.05	1.005	0.9	0.453	1.80	
0.0	0.326	0.70	0.774	-0.1	0.380	0.71	1.029	3.1	0.651	2.56	
1.2	0.397	0.94	0.684	0.8	0.472	0.73	0.967	5.5	0.843	3.06	
3.3	0.586	1.72	0.605	3.0	0.618	1.49	0.785	7.7	0.956	4.66	
5.4	0.771	3.56	0.463	5.3	0.805	2.83	0.660	9.5	0.898	12.67	
7.0	0.875	6.85	0.616	7.7	0.939	6.38	0.609	11.3	0.832	18.00	
8.0	0.883	9.15	0.818	8.7	0.945	8.91	0.754				
11.2	0.829	15.66	1.126	10.9	0.900	14.65	1.071				
<b>Gö 622: <math>R = 4 \cdot 2 \cdot 10^5</math></b>				<b>Gö 623: <math>R = 1 \cdot 2 \cdot 10^5</math></b>				<b>Gö 623: <math>R = 4 \cdot 2 \cdot 10^5</math></b>			
-7.2	-0.393	5.01	0.307	-7.7	-0.292	7.10		-7.7	-0.279	3.94	0.155
-5.1	-0.177	1.23	0.517	-5.8	-0.052	2.69		-5.8	-0.047	1.46	0.762
-3.1	0.039	1.00	0.473	-3.7	0.150	2.04		-3.7	0.155	1.11	0.724
-1.0	0.237	0.82	0.457	-1.5	0.342	2.02		-1.5	0.352	1.10	0.700
0.9	0.442	0.94	0.442	0.5	0.557	2.18		0.4	0.566	1.28	0.681
3.1	0.642	1.25	0.425	2.6	0.740	2.63		2.5	0.763	1.56	0.678
5.2	0.830	1.63	0.401	5.0	0.885	3.08		4.7	0.954	1.92	0.665
7.5	0.981	2.68	0.331	7.2	1.063	4.34		6.8	1.135	2.90	0.644
8.9	1.000	3.90	0.299	9.7	1.192	5.54		9.2	1.258	4.06	0.572
10.7	0.940	14.27	0.790	11.0	1.238	6.84		12.2	1.260	8.52	0.644
				11.7	1.220	8.43		15.8	1.129	17.49	0.902
				14.2	0.840	22.69					
				17.2	0.836	28.20					
<b>Gö 623: <math>R = 4 \cdot 3 \cdot 10^5</math></b>				<b>Gö 624: <math>R = 1 \cdot 1 \cdot 10^5</math></b>				<b>Gö 624: <math>R = 4 \cdot 2 \cdot 10^5</math></b>			
-7.9	-0.243	4.27		-11.3	-0.141	11.97		-11.1	-0.191	9.66	0.300
-5.8	-0.061	1.26		-8.7	-0.082	6.05		-8.4	-0.132	1.71	0.947
-3.7	0.144	1.18		-6.3	0.082	4.02		-6.2	0.066	1.49	0.899
-1.6	0.349	0.97		-4.2	0.284	3.89		-4.2	0.268	1.41	0.863
0.5	0.555	1.10		-2.2	0.489	3.35		-2.1	0.467	1.36	0.842
2.6	0.747	1.43		-0.2	0.694	3.19		-0.0	0.672	1.29	0.865
4.8	0.940	1.53		2.3	0.834	3.95		2.0	0.870	1.60	0.888
7.0	1.105	2.30		4.0	1.030	4.40		4.1	1.056	1.96	0.875
9.3	1.246	3.31		6.7	1.181	4.98		6.5	1.214	2.47	0.853
10.7	1.282	4.40		9.0	1.318	6.84		8.8	1.360	3.49	0.820
12.2	1.284	6.75		9.7	1.332	9.30		10.1	1.404	4.59	0.786
15.6	1.220	14.54		10.6	1.310	13.76		11.6	1.408	6.62	0.818
				12.9	1.143	20.30		14.7	1.370	12.01	0.795





$\alpha$	$C_L$	$100 \cdot C_D$	$-10 \cdot C_m$	$\alpha$	$C_L$	$100 \cdot C_D$	$-10 \cdot C_m$	$\alpha$	$C_L$	$100 \cdot C_D$	$-10 \cdot C_m$
<b>Gö 766: <math>R = 1.5 \cdot 10^6</math></b>				<b>Gö 766: <math>R = 1.9 \cdot 10^6</math></b>				<b>Gö 766: <math>R = 2.4 \cdot 10^6</math></b>			
-10.1	-0.652	21.19	0.730	7.4	0.851	1.28	0.120	5.6	0.644	1.09	0.130
-13.1	-1.182	2.58	0.160	9.3	1.043	1.61	0.130	7.4	0.846	1.36	0.130
-11.7	-1.078	1.85	0.200	11.3	1.223	2.33	0.130	9.5	1.024	1.80	0.130
-9.7	-0.909	1.33	0.150	12.0	1.279	2.50	0.140	11.3	1.222	2.24	0.140
-7.9	-0.719	1.11	0.130	12.4	1.302	2.71	0.140	12.7	1.340	2.95	0.130
-5.8	-0.526	1.02	0.110	14.1	1.099	9.62	0.180	15.0	1.008	12.59	0.360
-3.9	-0.331	0.93	0.070								
-2.0	-0.135	0.93	0.030								
-0.1	0.049	0.89	0.010								
0.5	0.111	0.90	0.030								
1.2	0.176	0.91	0.050								
1.9	0.239	0.94	0.070								
3.7	0.435	1.02	0.110								
5.6	0.646	1.13	0.100								
7.4	0.850	1.38	0.090								
9.4	1.031	1.76	0.090								
11.4	1.205	2.42	0.090								
11.8	1.226	2.78	0.080								
12.9	1.111	7.15	0.210								
15.1	1.080	11.50	0.400								
<b>Gö 767: <math>R = 1.5 \cdot 10^6</math></b>				<b>Gö 767: <math>R = 1.9 \cdot 10^6</math></b>				<b>Gö 767: <math>R = 2.4 \cdot 10^6</math></b>			
-17.1	-0.657	17.25	0.030	0.1	0.038	0.88	0.030	0.1	0.036	0.90	0.030
-12.9	-1.236	2.62	0.100	2.1	0.239	0.93	0.070	2.1	0.238	0.99	0.070
-11.5	-1.112	1.81	0.110	3.9	0.437	0.93	0.100	3.9	0.437	0.99	0.100
-7.6	-0.748	1.03	0.100	5.7	0.648	1.03	0.100	5.8	0.647	1.09	0.110
-5.8	-0.550	1.90	0.070	7.6	0.854	1.18	0.100	7.6	0.845	1.39	0.110
-3.9	-0.350	0.94	0.060	9.4	1.054	1.53	0.090	9.5	1.051	1.53	0.090
-1.7	-0.150	0.95		11.5	1.239	2.07	0.070	11.5	1.242	2.12	0.070
0.1	0.038	0.96	0.030	12.1	1.300	2.35	0.050	12.1	1.304	2.18	0.060
2.1	0.234	1.02	0.070	12.4	1.338	2.38	0.050	12.7	1.367	2.67	0.040
4.0	0.431	1.03	0.110	12.8	1.363	2.84	0.040	13.0	1.394	2.87	0.030
5.8	0.640	1.13	0.100	15.0	1.138	11.95	0.530	15.1	1.119	12.04	0.640
7.6	0.846	1.27	0.100								
9.5	1.040	1.65	0.090								
11.5	1.226	2.28	0.070								
12.2	1.283	2.54	0.060								
13.9	1.164	8.16	0.330								
<b>Gö 769: <math>R = 1.51 \cdot 10^6</math></b>				<b>Gö 769: <math>R = 1.87 \cdot 10^6</math></b>				<b>Gö 769: <math>R = 2.07 \cdot 10^6</math></b>			
-5.8	0.004	1.03	0.590	-7.8	-0.201	1.14	0.650	-7.8	-0.202	1.11	0.660
-3.7	0.204	1.02	0.530	-6.7	-0.100	1.07	0.620	-6.7	-0.102	1.03	0.620
-1.8	0.411	0.94	0.480	-5.8	-0.096	0.98	0.590	-5.7	-0.004	0.97	0.580
0.2	0.609	0.98	0.440	-4.8	-0.096	0.92	0.550	-4.6	-0.096	0.95	0.550
2.3	0.808	1.06	0.410	-3.7	-0.196	0.90	0.520	-3.5	-0.200	0.91	0.520
4.2	1.013	1.09	0.410	-1.7	-0.401	0.89	0.480	-2.7	-0.301	0.89	0.490
6.3	1.199	1.36	0.410	0.2	0.604	0.92	0.430	-1.7	-0.400	0.91	0.470
8.5	1.384	1.85	0.430	2.3	0.813	0.95	0.410	0.2	0.606	0.90	0.420
10.0	1.479	2.50	0.440	4.2	1.013	0.97	0.400	2.2	0.814	0.94	0.400
10.4	1.488	3.33	0.520	6.3	1.209	1.34	0.410	4.2	1.017	1.03	0.410
11.0	1.461	5.11	0.570	8.4	1.395	1.67	0.430	6.3	1.216	1.19	0.430
12.0	1.470	6.26	0.600	9.1	1.453	1.91	0.460	8.4	1.400	1.68	0.440
13.0	1.480	7.69	0.660	9.5	1.474	2.12	0.450	9.0	1.463	1.77	0.440
14.0	1.476	9.58	0.720	9.9	1.506	2.05	0.440	9.5	1.478	2.25	0.440
15.1	1.448	11.99	0.790	10.2	1.543	2.19	0.460	10.2	1.436	4.75	0.590
				11.0	1.474	4.88	0.580	10.7	1.436	6.09	0.660
				12.0	1.475	6.31	0.610	11.1	1.439	7.26	0.690
				13.0	1.478	7.93	0.670	12.2	1.416	9.58	0.750
				15.1	1.450	12.18	0.800	13.2	1.417	11.39	0.800
				17.4	1.395	16.57	0.950	15.5	1.368	17.09	1.010
								17.5	1.376	20.78	1.150

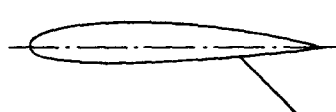
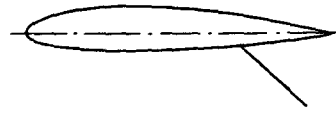
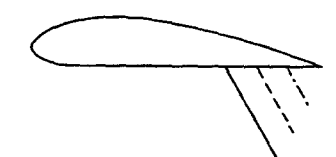
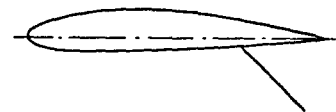
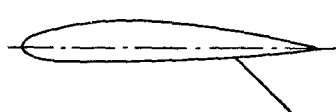
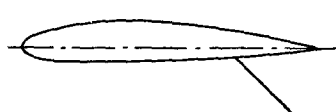
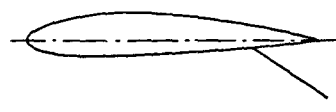
$\alpha$	$C_L$	$100 \cdot C_D$	$-10 \cdot C_m$	$\alpha$	$C_L$	$100 \cdot C_D$	$-10 \cdot C_m$	$\alpha$	$C_L$	$100 \cdot C_D$	$-10 \cdot C_m$
<b>Gö 771: <math>R = 2 \cdot 4 \cdot 10^6</math></b>				<b>Gö 771: <math>R = 2 \cdot 4 \cdot 10^6</math></b>				<b>Gö 795: <math>R = 3 \cdot 8 \cdot 10^6</math></b>			
-2.8	0.011	0.77	0.470	-2.2	0.075	0.82	0.470	-6.8	-0.394	5.76	0.262
-2.1	0.072	0.79	0.460	-1.0	0.208	0.83	0.460	-6.2	-0.351	4.25	0.393
-1.6	0.140	0.78	0.450	0.1	0.339	0.82	-0.450	-5.7	-0.301	2.20	0.452
-1.0	0.201	0.76	0.440	1.3	0.467	0.73	-0.450	-4.4	-0.158	1.40	0.563
-0.3	0.287	0.79	0.430	2.6	0.597	0.76	-0.430	-3.2	0.007	1.19	0.650
0.2	0.325	0.69	-0.420	3.8	0.728	0.77	-0.420	-1.9	0.147	0.87	0.651
0.9	0.390	0.75	-0.410	5.0	0.860	0.81	-0.420	0.1	0.355	1.00	0.642
1.5	0.449	0.80	-0.400	6.2	0.987	0.93	-0.420	2.1	0.557	1.08	0.605
2.1	0.512	0.78	-0.390	7.5	1.103	1.25	-0.410	4.2	0.741	1.52	0.543
2.7	0.574	0.85	-0.380	8.2	1.154	1.50	-0.390	6.4	0.896	2.34	0.459
3.4	0.641	0.90	-0.400	8.9	1.204	1.76	-0.390	7.3	0.928	3.82	0.423
4.0	0.703	0.96	-0.390	9.3	1.228	1.88	-0.390	8.3	0.930	7.97	0.579
4.7	0.766	1.01	-0.380	10.3	1.135	5.17	-0.370	9.3	0.918	11.36	0.722
6.5	0.945	1.38	-0.390	11.3	1.143	6.34	-0.520				
8.6	1.111	2.08	-0.370	14.3	1.135	10.93	-0.640				
9.3	1.157	2.36	-0.360								
9.7	1.176	2.72	-0.370								
10.8	1.085	5.88	-0.470								
11.7	1.094	6.77	-0.490								
15.7	1.095	10.98	-0.600								
<b>Gö 796: <math>R = 3 \cdot 8 \cdot 10^6</math></b>				<b>Gö 797: <math>R = 3 \cdot 8 \cdot 10^6</math></b>				<b>Gö 798: <math>R = 3 \cdot 8 \cdot 10^6</math></b>			
-9.0	-0.296	7.72	0.376	-19.2	-0.237	19.84	0.095	-10.1	-0.134	2.26	0.514
-8.0	-0.241	4.75	0.782	-13.6	-0.156	12.83	0.331	-9.5	-0.040	2.10	1.359
-7.8	-0.234	1.80	0.934	-10.0	-0.106	7.14	0.501	-8.8	0.017	2.02	1.300
-7.4	-0.204	1.71	0.946	-9.4	-0.205	1.96	1.121	-7.7	0.111	2.00	1.282
-6.7	-0.137	1.68	0.952	-8.7	-0.143	1.72	1.107	-5.7	0.301	1.84	1.261
-4.7	+0.052	1.45	0.889	-5.9	+0.107	1.81	1.090	-2.6	0.599	1.83	1.214
-2.6	0.244	1.31	0.831	-1.8	0.496	1.58	0.986	-0.6	0.799	1.58	1.259
-0.6	0.458	1.21	0.925	0	0.735	1.45	1.046	+1.4	0.992	1.59	1.185
1.3	0.672	1.04	0.841	2.0	0.933	1.20	1.042	3.7	1.147	1.90	1.142
3.4	0.864	1.15	0.808	4.2	1.106	1.19	0.948	5.9	1.298	2.29	1.016
5.5	1.043	1.39	0.702	6.5	1.241	1.76	0.844	8.5	1.386	3.01	1.007
8.0	1.151	2.53	0.761	9.1	1.333	3.64	0.766	10.9	1.512	4.95	0.860
9.5	1.137	4.86	0.554	11.9	1.361	6.99	0.702	13.6	1.572	8.37	0.969
11.2	1.112	7.63	0.599	15.3	1.291	13.10	0.818	15.0	1.585	10.43	0.897
14.6	1.037	14.41	0.787	24.6	-0.240	22.64	0.055	16.8	1.525	14.33	1.038
<b>DVL 0 00 09 — 0.825 40</b>				<b>DVL 0 00 09 — 0.55 40</b>				<b>DVL 0 00 09 — 0.55 45</b>			
$R = 2 \cdot 59 \cdot 10^6$				$R = 2 \cdot 66 \cdot 10^6$				$R = 2 \cdot 60 \cdot 10^6$			
-3.4	-0.303	0.80	0.111	-1.4	-0.114	0.60	0.050	-1.0	-0.096	0.47	0.056
-1.4	-0.114	0.61	0.059	-0.5	-0.043	0.52	0.010	-0.3	-0.035	0.39	0.013
0.0	-0.002	0.48	0	-0.0	0.005	0.50	0	0.2	0.009	0.37	-0.007
0.6	0.082	0.50	-0.029	0.3	0.036	0.49	-0.011	0.7	0.053	0.38	-0.029
1.4	0.120	0.55	-0.057	1.7	0.066	0.49	-0.022	2.1	0.181	0.55	-0.116
2.7	0.243	0.64	-0.092	1.3	0.126	0.54	-0.048	6.2	0.531	0.88	-0.206
4.7	0.432	0.75	-0.133	2.0	0.186	0.60	-0.071	8.2	0.724	1.24	-0.199
7.4	0.688	1.10	-0.145	2.7	0.249	0.64	-0.086	8.6	0.756	1.31	-0.196
10.1	0.934	1.73	-0.154	4.0	0.373	0.75	-0.117	9.0	0.684	5.18	-0.064
11.6	1.037	2.36	-0.170	5.4	0.498	0.88	-0.126	10.6	0.657	11.78	0.245
12.3	1.072	2.77	-0.175	6.7	0.624	1.07	-0.134	16.9	0.596	20.59	0.500
14.6	0.632	19.06	0.626	7.4	0.662	1.18	-0.136				
15.8	0.606	20.18	0.627	7.6	0.616	3.64	-0.205				
16.8	0.598	21.57	0.702	7.7	0.631	4.39	-0.193				
17.9	0.590	22.84	0.677	9.1	0.666	8.39	-0.055				
				10.0	0.672	11.17	-0.270				
				11.7	0.627	14.35	-0.492				
				13.8	0.601	17.68	-0.573				



$\alpha$	$C_L$	$100 \cdot C_D$	$-10 \cdot C_m$	$\alpha$	$C_L$	$100 \cdot C_D$	$-10 \cdot C_m$	$\alpha$	$C_L$	$100 \cdot C_D$	$-10 \cdot C_m$
<b>DVL 000 15 — 0·55 45</b>				<b>DVL 000 15 — 1·1 50</b>				<b>DVL 000 18 — 1·1 40</b>			
$R = 2 \cdot 73 \cdot 10^6$				$R = 2 \cdot 69 \cdot 10^6$				$R = 2 \cdot 63 \cdot 10^6$			
—3·8	—0·236	0·78	0·322	—5·4	—0·306	1·07	0·560	—3·3	—0·208	0·86	0·318
—1·6	—0·113	0·69	0·163	—3·3	—0·126	0·88	0·476	—1·9	—0·106	0·74	0·218
—0·8	—0·038	0·53	0·067	—1·4	—0·003	0·76	0·348	—0·8	—0·040	0·65	0·099
0·6	0·063	0·51	—0·057	—1·0	0·014	0·70	0·277	—0·0	0·005	0·63	0·015
1·0	0·089	0·49	—0·087	—0·5	0·008	0·63	0·157	0·8	0·046	0·62	—0·060
2·1	0·156	0·56	—0·197	0·0	—0·004	0·59	0·002	2·3	0·129	0·70	—0·217
5·2	0·360	0·86	—0·330	1·0	—0·016	0·68	—0·280	5·2	0·350	0·91	—0·382
9·3	0·702	1·38	—0·499	1·9	0·010	0·74	—0·410	9·4	0·686	1·57	—0·505
13·6	1·032	2·78	—0·503	2·6	0·060	0·78	—0·462	13·7	1·013	2·78	—0·528
15·2	1·108	3·59	—0·513	4·4	0·197	0·83	—0·552	15·0	1·076	3·36	—0·537
15·7	1·124	3·88	—0·509	7·6	0·460	1·09	—0·663	15·4	1·088	3·85	—0·518
17·1	0·808	13·55	—0·038	11·8	0·804	1·78	—0·734	15·8	1·056	5·32	—0·459
17·8	0·803	14·12	—0·001	16·1	1·142	3·30	—0·671	16·9	0·982	8·84	—0·261
18·3	0·759	18·95	0·007	17·3	1·210	4·10	—0·654	19·0	0·968	13·42	—0·102
19·5	0·773	19·74	0·043	17·6	1·226	4·23	—0·648	20·3	0·899	16·40	0·016
21·3	0·523	29·99	0·243	17·8	1·236	4·38	—0·648				
22·2	0·528	28·65	0·249	21·6	0·530	24·74	0·007				
				22·2	0·539	25·75	0·023				
<b>DVL 000 18 — 0·55 40</b>				<b>DVL 000 18 — 1·1 50</b>				<b>DVL 000 18 — 0·825 45</b>			
$R = 2 \cdot 74 \cdot 10^6$				$R = 2 \cdot 59 \cdot 10^6$				$R = 2 \cdot 74 \cdot 10^6$			
—0·7	—0·053	0·67	0·069	—5·3	—0·207	1·19	0·769	—1·6	—0·065	0·64	0·270
—0·0	0·002	0·65	0·014	—2·9	0·88	0·632	—0·4	—0·017	0·57	0·100	
0·6	0·054	0·66	—0·040	—1·7	0·067	0·75	0·518	0·6	0·031	0·55	—0·030
2·1	0·156	0·68	—0·148	—0·7	0·053	0·69	0·237	2·0	0·084	0·65	—0·250
5·8	0·419	0·94	—0·362	1·1	—0·013	0·86	—0·325	4·0	0·177	0·84	—0·460
10·2	0·742	1·56	—0·497	2·9	0·045	0·92	—0·590	8·3	0·508	1·29	—0·630
13·1	0·952	2·40	—0·514	5·0	0·196	0·99	—0·739	12·7	0·830	2·27	
14·2	1·010	3·20	—0·497	8·2	0·457	1·29	—0·828	15·6	1·040	3·58	—0·630
14·8	0·983	4·60	—0·416	11·8	0·740	1·98	—0·842	16·6	1·091	4·15	—0·610
15·2	0·975	5·34	—0·388	16·2	1·052	3·63	—0·725	17·6	0·914	10·46	—0·350
16·1	0·954	7·16	—0·323	16·9	1·096	4·14	—0·714	19·2	0·912	13·01	—0·230
20·6	0·861	16·48	—0·012	17·7	1·145	4·69	—0·670				
				19·3	0·869	1·34	—0·345				
				21·4	0·804	1·87	—0·168				
				22·5	0·778	20·90	—0·095				

Table 11.6

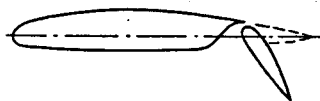
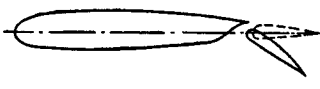
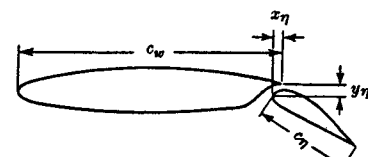
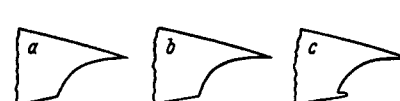
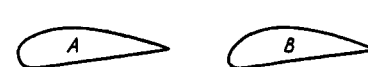
Profiles with High-lift Devices

	Arrangement	Profile	Source	$A = \frac{b^2}{S}$	$t/c$	$c_{\eta}/c$
1		Wa 192	FB 1655 Wysocki	7	0.12	0.30
2		Wa 743	FB 1655 Wysocki	6	0.14	0.30
3		Wa 284	FB 1655 Wysocki	5	0.175	0 0.15 0.25 0.35
4		Clark Y	N 422	6	0.115	0 0.20 0.30 0.40
5		Various	Jahrbuch d. Lufo 1939, I 79 Schrenk		0.09 0.12 0.15 0.18 0.21	0.20
6		NACA 2409 2412 2415 2418 2421	FB 642 Kramer, Doetsch	5	0.09 0.12 0.15 0.18 0.21	0.10
6		NACA 2409 2412 2415 2418 2421	"	5	0.09 0.12 0.15 0.18 0.21	0.20
7		Wa 743 Zap	FB 1655	5	0.14	0.30

$\eta$	$R$	$C_{L_{\max}}$	$aC_{L_{\max}}$	$\Delta C_{L_{\max}}$	$\Delta aC_{L_{\max}}$	$(L/D)C_{L_{\max}}$	$\frac{C_{L_{\max}}}{C_{D_{\min}}(\eta=0)}$	Remarks
0 20 40 60	$2 \cdot 2 \cdot 10^5$	1.20 1.65 1.86 1.99	16 — 11.5 11.5	— 0.45 0.66 0.79	— — —4.5 —4.5	9.50 — 5.40 4.30	86 118 133 142	Warsaw
0 20 40 60	$3 \cdot 10^5$	1.07 1.54 1.90 1.87	17.5 13.5 13.5 11.0	— 0.47 0.83 0.80	— —4.0 —4.0 —6.5	7.50 — — 3.70	112 160 198 195	"
60	$7 \cdot 1 \cdot 10^5$	1.40 2.05 2.12 2.16	14.5 11.5 11.5 11.5	— 0.65 0.72 0.76	— —3.0 —3.0 —3.0	7.80 4.80 3.80 3.40	93 137 141 144	"
0 68 62 54	$6 \cdot 10^5$	1.27 2.27 2.45 2.52	14.0 14.0 13.0 12.5	— 1.00 1.18 1.25	— 0 —1.0 —1.5	9.16 4.20 3.60 3.90		Position of axis of rotation $\frac{x_R}{c} = 1.0$ 0.93 0.90 NACA
75	$> 2 \cdot 10^6$			0.66 0.81 0.97 1.14 1.28				Mean values from German and other measurements
0	$2 \cdot 7 \cdot 10^6$	1.43 1.35 1.28 1.18 1.16	20.6 20.0 19.2 23.0 24.0	— — — — —	— — — — —	8.4 8.6 9.3 9.0 5.0	213 190 164 151 141	DVL
60	$2 \cdot 7 \cdot 10^6$	2.07 2.40 2.50 2.48 2.46	19.0 24.5 24.5 23.0 21.5	0.64 1.05 1.22 1.30 1.30	—1.6 +4.5 +5.3 0 —2.5	4.2 3.9 4.0 4.0 4.1	308 338 320 317 300	"
0 20 40 60 97	$3 \cdot 10^5$	1.07 1.55 1.97 2.05 2.09	17.5 14.0 13.5 10.7 10.7	— 0.48 0.90 0.98 1.02	— —3.5 —4.0 —6.8 —6.8	9.1 5.3 4.5 3.8 3.3	107 155 197 205 209	Warsaw

	Arrangement	Profile	Source	$A = \frac{b^2}{S}$	$t/c$	$c_{\eta}/c$
8		Wa 192	FB 1655	7 6	0.12 0.12	0.4
9		Wa 829	FB 1655 Wysocki	7	0.12	0.15
10		Clark Y	R 554 Wenzinger	6	0.115	0.20
11		Wa 859	FB 1655 Wysocki	7	0.126	0.33 0.33 0.28
12		B 106-04 R	FB 543 M. Schiller	5	0.137	0 0.1 0.2 0.3 0.4
13	see No. 12	NACA 23012	R 554 Wenzinger	6	0.12	0.20
14	see No. 12	23015	N 763 Ames	6	0.15	0.25
15	see No. 12	23021	R 554	6	0.21	0.20

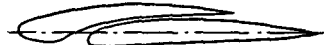
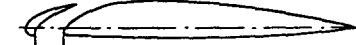
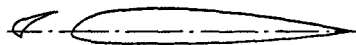
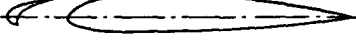
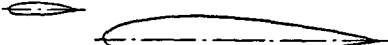
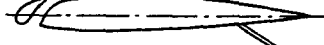
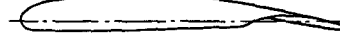
$\eta$	$R$	$C_{L\max}$	$\alpha C_{L\max}$	$\Delta C_{L\max}$	$\Delta \alpha C_{L\max}$	$(L/D)C_{L\max}$	$\frac{C_{L\max}}{C_{D\min}(\eta=0)}$	Remarks
0 60	$7 \cdot 1 \cdot 10^5$	1.20 1.65	14.0 12.5	— 0.45	— —1.5	6.2 3.9	89 147	Warsaw
0 60	$2 \cdot 9 \cdot 10^5$	0.95 1.63	14.0 9.0	— 0.68	— —5.0	10.2 6.3	100 172	"
50 opt 60 opt	$6 \cdot 0 \cdot 10^5$	1.67 2.02		0.50 0.77		4.3 4.9		Slot open Slot closed NACA
0 13 20	$2 \cdot 9 \cdot 10^5$	1.32 1.51 1.65	14.0 12.5 12.5	— 0.19 0.33	— —1.5 —1.5	10.4 7.8 7.3	94 108 118	Warsaw
0 76 opt 80 opt 60 opt 60 opt	$6 \cdot 1 \cdot 10^5$	1.08 1.74 1.85 1.82 1.68	14.5 14.2 15.0 13.0 10.0	— 0.66 0.77 0.74 0.60	— —0.3 +0.5 —1.5 —4.5	8.3 5.1 3.9 3.8 3.3	108 174 185 182 168	DVL
0° 30° 60°	$6 \cdot 1 \cdot 10^5$	1.14 1.68 1.96		— 0.54 0.82				NACA
0° 30° 60°	$6 \cdot 1 \cdot 10^5$	1.10 1.69 1.98	14.5 13.7 12.7	— 0.59 0.88	— —0.8 —1.8	11.9 6.6 4.8	115 178 210	"
0° 30° 60°	$6 \cdot 1 \cdot 10^5$	1.18 1.70 2.15		— 0.62 0.97				"

	Arrangement	Profile	Source	$A = \frac{b^2}{S}$	$t/c$	$c_{\eta}/c$
16	see No. 12	66 (215)—216	R 824	$\infty$	0.16	0.20
17		Wa 743	FB 1655 Doetsch-König	5	0.14	0.30
18		2412	FB 762	5	0.12	0.2
19		23012	R 679 ACR (1940) ACR (1940) R 664 R 664 R 679 R 664 N 808 N 808 N 808 N 808 N 715 N 715	$\infty$	0.12 0.12 0.12 0.12 0.12 0.12 0.12 0.12 0.12 0.12 0.12 0.12 0.12 0.12	0.10 0.15 0.25 0.256 0.257 0.257 0.267 0.30 0.30 0.30 0.30 0.40 0.40
20		23021	N 782 ACR (1941) ACR (1941) R 677 R 677 R 677 R 677 N 728 N 728	$\infty$	0.21 0.21 0.21 0.21 0.21 0.21 0.21 0.21	0.15 0.15 0.25 0.257 0.257 0.257 0.40 0.40
21		23030	N 755	$\infty$	0.30 0.30 0.30 0.30	0.257 0.257 0.40 0.40
22		63.4—420 63.4—421 (approx.)	R 824 MR (1943)	$\infty$	0.20 0.21	0.25 0.243

$\eta$	$R$	$C_{L_{\max}}$	$\alpha C_{L_{\max}}$	$\Delta C_{L_{\max}}$	$\Delta \alpha C_{L_{\max}}$	$(L/D)C_{L_{\max}}$	$\frac{C_{L_{\max}}}{C_{D_{\min}}(\eta=0)}$	Remarks	
0°	$6 \cdot 10^6$	1.43	16.5				358	NACA	
30°		2.01	14.0	0.58	-2.5		503		
60°		2.37	10.5	0.94	-6		593		
0	$3.1 \cdot 10^6$	1.05	16.5	—	—	8.51	82	Warsaw	
15		1.38	15.5	0.33	-1.0	6.2	108		
45		1.77	13.5	0.72	-3.0	5.0	138		
60		1.84	11.0	0.79	-5.5	4.4	144		
0	$1.55 \cdot 10^6$	1.27	19.0	—	—	9.1	106	DVL	
20		1.80	19.0	0.53	0	7.5	150		
45		2.34	21.0	1.07	+2.0	5.5	195		
				$c_w/c$	Type				
					$w$	$\eta$	$x_\eta$	$y_\eta$	
50	$3.5 \cdot 10^6$	2.25		0.93	a	A	0.004	0.005	NACA
30	$3.5 \cdot 10^6$	2.68		1.00	b	A	0	0.015	
40	$3.5 \cdot 10^6$	3.22		1.00	b	A	0	0.015	
50	$3.5 \cdot 10^6$	2.76		0.80	a	B	0.005	0.018	
50	$3.5 \cdot 10^6$	2.81		0.83	a	A	0.005	0.016	
40	$3.5 \cdot 10^6$	2.83		0.83	a	A	0.013	0.024	
30	$3.5 \cdot 10^6$	2.90		1.00	b	A	0	0.025	
50	$3.5 \cdot 10^6$	2.92		0.90	c	A	0.002	0.010	
40	$3.5 \cdot 10^6$	2.92		0.90	c	A	0.002	0.020	
30	$3.5 \cdot 10^6$	2.93		0.90	c	A	0.002	0.030	
40	$3.5 \cdot 10^6$	2.88		0.90	b	A	0.002	0.020	
40	$3.5 \cdot 10^6$	3.29		1.00	b	A	0	0.015	
50	$3.5 \cdot 10^6$	2.87		0.715	b	A	0.015	0.015	
50	$3.5 \cdot 10^6$	2.90		0.715	a	A	0.015	0.015	
60	$3.5 \cdot 10^6$	2.59		1.00	b	A	0	0.015	NACA
60	$3.5 \cdot 10^6$	2.66		1.00	b	A	0.050	0.030	
40	$3.5 \cdot 10^6$	3.17		1.00	b	A	0.025	0.015	
60	$3.5 \cdot 10^6$	2.69		0.827	b	B	0	0.015	
60	$3.5 \cdot 10^6$	2.74		0.827	a	B	0	0.015	
60	$3.5 \cdot 10^6$	2.71		0.827	b	A	0.005	0.020	
50	$3.5 \cdot 10^6$	2.82		0.827	a	A	0	0.025	
50	$3.5 \cdot 10^6$	2.79		0.715	b	A	0.015	0.025	
50	$3.5 \cdot 10^6$	2.88		0.715	a	A	0.015	0.045	
60	$3.5 \cdot 10^6$	2.59		0.860	b	B	-0.025	0.040	NACA
60	$3.5 \cdot 10^6$	2.68		0.860	a	B	-0.005	0.040	
50	$3.5 \cdot 10^6$	2.82		0.775	b	B	0.025	0.060	
50	$3.5 \cdot 10^6$	2.90		0.775	a	B	0.025	0.060	
35	$6.0 \cdot 10^6$	3.00		0.88	b	B	0.018	0.045	NACA
40	$9.0 \cdot 10^6$	3.21		0.835	a	A	0	0.027	

	Arrangement	Profile	Source	$A = \frac{b^2}{S}$	$t/c$	$c_{\eta}/c$
23	see No. 19-22	65-210	N 1191	$\infty$ $\infty$ $\infty$ $\infty$ $\infty$	0-10 0-10 0-10 0-10 0-10	— 0-25 0-25 0-25 0-25
24		66-2-218 $a = 0-6$	R 824	$\infty$	0-16	0-30
25		Wa 743	FB 1655	5	0-14	0-68
26		Wa 743	FB 1655	5	0-14	0-50
27		Wa 859	FB 1655	7	0-126	0-435
28		Wa 828	FB 1655	7	0-10	AB: 0-335 CD: 0-25
29		23012	R 573	5	0-12	0 0-20
30		P II p	ZAHN No. 159 Krasilschikoff 1934		0-14	0-20

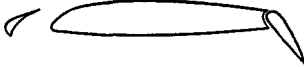
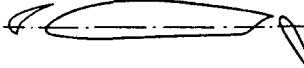
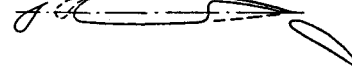
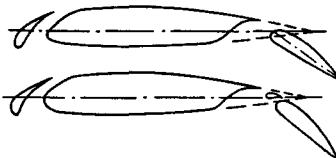
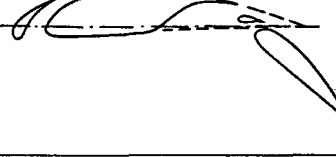
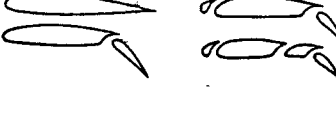
$\eta$	$R$	$C_{L_{\max}}$	$\alpha C_{L_{\max}}$	$c_w/c$	Type	$x_\eta$	$y_\eta$	Remarks	
					$w$				
0	$6 \cdot 10^6$	1.3			—	—	—	NACA	
0		1.4			0.84	c A	0.009		
45		2.47			0.80	c A	0.014		
41.3		2.48			0.975	c A	0.004		
35		2.45			0.975	c A	0.004		
35		2.43			0.975	c A	0.020		
37					0.90	c A	0		
					$\Delta C_{L_{\max}}$	$\Delta \alpha C_{L_{\max}}$	$(L/D)C_{L_{\max}}$	$\frac{C_{L_{\max}}}{C_{D_{\min}} (\eta = 0)}$	
0	$3 \cdot 10^5$	1.37	18.5		—0.02	—0.2	8.1	67	Warsaw
15		1.35	16.5		0.05	—7.0	4.8	66	
45		1.42	11.5		—0.10	—12.0	2.6	70	
60		1.27	6.5				1.8	62	
—20	$3 \cdot 1 \cdot 10^5$	0.60	19.5				6.0		"
10		1.47	15.0				6.7		
45		1.97	11.0				4.4		
—25	$2 \cdot 9 \cdot 10^5$	0.99	18.5				6.0		"
4		1.41	14.0				9.2		
10		1.48	14.0				7.7		
—25	$2 \cdot 9 \cdot 10^5$	0.77	16.2		—0.16	+2.5	4.3	75	"
0		0.93	13.7		—	—	9.8	91	
10		1.20	11.7		0.27	—2.0	8.5	118	
—25	60		1.36	12.5	0.43	—1.2	2.9	133	"
0			1.68	8.9	0.75	—4.8	4.3	164	
15			1.77	6.3	0.84	—7.4	5.3	173	
0	$7 \cdot 3 \cdot 10^5$	1.12	15.0		—	—	12.2	112	NACA
30		1.91	14		0.79	—1.0	7.6	74	
Without flap	$3 \div 5 \cdot 10^5$	1.45	$a_\infty =$		—	—			ZAH
0		1.45	15.0		—	—			
30		2.05	13.5		0	—1.5			
40		2.15	7.5		0.60	—7.5			
			5.0		0.70	—10.0			

	Arrangement	Profile	Source	<i>A</i>	<i>t/c</i>	$c_{\eta}/c$
31		Wa 743	FB 1655	7	0·14	—
32		Wa 192	FB 1655	5	0·12	$\frac{c_s}{c} = 0·154$
33		Wa 755	FB 1655	5	0·12	without slat $\frac{c_s}{c} = 0·10$ $0·16$
34		NACA 23012	FB 1623 Krüger	5 with end plates	0·12	$\frac{c_s}{c} = 0·13$
35		Clark Y	R 428		0·115	$\frac{c_s}{c} = 0·145$
36	 Maxwell Slot	Clark Y	N 598	6	0·115	0·211
37	 Short flap	Wa 192	FB 1655	7	0·12	0·25
38	 Fowler	Clark Y	N 419 R 534	6	0·115	0 0·40 0·20 0·30

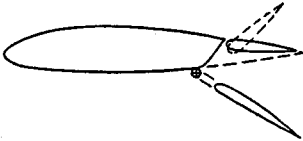
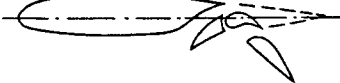
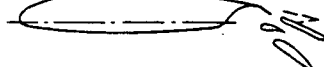
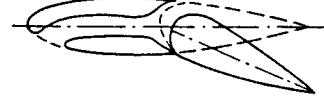
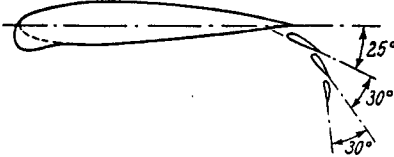
$\eta$	$R$	$C_{L_{\max}}$	$\alpha C_{L_{\max}}$	$\Delta C_{L_{\max}}$	$\Delta \alpha C_{L_{\max}}$	$(L/D)C_{L_{\max}}$	$\frac{C_{L_{\max}}}{C_{D_{\min}} (\eta = 0)}$	Remarks
—	$2 \cdot 9 \cdot 10^5$	1.07 1.18	16.5 16.5	— 0.11	— 0	9.2 9.2	100 56	without slat with slat Warsaw
—	$7 \cdot 1 \cdot 10^5$	1.21 1.46 1.75 1.70	17.5 24.5 26.5 27.0	— 0.25 0.54 0.49	— 7.0 9.0 9.5	7.5 5.6 5.4 5.1	92 111 133 129	without slat $x_s/c = 0.020$ 0.060 0.112 Warsaw
—	$2 \cdot 9 \cdot 10^5$	0.95 1.48 1.64	15.5 26.5 25.5	— 0.53 0.69	— 11.0 11.0	9.4 4.6 4.0	79 123 137	"
		1.27 2.00	$\alpha_{\infty} =$ 10.8 17.5	— 0.73	— 6.7			AVA
	$6 \cdot 10^5$	1.30 1.81	14.0 26.5	— 0.47	— 12.5			without slat with slat NACA
0 0 0	$6 \cdot 10^5$	1.26 1.81 2.07	14.0 23.0 25.8	— 0.55 0.81	— +9.0 +11.8	10.7 6.9 6.4	.84 121 138	original profile with slat $c_s/c = 0.175$ with slat $c_s/c = 0.300$
60 60 60	$6 \cdot 10^5$	2.09 2.31 2.53	11.8 16.7 21.6	0.83 1.05 1.27	—2.2 +2.7 +7.6	4.9 4.7 4.5	139 154 169	without slat with slat $c_s/c = 0.175$ with slat $c_s/c = 0.300$
0 13	$2 \cdot 9 \cdot 10^5$	1.20 1.72	16.0 12.0	— 0.52	— —4.0	9.6 8.7	91 130	Warsaw
0 40 30 40	$6 \cdot 1 \cdot 10^5$	1.27 3.17 2.45 2.85	16.0 14.0 15.0 13.0	— 1.90 1.18 1.58	— —2.0 —1.0 —3.0	7.0 4.2 5.2 4.6		NACA

	Arrangement	Profile	Source	$A$	$t/c$	$c_{\eta}/c$
39		NACA 2410	Jahrbuch d. D. Lufo 1939 Seiferth	4 4 6.67	0.10 0.10 0.10	0.40 0.40 0.27
40		Wa 433/349	FB 1655	7	0.189/0.165	0.7
41		NACA 2412	FB 1510 FB 548	5	0.12	0.3
42		23012	R 679 R 723 ARR 3 L 10	8	0.12	0.10 0.257 0.257
43		23021	R 723 ARR L 4 J 05		0.21	0.257 0.257
44		63-210	N 1545		0.10	0.25
45		64-208	N 1545		0.08	0.25 0.25
46		64-210	N 1545		0.10	0.25
47		64-212	N 1545		0.12	0.25
48		64 <sub>1</sub> A212	N 1293		0.12	0.229
49		65-210	N 1545		0.10	0.25
50		65 (216)-215 $a = 0.8$	RM L7A30		0.15	0.248
51		65 <sub>3</sub> -418	N 1071		0.18	0.238
52		66-210	N 1545		0.10	0.25

$\eta$	$R$	$C_{L_{\max}}$	$\alpha C_{L_{\max}}$	$\Delta C_{L_{\max}}$	$\Delta \alpha C_{L_{\max}}$	$(L/D)C_{L_{\max}}$	$\frac{C_{L_{\max}}}{C_{D_{\min}} (\eta = 0)}$	Remarks
32.5 0 42.5 0 $17.5 \div 55$ 0	$6.3 \cdot 10^5$	2.43 $\sim 1.20$ 2.82 $\sim 1.20$ 2.92 1.20	14.9 $\sim 16.9$ 12.6 $\sim 16.9$ 14.8 16.9	$\sim 1.23$ $\sim 1.62$ $\sim 4.3$ $\sim 2.1$ $\sim 2.1$	$\sim -2.0$ $\sim -4.0$ $\sim -4.8$	4.2 4.0 4.8		AVA
0 20	$2.2 \cdot 10^5$	1.70 3.55	21.0 21.0	— 1.85	— 0	5.6 3.0	31 64	Warsaw
0 45	$2.1 \cdot 10^6$	1.32 2.97	18	1.65		4.2		DVL
			$c_w/c$	$c_h/c$	$\eta_h$	$x_\eta$	$y_\eta$	$x_k$ $y_k$
70 70 60	$3.5 \cdot 10^6$ $3.5 \cdot 10^6$ $3.5 \cdot 10^6$	2.99 3.47 3.30	0.83 0.715 0.826	0.189 0.227 0.117	40 30 25	0.009 0.014 —0.016	0.009 0.012 0.010	NACA 0.014   0.024 0.015   0.035 —0.004   0.017
60 70	$3.5 \cdot 10^6$ $3.5 \cdot 10^6$	3.56 3.32	0.715 0.827	0.227 0.147	30 30	0.019 0.017	0.024 0.027	0.025   0.065 0.007   0.024
50	$6.0 \cdot 10^6$	2.91	0.84	0.075	25	0.022	0.024	0.024   0.018
45 50	$6.0 \cdot 10^6$ $6.0 \cdot 10^6$	2.51 2.40	0.84 0.84	0.075 0.056	30 25	0.015 0.018	0.015 0.014	0.015   0.019 0.015   0.024
55	$6.0 \cdot 10^6$	2.82	0.84	0.075	30	0.023	0.006	0.012   0.018
50	$6.0 \cdot 10^6$	3.03	0.84	0.075	30	0.021	0.020	0.010   0.019
55	$6.0 \cdot 10^6$	2.83	0.833	0.083	26	0.044	0.005	0.004   0.014
50	$6.0 \cdot 10^6$	2.72	0.84	0.075	25	0.025	0.011	0.009   0.024
70	$6.3 \cdot 10^6$	3.38	0.82	0.096	12	0.024	0.010	0.025   0.032
65	$6.0 \cdot 10^6$	3.50	0.851	0.106	21	0.027	0.007	0.012   0.028
60	$6.0 \cdot 10^6$	2.72	0.84	0.100	25	0.027	0.039	0.024   0.021

	Arrangement	Profile	Source	A	t/c	$c_{\eta}/c$
53		B 106—0·4R	FB 543 M. Schiller	5	0·137	0·2
54		Wa 192	FB 1655	7	0·12	0·228
55		Clark Y	N 459	6	0·115	0 0 0·4
56		NACA 2413	Jahrbuch d. D. Lufo. 1939 Seiferth	4	0·13	0·4
57		NACA 2412—34	Jahrbuch d. D. Lufo. 1939 Seiferth	4	0·12	0·325
58		NACA 2416	Jahrbuch d. D. Lufo. 1939 Seiferth	4	0·16	0·325
59		NACA 6416	Jahrbuch d. D. Lufo. 1939 Seiferth	4	0·16	0·50
60		Clark Y	R 427		0·115	0·3

$\eta$	$R$	$C_{L_{\max}}$	$\alpha C_{L_{\max}}$	$\Delta C_{L_{\max}}$	$\Delta \alpha C_{L_{\max}}$	$(L/D)C_{L_{\max}}$	$\frac{C_{L_{\max}}}{C_{D_{\min}}(\eta=0)}$	Remarks
0 80 80	$6 \cdot 1 \cdot 10^5$	1.08 1.85 2.15	14.5 15.0 20.0	— 0.77 1.07	— +0.5 +5.5	8.3 3.9 4.0	108 185 215	original profile without slat with slat
0 0 20 40	$2 \cdot 9 \cdot 10^5$	1.28 1.83 2.21 2.31	16.5 21.5 18.5 18.5	— 0.55 0.93 1.03	— 5.0 2.0 2.0	8.6 8.0 7.0 5.6	68 97 117 122	slot open with slat with slat and flap with slat and flap Warsaw
0 0	$6 \cdot 1 \cdot 10^5$	1.27 2.08 3.62	14.0 30.0 21.0	— — —	— — —	8.8 4.5 3.8	— — —	original profile with slat with slat and Fowler NACA
35	$6 \cdot 3 \cdot 10^5$	3.22 2.61	30.4 20.3	— 0.61	— 10.1	3.0 3.7	— —	AVA
0 35	$6 \cdot 3 \cdot 10^5$	0.94 2.67	16.4 21.9	— 1.73	— 5.6	— 3.6	80 226	without slat with slat AVA
35 35	$6 \cdot 3 \cdot 10^5$	2.61 3.40	20.3 36.9	— —	— —	3.8 2.9	— —	without slat with slat AVA
45 45		2.75 3.49	20.2 35.7	— —	— —	3.4 2.6	— —	without slat with slat
40	$6 \cdot 3 \cdot 10^5$	4.05	38.3	— — — —	— — — —	2.3	— — — —	$\frac{c_t}{c} = 0.18$ AVA
0	$6 \cdot 1 \cdot 10^5$	1.27 1.98 2.26 2.60	15.0 12.0 19.0 20.0	— 0.71 0.99 1.33	— —3.0 +4.0 +5.0	7.5 4.0 3.8 3.8	84 131 150 173	original profile with flap NACA

	Arrangement	Profile	Source	$A = \frac{b^2}{S}$	$t/c$	$c_{\eta}/c$
61		NACA 2415	Aero Digest VIII, 1938 R. F. Hall		0.15	~0.33
62		NACA 23014	Jahrbuch d. D. Lufc. 1940 Stauffer	5.16	0.14	0.26
63		NACA 23012	FB 1253 Holstein	4.7	0.12	
64		NACA 0020	FB 1576 Kramer		0.20	0.50
65		NACA 6215	AVA Bericht 37/4/24	4.5	0.15	$c_{\eta_1}/c = 0.13$ $c_{\eta_2}/c = 0.10$ $c_{\eta_3}/c = 0.07$
66			Aeron. Journal 1921 p. 270			

$\eta$	$R$	$C_{L\max}$	$aC_{L\max}$	$\Delta C_{L\max}$	$\Delta aC_{L\max}$	$(L/D)C_{L\max}$	$\frac{C_{L\max}}{C_{D\min}(\eta = 0)}$	Remarks
0 45		1.52 2.32	—	— 0.80				Dornier wind-tunnel
0 60	$1.6 \cdot 10^6$	1.42 3.00	20.4 21.1	1.58	0.7	7.5 3.5	119 250	AVA
0 55		1.43 2.70						DVL
0 10 20	$1.97 \cdot 10^6$	1.14 2.10 2.58	19.0 $\infty$	0.96 1.44				
25	$5.6 \cdot 10^5$	1.58 3.37	21.5 16.5	1.79	—5.0	6.3 4.0	42 89	without flaps with flaps
	$1.1 \cdot 10^6$	3.92	45					

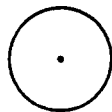
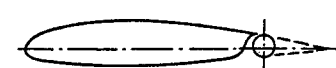
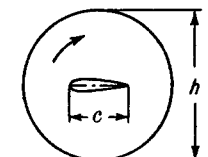
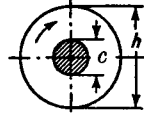
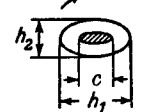
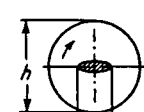
	Special arrangements	Source	<i>A</i>	<i>R</i>	<i>u/v</i>	$\eta$	$C_L$	$\alpha$	Remarks
67		E IV Busemann	12		2.0 4.0  2.0 4.0 8.0 12.0 13.0		max 4.0 8.4  4.2 11.8 14.9 16.0 16.5		without end plates  with end plates 3.1  AVA
68		FB 826 Regenscheit	4	$9 \cdot 10^4$	0 1.0 2.0 3.0 4.0 5.0 6.0		1.00 1.20 1.70 2.07 2.23 2.27 2.35	15	Profile 23015 AVA
69		FB 1513 Küchemann		$6 \cdot 10^5$	0 1.0 2.0 4.0 0	0 — — — 45	max 1.60 2.40 2.75 3.80 2.10	max 20.0 21.0 21.0 18.0 21.0	Profile 23015 AVA
70		FB 1308 v. Holst	5.3		1.0 3.0 5.0 3.0 5.0 7.0		max 2.0 7.5 16.5  5.3 7.7 8.3	max 20.0 21.0 21.0 18.0 21.0	with end plates $h/b = 0.47$ AVA  without end plates
71		FB 1651 Küchemann	1.7		2.0 4.0 8.0 10.0		1.3 1.8 2.3 2.6		without end plates AVA
72		FB 1651 Küchemann	12		2.0 4.0 8.0		4.0 11.7 14.9		AVA
73		FB 1651 Küchemann	5		2.0 4.0 8.0 10.0		2.8 3.4 2.4 2.2		Symmetrical circular arc $t/c = 0.167$ AVA
74		FB 1651 Küchemann	5		2.0 4.0 8.0 10.0		2.9 4.1 8.9 7.7		AVA
75		FB 1651 Küchemann	5		2.0 4.0 8.0 10.0		2.9 4.3 10.4 12.6		AVA

Table 11.7

Coefficients for the Determination of Theoretical Lift and Drag Coefficients

$$\begin{aligned} dC_L/d\alpha &= 2\pi(1 + \sum_{m=1}^{N-1} A_m \cdot 2y_m^{(t)}/c) \\ dC_m/dC_L &= -\frac{1}{4}(1 + \sum_{m=1}^{N-1} C_m \cdot 2y_m^{(t)}/c) \\ \alpha^* &= \sum_{m=1}^{N-1} E_m \cdot 2y_m^{(e)}/c \end{aligned} \quad \begin{aligned} \alpha_0 &= \frac{2\pi}{dC_L/d\alpha} \sum_{m=1}^{N-1} B_m \cdot 2^4 y_m^{(e)}/c \\ C_{m_0} &= \sum_{m=1}^{N-1} D_m \cdot 2^4 y_m^{(e)}/c \\ C_{L^*} &= \sum_{m=1}^{N-1} F_m \cdot 2^4 y_m^{(e)}/c \end{aligned}$$

**N = 6**

<i>m</i>	<i>x<sub>m</sub>/c</i>	<i>A<sub>m</sub></i>	<i>B<sub>m</sub></i>	<i>C<sub>m</sub></i>	<i>D<sub>m</sub></i>	<i>E<sub>m</sub></i>	<i>F<sub>m</sub></i>
1	0.93302	0.66667	-2.48812	0.82136	-4.36179	-1.15471	8.37760
2	0.75000	0	0	0.57736	-0.26180	0	0
3	0.50000	0.33333	-0.33333	0.33333	-0.52360	0	2.09440
4	0.25000	0	0	0.57736	0.26180	0	0
5	0.06699	0.66667	-0.17863	-1.48804	0.17286	1.15471	8.37760

**N = 12**

<i>m</i>	<i>x<sub>m</sub>/c</i>	<i>A<sub>m</sub></i>	<i>B<sub>m</sub></i>	<i>C<sub>m</sub></i>	<i>D<sub>m</sub></i>	<i>E<sub>m</sub></i>	<i>F<sub>m</sub></i>
1	0.98297	0.64395	-4.89189	0.68634	-7.93704	-2.40322	15.63328
2	0.93302	0	0	0.16667	-0.22673	0	0
3	0.85356	0.23570	-0.56904	0.33333	-1.07896	-0.23571	2.09440
4	0.75000	0	0	0.28868	-0.13091	0	0
5	0.62941	0.17255	-0.22487	0.23874	-0.42099	-0.04623	1.12238
6	0.50000	0	0	0.33333	0	0	0
7	0.37059	0.17255	-0.13240	0.06012	-0.14021	0.04623	1.12238
8	0.25000	0	0	0.28868	0.13091	0	0
9	0.14645	0.23570	-0.09763	-0.33333	0.03178	0.23571	2.09440
10	0.06699	0	0	0.16667	0.22673	0	0
11	0.01704	0.64393	-0.08478	-1.80170	0.11971	2.40322	15.63328

Table 11.8

Coefficients for Determining the Velocity Distribution (Given the Co-ordinates)  
(see p. 88)

Table 11.8 a

$N = 12$	$N = 6$	$N = 12$	$N = 6$	$\frac{x_m}{c}$	$a_n$	$b_n$	$c_n$
Upper side	Lower side						
0	0	24	12	1.00000	0	0	0
1		23		0.98297	0.12941	0.01704	0.01675
2	1	22	11	0.93302	0.25000	0.06698	0.06250
3		21		0.85356	0.35356	0.14644	0.12500
4	2	20	10	0.75000	0.43302	0.25000	0.18751
5		19		0.62941	0.48296	0.37059	0.23325
6	3	18	9	0.50000	0.50000	0.50000	0.25000
7		17		0.37059	0.48296	0.62941	0.23325
8	4	16	8	0.25000	0.43302	0.75000	0.18751
9		15		0.14645	0.35356	0.85356	0.12500
10	5	14	7	0.06699	0.25000	0.93302	0.06250
11		13		0.01704	0.12941	0.98296	0.01675
12	6	12	6	0.00000	0	1.00000	0

Table 11.8 b

 $A_{mn}$  $N = 6$ 

$m$	1	2	3	4	5
$n = 0$	0	0	0	0	0
1	+1.50000	-0.53867		-0.03868	
2	-0.53867	+1.50000	-0.57735	0	-0.03868
3	0	-0.57735	+1.50000	-0.57735	0
4	-0.03868	0	-0.57735	+1.50000	-0.53867
5	0	-0.03868	0	-0.53867	+1.50000
6	0	0	0	0	0

Table 11.8 c

 $S_{mn}$  $N = 6$ 

$m$	1	2	3	4	5
$n = 1$	2.74400	-0.70533	0.16666	-0.12799	0.08932
2	0.53867	+1.50000	-0.5	0	-0.03867
3	1.24400	-0.66666	+1.66666	-0.66666	+0.08932
4	1.11601	0	-0.5	+1.50000	-0.61601
5	1.24400	-0.12799	0.16666	-0.70533	+1.58932

Table 11.8 d

 $H_{mn}$  $N = 6$ 

$m$	1	2	3	4	5
$n = 1$	+0.71126	+0.09967	+0.07735	-0.03975	0
2	+0.14433	+0.86602	-0.50000	0	-0.14434
3	+0.28867	-0.28870	+1.50000	-0.53273	-0.28867
4	+0.29904	0	-1.00000	+2.59806	-2.29907
5	0	+0.69063	-1.15475	+1.00000	+1.38105

Table 11.8 e

 $A_{mn}$  $N = 12$ 

$m$	1	2	3	4	5	6	7	8	9	10	11
$n = 0$	0	0	0	0	0	0	0	0	0	0	0
1	3.00000	-1.08071	0	-0.08604	0	-0.02312	0	-0.00869	0	-0.00322	0
2	-1.08071	3.00000	-1.18675	0	-0.10916	0	-0.03181	0	-0.01191	0	-0.00322
3	0	-1.18675	3.00000	-1.18987	0	-0.11785	0	-0.03503	0	-0.01191	0
4	-0.08604	0	-1.18987	3.00000	-1.19856	0	-0.12107	0	-0.03503	0	-0.00869
5	0	-0.10916	0	-1.19856	3.00000	-1.20178	0	-0.12107	0	-0.03181	0
6	-0.02312	0	-0.11785	0	-1.20178	3.00000	-1.20178	0	-0.11785	0	-0.02312
7	0	-0.03181	0	-0.12107	0	-1.20178	3.0000	-1.19856	0	-0.10916	0
8	0.00869	0	-0.03503	0	-0.12107	0	-1.19856	3.00000	-1.18987	0	-0.08604
9	0	-0.01191	0	-0.03503	0	-0.11785	0	-1.18987	3.00000	-1.18675	0
10	-0.00322	0	-0.01191	0	-0.03181	0	-0.10916	0	-1.18675	3.00000	-1.08071
11	0	-0.00322	0	-0.00869	0	-0.02312	0	-0.08604	0	-1.08071	3.00000
12	0	0	0	0	0	0	0	0	0	0	0

Table 11.8 f

 $S_{mn}$  $N = 12$ 

$m$	1	2	3	4	5	6	7	8	9	10	11
$n=1$	5.44565	-1.36523	+0.28452	-0.19848	+0.11244	-0.08932	+0.06620	-0.05751	+0.04882	-0.04560	+0.04238
2	1.08042	+3.00000	-0.99487	0	-0.06292	0	-0.01443	0	-0.00547	0	-0.00322
3	2.44565	-1.27919	+3.28452	-1.25607	+0.11244	-0.16667	+0.06620	-0.07741	+0.04882	-0.05420	+0.04238
4	2.24717	0	-0.97155	+3.00000	-1.13494	0	-0.09725	0	-0.02859	0	-0.01513
5	2.44565	-0.17536	+0.28452	-1.24738	+3.11244	-1.24418	+0.06620	-0.16345	+0.04882	-0.08063	+0.04238
6	2.35633	0	+0.11785	0	-1.13172	+3.00000	-1.17796	0	-0.11775	0	-0.04694
7	2.44565	-0.08063	+0.28452	-0.16345	+0.11244	-1.24416	+3.06620	-1.24738	+0.04882	-0.17536	+0.04238
8	2.38814	0	+0.20711	0	-0.05101	0	-1.18118	+3.00000	-1.20725	0	-0.15610
9	2.44565	-0.05429	+0.28452	-0.07741	+0.11244	-0.16667	+0.06620	-1.25607	+0.04882	-1.27919	+0.04238
10	2.40005	0	+0.23023	0	+0.03181	0	-0.10916	0	-1.23027	+3.00000	-1.32285
11	2.44565	-0.04560	+0.28452	-0.05751	+0.11244	-0.08932	+0.06620	-0.19848	+0.04882	-1.36523	+3.04238

Table 11.8 g

 $H_{mn}$  $N = 12$ 

$m$	1	2	3	4	5	6	7	8	9	10	11
$n=1$	+0.71151	-0.35448	+0.10032	-0.09014	+0.05376	-0.04694	+0.03104	-0.02619	+0.01552	-0.01200	0
2	+0.14220	+0.80376	-0.41194	0	-0.04828	0	-0.01880	0	-0.01323	0	-0.02441
3	+0.31554	-0.32968	+1.34019	-0.69694	+0.04881	-0.11784	+0.02265	-0.04953	0	-0.02045	+0.04881
4	+0.29584	0	-0.40245	+1.73202	-0.87083	0	-0.12675	0	-0.06904	0	-0.11483
5	+0.31327	-0.02875	-0.09043	-0.68198	+2.33747	-1.17794	0	-0.16846	-0.04197	-0.05383	-0.18086
6	+0.31021	0	+0.04882	0	-0.86345	+3.00000	-1.53511	0	-0.28452	0	-0.35645
7	+0.30718	+0.00852	+0.07128	-0.2946	0	-1.13179	+3.84945	-1.96573	-0.15350	-0.23569	-0.53205
8	+0.31440	0	+0.08577	0	-0.03916	0	-1.53937	+5.19607	-2.91443	0	-1.18557
9	+0.28452	+0.06170	0	+0.11957	-0.13205	+0.11785	-0.28452	-1.68285	+6.67352	-3.71188	-1.83918
10	+0.31596	0	+0.09535	0	+0.02441	0	-0.14227	0	-2.97059	+11.19624	-10.04747
11	0	+0.64317	-0.89525	+1.37900	-1.79054	+2.35661	-3.10132	+3.89268	-5.78712	+4.03104	+4.53036

Table 11.9

Coefficients for Determining the Co-ordinates (Given the Velocities) (see p. 90)

Table 11.9 a

 $d_m$  and  $d_{mn}$  $N = 12$ 

$m$	1	2	3	4	5	6	7	8	9	10	11	12
$d_m$	-0.04530	-0.05399	-0.05248	-0.03932	-0.02147	0	0.02147	0.03932	0.06248	0.05399	0.04530	0.15652
$n = 0$	0	0	0	0	0	0	0	0	0	0	0	0
1	0.00070	0.00978	0.00300	0.00427	0.00148	0.00204	0.00029	0.00050	-0.00054	-0.00038	-0.00066	-0.00216
2	-0.11005	0.04079	0.02319	0.01342	0.00965	0.00590	0.00314	0.00072	-0.00109	-0.00207	-0.00227	-0.00805
3	-0.09216	-0.0696	0.07116	0.04083	0.02199	0.01528	0.00695	0.00248	-0.00241	-0.00418	-0.00498	-0.01947
4	-0.17831	-0.00703	0.02494	0.10089	0.05325	0.02813	0.01531	0.00466	-0.00284	-0.00703	-0.00815	-0.03316
5	-0.01763	-0.01022	0.00560	0.04412	0.12007	0.05977	0.02659	0.01065	-0.00304	-0.00925	-0.01178	-0.04817
$d_{mn}$	-0.01494	-0.01111	0	0.01925	0.05577	0.12778	0.05577	0.01925	0	-0.01111	-0.01494	-0.06389
6	-0.01178	-0.00925	-0.00304	0.01065	0.02659	0.05977	0.12007	0.04412	0.00550	-0.01022	-0.01763	-0.07757
7	-0.00815	-0.00703	-0.00284	0.00466	0.01531	0.02813	0.05325	0.10089	0.02494	-0.00703	-0.01831	-0.08872
8	-0.00498	-0.00418	-0.00241	0.00248	0.00695	0.01528	0.02199	0.04083	0.07116	0.00696	-0.01716	-0.09303
9	-0.00227	-0.00207	-0.00109	0.00072	0.00314	0.00590	0.00965	0.01342	0.02319	0.04079	-0.00925	-0.09061
10	-0.00066	-0.00038	-0.00054	0.00050	0.00029	0.00204	0.00148	0.00427	0.00300	0.00978	0.01007	-0.06584
11	0	0	0	0	0	0	0	0	0	0	0	0
12	0	0	0	0	0	0	0	0	0	0	0	0

Table 11.9 b

 $a_m$  and  $a_{mn}$  $N = 12$ 

$m$	1	2	3	4	5	6	7	8	9	10	11
$a_m$	0.12941	0.25000	0.35356	0.43302	0.48296	0.50000	0.48296	0.43302	0.35356	0.25000	0.12941
$n = 0$	0.16383	0	0.14226	0	0.10490	0	0.06177	0	0.02441	0	0.00284
1	0	0.20854	0	0.13414	0	0.08627	0	0.04264	0	0.01137	0
2	-0.05588	0	0.26219	0	0.12805	0	0.06912	0	0.02649	0	0.00305
3	0	-0.13109	0	0.30178	0	0.11785	0	0.05178	0	0.01324	0
4	-0.01198	0	-0.20119	0	0.32237	0	0.10246	0	0.03452	0	0.00381
5	0	-0.03431	0	-0.25915	0	0.32197	0	0.08237	0	0.01852	0
6	-0.00578	0	-0.05893	0	-0.30040	0	0.30040	0	0.05893	0	0.00578
7	0	-0.01852	0	-0.08237	0	-0.32197	0	0.25915	0	0.03431	0
8	-0.00381	0	-0.03452	0	-0.10246	0	-0.32237	0	0.20119	0	0.01198
9	0	-0.01324	0	-0.05178	0	-0.11785	0	-0.30178	0	0.13109	0
10	-0.00305	0	-0.02649	0	-0.06912	0	-0.12805	0	-0.26219	0	0.05588
11	0	-0.01137	0	-0.04264	0	-0.08627	0	-0.13414	0	-0.20854	0
12	-0.00284	0	-0.02441	0	-0.06177	0	-0.10490	0	-0.14226	0	-0.16383

Table 11.9 c

 $b_{mn}$  $N = 12$ 

$m$	1	2	3	4	5	6	7	8	9	10	11
$b_{mn}$	$n = 0$	0	0	0	0	0	0	0	0	0	0
1	0.02616	0.02372	0.01892	0.01899	0.01382	0.01111	0.00811	0.00552	0.00320	0.00148	0.00037
2	0.01228	0.06392	0.04742	0.03556	0.02968	0.02270	0.01689	0.01120	0.00660	0.00299	0.00076
3	0.00692	0.03353	0.10052	0.06770	0.04777	0.03711	0.02631	0.01770	0.01016	0.00466	0.00117
4	0.00508	0.02053	0.05528	0.13038	0.08167	0.05399	0.03869	0.02483	0.01445	0.00647	0.00165
5	0.00370	0.01537	0.03497	0.07323	0.14979	0.08750	0.06354	0.03469	0.01926	0.00874	0.00217
6	0.00288	0.01135	0.02624	0.04675	0.08452	0.15652	0.08452	0.04675	0.02624	0.01135	0.00288
7	0.00217	0.00874	0.01926	0.03469	0.05354	0.08750	0.14979	0.07323	0.03497	0.01537	0.00370
8	0.00165	0.00647	0.01445	0.02483	0.03869	0.05399	0.08167	0.13038	0.05528	0.02053	0.00508
9	0.00117	0.00466	0.01016	0.01770	0.02631	0.03711	0.04777	0.06770	0.10052	0.03353	0.00662
10	0.00076	0.00299	0.00660	0.01120	0.01689	0.02270	0.02968	0.03556	0.04742	0.06392	0.01228
11	0.00037	0.00148	0.00320	0.00552	0.00811	0.01111	0.01382	0.01699	0.01892	0.02372	0.02616
12	0	0	0	0	0	0	0	0	0	0	0

Table 11.9 d

 $p_n$  and  $q_n$  $N = 12$ 

$n$	$x/l$	$p_n$	$q_n$
1	0.98297	0.13165	0.03407
2	0.93302	0.26795	0.13397
3	0.85356	0.41421	0.29289
4	0.75000	0.57735	0.50000
5	0.62941	0.76733	0.74118
6	0.50000	1.00000	1.00000
7	0.37059	1.30323	1.25882
8	0.25000	1.73205	1.50000
9	0.14845	2.41421	1.70711
10	0.06899	3.73205	1.86603
11	0.01704	7.59575	1.96593

## 12. CATALOGUE OF THEORETICAL AND EXPERIMENTAL RESULTS

### **12.1 Pressure Distributions of Camber Lines**

BIRNBAUM-GLAUERT . . . . .	198
KAWALKI . . . . .	198
NACA 62—67 . . . . .	198
NACA 210—250 . . . . .	199
NACA $\alpha = 0$ to $\alpha = 1$ . . . . .	199

### **12.2 Pressure Distributions of Symmetrical Profiles**

Circular Arc with Parabolic Nose . . . . .	199
Bodies with Semicircular Ends . . . . .	199
J 005; 015; 025. NACA 0006 to 0030 . . . . .	200
DVL 0 00 09—0·825 40; 0 00 09—0·55 40 . . . . .	203
0 00 09—0·55 45; 0 00 09—0·55 50 . . . . .	203
0 00 12—1·1 40; 0 00 12—0·825 40 . . . . .	204
0 00 12—0·55 40; 0 00 12—0·275 40 . . . . .	204
0 00 15—0·55 40; 0 00 15—1·1 50 . . . . .	205
0 00 18—0·55 40; 0 00 18—1·1 50 . . . . .	205
NACA 16—009; 16—012; 16—015; 16—018 . . . . .	206
63—009 to 63 <sub>4</sub> —021 . . . . .	207
64—009 to 64 <sub>4</sub> —021; 65·2—023 . . . . .	208
65—006 to 65 <sub>4</sub> —021 . . . . .	208
RAE 100 to 104 . . . . .	209

### **12.3 Pressure Distributions of Cambered Profiles**

J 215; 415; 815 . . . . .	210
Gö 436; 549 . . . . .	211
Gö 622—625 . . . . .	212
Clark Y 6%—14% . . . . .	213
N 85—N 87 . . . . .	214
NACA 2409 to 2421 . . . . .	215
23009 to 23021 . . . . .	216
4409 to 4421 . . . . .	217
63 <sub>2</sub> —415; 64 <sub>2</sub> —415; 65 <sub>2</sub> —415; 66 <sub>2</sub> —415 .	218
6409 to 6421 . . . . .	219
63 <sub>2</sub> —615; 64 <sub>3</sub> —618 . . . . .	220

Comparison of a Calculated and a Measured Pressure Distribution for the Profile NACA 4412, at $C_L = 1·02$ .	220
Circular Arcs of Large Camber . . . . .	221
Flat Plate with Flap and Dead-water Region . . .	221

### **12.4 Measured Pressure Distributions**

#### **12.4.1 For Incompressible Flow**

Gö 738, 741, 744, 746 . . . . .	222
NACA 2412, 2418 . . . . .	223
Gö 616 with Flap . . . . .	224
Profile with Landing Flap . . . . .	225
Clark Y with Split Flap . . . . .	226
Clark Y with Flap . . . . .	226
Profile with Boundary Layer Suction . . . . .	226
NACA 4412 at Various Reynolds Numbers . . . . .	227

#### **12.4.2 For Compressible Flow**

NACA 0006—0018 . . . . .	228
NACA 0015 . . . . .	230
NACA 23009, 23015 . . . . .	231
NACA 65 <sub>2</sub> —215 $\alpha = 0·5$ ; 4415 . . . . .	233
Circular Segment Profile at $M = 1·85$ . . . . .	235
Biconvex Profile at $M = 1·85$ and 2·13 . . . . .	235
Double Wedge Profile . . . . .	236

### **12.5 Polars**

#### **12.5.1 For Incompressible Flow**

Flat Plate . . . . .	237
Gö 227, 242, 243, 289, 335, 342 . . . . .	237
409, 410, 417a, 420 . . . . .	238
436, 449, 508, 535, 537, 549, 558, 564, 576, 579, 596	239
608—610, 622—625 . . . . .	240
652, 708, 711, 735 . . . . .	241
738, 741, 744, 746, 769, 770 . . . . .	243
775, 776, 777 . . . . .	243
795—797 . . . . .	244
DVL . . . . .	245
NACA 0012, 4412, 4415, 23012, 23015 . . . . .	247
63—006, 64—009, 63—209 . . . . .	249
63 <sub>1</sub> —012, 63 <sub>1</sub> —212, 63 <sub>2</sub> —415,	
63 <sub>3</sub> —018, 64—006 . . . . .	250
64—009, 64—409, 64 <sub>1</sub> —012, 64 <sub>1</sub> A212 .	252
64 <sub>1</sub> —412, 64 <sub>1</sub> —612, 64 <sub>2</sub> —415, 64 <sub>3</sub> —418 .	253
65—006, 65 <sub>2</sub> —415, 66 <sub>2</sub> —415 . . . . .	254
0010 $C_L^* = 0·3$ , $\alpha = 1$ , and 64 A 310 . . . . .	255

**12.5.2 For Compressible Flow**

NACA 0015, 4415, 23015 . . . . .	256
16—009 to 16—1009 . . . . .	260
16—506 to 16—530 . . . . .	260
65 <sub>2</sub> —215 $\alpha = 0.5$ . . . . .	263
836D110, 847B110 . . . . .	265
Circular Segment Profile, $\frac{t}{c} = 0.088$ , at $M = 1.47$ and $2.13$ . . . . .	266

Circular Segment Profiles of Various Thickness Ratios (Theory) . . . . .	266
Double Wedge Profile in Supersonic Flow (Theory) . . . . .	266

**12.5.3 With Cavitation**

Gö 1K, 2K, 4K, 5K—16K . . . . .	267
---------------------------------	-----

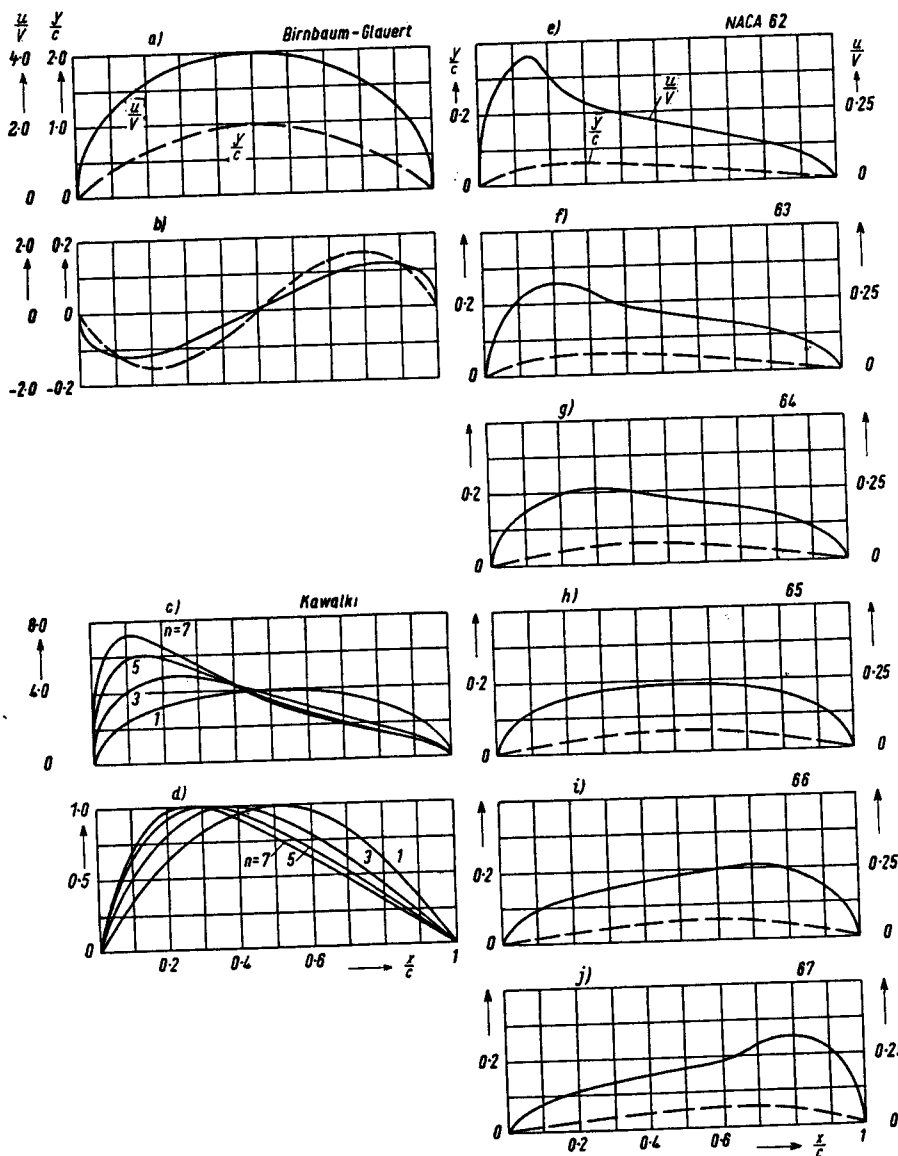


Fig. 12.1 a, b. Velocity distribution of the Birnbaum-Glaert camber lines

Fig. 12.1 c, d. Velocity distribution of the Kawalki camber lines

Fig. 12.1 e—j. Velocity distribution of the camber lines NACA 62—67

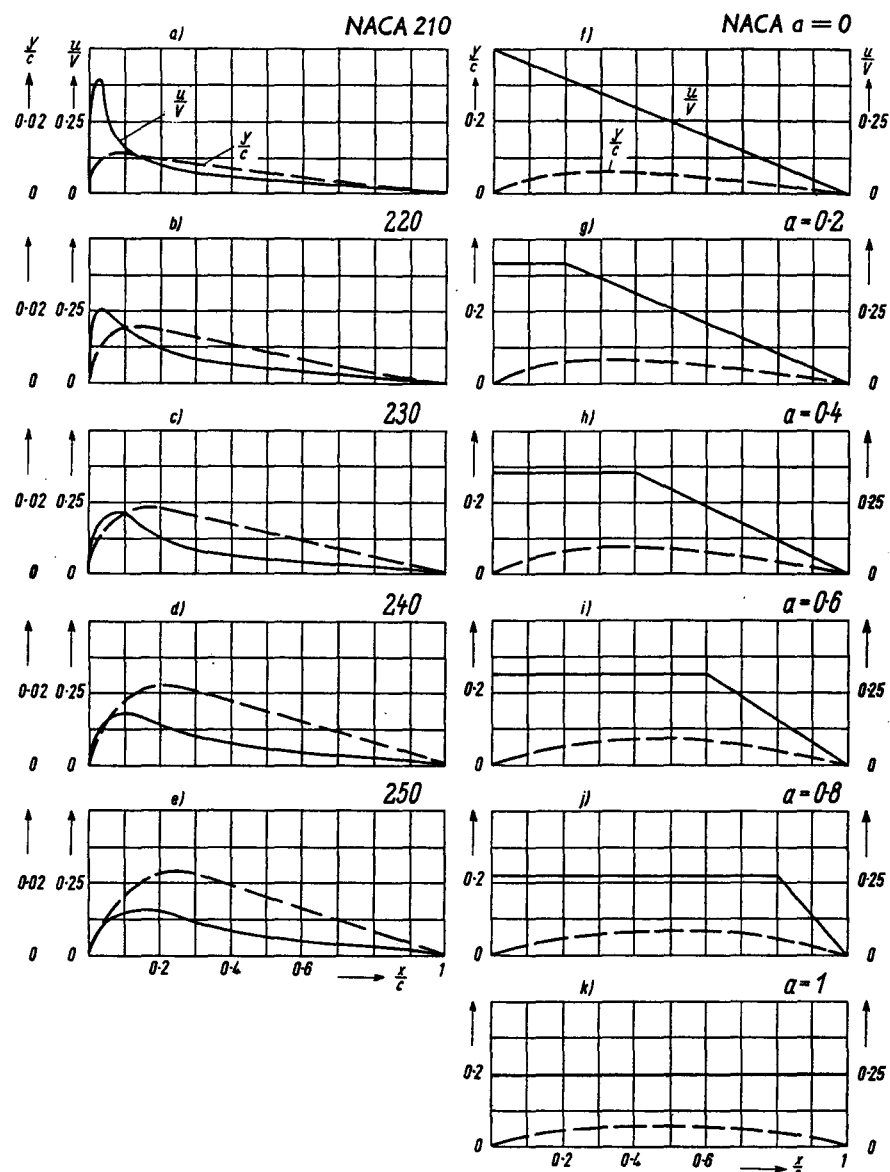


Fig. 12.2 a—e. Velocity distributions of the camber lines NACA 210—250

Fig. 12.2 f—k. Velocity distributions of the camber lines NACA  $\alpha = 0$  to  $\alpha = 1$

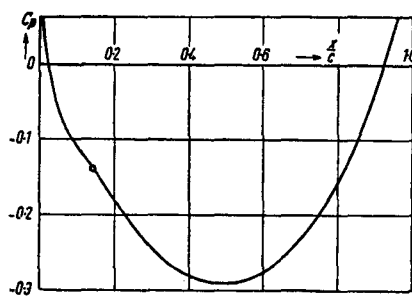


Fig. 12.3. Pressure distribution of the circular arc profile 00010.5—0.356 46.7 with parabolic nose ("kink" in curvature at the join:  $y'''_I + y'''_{II}$ )

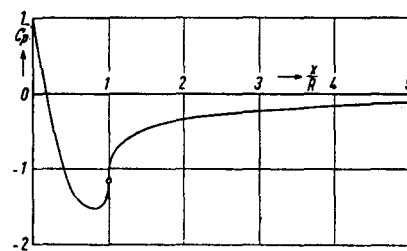


Fig. 12.4. Pressure distribution of semi-infinite body with semicircular nose. Effect of discontinuity in curvature ( $y''_I \neq y''_{II}$ )

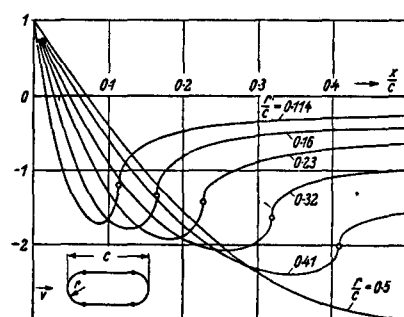


Fig. 12.5. Pressure distributions on bodies with semicircular ends, for various thickness ratios (Schmieden)

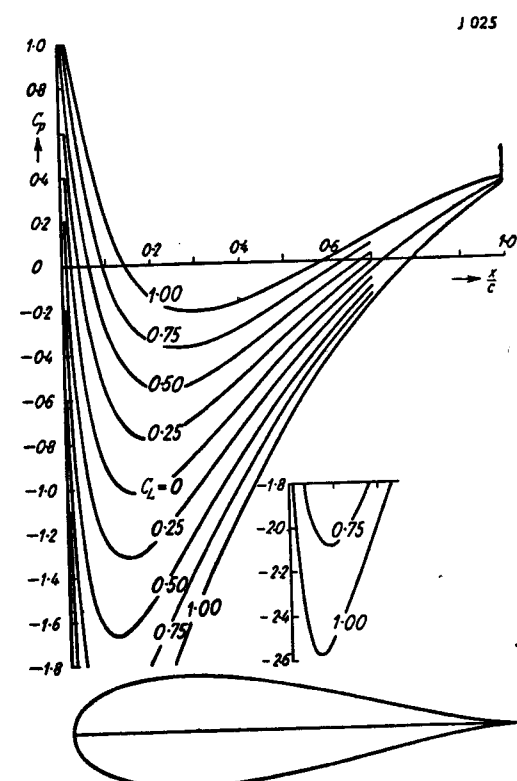
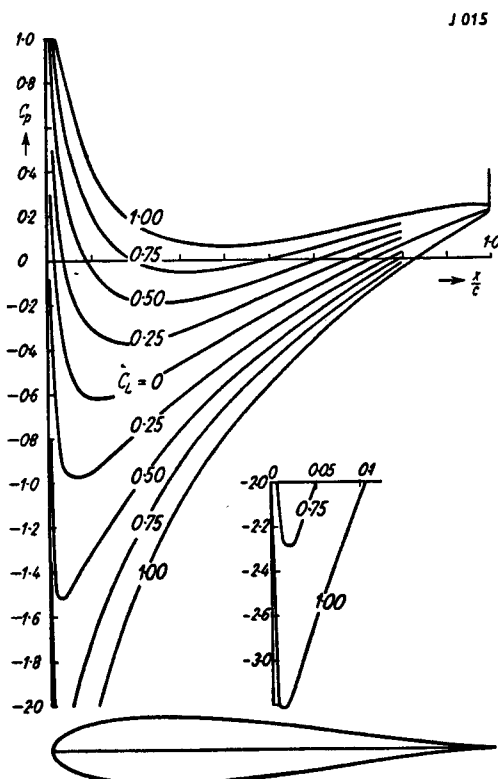
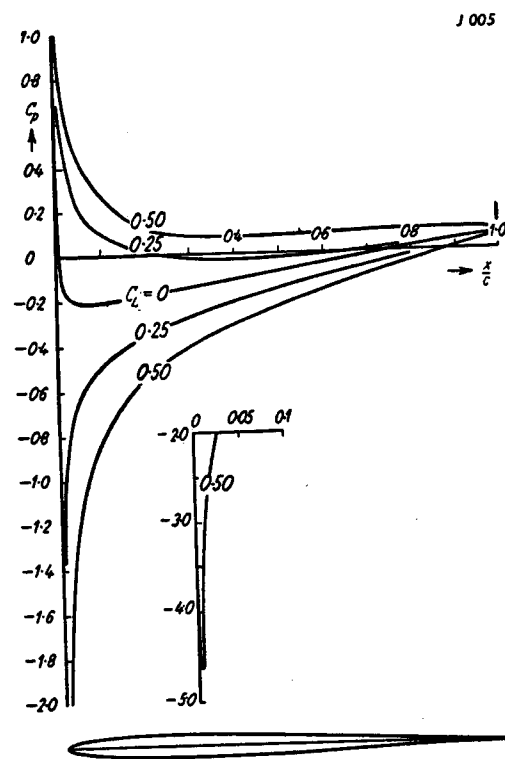
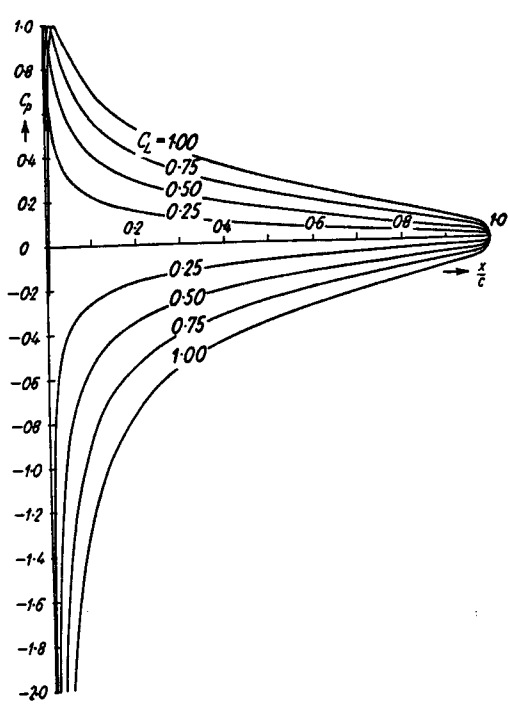


Fig. 12.6 a—d. Pressure distributions of the flat plate and the Joukowski profiles: J 005; 015; 025; (according to potential theory)

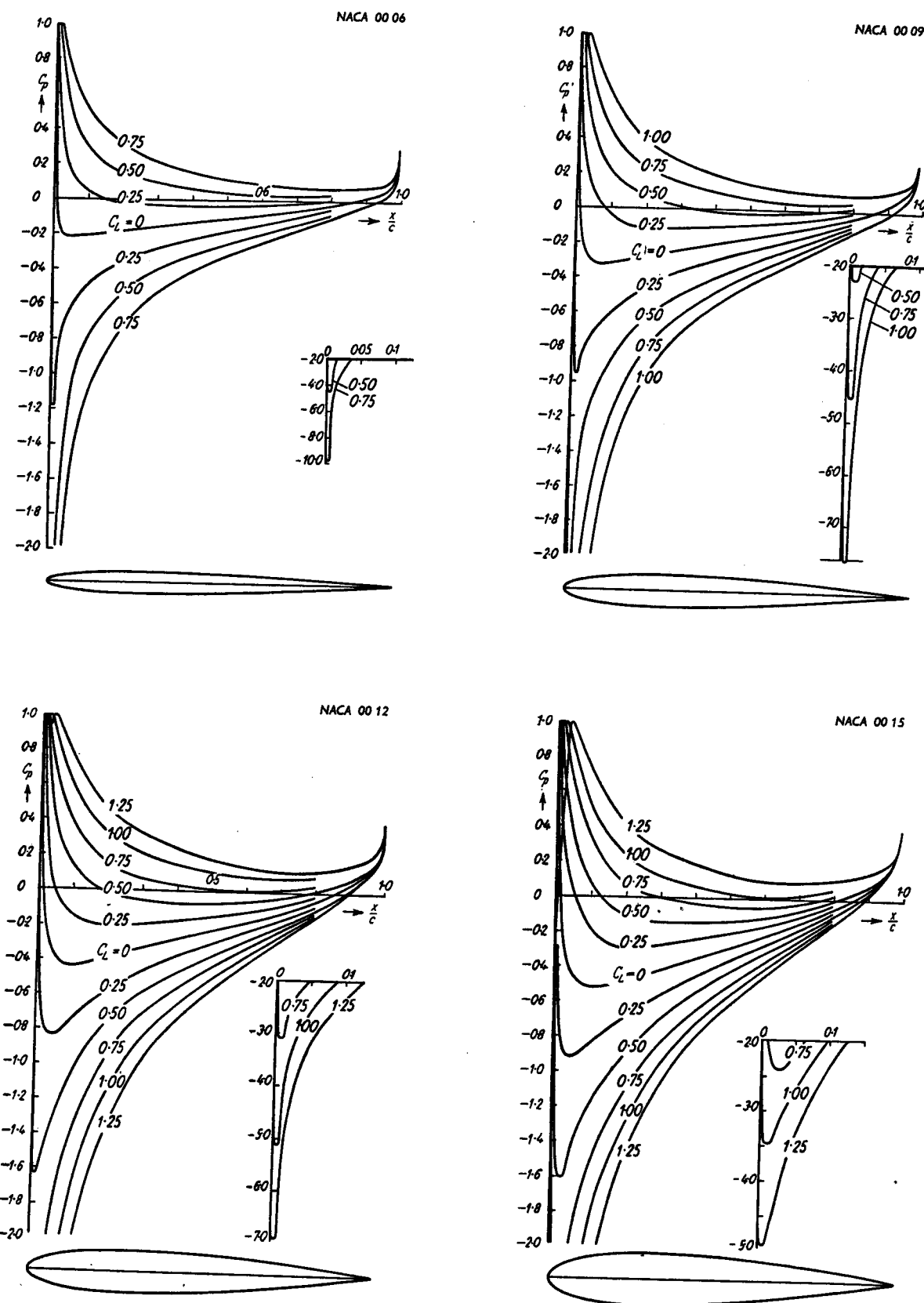


Fig. 12.7 a—d. Pressure distributions of the profiles: NACA 00 06; 00 09; 00 12; 00 15; (with effect of viscosity included,  $R = 2 \cdot 7 \cdot 10^4$ )

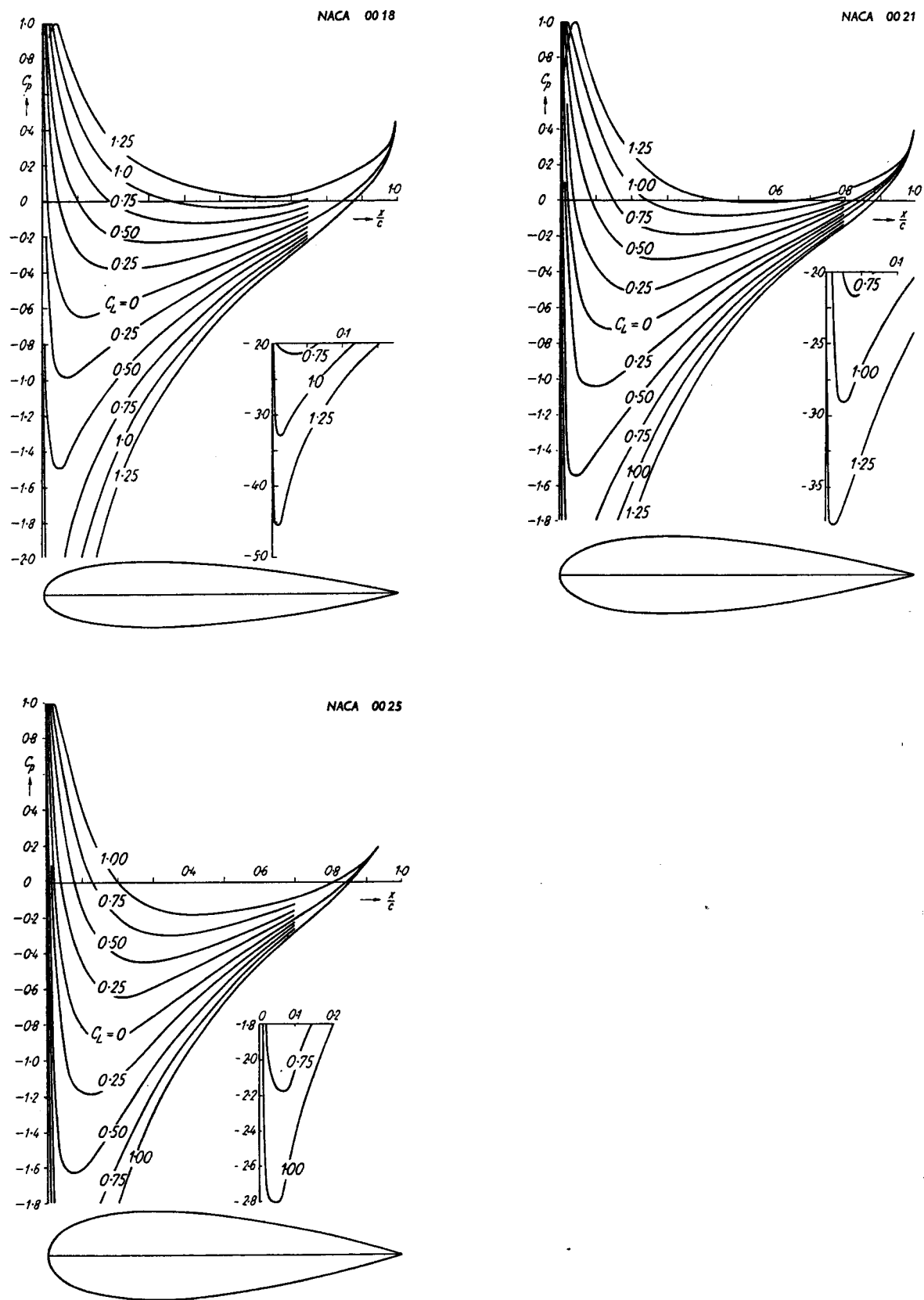


Fig. 12.7 e—g. Pressure distributions of the profiles: NACA 0018; 0021; 0025; (with effect of viscosity included,  $R = 2.7 \cdot 10^4$ )

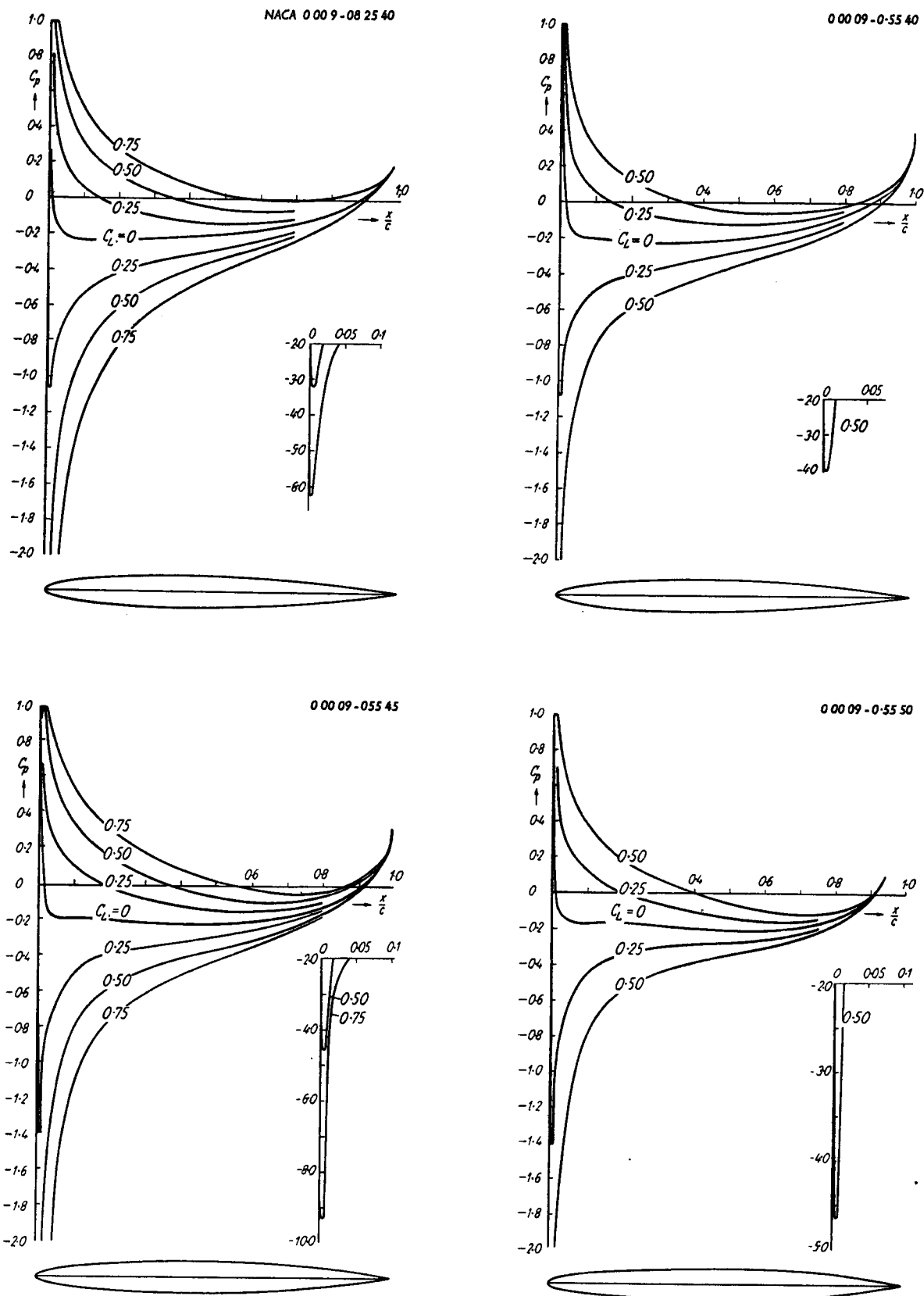


Fig. 12.8 a—d. Pressure distributions of the profiles: 0 00 09—0.825 40; 0 00 09—0.55 40; 0 00 09—0.55 45; 0 00 09—0.55 50; (with effect of viscosity included,  
 $R = 2.7 \cdot 10^6$ )

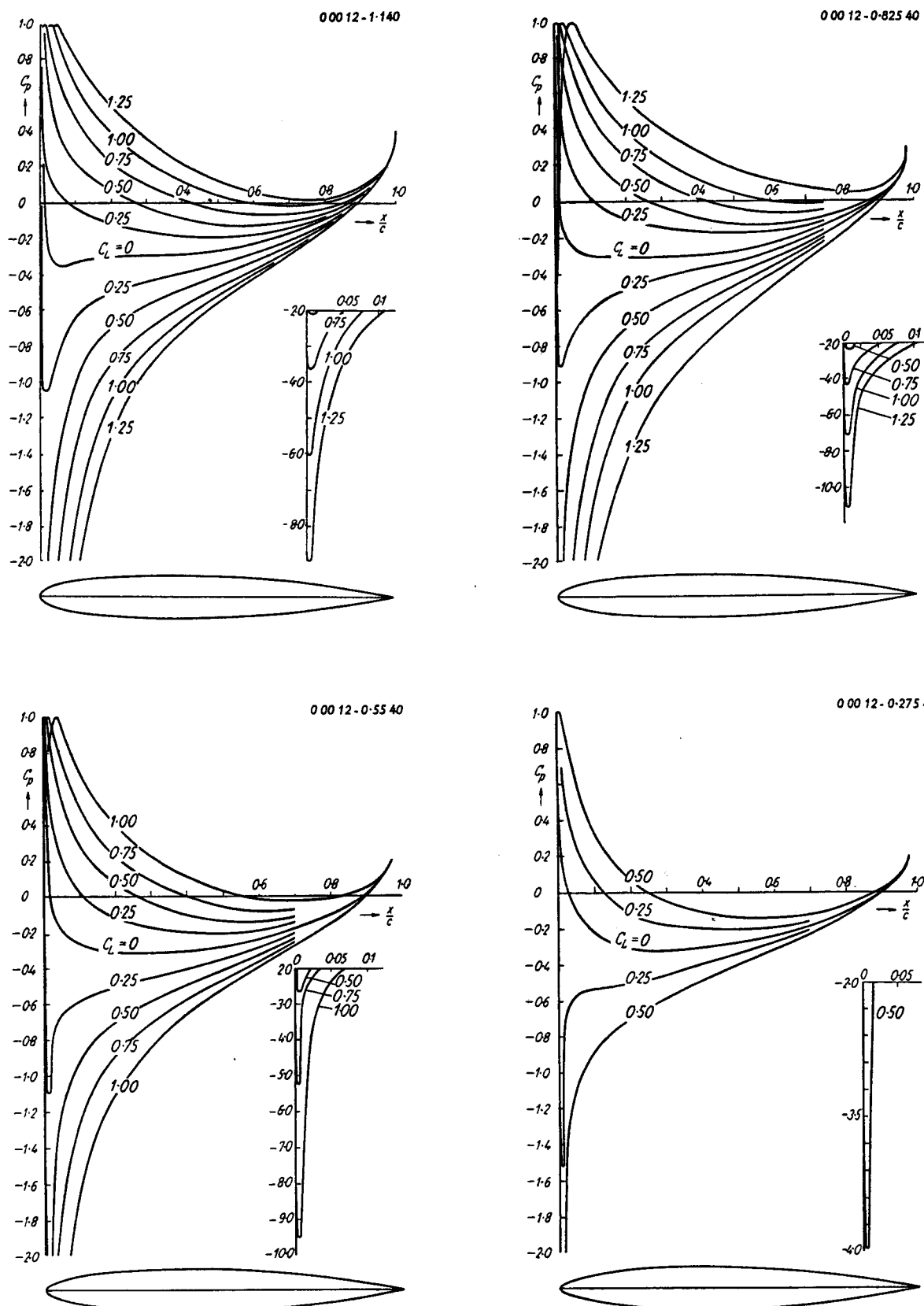


Fig. 12.9 a—d. Pressure distributions of the profiles: 0 00 12—1.14 0; 0 00 12—0.825 40; 0 00 12—0.55 40; 0 00 12—0.275 40; (with effect of viscosity included,  $R = 2.7 \cdot 10^4$ )

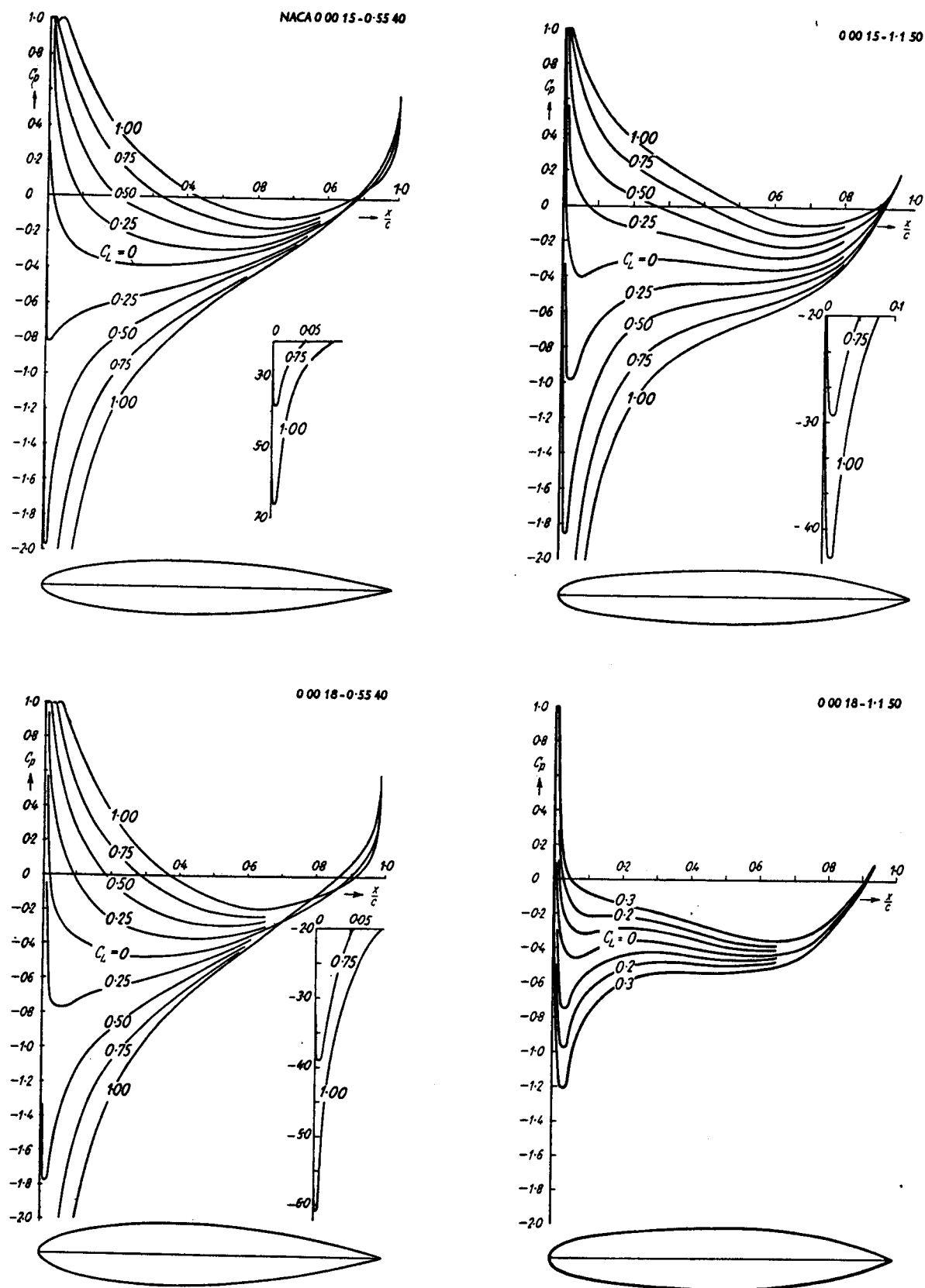


Fig. 12.10 a—d. Pressure distributions of the profiles: 0 00 15—0.55 40; 0 00 15—1.15 0; 0 00 18—0.55 40; 0 00 18—1.15 0 (with effect of viscosity included,  
 $R = 2 \cdot 7 \cdot 10^6$ )

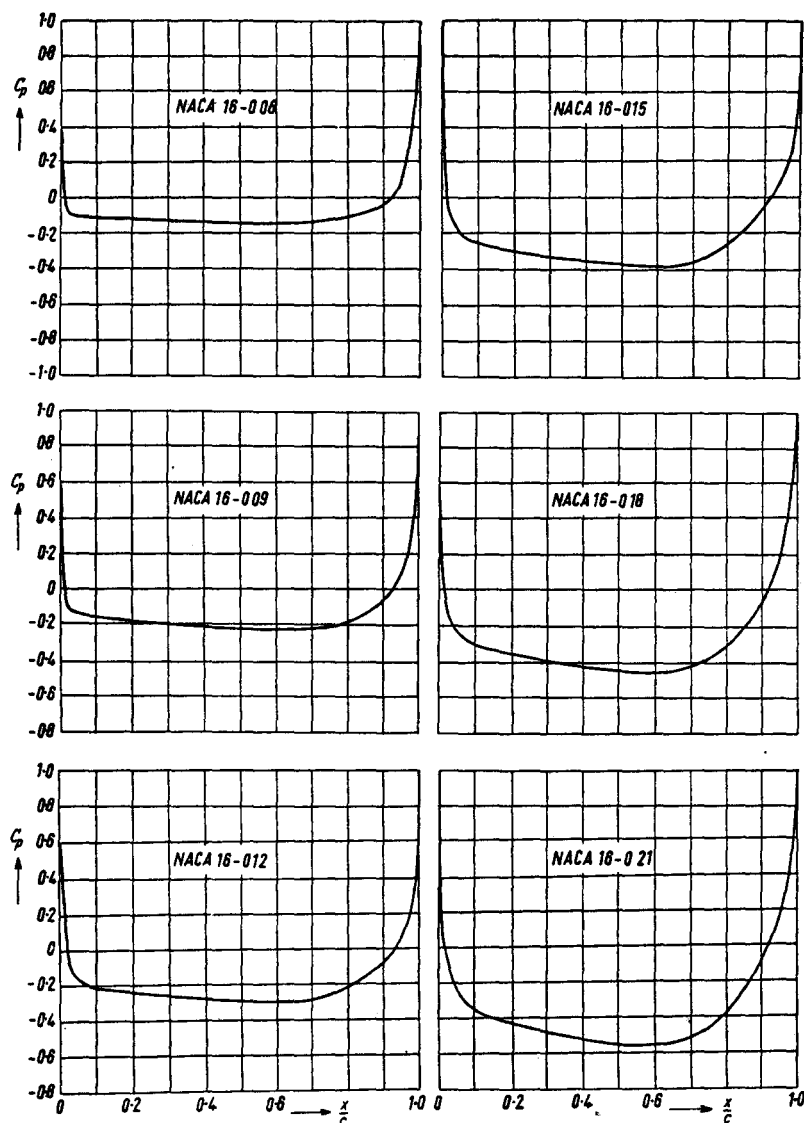


Fig. 12.11 a—f. Pressure distributions of some symmetrical profiles of the NACA 1-series; according to potential theory

*Remarks on the figures on pages 207 to 225.* The pressure distributions for the older NACA and DVL profiles were available by the end of the war; those for the later NACA series were calculated in 1953. Viscosity has been allowed for according to Equation (9.1);  $\Delta\alpha$  was taken from the Göttingen NACA or DVL measurements (giving  $C_L$  as a function of  $\alpha$ ); it corresponds to the Reynolds numbers of those measurements. For the later profiles the process described in 1948 in the Ingenieur-Archiv has been used (see Chapter 8);  $\Delta\alpha$  is taken from NACA Report 824, the Reynolds number being  $3 \cdot 10^4$ .

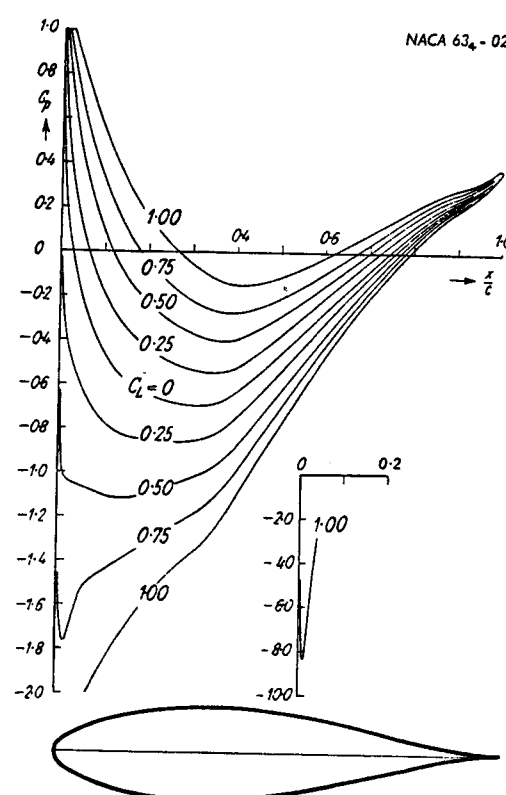
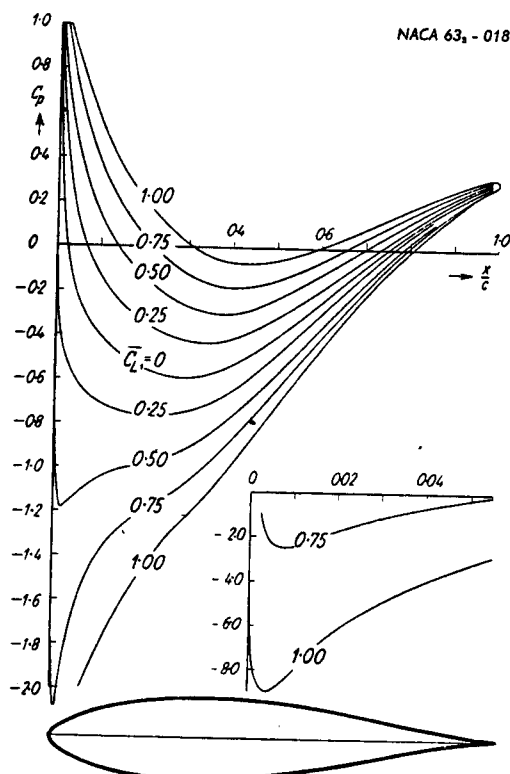
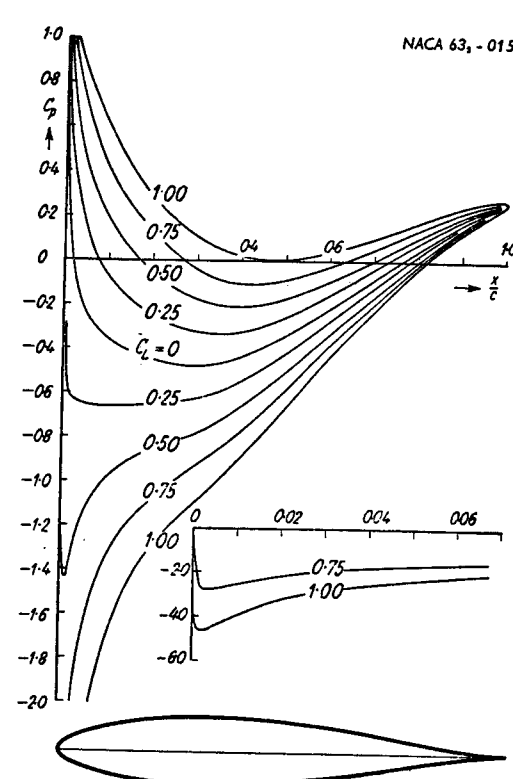
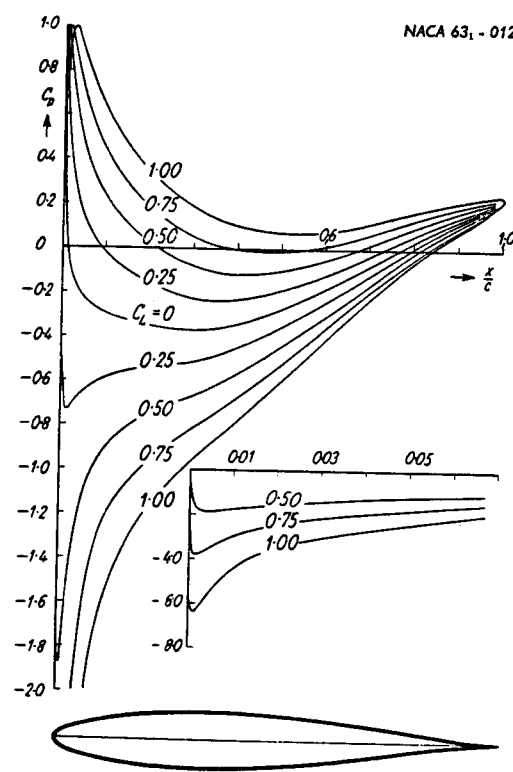


Fig. 12.12 a—d. Pressure distributions of the profiles: 63<sub>1</sub>—012; 63<sub>3</sub>—015; 63<sub>2</sub>—018; 63<sub>4</sub>—021; (with effect of viscosity included,  $R = 3 \cdot 10^6$ )

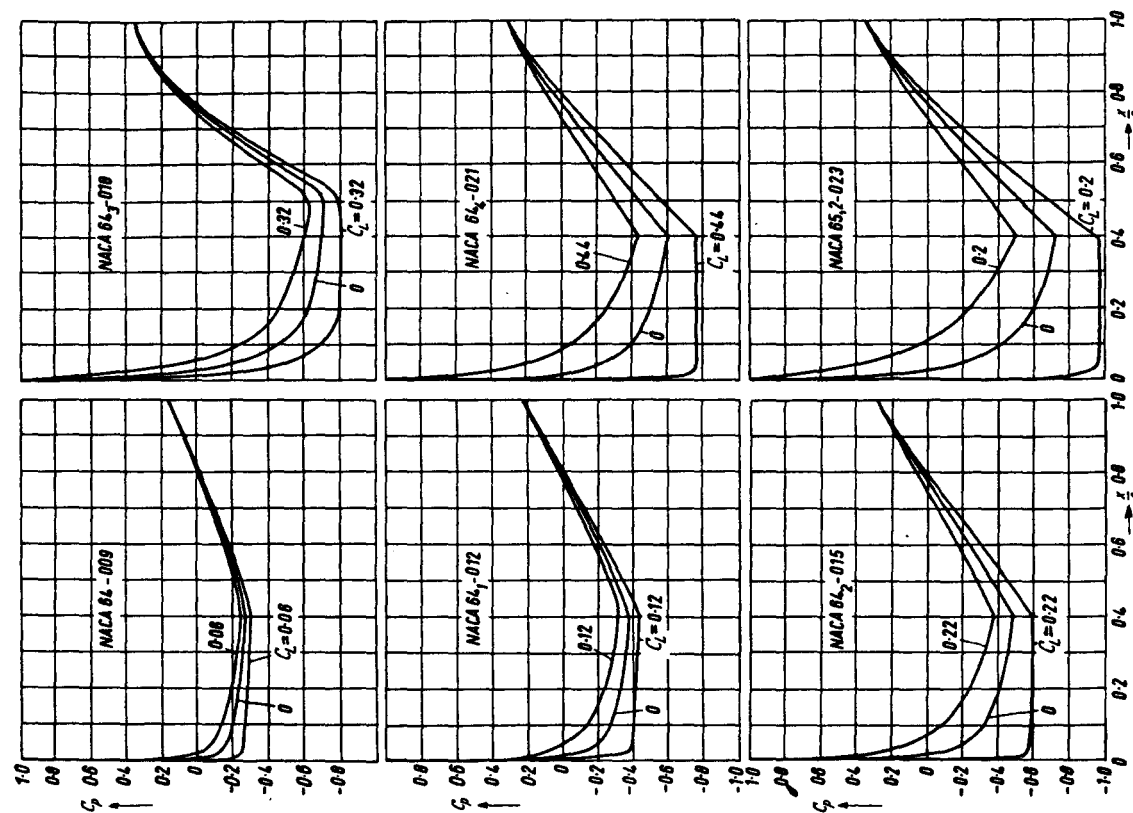


FIG. 12.13 a—f. Pressure distributions of some symmetrical profiles of the NACA 64-series;  
(according to potential theory)

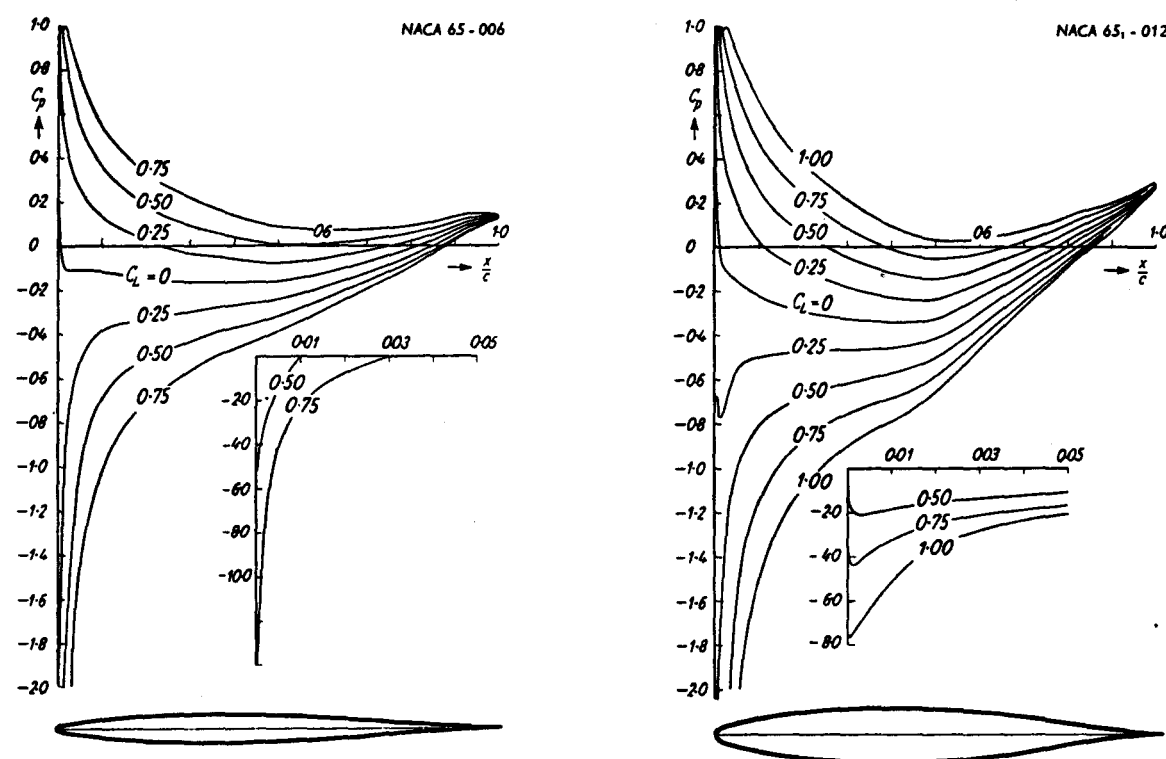


Fig. 12.14 a—b. Pressure distributions of the profiles: 65—006; 65<sub>1</sub>—012 (with effect of viscosity included,  $R = 3.106$ )

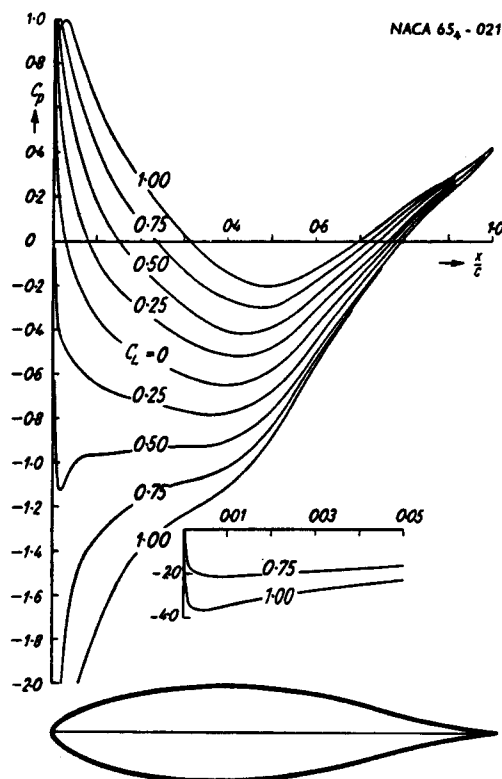


Fig. 12.14c. Pressure distribution of the profile: 65<sub>4</sub>-021 (with effect of viscosity included,  $R = 3 \cdot 10^4$ )

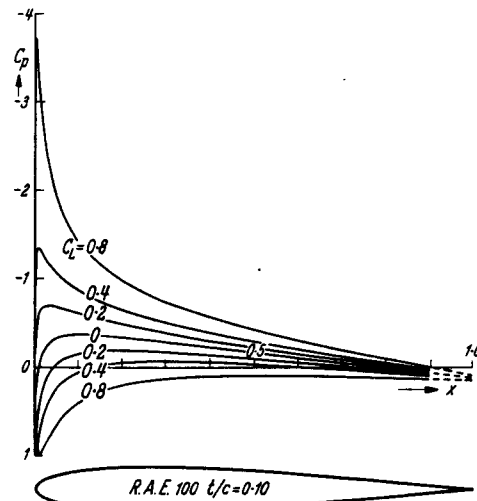
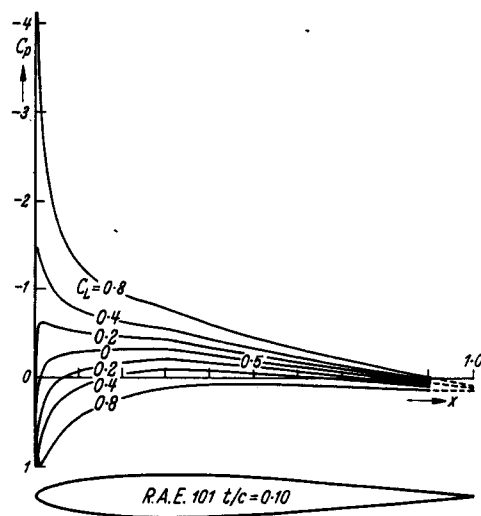
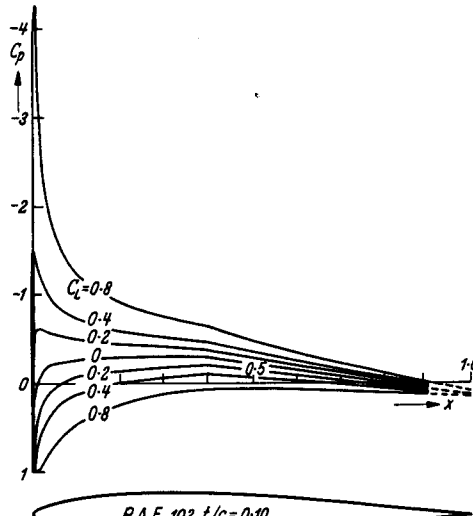
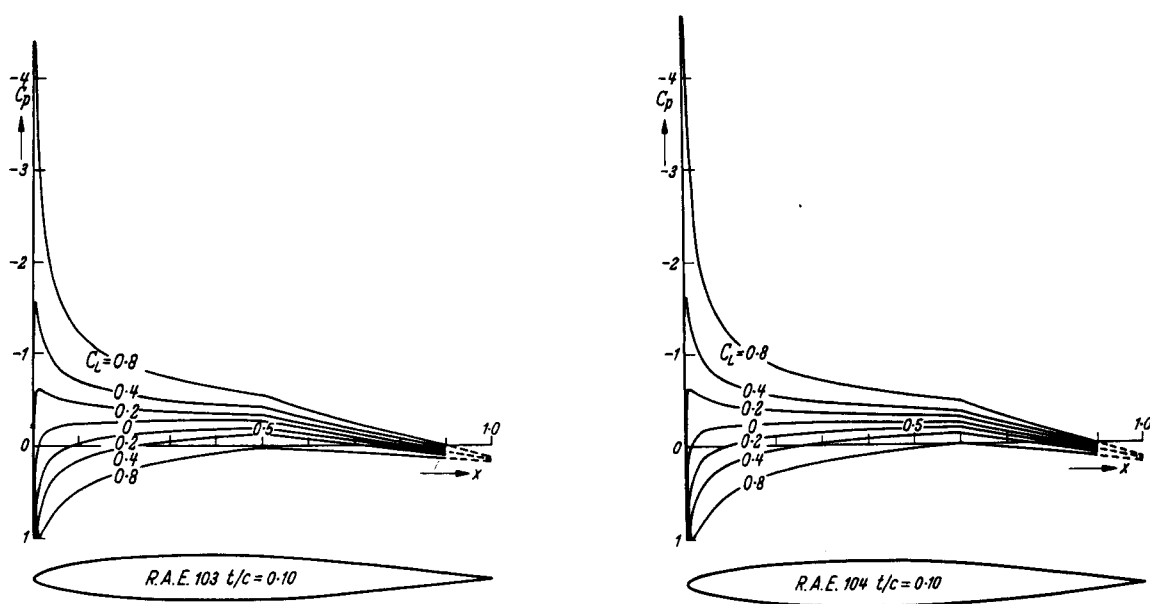


Fig. 12.14.1 a. Theoretical pressure distribution, RAE 100. From RAE Tech. Note Aero. 2039. Crown copyright reserved. Reproduced by permission of the Controller, H.M. Stationery Office



Figs. 12.14.1. b and c. Theoretical pressure distributions, RAE 101 and RAE 102. From RAE Tech. Note Aero. 2039. Crown copyright reserved. Reproduced by permission of the Controller, H.M. Stationery Office





Figs. 12.14.1. d and e. Theoretical pressure distributions, RAE 103 and RAE 104. From RAE Tech. Note Aero 2039. Crown copyright reserved. Reproduced by permission of the Controller, H.M. Stationery Office

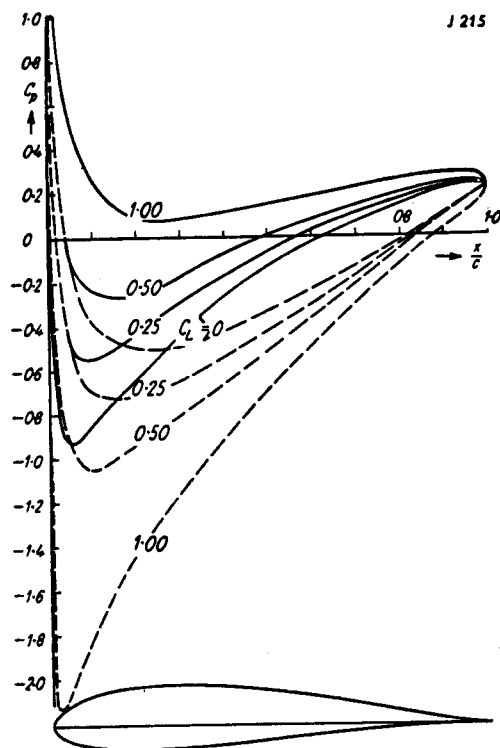


Fig. 12.15 a. Pressure distribution of the Joukowsky profile J 215; (according to potential theory)

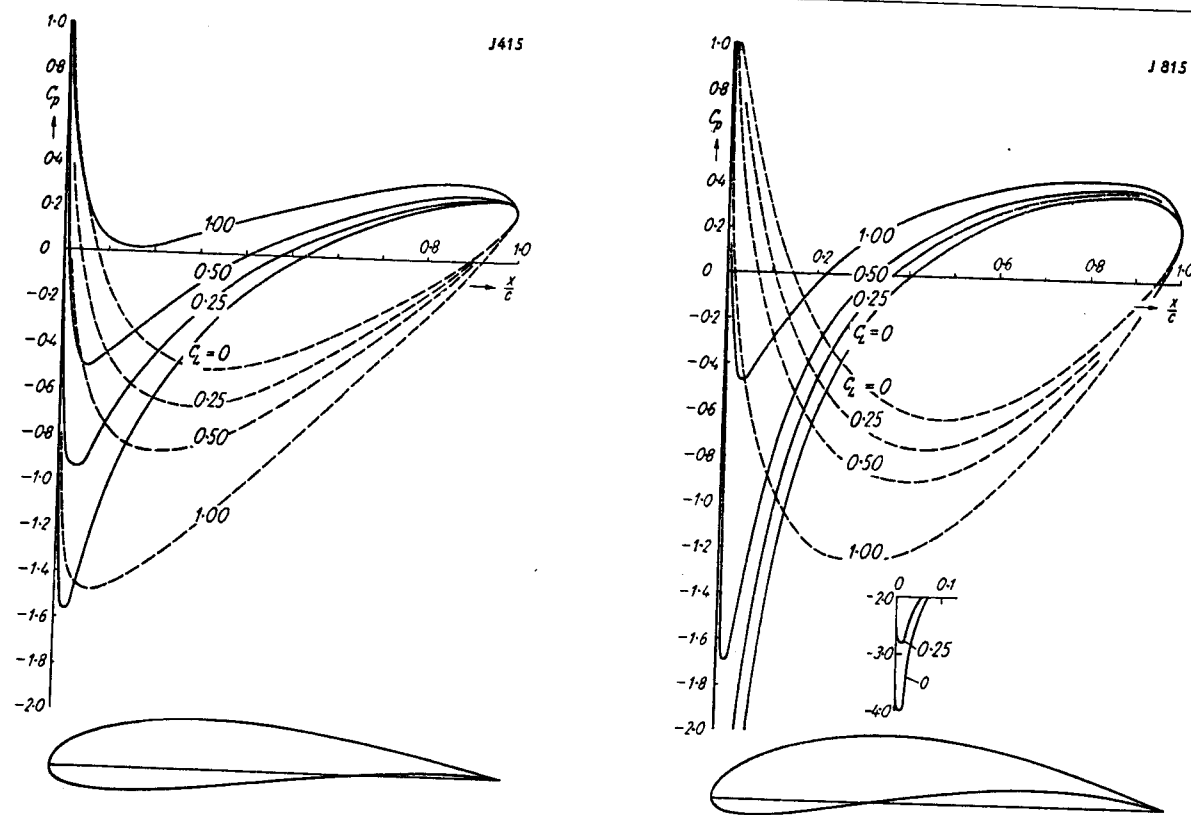


Fig. 12.15 b, c. Pressure distributions of the Joukowsky profiles: J 415; J 815; according to potential theory

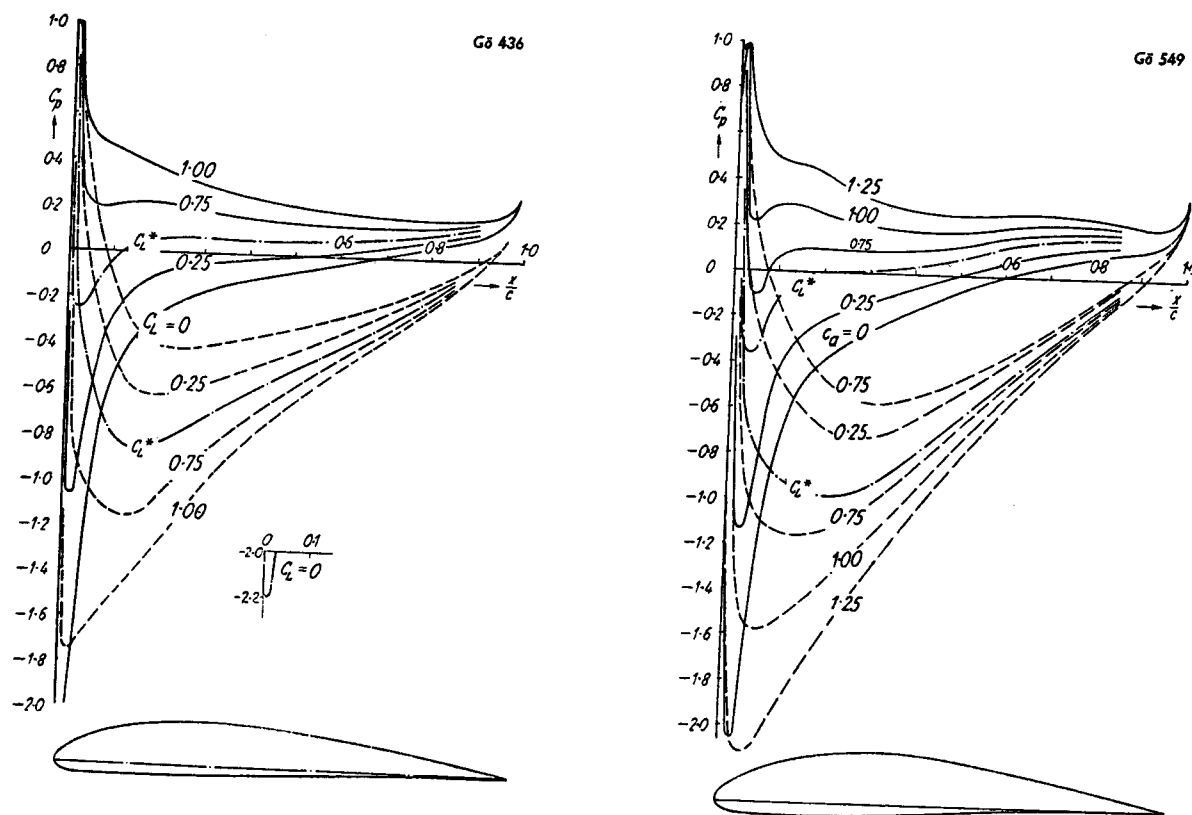


Fig. 12.16 a—b. Pressure distributions of the profiles: GÖ 436; GÖ 549; (with effect of viscosity included,  $R = 4 \cdot 2 \cdot 10^4$ )

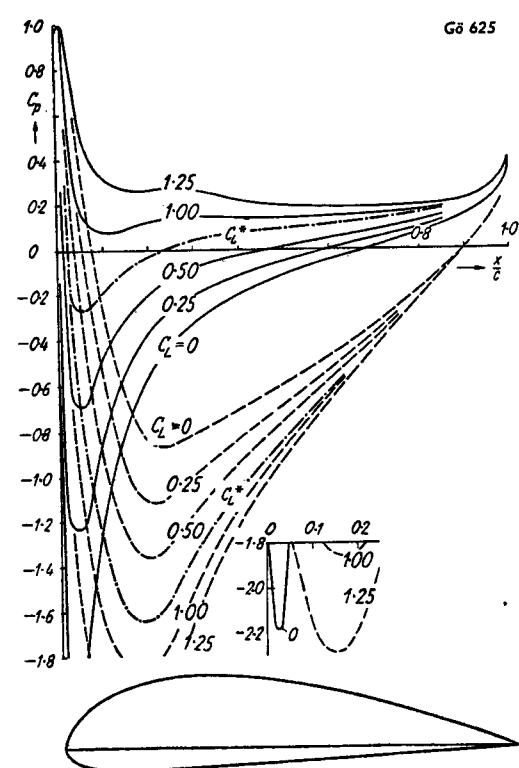
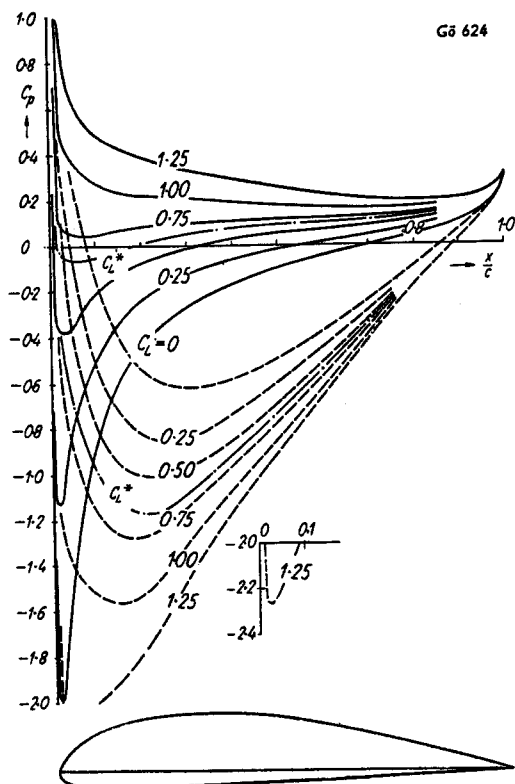
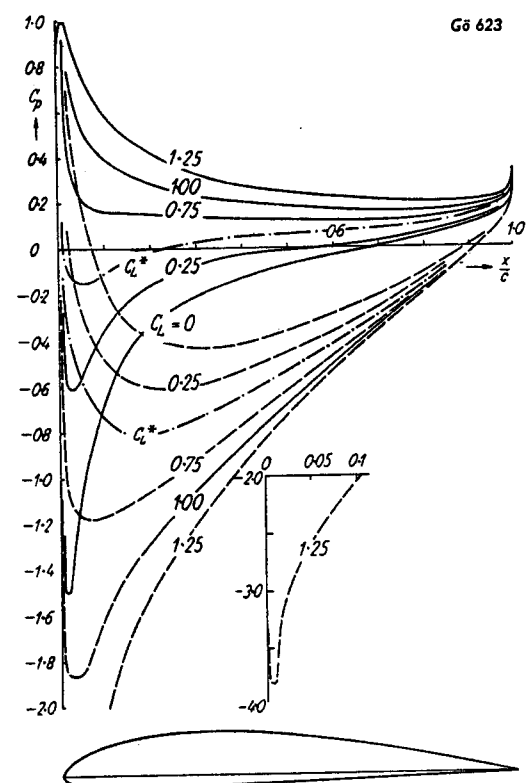
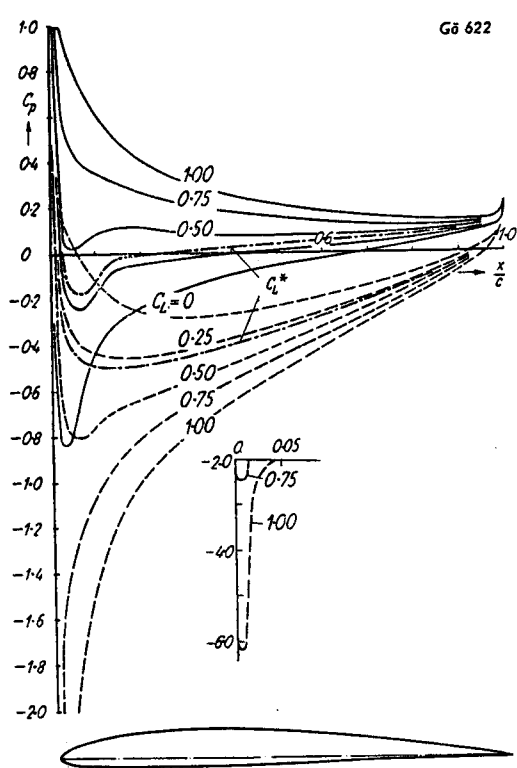


Fig. 12.17 a—d. Pressure distributions of the profiles Gö 622—625; (with effect of viscosity included,  $R = 4 \cdot 2 \cdot 10^4$ )

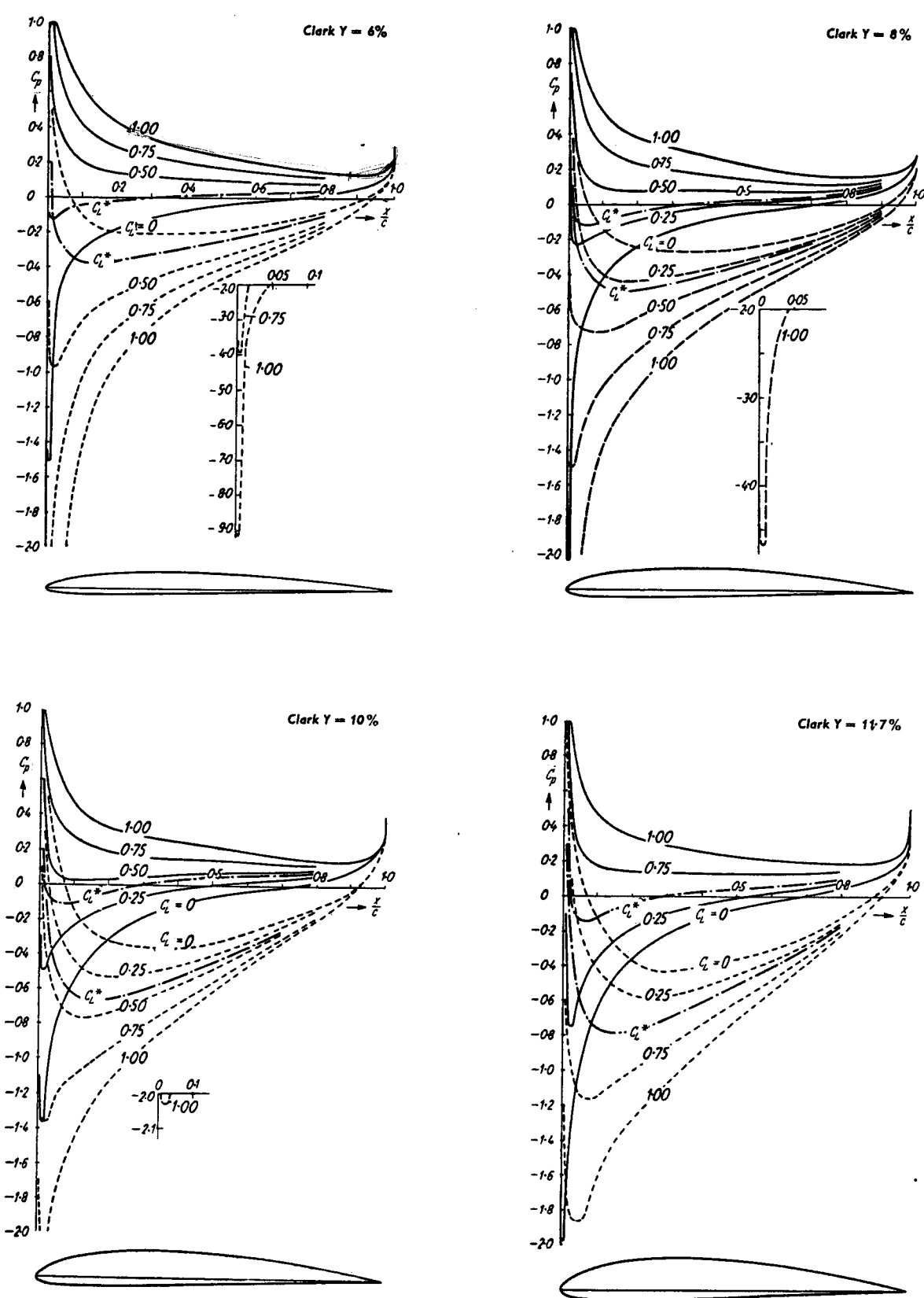


Fig. 12.18 a—d. Pressure distributions of the profiles: Clark Y 6%, 8%, 10%, 11.7%; (with effect of viscosity included)

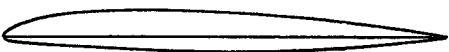
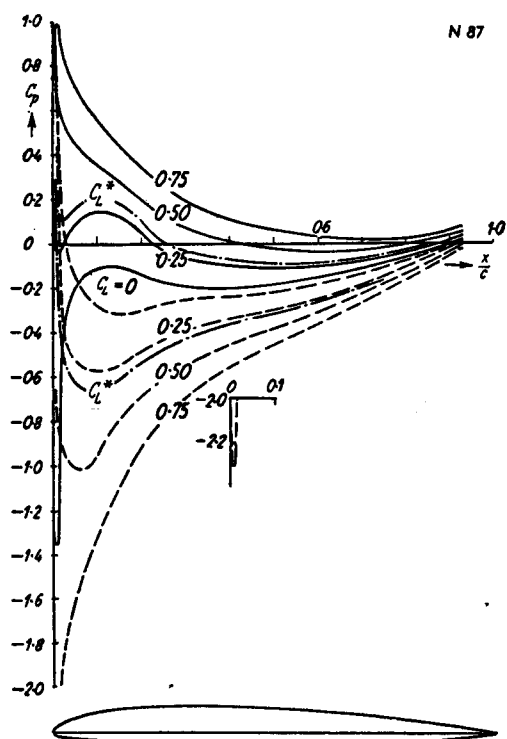
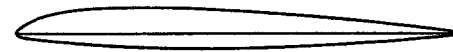
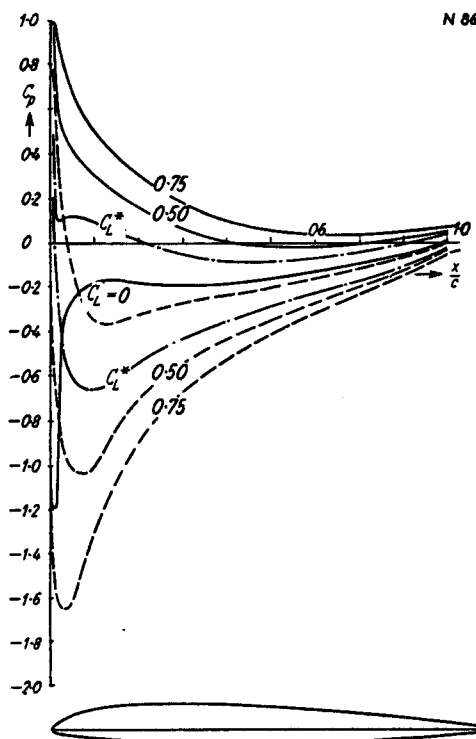
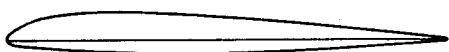
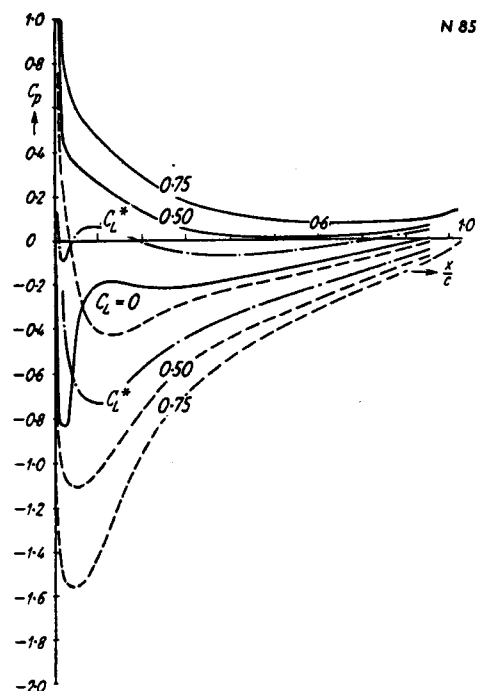
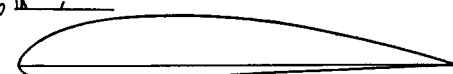
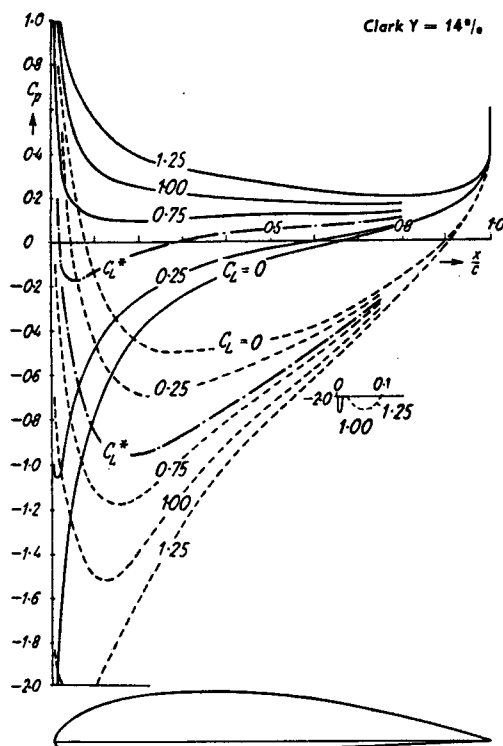


Fig. 12.19 a—d. Pressure distributions of the profiles: Clark Y 14%; N 85—87; (with effect of viscosity included)

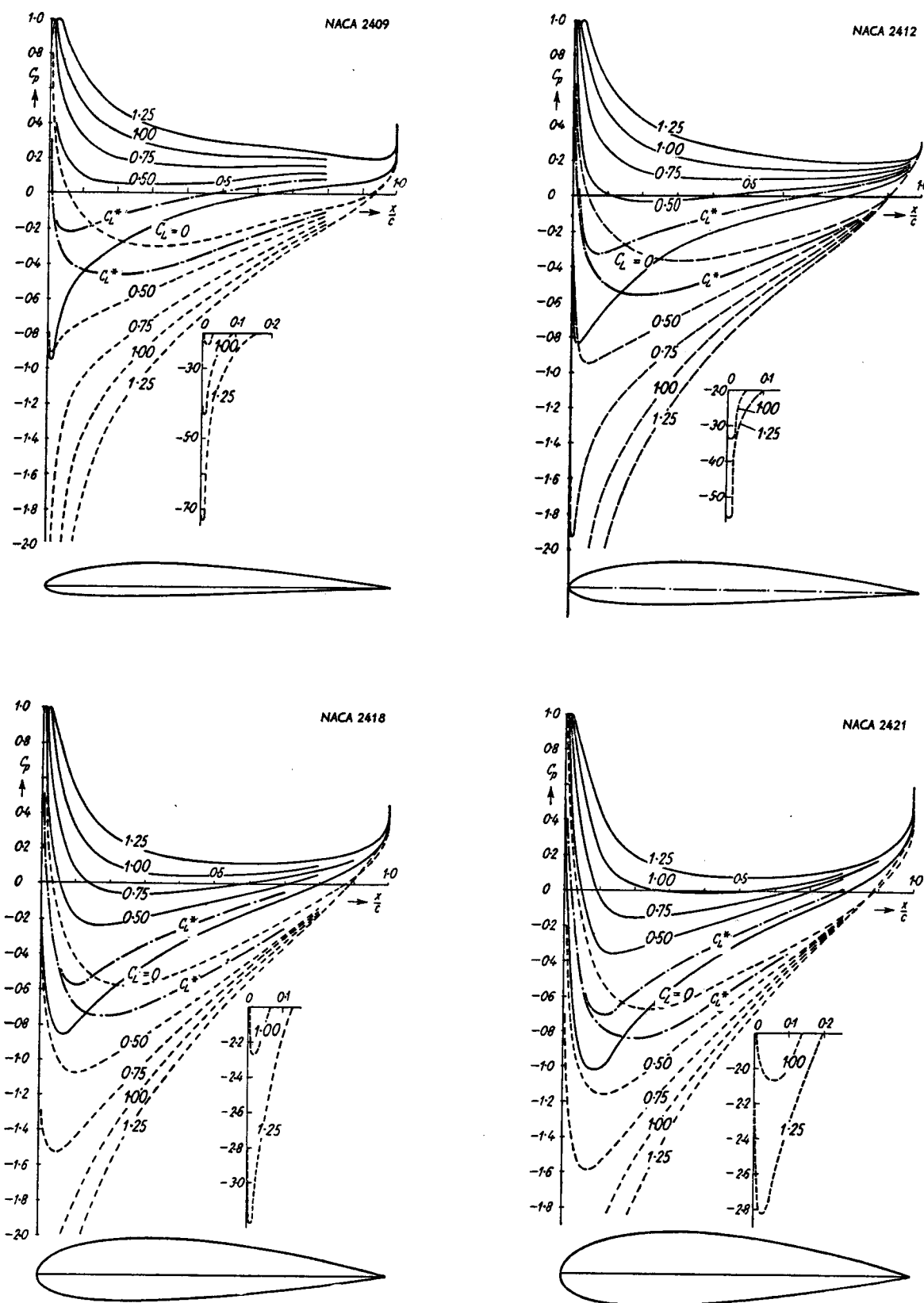


Fig. 12.20 a—d. Pressure distributions of the profiles: NACA 2409, 2412, 2418, 2421; (with effect of viscosity included,  $R = 3.10^4$ )

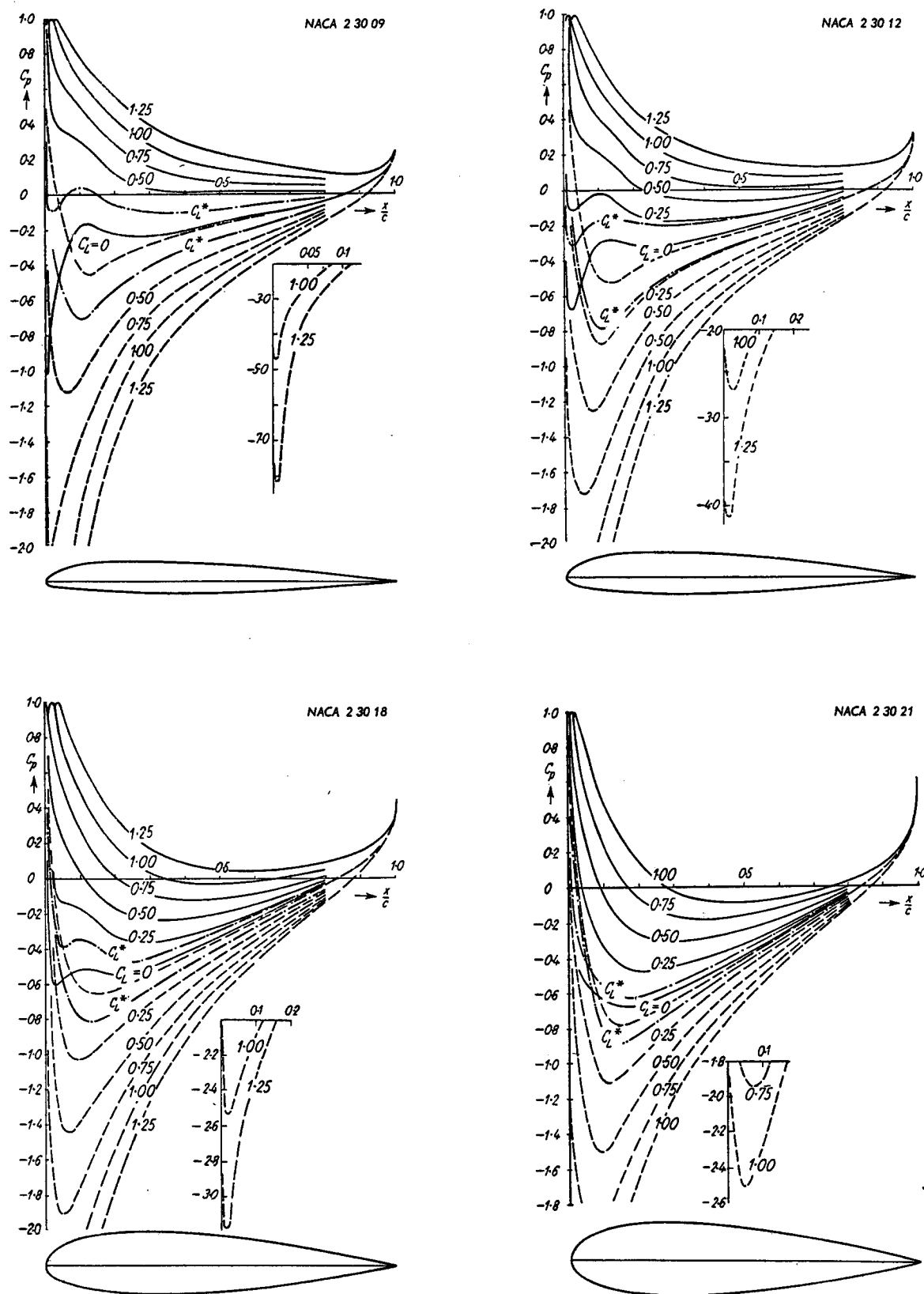


Fig. 12.21 a—d. Pressure distributions of the profiles: NACA 230 09, 230 12, 230 18, 230 21; (with effect of viscosity included,  $R = 3 \cdot 10^4$ )

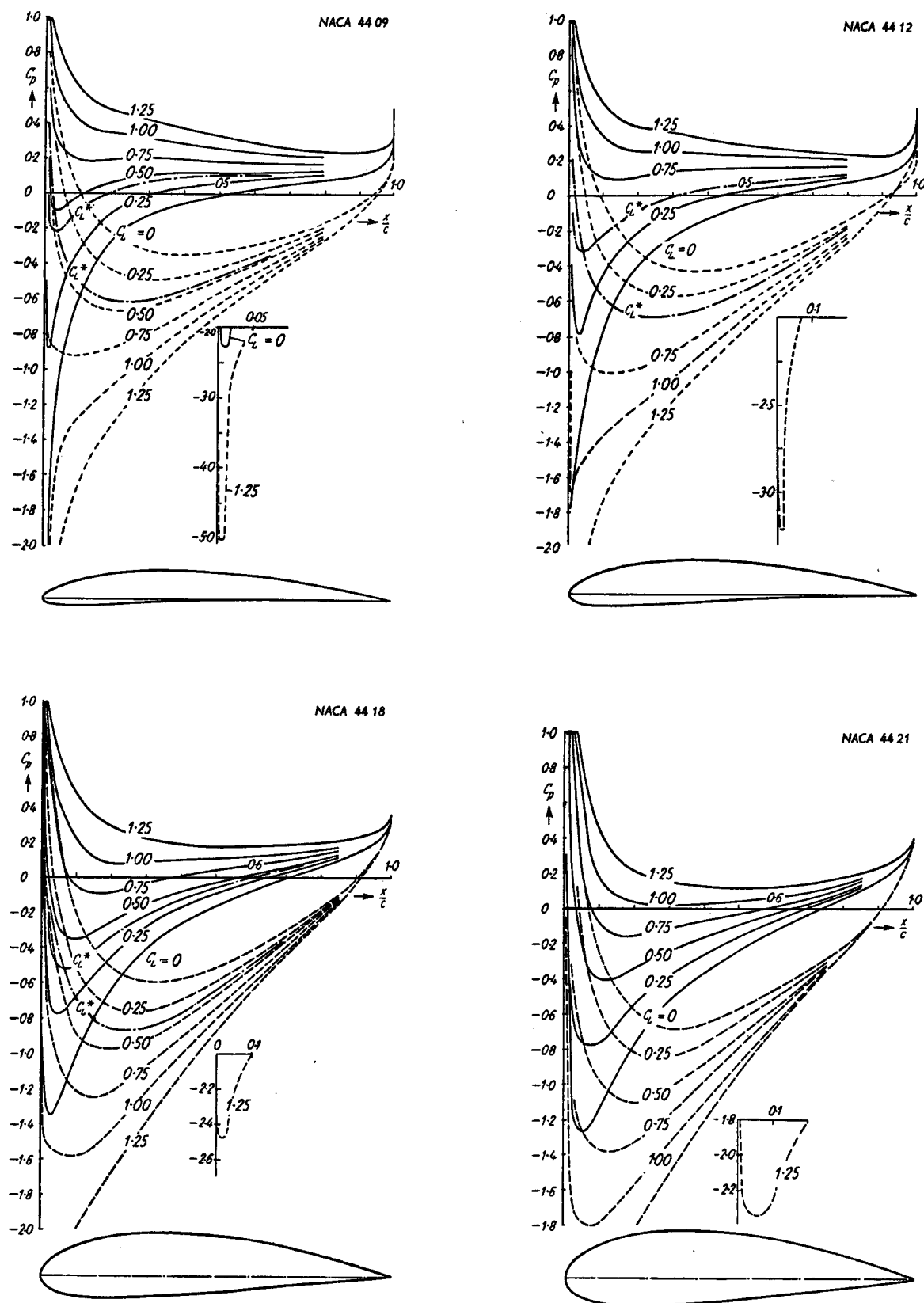


Fig. 12.22 a-d. Pressure distributions of the profiles: NACA 44 09, 44 12, 44 18, 44 21; (with effect of viscosity included,  $R = 3 \cdot 10^6$ )

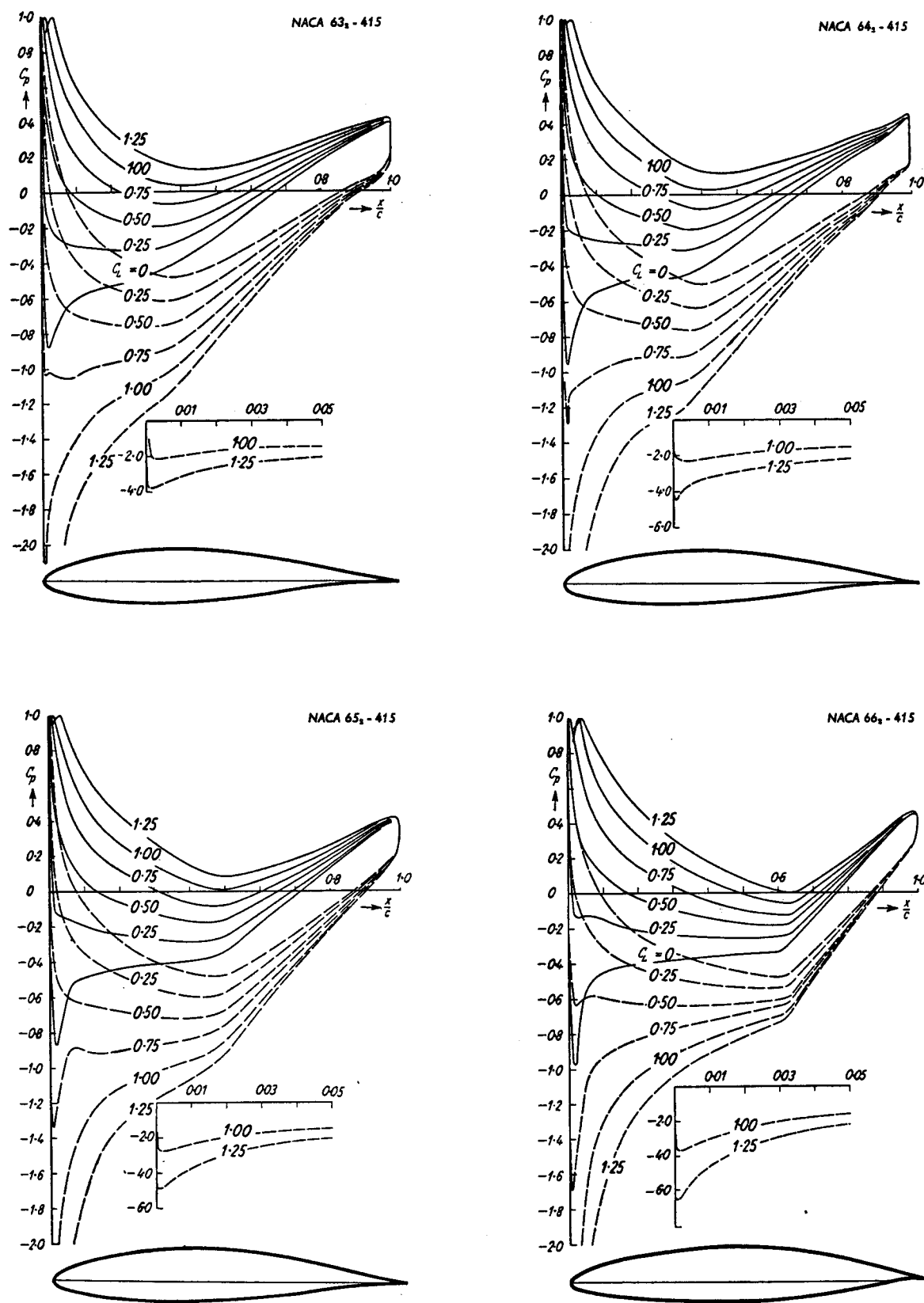


Fig. 12.23 a—d. Pressure distributions of the profiles: 63<sub>s</sub>-415; 64<sub>s</sub>-415; 65<sub>s</sub>-415; 66<sub>s</sub>-415; (with effect of viscosity included,  $R = 3 \cdot 10^4$ )

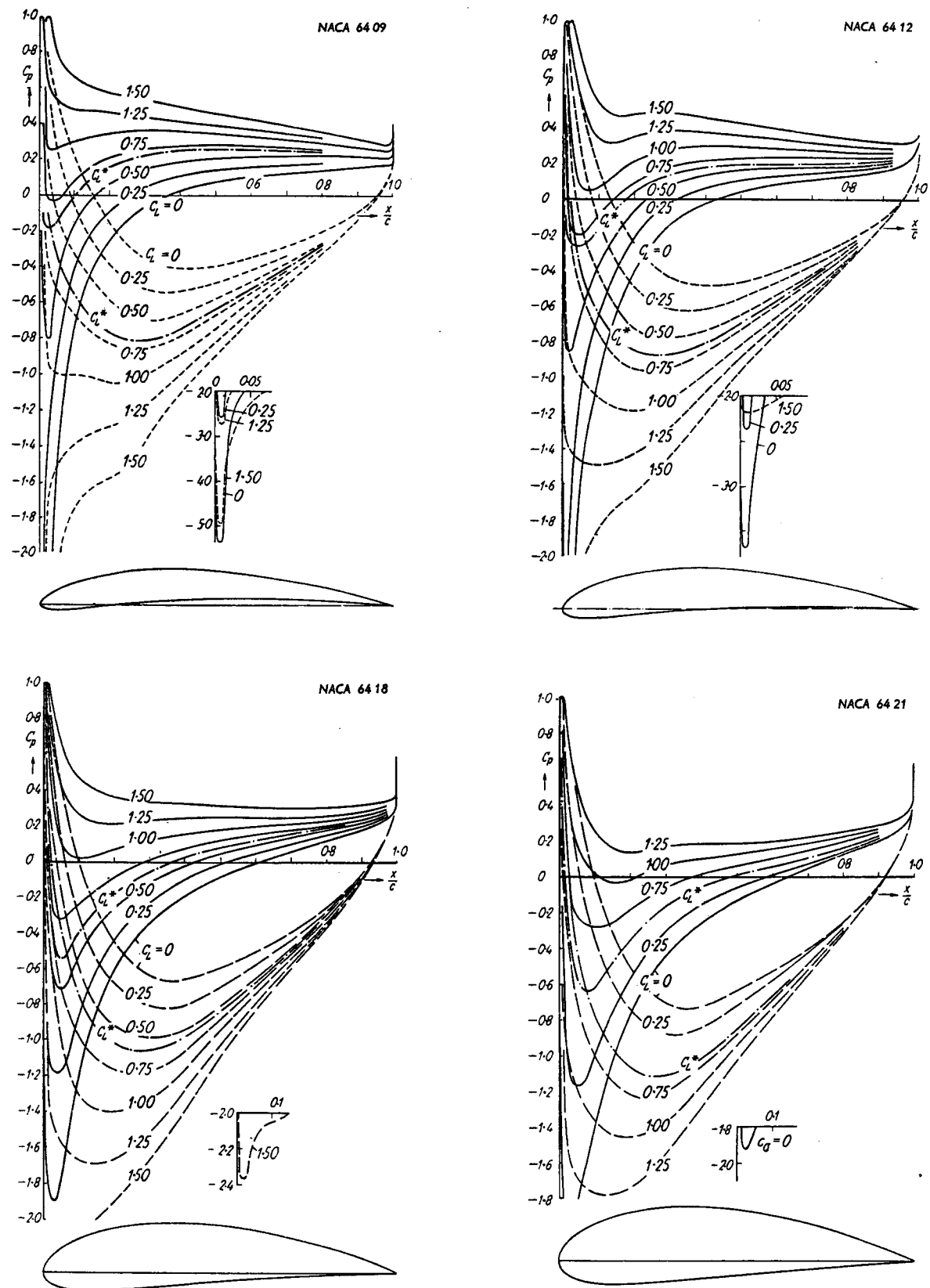


Fig. 12.24 a—d. Pressure distributions of the profiles: NACA 64 09, 64 12, 64 18, 64 21; (with effect of viscosity included,  $R = 3.10^6$ )

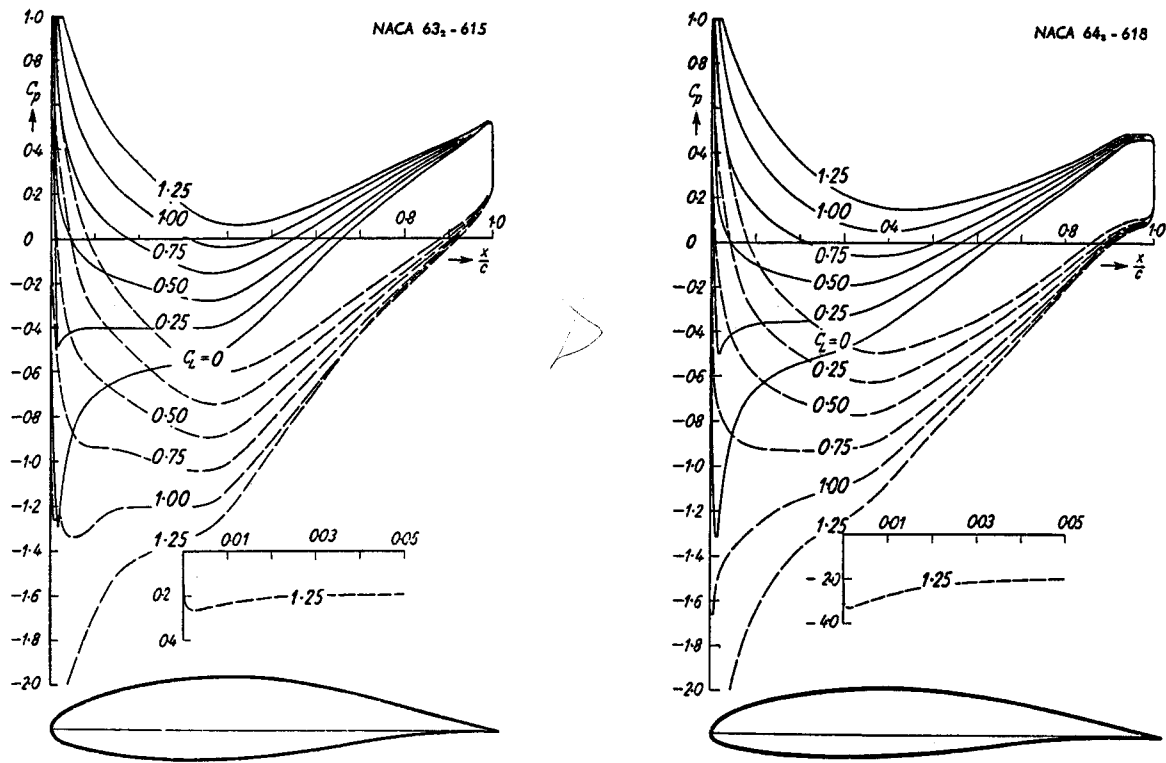


Fig. 12.25 a—b. Pressure distributions of the profiles: 64<sub>3</sub>—618; 63<sub>4</sub>—615; (with effect of viscosity included,  $R = 3 \cdot 10^6$ )

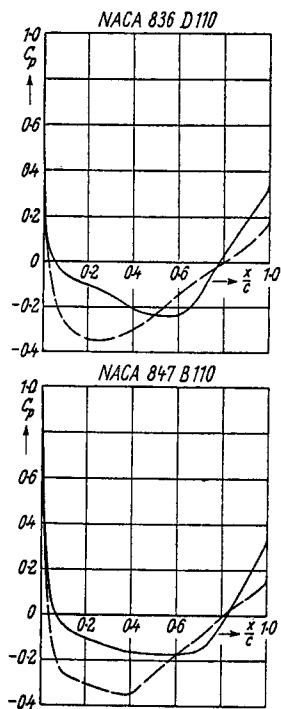


Fig. 12.26. Pressure distributions of the profiles: NACA 836 D 110, 847 B 110;  $\alpha = 0^\circ$ ; (according to potential theory)

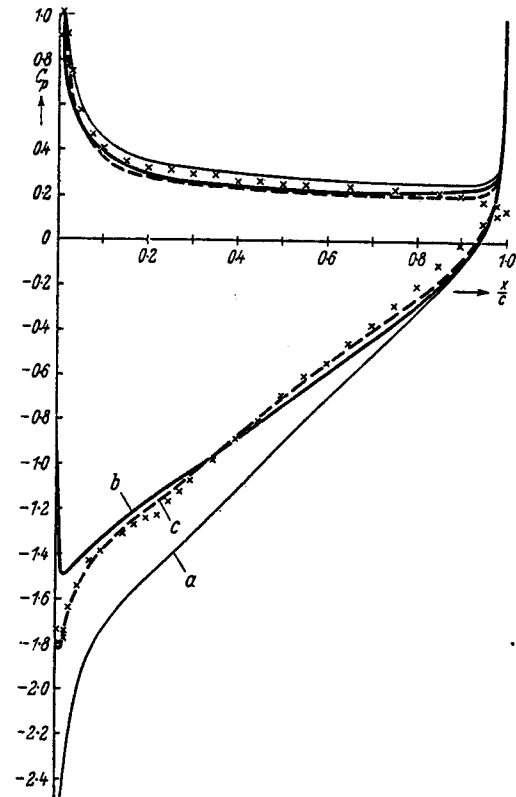
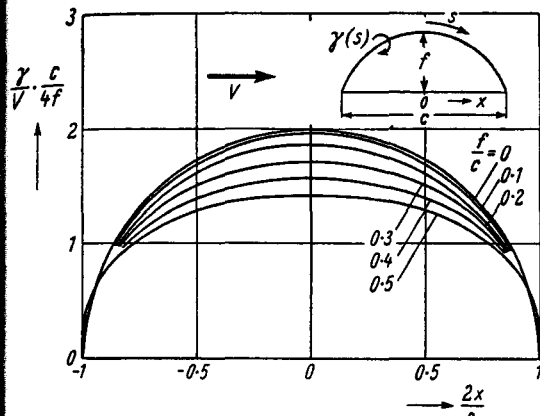
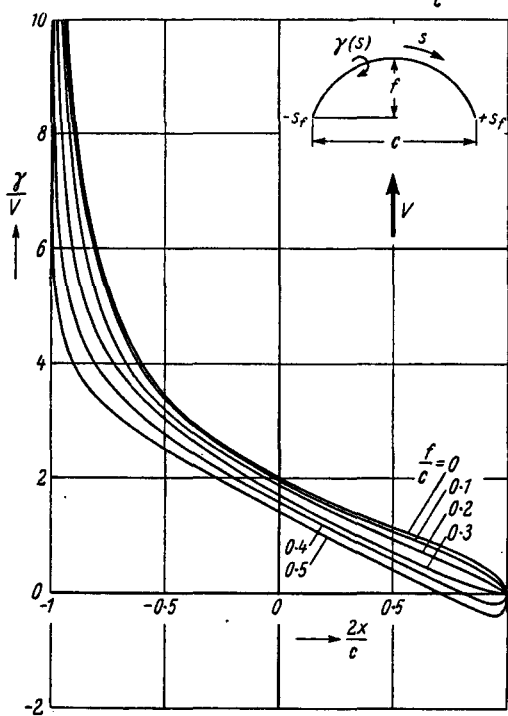


Fig. 12.27. Comparison of theoretical and experimental ( $\times \times \times$ ) pressure distributions for the profile NACA 4412 at  $C_L = 1.02$ :  
 (a) on potential theory, at the angle of incidence of the experiment;  
 (b) on potential theory, at the  $C_L$  of the experiment;  
 (c) with effect of viscosity included, at the angle of incidence of the experiment



a



b

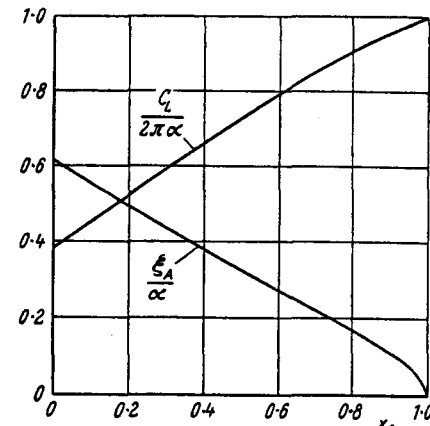
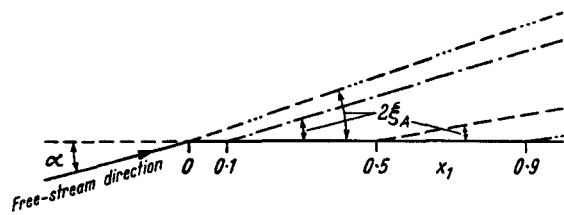
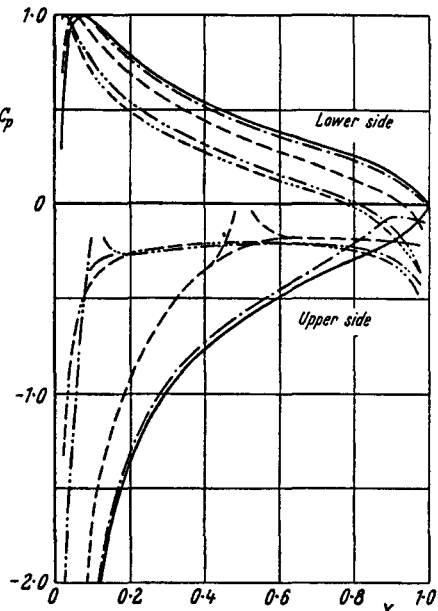


Fig. 12.28 a, b. Effect of large camber. Distribution of circulation on circular-arc profiles of various cambers; (according to potential theory).  
 (a) horizontal free-stream;  
 (b) vertical free-stream.  
 (H. KRÜGER, unpublished)

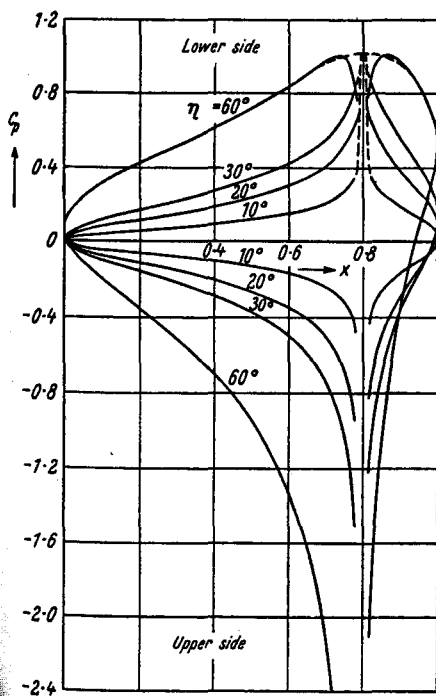


Fig. 12.29. Pressure distribution of flat plate with flap, at the ideal angle of incidence; (according to potential theory). Flap chord, 0.2. Flap deflection, \$\eta\$

Fig. 12.30 a, b. Approximate pressure distribution of a flat plate with dead-water region, for arbitrarily chosen separation points \$x\_1\$; (according to potential theory)

- |                        |                        |
|------------------------|------------------------|
| ... - - - \$x_1 = 0\$; | \$\xi_A = 9.2^\circ\$; |
| — - - \$x_1 = 0.1\$;   | \$\xi_A = 8.3^\circ\$; |
| — - - \$x_1 = 0.5\$;   | \$\xi_A = 4.8^\circ\$; |
| — - - \$x_1 = 0.9\$;   | \$\xi_A = 1.7^\circ\$; |
| — - - \$x_1 = 1.0\$;   | \$\xi_A = 0^\circ\$.   |

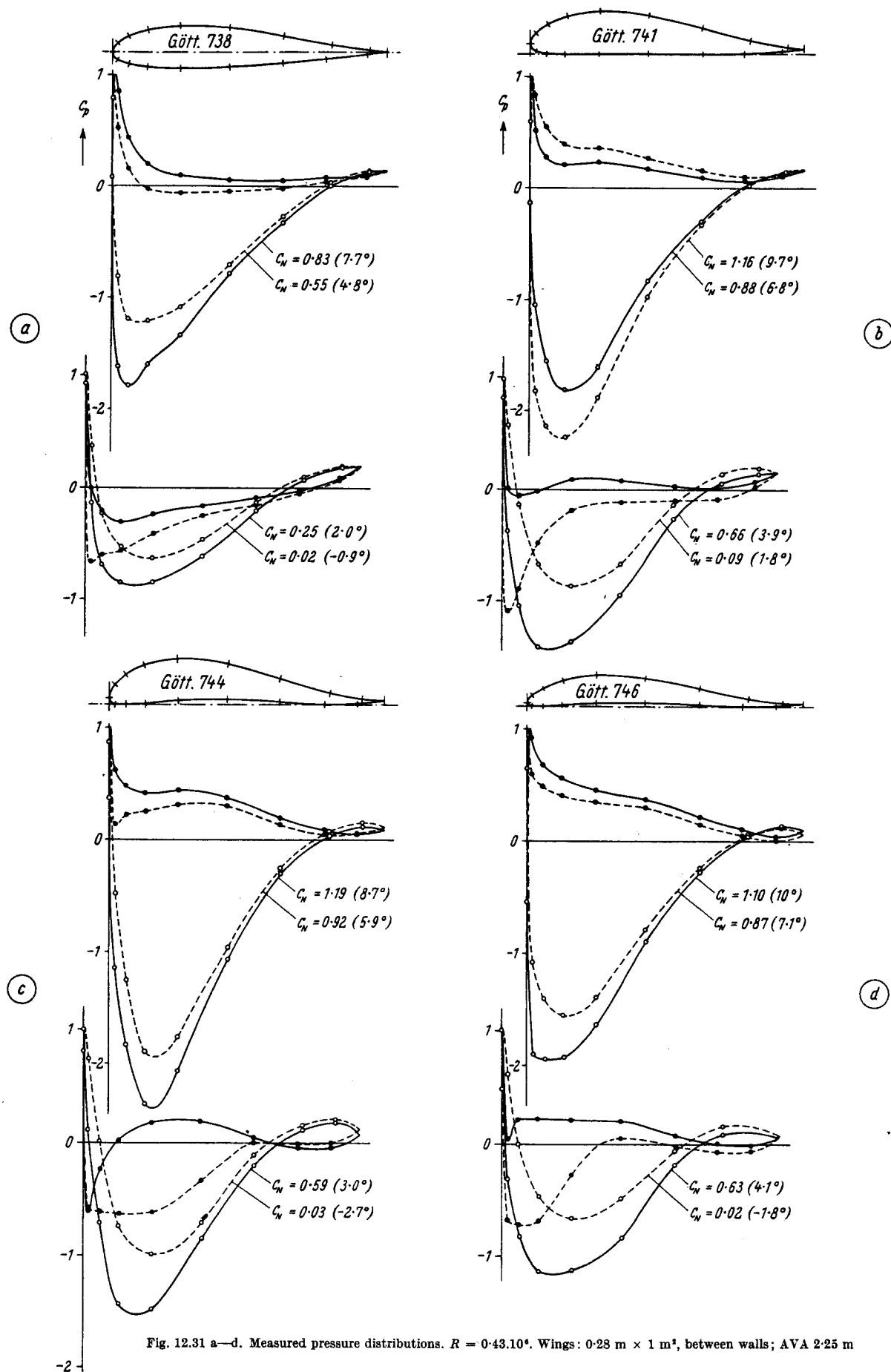


Fig. 12.31 a—d. Measured pressure distributions.  $R = 0.43 \cdot 10^6$ . Wings:  $0.28 \text{ m} \times 1 \text{ m}^2$ , between walls; AVA 2.25 m

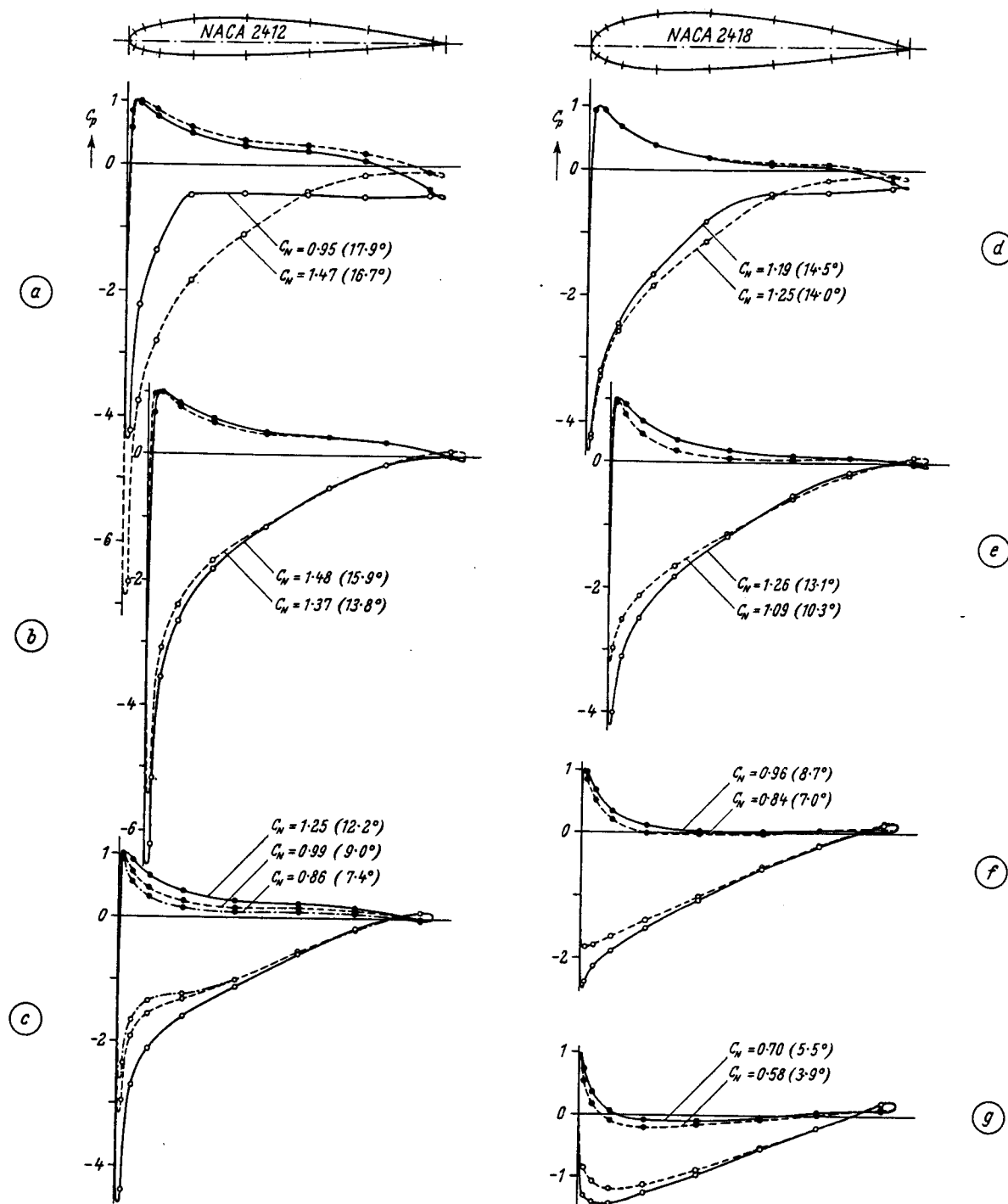


Fig. 12.32 a—g. Measured pressure distributions.  $R = 2 \cdot 7 \cdot 10^6$ . Rectangular wing (1:5), with rounded tips; DVL 5 m  $\times$  7 m

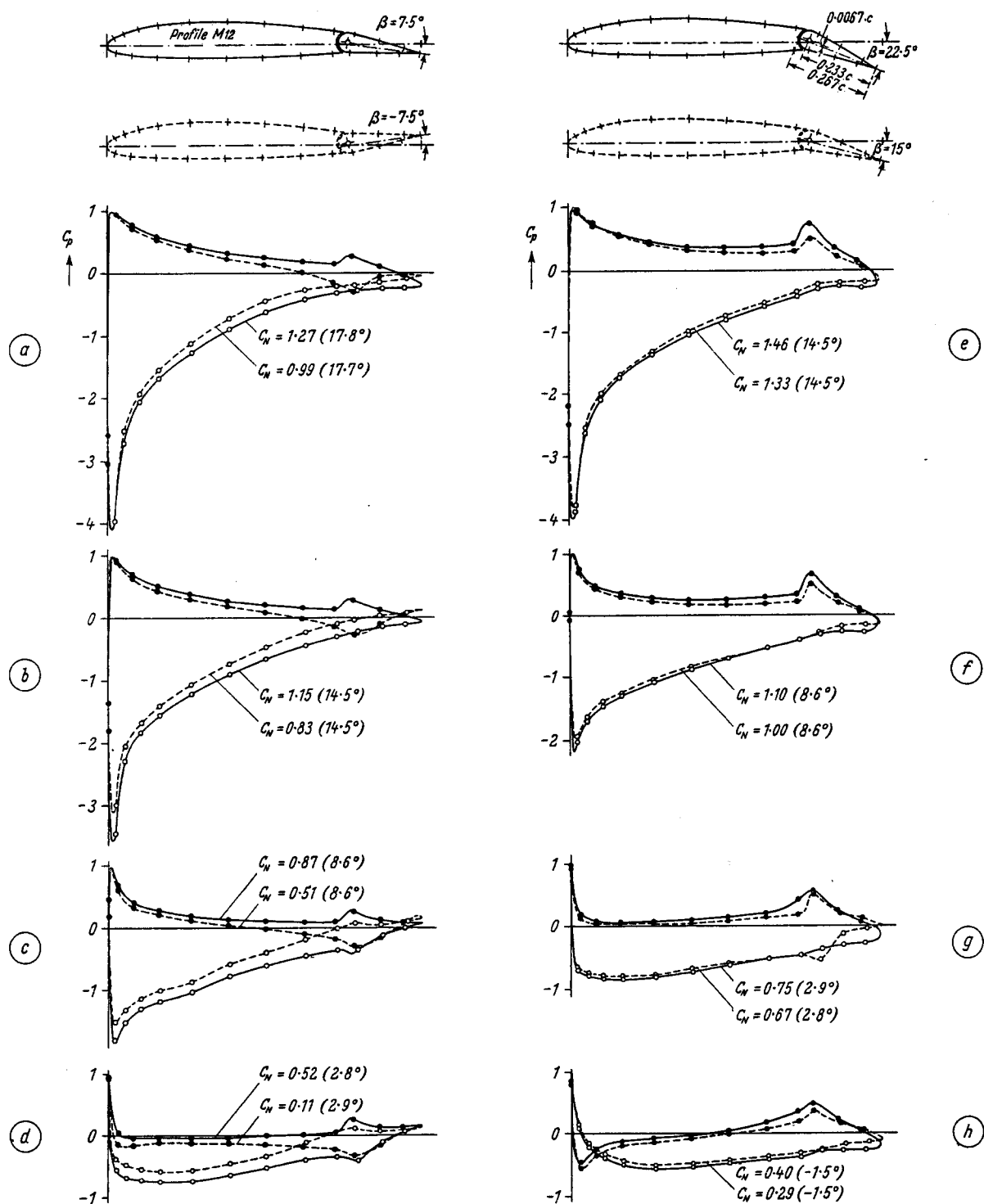


Fig. 12.33 a—h. Measured pressure distributions on the profile Gö 676 (M 12), with flap deflected.  $R = 0.5 \cdot 10^6$ . Elliptical wing,  $A = 6.25$ ; AVA 2.25 m

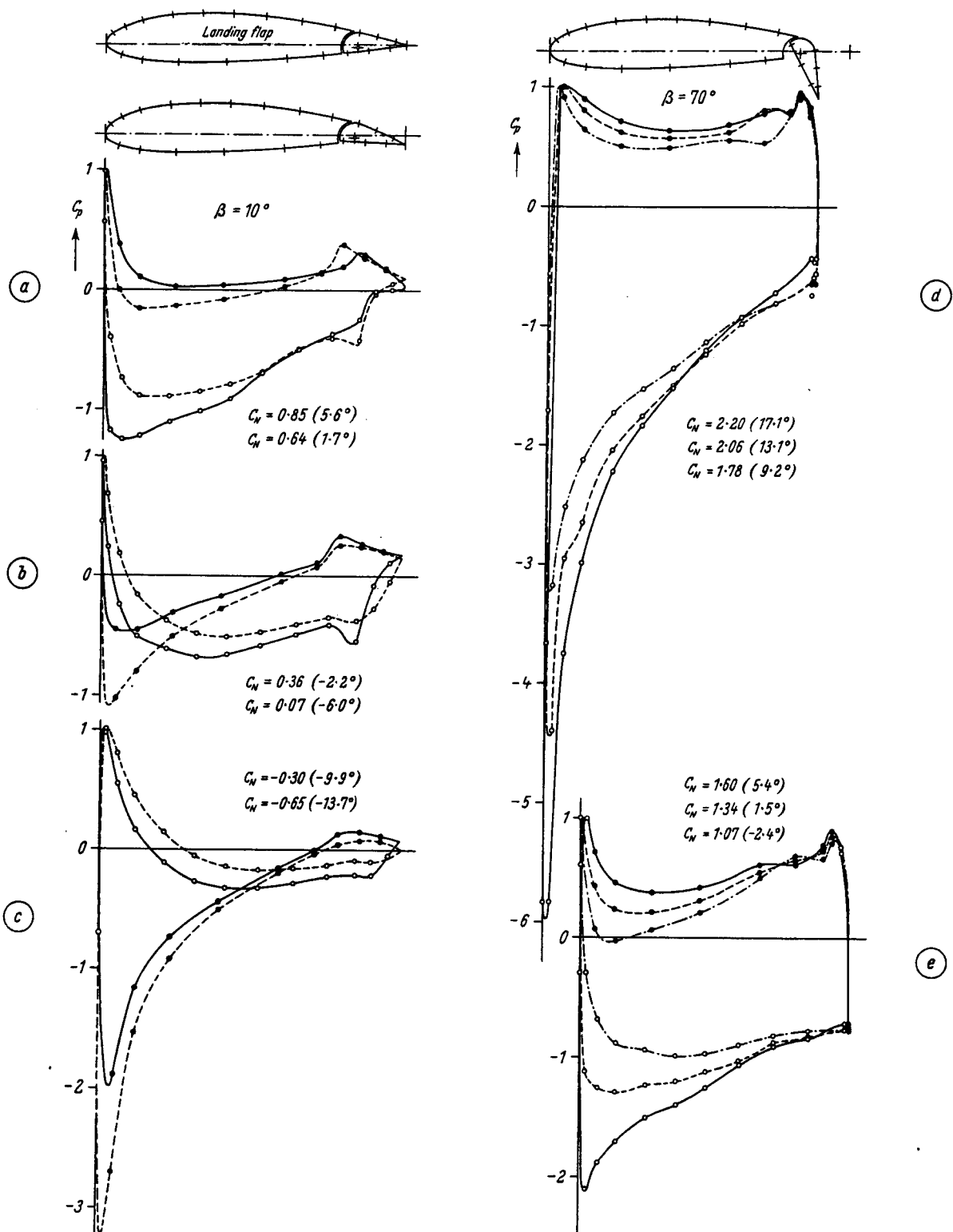


Fig. 12.34 a—e. Measured pressure distributions on a profile with flap deflected.  $R = 0.53 \cdot 10^6$ . Rectangular wing (1:5); AVA 2.25 m

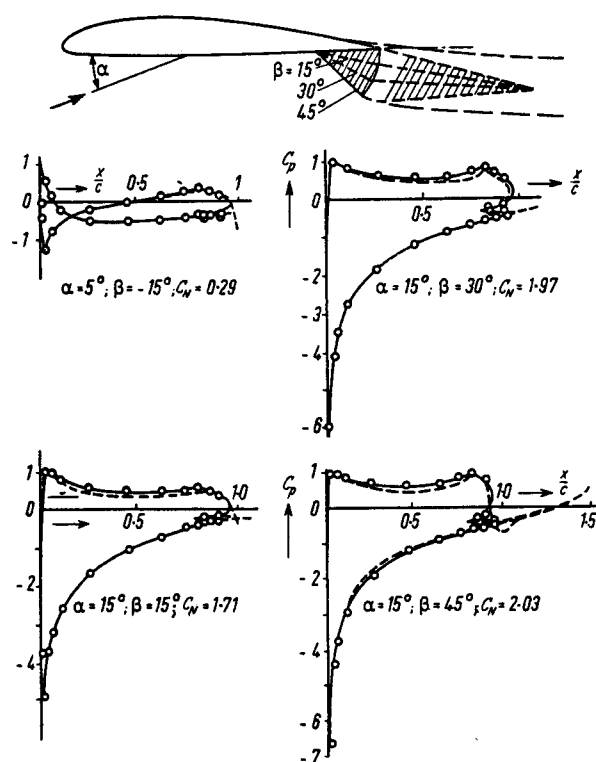


Fig. 12.35 a—e. Comparison between theoretical (—) and experimental (—o—) pressure distributions on a Clark Y profile, with various split-flap deflections. Dashed line: extended body, as suggested by WALZ

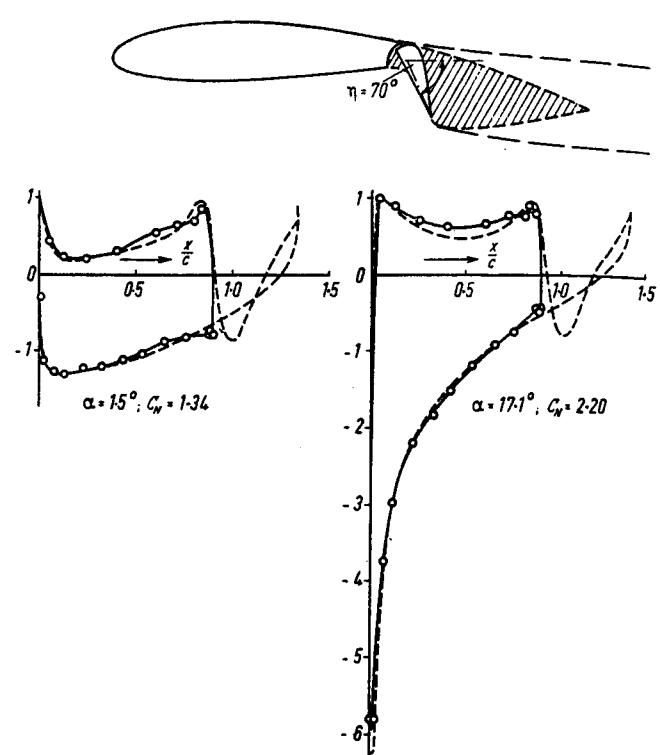


Fig. 12.36 a, b. Comparison between theoretical (—) and experimental (—o—) pressure distributions, on a profile with deflected flap (WALZ)

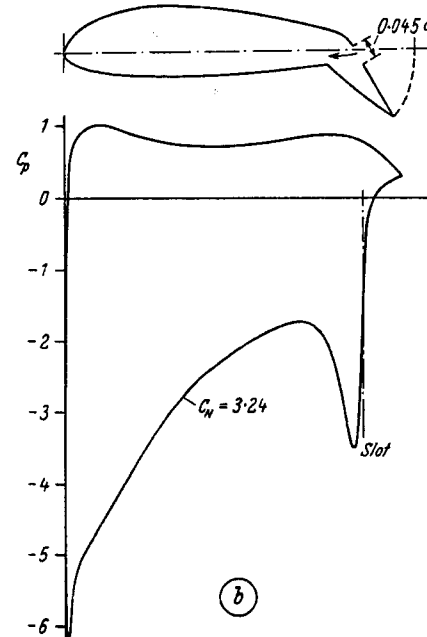
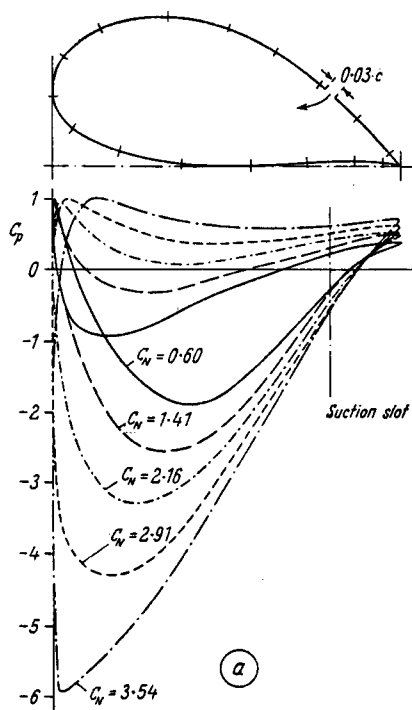


Fig. 12.37 a, b. Measured pressure distributions on two thick profiles, with boundary layer suction. (SCHRENK)

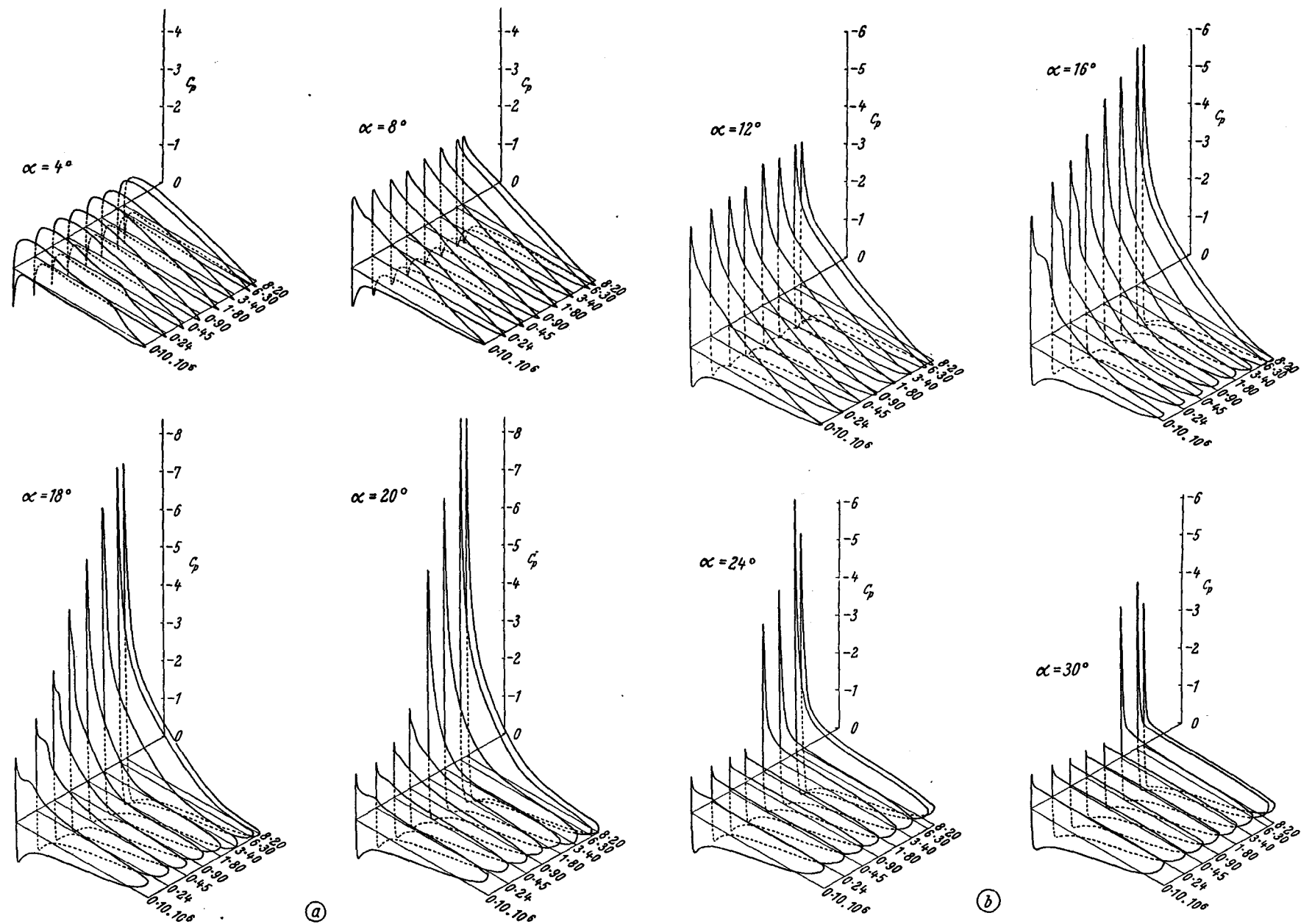


Fig. 12.38 a, b. Influence of Reynolds number on the pressure distribution. Profile: 4412. VDT [R 613]

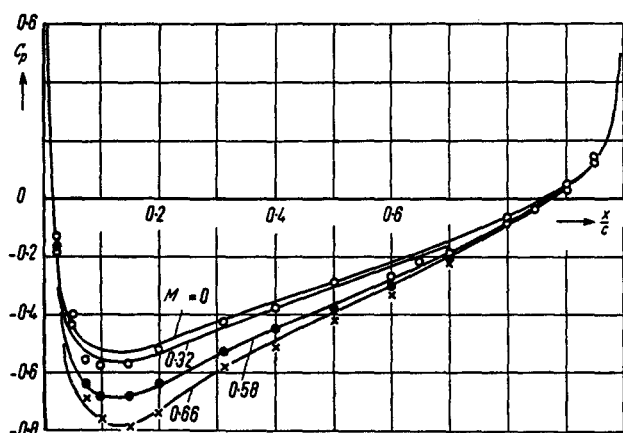


Fig. 12.39. Comparison between experimental and theoretical (full line) pressure distributions, at sub-critical Mach numbers. Profile 0015. Wind tunnel: DVL 2.7 m

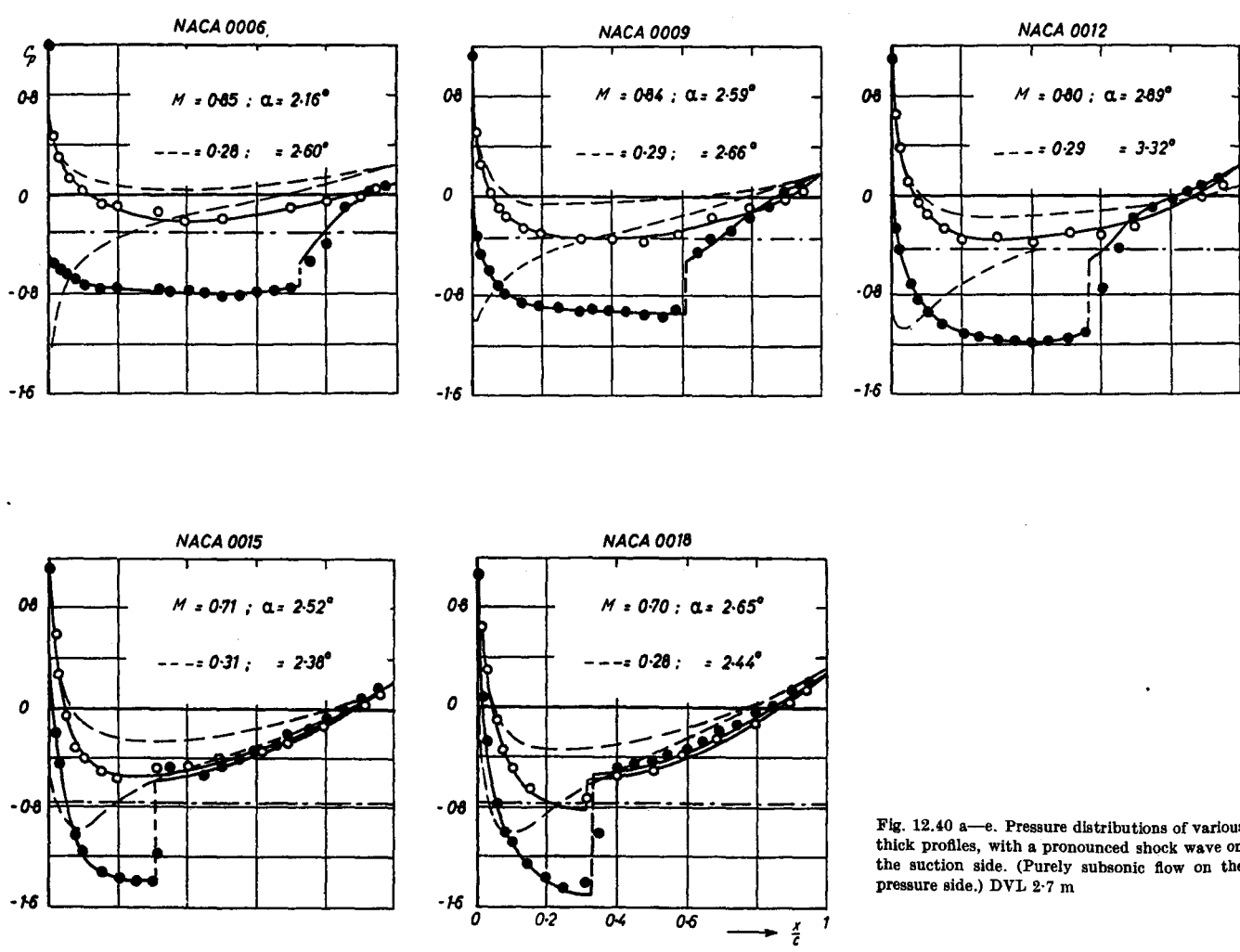


Fig. 12.40 a—e. Pressure distributions of various thick profiles, with a pronounced shock wave on the suction side. (Purely subsonic flow on the pressure side.) DVL 2.7 m

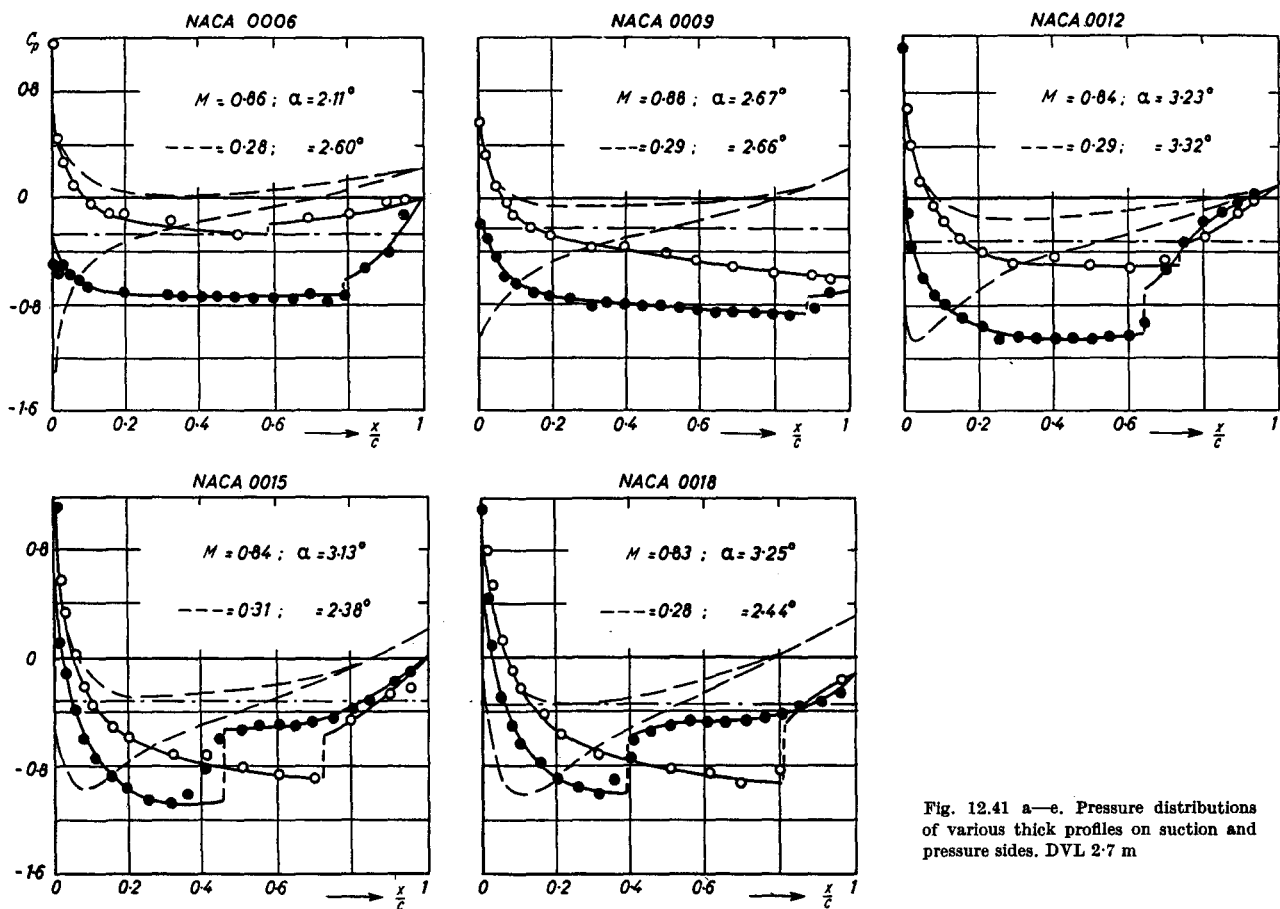


Fig. 12.41 a—e. Pressure distributions of various thick profiles on suction and pressure sides. DVL 2.7 m

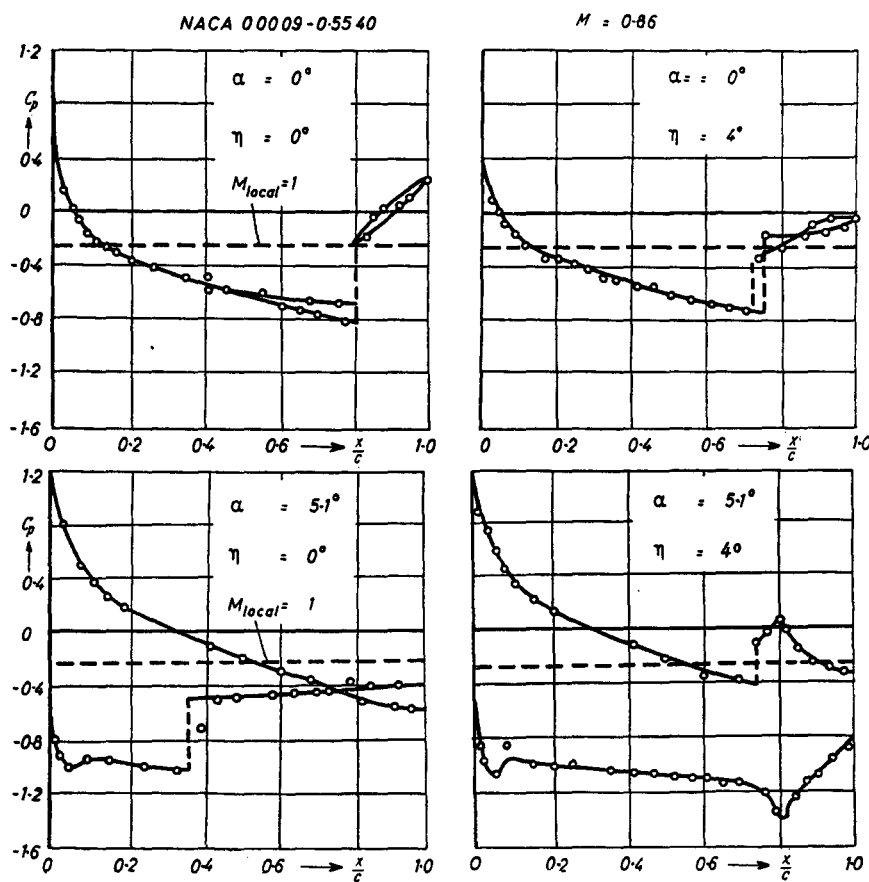


Fig. 12.42 a—d. Pressure distributions in subsonic flow on a profile with maximum thickness further back and nose radius smaller than normal profile, Profile: 00 09-0.55 40. DVL 2.7 m

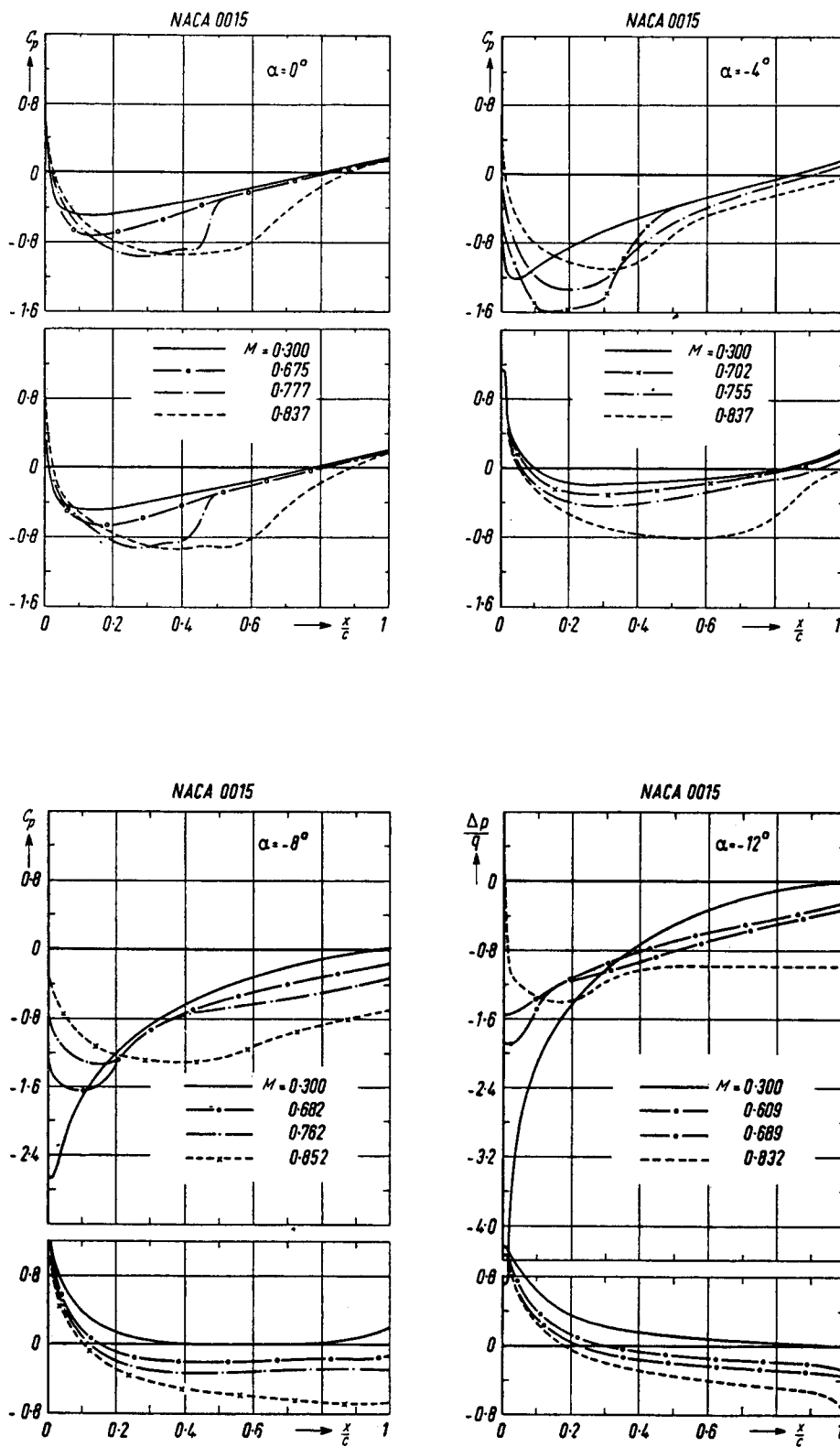


Fig. 12.43 a-d. Measured pressure distributions at various Mach numbers and angles of incidence. Profile: NACA 0015. Ames Lab 1 ft  $\times$  3½ ft

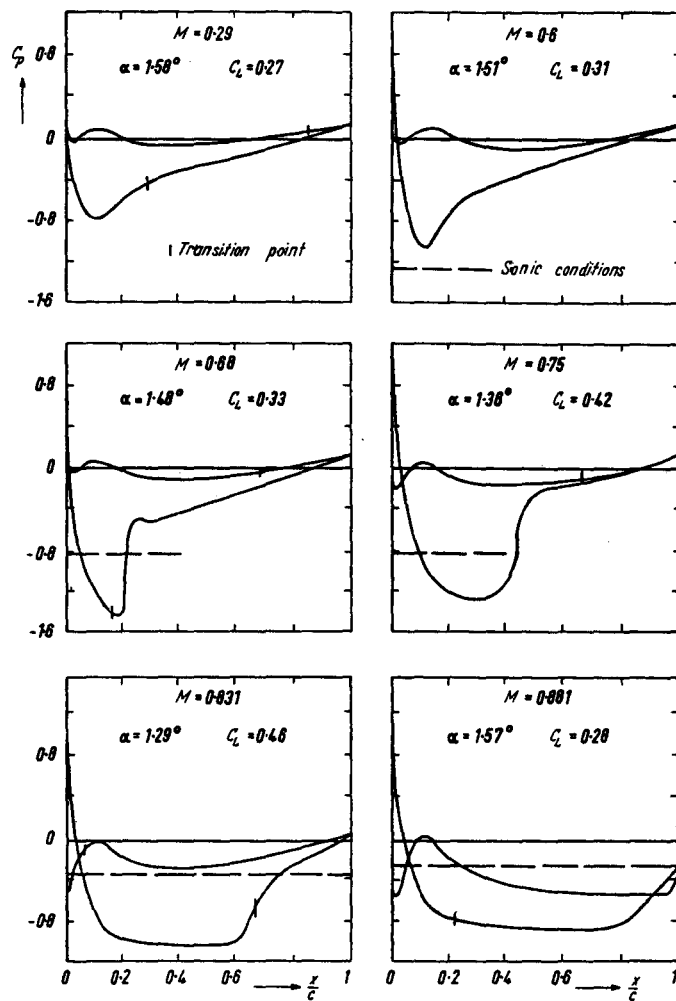


Fig. 12.44 a-f. Measured pressure distributions at various Mach numbers.  
Profile: NACA 230 09. DVL 2.7 m tunnel

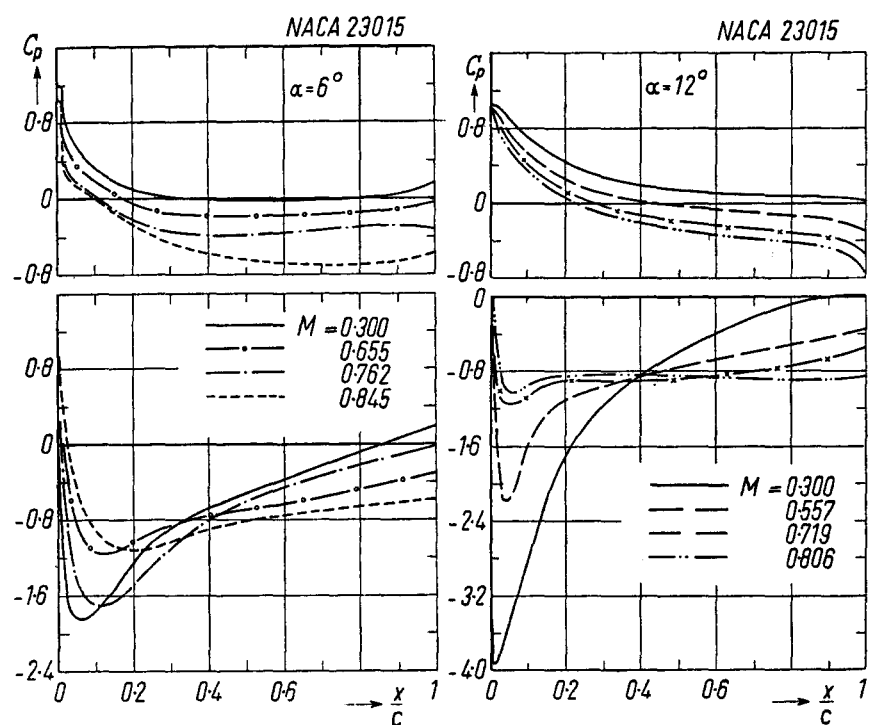
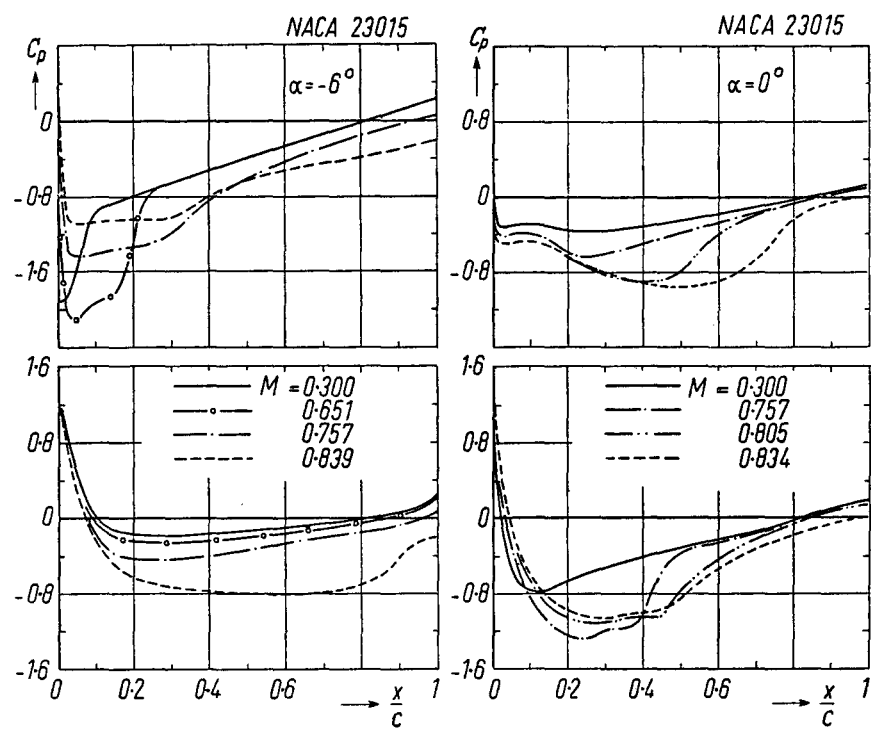


Fig. 12.45 a-d. Measured pressure distributions at various Mach numbers and angles of incidence.  
Profile: NACA 23015. Ames Lab 1 ft  $\times$   $3\frac{1}{2}$  ft

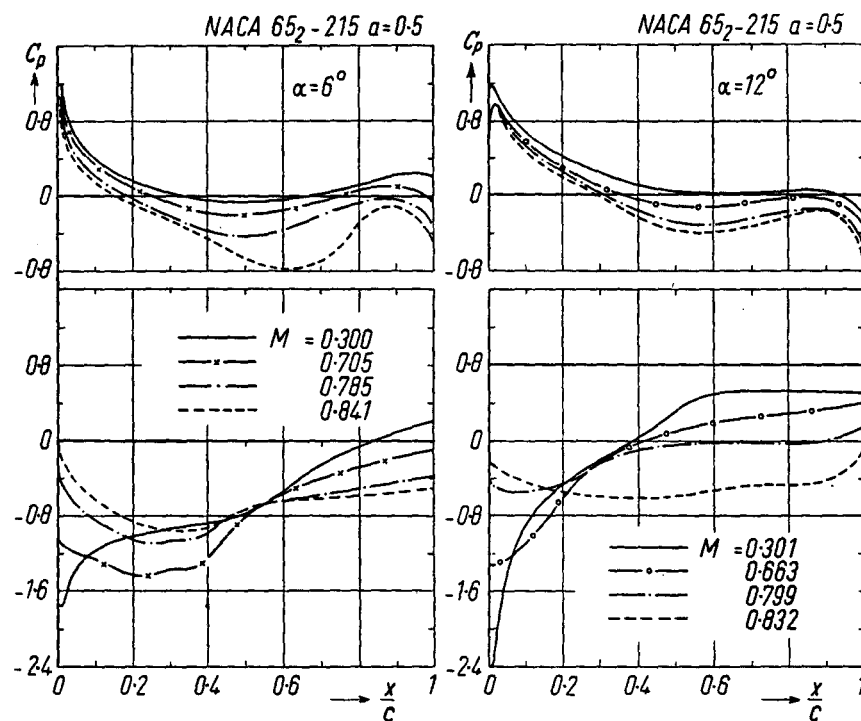
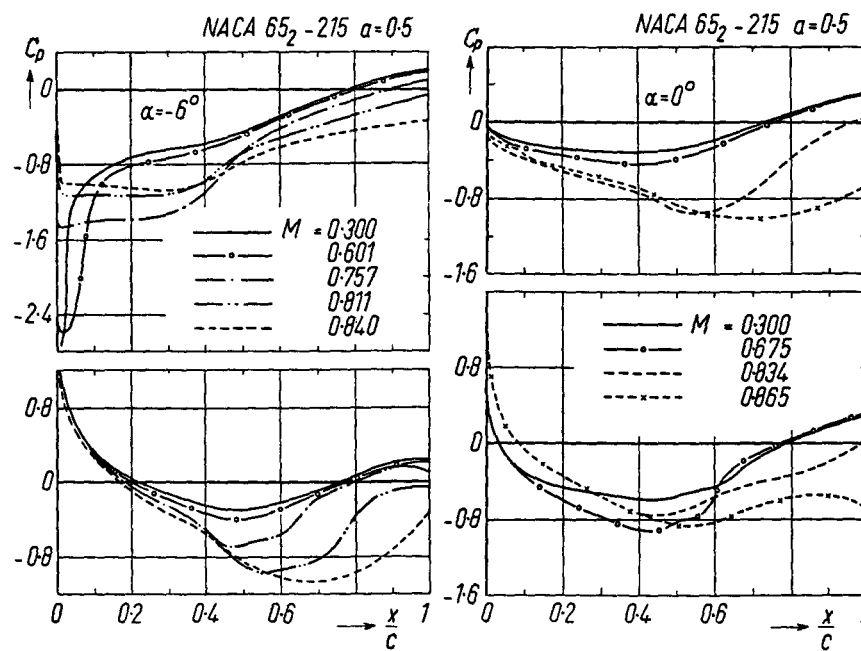


Fig. 12.46 a—d. Measured pressure distributions at various Mach numbers and angles of incidence.  
Profile: NACA 65<sub>2</sub>-215 ( $\alpha = 0.5$ ). Ames Lab 1 ft  $\times$  3½ ft

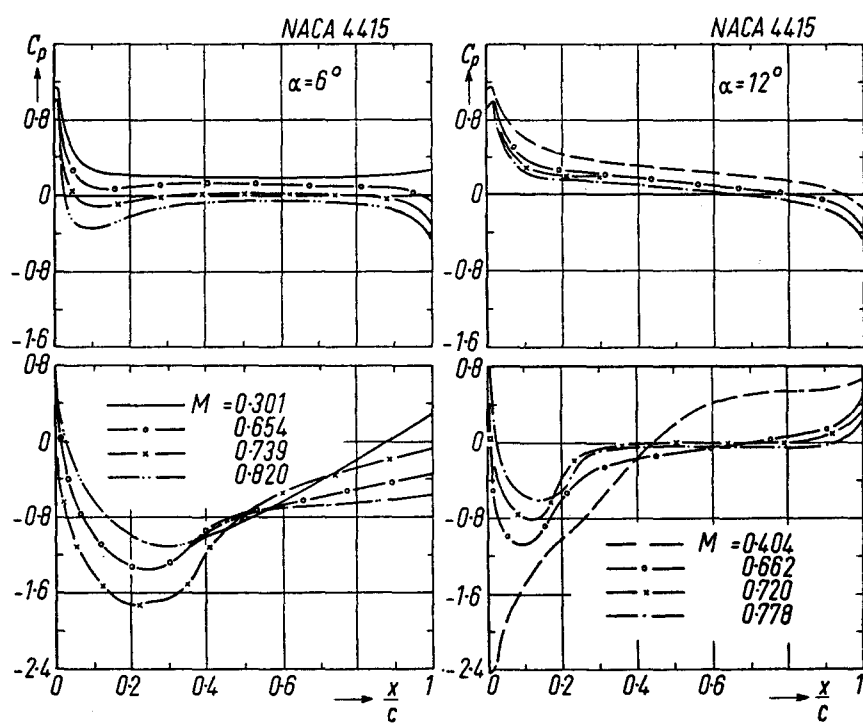
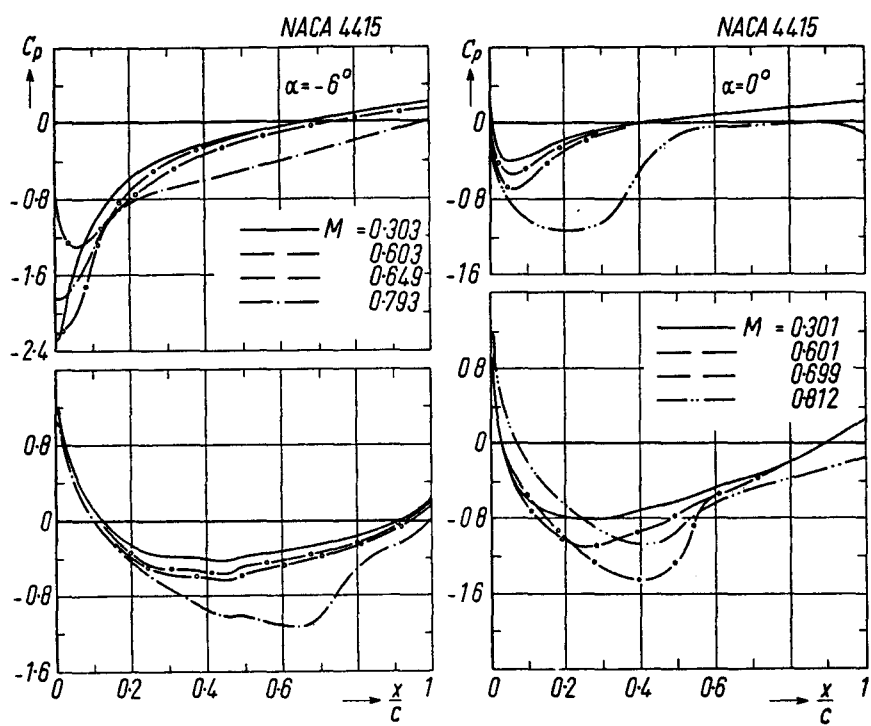


Fig. 12.47 a—d. Measured pressure distributions at various Mach numbers and angles of incidence.  
Profile: NACA 4415. Ames Lab 1 ft  $\times$   $3\frac{1}{2}$  ft

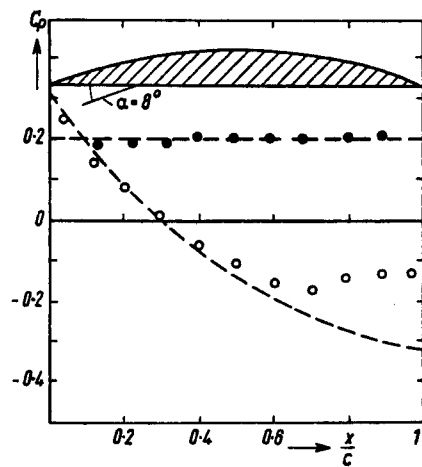


Fig. 12.48. Experimental and theoretical (—) pressure distributions on a circular-segment profile ( $t/c = 0.088$ ) in a supersonic flow ( $M = 1.85$ ). Wind tunnel: Guidonia



G.U.2

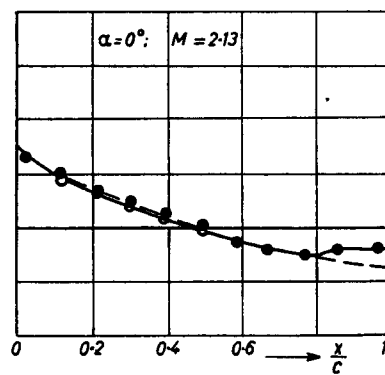
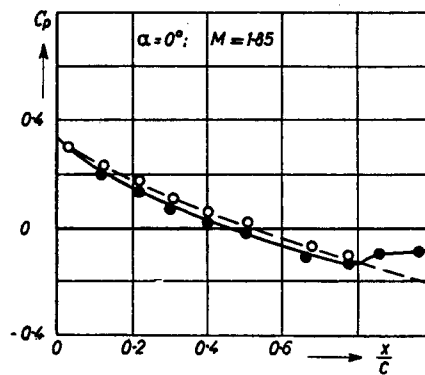
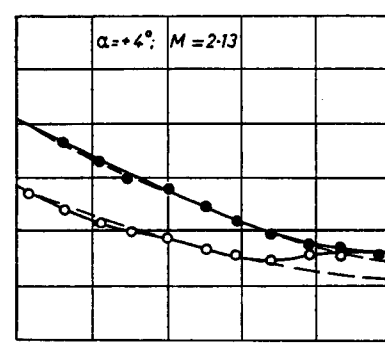
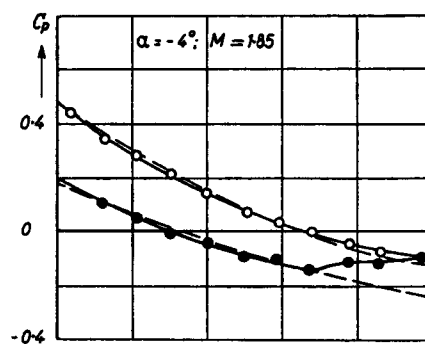
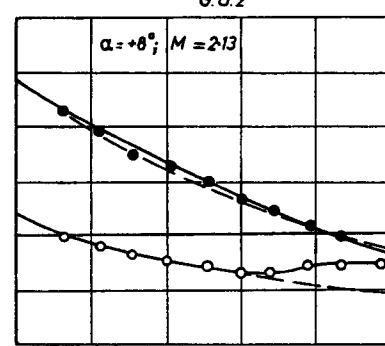
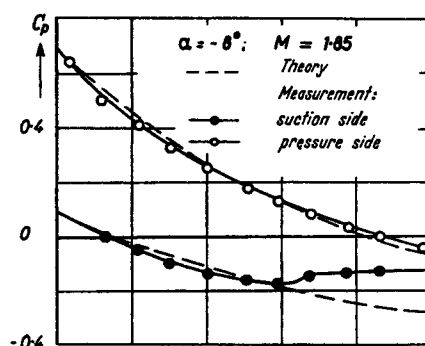


Fig. 12.49 a-f. Experimental and theoretical (—) pressure distributions on a biconvex profile G. U. 2. Wind tunnel: Guidonia

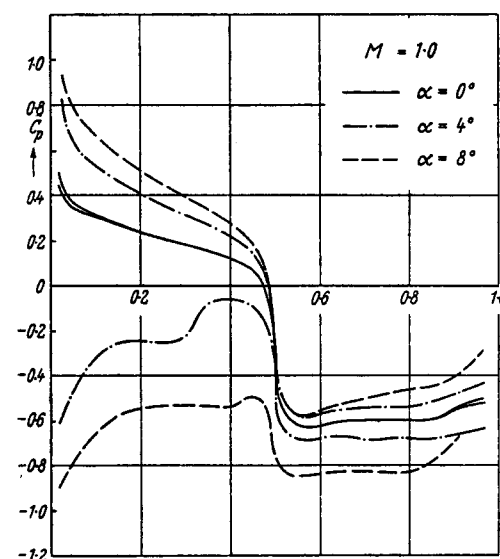
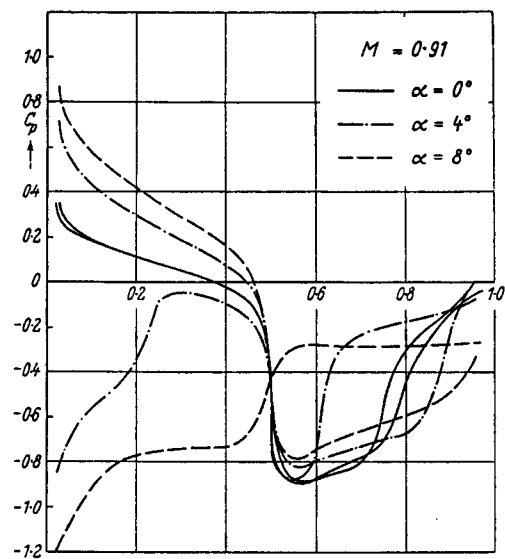
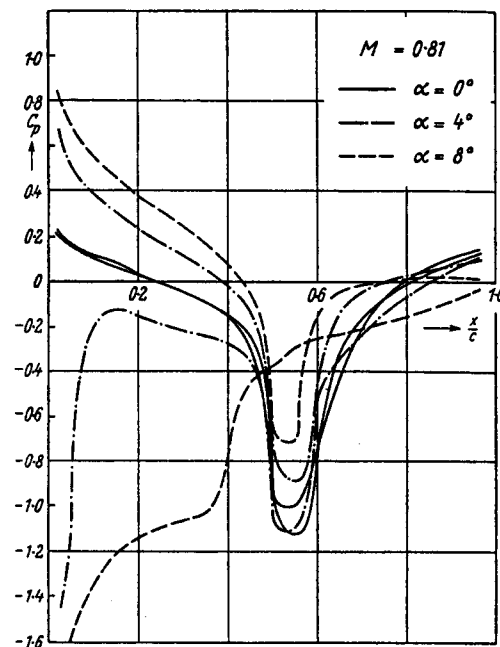
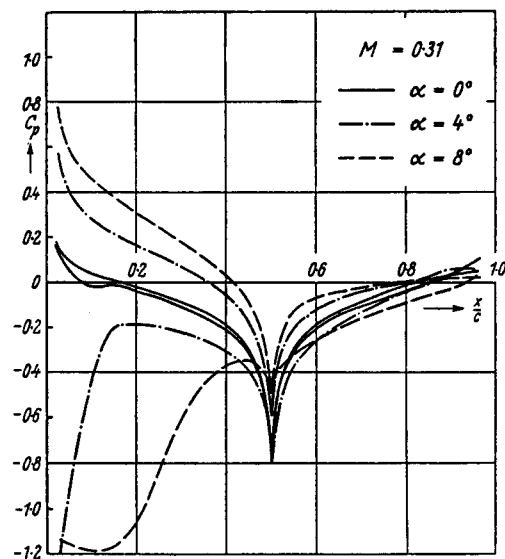


Fig. 12.50 a—d. Measured pressure distributions on a double wedge profile ( $t/c = 0.1$ ) at the angles of incidence  $\alpha = 0^\circ, 4^\circ, 8^\circ$ , and at various Mach numbers. [N 3306]

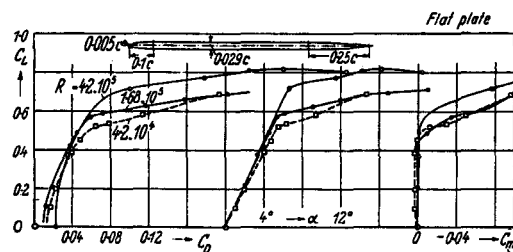


Fig. 12.51 a. Polars for flat plate,  $A = 5$ . Cologne 0.7 m.  
(SCHMITZ)

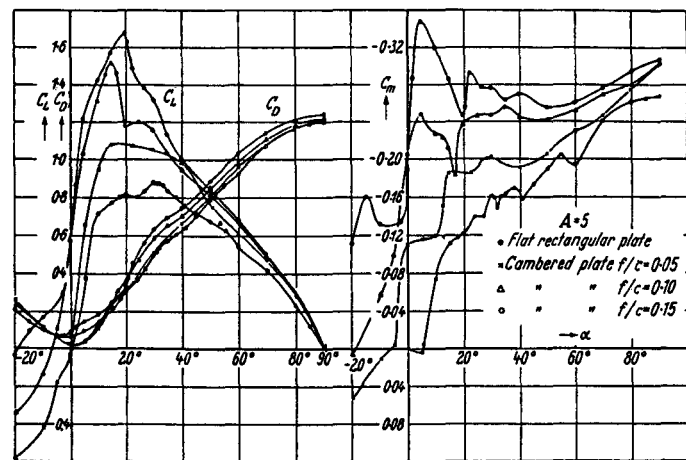


Fig. 12.51 b. Polars for flat and cambered plates,  $A = 5$ . AVA 2.25 m

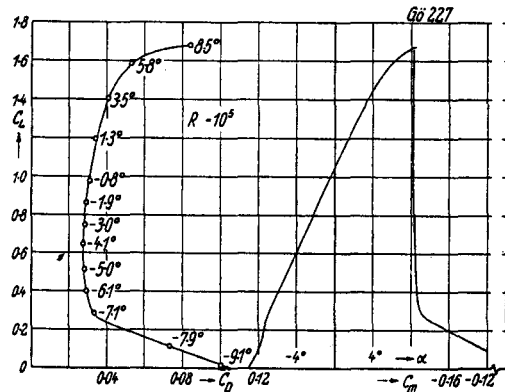


Fig. 12.52. Polars for Gö 227. MVA;  $R = 10^6$

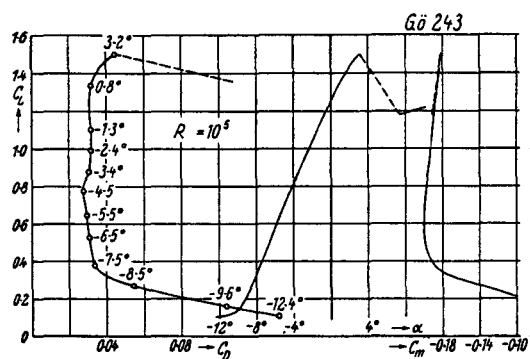


Fig. 12.54. Polars for Gö 243. MVA;  $R = 10^6$

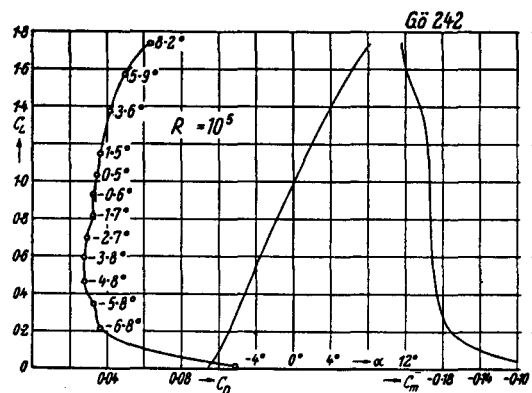


Fig. 12.53. Polars for Gö 242. MVA;  $R = 10^6$

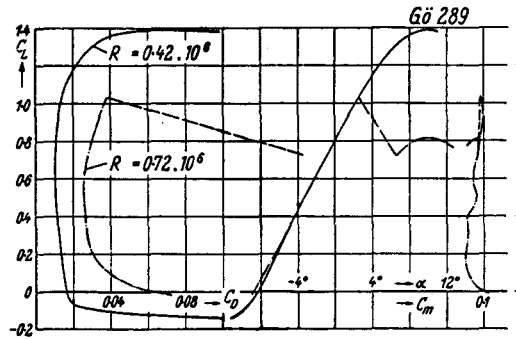


Fig. 12.55. Polars for Gö 289. MVA;  $R = 4.2 \cdot 10^6$  and  $7.2 \cdot 10^6$

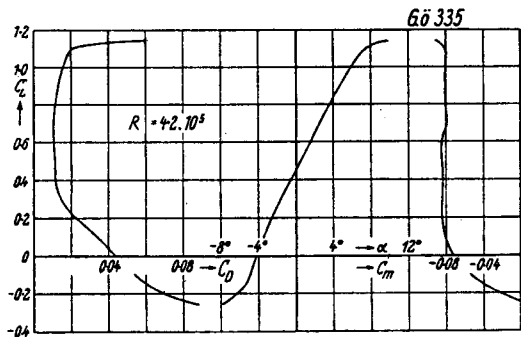


Fig. 12.56. Gö 335. MVA

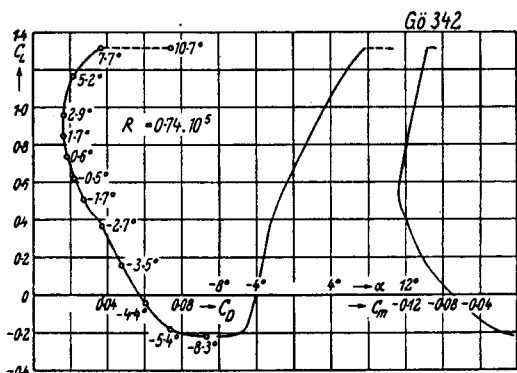
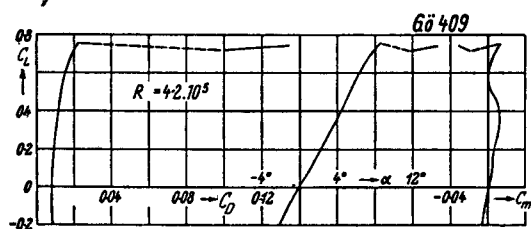
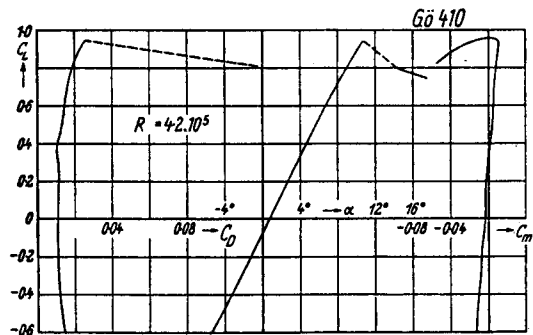
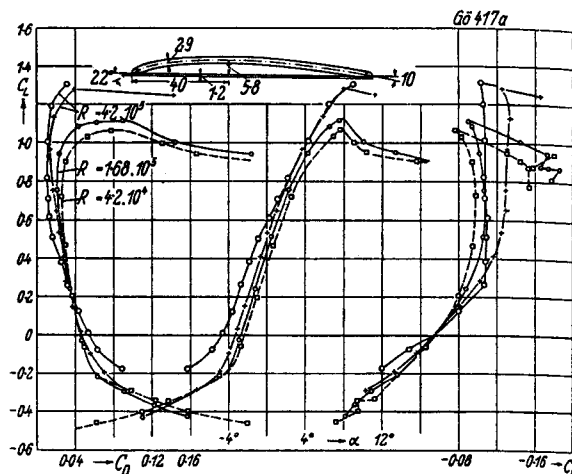
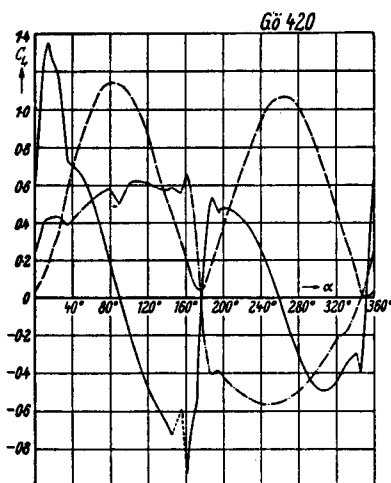
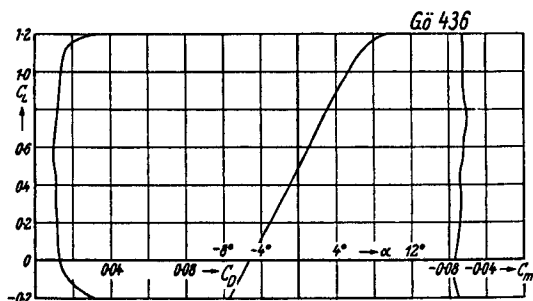
Fig. 12.57. Gö 342. MVA ;  $R = 0.74 \cdot 10^5$ Fig. 12.58. Gö 409. AVA 2.25 m;  $R = 4.2 \cdot 10^5$ Fig. 12.59. Gö 410. AVA 2.25 m;  $R = 4.2 \cdot 10^5$ 

Fig. 12.60. Gö 417a. Cologne 0.7 m (SCHMITZ)

Fig. 12.61. Gö 420 ( $0^\circ \leq \alpha \leq 360^\circ$ ). AVA 2.25 m;  $R = 4.2 \cdot 10^5$ Fig. 12.62. Gö 436. AVA 2.25 m;  $R = 4.2 \cdot 10^5$

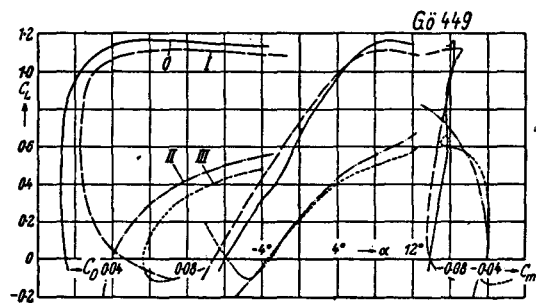


Fig. 12.63 a. Gö 449. Wind tunnel AVA 2.25 m;  $R = 6 \cdot 3 \cdot 10^6$ . O, smooth; I, pressure side rough; II, suction side rough; III, both sides rough

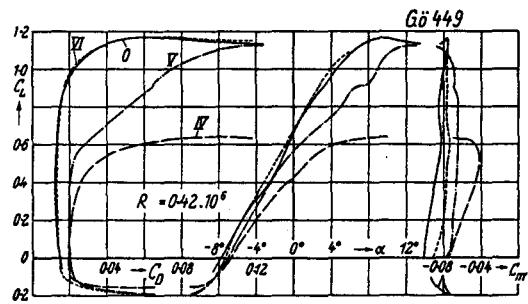


Fig. 12.63 b. Gö 449. AVA 2.25 m;  $R = 6 \cdot 3 \cdot 10^6$ . O, smooth; IV, suction side rough at front; V, suction side rough in middle; VI, suction side rough at rear

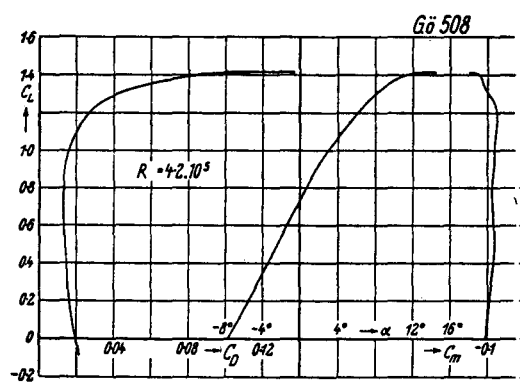


Fig. 12.64. Gö 508. AVA 2.25 m;  $R = 4 \cdot 2 \cdot 10^6$

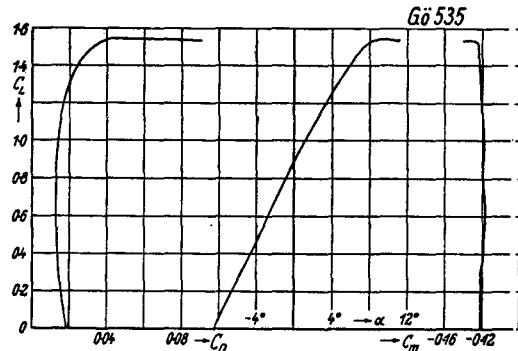


Fig. 12.65. Gö 535. AVA 2.25 m;  $R = 4 \cdot 2 \cdot 10^6$

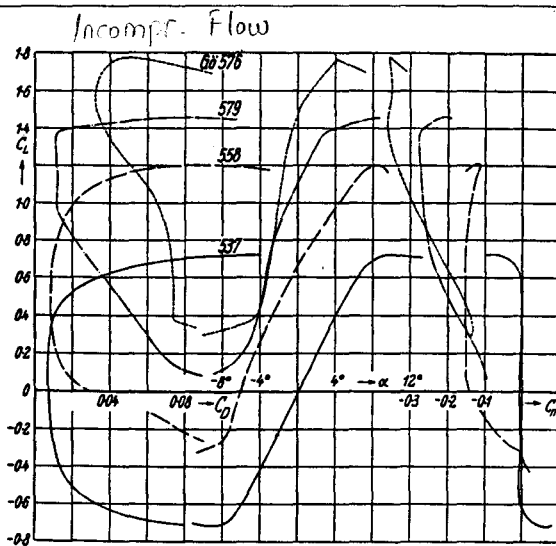


Fig. 12.66. Polars of Joukowsky profiles of various cambers. Gö 537, 558, 579, 576. AVA 2.25 m;  $R = 4 \cdot 2 \cdot 10^6$

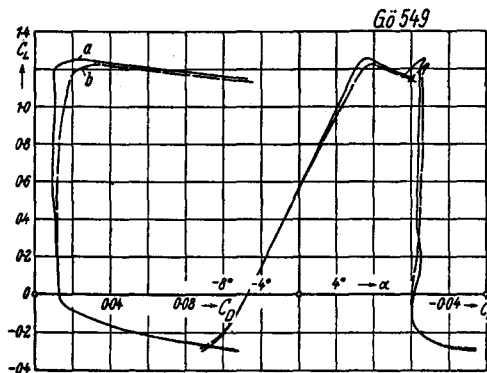


Fig. 12.67. Gö 549. AVA 4 m  $\times$  5.4 m;  $R = 1 \cdot 24 \cdot 10^6$ . (a: without, b: with tip-fairings)

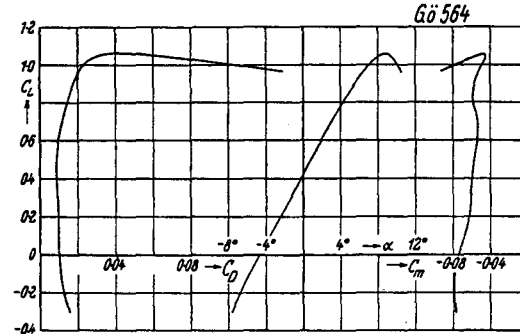


Fig. 12.68. Gö 564. AVA 2.25 m;  $R = 4 \cdot 2 \cdot 10^6$

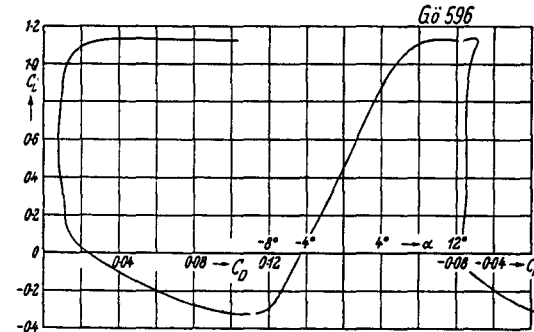


Fig. 12.69. Gö 596. AVA 2.25 m;  $R = 4 \cdot 2 \cdot 10^6$

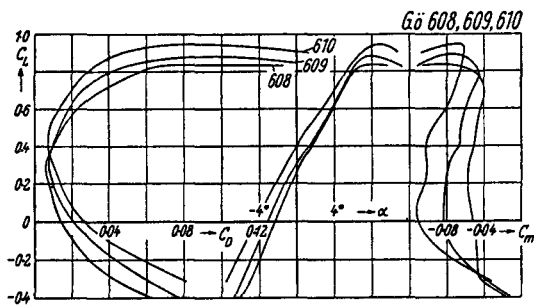


Fig. 12.70. Gö 608-610. AVA 2.25 m;  $R = 4 \cdot 2 \cdot 10^4$ . Circular segment profiles:  $f/c = 0.045, 0.051, 0.066$

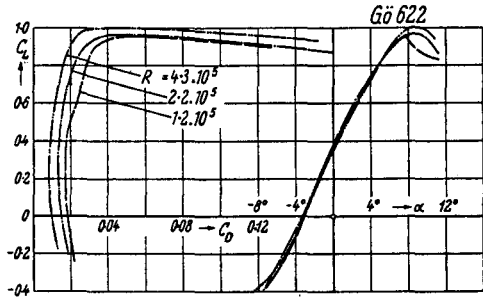


Fig. 12.71. Gö 622. AVA 2.25 m;  $R = 4 \cdot 2 \cdot 10^4$

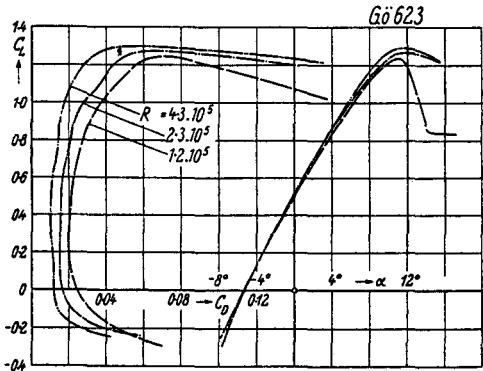


Fig. 12.72 a. Gö 623. AVA 2.25 m;  $R = 4 \cdot 2 \cdot 10^4$

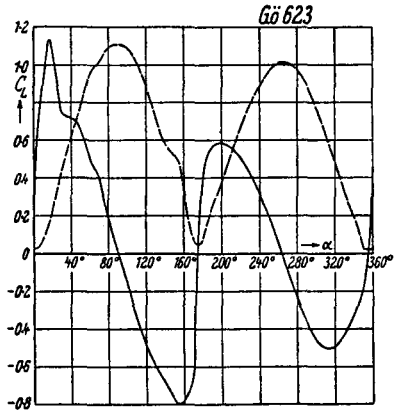


Fig. 12.72 b. Gö 623 for  $0^\circ \leq \alpha \leq 360^\circ$ . Wind tunnel: Aachen

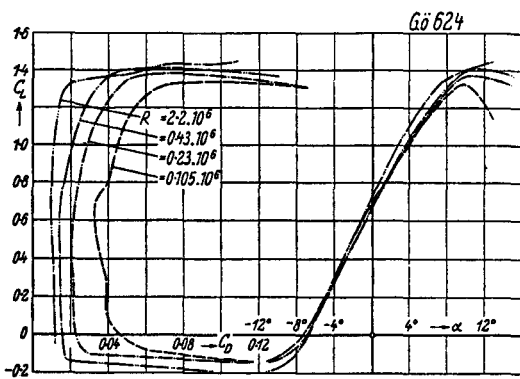


Fig. 12.73. Gö 624. AVA 2.25 m and (at  $R = 2 \cdot 2 \cdot 10^4$ )  $4 \text{ m} \times 5.4 \text{ m}$

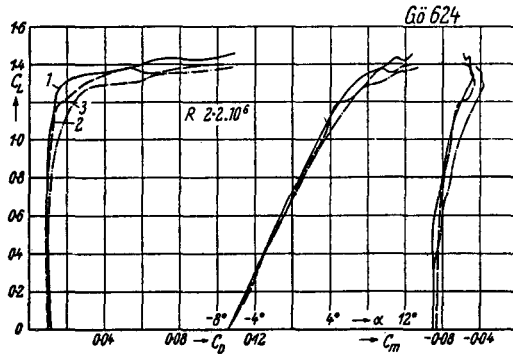


Fig. 12.74. Gö 624. AVA  $4 \text{ m} \times 5.4 \text{ m}$ .

1: without tip-fairings.

2: with normal tip-fairings.

3: with modified tip-fairings (see Section 2.3.3)

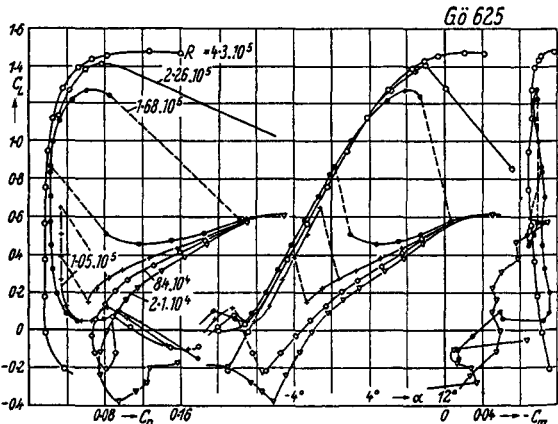


Fig. 12.75. Gö 625. AVA 2.25 m ( $R = 4 \cdot 3 \cdot 10^4$ ), and Cologne (SCHMITZ)

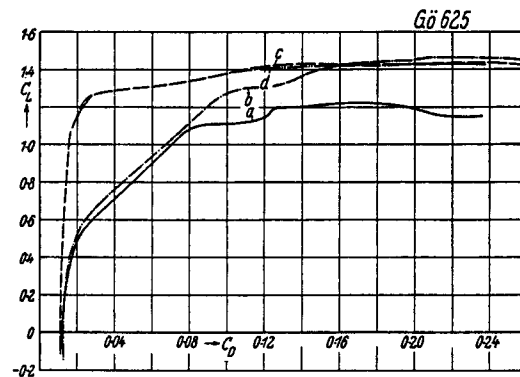


Fig. 12.76 a

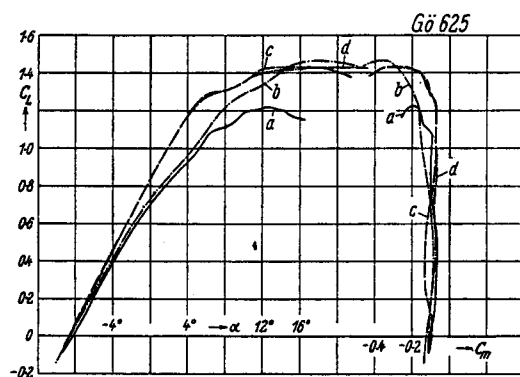


Fig. 12.76 b

Fig. 12.76 a, b. Gö 625. AVA 4 m  $\times$  5.4 m. Wing with tip-fairings.  
 (a) Surface plastered, slits open ( $R = 1.68 \cdot 10^4$ )  
 (b) Surface plastered and ground, slits open ( $R = 1.61 \cdot 10^4$ )  
 (c) Surface plastered and ground, slits closed ( $R = 1.61 \cdot 10^4$ )  
 (d) Surface lacquered and ground, slits closed ( $R = 1.57 \cdot 10^4$ )

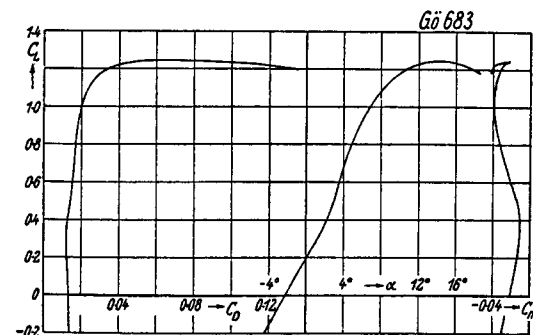
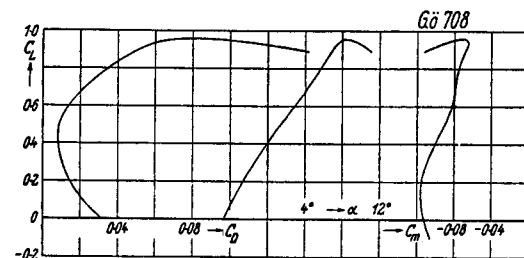
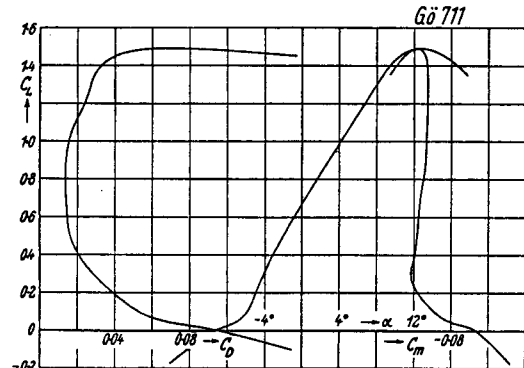
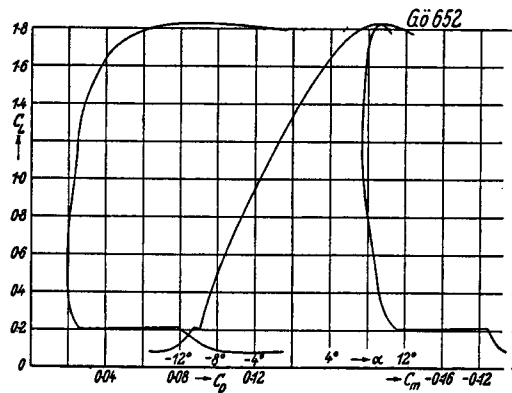
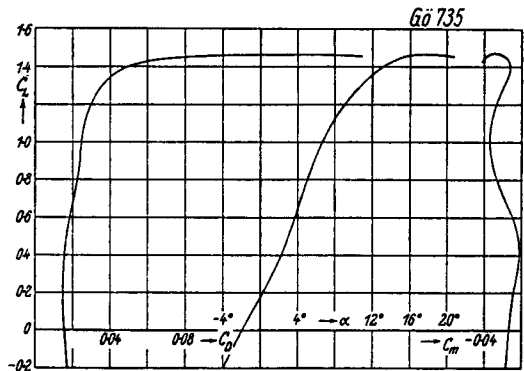
Fig. 12.78. Gö 683. AVA 2.25 m.  $R = 4.2 \times 10^4$ 

Fig. 12.79. Gö 708. AVA 2.25 m.  $R = 4.2 \cdot 10^4$ . Circular segment profile:  $f/c = 0.073$

Fig. 12.80. Gö 711. AVA 2.25 m.  $R = 4.2 \cdot 10^4$ Fig. 12.77. Gö 652. AVA 2.25 m.  $R = 4.2 \cdot 10^4$ Fig. 12.81. Gö 735. AVA 2.25 m.  $R = 4.2 \cdot 10^4$

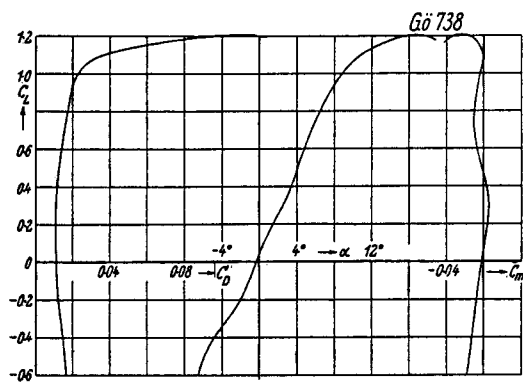
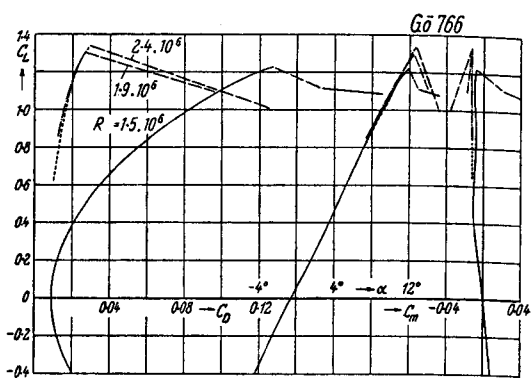
Fig. 12.82. Gö 738, AVA 2.25 m.  $R = 4 \cdot 2 \cdot 10^6$ 

Fig. 12.86. Gö 766, AVA 4 m × 5.4 m

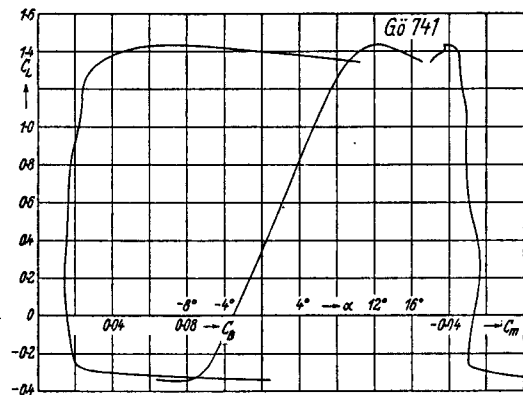
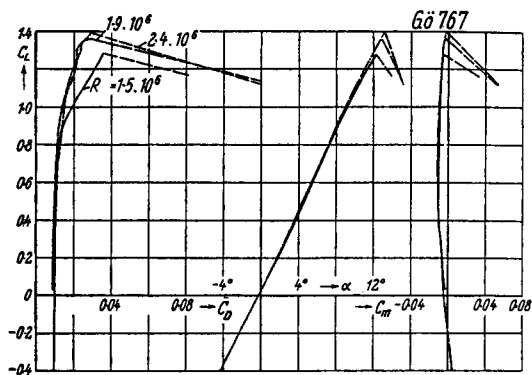
Fig. 12.83. Gö 741, AVA 2.25 m.  $R = 4 \cdot 2 \cdot 10^6$ 

Fig. 12.87. Gö 767, AVA 4 m × 5.4 m

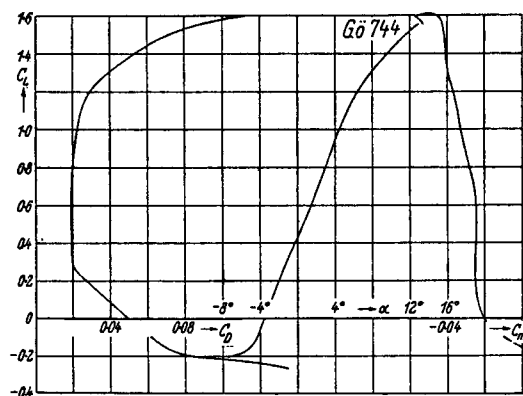
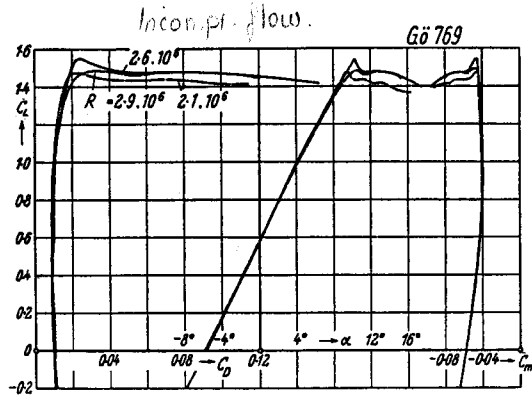
Fig. 12.84. Gö 744, AVA 2.25 m.  $R = 4 \cdot 2 \cdot 10^6$ 

Fig. 12.88. Gö 769, AVA 4 m × 5.4 m

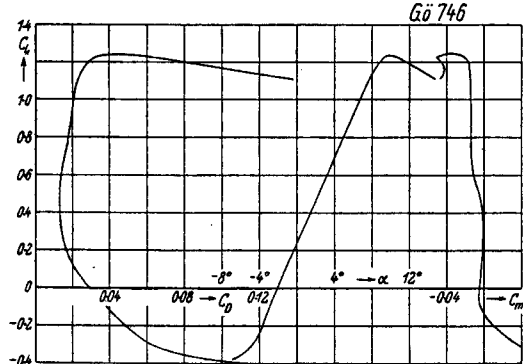
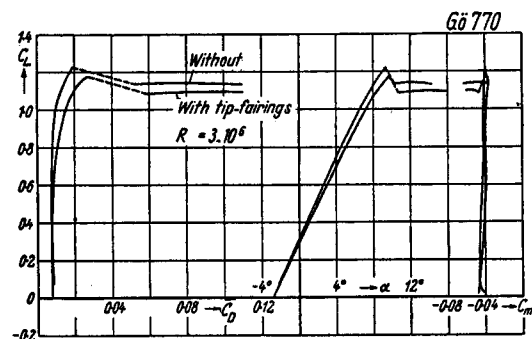
Fig. 12.85. Gö 746, AVA 2.25 m.  $R = 4 \cdot 2 \cdot 10^6$ 

Fig. 12.89. Gö 770, AVA 4 m × 5.4 m

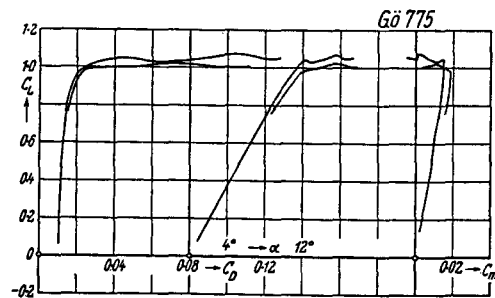
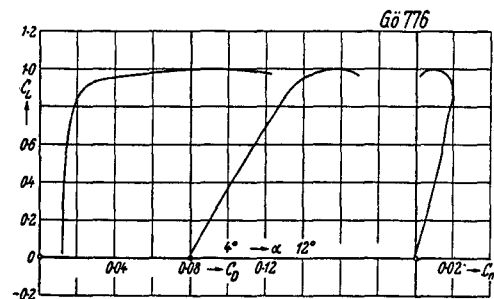
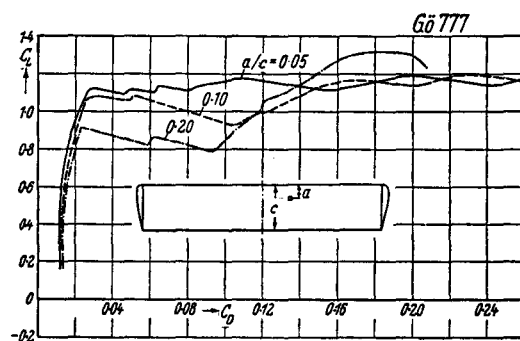
Fig. 12.90 a. Gö 775. AVA 4 m  $\times$  5.4 m.  $R = 10^6$ Fig. 12.90 b. Gö 776. AVA 4 m  $\times$  5.4 m.  $R = 10^6$ 

Fig. 12.91 a

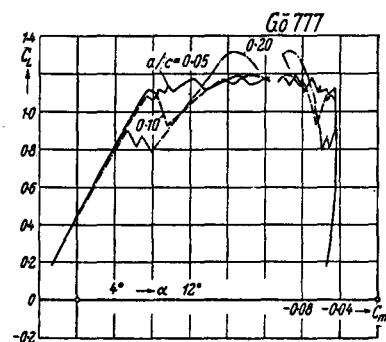


Fig. 12.91 b

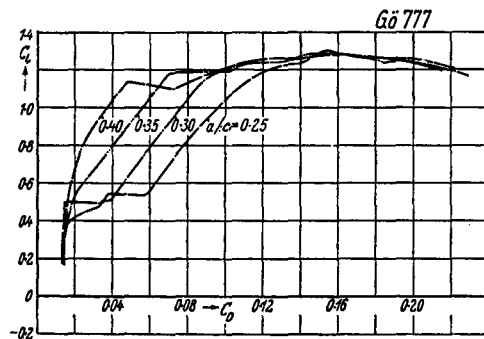


Fig. 12.91 c

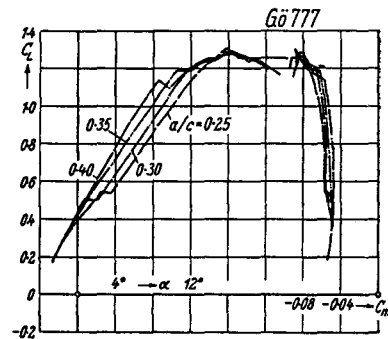


Fig. 12.91 d

Fig. 12.91 a-d. Flow disturbed by square plates ( $0.22 \times 0.022$  m) at a distance  $a$  from the leading edge. Chord: 0.5 m.  $R = 2.3 \cdot 10^6$ . Wind tunnel: AVA 4 m  $\times$  5.4 m.

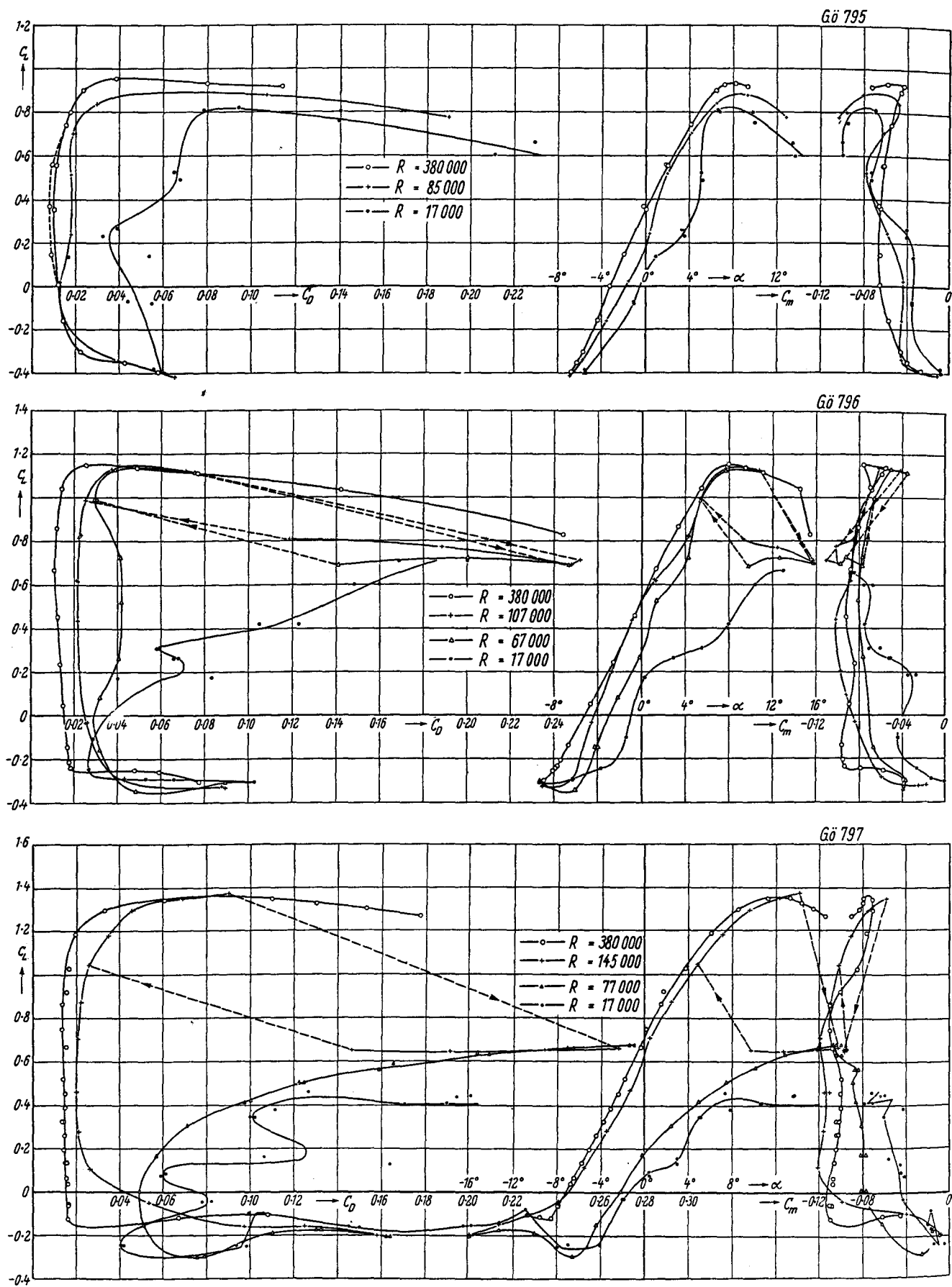


Fig. 12.92 a—c. Gö 795—797. Wind tunnel: Göttingen 0.7 m × 1 m. (MUESMANN-EGGERT, 1956)

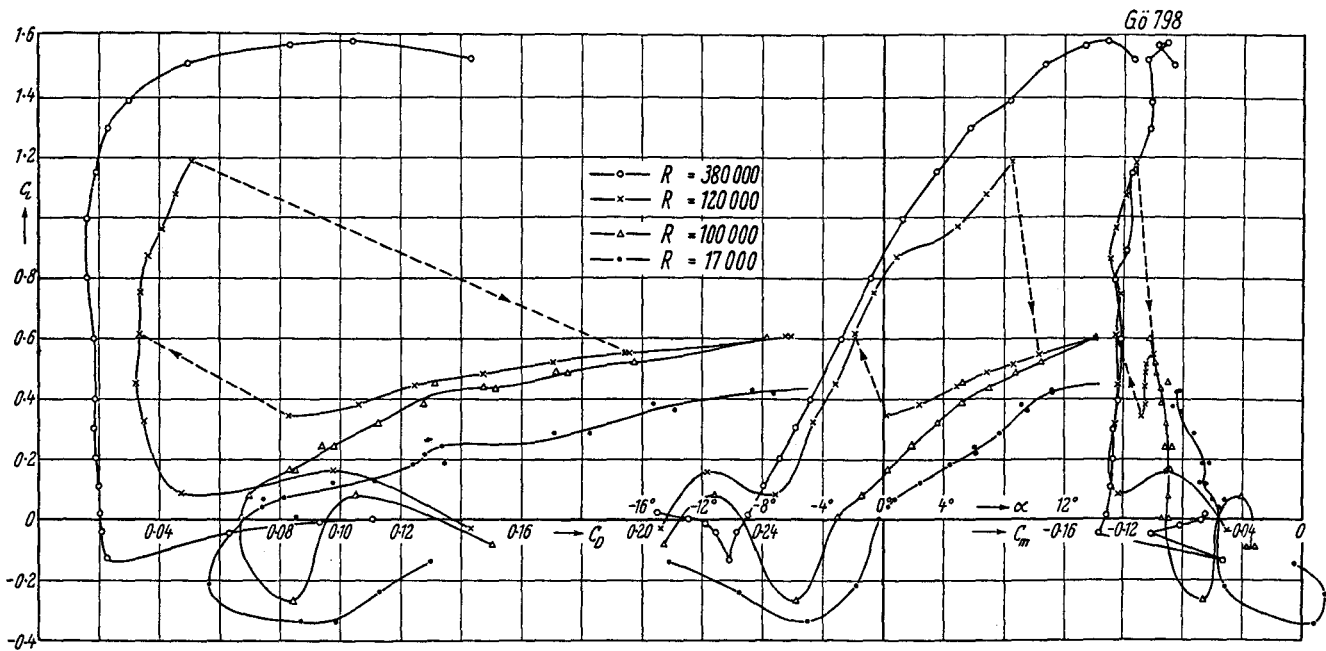


Fig. 12.92 d. Gö 798. Wind tunnel: Göttingen 0.7 m × 1 m (MUESMANN-EGGERT, 1956)

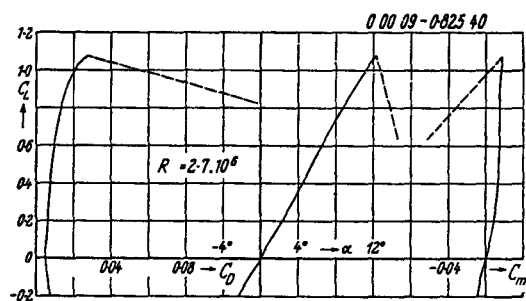


Fig. 12.93. Profile 0 00 09—0.825 40.  $R = 2.7.10^6$ .  
Wind tunnel: DVL 5 m × 7 m

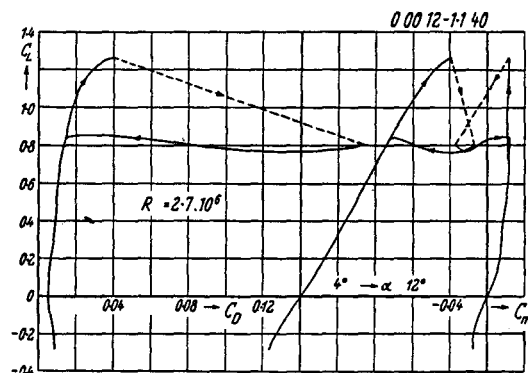


Fig. 12.95. Profile 0 00 12—1.1 40.  $R = 2.7.10^6$ .  
Wind tunnel: DVL 5 m × 7 m

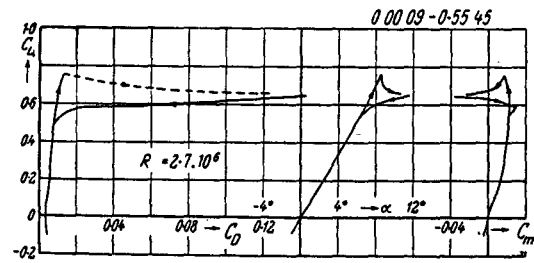


Fig. 12.94. Profile 0 00 09—0.55 45.  $R = 2.7.10^6$ .  
Wind tunnel: DVL 5 m × 7 m.

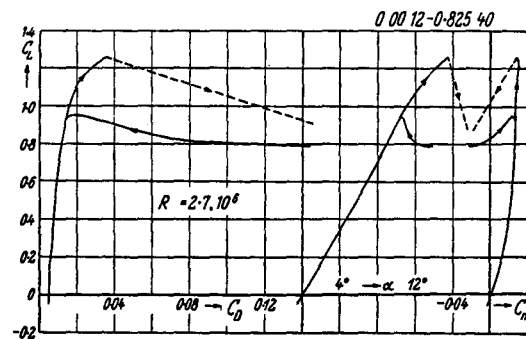


Fig. 12.96. Profile 0 00 12—0.825 40.  $R = 2.7.10^6$ .  
Wind tunnel: DVL 5 m × 7 m

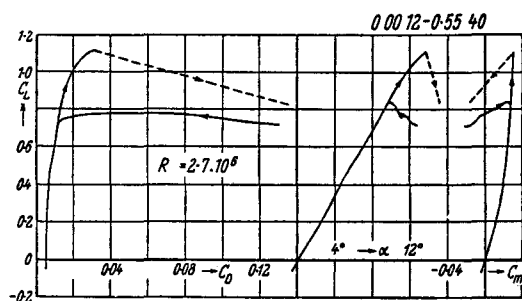
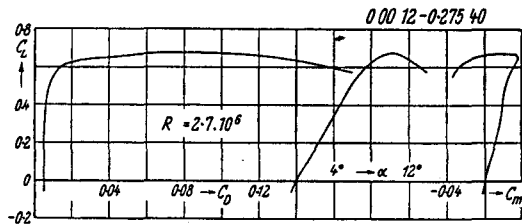
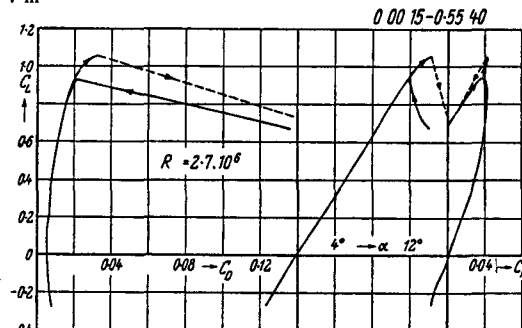
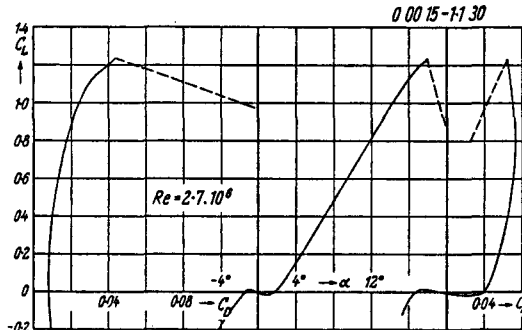
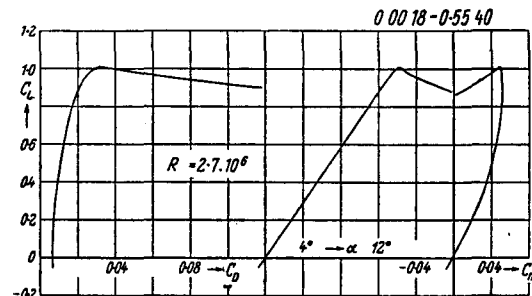
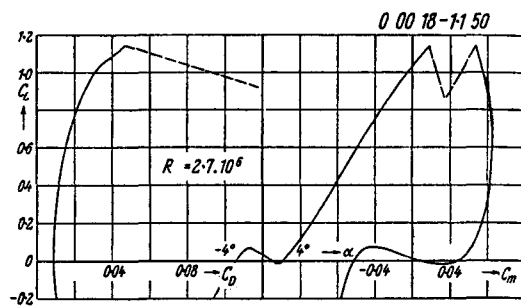
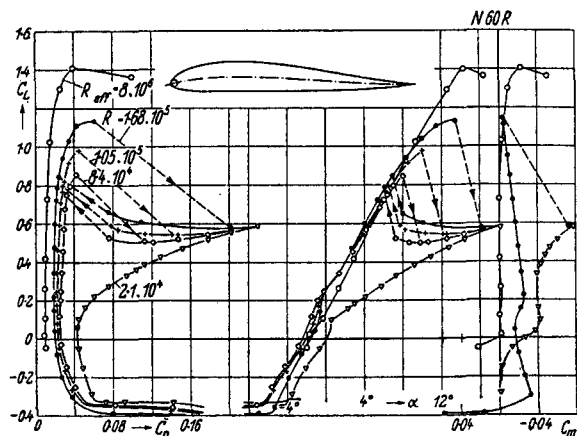
Fig. 12.97. Profile 0 00 12—0 55 40.  $R = 2.7 \cdot 10^6$ . Wind tunnel: DVL 5 m × 7 mFig. 12.98. Profile 0 00 12—0 275 40.  $R = 2.7 \cdot 10^6$ . Wind tunnel: DVL 5 m × 7 mFig. 12.99. Profile 0 00 15—0 55 40.  $R = 2.7 \cdot 10^6$ . Wind tunnel: DVL 5 m × 7 mFig. 12.100. Profile 0 00 15—1 150.  $R = 2.7 \cdot 10^6$ . Wind tunnel: DVL 5 m × 7 mFig. 12.101. Profile 0 00 18—0 55 40.  $R = 2.7 \cdot 10^6$ . Wind tunnel: DVL 5 m × 7 mFig. 12.102. Profile 0 00 18—1 150.  $R = 2.7 \cdot 10^6$ . Wind tunnel: DVL 5 m × 7 m

Fig. 12.103. N 60 R. Wind tunnel: Cologne 0.7 m (SCHMITZ)

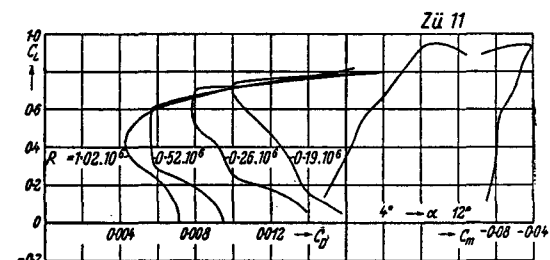


Fig. 12.104. Zü 11. Wind tunnel: Zürich (PFENNINGER)

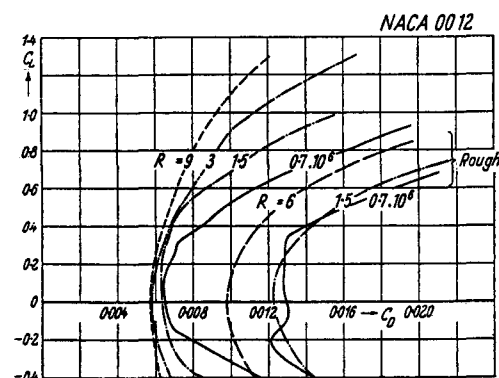
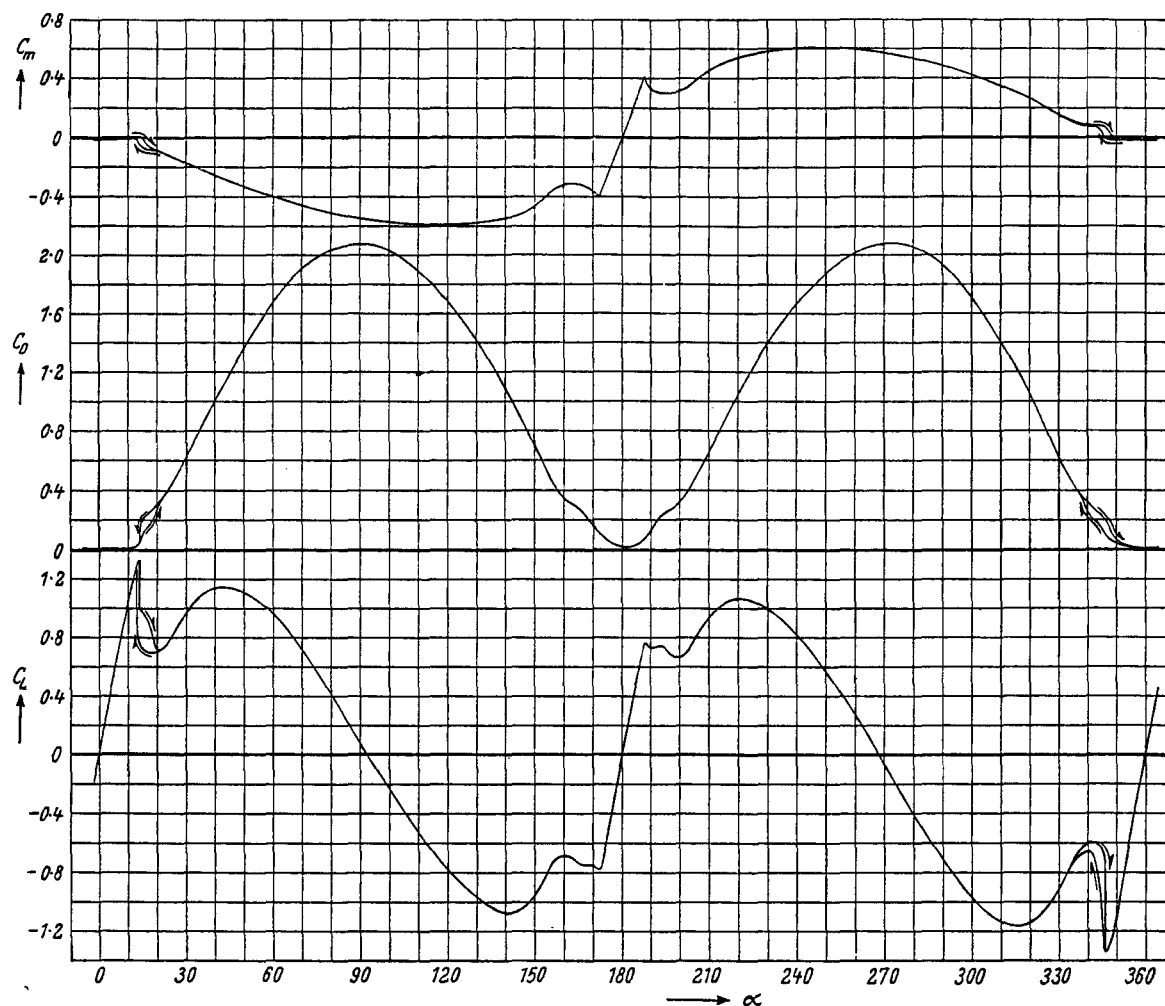


Fig. 12.105. NACA 0012 at various Reynolds numbers. Wind tunnel: TDT

Fig. 12.105a. NACA 0012.  $R = 1.8 \cdot 10^6$ . Wind tunnel: TDT. [N 3361]

Profile NACA 0012

$R \cdot 10^{-6}$	w'o	0·7 w	w'o	1·5 w	3	w'o	6 w	9
$C_{L\max}$	1.06 0.85	2.021 1.741	1.24 0.94	2.15 1.82	1.525	1.595 1.035	2.39 1.93	1.59
$\alpha C_{L\max}$	13.2 12.2	8.1° 5°	15.3° 11°	9.2° 5°	16.7°	16.3° 12.2°	10.2° 5.5°	15.7°
$a_s$	$\pm 0^\circ$	-12.4° -11.1°	-0.1°	-12.4° -11.2°		-0.1°	-12.6° -12.2°	$\pm 0^\circ$

w'o: without, w: with split flap, 60° deflection. The lower values include the effect of standard roughness.

Profile NACA 4412

$R \cdot 10^{-6}$	w'o	0·7 w	w'o	1·5 w	3	w'o	6 w	9
$C_{L\max}$	1.37 1.15	2.094 2.17	1.44 1.18	2.453 2.345	1.505	1.63 1.38	2.696 11°	1.668 14°
$\alpha C_{L\max}$	15.2° 11.2°	9.1° 8°	14.2° 12.2°	10.2° 9.5°	13.4°	14.5° 13.1°		
$a_s$	-4.02° -4.17°	-12.2°	-3.97° -3.7°	-11.4°	-3.83°	-3.9° -3.65°		-3.85°

w'o: without, w: with split flap, 60° deflection. The lower values include the effect of standard roughness.

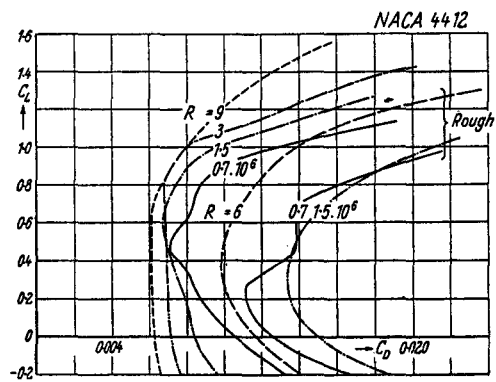


Fig. 12.106. NACA 4412. Wind tunnel: TDT

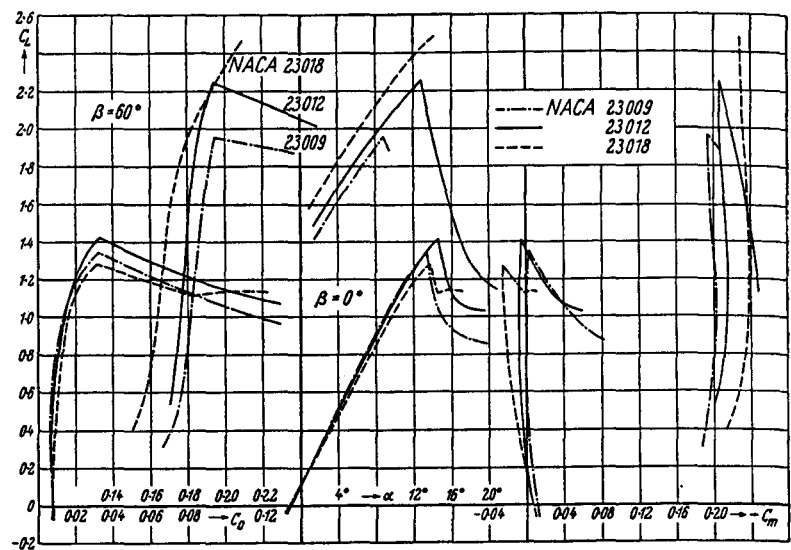
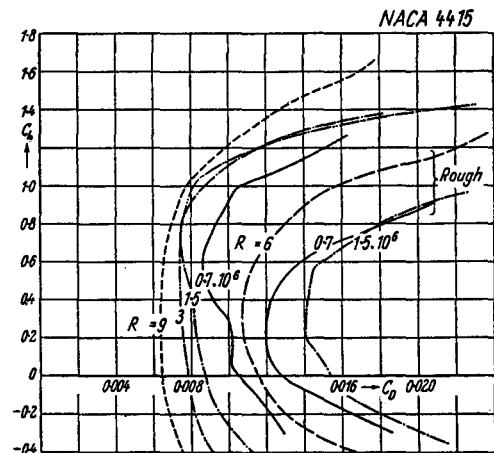
Fig. 12.108. NACA 23009, 23012, 23018. Wind tunnel: DVL 5 m  $\times$  7 m

Fig. 12.107. NACA 4415. Wind tunnel: TDT

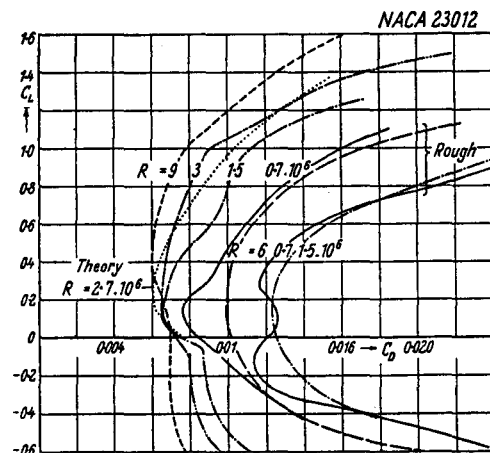


Fig. 12.109. NACA 23012. Wind tunnel: TDT

## Profile NACA 4415

$R \cdot 10^{-6}$	w'o	0.7	w	w'o	1.5	w	3	w'o	6	w	9
$C_{L_{\max}}$	1.415		2.37	1.417		2.6	1.422	1.57		2.772	1.635
$\alpha C_{L_{\max}}$	1.045		2.16	1.09		2.345		1.291			
$\alpha_0$	15.2°		8.2°	13.2°		9°	12.8°	14.2°		11°	14.2°
	12.2°		6.2°	12.2°		7°		12.2°			
	-4.87°		-12.1°	-4.9°		-13.3°	-4.3°	-4.22°		-15.7°	-4.05°
	-4.6°			-4.2°		-12.2°		-3.8°			

w'o: without, w: with split flap, 60° deflection. The lower values include the effect of standard roughness.

## Profile NACA 23012

$R \cdot 10^{-6}$	w'o	0.7	w	w'o	1.5	w	3	w'o	6	w	9
$C_{L_{\max}}$	1.173		2.21	1.425		2.46	1.611	1.75		2.73	1.795
$\alpha C_{L_{\max}}$	0.95		2.08	1.08		2.122		1.235		2.25	
	14.2°		10.1°	15.2°		11.1°	16.2°	17.8°		14.3°	17.8°
	10.1°		8.1°	11.1°		8.1°		13.2°		8.7°	
$\alpha_0$	-1.34°			-1.3°			-1.05°	-1.1°		-13.5°	-1.15°
	-1.2°			-1.3°				-1.39°		-11.4°	

w'o: without, w: with split flap, 60° deflection. The lower values include the effect of standard roughness.

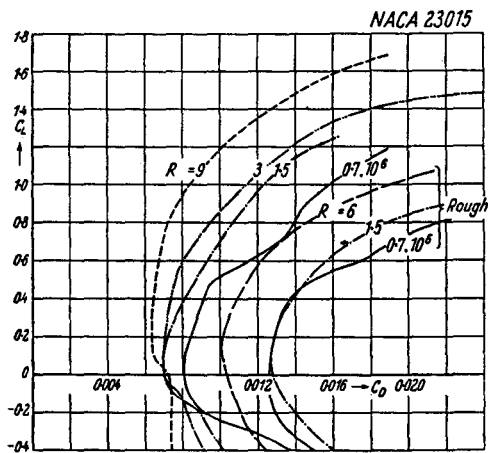


Fig. 12.110. NACA 23015. Wind tunnel: TDT

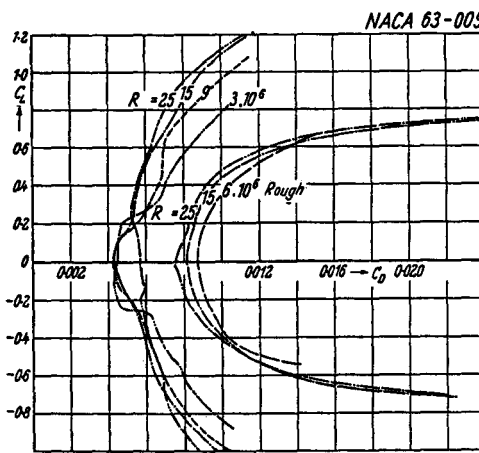


Fig. 12.112. NACA 63-009. Wind tunnel: TDT

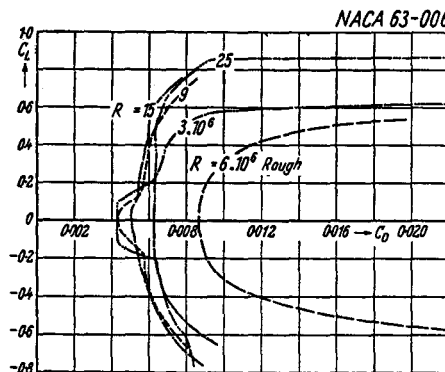


Fig. 12.111. NACA 63-006. Wind tunnel: TDT

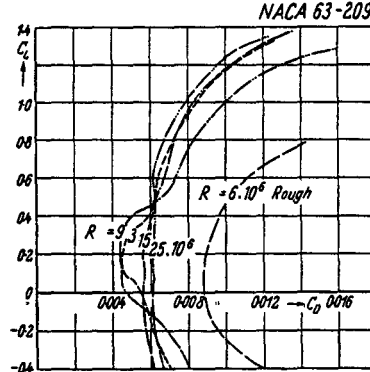


Fig. 12.113. NACA 63-209. Wind tunnel: TDT

## Profile NACA 23015

$R \cdot 10^{-6}$	w'o	0.7	w	w'o	1.5	w	2.6	w'o	6	w	9
$C_{L\max}$	1.31		2.39	1.393		2.532		1.487		1.7	2.9
$\alpha C_{L\max}$	0.973		2.2	1.014		2.27		1.53°		1.19	2.39
$\alpha_0$	14.2°		10.1°	15.2°		11°		-1.1°		12.6°	15.2°
	11°		8°	11.1°		8.1°				9°	18.2°
	-1.1°			-1.12°						-1.16°	-1.05°
	-1.31°			-1.12°						-1.15°	

w'o: without, w: with split flap, 60° deflection. The lower values include the effect of standard roughness.

## Profile NACA 63-009

$R \cdot 10^{-6}$	3	w'o	6	w	w'o	9	w	w'o	15	w	w'o	25	w
$C_{L\max}$	1.09		1.095	1.775		1.155		1.85		1.225		1.225	1.91
$\alpha C_{L\max}$	10.1°		0.895	19.6°		5.6°		11.2°		0.895		0.905	6.1°
$\alpha_0$			11.2°			-11.5°				11.2°		11.7°	10.2°
			-0.2							7°			-12.4°
										-12.2°			

w'o: without, w: with split flap, 60° deflection. The lower values include the effect of standard roughness.

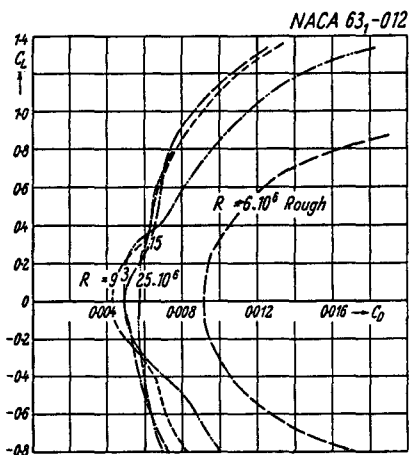
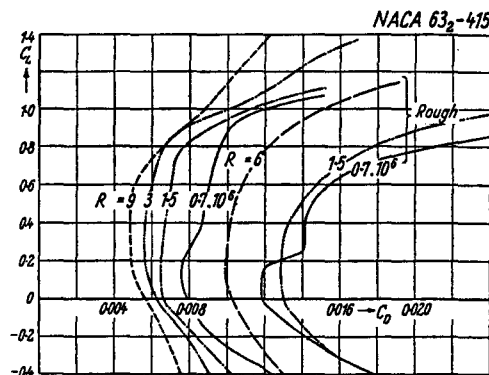
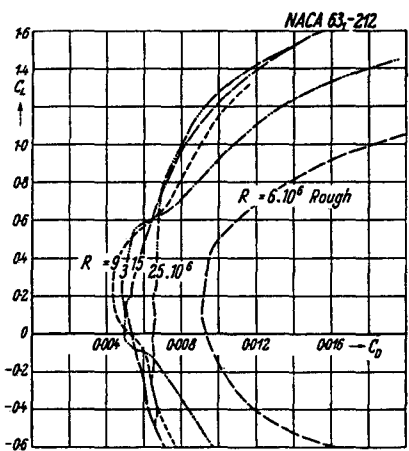
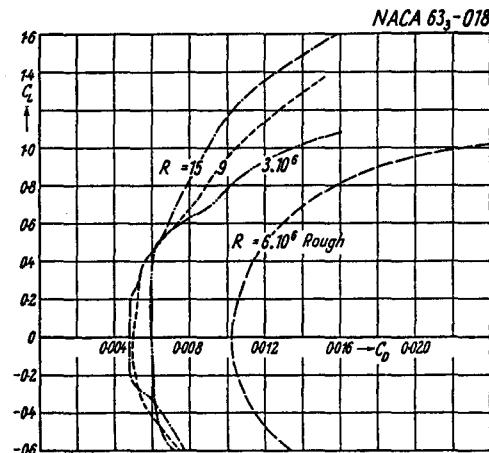
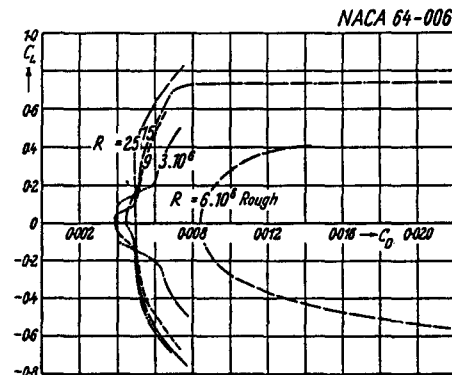
Fig. 12.114. NACA 63<sub>1</sub>-012. Wind tunnel: TDTFig. 12.116. NACA 63<sub>2</sub>-415. Wind tunnel: TDTFig. 12.115. NACA 63<sub>1</sub>-212. Wind tunnel: TDTFig. 12.117. NACA 63<sub>2</sub>-018. Wind tunnel: TDT

Fig. 12.118. NACA 64-006. Wind tunnel: TDT

Profile NACA 63<sub>2</sub>-415

$R \cdot 10^{-6}$	w'o	0.7	w	w'o	1.5	w	3	w'o	6	w	9
$C_{L_{max}}$	1.26 1.023		2.21 2.075		1.36 1.18		2.425 2.143		1.538 1.42°		2.678 2.425
$\alpha C_{L_{max}}$	13.1° 11°		9.1° 7°		13.9° 14.2°		11° 7°		15.3° 12.2°		12.2° 9.1°
$\alpha_0$	-2.55° -2.7°		-12.2° -12.58°		-2.79° -2.58°		-2.93°		-2.78° -2.73°		-12.7°

w'o: without, w: with split flap, 60° deflection. The lower values include the effect of standard roughness.

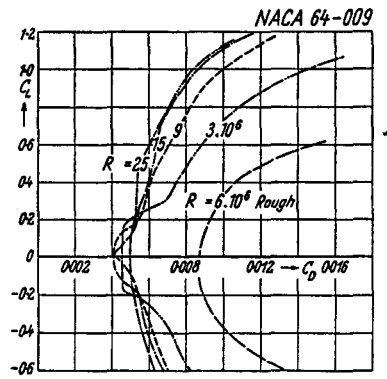


Fig. 12.119. NACA 64-009. Wind tunnel: TDT

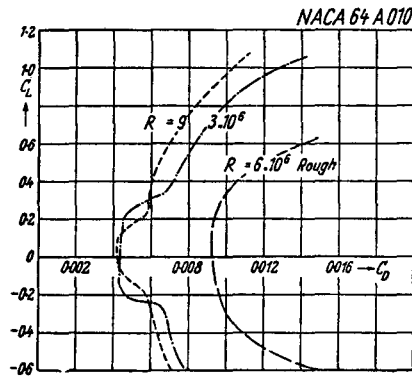


Fig. 12.121. NACA 64 A 010. Wind tunnel: TDT

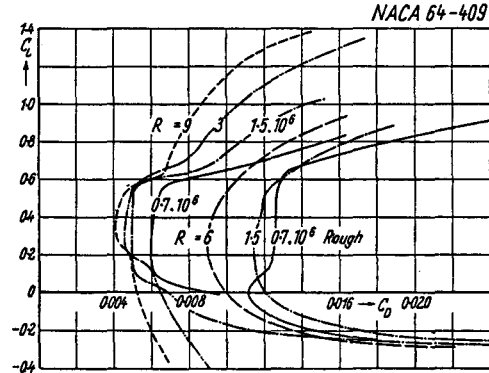


Fig. 12.120. NACA 64-409. Wind tunnel: TDT

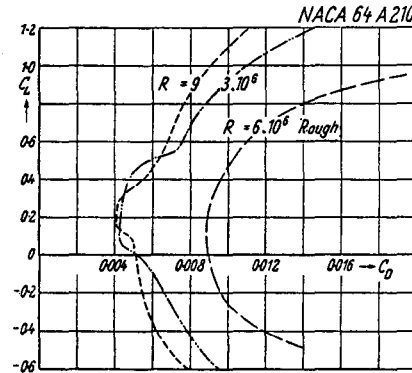


Fig. 12.122. NACA 64 A 210. Wind tunnel: TDT

## Profile NACA 64-409

$R \cdot 10^{-6}$	w'o	0.7 w	w'o	1.5 w	3	w'o	6 w	9
$C_{L_{\max}}$	1.085 1.1	1.855 1.78	1.200 1.12	1.824 1.81	1.418 11.5°	1.5 1.109 13.4°	2.07 1.87 6.7°	1.488 13.6°
$\alpha C_{L_{\max}}$	11.4° 11°	6° 6.1°	9° 12°	6° 7°	0.1115 -2.96°	0.114 0.11 -2.8° -2.42°	0.1119 -2.5°	-0.1119
$C_{L_a} (\alpha \text{ in degrees})$	0.0975 0.092	0.10 0.099	-3.2° -3.3°	-0.067	-0.07 -0.07	0.264 0.259	-0.020 -0.020	-0.025
$a_s$	-3.6° -3.43°	-3.2° -3.3°	-0.065	-0.067	-0.07 -0.07	0.260	-0.025	-0.025
$(C_m)_a$	-0.065	-0.067	-0.020	-0.020	-0.067	-0.020	-0.020	-0.020
$x_a$	0.258	0.263						
$y_a$	-0.035							

w'o: without, w: with split flap, 60° deflection. The lower values include the effect of standard roughness.

## Profile NACA 64 A 010

$R \cdot 10^{-6}$	3	w'o	6 w	9
$C_{L_{\max}}$	1.065	1.17 0.865	1.925 1.77	1.225
$\alpha C_{L_{\max}}$	10.2°	11.2° 12.05°	6.2° 6.1°	12.3°
$C_{L_a} (\alpha \text{ in degrees})$	0.107	0.107 0.102	0.107	
$a_s$	-0.4°	-0.4° -0.4°	-12.3° -11.8°	-0.4°
$(C_m)_a$	0	0	0	
$x_a$	0.250	0.253	0.253	
$y_a$	-0.018	-0.007	-0.017	

w'o: without, w: with split flap, 60° deflection. The lower values include the effect of standard roughness.

## Profile NACA 64 A 210

$R \cdot 10^{-6}$	3	w'o	6 w	9
$C_{L_{\max}}$	1.35	1.415 1.055	2.15 1.85	1.44
$\alpha C_{L_{\max}}$	12.2°	13.2° 10.05°	8.05° 8.05°	13.2°
$C_{L_a} (\alpha \text{ in degrees})$	0.1065	0.1065 0.105	0.1065	0.1065
$a_s$	-1.6°	-1.6° -1.3°	-12.3° -12.5°	-1.6°
$(C_m)_a$	-0.04	-0.04	-0.04	-0.04
$x_a$	0.251	0.251	0.251	0.251
$y_a$	-0.012	-0.006	-0.006	-0.013

w'o: without, w: with split flap, 60° deflection. The lower values include the effect of standard roughness.

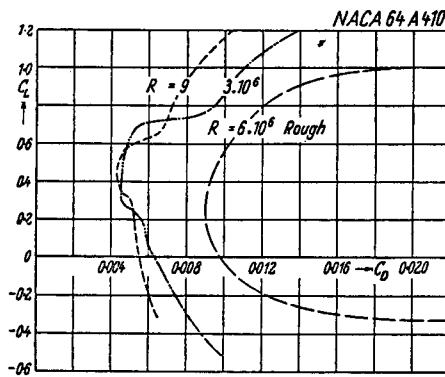


Fig. 12.123. NACA 64 A 410. Wind tunnel: TDT

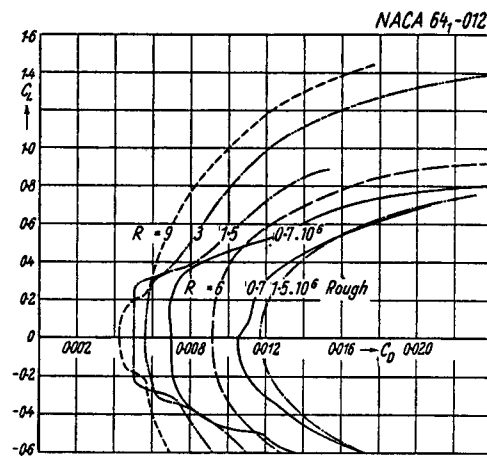


Fig. 12.124. NACA 64-012. Wind tunnel: TDT

Profile NACA 64 A 410

$R \cdot 10^{-6}$	3	w'o	6	w	9
$C_{L_{\max}}$	1.57	1.605	2.365	1.615	
$\alpha C_{L_{\max}}$	15.4°	15.4°	9.3°	15.4°	
$C_{L_a}$ (α in degrees)	0.105	0.105	0.105	0.105	
$a_0$	-3.5°	-3.1°	-13.9°	-3.1°	
$(C_m)_a$	-0.083	-0.083	-0.083	-0.083	
$x_a$	0.256	0.255	0.254	0.254	
$y_a$	-0.049	-0.067	-0.033	-0.033	

w'o: without, w: with split flap, 60° deflection.  
The lower values include the effect of standard roughness.

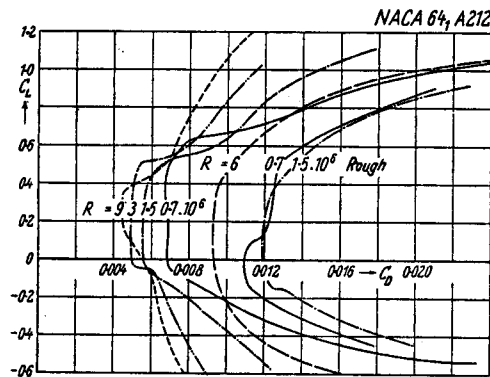


Fig. 12.125. NACA 64 A 212. Wind tunnel: TDT

Profile NACA 64-012

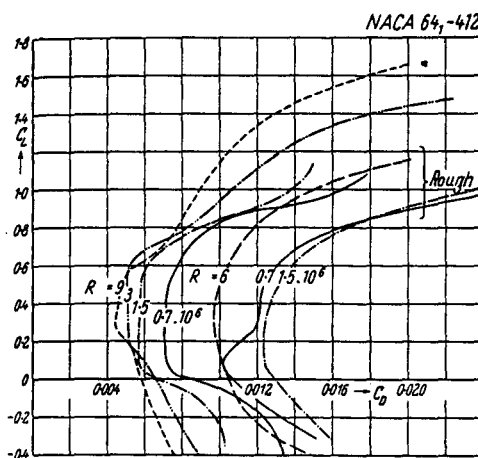
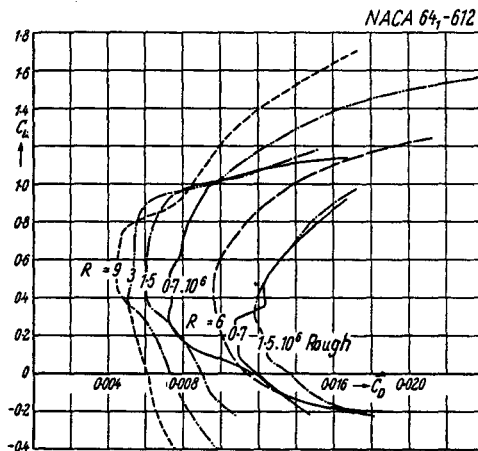
$R \cdot 10^{-6}$	w'o	0.7	w	w'o	1.5	w	3	w'o	6	w	9
$C_{L_{\max}}$	0.86		1.74		1.135		1.98		1.435		1.443
$\alpha C_{L_{\max}}$	0.906		1.75		0.909		1.754		0.945		1.811
$a_0$	12.2°		7°		14.3°		7.1°		15.3°		14.4°

w'o: without, w: with split flap, 60° deflection. The lower values include the effect of standard roughness.

Profile NACA 64 A 212

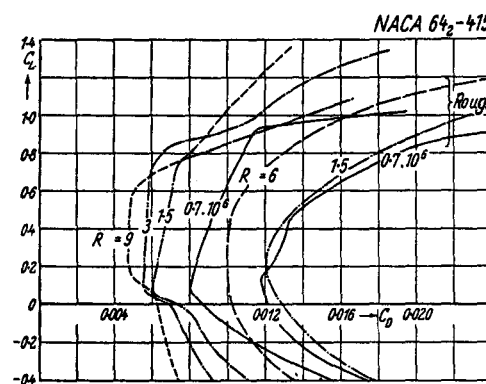
$R \cdot 10^{-6}$	0.7	1.5	3	6	9
$C_{L_{\max}}$	1.089	1.266	1.49	1.505	1.535
$\alpha C_{L_{\max}}$	1.065	1.07	1.135	1.135	
$a_0$	11.1°	13.2°	15.1°	14.2°	14.2°

The lower values include the effect of standard roughness.

Fig. 12.126. NACA 64<sub>1</sub>-412. Wind tunnel: TDTFig. 12.127. NACA 64<sub>1</sub>-612. Wind tunnel: TDT

$R \cdot 10^{-6}$	Profile NACA 64 <sub>1</sub> -412									
	w'o	0.7	w	w'o	1.5	w	3	w'o	6	w
$C_{L_{\max}}$	1.181	1.974	1.35	2.285	1.55	1.66	2.52	1.67		
$\alpha C_{L_{\max}}$	13.2°	6°	13.2°	10.2°	14.2°	15.3°	12.2°	11.6°	15.2°	
$\alpha_0$	12.3°	5.2°	12.2°	5.5°	2.76°	-2.6°	6.1°	-13.4°	-2.55°	
	2.8°	-3.05°	-2.75°	-2.75°	-2.9°	-2.9°	-12.7°			

w'o: without, w: with split flap, 60° deflection. The lower values include the effect of standard roughness.

Fig. 12.128. NACA 64<sub>1</sub>-415. Wind tunnel: TDTProfile NACA 64<sub>1</sub>-612

$R \cdot 10^{-6}$	Profile NACA 64 <sub>1</sub> -612										
	w'o	0.7	w	w'o	1.5	w	3	w'o	6	w	9
$C_{L_{\max}}$	1.325	1.94	1.397	2.285	1.605	1.77	2.574	1.775			
$\alpha C_{L_{\max}}$	1.21	1.89	1.328	2.09	14.2°	1.391	2.115				
$C_{L_{\alpha}} (\alpha \text{ in degrees})$	12.2°	6°	13.2°	8.1°	0.1125	16.2°	11.1°	6°	16.2°		
$\alpha_0$	12.2°	7°	13.4°	7.1°	0.1165	0.111					
$(C_m)_\alpha$	0.1019	0.097	0.111	0.101	-4.15°	-4.06°	-11.7°	0.1162			
$x_\alpha$	-4.12°	-11.8°	-4°	-12.2°	-4.15°	-4.03°	-11.3°	-3.93°			
$y_\alpha$	-3.9°	-11.8°	-3.94°	-12.2°	-0.104	-0.104	-0.104	-0.11			
	-0.1	-0.101	-0.101	-0.271	-0.270	-0.268	-0.268	-0.264			
	0.260	-0.041	-0.048	-0.028	-0.028	-0.039	-0.039	-0.003			

w'o: without, w: with split flap, 60° deflection. The lower values include the effect of standard roughness.

Profile NACA 64<sub>1</sub>-415

$R \cdot 10^{-6}$	Profile NACA 64 <sub>1</sub> -415										
	w'o	0.7	w	w'o	1.5	w	3.1	w'o	6	w	9
$C_{L_{\max}}$	1.2	2.14	1.31	2.34	1.48	1.615	2.66	1.645			
$\alpha C_{L_{\max}}$	1.13	2.12	1.22	2.2	14.2°	1.31	2.32				
$\alpha_0$	14.2°	8.1°	14.2°	9.1°	14.2°	16.2°	12.2°	16.2°			
	14.2°	8.2°	15.2°	8.1°	-3.05°	13.2°	7.7°	-2.87°			
$x_\alpha$	-3°	-2.95°	-3°	-2.95°	-3.05°	-2.99°	-2.95°				
$y_\alpha$	-3.1°	-	-	-	-	-	-	-			

w'o: without, w: with split flap, 60° deflection. The lower values include the effect of standard roughness.

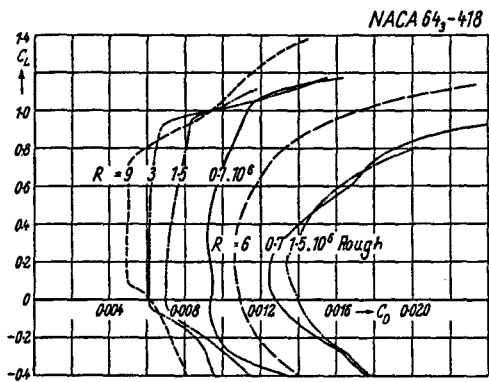
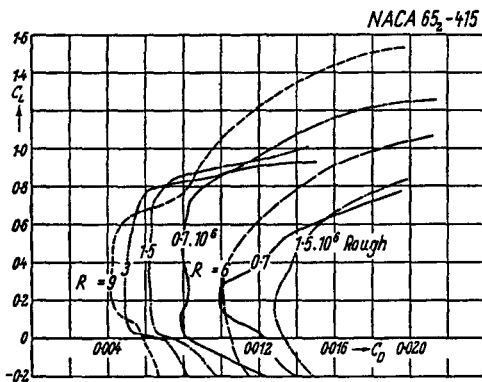
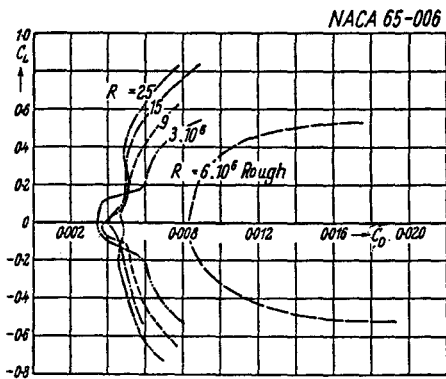
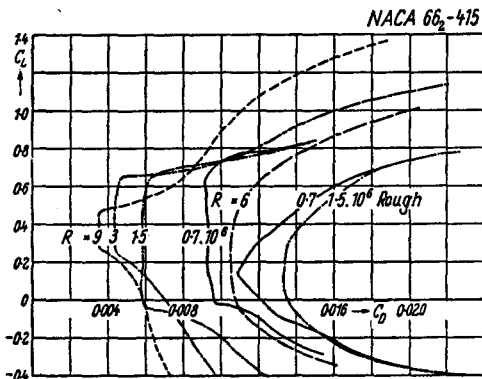
Fig. 12.129. NACA 64<sub>3</sub>-418. Wind tunnel: TDTFig. 12.131. NACA 65<sub>2</sub>-415. Wind tunnel: TDT

Fig. 12.130. NACA 65-006. Wind tunnel: TDT

Fig. 12.131 a. NACA 66<sub>3</sub>-415. Wind tunnel: TDTProfile NACA 64<sub>3</sub>-418

$R \cdot 10^{-6}$	w'o	0.7	w	w'o	1.5	w	3	w'o	6	w	9
$C_{L_{\max}}$	1.225 1.04°	2.2 8.2°	1.29 1.09°	2.33 2.26°	1.35	1.48 1.25°	2.82 2.509°	1.57			
$\alpha C_{L_{\max}}$	10.2° 11.2°	7.2° 7.2°	16.2° 16.2°	9.3° 9.3°	16.2°	16.2° 14.2°	12.4° 9.4°	20.2°			
$\alpha_0$	-2.35° -2.55°		-2.79° -2.25°		-2.86°	-2.75° -2.85°	-13.6° -13.2°	-2.68°			

w'o: without, w: with split flap, 60° deflection. The lower values include the effect of standard roughness.

Profile NACA 65<sub>2</sub>-415

$R \cdot 10^{-6}$	w'o	0.7	w	w'o	1.5	w	3	w'o	6	w	9
$C_{L_{\max}}$	1.169 1.065	2.075 2.045	1.297 1.19	2.4 2.11	1.44	1.588 1.245	2.605 2.175	1.62			
$\alpha C_{L_{\max}}$	15.2° 13.3°	7° 7°	14.2° 13.2°	9.2° 6.1°	16.2°	17.3° 13.2°	11.2° 6.1°	16.2°			
$\alpha_0$	-3.1° -2.83°	-12.6° -12.6°	-3.16° -2.65°	-12.6°	-2.75°	-2.76° -2.73°	-14.2° -12.8°	-2.75°			

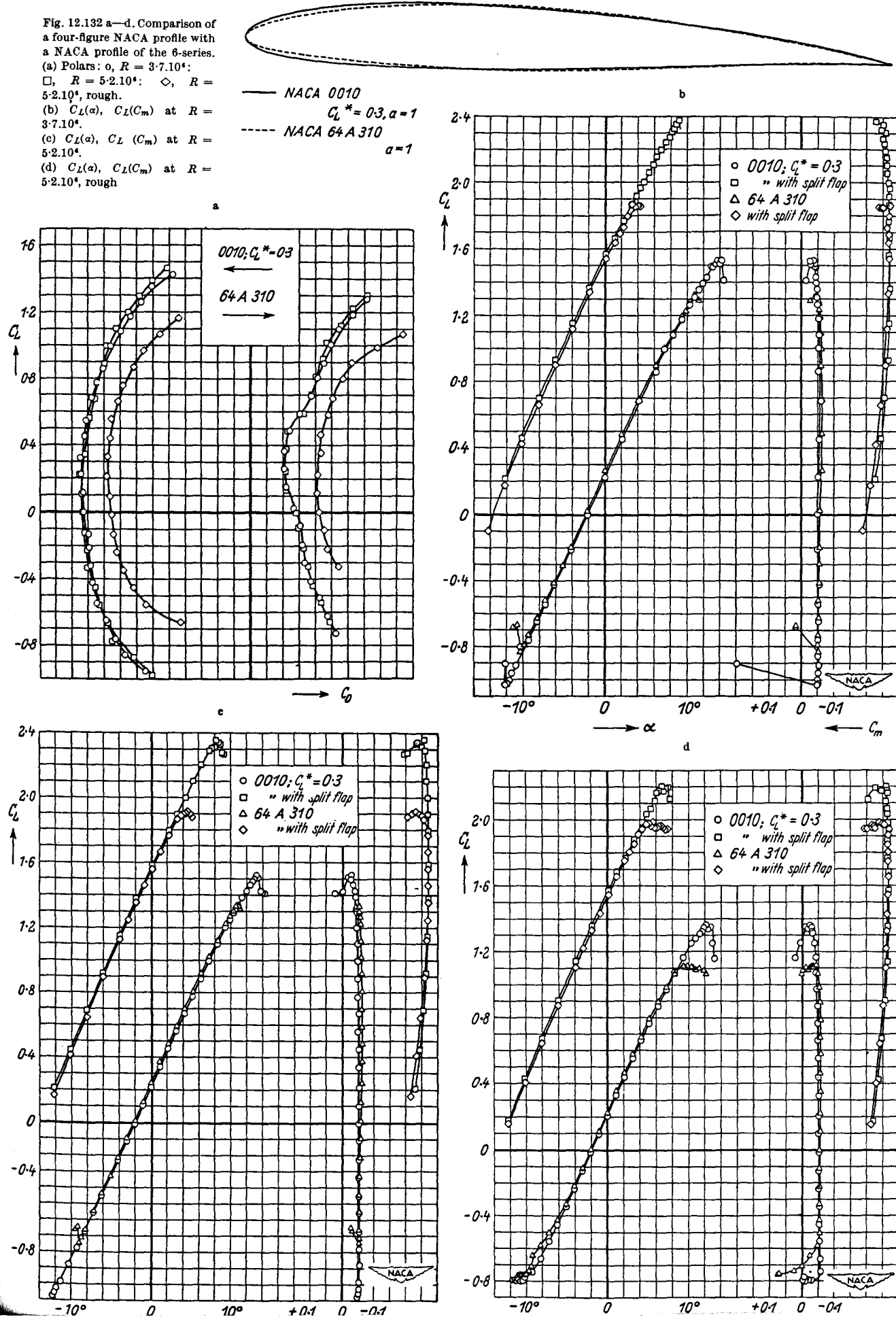
w'o: without, w: with split flap, 60° deflection. The lower values include the effect of standard roughness.

Profile NACA 66<sub>3</sub>-415

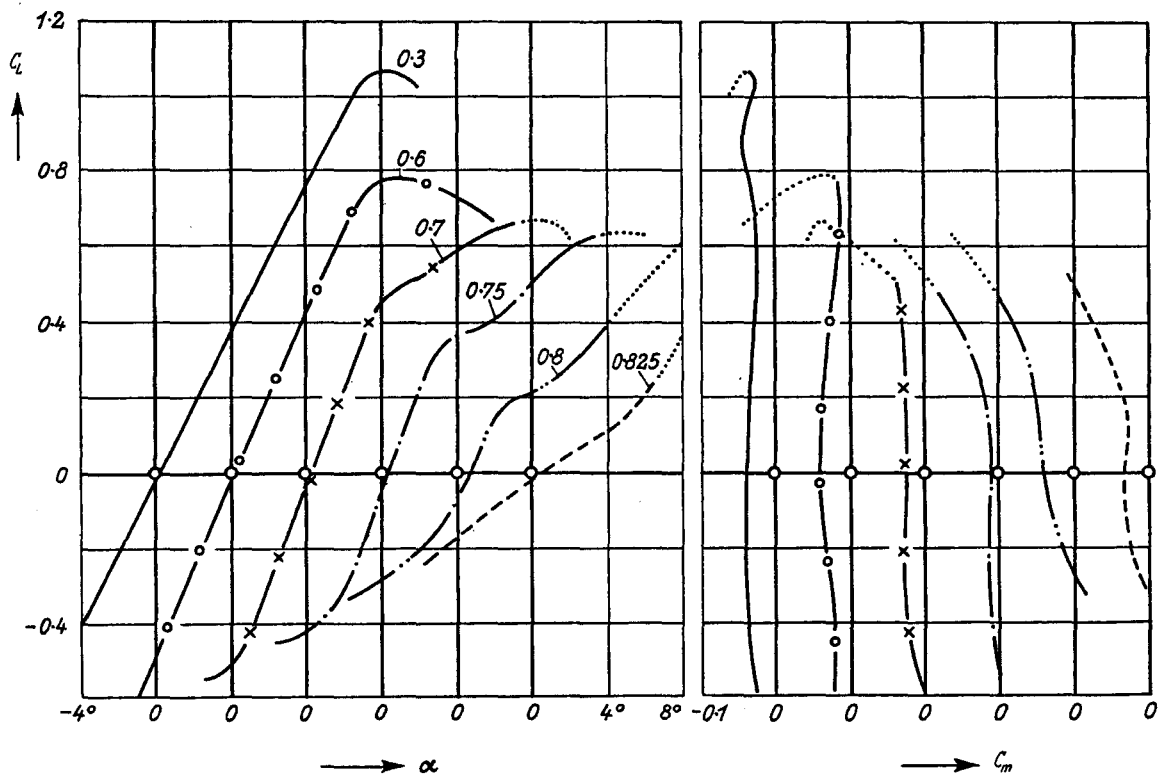
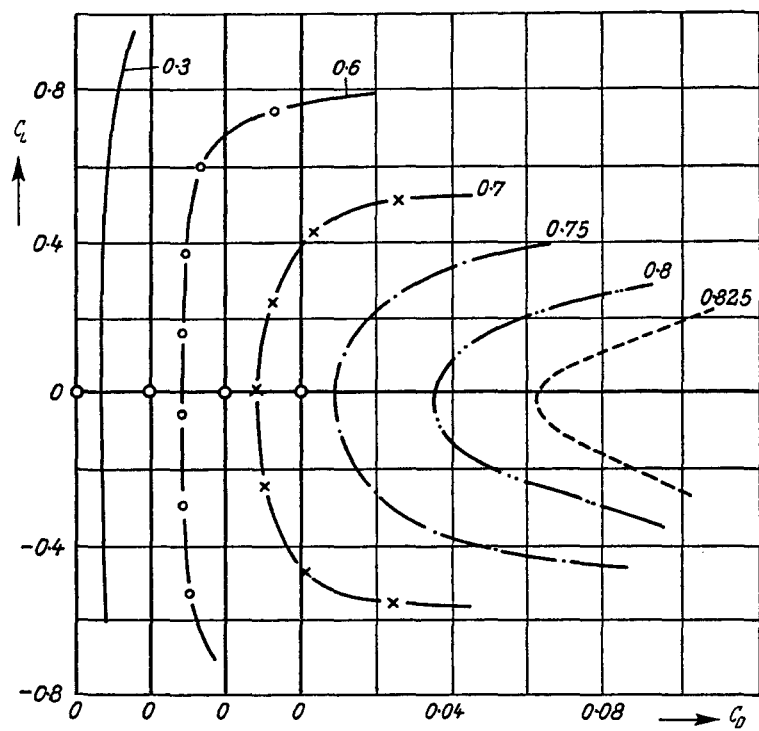
$R \cdot 10^{-6}$	w'o	0.7	w	w'o	1.5	w	3	w'o	6	w	9
$C_{L_{\max}}$	1.145 1.026	1.98 1.992	1.228 1.155	2.155 2.054	1.47	1.605 1.215	2.578 2.19	1.608			
$\alpha C_{L_{\max}}$	14.4° 15.3°	6.1° 6.2°	16.4° 13.2°	6° 6°	18.4°	18.4° 12.4°	11.2° 6.1°	17.2°			
$\alpha_0$	-2.7 -2.74	-13.1 -13.3	-2.63 -2.25	-13.2 -13.2	-2.51	-2.48° -2.38°	-14.2° -13.2°	-2.5°			

w'o: without, w: with split flap, 60° deflection. The lower values include the effect of standard roughness.

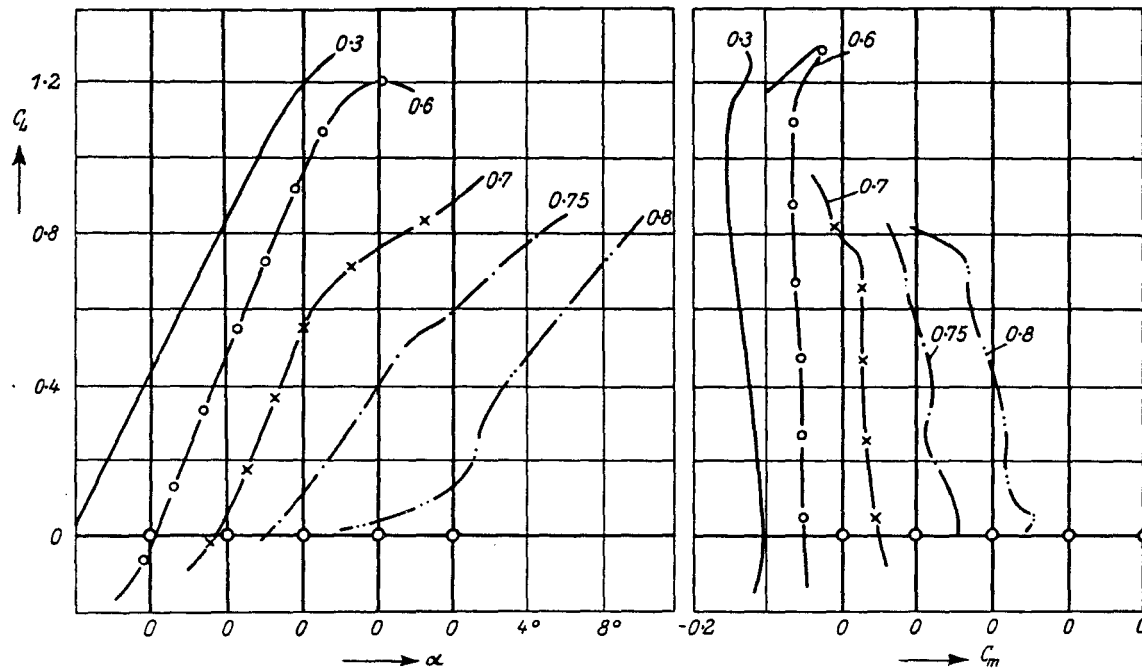
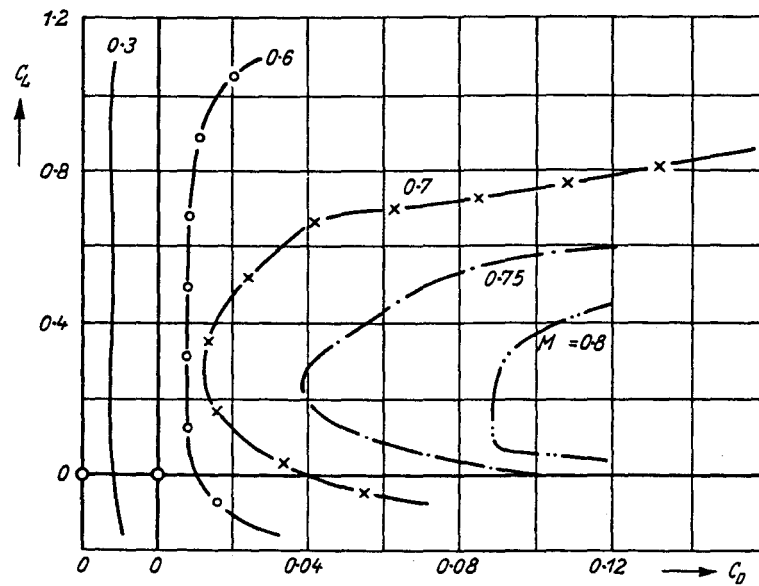
Fig. 12.132 a-d. Comparison of a four-figure NACA profile with a NACA profile of the 6-series.  
 (a) Polars:  $\alpha = 3.7 \cdot 10^4$ :  
 $\square$ ,  $R = 3.7 \cdot 10^4$ ;  $\diamond$ ,  $R = 5.2 \cdot 10^4$ , rough.  
 (b)  $C_L(\alpha)$ ,  $C_L(C_m)$  at  $R = 3.7 \cdot 10^4$ .  
 (c)  $C_L(\alpha)$ ,  $C_L(C_m)$  at  $R = 5.2 \cdot 10^4$ .  
 (d)  $C_L(\alpha)$ ,  $C_L(C_m)$  at  $R = 5.2 \cdot 10^4$ , rough.



## NACA 0015

Fig. 12.133. NACA 0015 for various Mach numbers. Wind tunnel: Ames Lab 1 ft  $\times$  3½ ft

NACA 4415

Fig. 12.134. NACA 4415 for various Mach numbers. Wind tunnel: Ames Lab 1 ft  $\times$  3½ ft

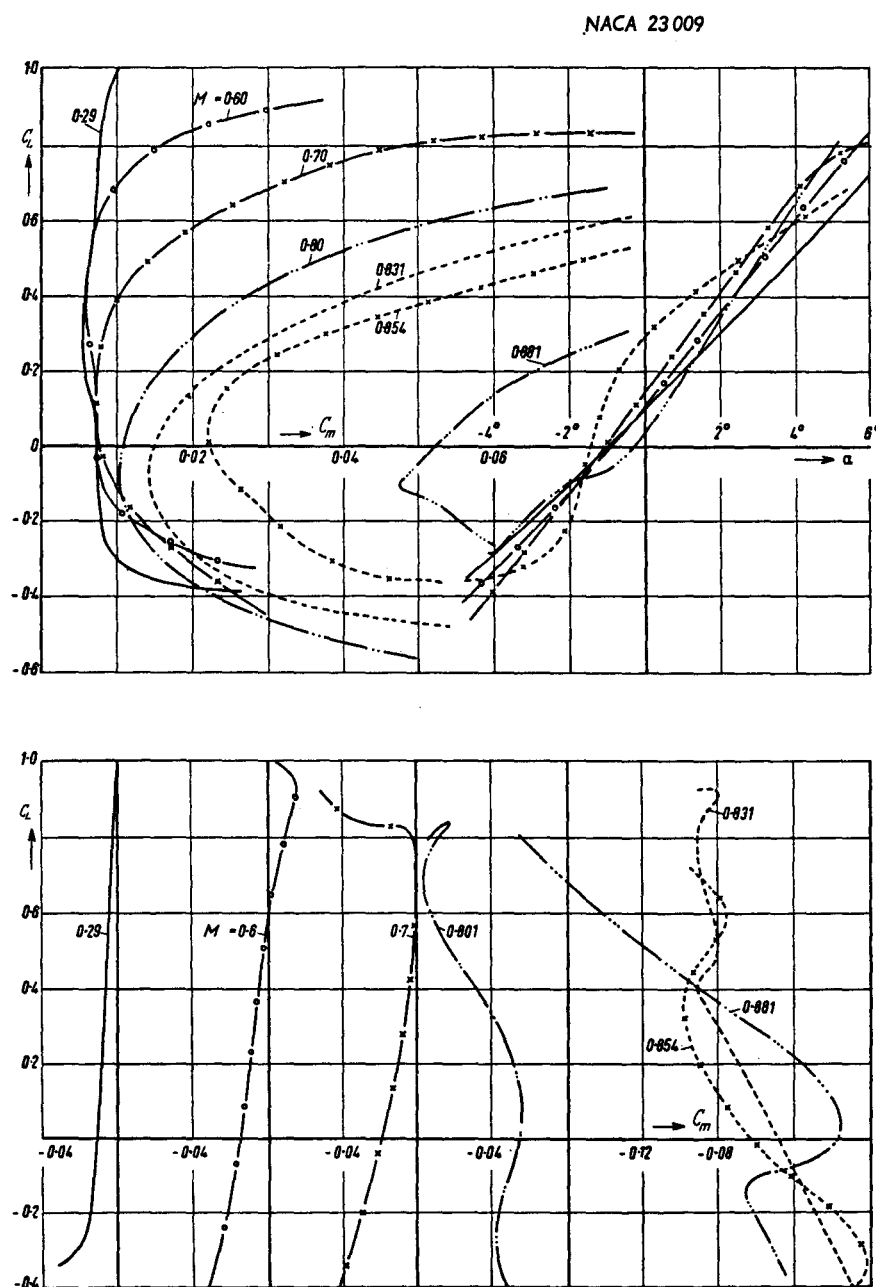
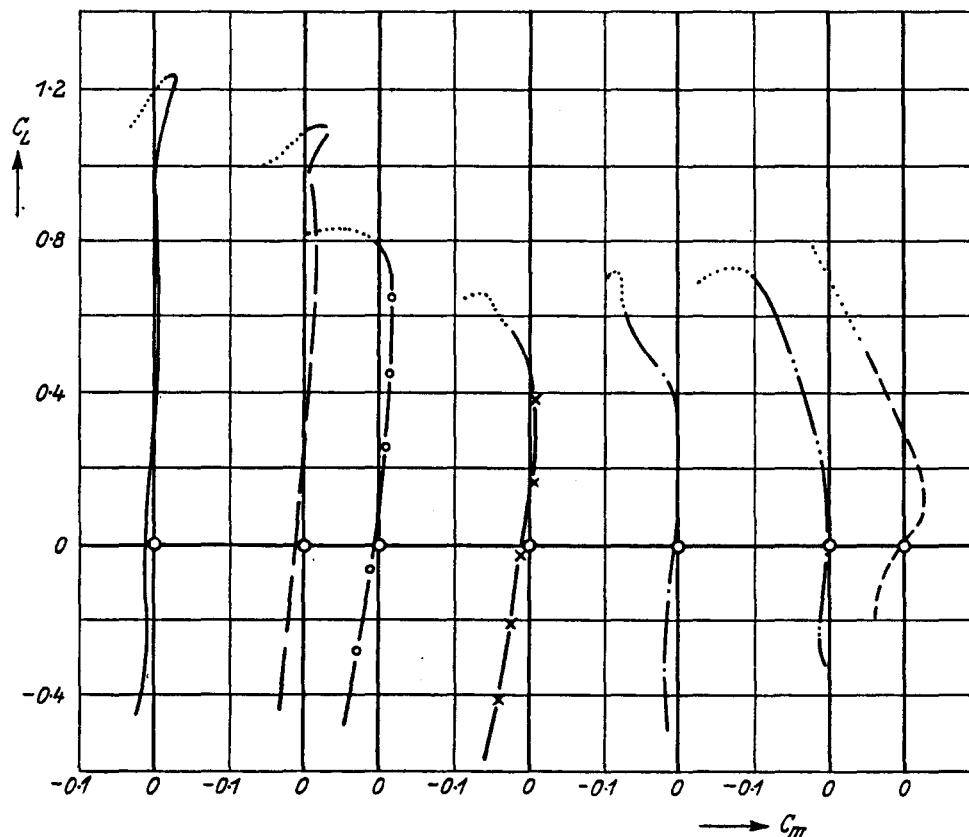
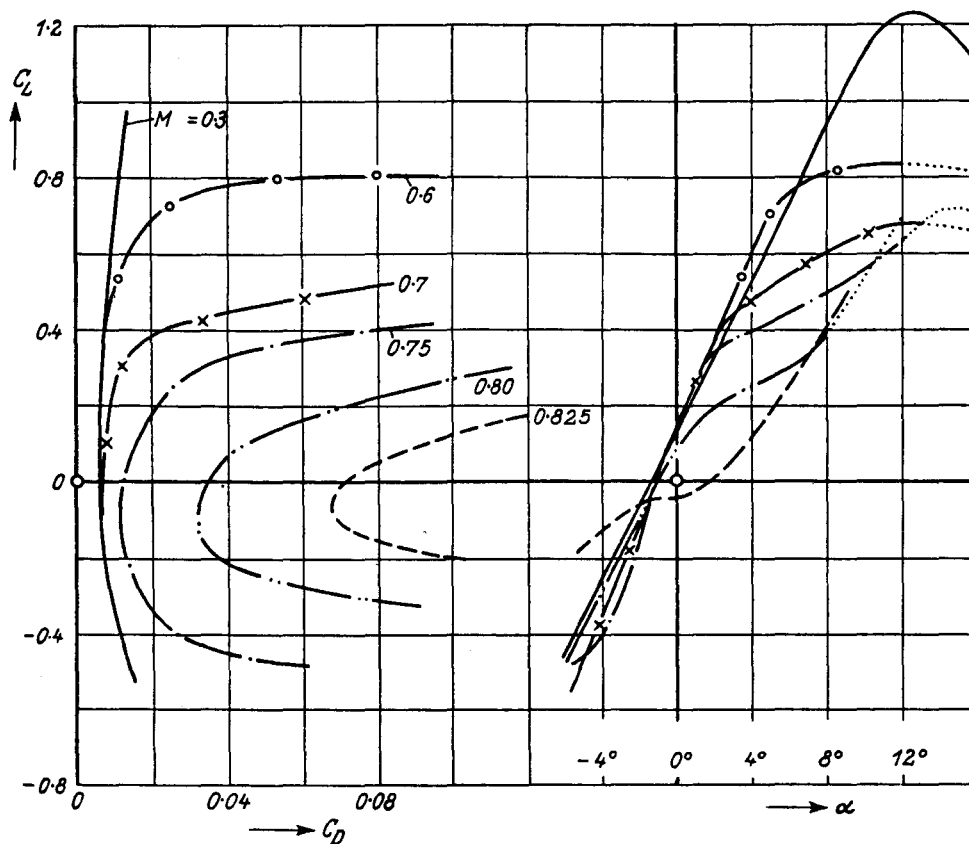
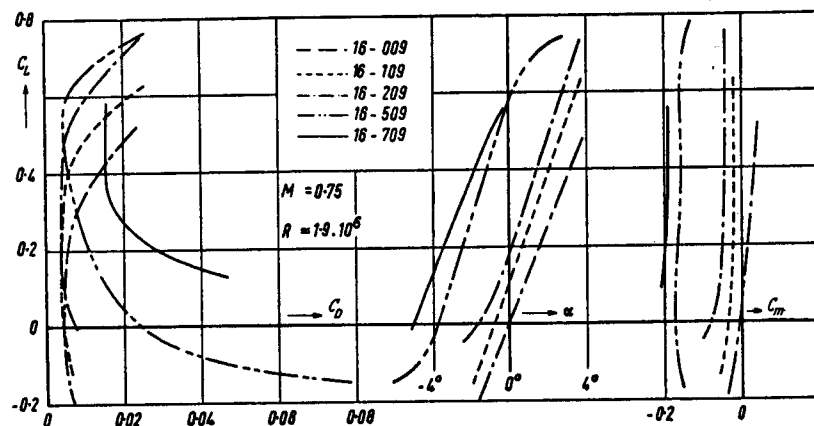


Fig. 12.135. NACA 23009 for various Mach numbers. Wind tunnel: DVL 2.7 m

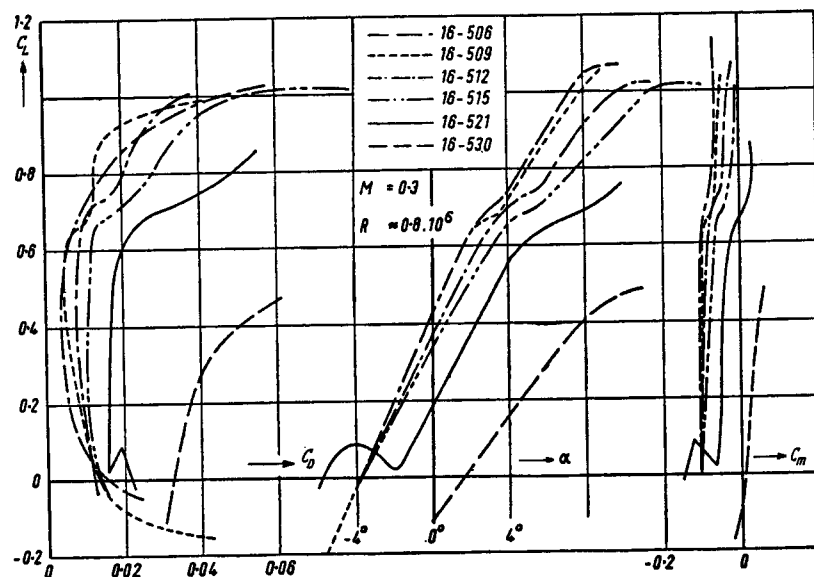
NACA 23015

Fig. 12.136. NACA 23015 for various Mach numbers. Wind tunnel: Ames Lab 1 ft  $\times$  3½ ft

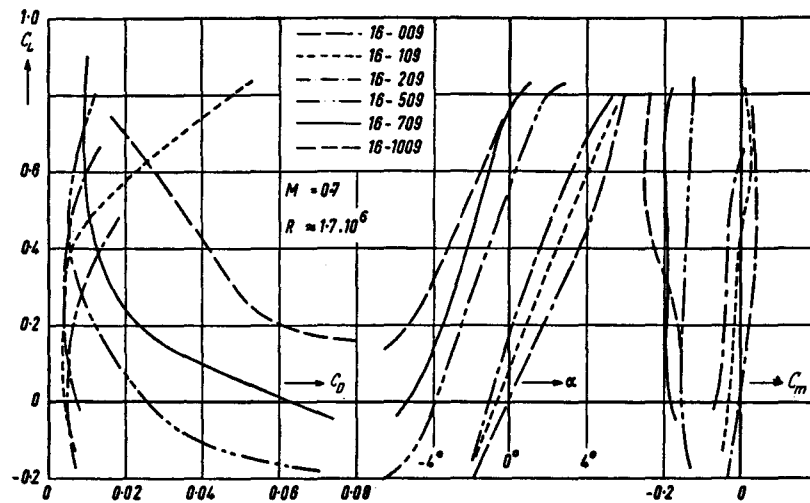
NACA 16-x 09

Fig. 12.137. NACA 16-x 09 at  $M = 0.3$ . Wind tunnel: Langley 2 ft HST

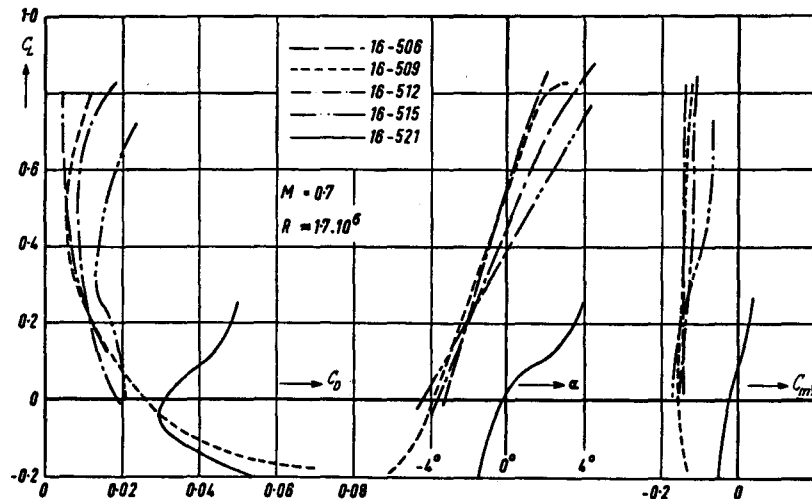
NACA 16-5 xx

Fig. 12.138. NACA 16-5 xx at  $M = 0.3$ . Wind tunnel: Langley 2 ft HST

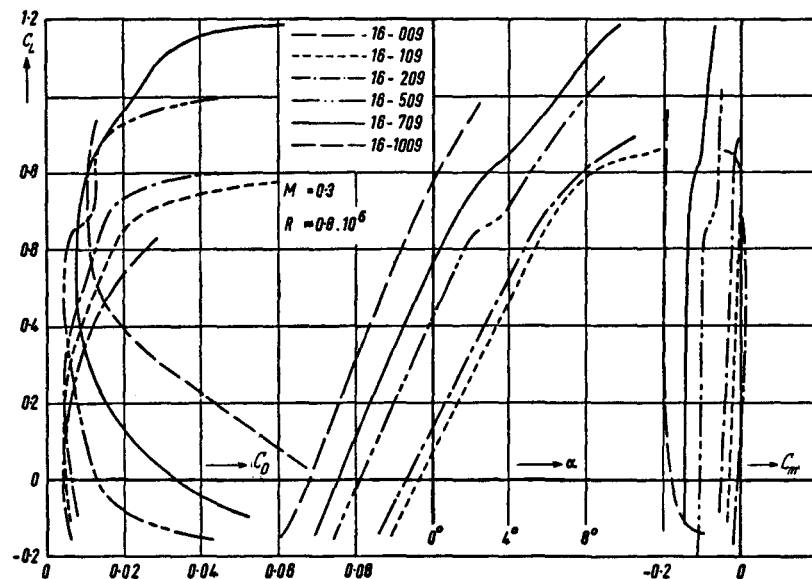
NACA 16-x09

Fig. 12.139. NACA 16—x 09 at  $M = 0.7$ . Wind tunnel: Langley 2 ft HST

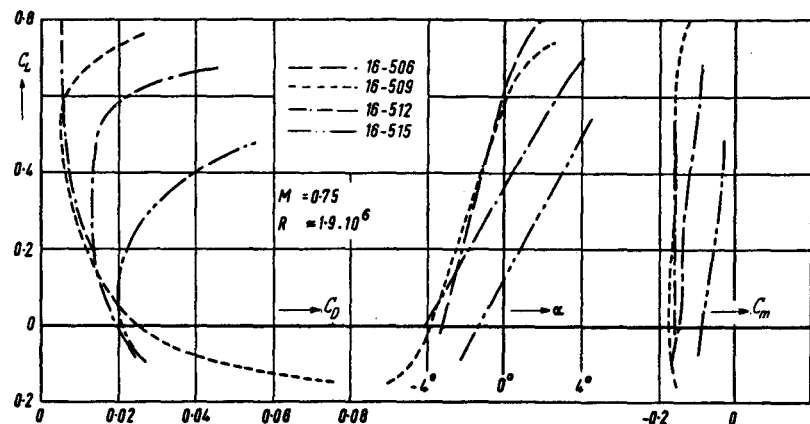
NACA 16-5xx

Fig. 12.140. NACA 16—5 xx at  $M = 0.7$ . Wind tunnel: Langley 2 ft HST

NACA 16-x09

Fig. 12.141. NACA 16—x 09 at  $M = 0.75$ . Wind tunnel: Langley 2 ft HST

NACA 16-5xx

Fig. 12.142. NACA 16—5 xx at  $M = 0.75$ . Wind tunnel: Langley 2 ft HST

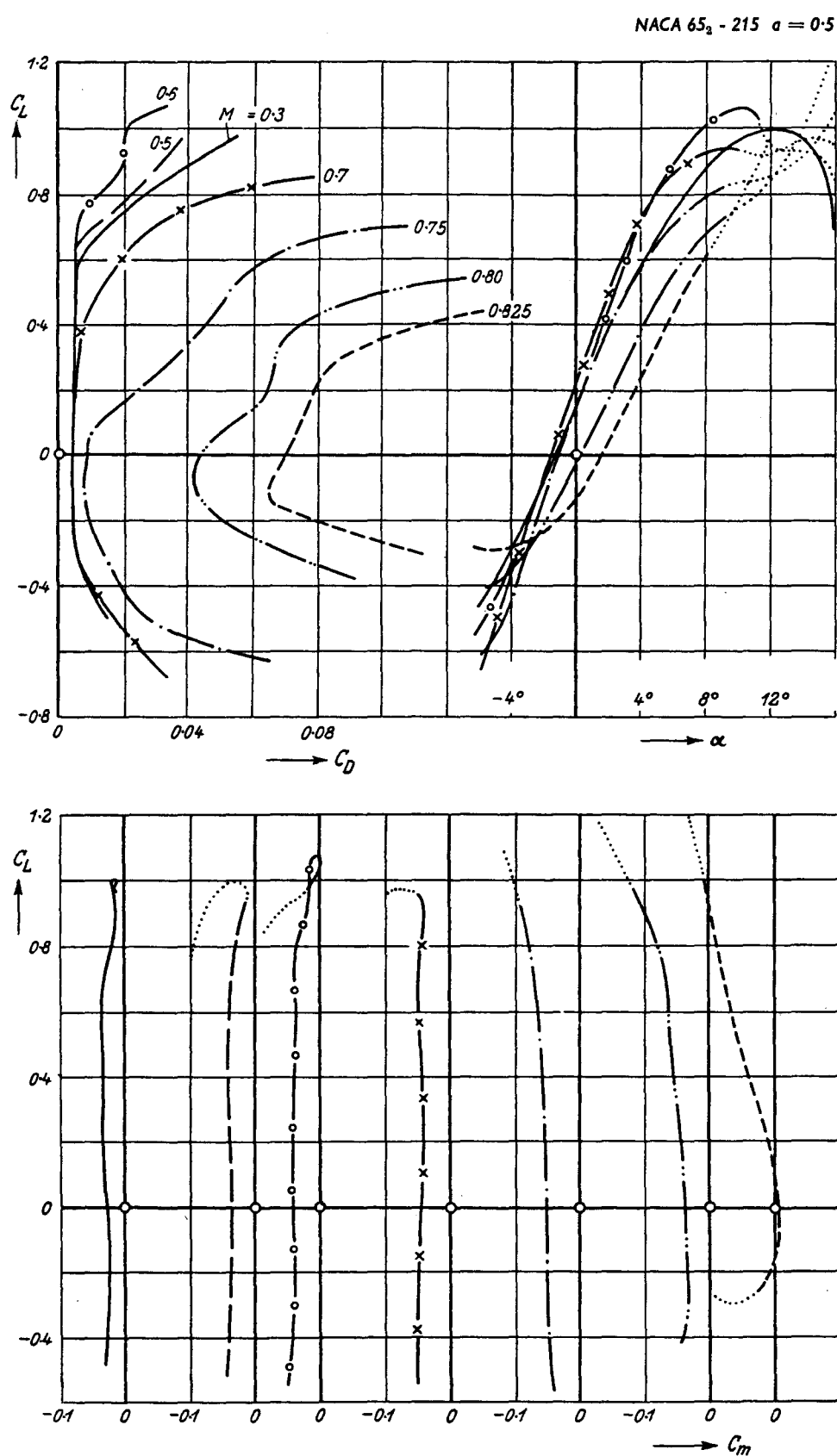


Fig. 12.143. NACA 65<sub>2</sub> - 215 ( $\alpha = 0.5$ ). Ames Lab 1 ft  $\times$  3½ ft

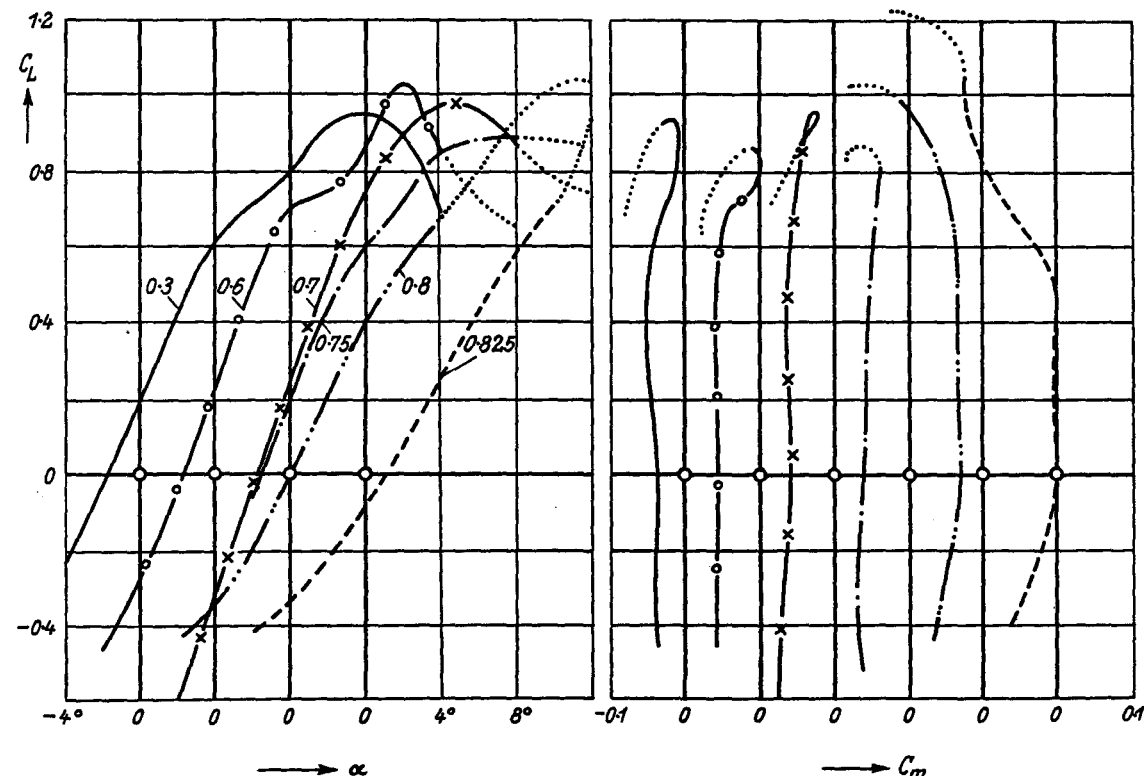
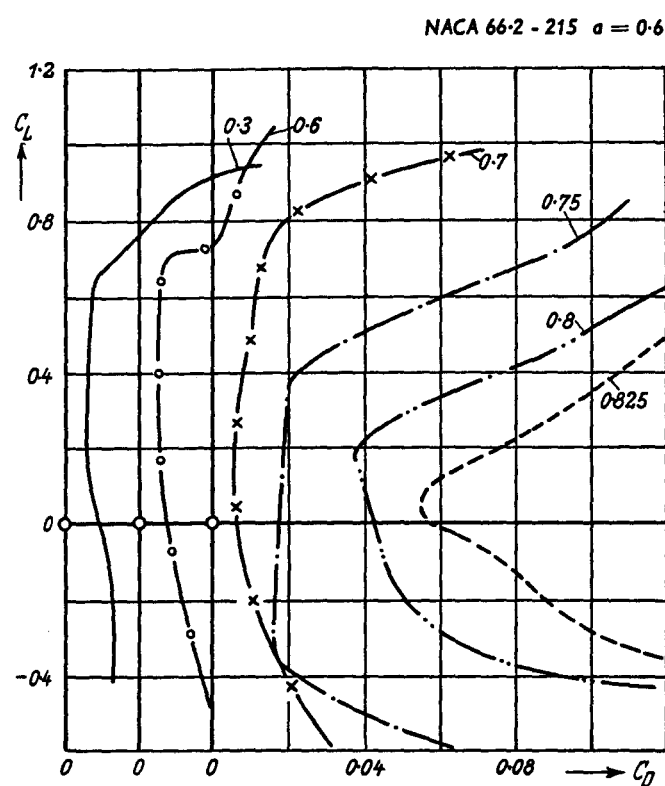


Fig. 12.144. NACA 66,2—215 ( $\alpha = 0\cdot6$ ). Ames Lab 1 ft  $\times$   $3\frac{1}{2}$  ft

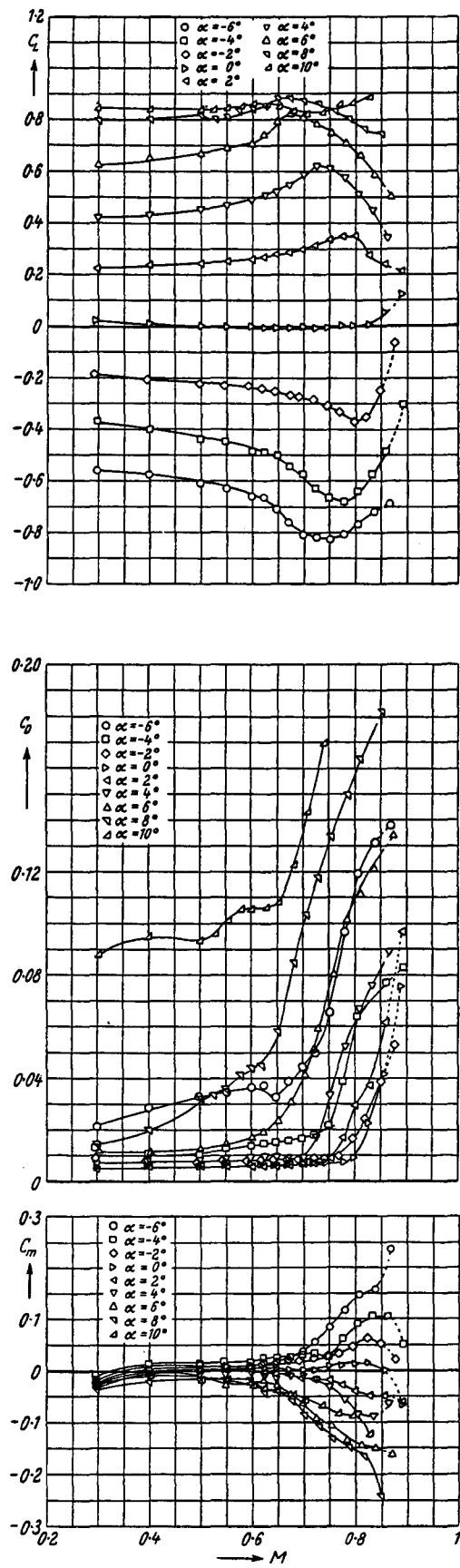


Fig. 12.145. NACA 836D110

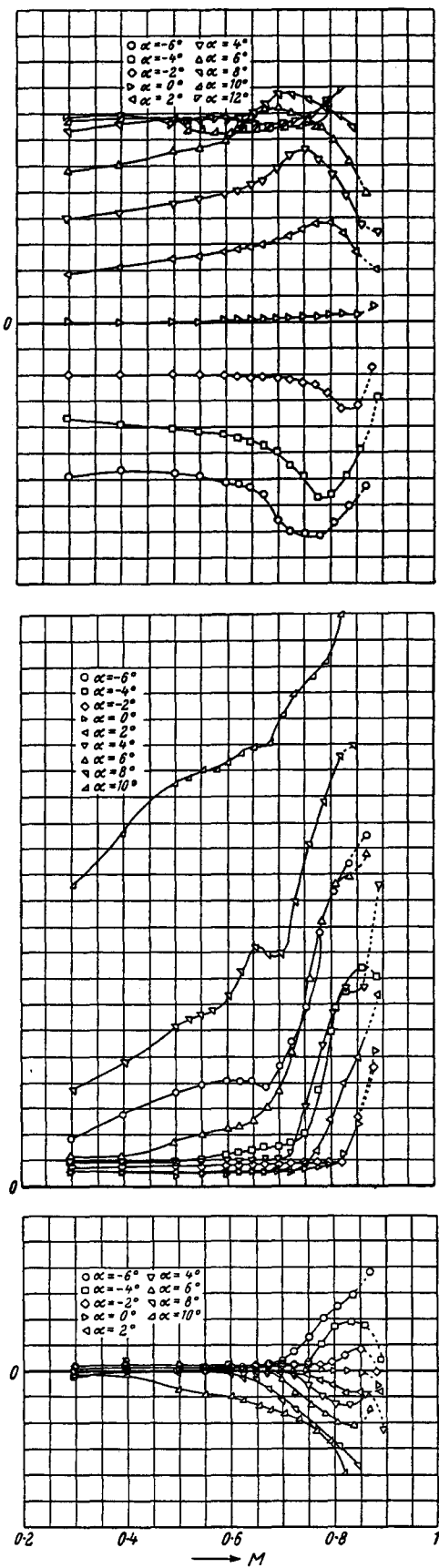


Fig. 12.146. NACA 847B110

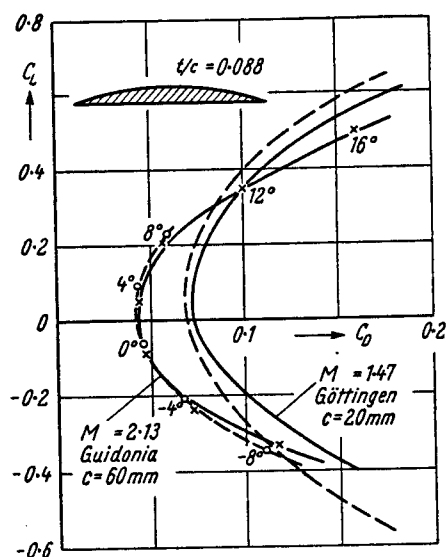


Fig. 12.147. Circular segment profile at two supersonic Mach numbers.  
Full line : experiment. Dashed line : theory. (BUSEMANN-WALCHNER)

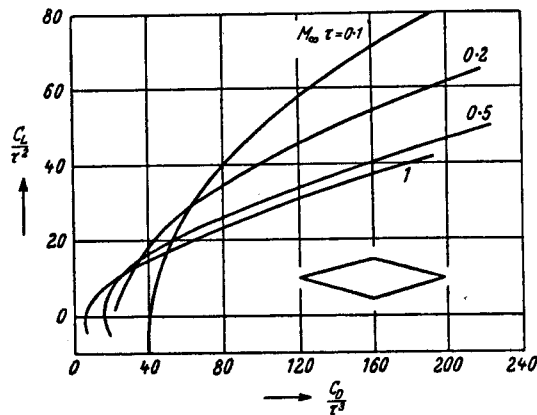


Fig. 12.149. Double wedge profile at hypersonic speeds (theory). [SAENGER]

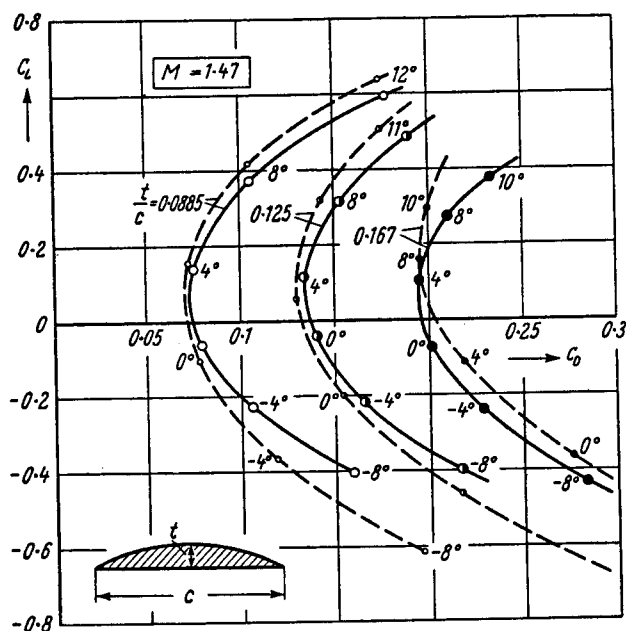
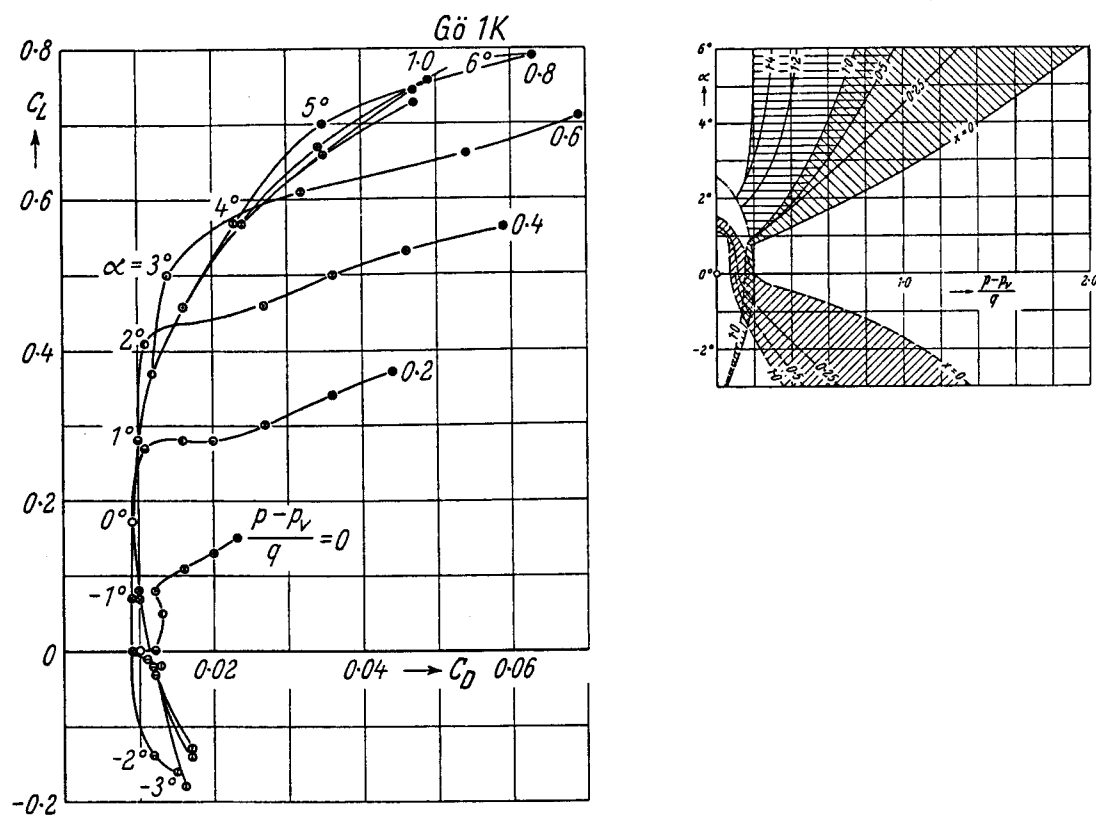
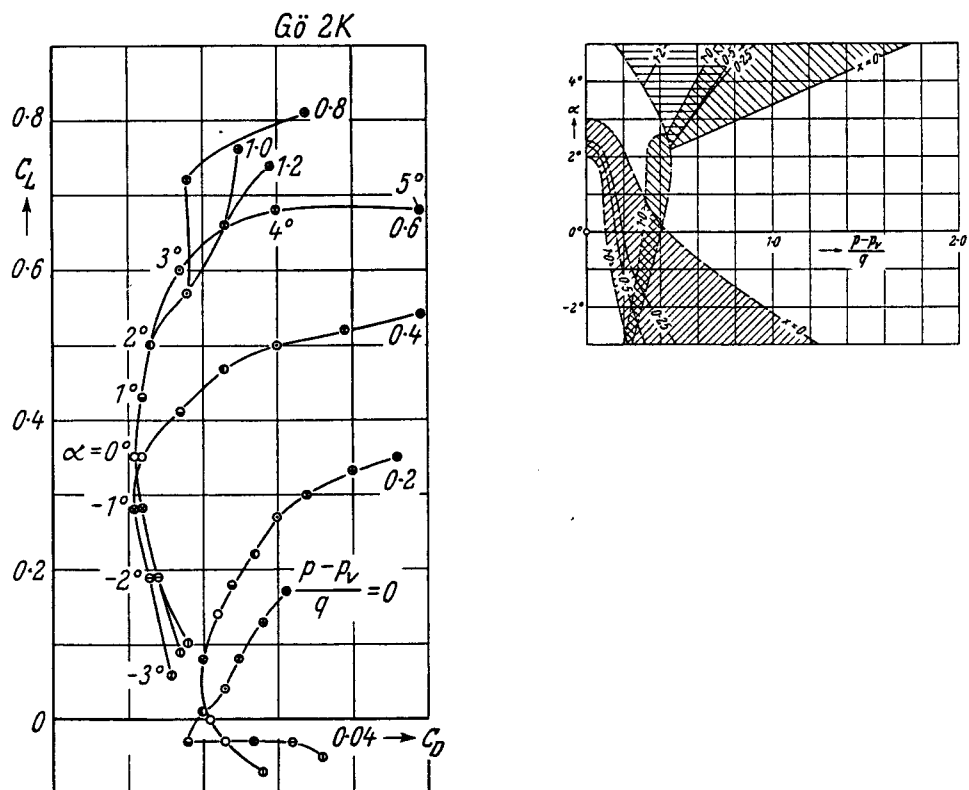


Fig. 12.148. Circular segment profiles with various thickness ratios in supersonic flow ( $M = 1.47$ ). Full line : experiment. Dashed line : theory.  
(BUSEMANN-WALCHNER)

Fig. 12.150. Circular segment profile, Gö 1 K ( $t/c = 0.0385$ ) for various cavitation numbers. (WALCHNER)Fig. 12.151. Circular segment profile, Gö 2 K ( $t/c = 0.0735$ ) for various cavitation numbers. (WALCHNER)

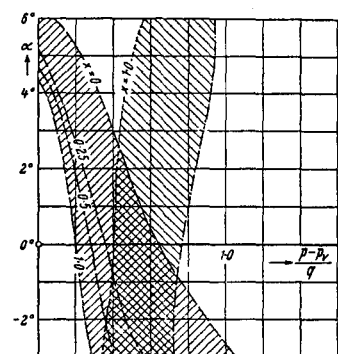
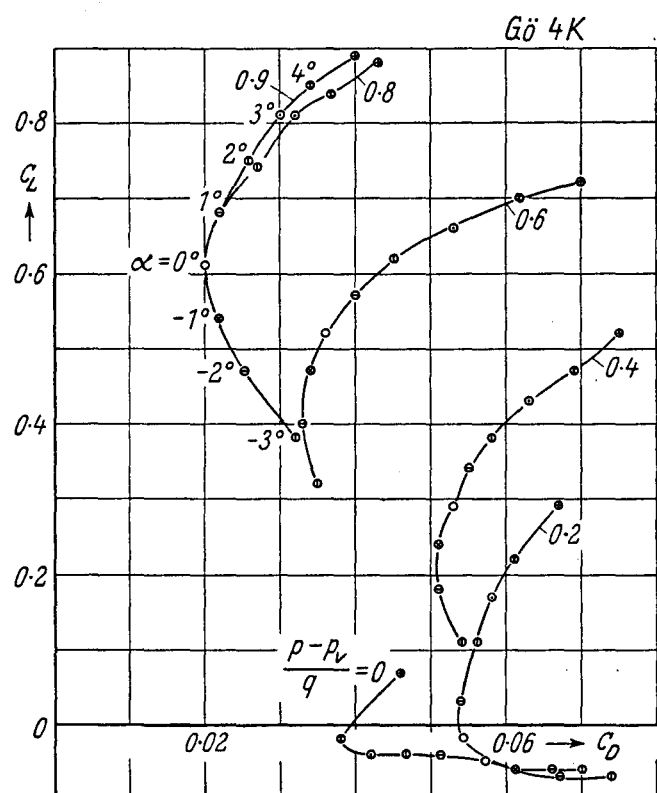


Fig. 12.152. Circular segment profile, Gö 4K ( $t/c = 0.1475$ ) for various cavitation numbers. (WALCHNER)

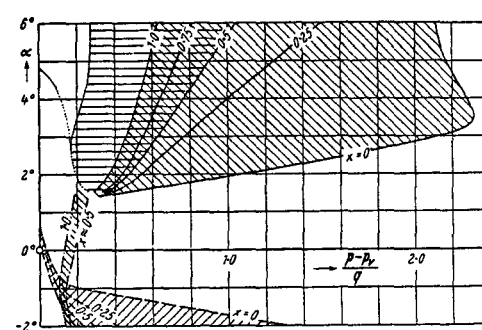
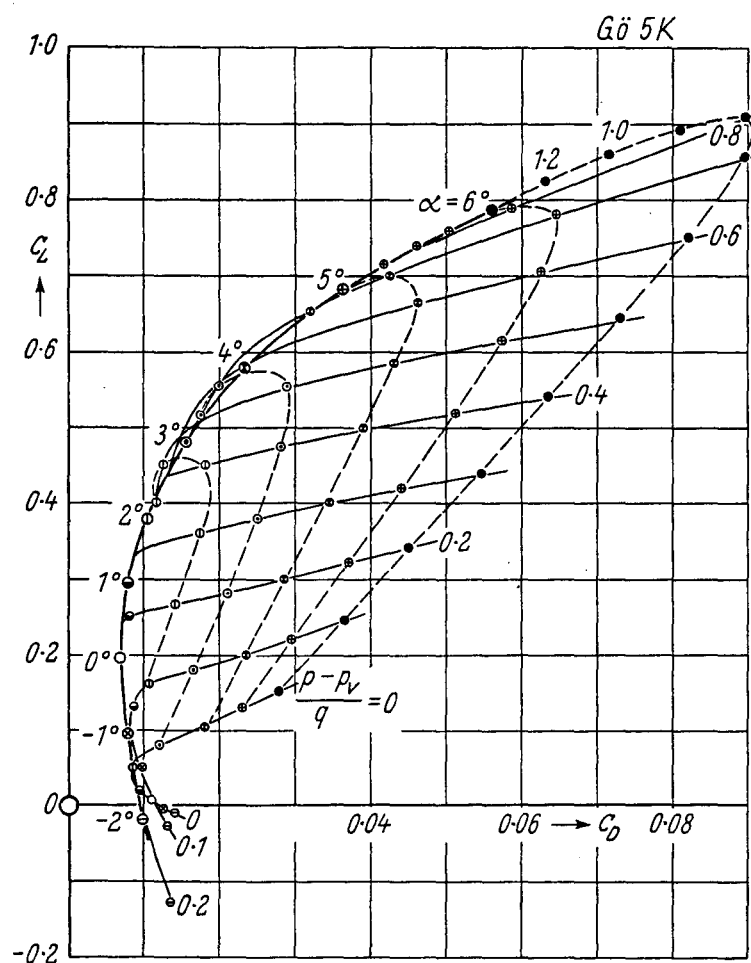


Fig. 12.153. a, b. Gö 5K for various cavitation numbers. (WALCHNER)

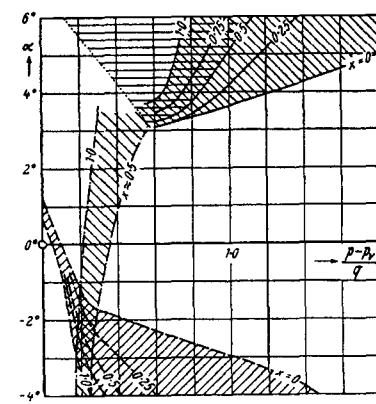
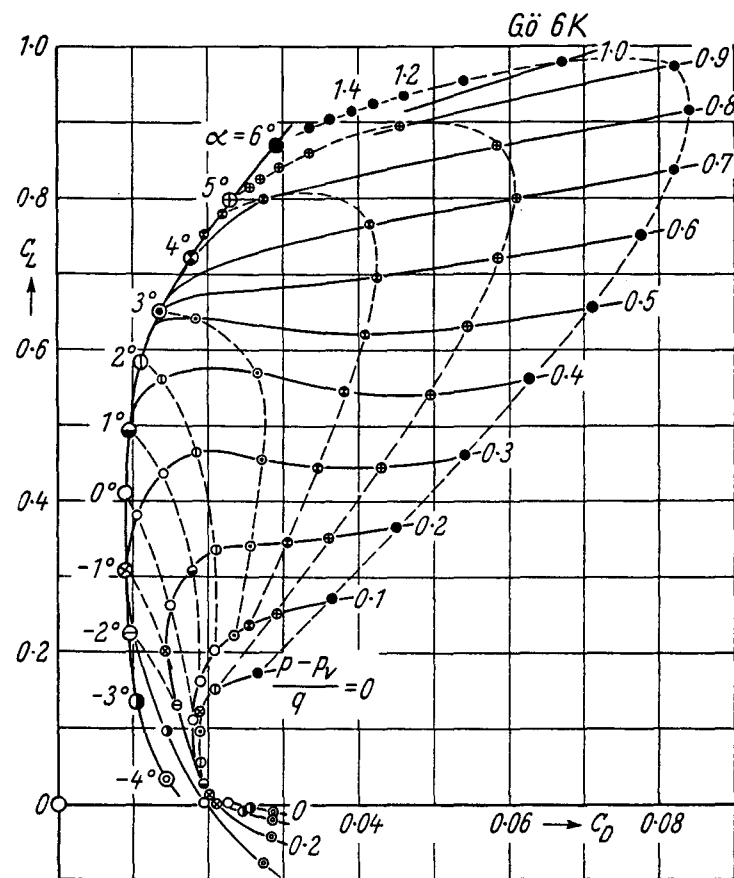


Fig. 12.154 a, b. Gö 6K for various cavitation numbers

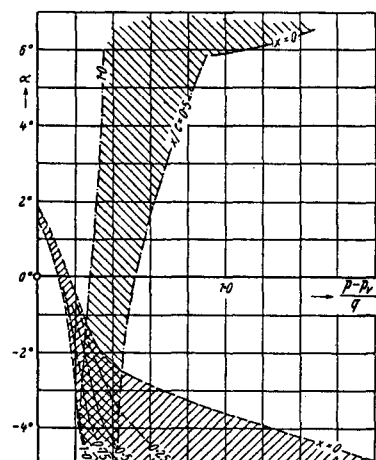
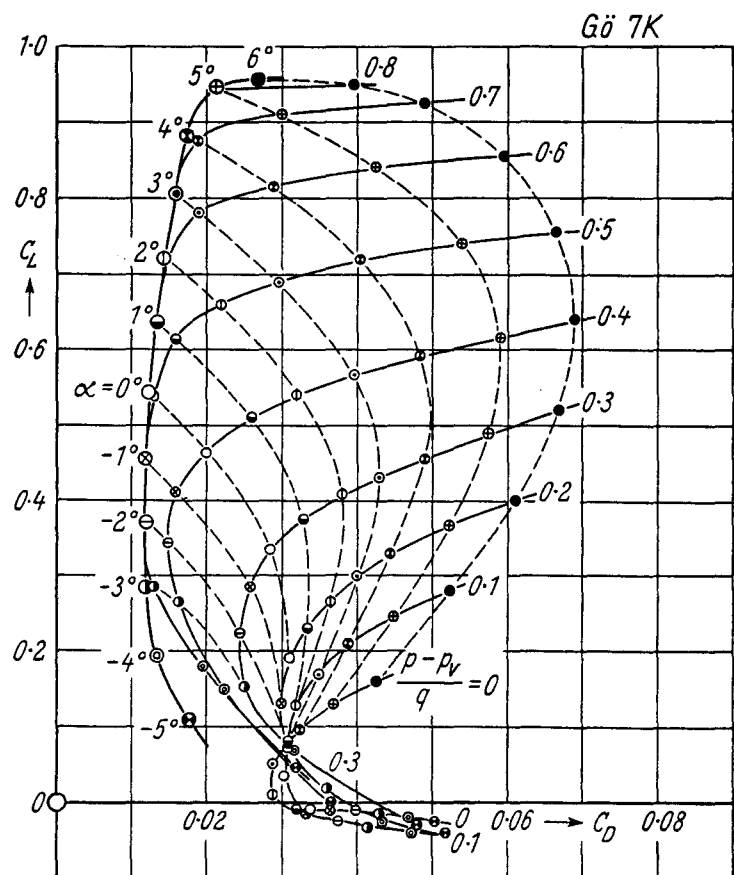


Fig. 12.155 a, b. Gö 7K for various cavitation numbers

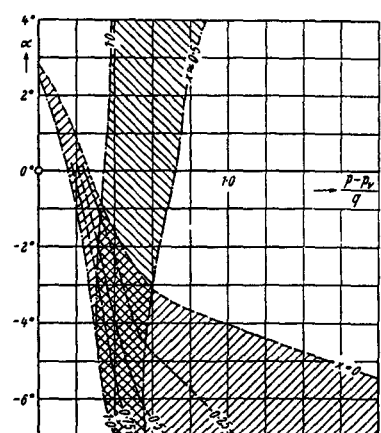
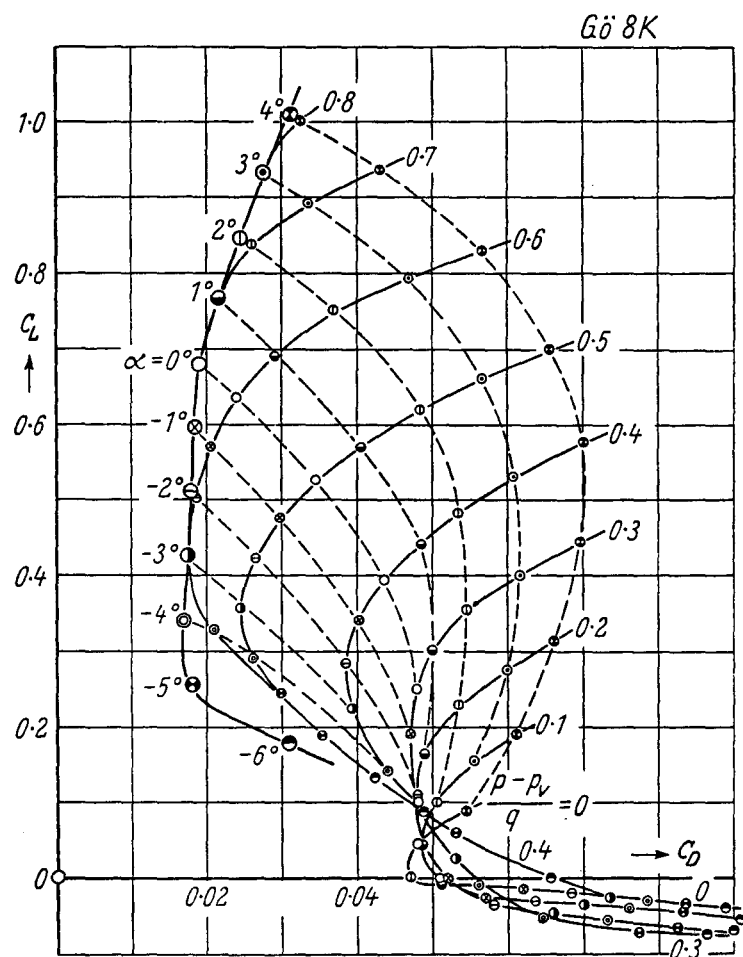


Fig. 12.156 a, b. Gö 8K for various cavitation numbers

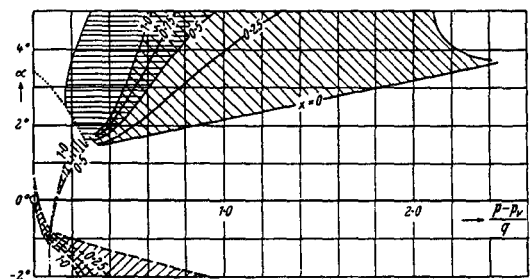
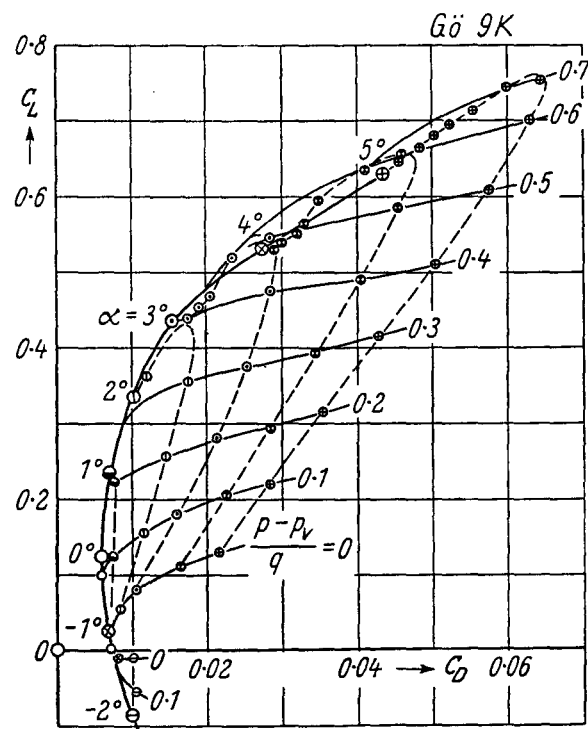


Fig. 12. 157 a, b. Gö 9K for various cavitation numbers. (WALCHNER)

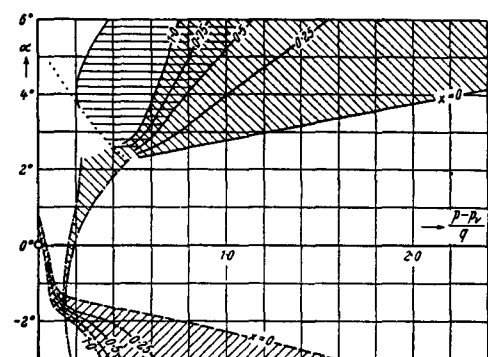
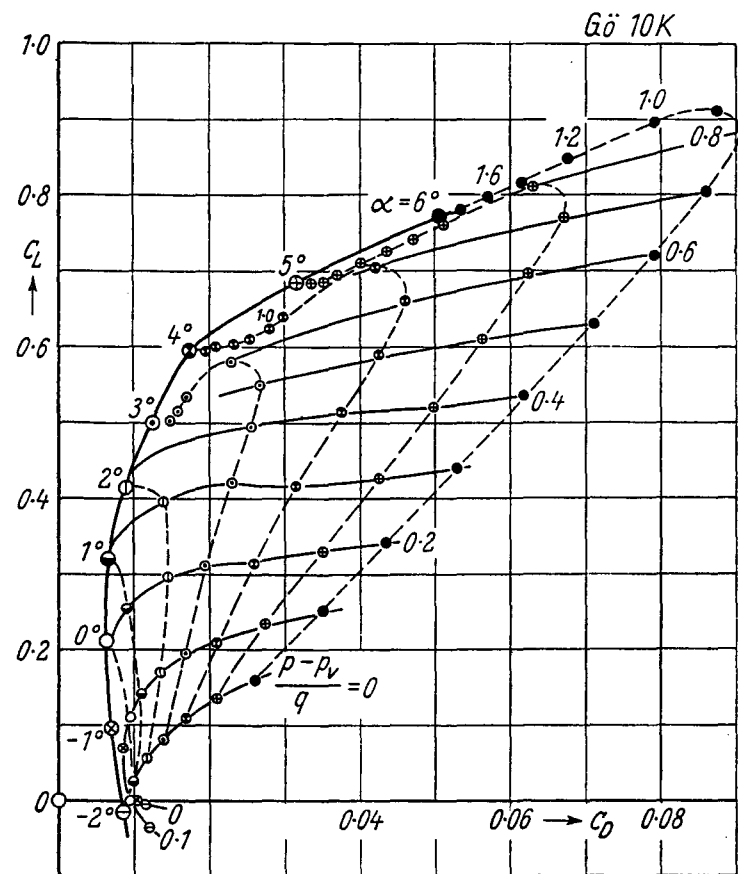


Fig. 12.158 a, b. Gö 10K for various cavitation numbers

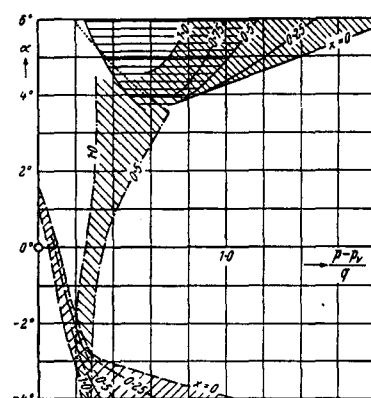
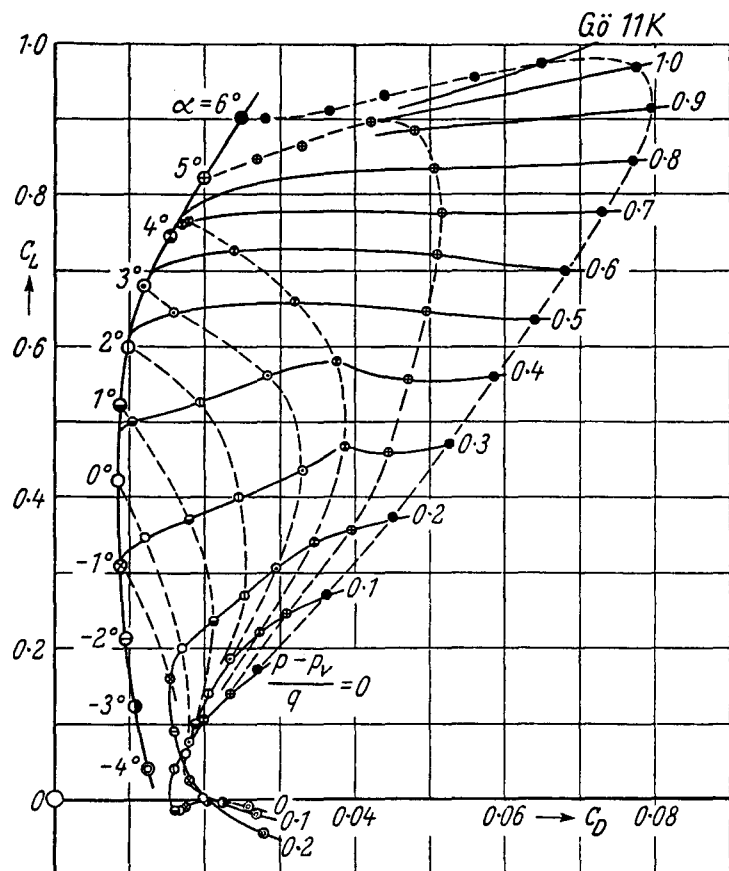


Fig. 12.159 a, b. Gö 11K for various cavitation numbers

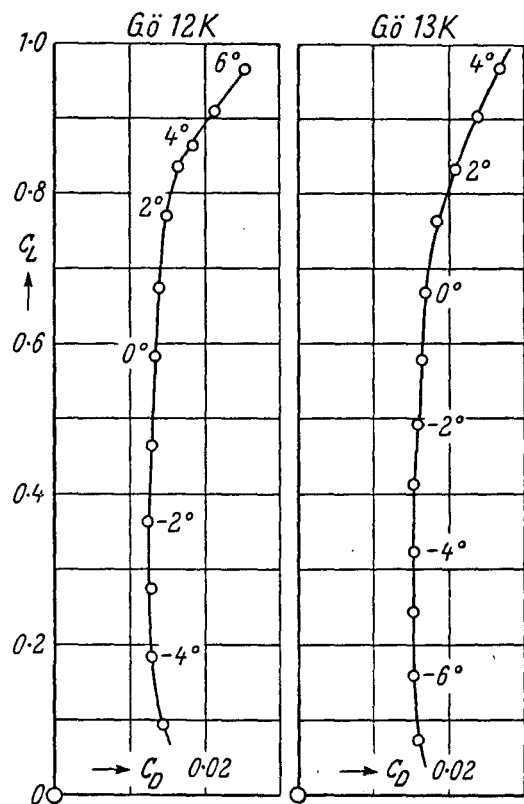


Fig. 12.160. Gö 12K, 13K, without cavitation

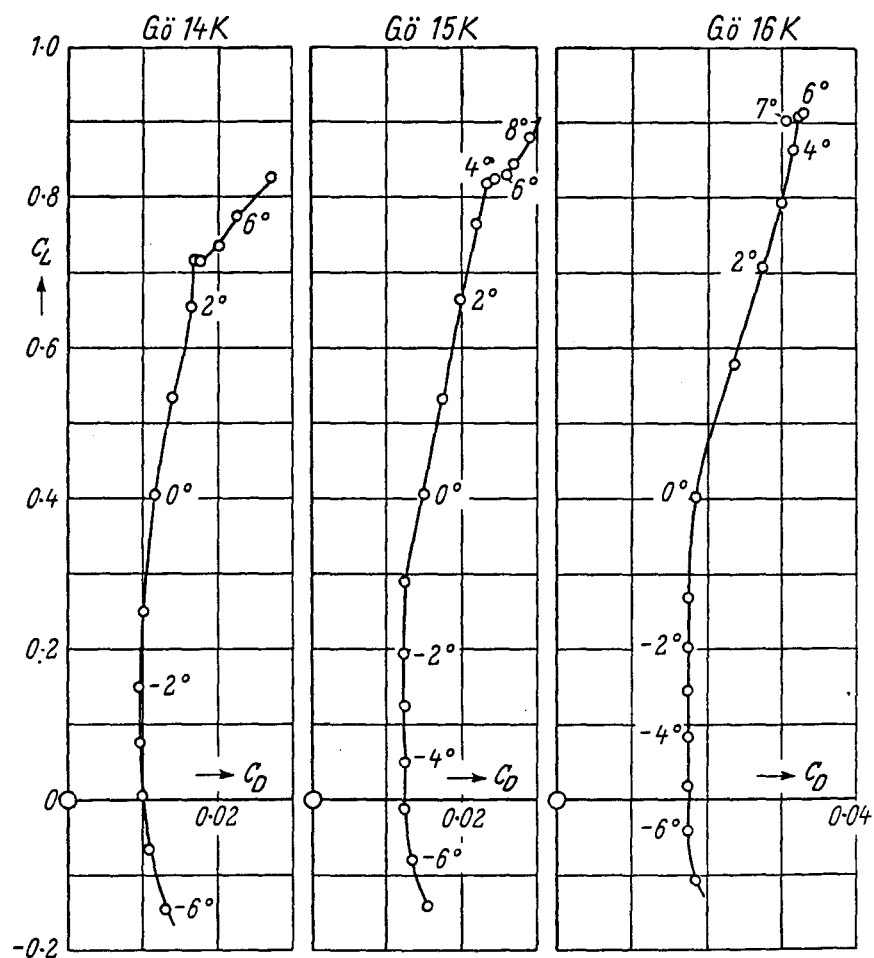


Fig. 12.161. Gö 14K, 15K, 16K, without cavitation. (WALCHNER)

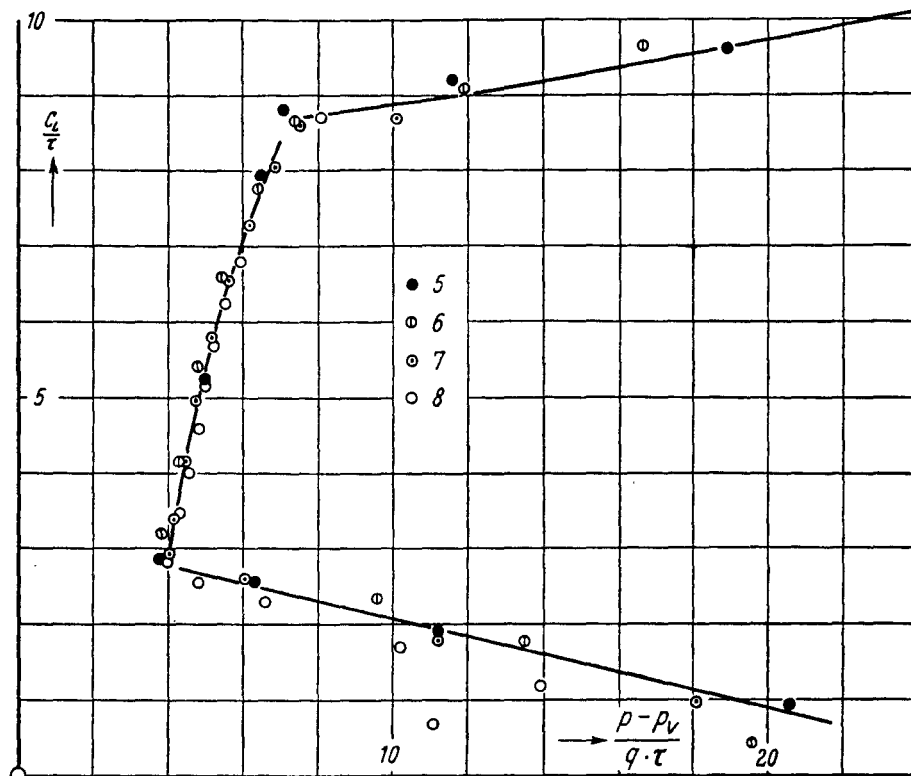
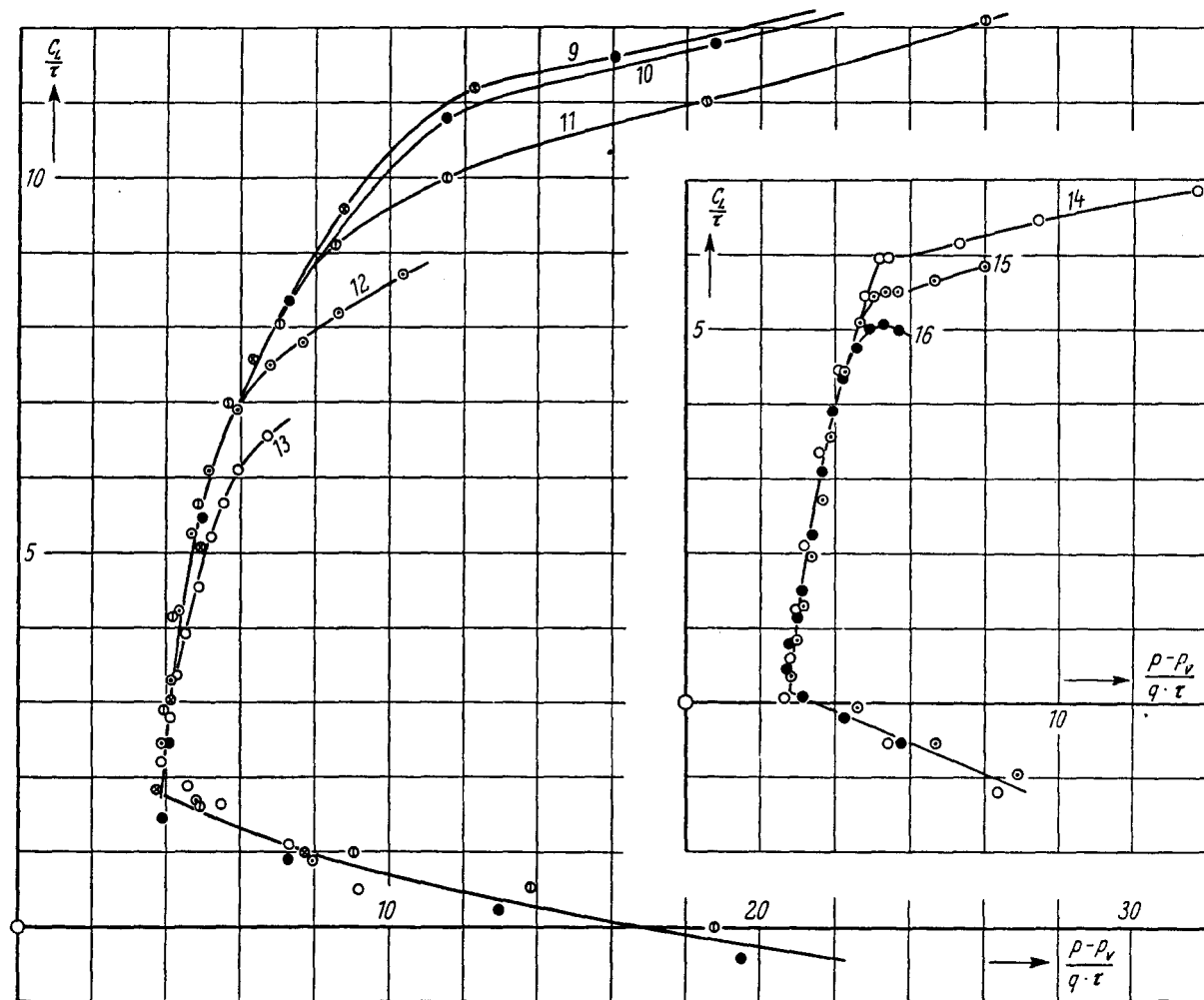
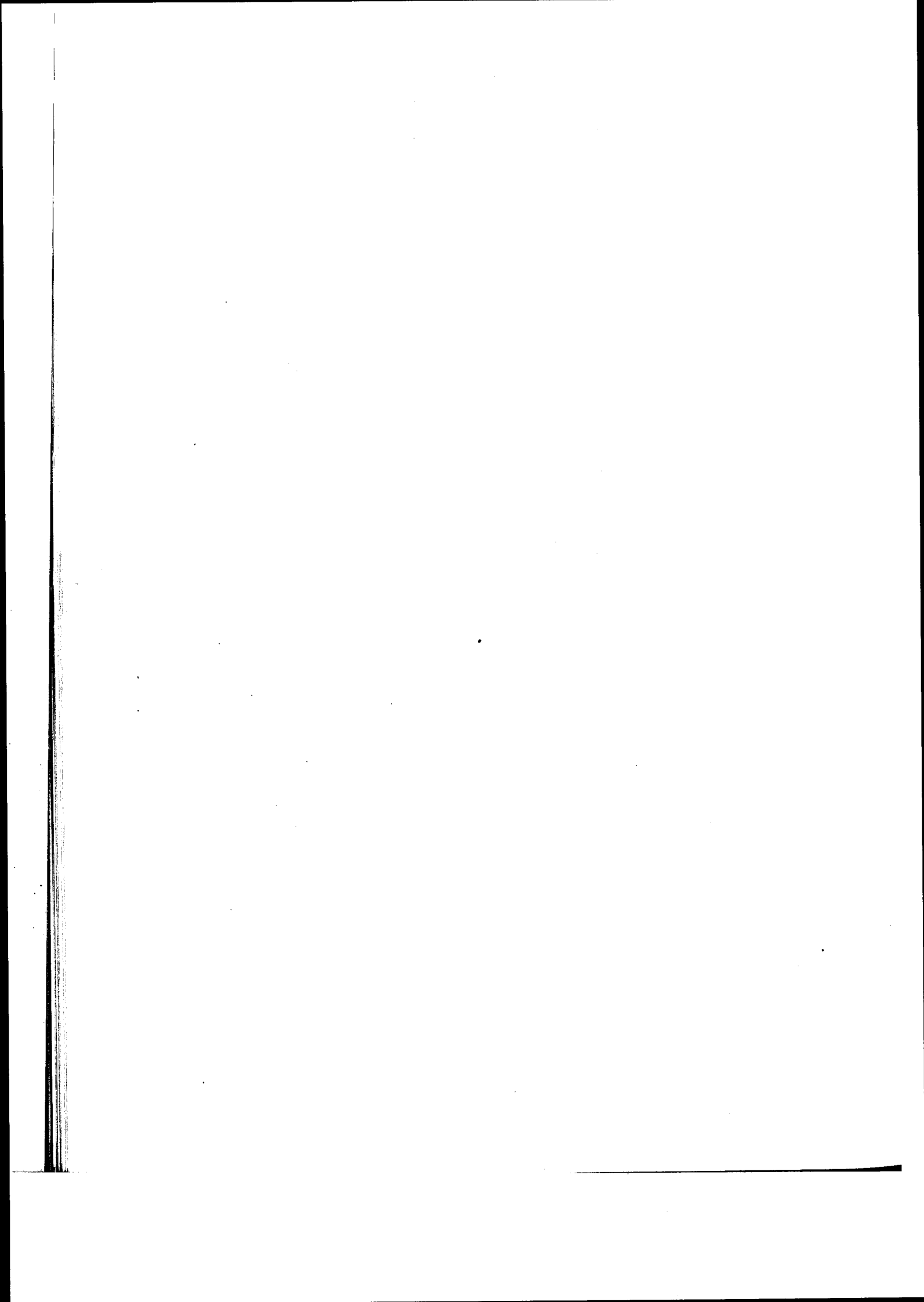


Fig. 12.163 (below). Beginning of cavitation for the affine series Gō 9K, 10K, 11K, 12K, 13K

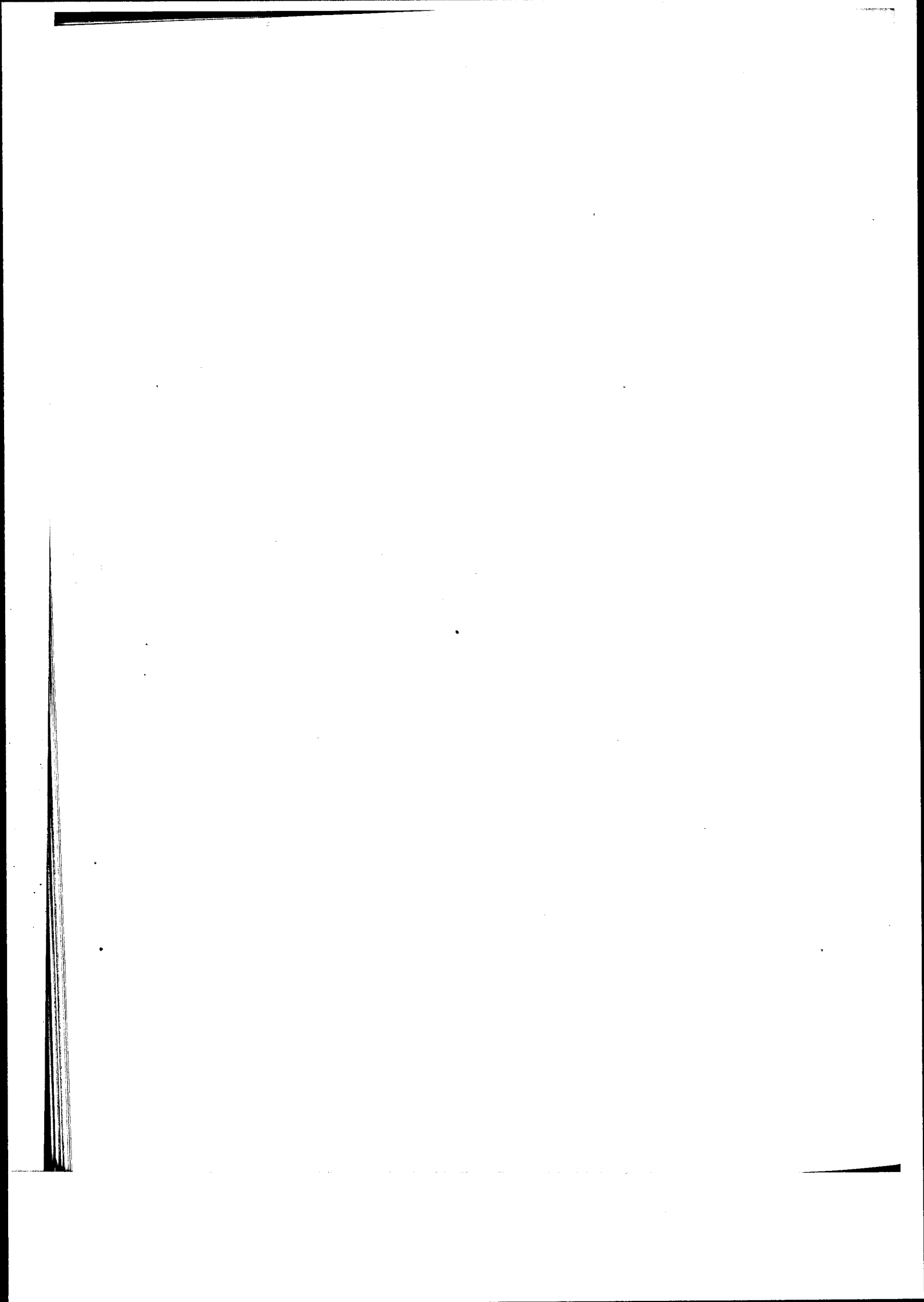
Fig. 12.164. Beginning of cavitation for the affine series Gō 14K, 15K, 16K. (WALCHNER)





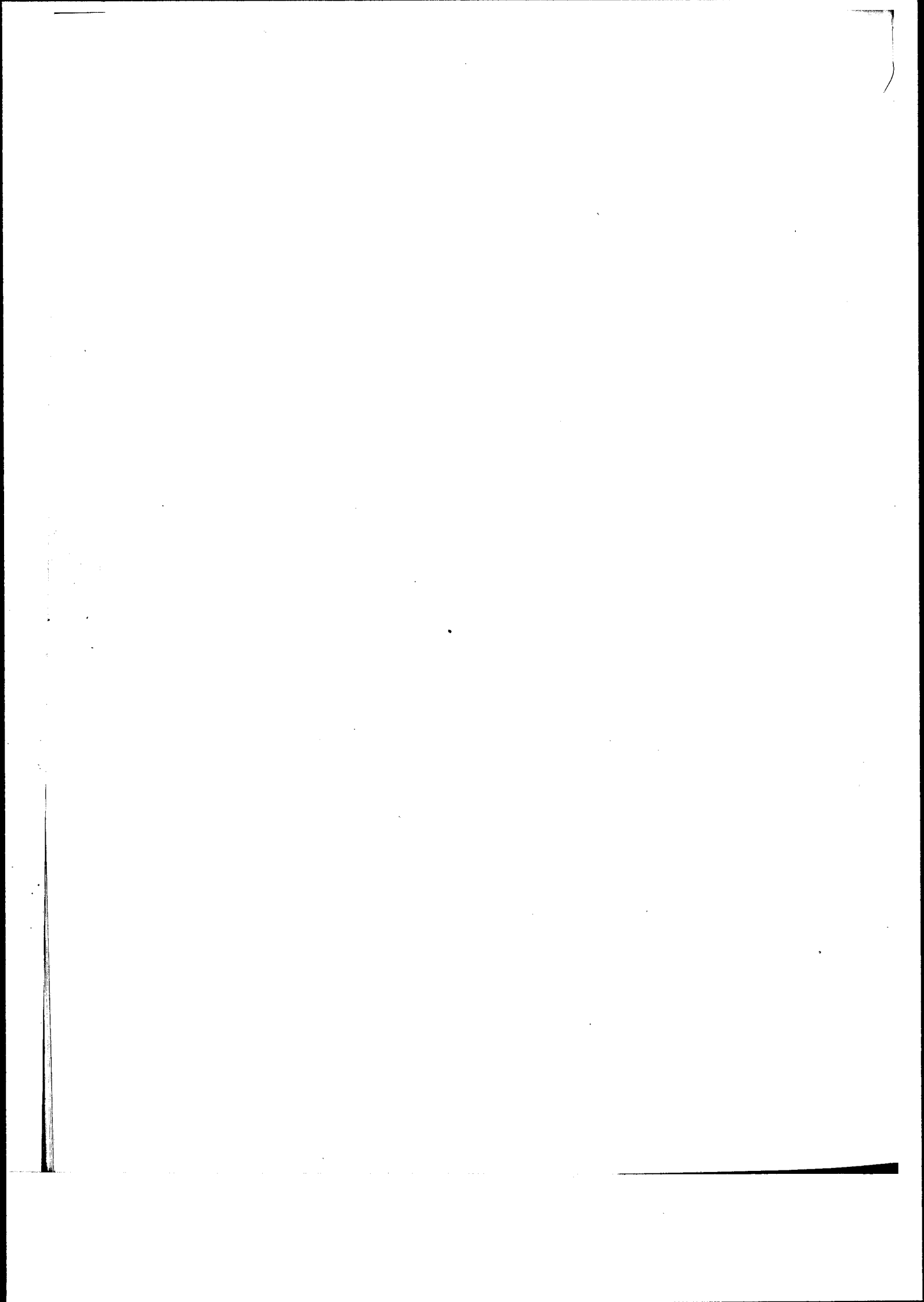
## LIST OF MAIN SYMBOLS

$A$	Aspect ratio, $b^2/S$ .	$V$	Free-stream speed.
$a$	Speed of sound: strictly, local speed; free-stream speed when no confusion possible.	$v_s$	Suction velocity.
$a_\infty$	Free-stream speed of sound.	$w$	Local speed.
$b$	Span.	$w_x, w_y$	Local velocity components.
$C_D$	Drag coefficient, $D/qS$ .	$x, y$	Cartesian co-ordinates, explained in Section 1.2.1 (but see also Section 9.2.2).
$C_{D_{\text{tot}}}$	Total drag coefficient (see Section 6.4).	$x_f$	Distance of position of maximum camber from leading edge.
$C_f$	Skin-friction drag coefficient.	$x_t$	Distance of position of maximum thickness from leading edge.
$C_L$	Lift coefficient, $L/qS$ .	$y^{(c)}$	Camber line (see Section 1.2.1).
$C_{L^*}$	The design $C_L$ , for which $\alpha = \alpha^*$ .	$y^{(t)}$	Thickness distribution (see Section 1.2.1).
$C_m$	Pitching moment coefficient, $M/qSc$ . Suffix $l$ means measured from leading edge: suffix $a$ means measured from aerodynamic centre. For further details see Section 3.1.		
$C_{m_0}$	$C_m$ for $\alpha = \alpha_0$ .	$\alpha$	Incidence.
$C_N$	Coefficient of normal force, $N/qS$ .	$\alpha_R$	Angle between chords defined in different ways (see Section 1.2.1).
$C_P$	Power consumption coefficient (see Section 6.4).	$\alpha_0$	Incidence at which lift vanishes.
$C_p$	Pressure coefficient, $(p - p_\infty)/q$ .	$\alpha^*$	Ideal angle of incidence (see Section 3.1).
$C_T$	Coefficient of tangential force, $T/qS$ .	$\beta$	In Section 9.2.1, Hartree parameter. In Section 10.5.2, local slope.
$c$	Chord.	$\beta_i$	Defined in Section 9.3.2.
$c_\eta$	Flap chord.	$\gamma$	Ratio of specific heat at constant pressure to specific heat at constant volume.
$c_q$	Volume-flow-rate coefficient (see Section 6.1).	$\gamma(x)$	Distribution of circulation.
$D$	Drag. In Section 2.2, diameter of sphere. In Section 9.2, dissipation.	$\delta$	Boundary layer thickness.
$f$	Maximum camber.	$\delta^*$	Displacement thickness (see Section 9.2.2).
$H$	$\delta^*/\theta$ .	$\bar{\delta}$	Energy thickness (see Section 9.2.2).
$H$	$\bar{\delta}/\theta$ .	$\varepsilon_L$	$\frac{\tan \tau_L}{t/c}$
$h$	Distance of centre of pressure from leading edge.	$\varepsilon_T$	$\frac{\tan \tau_L}{t/c}$
$k$	Height of protuberance.	$\eta$	Flap deflection. In Section 3.3.1, efficiency factor.
$L$	Lift. In Section 2.2.1, scale of turbulence. In Section 9.2.3, a boundary layer quantity.	$\theta$	Momentum thickness (see Section 9.2.2).
$M$	Mach number: strictly, local Mach number; free-stream Mach number when no confusion possible. In Section 3.1, pitching moment.	$\mu$	Viscosity.
$M_\infty$	Free-stream Mach number.	$\nu$	Kinematic viscosity.
$N$	Normal force.	$\xi$	Profile co-ordinate (see Section 1.2.1).
$p$	Local pressure.	$\rho$	Local density.
$p_v$	Vapour pressure.	$\rho_0$	$\rho_0 c/2$ . In Chapter 10, stagnation density (see Section 10.2).
$p_0$	Stagnation pressure (see Section 10.2).	$\rho_1$	$\rho_1 c/2$ .
$p_\infty$	Free-stream pressure.	$\rho_\infty$	Free-stream density.
$q$	Kinetic pressure, $\frac{1}{2}\rho_\infty V^2$ .	$\sigma$	Cavitation number $(p - p_v)/q$ .
$R$	Reynolds number. In Section 3.1, total force.	$\tau$	Skin friction.
$r_0$	Nose radius.	$\tau_L$	Defined in (b) 1 of Section 1.2.2.
$r_1$	Radius of curvature at maximum thickness.	$\tau_T$	$\tan \tau_T$ is the slope at the trailing edge.
$S$	Wing area.	$\tau_0$	Wall skin friction.
$T$	In Section 2.2.1, degree of turbulence. In Section 3.1, tangential force. In Section 9.2, turbulent energy produced per unit time.	$\Phi$	Velocity potential.
$t$	Maximum thickness.	$\phi$	Parametric angle (see Section 1.2.3).
$t.f.$	Turbulence factor (see Section 2.2.3).	$\psi$	Stream-function.
$u, v$	In Section 9.2.2, velocity components in boundary layer. In Chapter 10, velocity components in main stream.	$l$ and $t$	$l$ and $t$ are used as suffixes for quantities in laminar and turbulent flow respectively.
		$u$ and $l$	$u$ and $l$ are used as suffixes for quantities on upper and lower sides of profile respectively.



## AUTHOR INDEX

- ABBOTT, F. T. jr., 22  
ACKERET, J., 53, 56, 107, 111, 112  
EL BADRAWY, R. M., 115, 116  
BAUSCH, K., 1, 2  
BETZ, A., 10, 11, 21, 46, 53, 56, 57, 71, 84,  
    87, 97, 106, 107  
BIRNBAUM, W., 75  
BÖMELBURG, H., 108, 110  
BRASLOW, A. L., 56  
BURGERS, J. M., 10, 83  
BUSEMANN, A., 105, 111, 112, 114, 192,  
    266  
BUSSMANN, K., 88  
CHAPLYGIN, S. A., 106  
COPE, W. F., 93  
VON DOENHOFF, A. E., 92  
DOETSCH, H., 21, 27, 40, 45, 70, 176, 180  
VAN DRIEST, E. R., 93  
DRYDEN, H. L., 19, 20, 21, 45  
EGGERT, H., 244, 245  
EHLERS, F., 54  
FELDMANN, F., 107  
FERRI, A., 114  
GARRICK, I. E., 83  
GERBER, A., 58  
GLAUERT, H., 21, 75  
GOETT, H. I., 21  
GOLDSTEIN, S., 56, 84  
GÖRTLER, H., 88  
GÖTHERT, B., 16, 21  
GRUSCHWITZ, E., 93  
HALL, R. F., 190  
HANTZSCHE, W., 105  
HARTREE, D. R., 88, 89  
HELBOLD, H. B., 46, 63, 98  
HOERNER, S., 19, 20, 32  
HÖNDORF, F., 83  
VON HOLST, E., 192  
HOLSTEIN, H., 56, 190  
IMAI, I., 85  
JACOBS, E. N., 22  
JANZEN, O., 105  
JONES, B. M., 21  
JOUKOWSKY, N., 10  
JUNGCLAUS, G., 64  
KAJI, J., 85  
VON KÁRMÁN, T., 10, 83, 88, 90, 106, 108  
KAWALKI, K. H., 66  
KATZOFF, S., 21  
KEUNE, F., 11, 63, 75, 84  
KLEIN, M., 15  
KÖNIG, G., 180  
KRAEMER, K., 89  
KRAHN, E., 106  
KRAMER, M., 16, 176, 190  
KRASSILSCHIKOFF, P. P., 182  
KRÜGER, W., 49, 59, 184, 221  
KÜCHEMANN, D., 192  
KUETHE, A. M., 19  
LEVY, S., 93  
LIGHILL, M. J., 84  
LOCK, C. N. H., 12  
LUDWIEG, H., 21, 90, 91, 97  
MALAVARD, L., 108  
MÄNGLER, K. W., 88, 93  
MARTENSEN, E., 108  
MEYER, T., 111  
VON MISES, R., 11  
MOORE, L. L., 93  
MUESMANN, G., 244, 245  
MÜLLER, W., 83  
MULTHOFF, H., 104  
MUTTRAY, H., 21  
PÉRÈS, J., 74  
PFENNINGER, W., 56  
PIERCEY, N. A. V., 12  
PINKERTON, R. M., 87, 100  
PIPER, R. W., 12  
PISTOLESI, E., 75  
PLATT, R. C., 19, 20  
POHLHAUSEN, K., 88, 89, 90  
PRANDTL, L., 19, 22, 44, 88, 104, 111, 112  
PRESTON, J. H., 12  
PRETSCH, J., 93, 94, 95, 97, 98  
QUINN, J. H. jr., 54  
RAS, M., 56  
RASPET, A., 57  
RAYLEIGH, LORD, 105  
REGENSCHEIT, B., 22, 53, 54, 55, 56, 57, 58,  
    192  
REICHARDT, H., 45  
RIEGELS, F. W., 21, 75, 77, 80, 85  
RINGLEB, F., 12, 84, 85  
ROSSNER, G., 84  
ROTT, N., 107  
ROTTA, J., 90, 91  
RUDEN, P., 74  
SAENGER, E., 266  
SCHILLER, M., 178, 188  
SCHLICHTING, H., 44, 88, 93, 94, 95, 98  
SCHMIEDEN, S., 71, 199  
SCHMITZ, F. W., 22, 27, 35, 36, 120, 121,  
    237, 238, 240, 246  
SCHRENK, O., 10, 53, 58, 74, 176, 226  
SCHUBAUER, G. B., 93  
SCHULTZ-GRUNOW, F., 96  
SCHWIER, W., 55  
SEIFERTH, R., 19, 20, 21, 186, 188  
SILVERSTEIN, A., 21  
SKRAMSTAD, H. K., 93  
SQUIRE, H. B., 97  
STAUFER, 190  
STÜPER, J., 53  
TANI, J., 45  
TAYLOR, G. I., 21  
TETERVIN, N., 92  
THEODORSEN, T., 83, 84  
THWAITES, B., 55, 84  
TILLMANN, W., 43, 90, 91, 97  
TOLLMIEN, W., 88, 93  
TREFFTZ, E., 10, 74, 83  
TRUCKENBRODT, E., 79, 81, 82, 90, 91, 92,  
    98  
TSIEN, H. S., 106  
ULRICH, A., 93, 94  
UMEDA, K., 85  
WALCHNER, O., 46, 114, 266, 267, 268, 270,  
    272, 273  
WALZ, A., 54, 57, 58, 74, 83, 92, 97, 98, 99,  
    226  
WEINIG, F., 74  
WENDT, K., 105  
WENZINGER, C. J., 178  
WIEGHARDT, K., 43, 89, 90  
WILSON, R. E., 93  
WITTICH, H., 84, 85  
WUEST, H., 94  
WYSOCKI, 176, 178  
YOUNG, A. D., 45, 93, 97  
ZOBEL, T., 109



## SUBJECT INDEX

- Ackeret rule, 108, 111  
Aerodynamic centre, 25, 35  
American profile, 4  
Ames Laboratory 1 ft  $\times$  3½ ft high-speed tunnel, 18  
Amplification of disturbances in boundary layer, 95  
Angle, parametric, 3  
Angle of incidence, design, 24  
ideal, 24, 63, 76, 78, 80  
Angle of incidence at zero lift, 24, 29, 63  
Asymptotic suction profile, 94  
AVA 4 m  $\times$  5·4 m wind-tunnel, 16, 22  
AVA 2·25 m wind-tunnel, 15, 22, 26  
Bernoulli's equation, 62, 103  
Betz-Keune profile, 11, 74  
Biconvex profile, 67, 113, 114, 235  
Birnbaum-Glauert camber line, 63, 198  
Blowing, 53, 55, 88, 94, 95  
Boundary layer  
calculation of, 88, 90  
control, 53, 96, 97, 226  
effect of compressibility, 92  
equations, 89  
laminar, 95  
separation, 53, 72, 87, 91, 99, 100, 107  
stability, 93, 94, 95, 97  
transition, 93, 95  
Bow wave, 107  
Camber, maximum, 2, 63  
Camber line, 1, 62, 72, 138, 198  
Birnbaum-Glauert, 63, 198  
flow past, 76  
Kawalki, 66, 198  
CAT, 18  
Cavitation, 45, 267  
Cavitation number, 45, 46  
Cavitation tunnel, 16  
Centre, aerodynamic, 25, 35  
Centre of pressure, 25, 35, 64  
Chord, 1  
Circular arc, 63, 221  
symmetrical, 67, 70  
Circular segment profile, 45, 46, 114, 235, 240, 241, 266, 267  
Clark Y profile, 27, 48, 136, 145, 213, 226  
Compressed air tunnel, 18  
Compressibility, effect on boundary layer, 92  
Conformal mapping, 83  
Constant pressure distribution, profile with, 65  
Control, boundary layer, 53, 96, 97, 226  
Conversion formulas, 21  
Corrections, wind-tunnel, 21  
Critical height of roughness, 44  
Critical Mach number, 29, 35  
Critical Reynolds number, 19, 30, 31, 93, 94  
Critical speed, 108  
Curvature, effect of discontinuity in, 45, 70, 199  
Degree of turbulence, 18  
Density, reservoir, 103  
stagnation, 103  
Design angle of incidence, 24  
Design of symmetrical profile, 81  
Design of thin profile, 81  
Design of unsymmetrical profile, 82  
Design lift coefficient, 63  
Discontinuity in curvature, effect of, 45, 70, 199  
Displacement thickness, 89  
Dissipation, 90  
Distribution, thickness, 1  
Disturbances, isolated, 42  
Double wedge profile, 236, 266  
Drag, 24, 40, 42, 43, 56  
minimum, 31  
profile, 31, 96, 97, 98, 99  
skin-friction, 31, 44, 91  
Drag coefficient, 24, 32, 46, 107, 113, 114, 116, 162, 193  
total, 59  
DVL extension of NACA profiles, 7, 122, 146  
DVL 5 m  $\times$  7 m wind-tunnel, 16, 27  
DVL 2·7 m wind-tunnel, 16  
EC profile, 12, 70, 137  
ECH profile, 70  
Efficiency factor, 28  
End plates, 192  
Energy theorem, 89, 90  
Energy thickness, 90  
EQ profile, 12, 70  
EQH profile, 70, 137  
ETH wind-tunnel, 18  
Factor, turbulence, 19  
First main problem of profile theory, 80  
Five-figure NACA profile, 5, 6, 32, 126, 147, 161  
Flap, 48  
nose, 49  
plain, 48  
Short, 184  
slotted, 48  
split, 48, 50, 56, 226, 247, 255  
Flat plate, 28, 44, 54, 63, 96, 97, 113, 114, 115, 116, 200, 221, 237  
exact compressible solution, 114, 115, 116  
flow past, 76  
Flow field about Joukowsky profile, 74  
Flow field at a distance from a profile, 75  
Flow past camber line, 76  
Flow past flat plate, 76  
Form parameter, 91

- Four-figure NACA profiles, 4, 6, 31, 32, 64, 70, 107, 122, 147, 160, 255  
 Fowler high-lift device, 184  
 Full-scale wind-tunnel, 17  
 Generalised Joukowsky profile, 10, 74  
 Göttingen low-turbulence wind-tunnel, 20, 21  
 Göttingen 1·3 m wind-tunnel, 20  
 Göttingen profiles, 3, 120, 141, 162  
 Grain size, permissible, 44  
 Griffith profile, 56, 137  
 Gruschwitz parameter, 92, 93  
 Guidonia wind-tunnel, 18  
 Handley-Page high-lift device, 190  
 Hantzsch-Wendt approximation, 105  
 Hartree boundary layer profiles, 88, 89, 94, 95  
 High-lift devices, 176  
 Hinge moment, 114  
 Hodograph method, 105, 106  
 Hot-wire measurements, 20  
 Hyperbola family of profiles, 12, 70  
 Ideal angle of incidence, 24, 63, 76, 78, 80  
 Incidence at zero lift, 24, 29, 63  
 Isolated disturbances, 42  
 Janzen-Rayleigh approximation, 105  
 Japanese profile, 31  
 Joukowsky profile, 4, 10, 32, 68, 74, 200, 239  
     flow field about, 74  
     generalised, 10, 74  
 Kármán similarity parameter, 108  
 Kármán-Trefftz profile, 11, 56, 74  
 Kármán-Tsien approximation, 106  
 Kawalki camber line, 66, 198  
 Kellner-Bechereau high-lift device, 186  
 Kinetic pressure, 103  
 Krahn's  $\sqrt{\rho}$  method, 106  
 Kutta condition, 75, 87  
 Laminar boundary layer, 95  
 Laminar profile, 7, 32  
 Langley two-dimensional low-turbulence pressure tunnel, 17  
 Langley two-dimensional low-turbulence tunnel, 17  
 Leading edge coefficient, 2  
 Lift, 24, 28, 53, 55  
     influence of viscosity, 87  
     maximum, 30, 40, 42, 49, 53, 99  
 Lift coefficient, 24, 32, 46, 79, 113, 114, 116, 162, 193  
     design, 63  
 Lift coefficient at ideal angle of incidence, 63, 80  
 Lift-curve slope, 24, 28, 42, 79  
 Lighthill profile, 137  
 Line, camber, 1, 62, 72, 138, 198  
     mean, 1  
     skeleton, 1  
 Liquid media, 45  
 LTT, 17  
 Mach cone, 111  
 Mach number, critical, 29, 35  
 Main problem of profile theory, first, 80  
     second, 75, 83  
 Mapping theorem, Riemann's, 83  
 Maximum camber, 2, 63  
 Maximum lift, 30, 40, 42, 49, 53, 99  
 Maxwell slot, 184  
 Mean line, 1  
 Metacentric parabola, 24  
 Minimum drag, 31  
 Moment, see *pitching moment*  
 Momentum theorem, 88, 90  
 Momentum thickness, 90  
 MVA 2 m × 2 m wind-tunnel, 15, 22  
 NACA profiles, DVL extension, 7, 122, 146  
     five-figure, 5, 6, 32, 126, 147, 161  
     four-figure, 4, 6, 31, 32, 64, 70, 107, 122, 147, 160, 255  
     series 1 to 6, 7, 28, 32, 99, 206, 255  
     series 7 and 8, 9, 32  
     series 24, 27  
     series 230, 27, 29, 30, 33, 36, 53  
 NACA wind-tunnels, 16  
 Neutral point, 25  
 Normal force, 24  
 Nose flap, 49  
 NPL compressed air tunnel, 18  
 NPL profiles, 137  
 NPL 20 in × 8 in high-speed tunnel, 18  
 Optimum suction, 97  
 Parabola, metacentric, 25  
 Parametric angle, 3  
 Permissible grain size, 44  
 Pitching moment, 24  
 Pitching moment at zero lift, 35, 80  
 Pitching moment coefficient, 24, 35, 63, 80, 100, 114, 167  
 Plain flap, 48  
 Pohlhausen parameter, 92  
 Pohlhausen polynomial distributions, 88, 89, 93, 94  
 Poisson integral, 83, 84  
 Polars, 32, 237  
 Power-consumption coefficient, 58  
 Prandtl-Glauert rule, 29, 30, 104, 108, 111  
 Prandtl-Meyer flow, 112  
 Prandtl's boundary layer equations, 89  
 Pressure, centre of, 25, 35, 64  
     kinetic, 103  
     reservoir, 103  
     stagnation, 103  
 Pressure coefficient, 103  
 Pressure distribution, influence of viscosity, 87  
 Pressure distribution in supersonic flow, 112  
 Pressure side, 1  
 Profile, 1  
     American, 4  
     asymptotic suction, 94  
     Betz-Keune, 11, 74  
     biconvex, 67, 113, 114, 235  
     circular segment, 45, 46, 114, 235, 240, 241, 266, 267  
     Clark Y, 27, 48, 136, 145, 213, 226  
     double wedge, 236, 266  
     DVL extension of NACA, 7, 122, 146  
     EC, 12, 70, 137  
     ECH, 70  
     EQ, 12, 70  
     EQH, 70, 137  
     five-figure NACA, 5, 6, 32, 122, 147, 161

- four-figure NACA, 4, 6, 31, 32, 64, 70, 107, 122, 147, 160, 255  
 generalised Joukowsky, 10, 74  
 Griffith, 56, 137  
 Japanese, 31  
 Joukowsky, 4, 10, 32, 68, 74, 200, 239  
 Kármán-Trefftz, 11, 56, 74  
 laminar, 7, 32  
 Lighthill, 137  
 NACA series 1 to 6, 7, 28, 32, 99, 206, 255  
 NACA series 7 and 8, 9, 32  
 NACA series 24, 27  
 NACA series 230, 27, 29, 30, 33, 36, 53  
 RAF, 136  
 symmetrical, 67, 200  
 Profile drag, 31, 96, 97, 98, 99  
 Profile theory, first main problem, 80  
     second main problem, 75, 83  
 Profile with constant pressure distribution, 65  
 Profiles, Göttingen, 3, 120, 141, 162  
     Hartree, 88, 89, 94, 95  
     hyperbola family, 12, 70  
     NPL, 137  
     RAE, 159, 209  
 Profiles with high-lift devices, 176  
 RAE profiles, 159, 209  
 RAF profile, 136  
 Ratio, thickness, 2  
 Reservoir density, 103  
 Reservoir pressure, 103  
 Reynolds number, critical, 19, 30, 31, 93, 94  
 Riemann's mapping theorem, 83  
 Rotating high-lift devices, 192  
 Roughness, critical height of, 44  
     standard, 28, 40, 247  
     surface, 40  
 Scale of turbulence, 18  
 Second main problem of profile theory, 75, 83  
 Separation of boundary layer, 53, 72, 87, 91, 99, 100, 107  
 Shearing stress, work done against, 90  
 Shock wave, 107, 111, 112, 114, 228  
 Short flap, 184  
 Similarity rules, 108  
 Skeleton line, 1  
 Skin friction, 88  
 Skin-friction coefficient, 91  
 Skin-friction drag, 31, 44, 91  
 Slat, 50  
 Slot, Maxwell, 184  
 Slotted flap, 48  
 Span, 1  
 Speed, critical, 108  
 Split flap, 48, 50, 56, 226, 247, 255  
 Stability of boundary layer, 93, 94, 95, 97  
 Stagnation density, 103  
 Stagnation pressure, 103  
 Standard roughness, 28, 40, 247  
 Subsonic flow, 104  
 Suction, 53, 56, 88, 94, 95, 97, 226  
     asymptotic, 94  
     optimum, 97  
 Suction side, 1  
 Supersonic flow, 111  
 Support interference, 22  
 Surface roughness, 40  
 Surface waviness, 45  
 Symmetrical circular arc, 67, 70  
 Symmetrical profile, 67, 200  
     design of, 81  
     velocity distribution on, 76  
 Tangential force, 24  
 TDT, 17  
 Theodorsen's mapping procedure, 83, 84  
 Thickness, displacement, 89  
     energy, 90  
     momentum, 90  
 Thickness distribution, 1  
 Thickness ratio, 2  
 Thin profile, design of, 81  
 Tip-fairing, 22, 239, 240, 341  
 Total drag coefficient, 59  
 Transition of boundary layer, 93, 95  
 Transition point, 99  
 Transonic equations, 108  
 Transonic flow, 107  
 Truckenbrodt's procedure for boundary layer calculation, 90  
 Turbulence, degree of, 18  
     scale of, 18  
 Turbulence factor, 19  
 Turbulence of wind-tunnels, 18  
 Unsymmetrical profiles, design of, 82  
     velocity distribution on, 77  
 Variable-density wind-tunnel, 16, 22  
 Velocity distribution on symmetrical profile, 76  
 Velocity distribution on unsymmetrical profile, 77  
 Viscosity, influence on lift, 87  
     influence on pressure distribution, 87  
 Volume-flow-rate coefficient, 53, 94  
 Vortex distribution, 75  
 Wave, bow, 107  
     shock, 107, 111, 112, 114, 228  
 Waviness, surface, 45  
 Wind-tunnel  
     Ames 1 ft  $\times$  3½ ft, 18  
     AVA 4 m  $\times$  5·4 m, 16, 22  
     AVA 2·25 m, 15, 22, 26  
     DVL 5 m  $\times$  7 m, 16, 27  
     DVL 2·7 m, 16  
     ETH, 18  
     full-scale, 17  
     Göttingen low-turbulence, 20, 21  
     Göttingen 1·3 m, 20  
     Guidonia, 18  
     Langley LTT, 17  
     Langley TDT, 17  
     MVA 2 m  $\times$  2 m, 15, 22  
     NPL CAT, 18  
     NPL 20 in  $\times$  8 in, 18  
     variable-density, 16, 22  
 Wind-tunnel corrections, 21  
 Wind-tunnel turbulence, 18  
 Wing-tip influence, 22  
 Work done against shearing stress, 90

